frontiers | Research Topics

Community series in translational insights into mechanisms and therapy of organ dysfunction in sepsis and trauma, volume II

Edited by
Christoph Thiemermann, Pietro Ghezzi, Sina Maren Coldewey, Lukas Martin and Borna Relja

Published in
Frontiers in Immunology

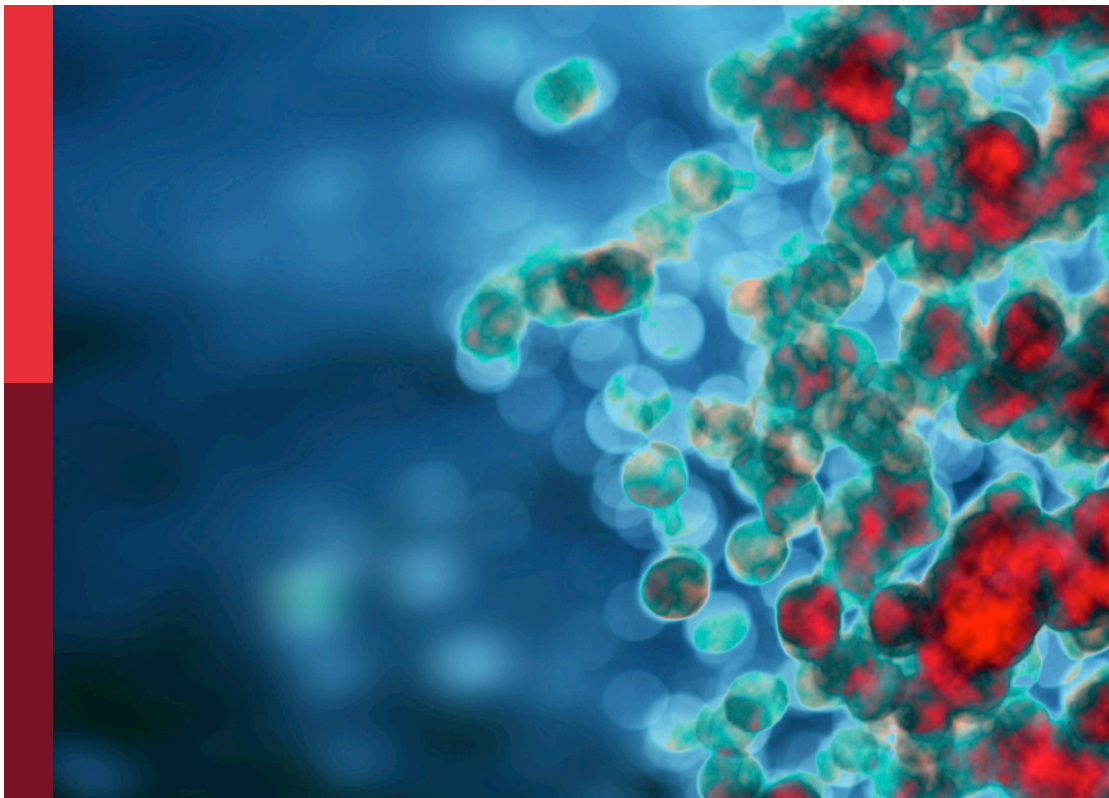

FRONTIERS EBOOK COPYRIGHT STATEMENT

The copyright in the text of individual articles in this ebook is the property of their respective authors or their respective institutions or funders. The copyright in graphics and images within each article may be subject to copyright of other parties. In both cases this is subject to a license granted to Frontiers.

The compilation of articles constituting this ebook is the property of Frontiers.

Each article within this ebook, and the ebook itself, are published under the most recent version of the Creative Commons CC-BY licence. The version current at the date of publication of this ebook is CC-BY 4.0. If the CC-BY licence is updated, the licence granted by Frontiers is automatically updated to the new version.

When exercising any right under the CC-BY licence, Frontiers must be attributed as the original publisher of the article or ebook, as applicable.

Authors have the responsibility of ensuring that any graphics or other materials which are the property of others may be included in the CC-BY licence, but this should be checked before relying on the CC-BY licence to reproduce those materials. Any copyright notices relating to those materials must be complied with.

Copyright and source acknowledgement notices may not be removed and must be displayed in any copy, derivative work or partial copy which includes the elements in question.

All copyright, and all rights therein, are protected by national and international copyright laws. The above represents a summary only. For further information please read Frontiers' Conditions for Website Use and Copyright Statement, and the applicable CC-BY licence.

ISSN 1664-8714
ISBN 978-2-8325-2660-6
DOI 10.3389/978-2-8325-2660-6

About Frontiers

Frontiers is more than just an open access publisher of scholarly articles: it is a pioneering approach to the world of academia, radically improving the way scholarly research is managed. The grand vision of Frontiers is a world where all people have an equal opportunity to seek, share and generate knowledge. Frontiers provides immediate and permanent online open access to all its publications, but this alone is not enough to realize our grand goals.

Frontiers journal series

The Frontiers journal series is a multi-tier and interdisciplinary set of open-access, online journals, promising a paradigm shift from the current review, selection and dissemination processes in academic publishing. All Frontiers journals are driven by researchers for researchers; therefore, they constitute a service to the scholarly community. At the same time, the *Frontiers journal series* operates on a revolutionary invention, the tiered publishing system, initially addressing specific communities of scholars, and gradually climbing up to broader public understanding, thus serving the interests of the lay society, too.

Dedication to quality

Each Frontiers article is a landmark of the highest quality, thanks to genuinely collaborative interactions between authors and review editors, who include some of the world's best academicians. Research must be certified by peers before entering a stream of knowledge that may eventually reach the public - and shape society; therefore, Frontiers only applies the most rigorous and unbiased reviews. Frontiers revolutionizes research publishing by freely delivering the most outstanding research, evaluated with no bias from both the academic and social point of view. By applying the most advanced information technologies, Frontiers is catapulting scholarly publishing into a new generation.

What are Frontiers Research Topics?

Frontiers Research Topics are very popular trademarks of the *Frontiers journals series*: they are collections of at least ten articles, all centered on a particular subject. With their unique mix of varied contributions from Original Research to Review Articles, Frontiers Research Topics unify the most influential researchers, the latest key findings and historical advances in a hot research area.

Find out more on how to host your own Frontiers Research Topic or contribute to one as an author by contacting the Frontiers editorial office: frontiersin.org/about/contact

Community series in translational insights into mechanisms and therapy of organ dysfunction in sepsis and trauma, volume II

Topic editors

Christoph Thiemermann — Queen Mary University of London, United Kingdom
Pietro Ghezzi — University of Urbino Carlo Bo, Italy
Sina Maren Coldewey — University Hospital Jena, Germany
Lukas Martin — University Hospital RWTH Aachen, Germany
Borna Relja — Universitätsklinikum Ulm, Germany

Citation

Thiemermann, C., Ghezzi, P., Coldewey, S. M., Martin, L., Relja, B., eds. (2023). *Community series in translational insights into mechanisms and therapy of organ dysfunction in sepsis and trauma, volume II*. Lausanne: Frontiers Media SA.
doi: 10.3389/978-2-8325-2660-6

The authors declare that the research was conducted in the absence of any commercial or financial relationships that could be construed as a potential conflict of interest

Table of contents

frontiers | Frontiers in Immunology

TYPE Editorial
PUBLISHED 25 May 2023
DOI 10.3389/fimmu.2023.1215888

Check for updates

OPEN ACCESS

EDITED AND REVIEWED BY
Yoram Vodovotz,
University of Pittsburgh, United States

*CORRESPONDENCE
Borna Relja
info@bornarelja.com

RECEIVED 02 May 2023
ACCEPTED 18 May 2023
PUBLISHED 25 May 2023

CITATION
Relja B, Coldewey SM, Ghezzi P, Martin L and Thiemermann C (2023) Editorial: Community series in translational insights into mechanisms and therapy of organ dysfunction in sepsis and trauma, volume II.
Front. Immunol. 14:1215888.
doi: 10.3389/fimmu.2023.1215888

COPYRIGHT
© 2023 Relja, Coldewey, Ghezzi, Martin and Thiemermann. This is an open-access article distributed under the terms of the Creative Commons Attribution License (CC BY). The use, distribution or reproduction in other forums is permitted, provided the original author(s) and the copyright owner(s) are credited and that the original publication in this journal is cited, in accordance with accepted academic practice. No use, distribution or reproduction is permitted which does not comply with these terms.

Editorial: Community series in translational insights into mechanisms and therapy of organ dysfunction in sepsis and trauma, volume II

Borna Relja[1]*, Sina Maren Coldewey[2], Pietro Ghezzi[3], Lukas Martin[4] and Christoph Thiemermann[5]

[1]Department of Trauma, Hand, Plastic and Reconstructive Surgery, Translational and Experimental Trauma Research, University Hospital Ulm, Ulm University, Ulm, Germany, [2]University Hospital Jena, Department of Anesthesiology and Intensive Care Medicine, Jena University Hospital, Jena, Germany, [3]University of Urbino Carlo Bo, Department of Biomolecular Sciences, Urbino, Italy, [4]University Hospital RWTH Aachen, Department of Intensive Care and Intermediate Care, Aachen, Germany, [5]Queen Mary University of London, William Harvey Research Institute, Barts and the London School of Medicine and Dentistry, Centre for Translational Medicine and Therapeutics, London, United Kingdom

KEYWORDS

sepsis, trauma, infections, complications, therapy, outcome

Editorial on the Research Topic
Community series in translational insights into mechanisms and therapy of organ dysfunction in sepsis and trauma, volume II

Critically ill patients with sepsis often experience life-threatening organ failure caused by a dysregulated response to inflammation. While there is a good understanding of some of the key signaling pathways involved in sepsis-related inflammation, the development of effective organ-protective therapeutic strategies is still limited. At present, therapeutic approaches for sepsis primarily involve source control, antibiotics, supportive care, and early goal-directed therapy. However, there is a lack of specific and effective treatments for the inflammatory response associated with sepsis, which can lead to multiple organ dysfunction in clinical patients. In addition, individuals who survive the initial acute stage of sepsis may develop an immuno-suppressive state, leaving them at an increased risk of detrimental secondary infections and high mortality rates. Therefore, relying solely on anti-inflammatory therapy may not be enough to successfully treat sepsis.

In their original article, Mohammad et al. discuss how Aquaporins, specifically RG100204, a new Aquaporin-9 inhibitor, can regulate crucial mechanisms in a cecal ligation and puncture (CLP) induced model of polymicrobial infection (sepsis) by reducing cardiac dysfunction (systolic and diastolic), renal dysfunction, and hepatocellular injury. One notable finding is that administering RG100204 orally, even 3 hours after the onset of polymicrobial sepsis, can reduce the activation of the NLRP3 inflammasome pathway and myeloperoxidase activity in the lungs, thereby reducing cardiac and renal dysfunction caused by severe sepsis. This and previous reports suggest that AQP9 could be a promising

drug target in the treatment of polymicrobial sepsis, and warrant further analysis in future trials.

Zhang et al. have shown that Erythropoietin (EPO), a glycoprotein that is regulated by hypoxia-inducible factor 1α (HIF-1α), is naturally induced in endotoxin-tolerant macrophages upon initial exposure to LPS. This study is the first to demonstrate that EPO plays a role in regulating the functional re-programming of endotoxin-tolerant macrophages.

When endotoxin-tolerized macrophages were exposed to EPO, they expressed fewer proinflammatory genes, such as *Il1b*, *Il6*, and *Tnfa*, and more host-protective genes, such as *Cnlp*, *Marco*, and *Vegfc*. This effect was achieved through the upregulation of *Irak3* and *Wdr5 via* the PI3K/AKT pathway upon secondary exposure to LPS. The authors also found that LPS-tolerized mice treated with EPO were protected against secondary infection with *E. coli* and had improved outcomes after sepsis. While more research is needed to translate these findings to clinical settings, this drug presents new opportunities for the treatment of sepsis.

Dennhardt et al. discovered that EPO and its non-hematopoietic analog, pyroglutamate helix B surface peptide (pHBSP), can provide tissue protection through the innate repair receptor (IRR), independent of their hematopoietic properties *via* the EPO receptor (EPO-R) homodimer. Their research also showed that EPO signaling plays a role in the pathology of Hemolytic-uremic syndrome (HUS) caused by infections with Shiga toxin (Stx)-producing *E. coli*, as evidenced by elevated levels of endogenous EPO in patients with HUS, piglets, and mice subjected to preclinical HUS models. Moreover, the protective effects of pHBSP and EPO were linked to decreased renal oxidative stress, and pHBSP was associated with reduced nitrosative stress and less KIM-1 expression in Stx-challenged mice, without any thromboembolic complications or other adverse side effects. The authors provide evidence that treating mice with HUS with EPO or pHBSP improves 7-day survival and disease outcome, and suggest that targeting the EPO-R/IRR axis could be a promising approach for treating patients with hemolytic anemia in HUS in future clinical trials.

Prior research has demonstrated that inhibiting Bruton's tyrosine kinase (BTK), a key factor in the recruitment and function of immune cells, can enhance renal function in experimental cases of sepsis and lupus nephritis. In a new study by Kröller et al., it was found that two FDA-approved BTK inhibitors, ibrutinib and acalabrutinib, can limit the progression of HUS in mice by reducing the activation of phospholipase-C-gamma-2 in the spleen, thereby decreasing the invasion of BTK-positive cells like neutrophils into the kidneys. Treatment with ibrutinib resulted in a decline in the infiltration of macrophages, improvement in acute kidney injury and dysfunction markers (NGAL and urea), and a decrease in hemolysis (bilirubin and LDH activity). These findings suggest that inhibiting BTK could be a promising and effective therapeutic approach for HUS by reducing the infiltration of immune cells in the kidneys, as demonstrated in a murine model.

Numerous clinical and experimental studies have indicated that the glycocalyx, which is involved in endothelial dysfunction that leads to sepsis-induced multiple organ failure, could be a promising early target for endothelial injury during infection. Urban et al. conducted experiments on mice with CLP-induced sepsis and administered Colivelin, a synthetic derivative of the mitochondrial peptide humanin. The results showed that Colivelin restored endothelial stability and reduced the infiltration of inflammatory cells in the lungs, kidneys, and liver, along with decreasing the systemic release of pro-inflammatory cytokines. These effects were associated with the inhibition of the signal transducer and activator of transcription 3 and the activation of the AMP-activated protein kinase in the aorta and lungs. When used in conjunction with standard fluid resuscitation and antibiotics, Colivelin improved the long-term recovery and health outcomes of septic mice.

Alves et al. evoked polymicrobial sepsis in WT mice and knockout mice for ICOS, ICOSL and OPN genes. Mice that received a soluble recombinant form of ICOS ICOS-Fc exhibited a decrease in plasma cytokine levels (TNF-α, IL-1β, IL-6, IFN-γ, and IL-10), liver injury (AST and ALT), kidney dysfunction (creatinine and urea), and local activation of FAK, P38 MAPK, and NLRP3 inflammasome caused by sepsis. The authors presented evidence that ICOS-Fc works on both sides of the ICOS-ICOSL interaction, as the protective effect was absent in septic knockout mice for the ICOS or ICOSL genes, while it was preserved in OPN knockout mice. These findings suggest that pharmacologically modifying the ICOS-ICOSL pathway may have beneficial effects and that there may be a potential cross-talk mechanism involving the FAK-p38-NLRP3 inflammasome axis in counteracting sepsis-induced inflammation and organ dysfunction.

Zheng et al. investigated the potential use of immune-related genes (IRGs) as biomarkers for developing diagnostic and prognostic models for sepsis outcomes. Their study aimed to understand the immune microenvironment of circulating immune cells, assess the immunosuppression state in sepsis, and develop a prognostic model based on IRGs to identify patients at high risk and predict 28-day mortality. The authors demonstrated that the immune response is critical in the development of sepsis. Using a Cox prediction model, they identified 22 differentially expressed immune-related genes (DEIRGs) that classified patients into low-risk and high-risk groups and constructed the prognostic model. The regulatory network between transcription factors (TFs) and prognostic DEIRGs provided novel molecular mechanisms in sepsis. The prognostic model showed high accuracy and performance in identifying patients at high risk and predicting 28-day mortality in sepsis patients.

Wang et al. conducted a study to evaluate the therapeutic effects of Human Umbilical Cord Mesenchymal Stem Cells (HUMSCs) intervention on lung tissue in juvenile septic rats. For the first time, they performed proteomic and phosphorylated proteomic screening and analysis on the lung tissue to identify differentially expressed proteins and significantly changed phosphorylation sites after 24 hours of HUMSCs intervention. The results revealed that 213 proteins and 971 phosphorylation sites showed significant changes in the therapy group. The authors found that Tenascin-C could be the key protein responsible for promoting lung injury repair in juvenile septic rats through HUMSCs intervention. Furthermore, the study suggested that HUMSCs may activate Tenascin-C-mediated

PGE2 release and improve endothelial cell functional barrier, leading to the recovery of gas-blood barrier function in lung tissue. Phosphorylation analysis revealed that HUMSCs may regulate the phosphorylation of VEGFA through the EGFR tight junction pathway, thus alleviating inflammatory injury and improving the permeability of the endothelial barrier in lung tissue. Overall, the study identified potential new therapeutic targets for HUMSCs to alleviate lung injury in a juvenile sepsis rat model.

Martinez-Orengo et al. have proposed a new approach for evaluating and measuring organ-level immunoreactivity and associated dysfunction in systemic inflammatory response syndrome (SIRS) and sepsis. Using a PET imaging tracer [^{18}F] DPA-714 for the translocator protein (TSPO), the authors were able to detect increased binding in the brain, lungs, liver, and bone marrow in a rat model of SIRS induced by LPS administration. The *in vivo* PET/CT scans were validated by *in vitro* measures of TSPO expression and immunofluorescent staining. The study revealed brain, liver, and lung inflammation, spleen monocytic efflux/lymphocytic activation, and suggested increased bone marrow hematopoiesis. The authors suggest that [^{18}F]DPA-714 PET could be used as a noninvasive tool to monitor organ-level inflammation in different organs (lung, liver, bone marrow, brain, and spleen) in SIRS and sepsis and to evaluate therapeutic interventions aimed at decreasing or controlling inflammation.

Amoafo et al. have shown that purinergic signaling, a newly identified regulatory mechanism in immune cell physiology, may be regulated differently in male and female mice in response to hormones. They found that deficiency in the $P2Y_{12}$ receptor but not the $P2Y_1$ receptor decreased activity of MPO in lungs and kidneys, platelet-leukocyte interaction, and platelet activation in male mice with sepsis, but not in female mice. Treatment with selective antagonists for $P2Y_{12}$ or $P2Y_1$ receptors also decreased sepsis-induced MPO levels, aggregate formation, and platelet activation in male mice, but not in female mice. These findings were supported by *in vitro* experiments with human T lymphocytes, where blocking $P2Y_1$ or $P2Y_{12}$ receptors had a sex-dependent effect on cell growth and secretion. These results suggest that drug targeting purinergic signaling in sepsis should be carefully tailored to the sex of the patient in future targeted therapies.

The focus of this Research Topic is to shed new light on the molecular mechanisms that contribute to inflammation during septic conditions, with particular attention given to preclinical and translational studies aimed at developing new therapeutic strategies to protect organs.

Author contributions

All authors listed have made a substantial, direct, and intellectual contribution to the work and approved it for publication.

Conflict of interest

The authors declare that the research was conducted in the absence of any commercial or financial relationships that could be construed as a potential conflict of interest.

Publisher's note

All claims expressed in this article are solely those of the authors and do not necessarily represent those of their affiliated organizations, or those of the publisher, the editors and the reviewers. Any product that may be evaluated in this article, or claim that may be made by its manufacturer, is not guaranteed or endorsed by the publisher.

frontiers | Frontiers in Immunology

ORIGINAL RESEARCH
published: 14 June 2022
doi: 10.3389/fimmu.2022.900906

RG100204, A Novel Aquaporin-9 Inhibitor, Reduces Septic Cardiomyopathy and Multiple Organ Failure in Murine Sepsis

Shireen Mohammad[1], Caroline E. O'Riordan[1], Chiara Verra[1], Eleonora Aimaretti[2], Gustavo Ferreira Alves[3], Klaus Dreisch[4], Johan Evenäs[4], Patrizia Gena[5], Angela Tesse[6], Michael Rützler[7,8], Massimo Collino[3], Giuseppe Calamita[5] and Christoph Thiemermann[1]**

[1] William Harvey Research Institute, Queen Mary University of London, London, United Kingdom, [2] Department of Clinical and Biological Sciences, University of Turin, Turin, Italy, [3] Department of Neurosciences "Rita Levi Montalcini", University of Turin, Turin, Italy, [4] Red Glead Discovery Akiebolag (AB), Lund, Sweden, [5] Department of Biosciences, Biotechnologies and Biopharmaceutics, University of Bari "Aldo Moro", Bari, Italy, [6] Nantes Université, Instite National de la Santé et de la Recherche Médicale (INSERM), Centre National de la Rescherche Scientifique (CNRS), l'institut du Thorax, Nantes, France, [7] Department of Biochemistry and Structural Biology, Lund University, Lund, Sweden, [8] Apoglyx Akiebolag (AB), Lund, Sweden

OPEN ACCESS

Edited by:
Manuela Mengozzi,
Brighton and Sussex Medical School, United Kingdom

Reviewed by:
Basilia Zingarelli,
Cincinnati Children's Hospital Medical Center, United States
Fei Tu,
University of Pittsburgh, United States

***Correspondence:**
Shireen Mohammad
s.mohammad@qmul.ac.uk
Christoph Thiemermann
c.thiemermann@qmul.ac.uk

Specialty section:
This article was submitted to Inflammation, a section of the journal Frontiers in Immunology

Received: 21 March 2022
Accepted: 09 May 2022
Published: 14 June 2022

Citation:
Mohammad S, O'Riordan CE, Verra C, Aimaretti E, Alves GF, Dreisch K, Evenäs J, Gena P, Tesse A, Rützler M, Collino M, Calamita G and Thiemermann C (2022) RG100204, A Novel Aquaporin-9 Inhibitor, Reduces Septic Cardiomyopathy and Multiple Organ Failure in Murine Sepsis. Front. Immunol. 13:900906. doi: 10.3389/fimmu.2022.900906

Sepsis is caused by systemic infection and is a major health concern as it is the primary cause of death from infection. It is the leading cause of mortality worldwide and there are no specific effective treatments for sepsis. Gene deletion of the neutral solute channel Aquaporin 9 (AQP9) normalizes oxidative stress and improves survival in a bacterial endotoxin induced mouse model of sepsis. In this study we described the initial characterization and effects of a novel small molecule AQP9 inhibitor, RG100204, in a cecal ligation and puncture (CLP) induced model of polymicrobial infection. *In vitro*, RG100204 blocked mouse AQP9 H_2O_2 permeability in an ectopic CHO cell expression system and abolished the LPS induced increase in superoxide anion and nitric oxide in FaO hepatoma cells. Pre-treatment of CLP-mice with RG100204 (25 mg/kg p.o. before CLP and then again at 8 h after CLP) attenuated the hypothermia, cardiac dysfunction (systolic and diastolic), renal dysfunction and hepatocellular injury caused by CLP-induced sepsis. Post-treatment of CLP-mice with RG100204 also attenuated the cardiac dysfunction (systolic and diastolic), the renal dysfunction caused by CLP-induced sepsis, but did not significantly reduce the liver injury or hypothermia. The most striking finding was that oral administration of RG100204 as late as 3 h after the onset of polymicrobial sepsis attenuated the cardiac and renal dysfunction caused by severe sepsis. Immunoblot quantification demonstrated that RG100204 reduced activation of the NLRP3 inflammasome pathway. Moreover, myeloperoxidase activity in RG100204 treated lung tissue was reduced. Together these results indicate that AQP9 may be a novel drug target in polymicrobial sepsis.

Keywords: aquaporin (AQP), sepsis, cecal ligation and puncture, inflammation, multiple organ failure

INTRODUCTION

Sepsis and septic shock result in multiple-organ failure that can lead to death (1). Aquaporins (AQPs) are a family of membrane channel proteins which are responsible for facilitating diffusion of water as well as glycerol across the plasma membrane (2). Briefly, there are 13 AQPs in mammals which are important for the regulation of water movement in and out of the cell. Some AQPs can also facilitate passive movement of glycerol and other small solutes including urea and hydrogen peroxide (H_2O_2) cross the cell membrane. Aquaporins can regulate crucial key mechanism of sepsis and hence could be promising drug targets (3).

In physiology, AQP9 is the principal facilitator of glycerol uptake into hepatocytes, for entry into gluconeogenesis, especially during fasting (4, 5). Previously described AQP9 functions in leukocytes include maturation of dendritic cells (6), glycerol metabolism in $CD8^+$ T memory cells, and an involvement in locomotion in neutrophils (7, 8). Moreover, when compared to healthy controls, neutrophils from patients with SIRS show increased AQP9 expression (9).

In addition to facilitating glycerol transmembrane diffusion, AQP9 is also permeable to water, and H_2O_2 (10–12). There is now increasing evidence that H_2O_2 permeability mediated by different AQP isoforms contributes to redox signaling in diverse cellular processes including locomotion (13, 14), growth factor signals (15), cytokine receptor signals (16), and toll-like receptor signal (17). Since AQP9 plays a role in metabolism and inflammation, it may also play a role in the progression of sepsis. Indeed, a recent study points towards a role for AQP9 in the pathophysiology of sepsis: when compared to wild-type mice, *Aqp9*$^{-/-}$ knockout mice challenged with a lethal dose of LPS had a longer survival time and 25% of these mice recovered fully. *Aqp9*$^{-/-}$ knockout mice subjected to endotoxemia also showed reduced iNOS expression (and NO formation) and COX-2 expression, secondary to a reduced expression/activation of NF-κB RelA/p65 in the kidney, aorta, liver, and heart compared to wild-type mice induced with LPS (18). The inflammasome component NLRP3 is upregulated in sepsis which leads to the cleavage of pro-caspase-1 to caspase-1, and subsequently maturation and release of the proinflammatory cytokine, IL-1β. As an intriguing hypothesis, a requirement of water influx *via* AQPs in the activation of the inflammasome has been introduced (19). However, experiments supporting this idea involved harsh osmotic conditions, and sometimes the use of the pleiotropic and cytotoxic AQP blocker $HgCl_2$ (19–21). Therefore, this idea requires further investigation. The development of specific aquaporin-inhibitors that are suitable for *in vivo* experiments has however been historically difficult (22, 23). We now describe the first use of a new AQP9 inhibitor, RG100204, in a cecal ligation and puncture (CLP) mouse model of peritoneal infection and systemic inflammation.

METHODS

RG100204

The compound RG100204 is described as example 29 in the patent US20190127360 (24) The patent contains description of the used synthetic route and the LC-MS and ^{1}H NMR data.

RG100204 Formulation for Oral Administration (25 mg/kg BW)

PEG 400 (polyethylene glycol 400, Acros Organics), Labrasol® (caprylocaproyl polyoxyl-8-glycerides, Gattefossé), and Kolliphor® EL (polyoxyl-35 castor oil, Sigma Aldrich) were mixed to a ratio of 50:30:20 w%. The components were mixed by stirring on a rolling mixer. Dry powder of RG100204 was solubilized in this blank vehicle to a concentration of 10 mg RG100204 per g vehicle. The formulation was homogenized by ultrasonication.

Cell Based Assays

Flp-In™-CHO Cells were purchased from Invitrogen (ThermoFisher) and modified as described previously (5, 11). Water permeability was measured as cell shrinking in response to extracellular sucrose addition, as described previously (5). Glycerol permeability was measured in the same way, except for the addition of 500 mM glycerol to the assay incubation buffer. The incubation time in glycerol buffer varied between 5 and 50 minutes, depending on the position of each well within a 96-well plate. No effect of incubation time was noted. Glycerol efflux was induced by replacing 250 mM of the extracellular glycerol with 250 mM sucrose, by 1:1 dilution with 500 mM sucrose containing buffer. Measurements of H_2O_2 permeability were conducted as described previously (11).

% Permeability Was Calculated as:

$$\%\,permeability = 1 - \frac{K\,[AQP9\ control] - K\,[AQP9\ inhibitor]}{K\,[AQP9\ control]\ - K\,[CHO]}$$

Whereby K corresponds to the rate constant, obtained from fitting the fluorescence intensity recordings after sucrose, and H_2O_2 addition, respectively, to a one-phase exponential function. [*AQP9 control*] describes AQP9 expressing cells incubated in 1% DMSO, the inhibitor vehicle; [*AQP9 inhibitor*] describes cells incubated at respective inhibitor concentration; and [*CHO*] describes recordings from CHO control cells, or CHO HyPer-3 (25) expressing control cells, respectively, that do not express ectopic AQP9.

NO and Superoxide Anion Measurements

Rat hepatoma FaO cells [The European Collection of Authenticated Cell Cultures (ECACC)] were grown in Coon's modified Ham's F12 with 10% fetal bovine serum (FBS) until 80% confluence. Cell incubations were made in humidified atmospheric air at 37°C with CO_2 added to 5%. Cell monolayers composed of about $5x10^5$ cells were exposed for 6 h at 37°C to the culture medium (1% DMSO) containing 25 μM RG100204, 1 μg/mL LPS (from Escherichia coli 0111:B4; Sigma) or 25 μM RG100204 plus 1 μg/mL LPS. For the basal condition cells were exposed to the culture medium containing the vehicle alone (1% DMSO). At the end of the treatment cell samples of each condition were harvested and handled to prepare the spin

traps for the subsequent nitric oxide (NO) and superoxide anion (O_2^-) measurements as described below.

The cytotoxicity of RG100204 in FaO cells was evaluated by MTT (3-(4,5-dimethylthiazol-2-yl)-2,5-diphenyltetrazolium bromide) cell viability assay (Biotium, Milan, Italy). FaO cells were seeded in a 96-well plate and incubated 24 h in humidified atmospheric air at 37°C with CO_2 added to 5%. After treated with the vehicle alone (1% DMSO) or 25 μM RG100204 (in 1% DMSO) for 24 h, cells were analyzed by adding MTT. The colorimetric absorbance was measured by an iMark™ microplate reader (BIO-RAD, Segrate, Italy) at 490 nm.

Electron paramagnetic resonance (EPR) for NO and O_2^- measurements with the spin traps of FaO cells prepared as above was carried out as previously described (18). Briefly, Fe^{2+} diethyldithiocarbamate ($Fe(DETC)_2$) was used as spin trap to evaluate NO production. For this purpose, Na-(DETC) (3.6 mg; Sigma) and $FeSO_4$-$7H_2O$ (2.3 mg; Sigma) were dissolved separately in equal volumes of ice-cold Krebs–Hepes buffer or distilled water, respectively, each one bubbled with nitrogen gas. The solutions were mixed to obtain a pale yellow-brown opalescent colloid $Fe(DETC)_2$ solution (0.4 mM), which was used immediately to incubate the FaO cells (45 min at 37°C). After incubation, the spin trap solution was removed, and cells were scraped off and frozen in liquid nitrogen.

To evaluate extracellular and intracellular production of O_2^-, FaO cells were incubated in a Krebs-Hepes solution containing 500 μM of 1-hydroxy-3methoxycarbonyl-2,2,5,5-tetramethylpyrrolidin (CMH; Noxygen, Denzlingen, Germany), 25 μM deferoxamin (Sigma) and 5 μM DETC (Sigma) for 45 min at 37°C. To measure the extracellular superoxide anion concentration, CMH solution was removed after the incubation step, and frozen in liquid nitrogen. Cells were then scraped off from the culture plate and frozen in liquid nitrogen. All the samples were analyzed using a table-top x-band spectrometer Miniscope (Magnettech, MS5000, Berlin, Germany). Recordings were made in liquid nitrogen, using a Dewar flask.

The instrument settings were 10 mW of microwave power, 1 mT of amplitude modulation, 100 kHz of modulation frequency, 180 s of sweep time and 3 scans for NO measurements, sweep time 60 s, and 3 scans for superoxide anion measurements. Signals were quantified by measuring the total amplitude of the spectra obtained, after correction of baseline for NO evaluation or by calculating the height of the central peak of the spectra for superoxide anion measurements.

Ethical Statement

All animal protocols in this study were approved by the Animal Use and Care Committee of Queen Mary University of London (QMUL), in accordance with the Home Office Guidance on the Operation of Animals (Scientific Procedure Act 1986), published by Her Majesty's Stationary Office and the Guide for the Care and Use of Laboratory Animals of the National Research Council and were approved by the Animal Welfare Ethics Review Board of QMUL. All research was conducted under the U.K. home office project license number: PC5F29685.

Animals

This study was carried out on 10-week-old, male C57BL/6 mice (Charles River Laboratories UK Ltd., Kent, UK) weighing 20-30 g kept under standard laboratory conditions. The animals were allowed to acclimatize to laboratory conditions for at least one week before undergoing experiments. Six mice were housed together in ventilated cages lined with absorbent bedding material. Tubes and chewing blocks were placed in all cages for environmental enrichment. All animals were subjected to 12-h light and dark cycles and the temperature was maintained at 19-23°C. All animals had access to a chow diet and water *ad libitum*. The cages were cleaned approximately every three days, with water being changed daily. Research staff inspected the animals each day for any signs of illness or abnormal behavior.

Cecal Ligation and Puncture (CLP) Model

CLP surgery was performed on 10-week-old C57BL/6 mice. Sham-operated mice underwent sham surgery, which involved the same treatment; however, these mice were not subjected to ligation and puncture of the caecum. Before starting surgery, mice were injected with buprenorphine (0.05 mg/kg i.p.) to provide analgesia. Mice were initially anaesthetized with 3% isoflurane and 1% oxygen and maintained under anaesthesia throughout surgery with 2% isoflurane and 1% oxygen *via* a nosecone. The temperature of the mice was monitored during surgery by a rectal thermometer and maintained at 37°C with a homoeothermic blanket. Abdominal hair was removed by Veet® hair removal cream and the area cleaned with 70% ethanol. The abdomen was opened *via* a 1.5 cm midline incision, exposing the caecum. The caecum was then totally ligated 1.5 cm from the end of the caecum (just below the ileocecal valve) and a G-18 needle was used to puncture both opposite ends of the ligated caecum. A small amount of faeces was squeezed out (~3mm) from both ends and the caecum was placed back into the abdomen in its anatomical position. Thereafter, 5 ml/kg of normal saline (0.9% NaCl) was placed into the abdominal cavity and the abdomen was closed. Normal saline (10 ml/kg) was also given s.c. directly after surgery for fluid resuscitation and this was repeated at both 6 h and 18 h after surgery. Antibiotics (Imipenem/Cilastin; 0.25mg/ml dissolved in the resuscitation fluid s.c.) and an analgesic (buprenorphine; 0.05 mg/kg body weight i.p.) were also administered at 6 h and 18 h after surgery. At 24 h after CLP, cardiac function was assessed by echocardiography *in vivo*. At 24 h, mice were anaesthetized (terminal anaesthesia) with isoflurane and blood was obtained by cardiac puncture. Mice were then killed by removing the heart. Organs were snap frozen in liquid nitrogen for further analysis.

At 24 h, a clinical score of each mouse that underwent surgery was taken to monitor the health of each mouse. The clinical score was based on the following signs: piloerection, diarrhoea, respiratory distress, tremors, lethargy, and periorbital exudates resulting in a potential, maximal score of 6. Mice with a clinical score of ≤ 3 were considered to have moderate sepsis, while mice with a clinical score of > 3 mice were considered to have severe sepsis.

Study Design

Pre-treatment study: Mice were randomised into three groups (sham, control, and drug treatment). Sham and CLP control mice received vehicle *via* oral gavage just before CLP surgery and 8 h after CLP, while drug treatment group received RG100204 *via* oral gavage just before CLP and 8 h after CLP surgery.

Post-treatment study: Mice were randomised into five groups (sham, control and three different drug treatments). Sham and CLP control mice received vehicle *via* oral gavage 1 h and 8 h after CLP surgery. The three different timepoints of the administration of RG100204 *via* oral gavage included: 1 h & 8 h, or 3 h & 8 h, or 3 h & 8 h & 18 h, after CLP surgery.

Assessment of Cardiac Function

At 24 h after surgery, cardiac function was assessed using the Vevo 3100 imaging system and MX550D transducer (FujiFilm VisualSonics). Mice were initially anaesthetized using 3% isoflurane together with 1 L/min oxygen in an anaesthesia chamber. Once mice were sedated, they were then transferred to the echocardiography table, where they were allowed to stabilize for at least 10 min and maintained under anaesthesia now using 2% isoflurane together with 1 L/min oxygen for the duration of the procedure *via* nosecone. The limbs of the mice were then taped down onto the metal ECG leads on the platform. The platform was heated to ensure the body temperature of the animals was maintained throughout the procedure (37°C). The temperature was continuously monitored with a rectal thermometer and the heart rate was monitored throughout the procedure from the ECG trace. The fur on the chest of the mice was removed using Veet® hair remover. Echocardiography gel, which was pre-warmed, was then placed on the shaven chest of the mice to allow measurements of the heart to be taken using the MX550D transducer. The following parameters were measured: left ventricular ejection fraction (LVEF), fractional shortening (FS), fractional area change (FAC), cardiac output (CO), stroke volume (SV), mitral valve E/A ratio, myocardial performance index, pulmonary artery VTI and pulmonary artery peak velocity. All data was analyzed offline on VevoLab (FujiFilm VisualSonics).

Organ and Blood Collection

At the end of the experiment mice were anaesthetized with isoflurane (3%) delivered in oxygen (1 L/min). They were then sacrificed by terminal cardiac puncture and exsanguination (removal of blood) with a G25 needle. Approximately 0.7 ml of blood was collected from each mouse and decanted immediately into 1.3 ml serum gel tubes (Sarstedt, Nümbrecht, Germany). All organs were collected and snap frozen in liquid nitrogen and were stored at -80°C. Blood serum was isolated after 3 min centrifugation at 9900 rpm, before snap-freezing in liquid nitrogen and storing at -80°C. 100 µl of serum samples were then analyzed in a blinded fashion by a commercial veterinary testing laboratory (MRC Harwell Institute, Oxfordshire, UK) to evaluate the biomarkers serum urea, and creatinine for renal dysfunction, serum alanine aminotransferase (ALT), and serum aspartate aminotransferase (AST) for hepatocellular injury, and lactate dehydrogenase (LDH) for general organ injury.

Western Blot Analysis

Immunoblot analyses of heart and kidney tissue were carried out using semi-quantitative Western blotting, as previously described (26). To assess the degree of phosphorylation of IKKα/β at $Ser^{176/180}$, IκBα at $Ser^{32/36}$, the expression and nuclear translocation of NF-κB p65, the expression of NLRP3, including the cleavage of pro-caspase to active caspase 1. The antibodies used were: rabbit anti-$Ser^{176/180}$-IKKα/β (1:1000, Cell Signalling Technology), rabbit anti-total IKKα/β (1:1000, Cell Signalling Technology), mouse anti-$Ser^{32/36}$-IκBα (1:1000, Cell Signalling Technology), mouse anti-total IκBα (1:1000, Cell Signalling Technology), rabbit anti-NFκB p65 (1:1000, Cell Signalling Technology), 1:1000 rabbit anti- NLRP3 inflammasome (AdipoGen) and 1:1000 mouse anti-caspase 1 (p20) (Cell Signalling).

The protein bands were visualized using enhanced chemiluminescence (ECL) detection system. Bio-Rad Image Lab Software 6.0.1 was used to analyze the immunoreactive bands and the results were normalized to sham.

Myeloperoxidase (MPO) Assay

Tissue was weighed and left on ice (~50 mg for lungs). Samples were homogenized in 500 µl of 20 mM phosphate buffer (pH 7.4) on ice. The homogenate was centrifuged at 13,000 x g at 4°C for 10 min. The supernatant was discarded, and the pellet was resuspended in 0.5 mL of hexadecyltrimethylammonium bromide (HTAB) solution. HTAB is a detergent that releases and solubilizes MPO from neutrophilic granules. Samples were centrifuged at 13,000 x g at 4°C for 10 min and supernatant was collected. The plate reader was set to 37°C. In a 96-well plate, 30 µL of the supernatant were added to each well (in duplicate). 180 µl of peroxide solution [sodium phosphate buffer (80 mM PBS, pH 5.4) with H_2O_2 (0.4 mM)] was added. The final concentration of H_2O_2 in the plate must be 0.3 mM. The reaction started with the addition of 20 µL of the TMB solution (18.4 mM). The final concentration on the TMB plate was 1.6 mM. The mixture was incubated for 2 min in the plate reader at 37°C, before 5 absorbance readings at 650 nm at 2 min intervals. MPO activity was expressed as optical density (O.D.) at 650nm per mg of protein.

Statistical Analysis

Dose-responses were calculated in GraphPad Prism 5.0 (GraphPad Software, San Diego, California, USA), after log transformation of compound concentrations and fitting to a standard sigmoidal model, with an assumed Hill slope of -1. All other data were analyzed using GraphPad Prism 7.0. All data in both text and figures are expressed as mean ± standard error of the mean (SEM) of *n* observations, where *n* represents the number of animals studied. Data was then assessed using One-way ANOVA followed by a Bonferroni's *post-hoc* test, except for **Figures 3C, E**, **8C, E**, where 2-way-ANOVA was performed. $P < 0.05$ was considered statistically significant.

RESULTS

RG100204 *In Vitro* Characterization

In order to characterize RG100204 for AQP isoform inhibition, we tested CHO cells with ectopic expression of either mouse AQP9, or its closest mouse AQP homologues, AQP3, and AQP7, respectively. AQP water permeability and AQP glycerol permeability were tested in Calcein loaded cells, a fluorescent cell volume indicator (**Figures 1A, B**). We observed a dose-dependent inhibition of both, AQP9 water permeability (IC_{50}~1.1×10^{-7} M) and AQP9 glycerol permeability (IC_{50}~7.6×10^{-8} M) by RG100204. By comparison, inhibition by the known, unspecific AQP9 inhibitor phloretin was less potent (IC_{50}~7.2×10^{-7} M), and for glycerol permeability also less efficacious (IC_{50}~1.6×10^{-6} M, mean observed remaining permeability 16%). No inhibition of water or glycerol permeability by RG100204 was observed in AQP3 expressing CHO cells, while only minor inhibition of AQP7 dependent water and glycerol permeability could be measured, thus establishing that RG100204 inhibits AQP9, while it does not inhibit closely related AQP isoforms.

In order to establish that RG100204 can inhibit AQP9 H_2O_2 permeability we utilized a cell line that expresses mouse AQP9 along with the H_2O_2 specific sensor HyPer-3. We observed inhibition of AQP9 H_2O_2 permeability by RG100204 with similar potency and efficacy as for water and glycerol permeability (**Figure 1C**).

To further establish that RG100204 affected similar biological processes as was established previously for *Aqp9* gene deletion, we next evaluated the effect of RG100204 on LPS-induced NO and O_2^- production in FaO cells, a rat hepatoma cell line expressing AQP9 (27). LPS increased the concentration of extracellular and intracellular O_2^- and intracellular NO in FaO cells compared to vehicle treated controls. This LPS induced increase in free radicals was completely prevented in cells incubated with RG100204 (**Figure 2**). At the dose used for the *in vitro* characterization RG100204 or LPS alone or RG100204 plus LPS did not show any significant toxic effect on FaO cells viability (**Supplementary Figure 1**).

RG100204 Treatment of Septic Shock in Mice

In order to address if RG100204 can affect systemic inflammation *in vivo* we utilized a CLP mouse model of polymicrobial sepsis resulting from intestinal perforation. The model includes fluid resuscitation and antibiotics treatment, thus mimicking the clinical standard of care in bacterial sepsis.

Pre-Treatment With RG100204 Maintains Physiological Parameters After CLP Surgery

When compared to sham-operated mice, mice subjected to CLP and treated with vehicle showed a significant increase in severity score and a decrease in heart rate after 24 h (**Figures 3A, B**). The

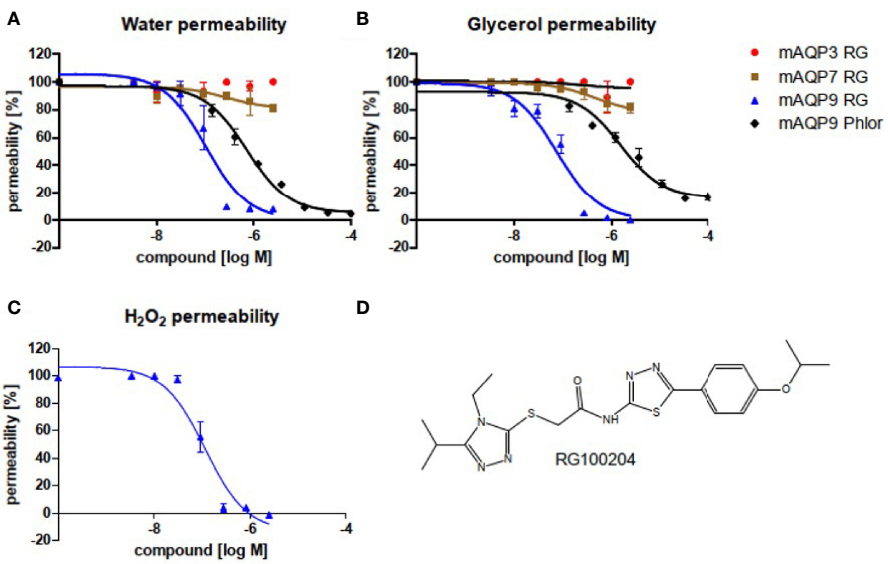

FIGURE 1 | Inhibitor characterization in CHO cells that ectopically express mouse AQP isoforms, as indicated. Water efflux **(A)** and glycerol efflux **(B)** were measured in Calcein loaded cells. H_2O_2 permeability was measured in a cell line that expressed mouse AQP9, along with the H_2O_2 sensitive fluorescence reporter protein HyPer3 **(C)**. Permeabilities were calculated in comparison to the respective parental cell lines, without AQP integration. **(D)** Chemical structure of RG100204.RG: RG100204, Phlor: Phloretin. Inhibition of water permeability: RG, IC_{50}~1.1×10^{-7} M, R^2 = 0.91; Phlor IC_{50}~7.2×10^{-7} M, R^2 = 0.98. Inhibition of glycerol permeability: RG, IC_{50}~7.6×10^{-8} M, R^2 = 0.94; Phlor IC_{50}~1.6×10^{-6} M, R^2 = 0.95. Inhibition of H_2O_2 permeability: RG, IC_{50}~1.2×10^{-7} M, R^2 = 0.94. n = 3.

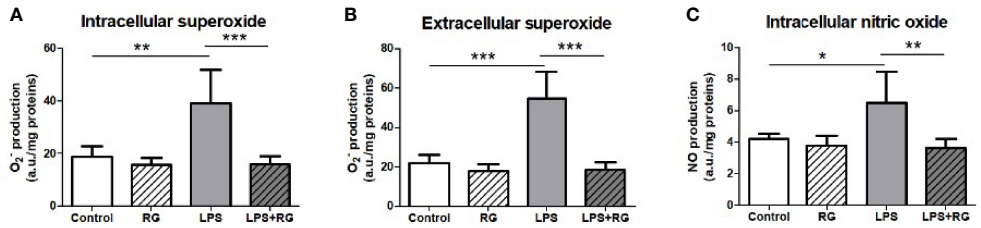

FIGURE 2 | LPS treatment of FaO rat hepatoma cells resulted in increased superoxide concentration, both intracellularly **(A)**, and extracellularly **(B)**, as well as increased intracellular nitric oxide concentration **(C)**. Oxide increases were diminished by RG100204 treatment. The levels of O_2^- and NO were assayed by electron paramagnetic resonance of spin traps prepared from the FaO cells submitted to the different experimental conditions. Control, cells exposed to the vehicle (1% DMSO) alone; RG, 25 μM RG100204 in 1% DMSO; LPS, 1 μg LPS/mL in 1% DMSO; LPS+RG, 25 μM RG100204 plus 1 μg LPS/mL in 1% DMSO; a.u., arbitrary units. Data were analyzed by one-way ANOVA, with Bonferroni's *post-hoc* test. Data are expressed as mean ± SEM, n=5, *P < 0.05, **P < 0.01 and ***P < 0.001.

temperature was also significantly decreased in this group of animals at 6 h, 18 h and 24 h (**Figure 3C**). When compared to CLP-animals treated with vehicle, treatment of CLP-animals with RG100204 just before CLP and 8 h after CLP surgery significantly attenuated the severity score and the decline in temperature at 6 h, 18 h and 24 h after CLP (**Figures 3A–D**). All mice showed a decline in body weight over the 24 h observation period, but no significant difference was detected between any of the three groups (sham + vehicle, CLP + vehicle and CLP + RG100204) (**Figure 3E**).

Pre-Treatment With RG100204 Attenuates CLP-Induced Systolic Cardiac Dysfunction

When compared to sham-operated mice, mice subjected to CLP and treated with vehicle demonstrated a significant reduction in the systolic parameters measured: % EF, % FS, % FAC, CO and SV after 24 h, indicating the development of systolic, cardiac dysfunction (**Figures 4A–F**). When compared to CLP-animals treated with vehicle, treatment of CLP-animals with RG100204 just before CLP and 8 h after CLP surgery improved systolic cardiac dysfunction with a significant increase in the following cardiac parameters: % EF, % FS, % FAC, CO and SV, demonstrating the ability of pre-treatment with RG100204 to effectively attenuate systolic dysfunction in septic mice (**Figures 4A–F**).

Pre-Treatment With RG100204 Attenuates CLP-Induced Diastolic Cardiac Dysfunction

When compared to sham-operated mice, mice subjected to CLP for 24 h and treated with vehicle demonstrated a significant reduction in the mitral valve E/A ratio (**Figure 5A**) and a significant increase in the myocardial performance index NFT and IV (**Figures 5B, C**) indicating the development of diastolic cardiac dysfunction. When compared to CLP-animals treated with vehicle, CLP-animals treated with RG100204 just before and 8 h after CLP significantly attenuated the decline in the mitral valve E/A ratio and the rise of the myocardial performance index NFT and IV (**Figures 5A–C**) and, hence, the diastolic, cardiac dysfunction caused by CLP.

Pre-Treatment With RG100204 Maintains Pulmonary Artery Flow

When compared to sham-operated mice, mice subjected to CLP for 24 h and treated with vehicle demonstrated a significant reduction in the pulmonary artery velocity time integral VTI and peak velocity (**Figures 6A, B**). However, CLP-animals treated with RG100204 just before CLP and 8 h after CLP, significantly attenuated the reduction in pulmonary artery VTI and peak velocity caused by CLP (**Figures 6A, B**).

Pre-Treatment With RG100204 Attenuates CLP-Induced Hepatocellular Injury and Renal Dysfunction

When compared to sham-operated mice, mice subjected to CLP for 24 h and treated with vehicle developed kidney dysfunction (indicated by a significant rise in serum urea and creatinine) and hepatocellular injury (indicated by a significant increase in serum ALT and AST). CLP-sepsis also caused a rise in the cell injury marker LDH (**Figures 7A–E**). When compared to CLP-animals treated with vehicle, CLP-animals treated with RG100204 just before CLP and 8 h after CLP showed significant reduction in serum creatinine, LDH and ALT, but no significant reductions in serum urea or AST (**Figures 7A–E**).

Effect of Post-Treatment (Therapeutic Administration) With RG100204 on Physiological Parameters After CLP

When compared to sham-operated mice, mice subjected to CLP and treated with vehicle showed a significant increase in severity score and a decrease in heart rate after 24 h (**Figures 8A, B**). The temperature was also significantly decreased in these animals at 6 h, 18 h and 24 h (**Figure 8C**). When compared to CLP-animals treated with vehicle, treatment of CLP-animals with RG100204 at all dosing times significantly attenuated the severity score and the rise in heart rate but did not have a significant effect on hypothermia (**Figures 8A–D**). Over the 24 h period, the body weight of all mice declined, but no significant differences were detected between any of the groups studied (**Figure 8E**).

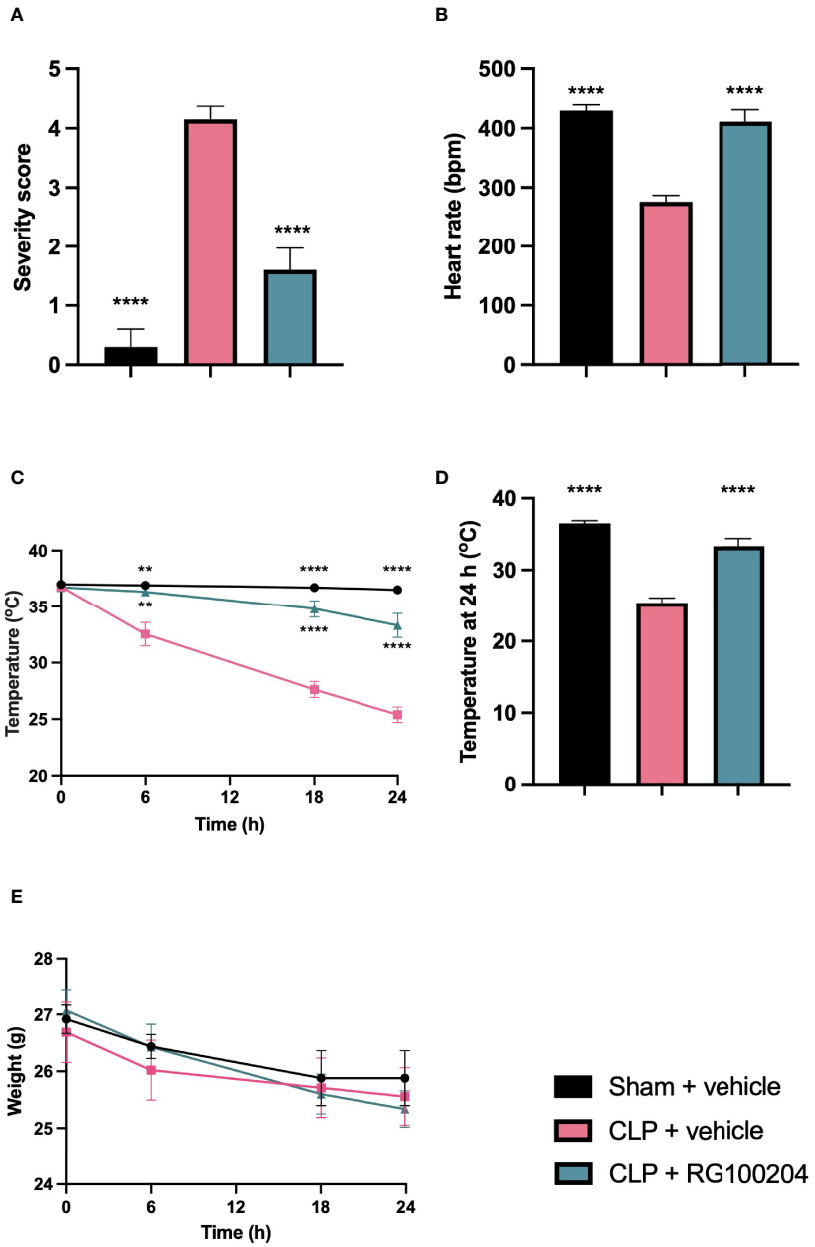

FIGURE 3 | Effect of pre-treatment with RG100204 on physiological parameters 24 h after CLP surgery. Mice were pre-treated with vehicle or RG100204 before CLP and 8 h after CLP surgery. Over the 24 h period after CLP physiological parameters were measured **(A)** Severity score at 24 h; **(B)** heart rate at 24 h (bpm); **(C)** temperature (°C); **(D)** temperature at 24 h (°C); and **(E)** weight (g). The following groups were studied: sham + vehicle (n = 5), CLP + vehicle (n = 10) and CLP + RG100204 (n = 10). All data were analyzed by one-way and two-way ANOVA, followed by a Bonferroni's *post-hoc* test. Data are expressed as mean ± SEM. **P < 0.01 and ****P < 0.0001 vs. CLP + vehicle.

Effect of Post-Treatment (Therapeutic Administration) With RG100204 on CLP-Induced Systolic, Cardiac Dysfunction

When compared to sham-operated mice, mice subjected to CLP for 24 h and treated with vehicle (control) demonstrated a significant reduction in % EF, % FS, % FAC, CO and SV (**Figures 9A–F**), indicating the development of systolic, cardiac dysfunction. When compared to CLP-animals treated with vehicle, treatment of CLP-animals with RG100204 significantly attenuated the decline in % EF, % FS, % FAC and CO caused by CLP except for the latest dosing time (**Figures 9A–F**).

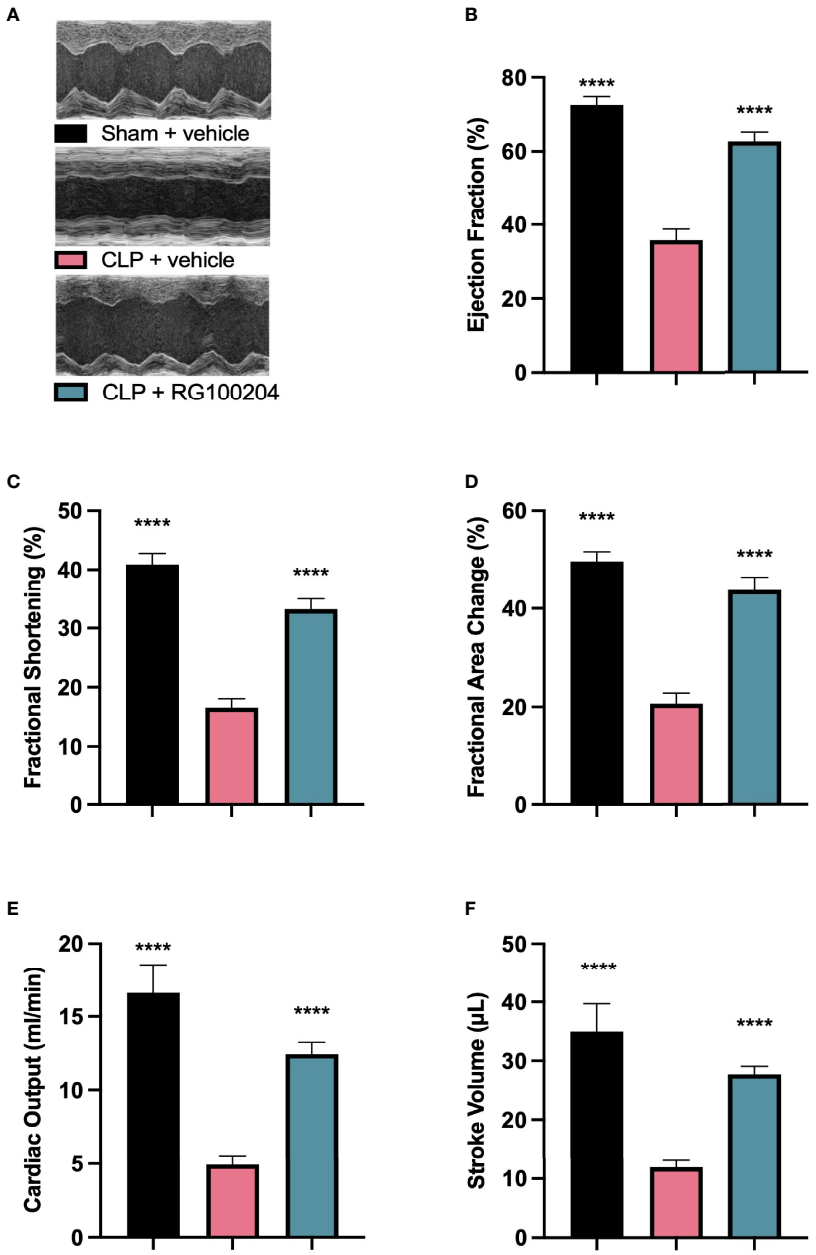

FIGURE 4 | Effect of pre-treatment with RG100204 on CLP-induced systolic cardiac dysfunction. Mice were pre-treated with vehicle or RG100204 before CLP and 8 h after CLP. Systolic cardiac function was assessed after 24 h. **(A)** Representative M-mode echocardiogram; **(B)** Ejection fraction (%); **(C)** Fractional shortening (%); **(D)** Fractional area change (%); **(E)** Cardiac output (ml/min); and **(F)** Stroke volume (µL). The following groups were studied: sham + vehicle (n = 5), CLP + vehicle (n = 10) and CLP + RG100204 (n = 10). All data were analyzed by one-way ANOVA, followed by a Bonferroni's *post-hoc* test. Data are expressed as mean ± SEM. ****P < 0.0001 vs. CLP + vehicle.

Effect of Post-Treatment (Therapeutic Administration) With RG100204 on CLP-Induced Diastolic Cardiac Dysfunction

When compared to sham-operated mice, mice subjected to CLP for 24 h and treated with vehicle (control) demonstrated a significant reduction in the mitral valve E/A ratio (**Figure 10A**) and a significant increase in the myocardial performance index NFT and IV (**Figures 10B, C**) indicating the development of diastolic, cardiac dysfunction. When compared to CLP-animals treated with vehicle, treatment of CLP-animals with RG100204 (except at the latest dosing time) significantly attenuated the decline in the mitral valve E/A ratio and the rise of the myocardial performance index (**Figures 10A, B**) and, hence, the diastolic, cardiac dysfunction caused by CLP.

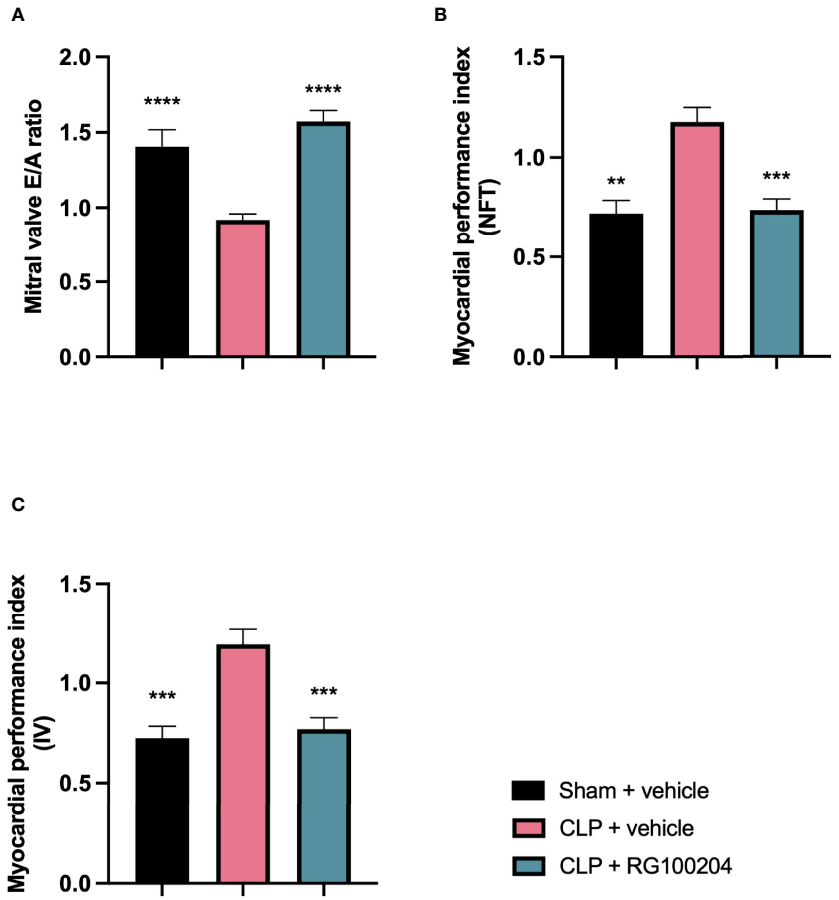

FIGURE 5 | Effect of pre-treatment with RG100204 on CLP-induced diastolic cardiac dysfunction. Mice were pre-treated with vehicle or RG100204 just before CLP and 8 h after CLP. Diastolic cardiac function was assessed after 24 h. **(A)** Mitral valve E/A ratio; **(B)** Myocardial performance index (NFT); and **(C)** Myocardial performance index (IV). The following groups were studied: sham + vehicle (n = 5), CLP + vehicle (n = 10) and CLP + RG100204 (n = 10). All data were analyzed by one-way ANOVA, followed by a Bonferroni's *post-hoc* test. Data are expressed as mean ± SEM. **P < 0.01, ***P < 0.001, and ****P < 0.0001 vs. CLP + vehicle.

Effect of Post-Treatment (Therapeutic Administration) With RG100204 on Pulmonary Artery Flow

When compared to sham-operated mice, mice subjected to CLP for 24 h and treated with vehicle (control) demonstrated a significant reduction in the pulmonary artery velocity time integral (VTI) and peak velocity (**Figures 11A, B**). When compared to CLP-animals treated with vehicle, CLP-animals treated with RG100204 showed a small but not significant increase in pulmonary artery VTI and peak velocity caused by CLP, with treatment at 1 h & 8 h, and 3 h & 8 h being more effective (**Figures 11A, B**).

Effect of Post-Treatment (Therapeutic Administration) With RG100204 on CLP-Induced Hepatocellular Injury and Renal Dysfunction

When compared to sham-operated mice, mice subjected to CLP for 24 h and treated with vehicle (control) developed both kidney dysfunction (rise in urea and creatinine) and hepatocellular injury (rise in ALT and AST) and a rise in the cell injury marker LDH (**Figures 12A–E**). When compared to CLP-animals treated with vehicle, CLP-animals treated with RG100204 at all dose times showed a decrease (although not significant in all) in serum urea, creatinine, LDH, ALT and AST (**Figures 12A–E**). Thus, post-treatment of CLP-mice with RG100204 had a more pronounced effect on renal dysfunction than on hepatocellular injury, caused by CLP.

Effect of Post-Treatment (Therapeutic Administration) With RG100204 on NF-κB Signalling and NLRP3 Inflammasome Activation in the Heart

When compared to sham-operated mice, mice subjected to CLP and treated with vehicle (control) showed significant increases in the phosphorylation of IKKα/β at $Ser^{176/180}$, the phosphorylation of IκBα at $Ser^{32/36}$ and the translocation of NF-κB subunit p65 to the nucleus in the heart (**Figures 13A–C**). When compared to

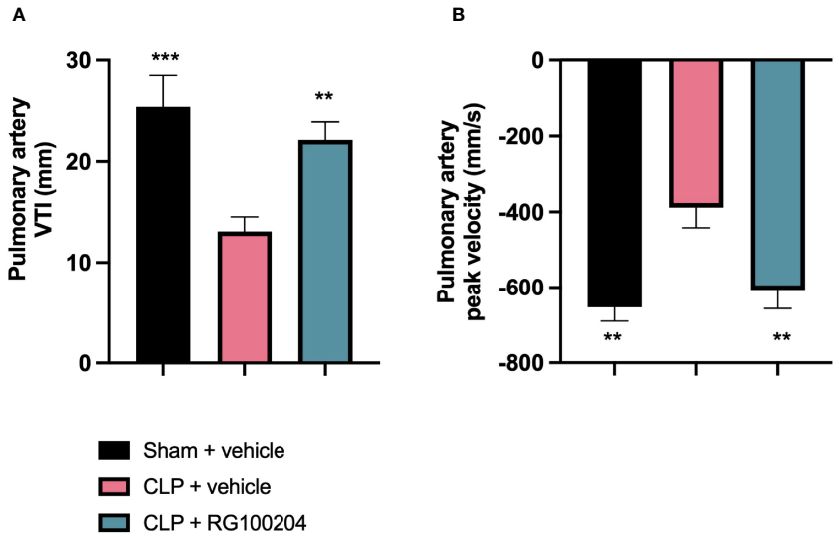

FIGURE 6 | Pre-treatment with RG100204 maintains pulmonary artery flow. Mice were pre-treated with vehicle or RG100204 before CLP and 8 h after CLP. Pulmonary artery flow was assessed after 24 h. **(A)** Pulmonary artery VTI; **(B)** Pulmonary artery peak velocity. The following groups were studied: sham + vehicle (n = 5), CLP + vehicle (n = 10) and CLP + RG100204 (n = 10). All data were analyzed by one-way ANOVA, followed by a Bonferroni's *post-hoc* test. Data are expressed as mean ± SEM. **P < 0.01 and ***P < 0.001 vs. CLP + vehicle.

CLP-animals treated with vehicle, treatment of CLP-animals with RG100204 at 1 h followed by 8 h after CLP significantly attenuated the degree of phosphorylation of IKKα/β at $Ser^{176/180}$, the phosphorylation of IκBα at $Ser^{32/36}$ and the translocation of the p65 subunit of NF-κB to the nucleus in the heart (**Figures 13A–C**), indicating the ability of RG100204 to block NF-κB activation in the heart. When compared to sham-operated mice, mice subjected to CLP and treated with vehicle (control) demonstrated a significant increase in the expression of the NLRP3 inflammasome and the cleavage of pro-caspase-1 to caspase-1 in the heart (**Figures 13D, E**). However, the expression of the NLPR3 inflammasome was significantly attenuated by the treatment with RG100204 given 1 h followed by 8 h after CLP surgery (**Figures 13D, E**).

Effect of Post-Treatment (Therapeutic Administration) With RG100204 on NF-κB Signalling and NLRP3 Inflammasome Activation in the Kidney

When compared to sham-operated mice, mice subjected to CLP and treated with vehicle (control) showed a significant increase in the phosphorylation of IKKα/β at $Ser^{176/180}$, in the phosphorylation of IκBα at $Ser^{32/36}$ and the translocation of NF-κB subunit p65 to the nucleus in the kidney (**Figures 14A–C**). When compared to CLP-animals treated with vehicle, treatment of CLP-animals with RG100204 given 1 h followed by 8 h after CLP surgery significantly attenuated the degree of phosphorylation of IKKα/β at $Ser^{176/180}$, the phosphorylation of IκBα at $Ser^{32/36}$ and the translocation of the p65 subunit of NF-κB to the nucleus in the liver (**Figures 14A–C**), indicating the ability of RG100204 to effectively inhibit the NF-κB signalling pathway in the kidney. When compared to sham-operated mice, mice subjected to CLP and treated with vehicle (control) demonstrated a significant increase in the expression of the NLRP3 inflammasome and the cleavage of pro-caspase-1 to caspase-1 in the liver (**Figures 14D, E**). However, the activation of the NLPR3 inflammasome was attenuated by the treatment with RG100204 given 1 h & 8 h after CLP surgery (**Figures 14D, E**).

Effect of Post-Treatment (Therapeutic Administration) With RG100204 on MPO Activity in the Lungs

When compared to sham-operated mice, mice subjected to CLP and treated with vehicle (control) demonstrated a significant increase in MPO activity in the lungs (**Figure 15**). However, the activity of MPO in the lungs was significantly attenuated by the treatment with RG100204 given 1 h followed by 8 h after CLP surgery (**Figure 15**).

DISCUSSION

A recent study demonstrated improved survival of *Aqp9*$^{-/-}$ knockout mice in an LPS induced mouse model of sepsis (18). While this model is well-suited to study mechanisms of systemic inflammation, which can be harmful when excessive, the LPS model does not include an infecting agent. Inflammation has however evolved to contain infections, and curtailing inflammation in infectious diseases is thus a strategy that may have concomitant beneficial and negative consequences. In the current study we thus asked if loss of *Aqp9* function can confer a net protective effect in a model of sepsis where a bacterial infection is present. This is the first study describing a novel

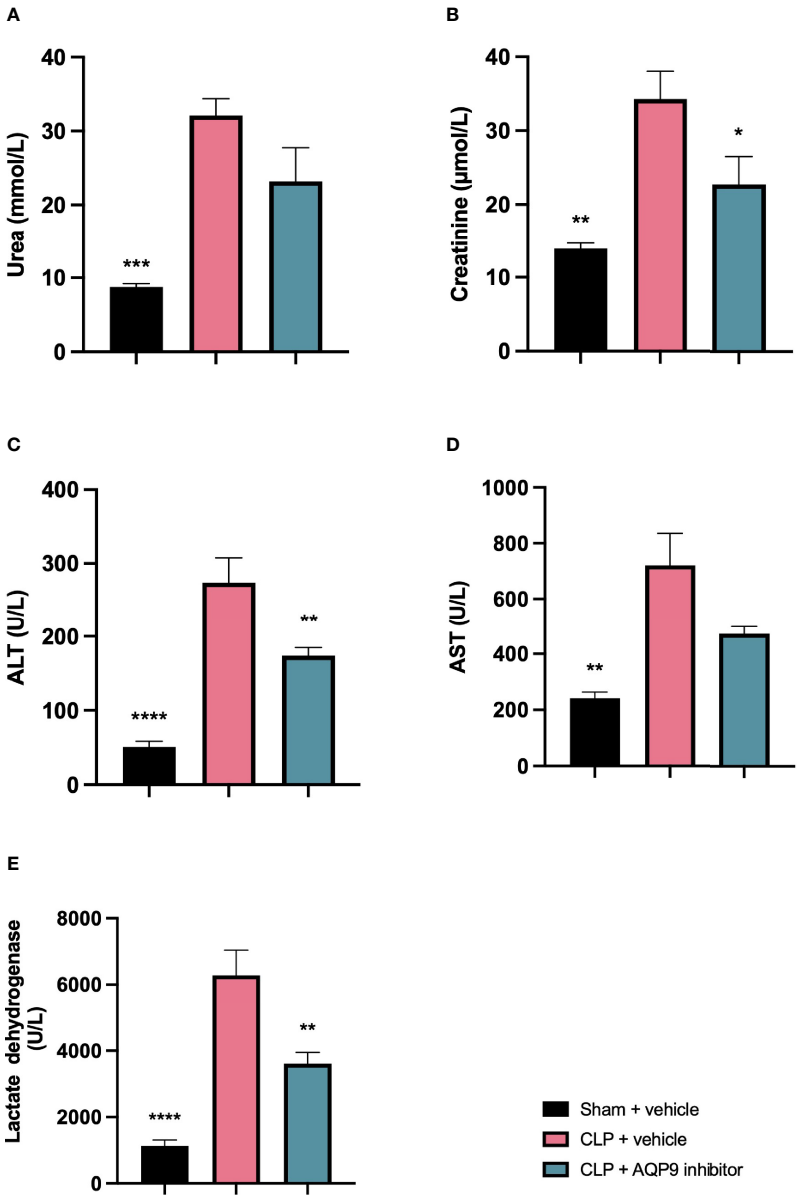

FIGURE 7 | Pre-treatment with RG100204 attenuates CLP-induced hepatocellular injury and renal dysfunction. Mice were pre-treated with vehicle or RG100204 just before CLP and 8 h after CLP. At 24 h after CLP surgery blood samples were collected to analyze. **(A)** Urea (mmol/L); **(B)** Creatinine (µmol/L); **(C)** Alanine aminotransferase (ALT) (U/L); **(D)** Aspartate transaminase (AST) (U/L); and **(E)** Lactate dehydrogenase (U/L). The following groups were studied: sham + vehicle (n = 5), CLP + vehicle (n = 10) and CLP + RG100204 (n = 10). All data were analyzed by one-way ANOVA, followed by a Bonferroni's *post-hoc* test. Data are expressed as mean ± SEM. *P < 0.05, **P < 0.01, ***P < 0.001, and ****P < 0.0001 vs. CLP + vehicle.

inhibitor, RG100204, that was developed and used for this purpose. In a rat hepatoma cell line RG100204 was able to ameliorate an LPS induced NO and O_2^- production, thus providing evidence that this substance can reproduce oxide-reducing effects that were previously observed in LPS treated mice (18).

Thus, we utilized RG10024 to further interrogate the potential of AQP9 as a drug target in polymicrobial sepsis. RG100204 administrated as pre- or post-treatment (prophylactic versus therapeutic administration) protected mice from sepsis-induced multiple organ dysfunction (cardiac dysfunction, renal dysfunction, and hepatocellular injury).

A mouse severity scoring system was used as a surrogate marker of mortality in this model of sepsis. Each mouse was assessed at 0 h, 6 h, 18 h, and 24 h after CLP surgery to determine the severity score. The physiological symptoms noted to calculate the score were symptoms of sepsis, which included piloerection, tremors, diarrhoea, respiratory distress, and periorbital exudates. At 24 h, severe sepsis was defined for mice with a severity score of > 3. This was present in CLP-mice treated with vehicle and a score of ≤ 3 in

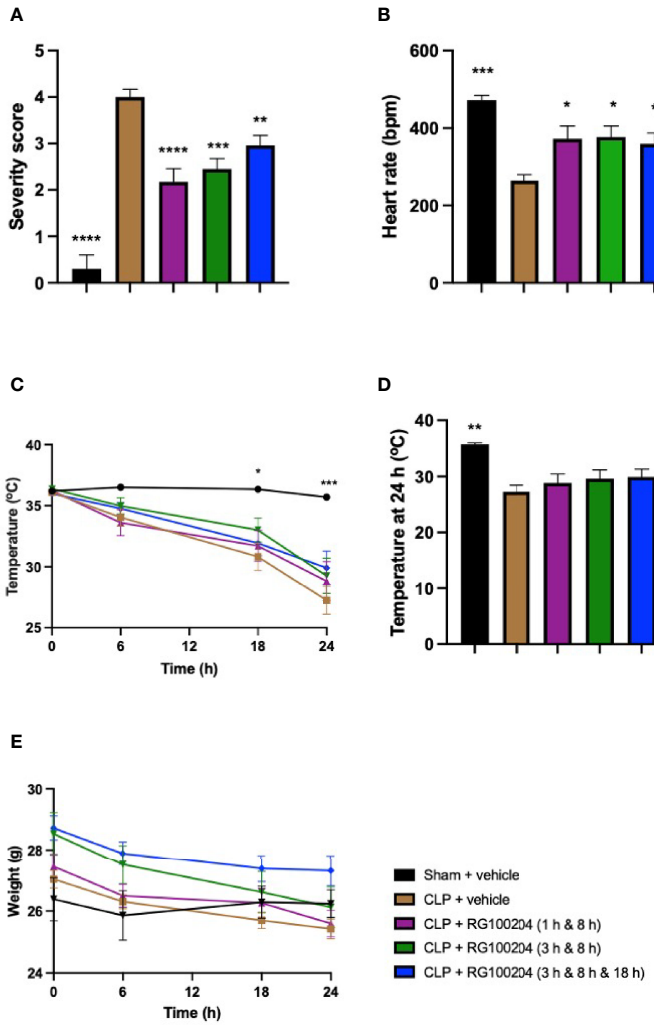

FIGURE 8 | Effect of post-treatment (therapeutic administration) with RG100204 on physiological parameters after CLP. Mice received post-treatment with vehicle or RG100204 at different dosing times after CLP. Over the 24 h period after CLP physiological parameters were measured. **(A)** Severity score; **(B)** heart rate at 24 h (bpm); **(C)** temperature (°C); **(D)** temperature at 24 h (°C); and **(E)** weight at 24 h (g). The following groups were studied: sham + vehicle (n = 5), CLP + vehicle (n = 10), CLP + RG100204 (1 h & 8 h) (n = 10), CLP + RG100204 (3 h & 8 h) (n = 10) and CLP + RG100204 (3 h & 8 h & 18 h) (n = 10). All data is expressed as mean ± SEM for n number of observations. All data were analyzed by one-way and two-way ANOVA, followed by a Bonferroni's *post-hoc* test. Data are expressed as mean ± SEM. *P < 0.05, **P < 0.01, ***P < 0.001, and ****P < 0.0001 vs. CLP + vehicle.

mice administered with RG100204 as a pre and post treatment in a CLP mouse model of sepsis. Body temperature was used as another surrogate marker of mortality. At 24 h, CLP mice treated with vehicle showed a gradual decrease in body temperature that was < 30°C. This suggests that these mice developed severe sepsis. However, at 24 h CLP mice treated with RG100204 as pre-treatment showed a body temperature > 30°C. This suggests that these mice had moderate sepsis and RG100204 treatment was effective at attenuating hypothermia in this CLP-mouse model.

Sepsis results in multiple organ failure and this includes cardiac dysfunction, renal dysfunction, and hepatocellular injury. In this study, pre-treatment of CLP-mice with RG100204 attenuated the cardiac dysfunction (systolic and diastolic), renal dysfunction and hepatocellular injury caused by CLP-sepsis. Hence, the next evaluation was whether the beneficial effect of this drug is maintained when given after the onset of CLP. Post-treatment administration of RG100204 attenuated both the cardiac dysfunction and renal dysfunction but did not significantly reduce the liver injury caused by CLP. However, the most striking finding was that administration as late as 3 h after the onset of polymicrobial sepsis (when followed by further drug administrations at 8 h and in some experiments also 18 h) attenuated the cardiac and renal dysfunction caused by severe sepsis.

What then is the evidence that inhibition of AQP9 exerts beneficial effects in sepsis? At 24 h, cardiac function was assessed by echocardiography investigating both systolic and diastolic function. The effect on systolic function of RG100204

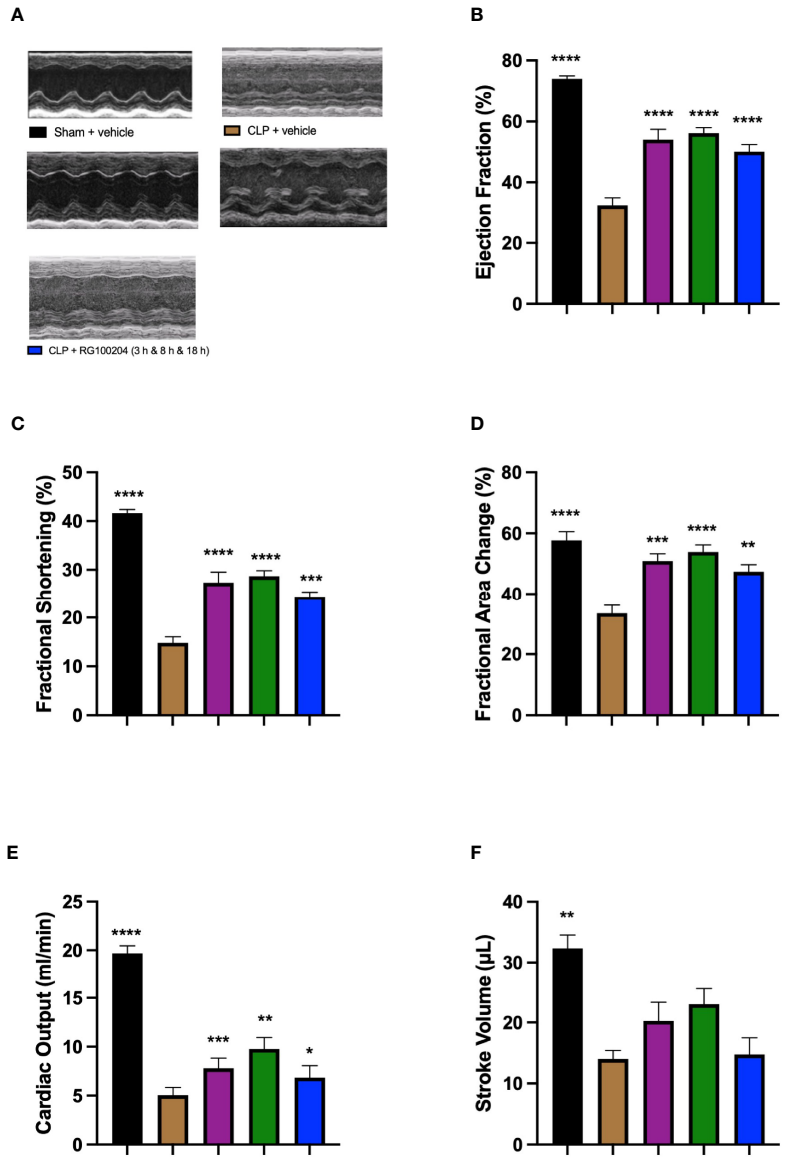

FIGURE 9 | Effect of post-treatment (therapeutic administration) with RG100204 on CLP-induced systolic, cardiac dysfunction. Mice received a post-treatment with vehicle or RG100204 at different dosing times after CLP. Cardiac function was assessed after 24 h. **(A)** Representative M-mode echocardiogram; **(B)** Ejection fraction (%); **(C)** Fractional shortening (%); **(D)** Fractional area change (%); **(E)** Cardiac output (ml/min); and **(F)** Stroke volume (µL). The following groups were studied: sham + vehicle (n = 5), CLP + vehicle (n = 10), CLP + RG100204 (1 h & 8 h) (n = 10), CLP + RG100204 (3 h & 8 h) (n = 10) and CLP + RG100204 (3 h & 8 h & 18 h) (n = 10). All data is expressed as mean ± SEM for n number of observations. All data were analyzed by one-way ANOVA, followed by a Bonferroni's *post-hoc test*. Data are expressed as mean ± SEM. *P < 0.05, **P < 0.01, ***P < 0.001, and ****P < 0.0001 vs. CLP + vehicle.

administered pre- and post-CLP surgery was evaluated by measuring % EF, % FS, % FAC, CO and SV. % EF is a common marker used to assess systolic cardiac function, as it reflects cardiac function and remodeling, and it is widely used for diagnostic and prognostic purposes (28). Since the early 1960s, estimated % EF and SV have been measured and both endpoints are now pivotal to the assessment of cardiac function in modern cardiology (28). CLP-sepsis caused a significant decrease in systolic function (as determined by a significant decrease in all parameters of the systolic function measured). In contrast, pre-treatment of CLP-mice with RG100204 attenuated the decline in all parameters used to measure left ventricular systolic function. Similarly, this was demonstrated for all post-treatment dosing times, however none of the dosing times had a significant effect on SV. Moreover, CLP-mice treated with vehicle showed impaired diastolic function which was improved by RG100204 given both as pre- or post-treatment (but not at the latest dosing time), since they exhibited a significant reduction in the mitral valve E/A ratio. The pre- and post-treatment administration (but not at the latest

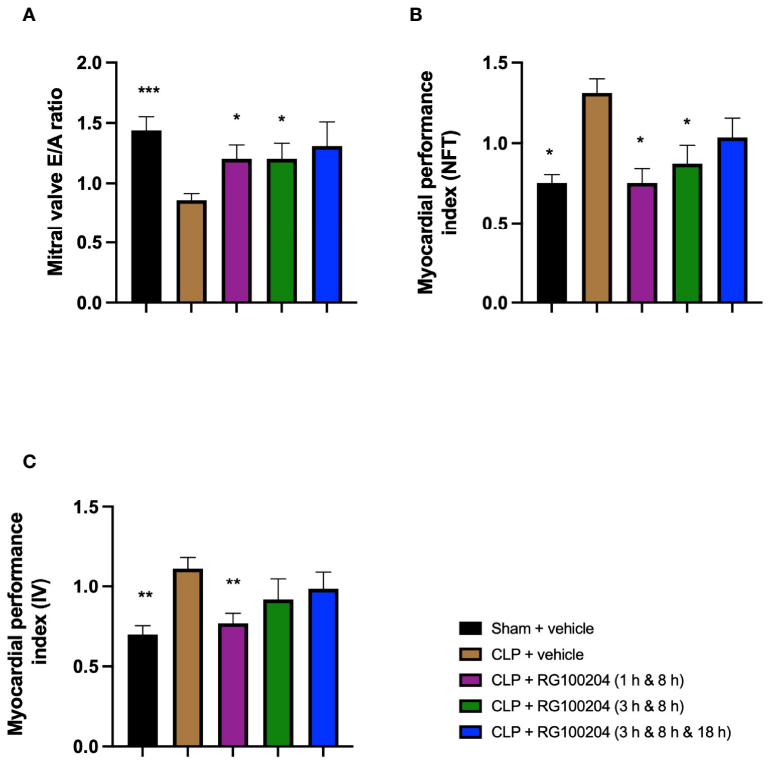

FIGURE 10 | Effect of post-treatment (therapeutic administration) with RG100204 on CLP-induced diastolic cardiac dysfunction. Mice received a post-treatment with vehicle or RG100204 at different dosing times after CLP. Cardiac function was assessed after 24 h. **(A)** Mitral valve E/A ratio; **(B)** Myocardial performance index (NFT); and **(C)** Myocardial performance index (IV). The following groups were studied: sham + vehicle (n = 5), CLP + vehicle (n = 10), CLP + RG100204 (1 h & 8 h) (n = 10), CLP + RG100204 (3 h & 8 h) (n = 10) and CLP + RG100204 (3 h & 8 h & 18 h) (n = 10). All data are expressed as mean ± SEM for n number of observations. All data were analyzed by one-way ANOVA, followed by a Bonferroni's *post-hoc* test. Data are expressed as mean ± SEM. *P < 0.05, **P < 0.01 and ***P < 0.001 vs. CLP + vehicle.

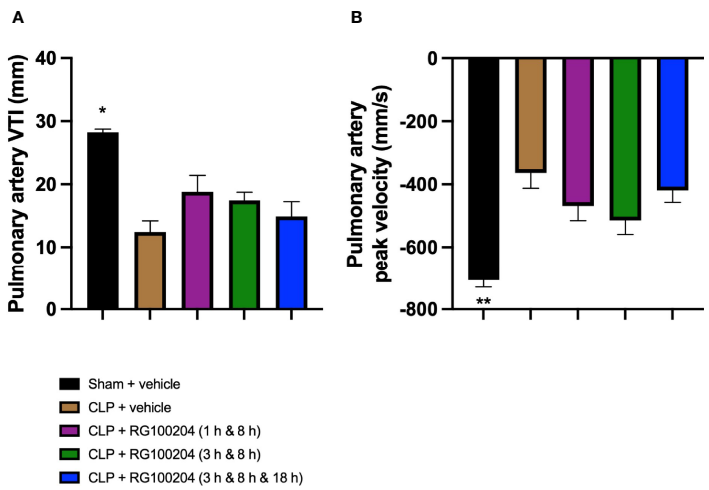

FIGURE 11 | Effect of post-treatment (therapeutic administration) with RG100204 on pulmonary artery flow. Mice received a post-treatment with vehicle or RG100204 at different dosing times after CLP. Cardiac function was assessed after 24 h. **(A)** Pulmonary artery VTI (mm); and **(B)** Pulmonary artery peak velocity (mm/s). The following groups were studied: sham + vehicle (n = 5), CLP + vehicle (n = 10), CLP + RG100204 (1 h & 8 h) (n = 10), CLP + RG100204 (3 h & 8 h) (n = 10) and CLP + RG100204 (3 h & 8 h & 18 h) (n = 10). All data are expressed as mean ± SEM for n number of observations. All data were analyzed by one-way ANOVA, followed by a Bonferroni's *post-hoc* test. Data are expressed as mean ± SEM. *P < 0.05 and **P < 0.01 vs. CLP + vehicle.

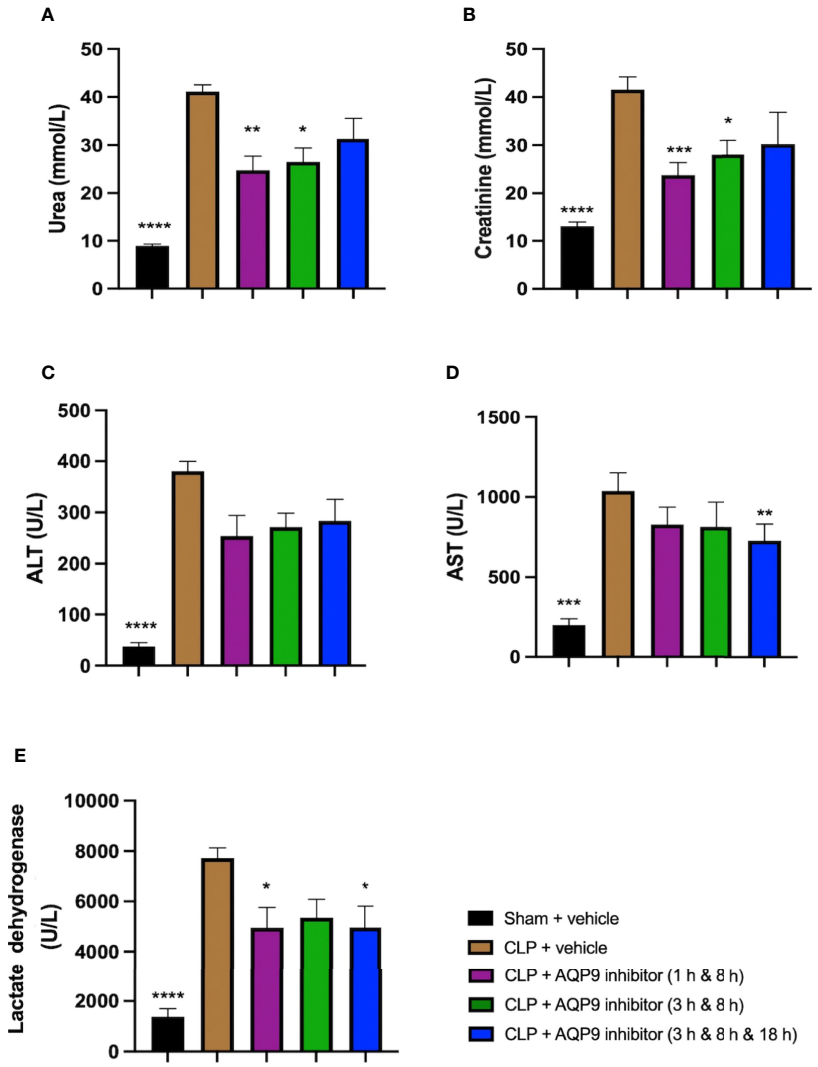

FIGURE 12 | Effect of post-treatment (therapeutic administration) with RG100204 on CLP-induced hepatocellular injury and renal dysfunction. Mice received a post-treatment with vehicle or RG100204 at different dosing times after CLP. Cardiac function was assessed after 24 h. **(A)** Urea (mmol/L); **(B)** Creatinine (μmol/L); **(C)** Alanine aminotransferase (ALT) (U/L); **(D)** Aspartate transaminase (AST) (U/L); and **(E)** Lactate dehydrogenase (U/L). The following groups were studied: sham + vehicle (n = 5), CLP + vehicle (n = 10), CLP + RG100204 (1 h & 8 h) (n = 10), CLP + RG100204 (3 h & 8 h) (n = 10) and CLP + RG100204 (3 h & 8 h & 18 h) (n = 10). All data are expressed as mean ± SEM for n number of observations. All data were analyzed by one-way ANOVA, followed by a Bonferroni's *post-hoc* test. Data are expressed as mean ± SEM. *P < 0.05, **P < 0.01, ***P < 0.001, and ****P < 0.0001 vs. CLP + vehicle.

timepoint) of RG100204 attenuated the rise in MPI NFT and MPI IV caused by CLP. The PV VTI and peak velocity are both used to evaluate how efficient blood flows through the pulmonary artery. CLP mice treated with vehicle caused a reduction in PV VTI and peak velocity. Pre-treatment with RG100204 in CLP mice caused a significant increase in PV VTI and peak velocity, therefore the administration of the drug pre-treatment was able to prevent right ventricular dysfunction. However, administration of the drug given post-treatment showed a small but not significant increase in both these parameters. The pre-treatment administration of RG100204 was more effective on systolic and diastolic function compared to post-treatment administration. It must be noted that 1 h administration of drug followed by 8 h administration after CLP was the most effective post-treatment dosing time.

Sepsis is a leading cause for acute kidney injury (29). Serum urea and creatinine are well established biomarkers used to assess renal function. CLP-sepsis was associated with a significant renal dysfunction (rise in both creatinine and urea). Pre-treatment of CLP-animals with RG100204 attenuated the rise in serum creatinine, but not serum urea, caused by sepsis. Most notably, therapeutic administration (post-treatment administration except the latest dosing time) significantly attenuated the renal dysfunction associated with sepsis. Serum levels of urea and creatinine are influenced by other factors (especially in sepsis) and, hence, the evaluation of further biomarkers, such as IL-18

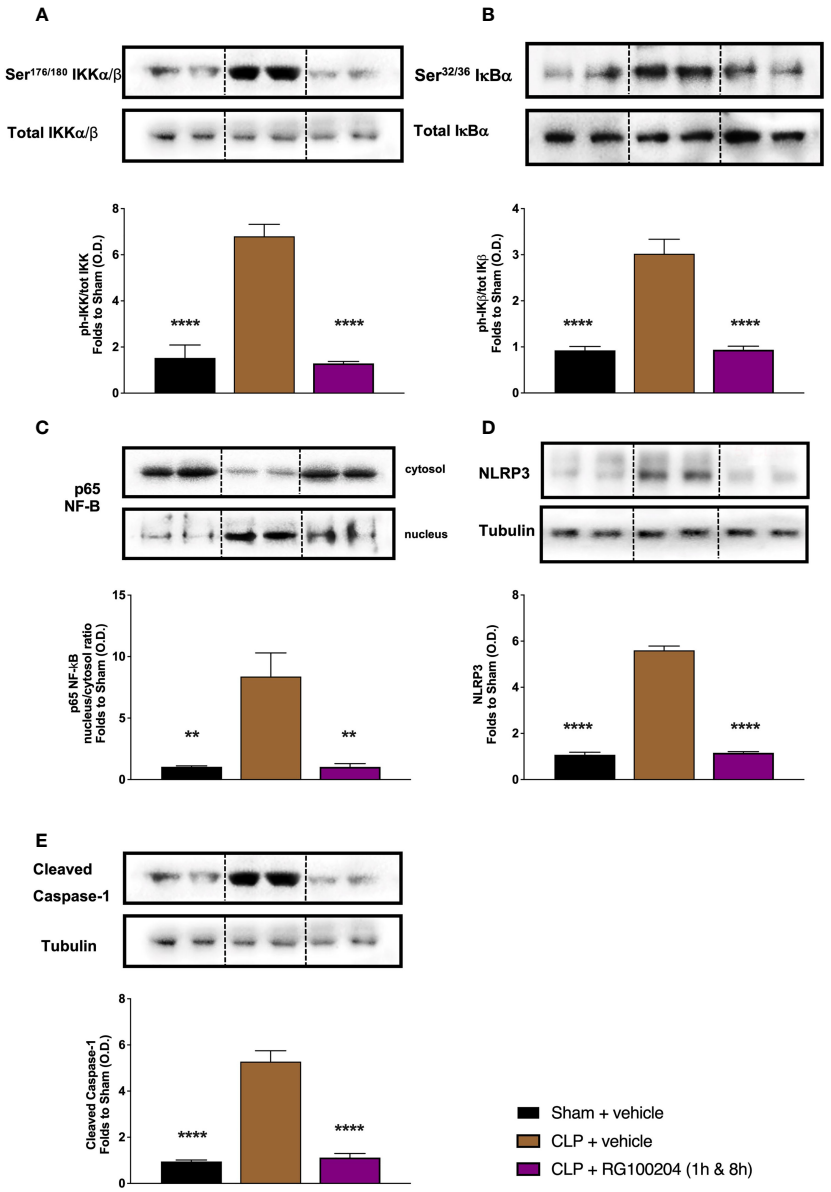

FIGURE 13 | Effect of post-treatment (therapeutic administration) with RG100204 on the NF-κB signalling pathway and the activation NLRP3 inflammasome in the heart. Heart samples were collected at the end of the experiment and the NF-κB signalling pathway, as well as the activation of the NLRP3 inflammasome. Densitometry analysis of the bands is expressed as relative optical density (O.D.) of the **(A)** phosphorylation of IKKα/β at $Ser^{178/180}$ corrected for the corresponding total IKKα/β content and normalized using the related sham band; **(B)** phosphorylation of IκBα at $Ser^{32/36}$ corrected for the corresponding total IκBα content and normalized using the related sham band; **(C)** NF-κB p65 subunit levels in both, cytosolic and nuclear fractions expressed as a nucleus/cytosol ratio normalized using the related sham bands; **(D)** NLRP3 activation, corrected against tubulin and normalized using the related sham bands; and **(E)** proteolytic cleavage of pro-caspase-1 to activated caspase-1 and normalized using the related sham band. The following groups were studied: sham + vehicle (n = 5), CLP + vehicle (n = 10), CLP + RG100204 (1 h & 8 h) (n = 10). All data were analyzed by one-way ANOVA, followed by a Bonferroni's *post-hoc* test. Data are expressed as mean ± SEM. **P < 0.01 and ****P < 0.0001 vs. the respective sham-operated group.

and kidney injury molecule-1 which are markers that have been found to be upregulated early after renal insult in sepsis (30). These are warranted to gain a better insight into the effects of AQP9 inhibition on renal dysfunction in sepsis. In terms of hepatocellular injury, pre- or post-treatment administration of RG100204 in CLP reduced liver injury. Only pre-treatment administration of RG100204 caused a significant reduction in serum ALT but had no effect on AST. None the less ALT is specific for liver injury, while AST is not. However, post-treatment administration had no significant effect on either serum ALT or AST, although in all cases there was a small reduction. Therefore, this provides a good indication that pre-

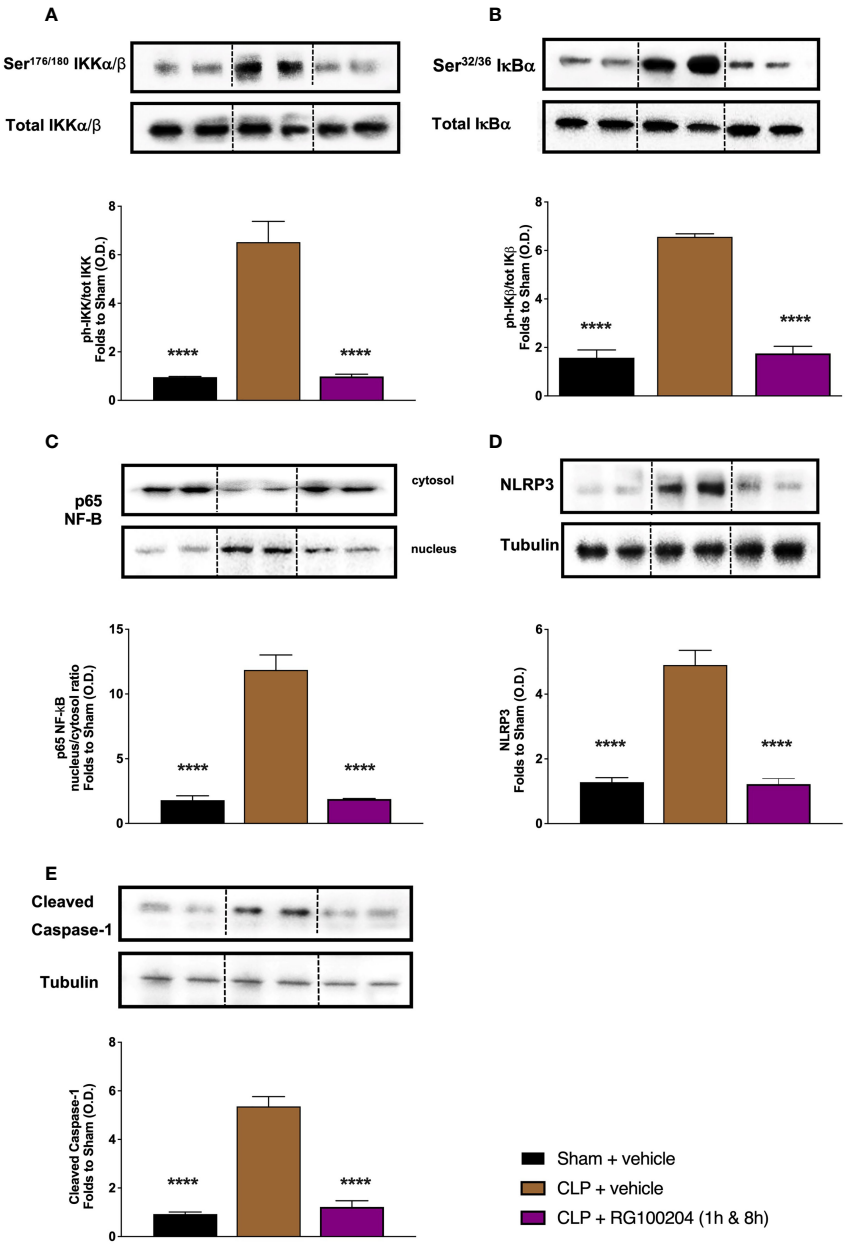

FIGURE 14 | Effect of post-treatment (therapeutic administration) with RG100204 on the NF-κB signalling pathway and the activation NLRP3 inflammasome in the kidney. Kidney samples were collected at the end of the experiment and the NF-κB signalling pathway, as well as the activation of the NLRP3 inflammasome. Densitometry analysis of the bands is expressed as relative optical density (O.D.) of the **(A)** phosphorylation of IKKα/β at $Ser^{178/180}$ corrected for the corresponding total IKKα/β content and normalized using the related sham band; **(B)** phosphorylation of IκBα at $Ser^{32/36}$ corrected for the corresponding total IκBα content and normalized using the related sham band; **(C)** NF-κB p65 subunit levels in both, cytosolic and nuclear fractions expressed as a nucleus/cytosol ratio normalized using the related sham bands; **(D)** NLRP3 activation, corrected against tubulin and normalized using the related sham bands; and **(E)** proteolytic cleavage of pro-caspase-1 to activated caspase-1 and normalized using the related sham band. The following groups were studied: sham + vehicle (n = 5), CLP + vehicle (n = 10), CLP + RG100204 (1 h & 8 h) (n = 10). All data were analyzed by one-way ANOVA, followed by a Bonferroni's *post-hoc* test. Data are expressed as mean ± SEM. ****P < 0.0001 vs. the respective sham-operated group.

treatment with AQP9 reduced the rise in ALT caused by sepsis and hence, liver injury. LDH is a biomarker used to evaluate tissue damage caused by sepsis. The observed rise in LDH in CLP-sepsis could be due to cellular injury related to bacterial toxins. Increased LDH levels are commonly seen in patients with sepsis, and a rise in LDH has been shown to reflect the degree of tissue damage (31). CLP-sepsis caused a significant increase in serum LDH and, hence, tissue injury. Pre-treatment of CLP-

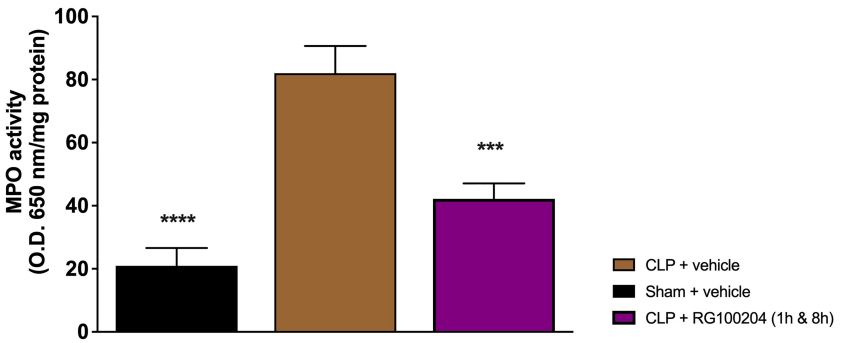

FIGURE 15 | Effect of post-treatment (therapeutic administration) with RG100204 on MPO activity in lung. MPO analysis was conducted on the lungs. The following groups were studied: sham + vehicle (n = 5), CLP + vehicle (n = 10), CLP + RG100204 (1 h & 8 h) (n = 10). All data are expressed as mean ± SEM for n number of observations. All data were analyzed by one-way ANOVA, followed by a Bonferroni's *post-hoc* test. Data are expressed as mean ± SEM. ***P < 0.001 and ****P < 0.0001 vs. the respective sham-operated group.

animals with RG100204 and post-treatment (given 1 h followed by 8 h after the onset of sepsis) prevented the rise in LDH caused by sepsis.

Sepsis results in multiple organ failure, including cardiac dysfunction, renal dysfunction, and hepatocellular injury. Taken together, we show that a novel AQP9 inhibitor, RG100204 demonstrates the ability to prevent sepsis-induced multiple organ dysfunction. What, then, is the mechanism by which RG100204 reduces the multiple organ failure associated with sepsis? To gain an insight into the potential mechanism of action of the observed beneficial effects of RG100204 in sepsis, we investigated NF-κB signalling and inflammasome expression in the heart and kidney. NF-κB plays a critical role in sepsis associated multiple organ failure, since NF-κB is involved in regulating the transcription of immunomodulatory mediators involved in the development of sepsis-induced multiple organ failure (32). In this study, we report that CLP mice subjected to polymicrobial sepsis have increased translocation of p65 in both the heart and kidneys which is attenuated by post-treatment with the AQP9 inhibitor RG100204. This is consistent with a recent study demonstrating that *Aqp9* gene deletion reduced NO, O_2^-, iNOS expression and COX-2 expression through impairment of NF-κB p65 expression/activation in an endotoxemic mouse model. Together, these observations suggest that AQP9 may play a role in the early stage of endotoxic shock, involving the NF-κB pathway. This role could potentially involve AQP9 dependent uptake of extracellular H2O2 (18). Inhibition of NF-κB activation prevents multiple organ injury in animal models of sepsis (33). This shows that NF-κB activation plays a pivotal role in sepsis and provides a potential explanation for the observed reduction in multiple organ injury and dysfunction observed in CLP-mice subjected to RG100204.

Activation of the NLRP3 inflammasome plays a further important role in sepsis (34). Inhibitors of NLRP3 (cortistatin and sulfur dioxide) can attenuate the inflammatory response in mouse models of sepsis and thereby prevent sepsis-induced cardiac dysfunction (35). The NLRP3 inflammasome is required by macrophages to release IL-1β. AQP9 is expressed in leukocytes and activation by an endotoxin challenge results in a modified mRNA expression of *Aqp9* (6). Inhibition of AQPs has been found to prevent inflammasome activation in macrophages (19, 20). Mechanisms involving AQP mediated water or glycerol influx, and cell swelling have been proposed. However, due to relatively large osmotic gradients used in these studies, indirect involvement of AQPs in inflammasome activation should not be discounted at this point. Nevertheless, these findings are consistent with the findings in this study, as we show that activation of the NLRP3 inflammasome (measured as NLRP3 and caspase-1 activation) in the heart and kidney was reduced in CLP mice treated with RG100204. NLRP3 activation involves both priming and triggering signals, hence inhibiting the inflammasome provides beneficial effects for controlling the inflammatory response in sepsis. Thereby, this provides evidence of a role of AQP9 in inflammatory diseases.

Finally, sepsis can affect the lungs, leading to lung failure, which is the most common cause of sepsis induced mortality (36). MPO is an enzyme stored in granules of neutrophils that are released upon neutrophil activation and serves as a marker for inflammation. During an inflammatory response, MPO catalyzes the conversion of chloride and hydrogen peroxide to hypochlorite (37). Neutrophils are involved in sepsis and MPO activity is used to investigate neutrophil infiltration. Uncontrolled migration of neutrophils into the lungs results in MPO sequestration, causing inflammation and lung dysfunction (38). Here we report that CLP mice showed a significant increase in MPO activity in the lungs, which was effectively attenuated by RG100204, hence demonstrating the protective effects of RG100204 on the lungs. This is in agreement with reduced migration of *Aqp9*$^{-/-}$ knockout neutrophils in a mouse model of contact hypersensitivity (7).

LIMITATIONS OF THIS STUDY

Due to restrictions by the held ethical permit, we are unable to measure death as an endpoint. Mortality of animals is not

acceptable to used and the "3Rs" in animal research strongly suggest the use of humane endpoints in animal models of sepsis in the UK. Therefore, we use surrogate markers of outcome in the CLP mouse model such as clinical severity score, body temperature, echocardiography, and biochemical markers of organ damage at 24 h after the induction of sepsis to be recorded. We are unable to do longer time evaluations, as this results in significant increase in mortality, which is prohibited by our home office license.

CONCLUSION

In conclusion, pre-treatment administration of RG100204 in CLP mice was effective at attenuating hypothermia, systolic and diastolic cardiac dysfunction and reduced renal dysfunction. However, hepatocellular injury was only slightly reduced. Post-treatment of CLP-mice with RG100204 attenuated the cardiac dysfunction (systolic and diastolic), ameliorated renal dysfunction, and reduced the rise in the cell injury marker LDH, which were all caused by CLP-sepsis, but it did not significantly reduce the liver injury and hypothermia. Most importantly, oral administration of RG100204 as late as 3 h after the onset of polymicrobial sepsis (when followed by further drug administrations at 8 h and in some experiments also 18 h) attenuated the cardiac and renal dysfunction caused by severe sepsis. RG100204 also demonstrated the ability to attenuate the activation of NF-κB as well as the expression of the NLRP3 inflammasome in the heart and kidney. Taken together our findings suggests that AQP9 inhibitors may hold promise for the use in sepsis.

DATA AVAILABILITY STATEMENT

The original contributions presented in the study are included in the article/**Supplementary Material**. Further inquiries can be directed to the corresponding authors.

ETHICS STATEMENT

All animal protocols in this study were reviewed and approved by the Animal Use and Care Committee of Queen Mary University of London (QMUL), in accordance with the Home Office Guidance on the Operation of Animals (Scientific Procedure Act 1986), published by Her Majesty's Stationary Office and the Guide for the Care and Use of Laboratory Animals of the National Research Council and were reviewed and approved by the Animal Welfare Ethics Review Board of QMUL.

AUTHOR CONTRIBUTIONS

SM, CO'R, EA, GA, MR, KD, AT, and PG performed the experiments. SM, CT, MR, AT, JE, and GC planned experiments. SM, CO'R, MC, EA, and GA analyzed the data. SM, CT, and MR contributed to the writing of the manuscript. All authors contributed to the article and approved the submitted version.

FUNDING

SM is supported by a MRes/PhD-Studentship awarded by the British Heart Foundation (BHF) (Award number: FS/17/69/33484). This work was, in part, supported by a commercial grant awarded to William Harvey Research Limited by Apoglyx, and (in part) by a grant from the William Harvey Research Foundation. GC was supported by a grant from the Italian Government ("Fondo Integrativo Speciale per la Ricerca 2020" - FISR 2020 CoVAPin, grant # FISR2020IP_04051).

ACKNOWLEDGMENTS

We would like to thank Stella Timpka and Jessica Larsson for expert preparation or RG100204 formulations.

SUPPLEMENTARY MATERIAL

The Supplementary Material for this article can be found online at: https://www.frontiersin.org/articles/10.3389/fimmu.2022.900906/full#supplementary-material

Supplementary Figure 1 | Effect of RG100204 on LPS-induced viability of FaO cells. Cultured FaO cells were treated with the vehicle alone (1% DMSO; Ctrl) or with a series of doses of RG100204 in presence or absence of LPS (1 μg/mL) for 6 h. Cell viability was measured by MTT assay. The effect of each concentration of RG100204 is compared to the corresponding basal condition (1% DMSO) in presence or absence of LPS. Data were analyzed by one-way ANOVA by Tukey's post-hoc test. Values are expressed as mean ± SD; n = 6. **P < 0.01.

REFERENCES

1. Berg D, Gerlach H. Recent Advances in Understanding and Managing Sepsis [version 1; peer review: 3 approved]. *F1000Research* (2018) 7:1570–77. doi: 10.12688/F1000RESEARCH.15758.1
2. Kozono D, Yasui M, King LS, Agre P. Aquaporin Water Channels: Atomic Structure Molecular Dynamics Meet Clinical Medicine. *J Clin Invest* (2002) 109(11):1395–9. doi: 10.1172/jci200215851
3. Rump K, Adamzik M. Function of Aquaporins in Sepsis: A Systematic Review. *Cell Biosci* (2018) 8(1):10–6. doi: 10.1186/s13578-018-0211-9
4. Calamita G, Gena P, Ferri D, Rosito A, Rojek A, Nielsen S, et al. Biophysical Assessment of Aquaporin-9 as Principal Facilitative Pathway in Mouse Liver Import of Glucogenetic Glycerol. *Biol Cell* (2012) 104(6):342–51. doi: 10.1111/boc.201100061
5. Jelen S, Wacker S, Aponte-Santamaria C, Skott M, Rojek A, Johanson U, et al. Aquaporin-9 Protein Is the Primary Route of Hepatocyte Glycerol Uptake for

Glycerol Gluconeogenesis in Mice. *J Biol Chem* (2011) 286(52):44319–25. doi: 10.1074/jbc.M111.297002
6. de Santis S, Fiorentino M, Galleggiante V, Verna G, Liso M, Massaro M, et al. Aquaporin 9 Contributes to the Maturation Process and Inflammatory Cytokine Secretion of Murine Dendritic Cells. *Front Immunol* (2018) 9:2355. doi: 10.3389/fimmu.2018.02355
7. Moniaga CS, Watanabe S, Honda T, Nielsen S, Hara-Chikuma M. Aquaporin-9-Expressing Neutrophils Are Required for the Establishment of Contact Hypersensitivity. *Sci Rep* (2015) 5:15319–31. doi: 10.1038/srep15319
8. Loitto V-M, Forslund T, Sundqvist T, Magnusson K-E, Gustafsson M. Neutrophil Leukocyte Motility Requires Directed Water Influx. *J Leukoc Biol* (2022) 71:212–22. doi: 10.1189/jlb.71.2.212
9. Matsushima A, Ogura H, Koh T, Shimazu T, Sugimoto H. Enhanced Expression of Aquaporin 9 in Activated Polymorphonuclear Leukocytes in Patients With Systemic Inflammatory Response Syndrome. *Shock* (2014) 42 (4):322–6. doi: 10.1097/SHK.0000000000000218
10. Watanabe S, Moniaga CS, Nielsen S, Hara-Chikuma M. Aquaporin-9 Facilitates Membrane Transport of Hydrogen Peroxide in Mammalian Cells. *Biochem Biophys Res Commun* (2016) 471(1):191–7. doi: 10.1016/j.bbrc.2016.01.153
11. Sonntag Y, Gena P, Maggio A, Singh T, Artner I, Oklinski M, et al. Identification and Characterization of Potent and Selective Aquaporin-3 and Aquaporin-7 Inhibitors. *J Biol Chem* (2019) 294(18):7377–87. doi: 10.1074/jbc.RA118.006083
12. Tsukaguchi H, Shayakul C, Berger U, Mackenzie B, Devidas S, Guggino W, et al. Molecular Characterization of a Broad Selectivity Neutral Solute Channel. *J Biol Chem* (1998) 273(38):24737–43. doi: 10.1074/jbc.273.38.24737
13. Satooka H, Hara-Chikuma M. Aquaporin-3 Controls Breast Cancer Cell Migration by Regulating Hydrogen Peroxide Transport and Its Downstream Cell Signaling. *Mol Cell Biol* (2016) 36(7):1206–18. doi: 10.1128/mcb.00971-15
14. Hara-Chikuma M, Chikum S, Sugiyama Y, Kabashima K, Verkman A. Chemokine-Dependent T Cell Migration Requires Aquaporin-3-Mediated Hydrogen Peroxide Uptake. *J Exp Med* (2012) 209(10):1743–52. doi: 10.1084/jem.20112398
15. Hara-Chikuma M, Watanabe S, Satooka H. Involvement of Aquaporin-3 in Epidermal Growth Factor Receptor Signaling via Hydrogen Peroxide Transport in Cancer Cells. *Biochem Biophys Res Commun* (2016) 471 (4):603–9. doi: 10.1016/j.bbrc.2016.02.010
16. Hara-Chikuma M, Satooka H, Watanabe S, Honda T, Miyachi Y, Watanabe T, et al. Aquaporin-3-Mediated Hydrogen Peroxide Transport Is Required for NF-Î° B Signalling in Keratinocytes and Development of Psoriasis. *Nat Commun* (2015) 6:7454–67. doi: 10.1038/ncomms8454
17. Bertolotti M, Farinelli G, Galli M, Aiuti A, Sitia R. AQP8 Transports NOX2-Generated H 2 O 2 Across the Plasma Membrane to Promote Signaling in B Cells. *J Leukocyte Biol* (2016) 100(5):1071–9. doi: 10.1189/jlb.2ab0116-045r
18. Tesse A, Gena P, Rützler M, Calamita G. Ablation of Aquaporin-9 Ameliorates the Systemic Inflammatory Response of LPS-Induced Endotoxic Shock in Mouse. *Cells* (2021) 10(2):435–51. doi: 10.3390/cells10020435
19. Schorn C, Fery B, Lauber K, Jamko C, Strysio M, Keppeler HC, et al. Sodium Overload and Water Influx Activate the NALP3 Inflammasome. *J Biol Chem* (2011) 286(1):35–41. doi: 10.1074/jbc.M110.139048
20. Rabolli V, Wallemme L, Lo Re S, Uwambayinema F, Palmai-Pallag M, Thomassen L, et al. Critical Role of Aquaporins in Interleukin 1β (IL-1β)-Induced Inflammation. *J Biol Chem* (2014) 289(20):13937–47. doi: 10.1074/jbc.M113.534594
21. V da Silva I, Soveral G. Aquaporins in Immune Cells and Inflammation: New Targets for Drug Development. *Int J Mol Sci* (2021) 22(4):1–16. doi: 10.3390/ijms22041845
22. Pimpão C, Wragg D, V da Silva I, Casini A, Soveral G. Aquaglyceroporin Modulators as Emergent Pharmacological Molecules for Human Diseases. *Front Mol Biosci* (2022) 9:845237. doi: 10.3389/fmolb.2022.845237
23. Verkman AS, Anderson MO, Papadopoulos MC. Aquaporins: Important But Elusive Drug Targets. *Nat Rev Drug Discov* (2014) 13(4):259–77. doi: 10.1038/nrd4226
24. Evenas J, Larsson J, Dreisch K. *Compounds for Modulating Aquaporins*. Apoglyx AB (Lund, SE), United States: Nature Publishing Group (2019). doi: 10.1038/nrd4226
25. Bilan DS, Pase L, Joosen L, Gorokhovatsky AY, Ermakova YG, Gadella TW, et al. HyPer-3: A Genetically Encoded H2O2 Probe With Improved Performance for Ratiometric and Fluorescence Lifetime Imaging. *ACS Chem Biol* (2013) 8(3):535–42. doi: 10.1021/cb300625g
26. Mohammad S, Al Zoubi S, Collotta D, Krieg N, Wissuwa B, Ferreira Alves G, et al. A Synthetic Peptide Designed to Neutralize Lipopolysaccharides Attenuates Metaflammation and Diet-Induced Metabolic Derangements in Mice. *Front Immunol* (2021) 12:701275. doi: 10.3389/fimmu.2021.701275
27. Baldini F, Portincasa P, Grasselli E, Damonte G, Salis A, Bonomo M, et al. Aquaporin-9 Is Involved in the Lipid-Lowering Activity of the Nutraceutical Silybin on Hepatocytes Through Modulation of Autophagy and Lipid Droplets Composition. *Biochim Biophys Acta - Mol Cell Biol Lipids* (2020) 1865(3):158586–95. doi: 10.1016/j.bbalip.2019.158586
28. Marwick TH. Ejection Fraction Pros and Cons: JACC State-Of-the-Art Review. *J Am Coll Cardiol* (2018) 72(19):2360–79. doi: 10.1016/j.jacc.2018.08.2162
29. Majumdar A. Sepsis-Induced Acute Kidney Injury. *Indian J Crit Care Med* (2010) 14(1):14–21. doi: 10.4103/0972-5229.63031
30. Zhang Z. Biomarkers, Diagnosis and Management of Sepsis-Induced Acute Kidney Injury: A Narrative Review. *Heart Lung Vessel* (2015) 7:64–73.
31. Zein JG, Lee GL, Tawk M, Dabaja M, Kinasewitz GT. Prognostic Significance of Elevated Serum Lactate Dehydrogenase (LDH) in Patients With Severe Sepsis. *Chest* (2004) 126(4):873S. doi: 10.1378/chest.126.4_meetingabstracts.873s
32. Abraham E. *Nuclear Factor-kB and Its Role in Sepsis-Associated Organ Failure* (2003). Available at: https://academic.oup.com/jid/article/187/Supplement_2/S364/814979.
33. Coldewey SM, Rogazzo M, Collino M, Patel NSA, Thiemermann C. Inhibition of Iκb Kinase Reduces the Multiple Organ Dysfunction Caused by Sepsis in the Mouse. *DMM Dis Models Mech* (2013) 6(4):1031–42. doi: 10.1242/dmm.012435
34. Kumar V. Inflammasomes: Pandora's Box for Sepsis. *J Inflammation Res* (2018) 11:477–502. doi: 10.2147/JIR.S178084
35. Yang L, Zhang H, Chen P. Sulfur Dioxide Attenuates Sepsis-Induced Cardiac Dysfunction *via* Inhibition of NLRP3 Inflammasome Activation in Rats. *Nitric Oxide - Biol Chem* (2018) 81:11–20. doi: 10.1016/j.niox.2018.09.005
36. Kremserova S, Perecko T, Soucek K, Klinke A, Baldus S, Eiserich JP, et al. Lung Neutrophilia in Myeloperoxidase Deficient Mice During the Course of Acute Pulmonary Inflammation. *Oxid Med Cell Longevity* (2016) 2016:273–80. doi: 10.1155/2016/5219056
37. Loria V, Dato I, Graziani F, Biasucci LM. Myeloperoxidase: A New Biomarker of Inflammation in Ischemic Heart Disease and Acute Coronary Syndromes. *Mediators Inflamm* (2008) 2008:S49–53. doi: 10.1155/2008/135625
38. Aziz M, Ode Y, Zhou M, Ochani M, Holodick NE, Rothstein TL, et al. B-1a Cells Protect Mice From Sepsis-Induced Acute Lung Injury. *Mol Med* (2018) 24(1):e0119784. doi: 10.1186/s10020-018-0029-2

Conflict of Interest: Author MR is an employee of ApoGlyx AB, which is pursuing AQP9 inhibitors for commercial applications. Authors KD and JE declare that they are employees of Red Glead Discovery AB, which is a shareholder of ApoGlyx AB. This study received funding from Apoglyx. The funder had the following involvement with the study: Study design, data collection and analysis (*in vitro* data only, see **Figure 1** and **2**) and the presentation of the manuscript.

The remaining authors declare that the research was conducted in the absence of any commercial or financial relationships that could be construed as a potential conflict of interest.

Publisher's Note: All claims expressed in this article are solely those of the authors and do not necessarily represent those of their affiliated organizations, or those of the publisher, the editors and the reviewers. Any product that may be evaluated in this article, or claim that may be made by its manufacturer, is not guaranteed or endorsed by the publisher.

Copyright © 2022 Mohammad, O'Riordan, Verra, Aimaretti, Alves, Dreisch, Evenäs, Gena, Tesse, Rützler, Collino, Calamita and Thiemermann. This is an open-access article distributed under the terms of the Creative Commons Attribution License (CC BY). The use, distribution or reproduction in other forums is permitted, provided the original author(s) and the copyright owner(s) are credited and that the original publication in this journal is cited, in accordance with accepted academic practice. No use, distribution or reproduction is permitted which does not comply with these terms.

frontiers | Frontiers in Immunology

TYPE Original Research
PUBLISHED 09 August 2022
DOI 10.3389/fimmu.2022.938944

Check for updates

OPEN ACCESS

EDITED BY
Christoph Thiemermann,
Queen Mary University of London,
United Kingdom

REVIEWED BY
Fausto Chiazza,
University of Eastern Piedmont, Italy
Sina Maren Coldewey,
University Hospital Jena, Germany

*CORRESPONDENCE
Bangwei Luo
bangwei_luo@outlook.com
Zhiren Zhang
zhangzhiren@tmmu.edu.cn
Fengxue Zhang
zhangfengxue@gzucm.edu.cn

†These authors have contributed equally to this work

SPECIALTY SECTION
This article was submitted to Inflammation, a section of the journal Frontiers in Immunology

RECEIVED 08 May 2022
ACCEPTED 12 July 2022
PUBLISHED 09 August 2022

CITATION
Zhang X, He D, Jia J, Liang F, Mei J, Li W, Liu T, Wang Z, Liu Y, Zhang F, Zhang Z and Luo B (2022) Erythropoietin mediates re-programming of endotoxin-tolerant macrophages through PI3K/AKT signaling and protects mice against secondary infection. *Front. Immunol.* 13:938944. doi: 10.3389/fimmu.2022.938944

COPYRIGHT
© 2022 Zhang, He, Jia, Liang, Mei, Li, Liu, Wang, Liu, Zhang, Zhang and Luo. This is an open-access article distributed under the terms of the Creative Commons Attribution License (CC BY). The use, distribution or reproduction in other forums is permitted, provided the original author(s) and the copyright owner(s) are credited and that the original publication in this journal is cited, in accordance with accepted academic practice. No use, distribution or reproduction is permitted which does not comply with these terms.

Erythropoietin mediates re-programming of endotoxin-tolerant macrophages through PI3K/AKT signaling and protects mice against secondary infection

Xue Zhang[1†], Dan He[2†], Jialin Jia[2†], Feihong Liang[3], Jie Mei[1], Wenhua Li[1], Tingting Liu[4], Zhiyu Wang[4], Yu Liu[4], Fengxue Zhang[1*], Zhiren Zhang[4*] and Bangwei Luo[4*]

[1]Research Center of Integrative Medicine, School of Basic Medical Sciences, Guangzhou University of Chinese Medicine, Guangzhou, China, [2]Medical College, Chongqing University, Chongqing, China, [3]Department of Medical Science, Shunde Polytechnic, Foshan, China, [4]Institute of Immunology, Army Medical University, Chongqing, China

Initial lipopolysaccharide (LPS) exposure leads to a hypo-responsive state by macrophages to a secondary stimulation of LPS, known as endotoxin tolerance. However, recent findings show that functions of endotoxin-tolerant macrophages are not completely suppressed, whereas they undergo a functional re-programming process with upregulation of a panel of molecules leading to enhanced protective functions including antimicrobial and tissue-remodeling activities. However, the underlying molecular mechanisms are still elusive. Erythropoietin (EPO), a glycoprotein regulated by hypoxia-inducible factor 1α (HIF-1α), exerts anti-inflammatory and tissue-protective activities. Nevertheless, the potential effects of EPO on functional re-programming of endotoxin-tolerant macrophages have not been investigated yet. Here, we found that initial LPS exposure led to upregulation of HIF-1α/EPO in macrophages and that EPO enhanced tolerance in tolerized macrophages and mice as demonstrated by suppressed proinflammatory genes such as *Il1b*, *Il6*, and *Tnfa* after secondary LPS stimulation. Moreover, we showed that EPO improved host protective genes in endotoxin-tolerant macrophages and mice, such as the anti-bacterial genes coding for cathelicidin-related antimicrobial peptide (*Cnlp*) and macrophage receptor with collagenous structure (*Marco*), and the tissue-repairing gene vascular endothelial growth factor C (*Vegfc*). Therefore, our findings indicate that EPO mediates the functional re-programming of endotoxin-tolerant macrophages. Mechanistically, we found that PI3K/AKT signaling contributed to EPO-mediated re-programming through upregulation of *Irak3* and *Wdr5* expression. Specifically, IL-1 receptor-associated kinase 3 (IRAK3) was responsible for inhibiting proinflammatory genes *Il1b*, *Il6*, and *Tnfa* in tolerized macrophages after LPS rechallenge, whereas WDR5 contributed to

the upregulation of host beneficial genes including *Cnlp*, *Marco*, and *Vegfc*. In a septic model of mice, EPO pretreatment significantly promoted endotoxin-tolerant re-programming, alleviated lung injury, enhanced bacterial clearance, and decreased mortality in LPS-tolerized mice after secondary infection of *Escherichia coli*. Collectively, our results reveal a novel role for EPO in mediating functional re-programming of endotoxin-tolerant macrophages; thus, targeting EPO appears to be a new therapeutic option in sepsis and other inflammatory disorders.

KEYWORDS

endotoxin tolerance, sepsis, macrophages, HIF-1α, erythropoietin

Introduction

Sepsis is a life-threatening pathology that arises from dysregulated host inflammatory response to severe bacterial infection, trauma, or cancer. The annual prevalence of sepsis worldwide is estimated at 19 million and it is a leading cause of death in intensive care units globally (1). Although great advance of therapeutic strategy has been made during the past 20 years, severe sepsis-related mortality still remains high at 20%–30% approximately (2). Therefore, novel effective therapeutic strategy is urgently required to improve the outcomes of septic patients. Severe proinflammatory response in sepsis results in multiple organ dysfunction in clinical patients; however, a number of clinical trials designed for blocking proinflammatory cytokines have failed in septic patients (3, 4). Nevertheless, increasing studies have found that patients who survived the initial acute stage of sepsis often developed an immuno-suppressive state, resulting in increased risks of detrimental secondary infections which are held responsible for high mortality in sepsis (5). These facts indicate that anti-inflammatory therapy alone might not be sufficient for the successful treatment of sepsis and it will be of great interest to achieve attenuation of cytokine response while enhancing protective immune function against secondary infections.

Endotoxin tolerance refers to a refractory state of macrophages induced by initial exposure to lipopolysaccharide (LPS) in response to a secondary dose of LPS (6). The endotoxin-tolerant macrophages are characterized by suppressed secretion of proinflammatory cytokines such as TNF-α, IL-6, and IL-1β after a secondary LPS stimulation (7). However, in animal models of experimental sepsis induced by bacterial challenge, for example, *Salmonella typhimurium*, *Pseudomonas aeruginosa*, and *Staphylococcus aureus*, results from prior works demonstrated that, although the inflammatory response was suppressed by LPS pretreatment, LPS-tolerant mice showed enhanced bacterial clearance and improved survival, suggesting that LPS tolerance upregulated the immune function to clear pathogenic bacteria despite cytokine response being attenuated (8–10). In addition, accumulating *in vitro* studies show that, in LPS-tolerant human peripheral blood mononuclear cells and murine macrophages, although genes encoding proinflammatory mediators such as *Il1b*, *Il6*, and *Tnfa* are silenced, genes encoding antimicrobial effectors such as cathelicidin-related antimicrobial peptide (CRAMP) coding gene *Cnlp* and macrophage receptor with collagenous structure coding gene *Marco* remain inducible (11). Most recently, investigations in clinical patients with sepsis reveal that rather than globally suppressed, septic blood monocytes undergo a functional re-programming from proinflammatory to an endotoxin-tolerant state. This re-programming process includes not only suppression of proinflammatory cytokines but also upregulation of several important host protective genes, for example, the antimicrobial gene coding for hepcidin antimicrobial peptide (HAMP) and the tissue-remodeling gene vascular endothelial growth factor (VEGF) (12). Therefore, endotoxin tolerance is different from post-injury immunosuppression of clinical patients and it may serve as an important mechanism to suppress proinflammatory response while enhancing the innate immune clearance of pathogens and tissue-repairing functions. Thus, exploring the re-programming mechanism of endotoxin tolerance and the development of novel tolerance regulators will be of great significance to achieve better outcomes in treating patients with sepsis and other diseases.

Hypoxia-inducible factor 1α (HIF-1α), a key transcriptional factor in the regulation of hypoxic response, plays a critical role in the development of immune re-programming in sepsis. For instance, recent studies reveal that expression of HIF-1α is significantly upregulated in monocytes isolated from sepsis patients and that HIF-1α mediates functional re-programming of monocytes by enhancing protective functions like phagocytosis, antimicrobial activity, and tissue-remodeling functions (12). However, the specific underlying molecular mechanisms have not been entirely clarified. Activation of HIF-1α is known to regulate numerous hypoxia-sensitive genes, for example, erythropoietin (EPO), a hematopoietic hormone that acts by

increasing oxygen availability *via* binding to its receptor EPOR (13). Recently, expression of EPOR has been found in several non-hematopoietic systems, especially the immune system such as macrophages (14). Treatment of EPO has been shown to exhibit potent anti-inflammatory functions in LPS-activated proinflammatory macrophages by inhibition of NF-κB (15). Moreover, EPO has been shown to enhance phagocytotic activity of macrophages (16). In addition, expression of EPOR has also been found in other non-hematopoietic systems such as the central nervous system, and EPO has been shown great tissue-protective effects in neurons (17, 18). However, there is still no report on the potential effect of EPO in the regulation of endotoxin tolerance. In this regard, we ask whether EPO is involved in the functional re-programming of endotoxin-tolerant macrophages and explore the underlying mechanisms.

Materials

Salidroside (SAL) (CAS 10338-51-9, purity >98%) and 5-aza-2′-deoxycytidine (5-AZA) were purchased from Solarbio (Beijing, China). LPS (*Escherichia coli* 055:B5) was purchased from Sigma Chemical Co. (St. Louis, MO, USA). Dulbecco's modified Eagle's medium (DMEM) and fetal bovine serum (FBS) were obtained from Invitrogen-Gibco (Grand Island, NY, USA). The neutralizing antibody to EPO (anti-EPO-16, Clone 16F1H11) was purchased from Stemcell Technologies (Vancouver, Canada). Recombinant mouse macrophage colony-stimulating factor (M-CSF) was purchased from Sinobiological (Beijing, China). Recombinant human EPO (rhEPO) was purchased from Sunshine Pharmaceutical (Shenyang, China). BAY87-2243 and MK2206 were purchased from Beyotime Biotechnology (Shanghai, China). WDR5-0103 was purchased from Selleck (Houston, TX, USA). *Irak3* siRNA(m) was purchased from Santa Cruz Biotechnology (Dallas, TX, USA).

Animals and mouse models

Wild-type C57BL/6 male mice approximately 8–12 weeks old were purchased from Army University Experimental Animal Center and acclimatized for 1 week before use. $Epor^{loxp/loxp}$LysM-$Cre^{+/+}$ mice were referred to as *EPOR-cKO* mice described previously (19). All mice were housed and bred in the animal facility at the Army Medical University under specific pathogen–free conditions. Rodent laboratory chow and tap water were provided and maintained under controlled conditions with a temperature of 24°C ± 1°C and a 12-h light/12-h dark cycle. All of the procedures were in strict accordance with the guide. *E. coli* serotype O6:K2:H1 cultured in Luria–Bertani (LB) broth was harvested at mid-log phase ($OD_{600} \approx 0.8$; 5×10^9 CFU/ml) and then washed twice in sterile PBS. Sepsis was induced *via* an intraperitoneal injection of 10^7 indicated CFU of *E. coli* into the abdominal cavity of mice. The peritoneal lavage fluids were collected aseptically by irrigating the peritoneal cavity with sterile PBS. Bacterial loads in peritoneal cavity were assessed to evaluate the bacterial clearance using the method described previously (19).

Cell culture

The RAW 264.7 murine macrophage cell line was obtained from the China Cell Line Bank (Beijing, China). Bone marrow cells were obtained from the femur and tibia of mice aged 8–12 weeks. After erythrocytes lysis and centrifugation, they were cultured in DMEM medium containing M-CSF (50 ng/ml) for 3 days. On day 4, fresh DMEM medium containing M-CSF into cell culture was added. After being cultured in DMEM medium containing M-CSF for a total of 6 days, adherent cells as bone marrow–derived macrophages (BMDMs) were collected. All cells were cultured in DMEM supplemented with 10% heat-inactivated FBS at 37°C under a humidified atmosphere of 5% CO2.

Real-time quantitative PCR

RNA was isolated from cultured cells or mice tissue samples with the RNA fast 200 Kit (Fastagen, Shanghai, China) according to the manufacturer's instructions. Reverse transcription was performed using a reverse transcription kit (Takara, Tokyo, Japan). qRT-PCR was performed using SYBR Green qPCR Master Mix (MedChemExpress, Monmouth Junction, NJ, USA). qRT-PCR was run on the CFX96 detection system (Bio-Rad Laboratories, Hemel Hempstead, UK); gene expression for each sample was normalized to β-actin for the mouse reference gene, and the differences were determined using the $2^{-\Delta\Delta CT}$ calculation. The sequences of primers used are listed in Supplementary methods.

Histological assessment

Lung samples were harvested, fixed in 4% paraformaldehyde, dehydrated, bisected, mounted in paraffin, and sectioned for H&E staining according to the manufacturer's protocol (Sigma-Aldrich, St Louis, MO, USA). For histological evaluation, the lung injury scores were quantified as previously described (19).

Statistics

All values in the figures and text are expressed as means ± SEM. Significance was calculated using one-way or two-way ANOVA with Tukey's *post-hoc* test for multiple comparisons or

Student's *t*-test for two groups meeting the normal distribution criteria. Survival rate was analyzed *via* the log-rank test. For all statistical analyses, the statistical significance was represented by a single asterisk ($P < 0.05$), two asterisks ($P < 0.01$), three asterisks ($P < 0.001$), or four asterisks ($P < 0.0001$) using GraphPad Prism 9.0.

Results

Blockade of endogenous EPO impaired re-programming of endotoxin-tolerant macrophages

Tolerance by macrophages to endotoxin can be elicited *in vitro* by long-term exposure to LPS. In order to determine whether the expression of endogenous EPO is induced by initial LPS exposure during the establishment of endotoxin tolerance, purified BMDMs from healthy wild-type (WT) C57BL/6 mice and a mouse cell line RAW264.7 macrophages were incubated with LPS (100 ng/ml) for 0, 6, 12, and 24 h, and mRNA levels of *Hif1a*, *Epo*, and its receptor *Epor* were measured by real-time quantitative reverse transcription PCR (qRT-PCR). Consistent with the previous study which established that HIF-1α expression was significantly upregulated in blood monocytes from septic patients (12), our results showed that gene expression of *Hif1a* was significantly elicited in BMDMs and RAW264.7 macrophages at 12 and 24 h by LPS tolerization (Figures 1A, B). We next measured the mRNA expression of *Epo* and its receptor *Epor* in LPS-tolerized macrophages. As demonstrated in Figures 1A, B, *Epo* and *Epor* mRNAs at 12 and 24 h were markedly upregulated in LPS-tolerized BMDMs and RAW264.7 macrophages. Therefore, our data demonstrated that the macrophage EPO pathway was induced endogenously by initial LPS exposure during the establishment of endotoxin tolerance. We thus hypothesized that the endogenously induced EPO might play a role in regulating the functional re-programming of endotoxin-tolerant macrophages. To address this question, a neutralizing antibody to EPO (anti-EPO-16) was used in our *in vitro* experiments to block endogenous EPO activities. Mice RAW264.7 macrophages were exposed to primary dose of LPS (100 ng/ml) for 24 h to induce tolerance, together with anti-EPO-16 or isotype IgG. Then, cells were washed with PBS twice and, subsequently, cells were given with a secondary LPS stimulation (10 ng/ml) for 6 h. As demonstrated in Figure 1C, our results showed that exposure of RAW264.7 macrophages to initial LPS induced an endotoxin-tolerant state indicated by the significant suppression of *Il1b*, *Il6*, and *Tnfa* mRNA after secondary LPS stimulation. However, anti-EPO-16 at a concentration of 10 μg/ml or higher significantly reversed the suppressed mRNA expression of *Il1b*, *Il6*, and *Tnfa* in tolerized macrophages following LPS rechallenge. Another hallmark of endotoxin-tolerant re-programming is the upregulation of antimicrobial and tissue-repairing genes. Our results showed that after LPS restimulation, tolerized macrophages showed a notable alteration in the pattern of host beneficial genes, with a remarkable upregulation of anti-bacterial genes, for example, *Cnlp* and *Marco*, as well as tissue-repairing gene *Vegfc* compared to non-tolerant macrophages (Figure 1D). However, when endogenous EPO was neutralized with anti-EPO-16, LPS-tolerant macrophages failed to upregulate expression of *Cnlp*, *Marco*, and *Vegfc* in response to secondary LPS stimulation (Figure 1D). Therefore, our data demonstrated that blockade of endogenous EPO significantly dampened the formation of functional re-programming in tolerized macrophages.

EPO-mediated functional re-programming of endotoxin-tolerant macrophages

Having established that endogenous EPO played an important role in the development of functional re-programming of endotoxin-tolerant macrophages, we anticipated that exogenous EPO could re-program LPS-tolerized macrophages in response to secondary LPS stimulation. To test directly whether exogenous EPO affects macrophage re-programming, we treated macrophages with rhEPO during the LPS-tolerization period. Specifically, BMDMs or RAW264.7 macrophages were exposed to a primary dose of LPS (100 ng/ml) for 24 h to induce tolerance, together with different doses of rhEPO or PBS. Then, cells were washed with PBS twice and, subsequently, cells were given with a secondary LPS stimulation (10 ng/ml) for 6 h. As shown in Figure 2A, B and Figure S1A, pretreatment of rhEPO during LPS-tolerization dose-dependently decreased mRNA expression and protein secretion of proinflammatory cytokines IL-1β, IL-6, and TNF-α but upregulated mRNA levels of protective genes *Cnlp*, *Marco*, and *Vegfc* in LPS-restimulated macrophages. Thus, our results showed that incubation of exogenous EPO during initial LPS tolerization promoted macrophage re-programming by suppressing inflammatory response while increasing host protective genes in response to secondary LPS stimulation. EPO is known to act *via* its receptor EPOR, we thus further verified the role of EPO-mediated endotoxin-tolerant re-programming with BMDMs from *EPOR-cKO* mice, a myeloid-specific *EPOR* knockout mice (19). As shown in Figure S1B, pretreatment of rhEPO failed to elicit endotoxin tolerance in tolerized BMDMs from *EPOR-cKO* mice, verifying that EPO mediated re-programming of endotoxin-tolerant macrophages *via* its receptor EPOR. Collectively, our *in vitro* studies demonstrated that exogenous EPO enhanced endotoxin-tolerant re-programming of tolerized macrophages in an EPOR-dependent manner.

In vivo effects of exogenous EPO on endotoxin tolerance were examined in WT C57BL/6 mice and *EPOR-cKO* mice. Mice were injected with LPS (1 mg/kg, i.p.) to induce tolerance, together with rhEPO (5,000 IU/kg) or an equal volume of PBS for 24 h, and then they were given with a secondary LPS injection (10 mg/kg, i.p.) for 6 h. The lung is one of the most vulnerable organs injured by

10.3389/fimmu.2022.938944

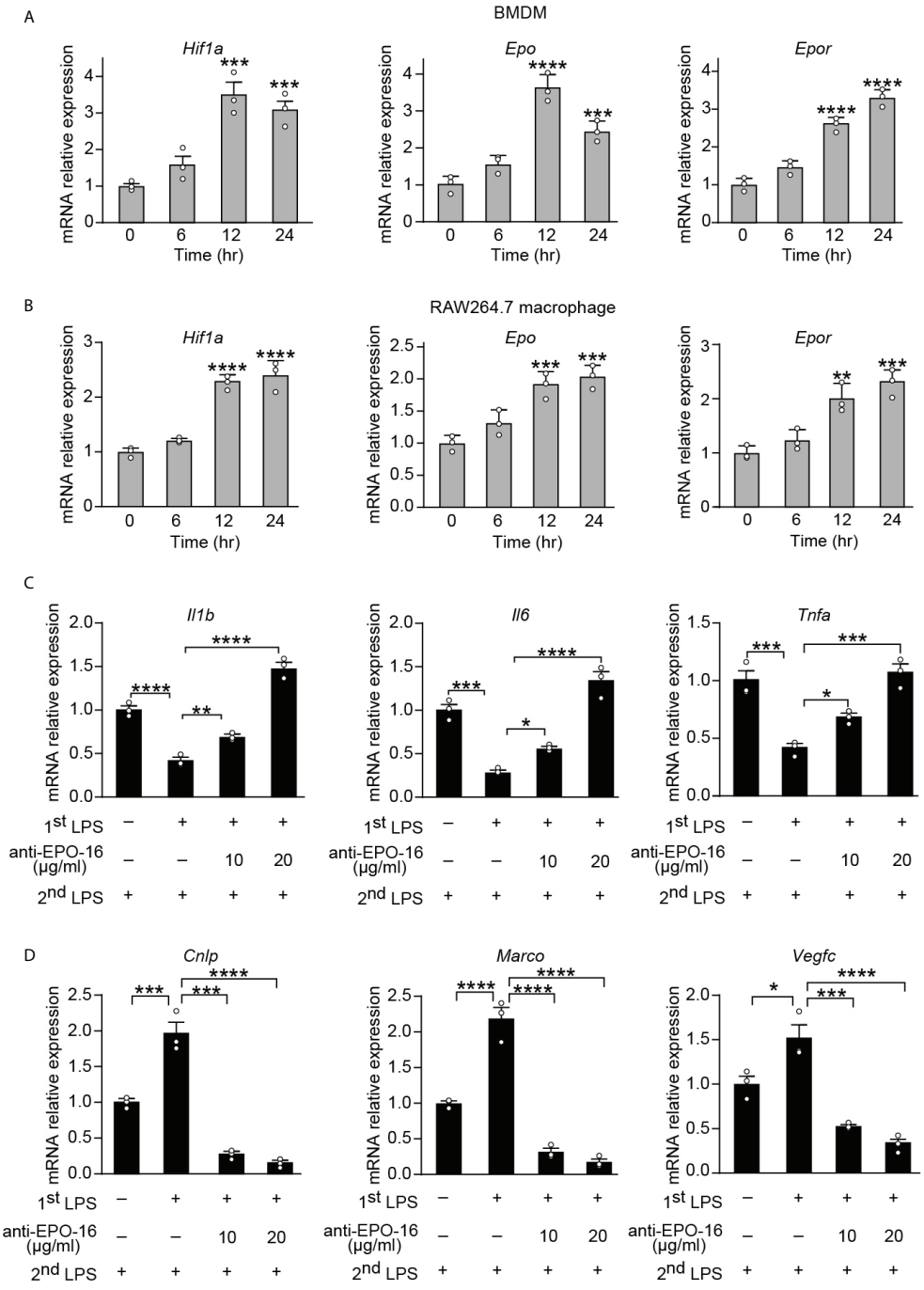

FIGURE 1
Blockade of endogenous EPO impaired re-programming of endotoxin-tolerant macrophages. **(A, B)**: *In vitro* cultured BMDMs from WT C57BL/6 mice **(A)** or mouse RAW264.7 macrophages **(B)** were incubated with LPS (100 ng/ml) for 0, 6, 12, and 24 h, and mRNA levels of *Hif1a*, *Epo*, and *Epor* in macrophages were measured by qRT-PCR (n = 3). (**C**, **D**): *In vitro* cultured RAW264.7 macrophages were pretreated with PBS (non-tolerant), LPS (100 ng/ml) (tolerant), or LPS (100 ng/ml) + anti-EPO-16 (10 or 20 μg/ml) for 24 h. Then, cells were washed with PBS twice. Subsequently, cells were given with a secondary LPS stimulation (10 ng/ml) for 6 h, and the mRNA levels of *Il1b*, *Il6*, *Tnfa* **(C)**, *Cnlp*, *Marco*, and *Vegfc* **(D)** were measured by qRT-PCR (n = 3). Data are representative of three independent experiments. Results were expressed as means ± SEM. *P < 0.05, **P < 0.01, ***P < 0.001, and ****P < 0.0001 (one-way ANOVA with Tukey's *post-hoc* test for multiple comparisons).

10.3389/fimmu.2022.938944

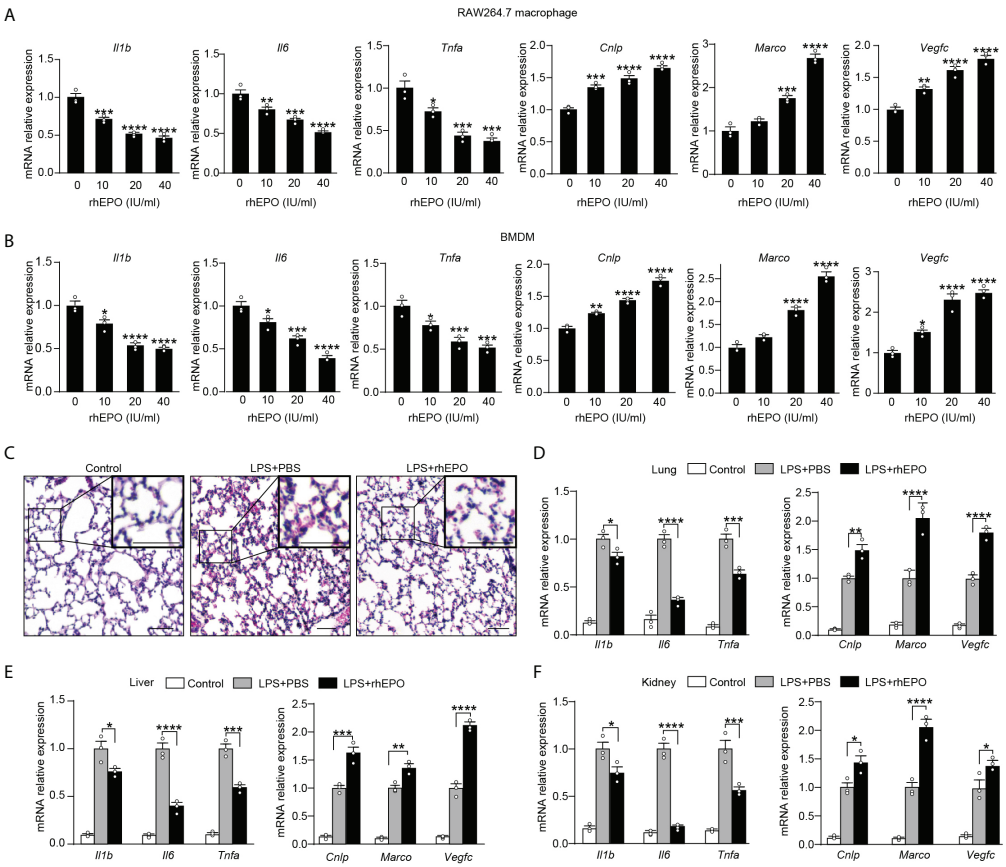

FIGURE 2
Exogenous EPO promoted endotoxin-tolerant re-programming.**(A, B)**: *In vitro* cultured RAW264.7 macrophages **(A)** or BMDMs from WT C57BL/6 mice **(B)** were incubated with different dose of rhEPO (0, 10, 20, and 40 IU/ml) in the presence of LPS (100 ng/ml) for 24 h, and then cells were washed with PBS twice followed by a secondary LPS stimulation (10 ng/ml) for 6 h; gene expression was measured by qRT-PCR (n = 3). **(C–F)**: WT C57BL/6 mice were intraperitoneally injected with LPS (1 mg/kg) together with rhEPO (5,000 IU/kg) or PBS for 24 h, and then mice were intraperitoneally given with a secondary LPS injection (10 mg/kg) for 6 h. Control mice were injected with PBS only. **(C)**: Lung specimens stained with H&E (bar = 100 μm, n = 3). **(D–F)**: qRT-PCR assay of gene expression in mice's lung **(D)**, liver **(E)**, and kidney **(F)** (n = 3). Data are representative of three independent experiments. Results were expressed as means ± SEM. *P < 0.05, **P < 0.01, ***P < 0.001, and ****P < 0.0001. Statistics: one-way ANOVA **(A, B)** or two-way ANOVA **(D-F)** with Tukey's *post-hoc* test for multiple comparisons.

sepsis, we examined the lung specimens after secondary LPS challenge by staining with H&E. As shown in Figure 2C and Figure S1C, lung tissues from the EPO group showed less interstitial edema, coagulation, and inflammatory cell infiltration, indicating a less inflammatory response and an increased tissue-protective effect by EPO pretreatment. Overexpression of proinflammatory cytokines contributes to lung injury in septic mice, and we observed a significantly lower level of proinflammatory *Il1b*, *Il6*, and *Tnfa* mRNA in the lungs from rhEPO-pretreated mice (Figure 2D), whereas mRNA expression of host beneficial genes *Cnlp*, *Marco*, and *Vegfc* was significantly increased in rhEPO-pretreated group (Figure 2D). Similar results were observed in the liver, kidney, and spleen of rhEPO-pretreated mice (Figures 2E, F, Figure S1D). Additionally, the *in vivo* roles of exogenous EPO were further validated in *EPOR-cKO* mice, and we found that pretreatment of rhEPO failed to induce endotoxin tolerance in tolerized *EPOR-cKO* mice to secondary LPS challenge (Figures S1E–H). Thus, our animal experiment results indicated that exogenous EPO mediated re-programming of endotoxin tolerance *in vivo* and this effect was macrophage EPOR–dependent.

EPO re-programmed endotoxin-tolerant macrophages through PI3K/AKT pathway *via* upregulation of IRAK3 and WDR5

We next explored pathways that participated in EPO-mediated re-programming of endotoxin-tolerant macrophages. One of the well-known EPO signaling pathways is the phosphatidyl-inositol-3 kinase (PI3K) and its downstream target protein kinase B (AKT) pathway (20), which is discovered to negatively regulate LPS

signaling in macrophages (21). Therefore, in the present study, we sought to determine whether PI3K/AKT pathway was responsible for the EPO-mediated re-programming of endotoxin-tolerant macrophages. To clarify this question, the PI3K inhibitor LY294002 and AKT inhibitor MK2206 were examined in our experiments. As shown in Figures 3A, B, inhibition of PI3K/AKT pathway with LY294002 (20 μM) or MK2206 (5 μM) remarkably reversed the suppressed expression of proinflammatory *Il1b*, *Il6* and *Tnfa*, whereas significantly impaired the upregulated expression of host beneficial genes *Cnlp*, *Marco* and *Vegfc* by rhEPO in tolerized RAW264.7 macrophages after secondary LPS stimulation. Thus, our results indicated that PI3K/AKT pathway was indeed responsible for the EPO-mediated re-programming of endotoxin-tolerant macrophage. Negative regulators of LPS response, for instance, IL-1 receptor–associated kinase 3 (IRAK3), play important roles in endotoxin tolerance by limiting overexpression of proinflammatory cytokines (22). On the other hand, the upregulation of tissue-protective genes in endotoxin tolerance is associated with epigenetic mechanisms, for example, trimethylation of histone H3 methylated at K4 (H3K4me3) (11). Therefore, we asked whether these negative feedback regulators and epigenetic modulation enzymes might play critical roles in EPO-mediated endotoxin-tolerant re-programming. We treated LPS-tolerized RAW264.7 macrophages with rhEPO during initial the LPS-tolerization period for 24 h; as shown in Figure S2, rhEPO significantly increased gene expression of *Irak3* and increased mRNA expression of WD repeat-containing protein 5 (*Wdr5*) which is essential for H3K4me3-specific histone methyl transferase activity. Additionally, this induction effect of EPO was inhibited by AKT inhibitor MK2206 (Figure 3C). Thus, our findings suggest that *Irak3* and *Wdr5* might be closely linked to the regulation of EPO-mediated macrophage re-programming. We then determined to investigate the role of IRAK3 and WDR5 in modulation of EPO-mediated re-programming in endotoxin-

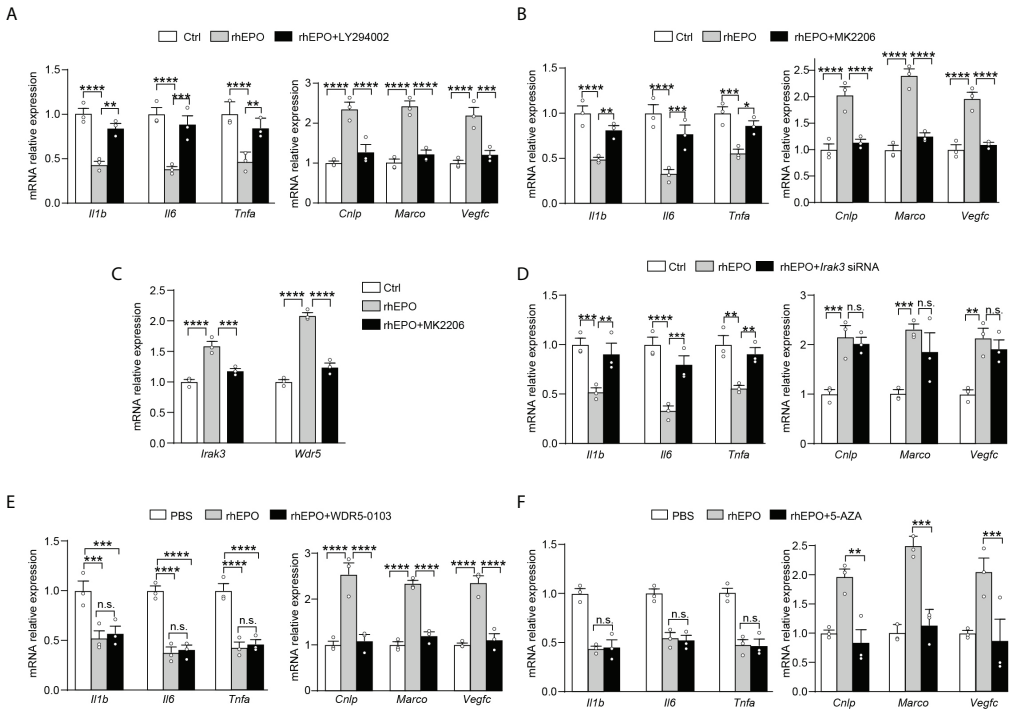

FIGURE 3
EPO mediated re-programming of endotoxin-tolerant macrophages through PI3K/AKT pathway *via* upregulation of IRAK3 and WDR5 **(A, B)**: *In vitro* cultured RAW264.7 macrophages were incubated with PBS, rhEPO (40 IU/ml), and rhEPO (40 IU/ml) + LY294002 (20 μM) **(A)** or PBS, rhEPO (40 IU/ml), and rhEPO (40 IU/ml) + MK2206 (5 μM) **(B)** the in presence of LPS (100 ng/ml) for 24 h, and then cells were washed with PBS twice followed by a secondary LPS stimulation (10 ng/ml) for 6 h; gene expression was measured by qRT-PCR (n = 3). **(C)**: *In vitro* cultured RAW264.7 macrophages were incubated with PBS, rhEPO (40 IU/ml), or rhEPO (40 IU/ml) + MK2206 (5 μM) in the presence of LPS (100 ng/ml) for 24 h, and then gene expression of *Irak3* and *Wdr5* was measured by qRT-PCR (n = 3). **(D–F)**: RAW264.7 macrophages were incubated with PBS, rhEPO (40 IU/ml), and rhEPO (40 IU/ml) + *Irak3* siRNA (50 nM) **(D)**; PBS, rhEPO (40 IU/ml), and rhEPO (40 IU/ml) + WDR5-0103 (500 nM) **(E)**; or PBS, rhEPO (40 IU/ml), and rhEPO (40 IU/ml) + 5-AZA (5 μM) **(F)** in the presence of LPS (100 ng/ml) for 24 h, and then cells were washed with PBS twice followed by a secondary LPS stimulation (10 ng/ml) for 6 h; gene expression was measured by qRT-PCR (n = 3). Data are representative of three independent experiments. Results were expressed as means ± SEM. *P < 0.05, **P < 0.01, ***P < 0.001, and ****P < 0.0001. n.s., not statistically significant. Statistics: two-way ANOVA with Tukey's *post-hoc* test for multiple comparisons. "n.s." stands for "not statistically significant".

tolerant macrophages. As shown in Figure 3D, treatment with *Irak3* siRNA reversed the expression of proinflammatory *Il1b*, *Il6*, and *Tnfa* suppressed by rhEPO pretreatment in tolerized RAW264.7 macrophages triggered by LPS restimulation, whereas levels of host beneficial genes *Cnlp*, *Marco* and *Vegfc* were not affected. On the other hand, treatment of WDR5-0103, an inhibitor of WDR5, did not change the expression of proinflammatory *Il1b*, *Il6*, and *Tnfa* but specifically reduced levels of host protective genes *Cnlp*, *Marco*, and *Vegfc* (Figure 3E). Therefore, our results indicated that IRAK3 was responsible for the regulation of proinflammatory genes, whereas WDR5 was countable for modulating host protective genes in EPO-mediated re-programming of endotoxin-tolerant macrophages.

Previous experiments showed that treatment with a demethylating agent 5-AZA significantly decreased H3K4me3 in tolerized macrophages and reduced expression of *Marco* upon LPS rechallenge without change in the inflammatory component of immune tolerance (23). Thus, from the current data and that published by others, we speculated that this mechanism might also work for EPO-mediated expression of *Cnlp*, *Marco*, and *Vegfc* in tolerized macrophages. As shown in Figure 3F, we testified that in LPS-tolerized RAW264.7 macrophages, treatment with 5-AZA indeed significantly impaired EPO-mediated *Cnlp*, *Marco*, and *Vegfc* mRNA expression upon secondary LPS stimulation but did not affect the inflammatory response as measured by the expression of *Il1b*, *Il6*, and *Tnfa*. In aggregate, our results suggested that WDR5-induced methylation played a critical role in EPO-mediated functional re-programming of tolerized macrophages.

Induction of endogenous EPO by salidroside promoted functional re-programming of endotoxin tolerance

While our findings promise beneficial effects of EPO, fear has also arisen that treatment of exogenous EPO may accelerate tumor growth in cancer patients in clinical studies (24, 25). In addition, there is an increased risk of thrombosis following EPO treatment and thus the pro-thrombotic effects of EPO therapy could not be neglected (26). To this end, it is of great interest to identify an alternative therapy without the potential risk of stimulating tumor growth or promoting thrombosis. SAL, a main bioactive component extracted from the root of *R. rosea* L., has long been used to prevent high-altitude sickness in traditional Chinese medicine (27). Recent studies have discovered that SAL is able to upregulate expression of HIF-1a and EPO even under non-hypoxia stress (28–31). Previous studies showed potent anti-inflammatory, anti-tumor, and anti-thrombosis activities of SAL (32–35). These findings, coupled with our data describing that blocking endogenous EPO impaired macrophage re-programming (Figures 1C, D), promoted us to conceive that SAL might serve as an optimal alternative therapy acting by inducing endogenous EPO without the risk of stimulating tumor growth or promoting thrombosis. In this event, we next determined to evaluate whether SAL was able to regulate the re-programming of endotoxin tolerance through induction of endogenous EPO in tolerized macrophages. To accomplish this, we treated RAW264.7 macrophages with different doses of SAL during LPS tolerization (100 ng/ml) for 24 h. As shown in Figure S3A, SAL incubation dose-dependently elicited gene expression of *Hif1a*, *Epo*, and *Epor* in LPS-tolerized RAW264.7 macrophages. Moreover, we conducted this experiment with BMDMs from healthy WT C57BL/6 mice and similar results were observed (Figure S3B), demonstrating that endogenous EPO could be induced by SAL in LPS-tolerized macrophages. Therefore, the pharmacological effects of SAL on mediating functional re-programming in endotoxin-tolerant macrophages were tested. As predicted, pretreatment of SAL dose-dependently reduced the expression of proinflammatory *Il1b*, *Il6*, and *Tnfa* mRNA but upregulated *Cnlp*, *Marco*, and *Vegfc* mRNA in tolerized RAW264.7 macrophages to LPS restimulation (Figure 4A). In addition, treatment with BAY87-2243 (20 μM), a potent HIF-1α inhibitor, eliminated the effects of SAL pretreatment on the re-programming of endotoxin-tolerant RAW264.7 macrophages (Figure S3C). Next, we performed *in vitro* experiments with BMDMs from healthy WT C57BL/6 mice and similar results were obtained (Figures 4B and S3D). To further testify whether SAL mediates the functional re-programming *via* endogenous EPO pathway, BMDMs from *EPOR*-cKO mice were used in our experiments and we found that after LPS tolerization and rechallenge, pretreatment of SAL failed to promote endotoxin tolerance in *EPOR*-cKO BMDMs (Figure S3E). Taken together, these data indicated that induction of endogenous EPO promoted the re-programming of endotoxin-tolerant macrophages *in vitro*.

We then investigated whether SAL could promote functional re-programming of endotoxin tolerance *in vivo* through the endogenous EPO pathway. Healthy WT C57BL/6 mice were injected with LPS (1 mg/kg, i.p.) to induce tolerance, together with SAL (40 mg/kg, i.p.) or an equal volume of PBS for 24 h, then these mice were given with a secondary LPS injection (10 mg/kg, i.p.) for 6 h. As shown in Figures 4C and S4A, the lung tissues from the SAL group showed less interstitial edema, coagulation, and inflammatory cell infiltration. As shown in Figure 4D, we found that SAL pretreatment lowered mRNA levels of proinflammatory *Il1b*, *Il6*, and *Tnfa*, whereas upregulated host beneficial genes *Cnlp*, *Marco*, and *Vegfc* in the lung. Similarly, we found lower levels of *Il1b*, *Il6*, and *Tnfa* mRNA and higher levels of *Cnlp*, *Marco*, and *Vegfc* mRNA in the liver, kidney, and spleen of SAL pretreated mice (Figure 4E–G). In addition, treatment with HIF-1α inhibitor BAY87-2243 (9 mg/kg, i.p.) markedly impaired SAL-induced endotoxin tolerance (Figures S4B–E). In accordance with *in vitro* results, SAL pretreatment failed to promote endotoxin tolerance in LPS-tolerized *EPOR-cKO* mice (Figures S4F–I), indicating that the *in vivo* effects of SAL in improving endotoxin tolerance were through macrophage EPOR. Taken together, our results

10.3389/fimmu.2022.938944

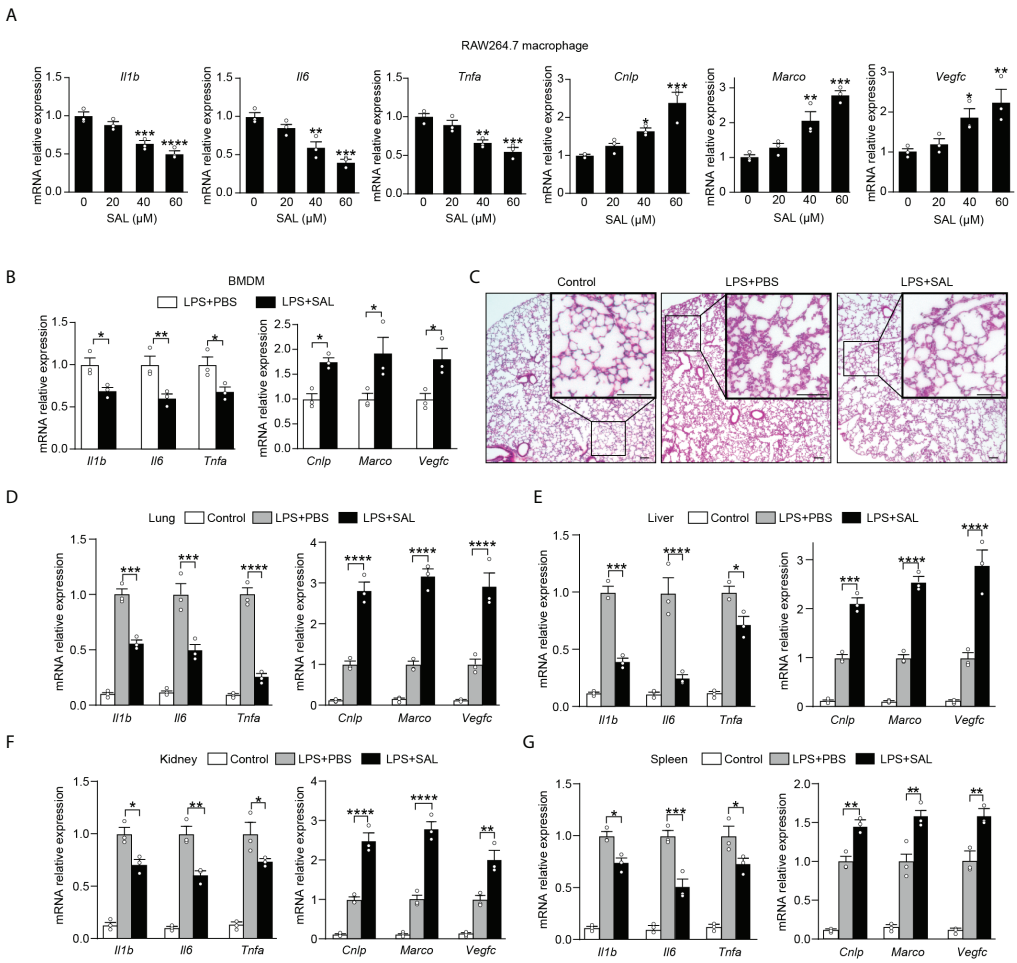

FIGURE 4
Induction of endogenous EPO by SAL improved endotoxin-tolerant re-programming **(A)**: *In vitro* cultured RAW264.7 macrophages were pretreated by LPS (100 ng/ml) together with different doses of SAL (0, 20, 40 and 60 μM) for 24 h. Then, cells were washed with PBS twice followed by a secondary LPS stimulation (10 ng/ml) for 6 h, and mRNA levels were measured by qRT-PCR (n = 3). **(B)**: *In vitro* cultured BMDMs from WT C57BL/6 mice were pretreated by LPS (100 ng/ml), together with SAL (60 μM) or PBS for 24 h. Then, cells were washed with PBS twice followed by a secondary LPS stimulation (10 ng/ml) for 6 h, and gene expression was measured by qRT-PCR (n = 3). For **(C–G)**: WT C57BL/6 mice were intraperitoneally injected with LPS (1 mg/kg) together with SAL (40 mg/kg) or PBS for 24 h, and then these mice were intraperitoneally given with a secondary LPS injection (10 mg/kg) for 6 h. Control mice were injected with PBS only. **(C)**: Lung specimens stained with H&E (bar = 100 μm, n = 3). **(D–G)**: qRT-PCR assay of gene expression in mice's lung **(D)**, liver **(E)**, kidney **(F)**, and spleen **(G)** (n = 3). Results were expressed as means ± SEM. *P < 0.05, **P < 0.01, ***P < 0.001, and ****P < 0.0001. Statistics: one-way ANOVA (A) or two-way ANOVA **(D–G)** with Tukey's *post-hoc* test for multiple comparisons.

provided a strong premise for SAL in mediated functional re-programming of endotoxin tolerance through the endogenous EPO pathway.

EPO and SAL protected tolerized mice from secondary infection of *Escherichia coli* sepsis

Sepsis is often caused by a secondary bacterial infection in clinical settings. The incidence of gram-negative bacterial sepsis has risen significantly during the last decade. *E. coli* is one of the most frequent gram-negative bacterial pathogens of bloodstream infections and a major cause of death due to sepsis (36). Therefore, compared to LPS restimulation which is a commonly used method to establish an immune tolerance mice model, rechallenge with *E. coli* is a more clinically relevant experimental sepsis model to validate our findings in secondary infections. Thus, given the striking impact of EPO and SAL on LPS tolerance, we further examined the effects of EPO and SAL on the re-programming of immune tolerance in *E. coli*–induced septic mice. WT C57BL/6 mice were intraperitoneally injected with LPS (1 mg/kg) to induce tolerance, together with rhEPO (5,000 IU/kg), SAL (40 mg/kg), or PBS for 24 h, and then

10.3389/fimmu.2022.938944

mice were challenged with secondary infection of *E. coli* (10^7 CFU, i.p.) for 6 h followed by detection. As shown in Figure 5A, compared to the PBS group, lung tissues from the rhEPO or SAL group showed less pulmonary hemorrhage, infiltration of inflammatory cells, and degeneration in the lung tissue. As shown in Figure 5B, in mice lung tissues, mRNA levels of proinflammatory *Il1b*, *Il6*, and *Tnfa* in the rhEPO and SAL groups were significantly lower compared to the PBS group, whereas mRNA levels of *Cnlp*, *Marco*, and *Vegfc* in the rhEPO and SAL groups were increased. Similar results were obtained in the liver, kidney, and spleen samples of septic mice (Figures 5C–E). Thus, these data indicated that EPO and SAL mediated endotoxin-tolerant re-programming in LPS-tolerized mice after secondary infection of *E. coli*. In addition, we discovered that treatment of rhEPO or SAL promoted the re-programming of host immunity to an antimicrobial state (Figure 5F) as indicated by diminished bacterial loads in peritoneal exudates. Moreover, as shown in Figure 5G, LPS-tolerant mice subjected to secondary *E. coli* sepsis had a 75% mortality rate, and we found a higher survival rate by rhEPO and SAL pretreatment in LPS-tolerized mice after secondary infection of *E. coli*. Collectively, we found that EPO and SAL protected LPS-tolerized mice against secondary infection of *E. coli*–induced sepsis.

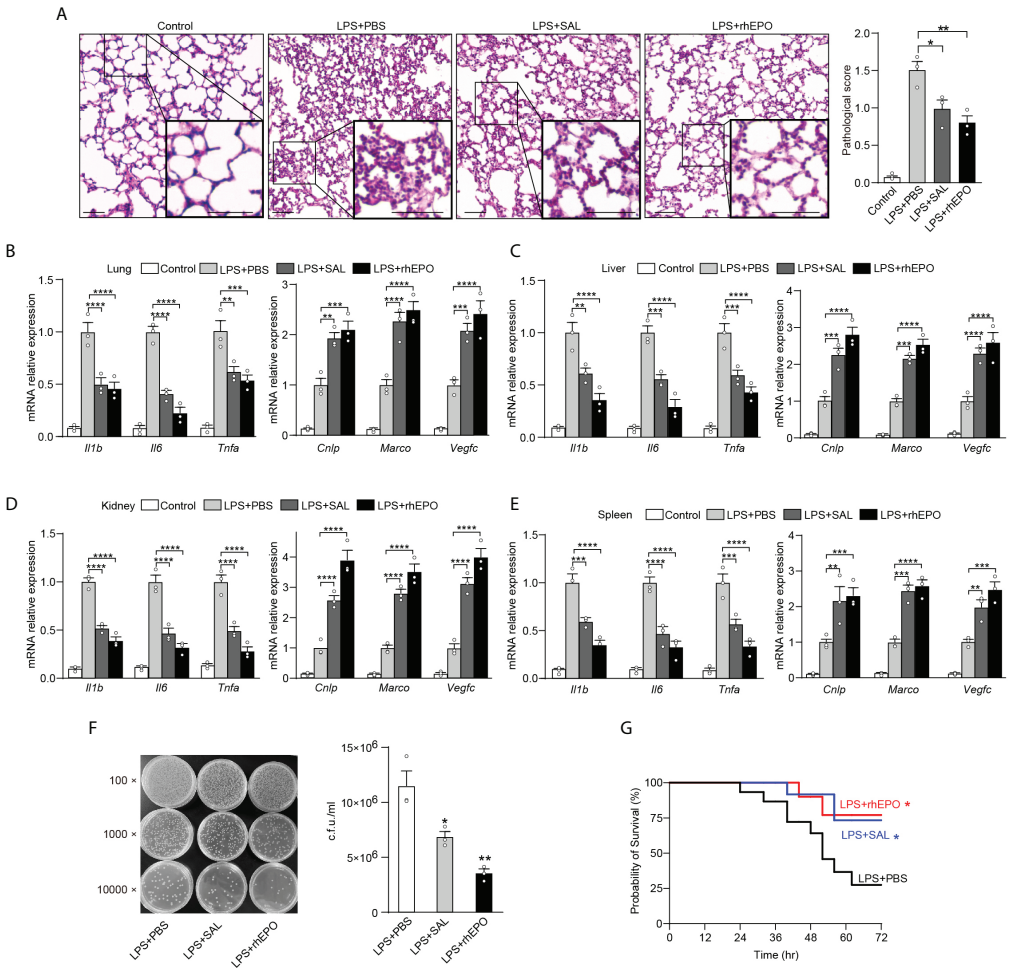

FIGURE 5
EPO and SAL protected LPS-tolerized mice from secondary infection of *E. coli* sepsis. WT C57BL/6 mice were intraperitoneally injected with LPS (1 mg/kg) + PBS, LPS (1 mg/kg) + rhEPO (5,000 IU/kg), or LPS (1 mg/kg) + SAL (40 mg/kg) for 24 h, and then mice were rechallenged with *E. coli* (10^7 CFU, i.p.) for 6 h. Control mice were injected with PBS only. **(A)**: Lung specimens stained with H&E for histological evaluation (bar = 100 μm, n = 3). **(B–E)**: qRT-PCR evaluation of gene expression in mice's lung **(B)**, liver **(C)**, kidney **(D)**, and spleen **(E)** (n = 3). **(F)**: Bacterial titers in peritoneal lavage fluids (n = 3). WT C57BL/6 mice were intraperitoneally injected with LPS (1 mg/kg) + PBS, LPS (1 mg/kg) + rhEPO (5,000 IU/kg), or LPS (1 mg/kg) + SAL (40 mg/kg) for 24 h, and then mice were rechallenged with *E. coli* (10^7 CFU, i.p.) for 72 h for survival observation. **(G)**: Survival of mice (n = 15, log-rank test). Data are representative of three independent experiments. Results were expressed as means ± SEM. *P < 0.05, **P < 0.01, ***P < 0.001, and ****P < 0.0001. Statistics: one-way ANOVA **(A, F)** or two-way ANOVA **(B–E)** with Tukey's *post-hoc* test for multiple comparisons.

Discussion

In the current study, we reveal that EPO is endogenously induced by initial LPS exposure in tolerized macrophages, and we show for the first time that EPO is a regulator of functional re-programming of endotoxin-tolerant macrophages (summarized in Figure 6). Endotoxin-tolerant macrophages are re-programmed by EPO to express less proinflammatory genes, for example, *Il1b*, *Il6*, and *Tnfa*, and more host protective genes such as *Cnlp*, *Marco*, and *Vegfc* in tolerized macrophages upon the secondary challenge of LPS. We established a mouse sepsis model by i.p. injection of *E. coli* to LPS-tolerized mice, and our results indicate that pretreatment of EPO mediated endotoxin-tolerant re-programming and protected mice from secondary infection of *E. coli*. Thus, EPO may be a potential target for the treatment of patients with sepsis.

Consistent with our findings in this study that EPO leads to a decreased level of proinflammatory cytokines in tolerized macrophages after LPS rechallenge, the anti-inflammatory activity of EPO has been reported in numerous models (37). On the other hand, we reveal a novel role of EPO in the functional re-programming of endotoxin-tolerant macrophages by upregulation of host protective genes including *Marco*, *Cnlp*, and *Vegfc*. Previous studies showed that the gene expression of *Marco* was selectively upregulated in LPS-tolerant macrophages and that MARCO contributed to the increased phagocytosis of tolerant macrophages (23, 38). *Cnlp* is responsible for the production of anti-bacterial effector CRAMP and an upregulated expression of *Cnlp* was also found in LPS-rechallenged macrophages (11, 39). In accordance with these studies, our data showed an upregulation of *Marco* and *Cnlp* gene expression by EPO and we observed an enhanced ability in bacterial clearance by EPO pretreatment in LPS-tolerized mice subjected to secondary infection of *E. coli*. Therefore, the upregulation of *Marco* and *Cnlp* by EPO-mediated re-programming of endotoxin-tolerant macrophages would be particularly helpful for septic patients who are at high risk of secondary infections.

VEGF plays a crucial role in wound healing and tissue repairing through the formation of blood and lymphatic vessels. VEGF-A regulates angiogenesis, whereas VEGF-C is responsible for lymphangiogenesis (40). Data from previous studies showed that the expression of *Vegfa* is upregulated in endotoxin-tolerant human monocytes (12). However, the enhanced circulating concentration of VEGF-A has been linked with sepsis severity and mortality (41). In addition, anti–VEGF-A antibody has been found to attenuate inflammation and decrease mortality in an experimental model of severe sepsis (42). Therefore, upregulation of VEGF-A seems not a protective mechanism in sepsis. In this regard, we focused on *Vegfc* rather than *Vegfa* in our current study. The gene expression of *Vegfc* was previously found to be upregulated in tolerized macrophages after LPS rechallenge (11). Moreover, VEGF-C secreted by macrophages was essential during tissue repair through lymphatic vessel formation (43, 44). Aside from targeting lymphatic vessels, recently, it has been reported that VEGF-C signaling in macrophages represents a self-control mechanism during anti-bacterial innate immunity and that VEGF-C protects mice against septic shock (45). These findings

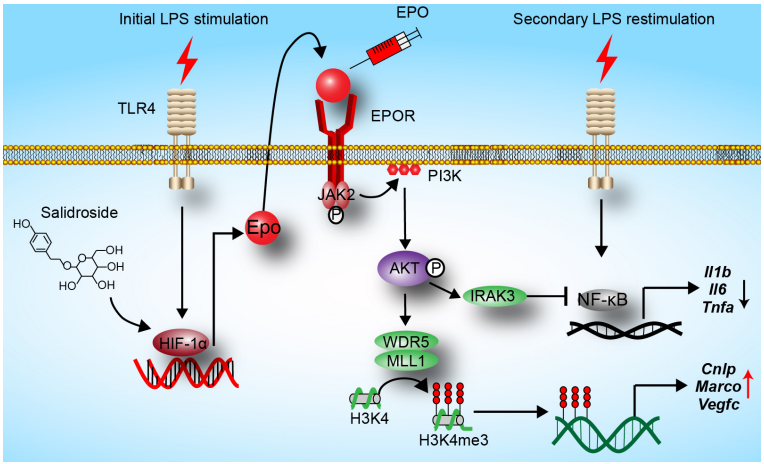

FIGURE 6
Hypothesis schema depicting the mechanism of endotoxin-tolerant re-programming mediated by EPO in macrophages. EPO is induced by initial LPS exposure through upregulation of HIF-1α. Binding of EPO to its receptor EPOR expressed on macrophages leads to activation of PI3K/AKT pathway, which further upregulated expressions of *Irak3* (a negative regulator of LPS response) and *Wdr5* (a core scaffolding component of histone methyltransferase complexes). When tolerized macrophages were challenged with a secondary dose of LPS, expression of proinflammatory genes such as *Il1b*, *Il6*, and *Tnfa* was robustly suppressed by IRAK3 *via* negative regulation of NF-κB, whereas the expression of host protective genes including *Cnlp*, *Marco*, and *Vegfc* in macrophages was upregulated by WDR5-induced histone methylation. In addition, SAL promotes re-programming of endotoxin-tolerant macrophages by inducing endogenous EPO through upregulation of *Hif1a*.

suggest that the upregulation of *Vegfc* might be an endotoxin tolerance–induced endogenous protective mechanism in sepsis. In our study, we found a dramatic increase of *Vegfc* by EPO in tolerized macrophages and mice following LPS restimulation. Therefore, the upregulated *Vegfc* by EPO-mediated re-programming in endotoxin-tolerant macrophages would be beneficial for the treatment of septic patients.

Identifying EPO-related pathways involved in re-programming may lead to potential targets for sepsis treatment. Therefore, our next focus was to identify the molecular mechanisms by which EPO mediated re-programming of endotoxin-tolerant macrophages. In previous studies, we found that EPO promoted infection resolution and ameliorated inflammatory response through a ligand-activated transcriptional factor peroxisome proliferator–activated receptor gamma (PPAR-γ) in macrophages (19). Nevertheless, recent study showed that PPAR-γ is not necessary for the development of LPS tolerance in macrophages (46). Therefore, we determined to examine other signaling pathways which may play important roles in the re-programming of endotoxin tolerance mediated by EPO. Binding of EPO triggers its receptor EPOR and activates multiple downstream signaling pathways including STAT5, MAPK, and PI3K/AKT (47). In the present study, we found that inhibition of PI3K/AKT with PI3K inhibitor LY294002 or AKT inhibitor MK2206 greatly dampened EPO-mediated functional re-programming of LPS-tolerant macrophages. In accordance with our observations, there have been increasing studies indicating that PI3K/AKT pathway is essential for LPS-induced tolerance. For example, it has been reported that blockade of PI3K with its inhibitor wortmannin reversed *in vivo* tolerance in LPS-pretreated mice (48, 49). For another example, results from Pik3r1$^{-/-}$-deficient mice (PI3K activity reduced) and PTEN$^{-/-}$ mice (AKT activity enhanced) demonstrated that PI3K/AKT pathway negatively regulated LPS signaling in macrophages and endotoxemic mice (50). Moreover, Androulidaki and colleagues reported that AKT$^{-/-}$ macrophages exhibited increased responsiveness to LPS and that AKT$^{-/-}$ mice did not develop endotoxin tolerance (51). However, previous experiments mainly focused on proinflammatory genes regulated by PI3K/AKT pathway in tolerized macrophages to secondary stimulation, and we revealed a novel role for PI3K/AKT signaling in EPO-mediated functional re-programming based on the significant enhancement of host protective genes including *Cnlp*, *Marco*, and *Vegfc* in endotoxin-tolerant macrophages.

Negative regulators play important roles in the development of endotoxin tolerance, for example, IRAK3 has been reported to suppress various Toll-like receptor (TLR)–mediated signal transduction in macrophages and essential for endotoxin tolerance (22, 52). In the present study, EPO markedly increased the expression of *Irak3* in LPS-tolerized macrophages and it was suppressed by AKT inhibitor MK2206. We next suppressed gene expression of *Irak3* with specific siRNA, and we found that this method effectively inhibited endotoxin tolerance induced by EPO, as reflected by the levels of *Il1b*, *Il6*, and *Tnfa* in tolerized RAW264.7 cells after LPS rechallenge. Consistent with our results, studies demonstrated that macrophages deficient in IRAK3 produced elevated levels of proinflammatory cytokines such as *Tnfa*, *Il6*, and *Il12* upon LPS challenge (22). However, we found that *Irak3* silencing did not change the expression of *Cnlp*, *Marco*, and *Vegfc* by EPO in LPS-restimulated macrophages. These observations demonstrated that other mechanisms could be responsible for the upregulation of protective genes in EPO-mediated re-programming of endotoxin-tolerant macrophages.

LPS-induced tolerance is an example of epigenetic re-programming and increasing studies have shown that chromatin modification plays a pivotal role in the modulation of re-programmed gene expression pattern. For example, H3K4me3, a well-known permissive histone modification, plays an important role in endotoxin tolerance by allowing upregulation of host beneficial genes in tolerized macrophages (11). Mixed-lineage leukemia 1 (MLL1) is a histone H3K4 methyl transferase, and WD repeat-containing protein 5 (WDR5) forms a core complex with MLL1 and is essential for catalyzing trimethylation of H3K4 on chromatin (53). We showed that EPO induced WDR5 expression in tolerized macrophages and it was blocked by AKT inhibitor MK2206. Consistent with our results, experiments in colorectal cancer showed that WDR5 expression could be increased through activating PI3K/AKT signaling (54). We further determined whether WDR5-induced methylation contributed to EPO-mediated functional re-programming of tolerant macrophages. We found that blocking WDR5 with WDR5-0103 or treatment with a demethylating agent (5-AZA) in tolerized macrophages remarkably dampened EPO-mediated functional re-programming, as indicated by diminished *Cnlp*, *Marco*, and *Vegfc* upon LPS restimulation, whereas proinflammatory *Il1b*, *Il6*, and *Tnfa* were not affected. Thus, we present a novel function of WDR5 in the contribution of EPO-mediated re-programming in tolerant macrophages.

The current study has some limitations. For instance, the effects of post-treatment should be validated scientifically, and the sample size should be increased for further investigations. In addition, increasing scientific literature has demonstrated that β common receptor (βCR) plays a crucial role in EPO-mediated protective effects by forming a heterodimeric receptor with EPOR (EPOR/βCR) (55). However, there is still controversy on how βCR interacts with EPOR. For example, a recent study demonstrated that the extracellular regions of the EPOR and the βCR do not specifically associate and that EPO does not promote interaction between the EPOR and the βCR (56). Therefore, further investigation would be required to confirm the possible involvement of EPOR/βCR in the mediation of macrophages endotoxin tolerance.

In summary, our present data indicate that EPO functionally re-programs endotoxin-tolerant macrophages through PI3K/AKT pathway–induced upregulation of *Irak3* and *Wdr5*. We report that EPO protected LPS-tolerized mice from secondary

infection of *E. coli* and improved the outcomes of septic mice. Our findings open further research of this drug to new opportunities beyond the limit of its actual clinical utility. However, additional research would be needed to transfer our findings into clinical settings.

Data availability statement

The raw data supporting the conclusions of this article will be made available by the authors, without undue reservation.

Ethics statement

The animal study was reviewed and approved by Laboratory Animal Welfare and Ethics Committee of the Army Medical University.

Author contributions

BL provided the idea and conceived and designed the experiments. XZ, DH and JJ performed the experiments. FL, JM, WL, TL, YL, and ZW provided the technical support. BL, ZZ and FZ analyzed and interpreted the data. BL wrote the draft of the manuscript. ZZ and FZ revised the manuscript. BL, FZ and ZZ supervised the study. All authors contributed to the article and approved the submitted version.

Funding

This work was supported by grants (32000638 and 82071778) from the National Natural Science Foundation of China (BL and ZZ).

Conflict of interest

The authors declare that the research was conducted in the absence of any commercial or financial relationships that could be construed as a potential conflict of interest.

Publisher's note

All claims expressed in this article are solely those of the authors and do not necessarily represent those of their affiliated organizations, or those of the publisher, the editors and the reviewers. Any product that may be evaluated in this article, or claim that may be made by its manufacturer, is not guaranteed or endorsed by the publisher.

Supplementary material

The Supplementary Material for this article can be found online at: https://www.frontiersin.org/articles/10.3389/fimmu.2022.938944/full#supplementary-material

References

1. Rudd KE, Kissoon N, Limmathurotsakul D, Bory S, Mutahunga B, Seymour CW, et al. The global burden of sepsis: barriers and potential solutions. *Crit Care* (2018) 22:232. doi: 10.1186/s13054-018-2157-z

2. Kaukonen KM, Bailey M, Suzuki S, Pilcher D, Bellomo R. Mortality related to severe sepsis and septic shock among critically III patients in Australia and new Zealand, 2000-2012. *JAMA J Am Med Assoc* (2014) 311(13):1308–16. doi: 10.1001/jama.2014.2637

3. Cavaillon JM, Singer M, Skirecki T. Sepsis therapies: learning from 30 years of failure of translational research to propose new leads. *EMBO Mol Med* (2020) 12 (4):e10128. doi: 10.15252/emmm.201810128

4. Marshall JC. Special issue: Sepsis why have clinical trials in sepsis failed? *Trends Mol Med* (2014) 20(4):195–203. doi: 10.1016/j.molmed.2014.01.007

5. Monneret G, Venet F, Pachot A, Lepape A. Monitoring immune dysfunctions in the septic patient: A new skin for the old ceremony. *Mol Med* (2008) 14(1-2):64–78. doi: 10.2119/2007-00102.Monneret

6. Bohannon JK, Hernandez A, Enkhbaatar P, Adams WL, Sherwood ER. The immunobiology of toll-like receptor 4 agonists: From endotoxin tolerance to immunoadjuvants. *Shock* (2013) 40(6):451–62. doi: 10.1097/SHK.0000000000000042

7. Biswas SK, Lopez-Collazo E. Endotoxin tolerance: new mechanisms, molecules and clinical significance. *Trends Immunol* (2009) 30(10):475–87. doi: 10.1016/j.it.2009.07.009

8. Lehner MD, Ittner J, Bundschuh DS, van Rooijen N, Wendel A, Hartung T. Improved innate immunity of endotoxin-tolerant mice increases resistance to salmonella enterica serovar typhimurium infection despite attenuated cytokine response. *Infect Immun* (2001) 69(1):463–71. doi: 10.1128/IAI.69.1.463-471.2001

9. Murphey ED, Fang GP, Varma TK, Sherwood ER. Improved bacterial clearance and decreased mortality can be induced by LPS tolerance and is not dependent upon IFN-gamma. *Shock* (2007) 27(3):289–95. doi: 10.1097/01.shk.0000245024.93740.28

10. Murphey ED, Fang GP, Sherwood ER. Endotoxin pretreatment improves bacterial clearance and decreases mortality in mice challenged with staphylococcus aureus. *Shock* (2008) 29(4):512–8. doi: 10.1097/SHK.0b013e318150776f

11. Foster SL, Hargreaves DC, Medzhitov R. Gene-specific control of inflammation by TLR-induced chromatin modifications. *Nature* (2007) 447 (7147):972–U4. doi: 10.1038/nature05836

12. Shalova IN, Lim JY, Chittezhath M, Zinkernagel AS, Beasley F, Hernandez-Jimenez E, et al. Human monocytes undergo functional re-programming during sepsis mediated by hypoxia-inducible factor-1 alpha. *Immunity* (2015) 42(3):484–98. doi: 10.1016/j.immuni.2015.02.001

13. Grimm C, Wenzel A, Groszer M, Mayser H, Seeliger M, Samardzija M, et al. HIF-1-induced erythropoietin in the hypoxic retina protects against light-induced retinal degeneration. *Nat Med* (2002) 8(7):718–24. doi: 10.1038/nm723

14. Lifshitz L, Tabak G, Gassmann M, Mittelman M, Neumann D. Macrophages as novel target cells for erythropoietin. *Haematol Hematol J* (2010) 95(11):1823–31. doi: 10.3324/haematol.2010.025015

15. Nairz M, Schroll A, Moschen AR, Sonnweber T, Theurl M, Theurl I, et al. Erythropoietin contrastingly affects bacterial infection and experimental colitis by inhibiting nuclear factor-kappa b-inducible immune pathways. *Immunity* (2011) 34(1):61–74. doi: 10.1016/j.immuni.2011.01.002

16. Bogdanova A, Mihov D, Lutz H, Saam B, Gassmann M, Vogel J. Enhanced erythro-phagocytosis in polycythemic mice overexpressing erythropoietin. *Blood* (2007) 110(2):762–9. doi: 10.1182/blood-2006-12-063602

17. Maiese K, Li FQ, Chong ZZ. New avenues of exploration for erythropoietin. *Jama J Am Med Assoc* (2005) 293(1):90–5. doi: 10.1001/jama.293.1.90

18. Kretz A, Happold CJ, Marticke JK, Isenmann S. Erythropoietin promotes regeneration of adult CNS neurons *via* Jak2/Stat3 and PI3K/Akt pathway activation. *Mol Cell Neurosci* (2005) 29(4):569–79. doi: 10.1016/j.mcn.2005.04.009

19. Liang FH, Guan HT, Li WH, Zhang X, Liu TT, Liu Y, et al. Erythropoietin promotes infection resolution and lowers antibiotic requirements in e. coli- and s. aureus-initiated infections. *Front Immunol* (2021) 12. doi: 10.3389/fimmu.2021.658715

20. Sivertsen EA, Hystad ME, Gutzkow KB, Dosen G, Smeland EB, Blomhoff HK, et al. PI3K/Akt-dependent epo-induced signalling and target genes in human early erythroid progenitor cells. *Br J Haematol* (2006) 135(1):117–28. doi: 10.1111/j.1365-2141.2006.06252.x

21. Fukao T, Koyasu S. PI3K and negative regulation of TLR signaling. *Trends Immunol* (2003) 24(7):358–63. doi: 10.1016/S1471-4906(03)00139-X

22. Kobayashi K, Hernandez LD, Galan JE, Janeway CAJr., Medzhitov R, Flavell RA. IRAK-m is a negative regulator of toll-like receptor signaling. *Cell* (2002) 110 (2):191–202. doi: 10.1016/S0092-8674(02)00827-9

23. Jing J, Yang IV, Hui L, Patel JA, Evans CM, Prikeris R, et al. Role of macrophage receptor with collagenous structure in innate immune tolerance. *J Immunol* (2013) 190(12):6360–7. doi: 10.4049/jimmunol.1202942

24. Cao YH. Erythropoietin in cancer: a dilemma in risk therapy. *Trends Endocrin Met* (2013) 24(4):190–9. doi: 10.1016/j.tem.2012.10.007

25. Sytkowski AJ. Does erythropoietin have a dark side? epo signaling and cancer cells. *Sci STKE* (2007) 2007(395):pe38. doi: 10.1126/stke.3952007pe38

26. Aydin Z, Mallat MJ, Schaapherder AF, van Zonneveld AJ, van Kooten C, Rabelink TJ, et al. Randomized trial of short-course high-dose erythropoietin in donation after cardiac death kidney transplant recipients. *Am J Transpl* (2012) 12 (7):1793–800. doi: 10.1111/j.1600-6143.2012.04019.x

27. Zhang XM, Xie L, Long JY, Xie QX, Zheng Y, Liu K, et al. Salidroside: A review of its recent advances in synthetic pathways and pharmacological properties. *Chem Biol Interact* (2021) 339:109268. doi: 10.1016/j.cbi.2020.109268

28. Guo QY, Yang J, Chen YM, Jin X, Li ZM, Wen XC, et al. Salidroside improves angiogenesis-osteogenesis coupling by regulating the HIF-1 alpha/VEGF signalling pathway in the bone environment. *Eur J Pharmacol* (2020) 884:173394. doi: 10.1016/j.ejphar.2020.173394

29. Xie RY, Fang XL, Zheng XB, Lv WZ, Li YJ, Rage HI, et al. Salidroside and FG-4592 ameliorate high glucose-induced glomerular endothelial cells injury *via* HIF upregulation. *BioMed Pharmacother* (2019) 118:109175. doi: 10.1016/j.biopha.2019.109175

30. Zheng KY, Zhang ZX, Guo AJ, Bi CW, Zhu KY, Xu SL, et al. Salidroside stimulates the accumulation of HIF-1alpha protein resulted in the induction of EPO expression: a signaling *via* blocking the degradation pathway in kidney and liver cells. *Eur J Pharmacol* (2012) 679(1-3):34–9. doi: 10.1016/j.ejphar.2012.01.027

31. Zhang JP, Liu AH, Hou RR, Zhang J, Jia X, Jiang WF, et al. Salidroside protects cardiomyocyte against hypoxia-induced death: A HIF-1 alpha-activated and VEGF-mediated pathway. *Eur J Pharmacol* (2009) 607(1-3):6–14. doi: 10.1016/j.ejphar.2009.01.046

32. Pu WL, Zhang MY, Bai RY, Sun LK, Li WH, Yu YL, et al. Anti-inflammatory effects of rhodiola rosea l.: A review. *BioMed Pharmacother* (2020) 121:109552. doi: 10.1016/j.biopha.2019.109552

33. Sun AQ, Ju XL. Advances in research on anticancer properties of salidroside. *Chin J Integr Med* (2021) 27(2):153–60. doi: 10.1007/s11655-020-3190-8

34. Wang XP, Yuan DY, Tian Y, Li WH. Multiple mechanisms of salidroside on anti-tumor effects. *Eur Rev Med Pharmaco* (2021) 25(17):5349–54. doi: 10.26355/eurrev_202109_26641

35. Wei G, Xu X, Tong H, Wang X, Chen Y, Ding Y, et al. Salidroside inhibits platelet function and thrombus formation through AKT/GSK3beta signaling pathway. *Aging (Albany NY)* (2020) 12(9):8151–66. doi: 10.18632/aging.103131

36. Cooke NM, Smith SG, Kelleher M, Rogers TR. Major differences exist in frequencies of virulence factors and multidrug resistance between community and nosocomial escherichia coli bloodstream isolates. *J Clin Microbiol* (2010) 48 (4):1099–104. doi: 10.1128/JCM.02017-09

37. Walden AP, Young JD, Sharples E. Bench to bedside: A role for erythropoietin in sepsis. *Crit Care* (2010) 14(4):227. doi: 10.1186/cc9049

38. Thuong NTT, Tram TTB, Dinh TD, Thai PVK, Heemskerk D, Bang ND, et al. MARCO variants are associated with phagocytosis, pulmonary tuberculosis susceptibility and Beijing lineage. *Genes Immun* (2016) 17(7):419–25. doi: 10.1038/gene.2016.43

39. Kovach MA, Ballinger MN, Newstead MW, Zeng XY, Bhan U, Yu FS, et al. Cathelicidin-related antimicrobial peptide is required for effective lung mucosal immunity in gram-negative bacterial pneumonia. *J Immunol* (2012) 189(1):304–11. doi: 10.4049/jimmunol.1103196

40. Bao P, Kodra A, Tomic-Canic M, Golinko MS, Ehrlich HP, Brem H. The role of vascular endothelial growth factor in wound healing. *J Surg Res* (2009) 153 (2):347–58. doi: 10.1016/j.jss.2008.04.023

41. van der Flier M, van Leeuwen HJ, van Kessel KP, Kimpen JL, Hoepelman AI, Geelen SP. Plasma vascular endothelial growth factor in severe sepsis. *Shock* (2005) 23(1):35–8. doi: 10.1097/01.shk.0000150728.91155.41

42. Jeong SJ, Han SH, Kim CO, Choi JY, Kim JM. Anti-vascular endothelial growth factor antibody attenuates inflammation and decreases mortality in an experimental model of severe sepsis. *Crit Care* (2013) 17(3):R97. doi: 10.1186/cc12742

43. Saaristo A, Tammela T, Farkkila A, Karkkainen M, Suominen E, Yla-Herttuala S, et al. Vascular endothelial growth factor-c accelerates diabetic wound healing. *Am J Pathol* (2006) 169(3):1080–7. doi: 10.2353/ajpath.2006.051251

44. Maruyama K, Asai J, Li M, Thorne T, Losordo DW, D'Amore PA. Decreased macrophage number and activation lead to reduced lymphatic vessel formation and contribute to impaired diabetic wound healing. *Am J Pathol* (2007) 170 (4):1178–91. doi: 10.2353/ajpath.2007.060018

45. Zhang YB, Lu Y, Ma L, Cao XD, Xiao J, Chen JX, et al. Activation of vascular endothelial growth factor receptor-3 in macrophages restrains TLR4-NF-kappa b signaling and protects against endotoxin shock. *Immunity* (2014) 40(4):501–14. doi: 10.1016/j.immuni.2014.01.013

46. Zingarelli B, Fan H, Ashton S, Piraino G, Mangeshkar P, Cook JA. Peroxisome proliferator activated receptor gamma is not necessary for the development of LPS-induced tolerance in macrophages. *Immunology*. (2008) 124 (1):51–7. doi: 10.1111/j.1365-2567.2007.02734.x

47. Zhang J, Ney PA. EPOR signaling: 450 million years' history. *Blood* (2007) 110(7):2225–6. doi: 10.1182/blood-2007-07-097683

48. Peck OM, Zingarelli B, Fan HK, Teti G, Tempel G, Halushka PV, et al. The phosphatidylinositol 3 kinase pathway regulates tolerance to lipopolysaccharide and priming responses to staphylococcus aureus and lipopolysaccharide. *Shock* (2006) 26(1):31–6. doi: 10.1097/01.shk.0000223128.79759.3d

49. Schabbauer G, Tencati M, Pedersen B, Pawlinski R, Mackman N. PI3K-akt pathway suppresses coagulation and inflammation in endotoxemic mice. *Arterioscl Throm Vas* (2004) 24(10):1963–9. doi: 10.1161/01.ATV.0000143096.15099.ce

50. Luyendyk JP, Schabbauer GA, Tencati M, Holscher T, Pawlinski R, Mackman N. Genetic analysis of the role of the PI3K-akt pathway in lipopolysaccharide-induced cytokine and tissue factor gene expression in monocytes/macrophages. *J Immunol* (2008) 180(6):4218–26. doi: 10.4049/jimmunol.180.6.4218

51. Androulidaki A, Iliopoulos D, Arranz A, Doxaki C, Schworer S, Zacharioudaki V, et al. The kinase Akt1 controls macrophage response to lipopolysaccharide by regulating MicroRNAs. *Immunity* (2009) 31(2):220–31. doi: 10.1016/j.immuni.2009.06.024

52. Liu ZJ, Yan LN, Li XH, Xu FL, Chen XF, You HB, et al. Up-regulation of IRAK-m is essential for endotoxin tolerance induced by a low dose of lipopolysaccharide in kupffer cells. *J Surg Res* (2008) 150(1):34–9. doi: 10.1016/j.jss.2007.12.759

53. Song JJ, Kingston RE. WDR5 interacts with mixed lineage leukemia (MLL) protein *via* the histone H3-binding pocket. *J Biol Chem* (2008) 283(50):35258–64. doi: 10.1074/jbc.M806900200

54. Tan X, Chen S, Wu JX, Lin JX, Pan CC, Ying XF, et al. PI3K/ AKT-mediated upregulation of WDR5 promotes colorectal cancer metastasis by directly targeting ZNF407. *Cell Death Dis* (2017) 8:e2686. doi: 10.1038/cddis.2017.111

55. Collino M, Thiemermann C, Cerami A, Brines M. Flipping the molecular switch for innate protection and repair of tissues: Long-lasting effects of a non-erythropoietic small peptide engineered from erythropoietin. *Pharmacol Therapeut* (2015) 151:32–40. doi: 10.1016/j.pharmthera.2015.02.005

56. Shing KSCT, Broughton SE, Nero TL, Gillinder K, Ilsley MD, Ramshaw H, et al. EPO does not promote interaction between the erythropoietin and beta-common receptors. *Sci Rep Uk* (2018) 8:12457. doi: 10.1038/s41598-018-29865-x

frontiers | Frontiers in Immunology

TYPE Original Research
PUBLISHED 02 September 2022
DOI 10.3389/fimmu.2022.984298

Check for updates

OPEN ACCESS

EDITED BY
Christoph Thiemermann,
Queen Mary University of London,
United Kingdom

REVIEWED BY
Lukas Martin,
University Hospital RWTH Aachen,
Germany
Sina Maren Coldewey,
University Hospital Jena, Germany

*CORRESPONDENCE
Basilia Zingarelli
basilia.zingarelli@cchmc.org

SPECIALTY SECTION
This article was submitted to Inflammation,
a section of the journal
Frontiers in Immunology

RECEIVED 01 July 2022
ACCEPTED 15 August 2022
PUBLISHED 02 September 2022

CITATION
Urban C, Hayes HV, Piraino G, Wolfe V, Lahni P, O'Connor M, Phares C and Zingarelli B (2022) Colivelin, a synthetic derivative of humanin, ameliorates endothelial injury and glycocalyx shedding after sepsis in mice.
Front. Immunol. 13:984298.
doi: 10.3389/fimmu.2022.984298

COPYRIGHT
© 2022 Urban, Hayes, Piraino, Wolfe, Lahni, O'Connor, Phares and Zingarelli. This is an open-access article distributed under the terms of the Creative Commons Attribution License (CC BY). The use, distribution or reproduction in other forums is permitted, provided the original author(s) and the copyright owner(s) are credited and that the original publication in this journal is cited, in accordance with accepted academic practice. No use, distribution or reproduction is permitted which does not comply with these terms.

Colivelin, a synthetic derivative of humanin, ameliorates endothelial injury and glycocalyx shedding after sepsis in mice

Catherine Urban[1], Hannah V. Hayes[2], Giovanna Piraino[3], Vivian Wolfe[3], Patrick Lahni[3], Michael O'Connor[3], Ciara Phares[4] and Basilia Zingarelli[3,5]*

[1]Division of Pediatric Critical Care, Stony Brook Children's, Stony Brook University, Stony Brook, NY, United States, [2]Department of Surgery, College of Medicine, University of Cincinnati, Cincinnati, OH, United States, [3]Division of Critical Care Medicine, Cincinnati Children's Hospital Medical Center, Cincinnati, OH, United States, [4]Department of Systems Biology and Physiology, College of Medicine, University of Cincinnati, Cincinnati, OH, United States, [5]Department of Pediatrics, College of Medicine, University of Cincinnati, Cincinnati, OH, United States

Endothelial dysfunction plays a central role in the pathogenesis of sepsis-mediated multiple organ failure. Several clinical and experimental studies have suggested that the glycocalyx is an early target of endothelial injury during an infection. Colivelin, a synthetic derivative of the mitochondrial peptide humanin, has displayed cytoprotective effects in oxidative conditions. In the current study, we aimed to determine the potential therapeutic effects of colivelin in endothelial dysfunction and outcomes of sepsis *in vivo*. Male C57BL/6 mice were subjected to a clinically relevant model of polymicrobial sepsis by cecal ligation and puncture (CLP) and were treated with vehicle or colivelin (100-200 μg/kg) intraperitoneally at 1 h after CLP. We observed that vehicle-treated mice had early elevation of plasma levels of the adhesion molecules ICAM-1 and P-selectin, the angiogenetic factor endoglin and the glycocalyx syndecan-1 at 6 h after CLP when compared to control mice, while levels of angiopoietin-2, a mediator of microvascular disintegration, and the proprotein convertase subtilisin/kexin type 9, an enzyme implicated in clearance of endotoxins, raised at 18 h after CLP. The early elevation of these endothelial and glycocalyx damage biomarkers coincided with lung histological injury and neutrophil inflammation in lung, liver, and kidneys. At transmission electron microscopy analysis, thoracic aortas of septic mice showed increased glycocalyx breakdown and shedding, and damaged mitochondria in endothelial and smooth muscle cells. Treatment with colivelin ameliorated lung architecture, reduced organ neutrophil infiltration, and attenuated plasma levels of syndecan-1, tumor necrosis factor-α, macrophage inflammatory protein-1α and interleukin-10. These therapeutic effects of colivelin were associated with amelioration of glycocalyx density and mitochondrial structure in the aorta. At molecular analysis, colivelin treatment was associated with inhibition of the signal transducer and activator of

transcription 3 and activation of the AMP-activated protein kinase in the aorta and lung. In long-term outcomes studies up to 7 days, co-treatment of colivelin with antimicrobial agents significantly reduced the disease severity score when compared to treatment with antibiotics alone. In conclusion, our data support that damage of the glycocalyx is an early pathogenetic event during sepsis and that colivelin may have therapeutic potential for the treatment of sepsis-associated endothelial dysfunction.

KEYWORDS

cecal ligation and puncture, colivelin, endothelial injury, glycocalyx, organ injury

Introduction

Sepsis is a life-threating organ dysfunction caused by dysregulated host responses to infection (1). A recent global study reported 49 million cases and 11 million sepsis-related deaths in 2017, accounting for approximately 20% of all annual deaths globally (2). Endothelial injury is a hallmark of systemic inflammatory response syndrome during sepsis and largely contributes to the serious clinical consequences of the infection such as increased vascular permeability, tissue edema, augmented adhesion of leukocytes and platelet aggregation, and loss of flow-dependent vasodilation leading to profound decrease in systemic vascular tone, and collapse of the microcirculation, and contributing to acute lung, kidney and liver injury (3, 4).

Clinical and experimental studies have proven that the glycocalyx is one of the earliest sites involved during the pathogenesis of endothelial injury (5). The glycocalyx is a gel-like mesh layer which covers the luminal surface of vascular endothelial cells. It is composed of membrane-attached proteoglycans, glycosaminoglycan sidechains, glycoproteins, and adherent plasma proteins such as albumin and antithrombin. This structure is known to play critical roles in maintaining hemostasis (6) and coagulation, regulating leukocyte adhesion and rolling (7, 8), and sensing mechanical forces, such as shear stress and pressure (9). It also shields cell surface receptors and can prevent their activation by presenting a physical barrier. In sepsis, there is a distinct alteration in the composition of the endothelial glycocalyx following the activation of proteases, such as metalloproteinases, heparanase, and hyaluronidase, by bacterial and inflammatory insults (10). These enzymes lead to glycocalyx degradation *via* release of glycosaminoglycan sidechains, and if severe enough, loss of core membrane proteins. As the glycocalyx is shed, circulating levels of glycocalyx components, including syndecans, can be measured and are considered biomarkers of endothelial injury (11).

Mitochondria have emerged as important players in maintaining vascular homeostasis (12). In addition to energy production, mitochondria affect a variety of complex processes including inflammation and cell survival (13). Mitochondria-derived peptides, including humanin, encoded by short open reading frame in the mitochondrial DNA (mtDNA), have been recently described to have biological effects (14, 15). Several experimental studies describe potent cytoprotective effects of humanin and its synthetic derivatives (15). For example, humanin is shown to protect endothelial cells from oxidative stress (16, 17) and to prevent glucose-induce endothelial expression of adhesion molecules and apoptosis (18, 19). At the molecular level, humanin appears to regulate metabolic homeostasis through involvement of the signal transducer and activator of transcription 3 (STAT3) (20–22) and AMP-activated protein kinase (AMPK) (15, 23, 24). Recently, colivelin, a new generation potent humanin derivative has also been reported to have cytoprotective effects by inhibiting apoptosis and inflammatory response *in vitro* and *in vivo* models of neuronal degeneration and ischemic injury (25–28). Despite the substantial literatures on colivelin-mediated beneficial effects in neurological diseases, the effect of colivelin on the endothelial damage during a systemic inflammation, like sepsis, has not been investigated.

In the present study, by employing a clinically relevant mouse model of sepsis we hypothesized that endothelial damage occurs early during sepsis and is characterized by structural damage of glycocalyx and associated with organ dysfunction. We also sought to evaluate the therapeutic efficacy of colivelin in sepsis and its potential molecular mechanisms of action.

Materials and methods

Murine model of polymicrobial sepsis

The investigation conformed to the National Institutes of Health Guide for the Care and Use of Laboratory Animals (Eighth Edition, 2011) and was approved by the Institutional Animal Care and Use Committee of the Cincinnati Children's

Hospital Medical Center. Male C57BL/6 mice were obtained from Charles River Laboratories International, Inc. (Wilmington, MA). Mice were used at 3-5 months of age to mimic the equivalent for human ranges from 20 - 25 years (29). Male mice only were chosen for the experimentation to avoid interference from female hormonal fluctuations in sepsis responses during the estrous cycle. Mice were housed in pathogen-free conditions under a 10-h light/14-h dark cycle with free access to food and water. Mice were anesthetized with 2.0% isoflurane in 50% oxygen and polymicrobial sepsis was induced by cecal ligation and puncture (CLP) (30). After a midline laparotomy, the cecum was exteriorized, ligated and punctured twice with a 23-G needle. The cecum was then returned into the peritoneal cavity and the abdominal incision was closed. After the procedure, mice were randomly assigned to three treatment groups: a vehicle-treated group received distilled water (200 µl/mouse) intraperitoneally (i.p.); a 100 µg colivelin-treated group received the colivelin at 100 µg/kg i.p., and a 200 µg colivelin-treated group received the colivelin at 200 µg/kg i.p. at 1 h after CLP. The intraperitoneal injection was chosen to allow for a rapid uptake and bioavailability of the peptide. All groups of mice also received fluid resuscitation (35 ml/kg normal saline solution subcutaneously) immediately after, at 3 h and 12 h after the CLP procedure. To minimize pain at the surgical incision site, lidocaine hydrochloride (1%, 4 mg/kg total dose) was applied locally immediately after the procedure. Control mice did not undergo any surgical procedure; sham mice underwent laparotomy only without CLP. Mice were then sacrificed at 0, 6 and 18 h after CLP. Blood, lungs, kidneys, liver, and thoracic aortas were collected for biochemical assays.

Long-term studies of severity of sepsis

In a separate study, another cohort of mice was subjected to the CLP procedure and was used for assessing health and moribundity conditions, and survival rate up to 7 days. Mice were divided into two treatment groups in a blind and random fashion: a vehicle-treated group received distilled water (200 µl/mouse), and a colivelin-treated group received colivelin (100 µg/kg subcutaneously) at 1 h, 3 h and 24 h after the CLP procedure. Twelve animals were included for each group. One animal was sacrificed because of unintentional extensive damage in the small intestine during surgical procedure and was excluded from the study. The subcutaneous injection was chosen to avoid further stress in the peritoneum since the animals also received intraperitoneal treatment of antibiotics. To mimic the clinical management of antimicrobial coverage, all mice received ceftriaxone (25 mg/kg) and metronidazole (12.5 mg/kg) intraperitoneally every 12 h after CLP for three days. To minimize pain, buprenorphine (0.05 mg/kg) was administered subcutaneously at 1 h after surgery and every 12 h for three days after surgery. All groups of mice also received fluid resuscitation (35 ml/kg normal saline with 5% dextrose subcutaneously) every 24 h for all the duration of the experimental period. Although some spontaneous death occurred given the acute severity of the disease, spontaneous death was not considered as endpoint for this study for ethical reasons. Animals were euthanized when they exhibited signs of moribundity. During the monitoring period a score system was developed according to the clinical signs of peritoneal sepsis (31, 32). Physical examination focused on four parameters: posture, feces consistency, eye appearance, hair coat. For each parameter a score 0 to 3 was given according to the abnormalities. Specifically, a score of 0 represents no symptoms; score of 1 represents minimum symptoms (awkward gait, loose stools, some watery ocular discharge, fuzzy facial fur); score of 2 represents mild symptoms (hunched or slow walk, watery stools, some yellow ocular discharge, rough hair coat); score of 3 represents severe symptoms (complete inability to move or lethargy, hemorrhagic diarrhea, red eyes with thick ocular discharge, pilo-erection). Weight loss of more than 20% was also considered a humane endpoint. Monitoring and weighing of the animals was performed daily by the laboratory personnel blinded to the treatment protocol and logged in a score sheet. Animals with cumulative scores >8 or weight loss > 20% from the initial body weight were euthanized. Therefore, mice experiencing spontaneous death or euthanized within 7 days were defined as non-survivor mice. Animals that survived the entire observation period of 7 days were also euthanized and were defined as survivor mice.

Myeloperoxidase activity

Myeloperoxidase (MPO) activity was measured as an indicator of neutrophil infiltration in lung, kidneys and liver tissue (33). Tissues were homogenized in a solution containing 0.5% hexa-decyl-trimethyl-ammonium bromide dissolved in 10 mM potassium phosphate buffer (pH 7.0) and centrifuged for 30 min at 4000 × g at 4°C. An aliquot of the supernatant was allowed to react with a solution of tetra-methyl-benzidine (1.6 mM) and hydrogen peroxide (0.1 mM). The rate of change in absorbance was measured by spectrophotometry at 650 nm. MPO activity was defined as the quantity of enzyme degrading 1 µmol of hydrogen peroxide/min at 37°C and expressed in units per 100 mg weight of tissue.

Histopathologic analysis

Paraffin-embedded sections of thoracic aortas and lungs were stained with hematoxylin and eosin for morphological

evaluation by three independent observers blinded to the treatment groups. Lung injury was also analyzed by a semiquantitative score based on the following histologic features: alveolar capillary congestion, infiltration of red blood cells and inflammatory cells into the airspace, alveolar wall thickness, and hyaline membrane formation (34). A score of 0 represented normal findings and scores of 1, 2, 3 and 4 represented minimal (<25% lung involvement), mild (25-50% lung involvement), significant (50-75% lung involvement) and severe (>75% lung involvement) injury, respectively. The four variables were summed to represent the lung injury score (total score, 0–16).

Transmission electron microscopy

Glycocalyx structure was assessed by transmission electron microscopy (35). At 6 h after CLP, mice were again anesthetized with 2.0% isoflurane in 50% oxygen and perfused *via* cardiac puncture with a solution for lanthanum staining composed of 2% glutaraldehyde, 2% sucrose, 0.1 M sodium cacodylate buffer (pH 7.3), and 2% lanthanum nitrate. Thereafter, the aorta was harvested and diced in three to four pieces of approximately 1 mm^3 each. Sections were immersed for 2 h in the lanthanum staining solution and then immersed overnight in a solution composed of 2% sucrose and 0.1 M sodium cacodylate buffer (pH 7.3). After washing in alkaline 2% sucrose and 0.03 M NaOH solution, sections were immersed in 2% osmium tetroxide and 2% lanthanum nitrate, embedded and cut with ultramicrotome. The sections were viewed and photographed on Hitachi H-7650 transmission electron microscope at 120 kV.

Plasma levels of cytokines and biomarkers of endothelial injury

Plasma levels of tumor necrosis factor-α (TNFα), interleukin (IL)-1β, IL-6, IL-10, keratinocytes-derived chemokine (KC), and macrophage inflammatory proteins (MIP-1α) were used as indices of the systemic inflammatory response and were evaluated by a commercially available multiplex array system (Milliplex, Millipore Corporation, Billerica, MA). Plasma levels of endoglin, intercellular adhesion molecule-1 (ICAM-1), P-selectin, proprotein convertase subtilisin/kexin type 9 (PCSK9), and angiopoietin-2 (Ang 2) were used as indices of endothelial injury and were evaluated by a commercially available multiplex array system (R&D Systems, Minneapolis, MN). Plasma levels of syndecan-1 were used as indices of glycocalyx damage and were evaluated by a mouse syndecan-1 sandwich-type enzyme-linked immunosorbent assay (ELISA) kit (Boster Biological Technology Co., California, US). Assays were performed using the protocols recommended by the manufacturer.

Subcellular fractionation

Subcellular fractionation was performed using a centrifugation model. Tissue samples of lung and thoracic aortas were homogenized in a buffer (50 mg tissue/100 µL) containing 0.32 M sucrose, 10 mM Tris-HCl (pH 7.4), 1 mM EGTA, 2 mM EDTA, 5 mM NaN3, 10 mM β-mercaptoethanol, 2 µM leupeptin, 0.15 µM pepstatin A, 0.2 mM phenylmethanesulfonyl fluoride, 50 mM NaF, 1 mM sodium orthovanadate and 0.4 nM microcystin. Samples were centrifuged at 1000x g for 10 min at 4°C and the supernatants collected as cytosol extracts, which also contain membrane and mitochondria. The pellets were then solubilized in Triton buffer (1% Triton X-100, 250 mM NaCl, 50 mM Tris HCl at pH 7.5, 3 mM EGTA, 3 mM EDTA, 1 mM phenylme-thanesulfonyl fluoride, 0.1 mM sodium orthovanadate, 10% glycerol, 2 mM p-nitrophenyl phosphate, 0.5% NP-40 and 46 µM aprotinin). The lysates were rocked for 1 h and subsequently centrifuged at 15,000x g for 30 min at 4° C and the supernatant collected as nuclear extracts. The Bradford protein assay was then used for quantitative determination of total proteins.

Western blot analysis

Cytosol content of total AMPKα1/α2 and its phosphorylated form pAMPKα1/α2 (Santa Cruz Biotechnology, Dallas, TX, USA), cytosol and nuclear content of STAT3 and its phosphorylated forms pSTAT3(Tyr705) and pSTAT3(Ser727) (Cell Signaling Technology, Danvers, MA, USA) were determined by immunoblot analyses; β-actin was concomitantly probed with mouse anti-β-actin (Santa Cruz Biotechnology) as a loading control for both cytosol and nuclear proteins. Extracts were heated at 70°C in equal volumes of 4x Protein Sample Loading Buffer. Twenty-five µg of proteins were loaded per lane on a 10% Bis-Tris gel. Proteins were separated electrophoretically and transferred to nitro-cellulose membranes. The immunoreaction was detected by near-infrared fluorescence. Membranes were blocked with Odyssey blocking buffer (LI-COR Biotechnology, Lincoln, NE, USA) and incubated with primary antibodies. Membranes were washed in PBS with 0.1% TWEEN 20 and incubated with near infrared fluorescent dye-conjugated secondary antibodies (IRDye goat anti-rabbit and anti-mouse IgG; LI-COR Biotechnology). Immunoblotting was performed by using the IBind Flex Western System (Thermo Fischer Scientific, Waltham, MA, USA) that uses sequential lateral flow to perform blocking and antibody binding. The Odyssey LI-COR scanner (LI-COR Biotechnology) was used for detection. Fold changes of relative intensity of proteins were calculated *versus* mean value of control mice upon data normalization with β-actin by NIH ImageJ 1.53k software (36). Normalization and

quantification for AMPKα1/α2 was also validated by Revert total protein stain and Empiria Studio analysis (LI-COR Biotechnology).

Materials

Unless otherwise stated, all chemicals were obtained from Sigma-Aldrich (St. Louis, MO).

Statistical analysis

Statistical analysis was performed using SigmaPlot 14.0 (Systat Software, San Jose, CA, USA). Data in figures and text are expressed means ± SEM or median with 25th and 75th percentile of n observations (n = 3–17 animals for each group). The results were examined by analysis of variance followed by the Student–Newman–Keuls correction *post hoc* t-test. Statistical analysis of damage scores was performed using the non-parametric Mann–Whitney test. The Gehan-Breslow test was used to compare differences in survival rates (n = 11-12 animals for each group). A value of $P<0.05$ was considered significant.

Results

Glycocalyx shedding and endothelial damage occur early during polymicrobial sepsis and are associated with lung injury

To determine the onset of endothelial damage, we performed histology of thoracic aortas and we measured plasma biomarkers at 6 h and 18 h after CLP. Hematoxylin and eosin-stained sections of the thoracic aorta did not reveal alteration of cellular density or irregularities in the tunica intima, tunica media, and adventitia layers at 6 h or 18 h after CLP (Supplementary Figure S1). However, an early elevation of plasma levels of syndecan-1, a marker of glycocalyx breakdown and shedding, was observed at 6 h in mice subjected to CLP when compared to control mice at baseline conditions (2.77 ± 0.34 *versus* 0.49 ± 0.13 ng/ml, $P<0.05$; Figure 1A). This early glycocalyx damage was also associated with an early increase of the angiogenetic factor endoglin (5.07 ± 0.69 ng/ml), the adhesion molecules ICAM-1 (156.72 ± 20.93 ng/ml) and P-selectin (58.26 ± 6.40 ng/ml) when compared to control mice (3.50 ± 0.24, 73.96 ± 6.62, and 31.04 ± 5.73 ng/ml, respectively; $P<0.05$). At 18 h after CLP plasma syndecan-1, endoglin, ICAM-1 and P-selectin were still maintained at high levels (Figures 1B–D). At 18 h after CLP, septic mice also exhibited higher plasma levels of angiopoietin-2 (154.80 ± 21.90 ng/mL), a mediator of microvascular disintegration, and levels of PCSK9 (59.27 ± 11.28 ng/mL), an enzyme implicated in low-density lipoprotein receptor degradation and clearance of endotoxins, when compared to control mice (63.19 ± 4.08 and 27.99 ± 2.80, respectively; $P<0.05$) (Figures 1E, F). Early degradation of endothelial glycocalyx was also associated with higher lung injury score at 6 h, which persisted at 18 h after CLP, and was characterized by reduced alveolar space, and accumulation of red and inflammatory cells when compared to control mice at basal condition (Figure 2). To distinguish whether early endothelial damage was secondary to specific sepsis-induced immune response, we also measured these circulating biomarkers in sham mice, which underwent laparotomy but not CLP. In sham mice at 6 h, levels were not significantly different when compared with baseline levels of control mice. Sham mice at 18 h exhibited a significant elevation of P-selectin, PCSK9 and angiopoietin-2 (Supplementary Figure S2). There was only a mild infiltration of neutrophil, as determined by MPO activity, in the lung at 6 h when compared with control mice, but levels were significantly lower than mice subjected to CLP (Supplementary Figure S3). Thus, these data suggested that the early occurrence of endothelial damage is a specific sepsis-induced response and not induced by the sterile inflammation caused by the surgical procedures.

Treatment with colivelin reduces neutrophil infiltration in lung, liver and kidney after CLP in a dose-independent manner

Considering the early elevation in plasma levels of adhesion molecules, we next determined the effects of treatment with the peptide colivelin on neutrophil infiltration by measuring MPO activity in major organs at 6 h after CLP. Vehicle-treated mice had higher MPO activity in lungs, liver and kidneys when compared to control mice at basal conditions. Treatment with colivelin significantly decreased MPO activity in lungs, liver and kidneys in a dose-independent manner when compared to vehicle treatment (Figures 3A–C). Microscopic examination of hematoxylin and eosin-stained lung sections confirmed that treatment with colivelin reduced infiltration of inflammatory cells and ameliorated alveolar damage in the lung (Figures 3D, E) when compared to vehicle treatment (Figure 2B).

Treatment with colivelin reduces plasma levels of cytokines after CLP in a dose-independent manner

To evaluate the effect of colivelin on systemic inflammatory response, a panel of Th1/Th2/Th17 cytokines was measured. At 6 h after CLP, plasma levels of IL-1β, IL-6, IL-10, KC, TNF-α, and MIP-1α were significantly increased in vehicle-treated mice compared to control mice. Colivelin treatment significantly decreased levels of TNF-α, MIP-1α and IL-10 in a dose independent-manner. Levels of KC were significantly reduced in the mice treated with colivelin at 200 μg/kg. There was also a

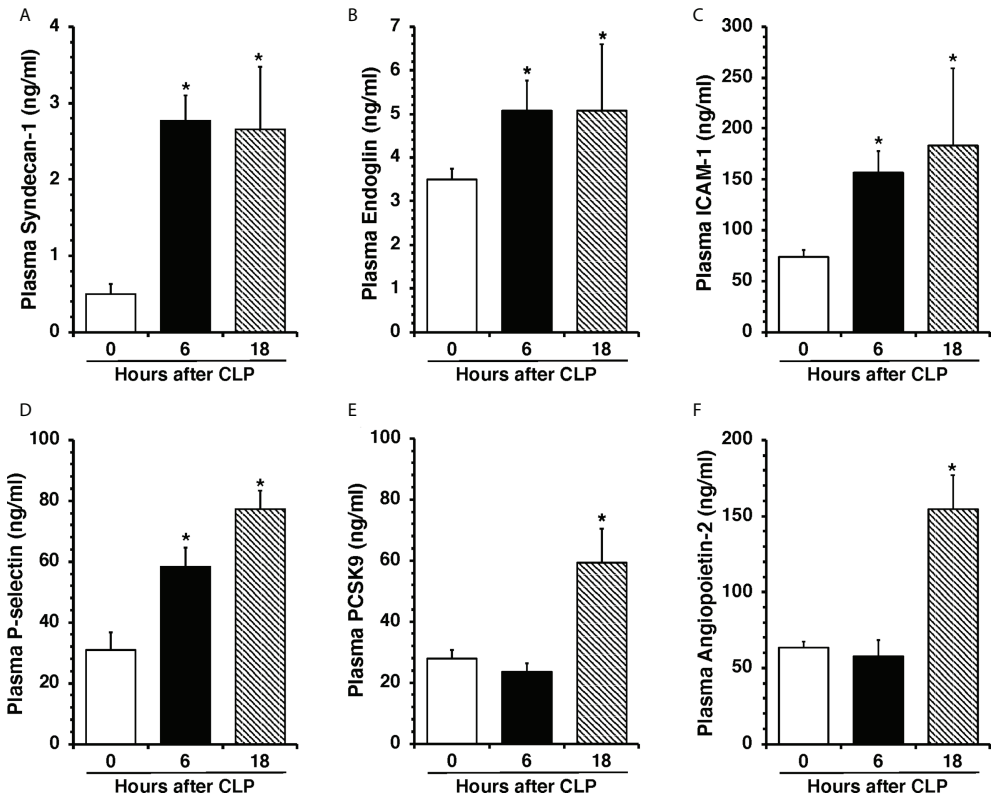

FIGURE 1
Plasma levels of Syndecan-1 **(A)**, Endoglin **(B)**, ICAM-1 **(C)**, P-selectin **(D)**, PCSK9 **(E)**, and Angiopoietin-2 **(F)** at 0 h, 6 h and 18 h after cecal ligation and puncture (CLP). Data represents the mean ± SEM of 10-13 mice for group (n=10 control group at 0 h, n=13 at 6 h, n=11 at 18 h). *Represents $P < 0.05$ *versus* control mice at time 0.

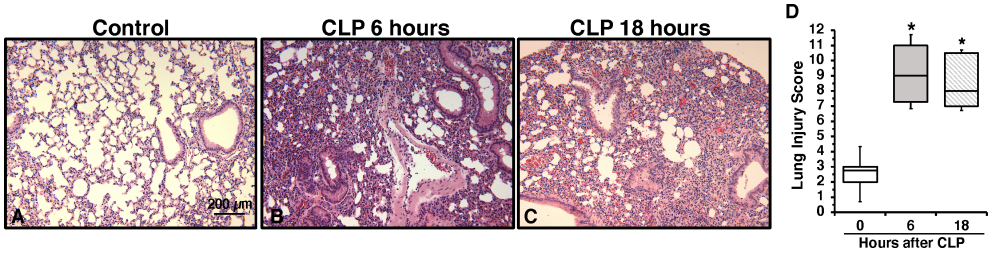

FIGURE 2
Representative histology photomicrographs of lung sections of a control mouse **(A)** or mice subjected to polymicrobial sepsis at 6 h **(B)** and 18 h **(C)** after cecal ligation and puncture (CLP). Lung damage at 6 h and 18 h after CLP was characterized by severe reduction of alveolar space, neutrophil adhesion along vascular wall, hemorrhage, and infiltration of inflammatory cells. Magnification x100. A similar pattern was seen in tissue sections of n=5 mice in each experimental group. **(D)** Histopathologic scores of lung sections (n=5 mice for each group). Lung injury was scored from 0 (no damage) to 16 (maximum damage). Box plots represent 25th percentile, median, and 75th percentile; error bars define 10th and 90th percentiles. *Represents $P < 0.05$ *versus* control mice at time 0.

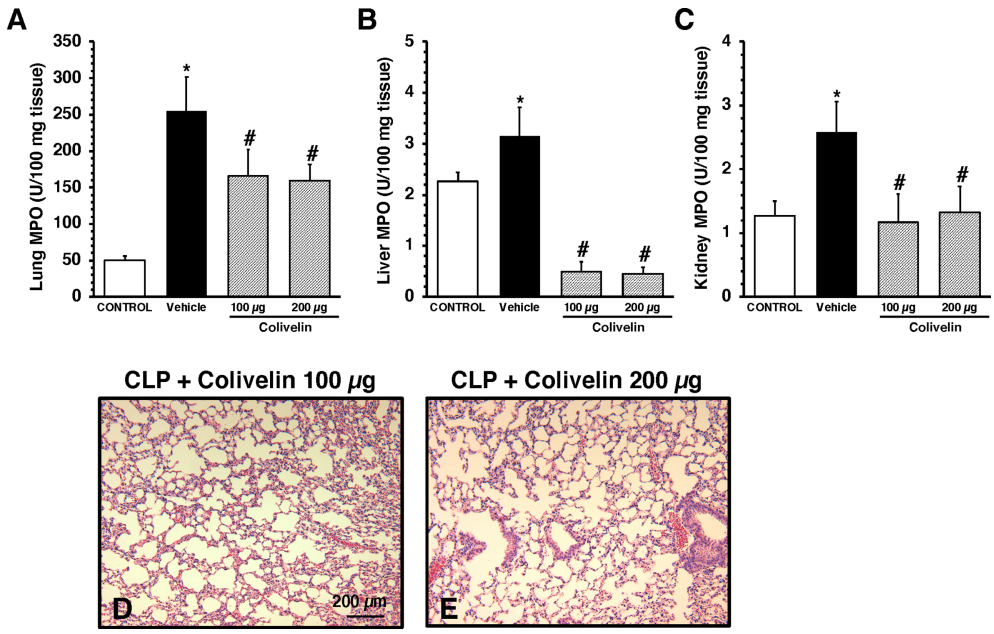

FIGURE 3
Activity of myeloperoxidase (MPO) in lung **(A)**, liver **(B)**, kidney **(C)** at 6 h after cecal ligation and puncture (CLP). Data represents the mean ± SEM of 7-17 mice for group (n=17 control group, n=13 vehicle group, n=7 colivelin 100 μg group, n=11 colivelin 200 μg group). *Represents $P < 0.05$ *versus* control mice; #represents $P < 0.05$ *versus* vehicle-treated mice. **(D-E)** Representative histology photomicrographs of lung sections of colivelin-treated mice at 6 h after CLP. Vehicle (200 μl distilled water) or colivelin (100 or 200 μg/kg) was administered intraperitoneally at 1 h after CLP. Magnification x100. A similar pattern was seen in tissue sections of n=5 mice in each experimental group.

trend towards reduction of IL-1β and IL-6 after treatment with colivelin, but levels of these cytokines were not statistically different when compared with vehicle treatment (Figure 4).

Treatment with colivelin ameliorates endothelial glycocalyx damage and mitochondrial damage in thoracic aortas after CLP

We next evaluated the effect of colivelin on endothelial injury. Colivelin treatment significantly decreased levels of plasma syndecan-1 in a dose-independent manner at 6 h after CLP, thus suggesting reduction in glycocalyx shedding (Figure 5). Since effects of the peptide were in a dose-independent manner, we next examined the ultrastructural changes of the thoracic aortas in mice treated with colivelin at 100 μg/kg only (Figure 6). At electron microscopic analysis, mitochondria damage was evident in smooth muscle and endothelial cells in vehicle-treated mice at 6 h after CLP and was characterized by swollen mitochondria and presence of autophagosomes when compared to control mice. On the luminal surface the lanthanum staining showed a thick endothelial glycocalyx layer with dense individual bundles in control mice. At 6 h after CLP, the glycocalyx layer appeared thinner with less dense bundles with loose structure in vehicle-treated mice. On the contrary, in colivelin-treated mice mitochondria appeared normal with dense matrix in all cell types and the dense structure of glycocalyx appeared well preserved when compared to vehicle treatment (Figure 6).

Treatment with colivelin inhibits STAT3 activation in thoracic aortas and lungs after CLP

Since colivelin has been reported to activate STAT3 *in vitro*, we next determined whether colivelin induced changes in STAT3 activation and intracellular localization in aortas and lungs. Control mice exhibited marginal levels of pSTAT3 (Ser727), whereas the pSTAT3(Tyr705) was undetectable in both cytosol and nuclear compartments of thoracic aortas (Figure 7). At 6 h after CLP, the levels of total STAT3 were reduced in the cytosol while they remained unchanged in the nucleus in vehicle-treated mice when compared to control mice. On the contrary, the expression of pSTAT3(Ser727) was significantly upregulated in the cytosol, while there was a trend towards increase in the nucleus; pSTAT3(Tyr705) was significantly upregulated in the cytosol and nuclear compartments when compared to basal levels of control

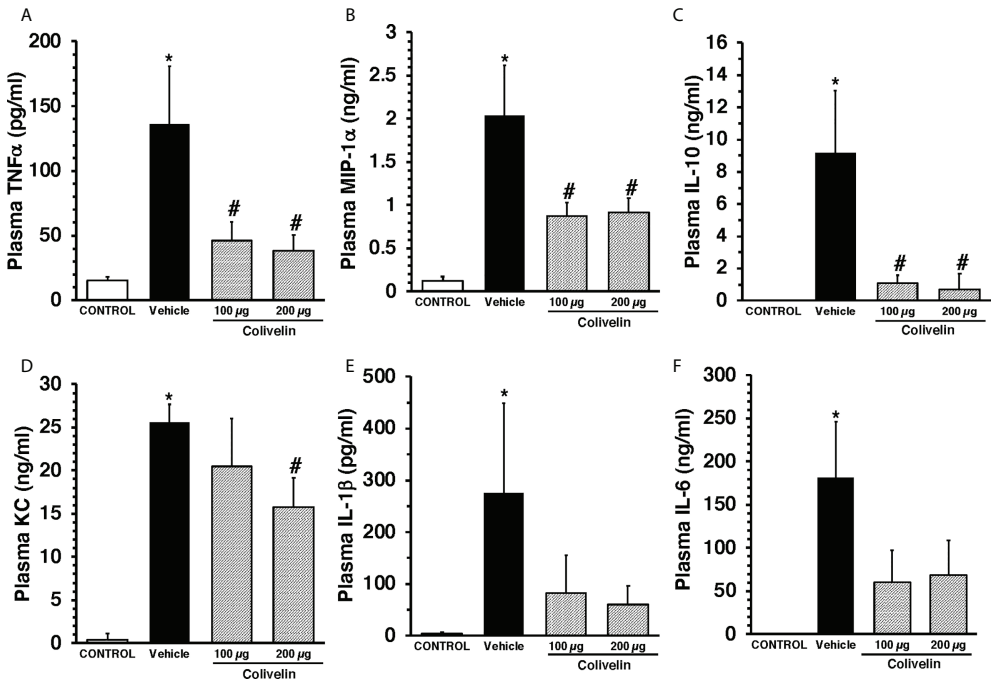

FIGURE 4
Plasma levels of TNFα **(A)**, MIP-1α **(B)**, IL-10 **(C)**, KC **(D)**, IL-1β **(E)**, and IL-6 **(F)** at 6 h after cecal ligation and puncture (CLP). Vehicle (200 µl distilled water) or colivelin (100 or 200 µg/kg) was administered intraperitoneally at 1 h after CLP. Data represents the mean ± SEM of 4-7 mice for group (n=4 control group, n=6 vehicle group, n=4 colivelin 100 µg group, n=7 colivelin 200 µg group). *Represents $P < 0.05$ *versus* control mice; #represents $P < 0.05$ *versus* vehicle-treated mice.

mice, thus suggesting an overall activation of the transcription factor after sepsis. Interestingly, in thoracic aortas of colivelin-treated mice, cytosolic expression of both pSTAT3(Ser727) and pSTAT3(Tyr705) was significantly reduced. Colivelin treatment did not affect nuclear expression of pSTAT3 (Ser727), while it inhibited pSTAT3(Tyr705) at the highest dose. Furthermore, the levels of total STAT3 were restored in the cytosol while they remained unchanged in the nucleus in colivelin-treated mice when compared to vehicle treatment (Figure 7). In the lung, there was a constitutive expression of both pSTAT3(Ser727) and pSTAT3(Tyr705) in the cytosol and nuclear compartments of control mice (Figure 8). At 6 h after CLP, the expression of pSTAT3(Ser727) was significantly upregulated in the cytosol, while there was a trend towards increase in the nucleus (P=0.063); pSTAT3(Tyr705) was significantly upregulated in the cytosol and nuclear compartments when compared to basal levels of control mice, thus suggesting an overall activation of the transcription factor also in the lung after sepsis. Interestingly, in the lung of colivelin-treated mice, cytosolic expression of both pSTAT3(Ser727) and pSTAT3(Tyr705) was significantly reduced when compared to vehicle-treatment. Nuclear expression of both pSTAT3(Ser727) and pSTAT3(Tyr705) was lower than vehicle-treated mice, but not statistically significant. In the lung, levels of total STAT3 were similar among the three groups of mice (Figure 8).

Treatment with colivelin activates AMPK in thoracic aortas after CLP

To further examine the molecular mechanism of colivelin, we also determined the cytosolic activation of AMPK, the crucial regulator of mitochondrial control quality. At 6 h after CLP, the phosphorylated active pAMPKα1/α2 were reduced in the cytosol of thoracic aortas in vehicle-treated mice when compared to basal levels of control mice. Colivelin treatment significantly increased the ratio of the phosphorylated/total forms in a dose-independent manner, thus suggesting the restoration of the kinase function (Figure 9).

Treatment with colivelin ameliorated long-term outcomes after CLP

Given the early beneficial effects of colivelin on organ and endothelial injury induced by sepsis, we sought to determine the effect of the peptide in long-term outcomes. In long-term

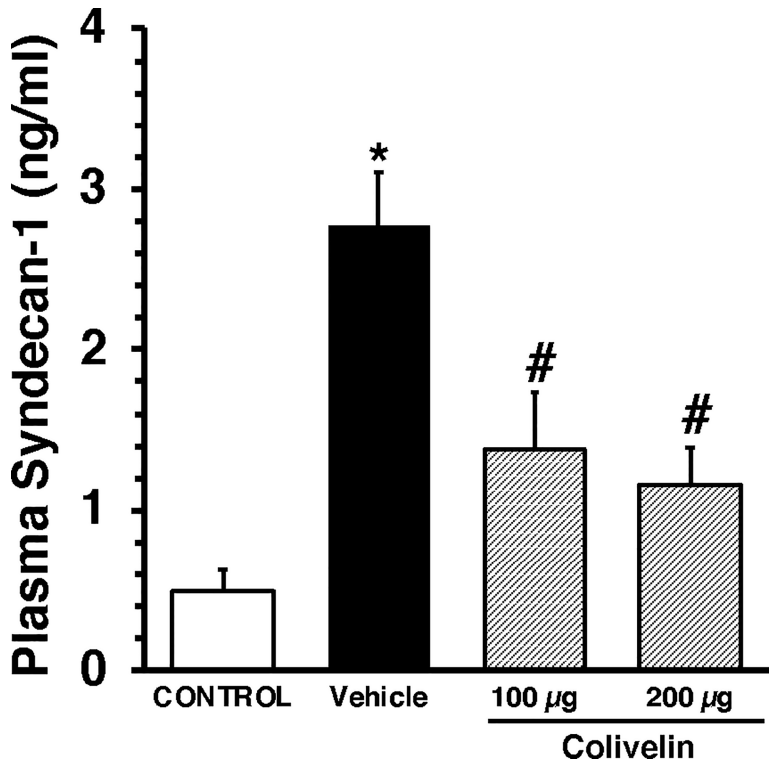

FIGURE 5
Plasma levels of Syndecan-1 at 6 h after cecal ligation and puncture (CLP). Vehicle (200 µl distilled water) or colivelin (100 or 200 µg/kg) was administered intraperitoneally at 1 h after CLP. Data represents the mean ± SEM of 7-13 mice for group (n=10 control group, n=13 vehicle group, n=7 colivelin 100 µg group, n=11 colivelin 200 µg group). *Represents $P < 0.05$ *versus* control mice; #represents $P < 0.05$ *versus* vehicle-treated mice.

studies, septic mice were treated with colivelin (100 µg/kg subcutaneously) or vehicle at 1 h, 3 h and 24 h after CLP and were monitored up to 7 days. To mimic the clinical condition, all mice also received antibiotic therapy for three days and fluid resuscitation for all the duration of the experimental period. The vehicle-treated group exhibited a survival rate of 50% as 6 out of 12 mice survived at 7 days after CLP. The colivelin-treated group experienced a slight, but not significant, increase of survival rate (72.6%) as 8 out of 11 mice survived at 7 days (Figure 10A). Both vehicle- and colivelin-treated mice exhibited diarrhea, pilo-erection and signs of lethargy in the early 36 h after CLP. Symptoms declined at 48 h but increased again at later time after antibiotics discontinuation in both vehicle and colivelin-treated groups. However, colivelin-treated mice exhibited less severe signs of sepsis for all the duration of the observation period and survivor colivelin-treated mice were significantly healthier than survivor vehicle-treated mice at 6 and 7 days after CLP (Figure 10B). Both vehicle- and colivelin-treated mice experienced a similar body weight loss in the first two days after CLP. However, at later time points vehicle-treated mice maintained a significant lower weight than colivelin-treated mice (Figure 10C).

Discussion

In the present work, we demonstrated that increased plasma levels of biomarkers of endothelial permeability, inflammation and adhesiveness occurred at the early stage of experimental sepsis in mice (i.e., at 6 h after CLP) and coincided with structural changes of endothelial glycocalyx in the aorta and with inflammation of major organs. We also demonstrated for the first time that colivelin, a potent synthetic humanin derivative, is a potential therapeutic compound to restore endothelial stability and improve outcomes of sepsis. We found, in fact, that colivelin treatment attenuated infiltration of inflammatory cells in lung, kidney and liver, reduced the systemic release of the pro-inflammatory cytokines, and, when given as an adjunctive treatment to the standard fluid resuscitation and antibiotics, improved long-term recovery and health conditions of septic mice.

Being responsible of important physiological functions, such as hemostasis, vasomotor control, barrier integrity and immunological function, the endothelium is a critical cellular system for host survival following severe injury, including sepsis (3, 4). Considering the systemic nature of sepsis, exposure to

10.3389/fimmu.2022.984298

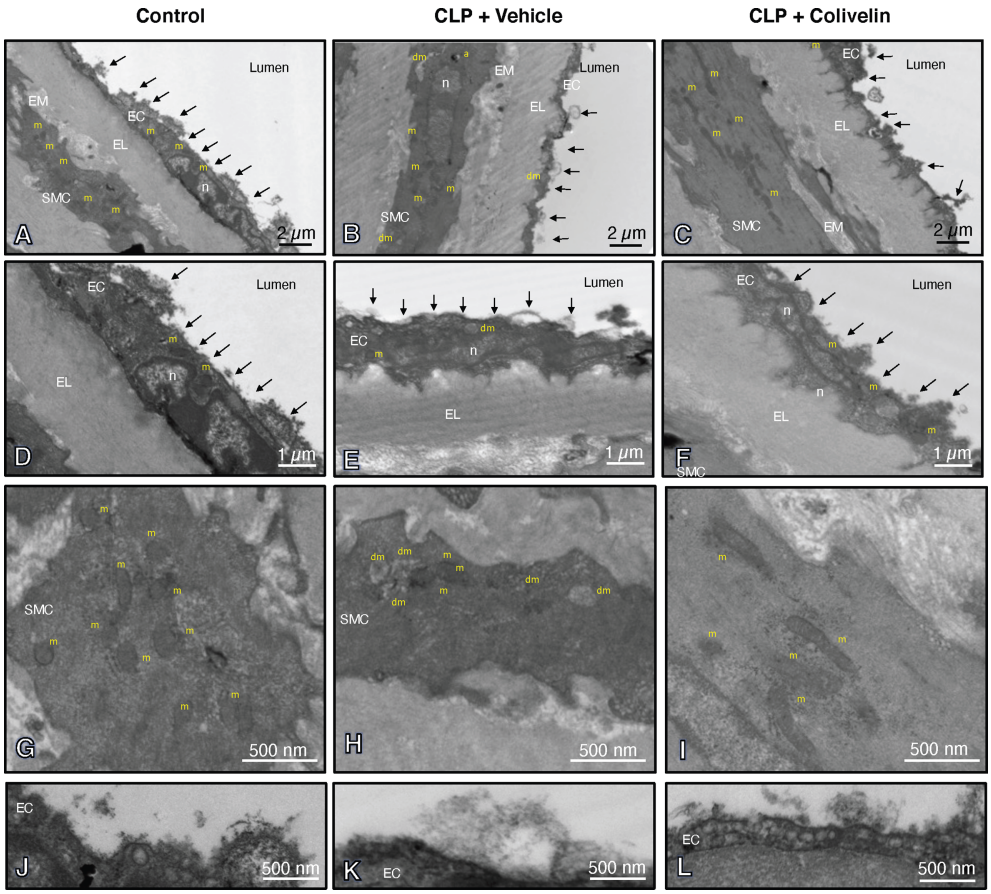

FIGURE 6
Transmission electron microscopy sections of thoracic aortas with lanthanum staining at 6 h after cecal ligation and puncture (CLP). Panels of control mice **(A, D, G, J)** show thick endothelial glycocalyx layer with dense individual bundles and normal mitochondria in endothelial and smooth muscle cells. Panels of vehicle-treated mice **(B, E, H, K)** show thin glycocalyx with bundles with loose structure and some damaged mitochondria and authophagic vesicles at 6 h after CLP. Panels of colivelin-treated mice **(C, F, I, L)** show well preserved thin glycocalyx and normal mitochondria at 6 h after CLP. Vehicle (200 µl distilled water) or colivelin (100 µg/kg) was administered intraperitoneally at 1 h after CLP. Arrows = glycocalyx; EC = endothelial cell; EL = elastica lamina; EM = extracellular matrix; RC = red cell; SMC = smooth muscle cell; a = authophagosome; n = nucleus; m = normal mitochondria; dm = damaged swollen mitochondria presenting translucent matrix and disrupted cristae.

pathogen-associated molecular patterns and endogenous damage-associated molecular patterns may impair the structure and function of the endothelium and its glycocalyx layer. Several clinical studies have demonstrated elevated circulating levels of syndecan-1 as a marker of glycocalyx degradation in sepsis and are associated with organ dysfunction and mortality (37–40). Clinical studies have also profiled protein markers of endothelial activation in both the adult and pediatric populations and have reported significant associations with the severity of sepsis and septic shock, organ failure and mortality risks (41–44). Adhesion molecules, such as ICAM-1 and P-selectin, have been associated with poor outcomes of acute lung injury (45–47). In adult patients circulating P-selectin, measured at ICU admission, appear to be associated with sepsis development in time (48) and it may have diagnostic value for sepsis when used with other endothelial markers (40). Angiopoietin-2, which is produced in endothelial cells and pre-stored in the Weibel-Palade bodies, has been correlated with sepsis severity and death (42–44, 49) and with acute kidney injury and respiratory failure (50). Other novel biomarkers have been proposed for the evaluation of endothelial dysfunction (51). Endoglin, or CD105, is a membrane-bound glycoprotein that serves as a co-receptor for members of the transforming growth factor-β and functions as an angiogenetic factor. Although not yet determined in sepsis, circulating levels of soluble endoglin have been shown to be higher in the serum of patients with cardiovascular diseases with a significant inflammatory component (52, 53). Recent experimental and clinical studies have also supported a central role of PCSK9 in the clearance of pathogenic lipids such as the

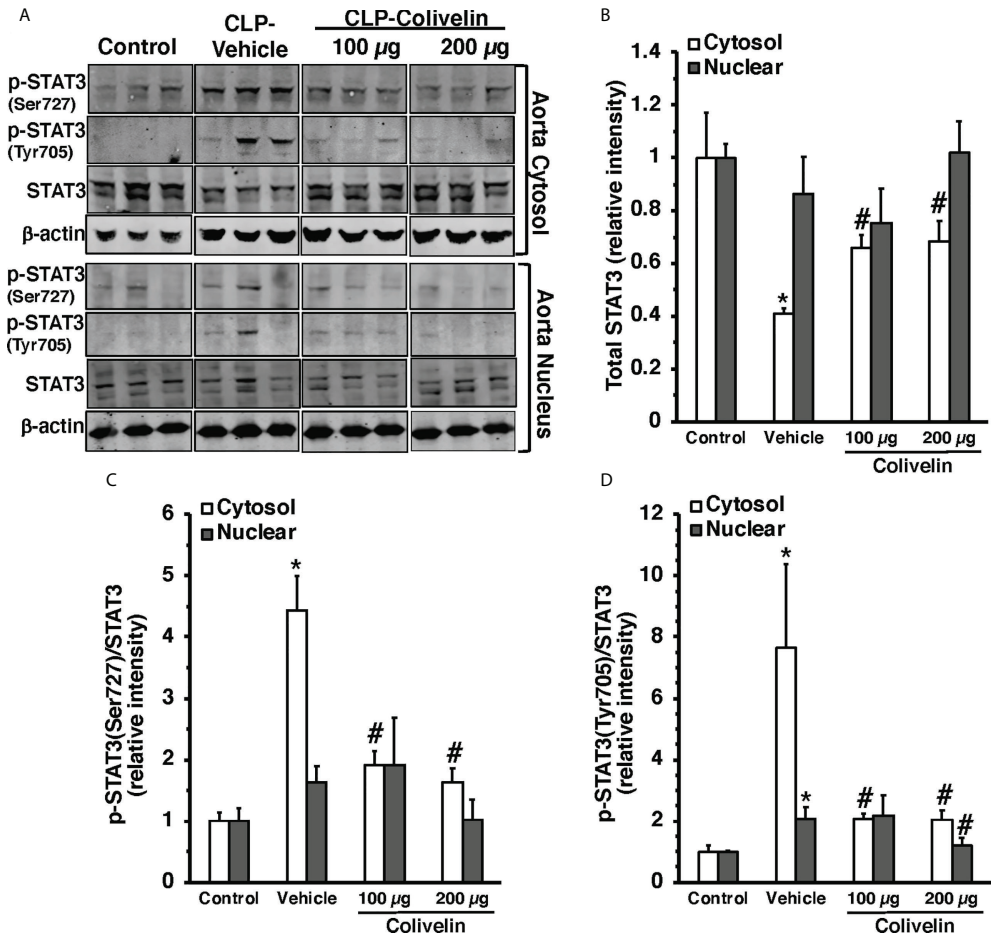

FIGURE 7
Representative Western blots of total STAT3, p-STAT3(Ser727) and p-STAT3(Tyr705) in cytosol and nuclear extracts of thoracic aorta; β-actin was used as loading control protein **(A)**. Image analyses of cytosol and nuclear of relative intensity of total STAT3 **(B)**, ratio of p-STAT3(Ser727)/STAT3 **(C)**, and ratio of p-STAT3(Tyr705)/STAT3 **(D)** as determined by densitometry. Vehicle (200 µl distilled water) or colivelin (100 µg/kg) was administered intraperitoneally at 1 h after CLP. Each data represents the mean ± SEM of 3-4 animals for each group. *Represents $P < 0.05$ versus control mice; #represents $P < 0.05$ versus vehicle-treated mice.

bacterial lipopolysaccharide (LPS) and in sepsis (54). Although mainly located in the liver PCSK9 is also expressed in vascular smooth muscle and endothelial cells and its expression is increased by stimulation with LPS (55), suggesting a critical role of PCSK9 in vascular function. Plasma PCSK9 levels have been shown to serve as a late biomarker of the severity of illness in patients with severe trauma injury in ICU (56) and sepsis (57) and have been correlated to endothelial dysfunction in patients with chronic kidney disease (58).

Despite these data on association with poor prognosis, the pathophysiology of glycocalyx injury and endothelial dysfunction and its potential role as therapeutic targets in improving sepsis outcomes remain unclear. In our study, we observed a distinct temporal profile of these circulating endothelial biomarkers and glycocalyx degradation. We observed that plasma elevation of the glycocalyx component syndecan-1 occurred early after CLP procedure and correlated with an early elevation of plasma levels of the adhesion molecules ICAM-1 and P-selectin. This early increased expression of circulating syndecan-1 support the hypothesis that the shedding of the glycocalyx concomitantly occurs with the critical period of the inflammatory process of the endothelium and may precede angiogenetic events as angiopoietin-2 was elevated only at 18 h after CLP. Interestingly, in our model we also have identified other novel markers, such as endoglin and PCSK9, whose pathophysiological role in sepsis deserves further investigation.

Neutrophil infiltration is a crucial pathophysiological event of organ injury. In normal conditions, adhesion molecules responsible for leukocyte adhesion are embedded in the glycocalyx and are shielded from leukocytes rolling. Therefore, shedding of the glycocalyx allows for neutrophil infiltration. In

10.3389/fimmu.2022.984298

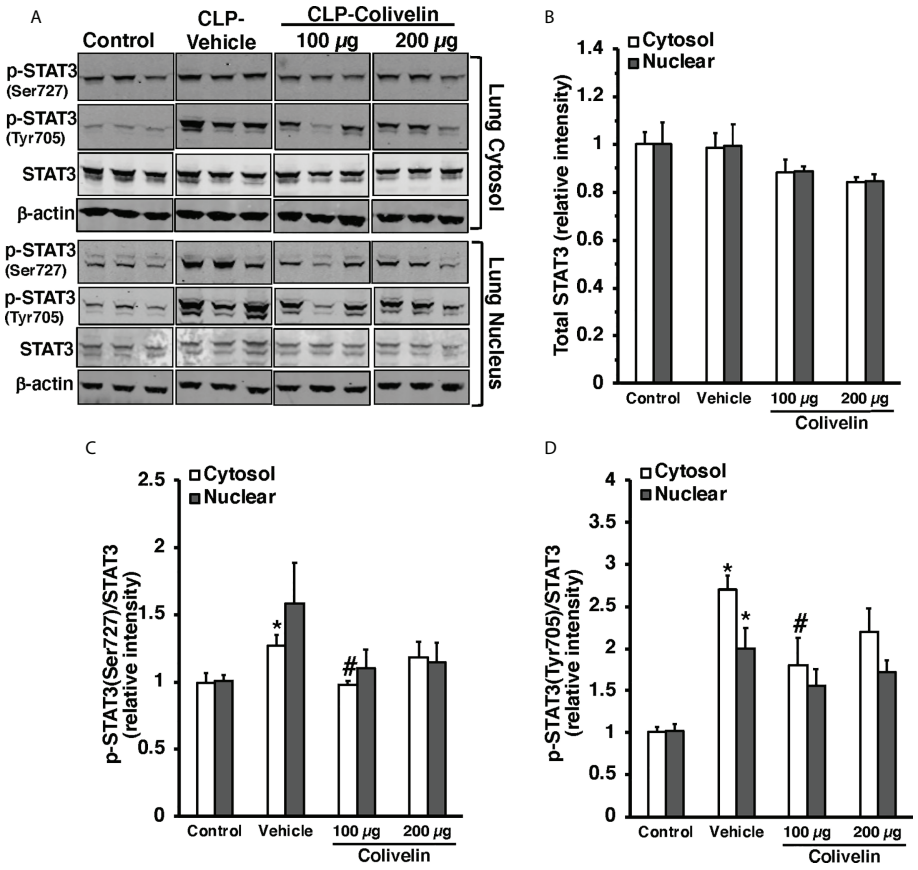

FIGURE 8
Representative Western blots of total STAT3, p-STAT3(Ser727) and p-STAT3(Tyr705) in lung cytosol and nuclear extracts; β-actin was used as loading control protein **(A)**. Image analyses of cytosol and nuclear of relative intensity of total STAT3 **(B)**, ratio of p-STAT3(Ser727)/STAT3 **(C)**, and ratio of p-STAT3(Tyr705)/STAT3 **(D)** as determined by densitometry. Vehicle (200 µl distilled water) or colivelin (100 µg/kg) was administered intraperitoneally at 1 h after CLP. Each data represents the mean ± SEM of 3-4 mice for group (n=3 control group, n=4 vehicle group, n=4 colivelin 100 µg group). *Represents $P < 0.05$ versus control mice; #represents $P < 0.05$ versus vehicle-treated mice.

our model, the early increase of syndecan-1 and adhesion molecules temporally correlated with neutrophil infiltration in lung, liver and kidney. In this regard, it is noteworthy that elevation of circulating syndecan-1 was associated with inflammatory biomarkers of neutrophil activation, including MPO, and was predictive of adverse clinical outcomes in patients with sepsis due to pneumonia (59).

To restore the endothelial permeability barrier and improve outcome in sepsis, we tested the efficacy of colivelin, a new generation humanin peptide derivative (25). Humanin is a polypeptide containing 24 amino acids, which is encoded encoded by short open reading frame in the mtDNA and acts as retrograde signaling molecule to regulate inflammation (14). Humanin was first identified in the cDNA associated with neuroprotective effects in Alzheimer's disease patients, and therefore recognized for its antiapoptotic properties (21). Previous *in vitro* studies have demonstrated that humanin has cytoprotective effects in human aortic endothelial cells against oxidative stress (16). A synthetic analogue with enhanced potency, humanin-G, has also been reported to inhibit cell death in high-glucose-induced apoptosis in human umbilical vein endothelial cells (17). Another potent humanin derivative is colivelin, a hybrid peptide named composed of activity-dependent neurotrophic factor and fused at the C-terminus to a fragment of humanin (25), which has been shown to provide beneficial effects in ischemia models *in vivo* (28). In our study, we demonstrated that *in vivo* treatment with colivelin reduced lung injury and reduced leukosequestration in lung, liver and kidney. These beneficial effects correlated with a significant reduction of circulating levels of syndecan-1, thus suggesting inhibition of glycocalyx shedding, when compared to vehicle treatment. To determine the beneficial effect of colivelin on

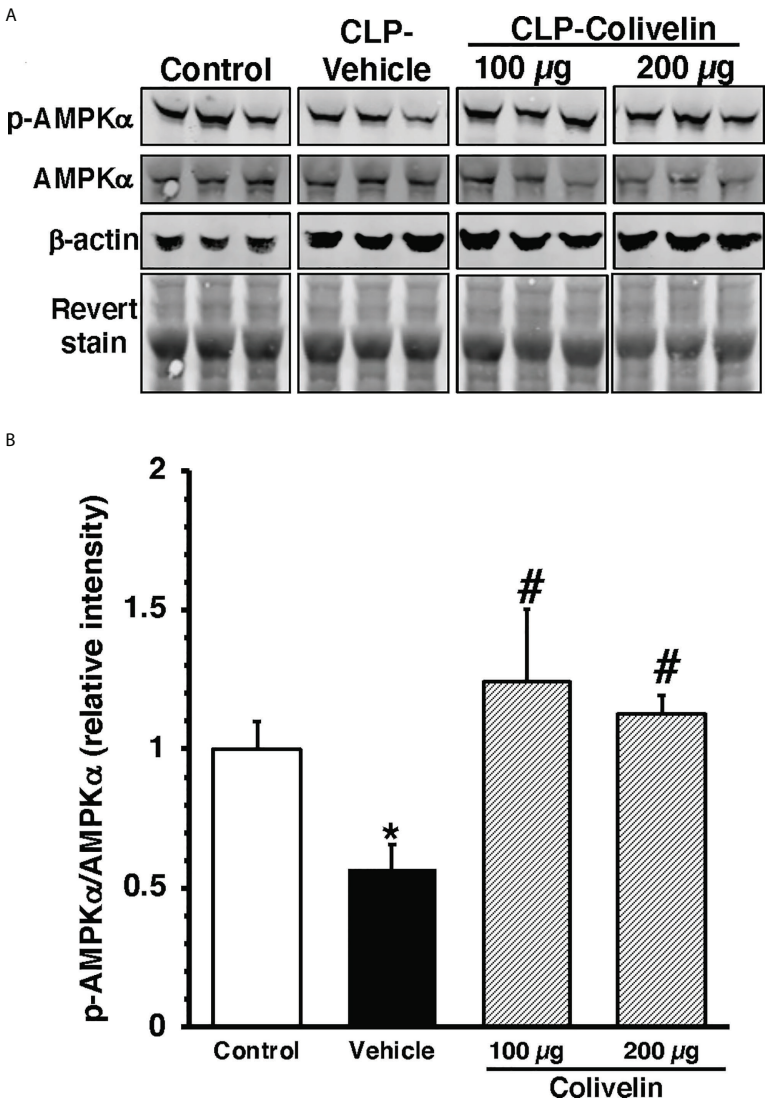

FIGURE 9
Representative Western blots of total AMPKα and pAMPKα in cytosol extracts of thoracic aorta; β-actin and Revert stain were used to verify loading of proteins **(A)**. Image analyses of ratio of relative intensity of p-AMPKα/AMPKα **(B)** as determined by densitometry. Vehicle (200 µl distilled water) or colivelin (100 µg/kg) was administered intraperitoneally at 1 h after CLP. Each data represents the mean ± SEM of 3-4 mice for group (n=3 control group, n=4 vehicle group, n=4 colivelin 100 µg group). *Represents $P < 0.05$ versus control mice; #represents $P < 0.05$ versus vehicle-treated mice.

glycocalyx and endothelium we comprehensively assessed the vascular damage of thoracic aortas by transmission electron microscopy and found that colivelin treatment was associated with amelioration of glycocalyx structure, as evidenced by the presence of thick and complex bundles when compared to the loose and thin structure in mice receiving vehicle. Although our analysis of the vascular wall was focused on glycocalyx structure, we also found that vascular damage in vehicle-treated mice was characterized by the presence of damaged mitochondria in both endothelial and smooth muscle cells. It must be considered that mitochondria in vascular smooth muscle and endothelial cells play a pivotal role in maintaining the structural integrity of the vascular wall, whereas their dysfunction leads to energy failure and contributes to inflammation *via* production of reactive oxygen species (12). In our study, colivelin treatment also ameliorated mitochondrial structure. Thus, taken together, our data demonstrated that the peptide affords multifactorial beneficial effects against oxidative and metabolic stress and against neutrophil adhesiveness and activation at the vascular level. Many preclinical and clinical studies have demonstrated an association between inflammatory cytokines and glycocalyx degradation biomarkers (35, 39, 60, 61). In our study colivelin

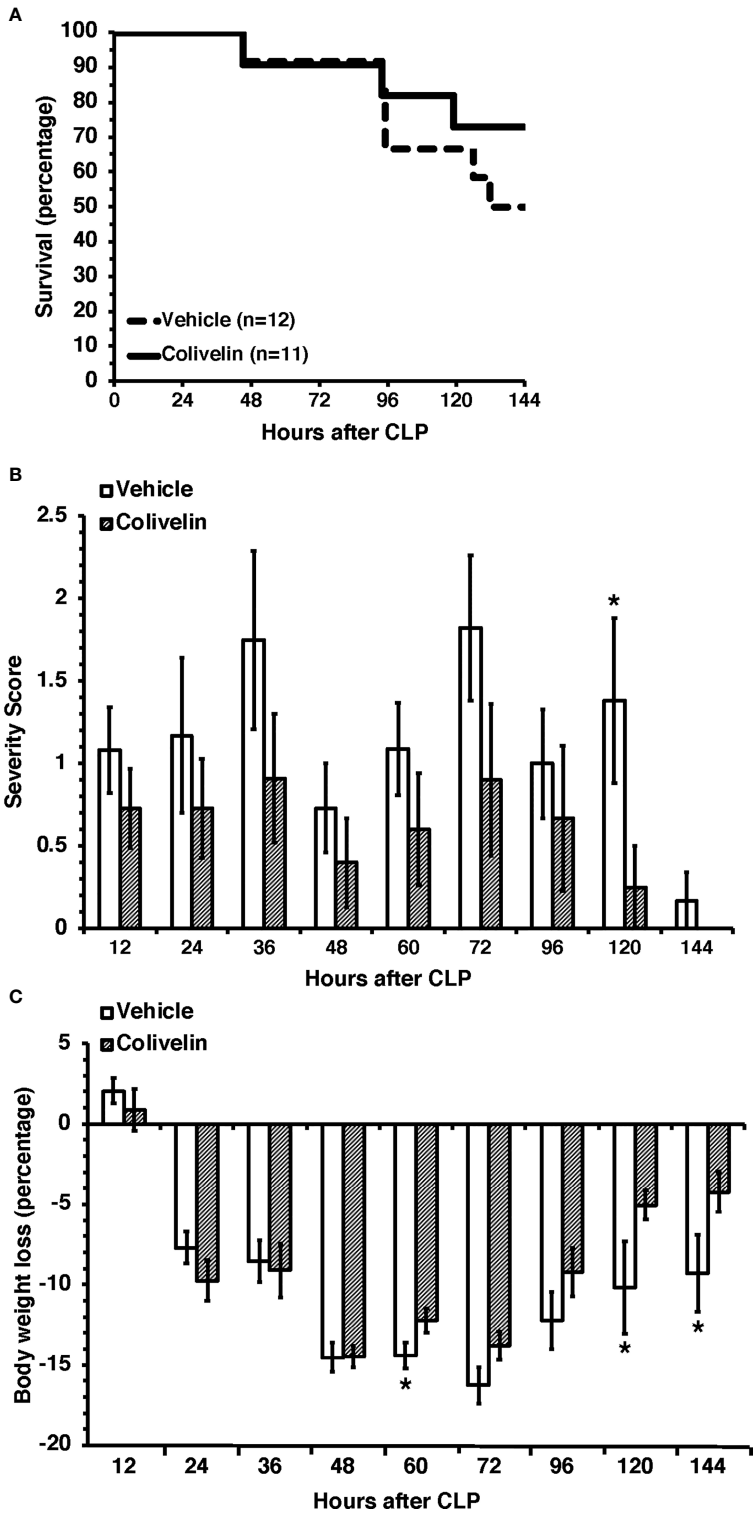

FIGURE 10
Survival rate **(A)**, severity score **(B)** and body weight loss **(C)** of mice at 7 days after cecal ligation and puncture (CLP). Mice were subjected to CLP and received colivelin (100 μg/kg subcutaneously) or vehicle at 1 h, 3 h and 24 h after CLP. All mice received fluid resuscitation (35 ml/kg normal saline with 5% dextrose subcutaneously) every 24 h up to 7 days and ceftriaxone (25 mg/kg) and metronidazole (12.5 mg/kg) intraperitoneally every 12 h up to 3 days after the CLP procedure. *Represents $P < 0.05$ versus colivelin-treated mice.

treatment significantly blunted the systemic elevation of TNFα, MIP-1α, KC and IL-10, suggesting that the peptide interferes with the vicious cycle between impaired endothelial glycocalyx and neutrophil activation.

One of the most notable observations in our study was that treatment with colivelin improved long-term wellbeing outcomes of mice subjected to sepsis. To mimic human sepsis management, mice were resuscitated with fluids and treated with antibiotics. We observed that mice treated with a combination of fluids, antibiotics and colivelin experienced less severe clinical signs of sepsis up to 7 days after CLP when compared with animals treated only with fluids and antibiotics, suggesting beneficial effects of colivelin on recovery. The group of mice that received the adjunct therapy of colivelin also exhibited a higher, but not significant, survival rate (72.6%) than the group that received only vehicle in combinations with fluids and antibiotics (50%). However, it must be noted that for ethical reasons mortality was not used as endpoint of our study and we did not use a large number of mice; furthermore, some mice were euthanized according to criteria that predicted moribundity, thus, most probably affecting statistical significance.

In evaluating the molecular mechanisms of colivelin, we investigated the contribution of both STAT-3 and AMPK since these signaling pathways have been reported to be activated by humanin and its derivatives. STAT3 is a crucial transcription factor, which plays a role in development, inflammation, immunity, metabolism and cancer (62). In addition to its established role as a nuclear transcription factor, a pool of STAT3 has been described in the mitochondria. STAT3 in the mitochondria requires Ser727 but not Tyr705 phosphorylation and functions as a positive regulator of mitochondrial electron transport chain for ATP production (63). *In vitro* studies have shown that treatment with humanin and its analogues may exert protective functions through STAT3 phosphorylation (20, 23, 64). In a murine model of ischemic stroke, the beneficial effects on neuronal death and axonal remodeling of colivelin have also been associated with activation of STAT3 signaling (28). Previous studies have reported that expression of pSTAT3(Tyr705) increases in the lung, liver, and kidney in murine models of sepsis (65–67). However, these studies have not examined the subcellular localization of the different phosphorylated forms of STAT3. In our study, we observed for the first time that in addition to the lung, pSTAT3(Tyr705) is also activated in the cytosol and nuclear compartments of the aorta at 6 h after CLP in vehicle-treated mice. Interestingly, we also found that distinct subcellular localization of the pSTAT3(Ser727), which increased in both aortas and lungs and was preferentially located in the cytosol. It is important to note that non-canonical STAT3 activation through Ser727 phosphorylation has been recently demonstrated to serve as a crucial signaling intermediary for TLR4-induced glycolysis, macrophage metabolic reprogramming and inflammation (68). An intriguing finding of our study was that colivelin treatment inhibited the activation of STAT3 in the aorta and lung and was associated with improvement of endothelial damage and pulmonary protection. These data are in discrepancy with previous *in vivo* and *in vitro* studies demonstrating that colivelin may act as a potent activator of STAT3 (25, 28). A potential reason for this discrepancy on STAT3 activation by colivelin may be due to the different disease models. Our study is the first to investigate the beneficial effects in an infection condition, while previous *in vivo* and *in vitro* studies have focused on conditions of neurodegeneration in Alzheimer's disease and ischemia and reperfusion injury models. On the contrary, our findings are consistent with previous studies demonstrating that inhibitors of STAT3, such as Stattic, ameliorate inflammatory responses in endotoxin-induced acute lung injury (69).

To further understand the molecular mechanisms of colivelin, we also investigated the contribution of AMPK signaling pathway. AMPK is a serine/threonine protein kinase, which is the crucial regulator of energy metabolism and mitochondrial quality control (70). In our study, we observed that the thoracic aorta of colivelin-treated mice had increased activation of AMPK. It must be noted that humanin and humanin analogues may exert beneficial effects in oxidative stress by activation of AMPK (71, 72). Furthermore, it has been proposed that AMPK activation exerts anti-inflammatory effects in endotoxic shock in mice by inhibiting STAT3 signaling (73). Thus, it is plausible that the molecular mechanisms of the protective effect of colivelin in sepsis may be related to increased AMPK, which in turn inhibits phosphorylation of STAT3. Our current findings also support our previous studies demonstrating that pharmacological activation of AMPK ameliorates organ injury in mice subjected to experimental sepsis (74, 75).

In our study, however, we did not investigate the direct mechanisms by which colivelin interferes with STAT3 or AMPK activation. Mitochondrial peptides have been described to interact with cell surface receptors, such as formylpeptide-like-1 receptor and insulin-like growth factor binding protein-3 (14). Specific *in vitro* studies in endothelial cells are, therefore, necessary to further establish the upstream molecular mechanisms of colivelin in preserving glycocalyx structure and function.

Limitations

As a limitation of our study, we did not include a colivelin-treated control group of healthy mice. Furthermore, we did not investigate potential sex-differences in colivelin beneficial effects as we used only male mice. However, at this preliminary stage of our investigation, the main goal of our study was to evaluate the effect of colivelin post-treatment in a disease state without the phenotypic variability of the estrous cycle. Previous studies have investigated the effect of colivelin on healthy animals/cells in the context of experimental model of neurodegenerative diseases. In

these studies, colivelin did not alter behavior parameters or cell viability (25). Further comprehensive studies and elucidations of hormonal influences are required to better understand the molecular mechanisms of this synthetic mitochondrial peptide.

Another limitation of our study is that we used two different routes of administration to explore the therapeutic efficacy of colivelin in short-term and long-term experiments. In the short-term studies, colivelin was injected intraperitoneally to allow for a rapid uptake and bioavailability of the peptide. However, for the wellness of the animals, we switched to subcutaneous injection for the long-term administration to avoid further stress in the peritoneum since the animals also required repetitive intraperitoneal injections of antibiotics. Thus, it can be speculated that differences in biodistribution might have resulted in less efficacy in long-term outcomes. However, it must be noted that the cytoprotective effects of colivelin or other humanin derivatives have been described through different routes of administration *in vivo* (76).

Conclusion

In conclusion, our data indicates that endothelial dysfunction and glycocalyx damage are early events of lung injury in a murine model of polymicrobial sepsis. Treatment with the novel synthetic mitochondrial peptide colivelin exerted pulmonary protective effects and improved long-term recovery *via* activation of AMPK and inhibition of STAT3 in thoracic aortas and lung. With the ability to rescue endothelium function and ameliorate glycocalyx structure, colivelin should be investigated as adjunct therapy for the treatment of sepsis.

Data availability statement

The raw data supporting the conclusions of this article will be made available by the authors, without undue reservation.

Ethics statement

This study was reviewed and approved by Institutional Animal Care and Use Committee of the Cincinnati Children's Hospital Medical Center.

Author contributions

BZ conceived and designed the projects. CU contributed to the design of the study. CU and VW performed the animal experiments. CU, VW, GP, CP, MO and PL performed the biochemical assays. CU, GP, and BZ performed the electron microscopy analysis. CU, GP, and BZ analyzed the data and prepared graphics. CU and BZ wrote the draft of the manuscript. All authors contributed to the article and approved the submitted version.

Funding

This work was supported by the National Institutes of Health grants R01 GM-067202 and GM-115973 to Basilia Zingarelli, and in part by grant P30 DK-078392 of the Digestive Research Core Center (Integrative Morphology Core). The content is solely the responsibility of the authors and does not necessarily represent the official views of the National Institutes of Health.

Conflict of interest

The authors declare that the research was conducted in the absence of any commercial or financial relationships that could be construed as a potential conflict of interest.

Publisher's note

All claims expressed in this article are solely those of the authors and do not necessarily represent those of their affiliated organizations, or those of the publisher, the editors and the reviewers. Any product that may be evaluated in this article, or claim that may be made by its manufacturer, is not guaranteed or endorsed by the publisher.

Supplementary material

The Supplementary Material for this article can be found online at: https://www.frontiersin.org/articles/10.3389/fimmu.2022.984298/full#supplementary-material

References

1. Singer M, Deutschman CS, Seymour CW, Shankar-Hari M, Annane D, Bauer M, et al. The third international consensus definitions for sepsis and septic shock (Sepsis-3). *JAMA* (2016) 315:801–10. doi: 10.1001/jama.2016.0287

2. Rudd KE, Johnson SC, Agesa KM, Shackelford KA, Tsoi D, Kievlan DR, et al. Global, regional, and national sepsis incidence and mortality, 1990-2017: analysis for the global burden of disease study. *Lancet* (2020) 395:200–11. doi: 10.1016/S0140-6736(19)32989-7

3. Ince C, Mayeux PR, Nguyen T, Gomez H, Kellum JA, Ospina-Tascón GA, et al. ADQI XIV workgroup. the endothelium in sepsis. *Shock* (2016) 45:259–70. doi: 10.1097/SHK.0000000000000473

4. Joffre J, Hellman J. Oxidative stress and endothelial dysfunction in sepsis and acute inflammation. *Antioxid Redox Signal* (2021) 35:1291–307. doi: 10.1089/ars.2021.0027

5. Chelazzi C, Villa G, Mancinelli P, De Gaudio AR, Adembri C. Glycocalyx and sepsis-induced alterations in vascular permeability. *Crit Care* (2015) 19:26. doi: 10.1186/s13054-015-0741-z

6. Curry FE, Adamson RH. Endothelial glycocalyx: permeability barrier and mechanosensor. *Ann BioMed Eng* (2012) 40:828–39. doi: 10.1007/s10439-011-0429-8

7. Lipowsky HH. The endothelial glycocalyx as a barrier to leukocyte adhesion and its mediation by extracellular proteases. *Ann BioMed Eng* (2012) 40:840–8. doi: 10.1007/s10439-011-0427-x

8. Mulivor AW, Lipowsky HH. Role of glycocalyx in leukocyte-endothelial cell adhesion. *Am J Physiol Heart Circ Physiol* (2002) 283:H1282–91. doi: 10.1152/ajpheart.00117.2002

9. Tarbell JM, Ebong EE. The endothelial glycocalyx: a mechano-sensor and -transducer. *Sci Signal* (2008) 1:pt8. doi: 10.1126/scisignal.140pt8

10. Becker BF, Jacob M, Leipert S, Salmon AH, Chappell D. Degradation of the endothelial glycocalyx in clinical settings: searching for the sheddases. *Br J Clin Pharmacol* (2015) 80:389–402. doi: 10.1111/bcp.12629

11. Iba T, Levy JH. Derangement of the endothelial glycocalyx in sepsis. *J Thromb Haemost* (2019) 17:283–94. doi: 10.1111/jth.14371

12. Kirkman DL, Robinson AT, Rossman MJ, Seals DR, Edwards DG. Mitochondrial contributions to vascular endothelial dysfunction, arterial stiffness, and cardiovascular diseases. *Am J Physiol Heart Circ Physiol* (2021) 320:H2080–100. doi: 10.1152/ajpheart.00917.2020

13. Lionaki E, Gkikas I, Tavernarakis N. Differential protein distribution between the nucleus and mitochondria: Implications in aging. *Front Genet* (2016) 7:162. doi: 10.3389/fgene.2016.00162

14. Lee C, Yen K, Cohen P. Humanin: a harbinger of mitochondrial derived peptides? trends endocrinol. *Metab* (2013) 24:222–8. doi: 10.1016/j.tem.2013.01.005

15. Lee C, Zeng J, Drew BG, Sallam T, Martin-Montalvo A, Wan J, et al. The mitochondrial-derived peptide MOTS-c promotes metabolic homeostasis and reduces obesity and insulin resistance. *Cell Metab* (2015) 21:443–54. doi: 10.1016/j.cmet.2015.02.009

16. Bachar AR, Scheffer L, Schroeder AS, Nakamura HK, Cobb LJ, Oh YK, et al. Humanin is expressed in human vascular walls and has a cytoprotective effect against oxidized LDL-induced oxidative stress. *Cardiovasc Res* (2010) 88:360–6. doi: 10.1093/cvr/cvq191

17. Shi D, Zhou X, Wang H. S14G-humanin (HNG) protects retinal endothelial cells from UV-b-induced NLRP3 inflammation activation through inhibiting egr-1. *Inflammation Res* (2021) 70:1141–50. doi: 10.1007/s00011-021-01489-4

18. Wang X, Wu Z, He Y, Zhang H, Tian L, Zheng C, et al. Humanin prevents high glucose-induced monocyte adhesion to endothelial cells by targeting KLF2. *Mol Immunol* (2018) 101:245–50. doi: 10.1016/j.molimm.2018.07.008

19. Xie Y, Liu ZH, Li XY, Zhou YD, Xu X, Hu LF, et al. Protection effect of [Gly14]-humanin from apoptosis induced by high glucose in human umbilical vein endothelial cells. *Diabetes Res Clin Pract* (2014) 106:560–6. doi: 10.1016/j.diabres.2014.09.020

20. Hoang PT, Park P, Cobb LJ, Paharkova-Vatchkova V, Hakimi M, Cohen P, et al. The neurosurvival factor humanin inhibits β-cell apoptosis *via* signal transducer and activator of transcription 3 activation and delays and ameliorates diabetes in non-obese diabetic mice. *Metabolism* (2010) 59:343–9. doi: 10.1016/j.metabol.2009.08.001

21. Hashimoto Y, Suzuki H, Aiso S, Niikura T, Nishimoto I, Matsuoka M. Involvement of tyrosine kinases and STAT3 in humanin-mediated neuroprotection. *Life Sci* (2005) 77:3092–104. doi: 10.1016/j.lfs.2005.03.031

22. Jia Y, Lue YH, Swerdloff R, Lee KW, Cobb LJ, Cohen P, et al. The cytoprotective peptide humanin is induced and neutralizes bax after pro-apoptotic stress in the rat testis. *Andrology* (2013) 1:651–9. doi: 10.1111/j.2047-2927.2013.00091.x

23. Ming W, Lu G, Xin S, Huanyu L, Yinghao J, Xiaoying L, et al. Mitochondria related peptide MOTS-c suppresses ovariectomy-induced bone loss *via* AMPK activation. *Biochem Biophys Res Commun* (2016) 476:412–9. doi: 10.1016/j.bbrc.2016.05.135

24. Qin Q, Jin J, He F, Zheng Y, Li T, Zhang Y, et al. Humanin promotes mitochondrial biogenesis in pancreatic MIN6 β-cells. *Biochem Biophys Res Commun* (2018) 497:292–7. doi: 10.1016/j.bbrc.2018.02.071

25. Chiba T, Yamada M, Hashimoto Y, Sato M, Sasabe J, Kita Y, et al. Development of a femtomolar-acting humanin derivative named colivelin by attaching activity-dependent neurotrophic factor to its n terminus: characterization of colivelin-mediated neuroprotection against alzheimer's disease-relevant insults *in vitro* and *in vivo*. *J Neurosci* (2005) 25:10252–61. doi: 10.1523/JNEUROSCI.3348-05.2005

26. Chiba T, Yamada M, Sasabe J, Terashita K, Aiso S, Matsuoka M, et al. Colivelin prolongs survival of an ALS model mouse. *Biochem Biophys Res Commun* (2006) 343:793–8. doi: 10.1016/j.bbrc.2006.02.184

27. Sari Y, Chiba T, Yamada M, Rebec GV, Aiso S. A novel peptide, colivelin, prevents alcohol-induced apoptosis in fetal brain of C57BL/6 mice: signaling pathway investigations. *Neuroscience* (2009) 164:1653–64. doi: 10.1016/j.neuroscience.2009.09.049

28. Zhao H, Feng Y, Wei C, Li Y, Ma H, Wang X, et al. Colivelin rescues ischemic neuron and axons involving JAK/STAT3 signaling pathway. *Neuroscience* (2019) 416:198–206. doi: 10.1016/j.neuroscience.2019.07.020

29. Flurkey K, Currer JM, Harrison DE. The mouse in aging research. In: JG Fox, editor. *The mouse in biomedical research, 2nd Edition*. Burlington, MA, USA: American College Laboratory Animal Medicine (Elsevier) (2007).

30. Hubbard WJ, Choudhry M, Schwacha MG, Kerby JD, Rue LW3rd, Bland KI, et al. Cecal ligation and puncture. *Shock* (2005) 24(Suppl 1):52–7. doi: 10.1097/01.shk.0000191414.94461.7e

31. Shrum B, Anantha RV, Xu SX, Donnelly M, Haeryfar SM, McCormick JK, et al. A robust scoring system to evaluate sepsis severity in an animal model. *BMC Res Notes* (2014) 7:233. doi: 10.1186/1756-0500-7-233

32. Zingarelli B, Coopersmith CM, Drechsler S, Efron P, Marshall JC, Moldawer L, et al. Part I: Minimum quality threshold in preclinical sepsis studies (MQTiPSS) for study design and humane modeling endpoints. *Shock* (2019) 51:10–22. doi: 10.1097/SHK.0000000000001243

33. Mullane KM, Kraemer R, Smith B. Myeloperoxidase activity as a quantitative assessment of neutrophil infiltration into ischemic myocardium. *J Pharmacol Methods* (1985) 14:157–67. doi: 10.1016/0160-5402(85)90029-4

34. Wolthuis EK, Vlaar AP, Choi G, Roelofs JJ, Juffermans NP, Schultz MJ. Mechanical ventilation using non-injurious ventilation settings causes lung injury in the absence of pre-existing lung injury in healthy mice. *Crit Care* (2009) 13:R1. doi: 10.1186/cc7688

35. Wiesinger A, Peters W, Chappell D, Kentrup D, Reuter S, Pavenstädt H, et al. Nanomechanics of the endothelial glycocalyx in experimental sepsis. *PloS One* (2013) 8:e80905. doi: 10.1371/journal.pone.0080905

36. Schneider CA, Rasband WS, Eliceiri KW. NIH Image to ImageJ: 25 years of image analysis. *Nat Methods* (2012) 9:671–5. doi: 10.1038/nmeth.2089

37. Steppan J, Hofer S, Funke B, Brenner T, Henrich M, Martin E, et al. Sepsis and major abdominal surgery lead to flaking of the endothelial glycocalix. *J Surg Res* (2011) 165:136–41. doi: 10.1016/j.jss.2009.04.034

38. Sallisalmi M, Tenhunen J, Yang R, Oksala N, Pettilä V. Vascular adhesion protein-1 and syndecan-1 in septic shock. *Acta Anaesthesiol Scand* (2012) 56:316–22. doi: 10.1111/j.1399-6576.2011.02578.x

39. Nelson A, Berkestedt I, Schmidtchen A, Ljunggren L, Bodelsson M. Increased levels of glycosaminoglycans during septic shock: relation to mortality and the antibacterial actions of plasma. *Shock* (2008) 30:623–7. doi: 10.1097/SHK.0b013e3181777da3

40. Burmeister DM, Heard TC, Chao T, Alcover K, Wagner A, Chung KK, et al. A prospective observational study comparing clinical sepsis criteria to protein biomarkers reveals a role for vascular dysfunction in burn sepsis. *Crit Care Explor* (2022) 4:e0610. doi: 10.1097/CCE.0000000000000610

41. Martin-Fernandez M, Vaquero-Roncero LM, Almansa R, Gómez-Sánchez E, Martín S, Tamayo E, et al. Endothelial dysfunction is an early indicator of sepsis and neutrophil degranulation of septic shock in surgical patients. *BJS Open* (2020) 4:524–34. doi: 10.1002/bjs5.50265

42. Giuliano JSJr, Lahni PM, Harmon K, Wong HR, Doughty LA, Carcillo JA, et al. Admission angiopoietin levels in children with septic shock. *Shock* (2007) 28:650–4.

43. Giuliano JSJr, Tran K, Li FY, Shabanova V, Tala JA, Bhandari V. The temporal kinetics of circulating angiopoietin levels in children with sepsis. *Pediatr Crit Care Med* (2014) 15:e1–8. doi: 10.1097/PCC.0b013e3182a553bb

44. Hahn WO, Mikacenic C, Price BL, Harju-Baker S, Katz R, Himmelfarb J, et al. Host derived biomarkers of inflammation, apoptosis, and endothelial activation are associated with clinical outcomes in patients with bacteremia and sepsis regardless of microbial etiology. *Virulence* (2016) 7:387–94. doi: 10.1080/21505594.2016.1144003

45. Agouridakis P, Kyriakou D, Alexandrakis MG, Prekates A, Perisinakis K, Karkavitsas N, et al. The predictive role of serum and bronchoalveolar lavage cytokines and adhesion molecules for acute respiratory distress syndrome development and outcome. *Respir Res* (2002) 3:25. doi: 10.1186/rr193

46. Flori HR, Ware LB, Glidden D, Matthay MA. Early elevation of plasma soluble intercellular adhesion molecule-1 in pediatric acute lung injury identifies patients at increased risk of death and prolonged mechanical ventilation. *Pediatr Crit Care Med* (2003) 4:315–21. doi: 10.1097/01.PCC.0000074583.27727.8E

47. -Calfee CS, Eisner MD, Parsons PE, Thompson BT, Conner ERJr, Matthay MA, et al. NHLBI acute respiratory distress syndrome clinical trials network. soluble intercellular adhesion molecule-1 and clinical outcomes in patients with acute lung injury. *Intensive Care Med* (2009) 35:248–57. doi: 10.1007/s00134-008-1235-0

48. Vassiliou AG, Mastora Z, Orfanos SE, Jahaj E, Maniatis NA, Koutsoukou A, et al. Elevated biomarkers of endothelial dysfunction/activation at ICU admission are associated with sepsis development. *Cytokine* (2014) 69:240–7. doi: 10.1016/j.cyto.2014.06.010

49. Wright JK, Hayford K, Tran V, Al Kibria GM, Baqui A, Manajjir A, et al. Biomarkers of endothelial dysfunction predict sepsis mortality in young infants: a matched case-control study. *BMC Pediatr* (2018) 18:118. doi: 10.1186/s12887-018-1087-x

50. Yu WK, McNeil JB, Wickersham NE, Shaver CM, Bastarache JA, Ware LB. Angiopoietin-2 outperforms other endothelial biomarkers associated with severe acute kidney injury in patients with severe sepsis and respiratory failure. *Crit Care* (2021) 25:48. doi: 10.1186/s13054-021-03474-z

51. Leite AR, Borges-Canha M, Cardoso R, Neves JS, Castro-Ferreira R, Leite-Moreira A. Novel biomarkers for evaluation of endothelial dysfunction. *Angiology* (2020) 71:397–410. doi: 10.1177/0003319720903586

52. Kapur NK, Heffernan KS, Yunis AA, Parpos P, Kiernan MS, Sahasrabudhe NA, et al. Usefulness of soluble endoglin as a noninvasive measure of left ventricular filling pressure in heart failure. *Am J Cardiol* (2010) 106:1770–6. doi: 10.1016/j.amjcard.2010.08.018

53. Yanavitski M, Givertz MM. Novel biomarkers in acute heart failure. *Curr Heart Fail Rep* (2011) 8:206–11. doi: 10.1007/s11897-011-0065-5

54. Walley KR, Francis GA, Opal SM, Stein EA, Russell JA, Boyd JH. The central role of proprotein convertase Subtilisin/Kexin type 9 in septic pathogen lipid transport and clearance. *Am J Respir Crit Care Med* (2015) 192:1275–86. doi: 10.1164/rccm.201505-0876CI

55. Ding Z, Liu S, Wang X, Deng X, Fan Y, Sun C, et al. Hemodynamic shear stress *via* ROS modulates PCSK9 expression in human vascular endothelial and smooth muscle cells and along the mouse aorta. *Antioxid Redox Signal* (2015) 22:760–71. doi: 10.1089/ars.2014.6054

56. Le Bras M, Roquilly A, Deckert V, Langhi C, Feuillet F, Sébille V, et al. Plasma PCSK9 is a late biomarker of severity in patients with severe trauma injury. *J Clin Endocrinol Metab* (2013) 98:E732–6. doi: 10.1210/jc.2012-4236

57. Vecchié A, Bonaventura A, Meessen J, Novelli D, Minetti S, Elia E, et al. ALBIOS biomarkers study investigators. PCSK9 is associated with mortality in patients with septic shock: data from the ALBIOS study. *J Intern Med* (2021) 289:179–92. doi: 10.1111/joim.1315

58. Dounousi E, Tellis C, Pavlakou P, Duni A, Liakopoulos V, Mark PB, et al. Association between PCSK9 levels and markers of inflammation, oxidative stress, and endothelial dysfunction in a population of nondialysis chronic kidney disease patients. *Oxid Med Cell Longev* (2021) 2021:6677012. doi: 10.1155/2021/6677012

59. Smart L, Bosio E, Macdonald SPJ, Dull R, Fatovich DM, Neil C, et al. Glycocalyx biomarker syndecan-1 is a stronger predictor of respiratory failure in patients with sepsis due to pneumonia, compared to endocan. *J Crit Care* (2018) 47:93–8. doi: 10.1016/j.jcrc.2018.06.015

60. Nieuwdorp M, Meuwese MC, Mooij HL, van Lieshout MH, Hayden A, Levi M, et al. Tumor necrosis factor-alpha inhibition protects against endotoxin-induced endothelial glycocalyx perturbation. *Atherosclerosis* (2009) 202:296–303. doi: 10.1016/j.atherosclerosis.2008.03.024

61. Nelson A, Berkestedt I, Bodelsson M. Circulating glycosaminoglycan species in septic shock. *Acta Anaesthesiol Scand* (2014) 58:36–43. doi: 10.1111/aas.12223

62. Yu H, Lee H, Herrmann A, Buettner R, Jove R. Revisiting STAT3 signalling in cancer: new and unexpected biological functions. *Nat Rev Cancer* (2014) 14:736–46. doi: 10.1038/nrc3818

63. Wegrzyn J, Potla R, Chwae YJ, Sepuri NB, Zhang Q, Koeck T, et al. Function of mitochondrial Stat3 in cellular respiration. *Science* (2009) 323(5915):793–7. doi: 10.1126/science.1164551

64. Kim SJ, Guerrero N, Wassef G, Xiao J, Mehta HH, Cohen P, et al. The mitochondrial-derived peptide humanin activates the ERK1/2, AKT, and STAT3 signaling pathways and has age-dependent signaling differences in the hippocampus. *Oncotarget* (2016) 7(30):46899–912. doi: 10.18632/oncotarget.10380

65. Xu S, Pan X, Mao L, Pan H, Xu W, Hu Y, et al. Phospho-Tyr705 of STAT3 is a therapeutic target for sepsis through regulating inflammation and coagulation. *Cell Commun Signal* (2020) 18:104. doi: 10.1186/s12964-020-00603-z

66. Williamson L, Ayalon I, Shen H, Kaplan J. Hepatic STAT3 inhibition amplifies the inflammatory response in obese mice during sepsis. *Am J Physiol Endocrinol Metab* (2019) 316(2):E286–92. doi: 10.1152/ajpendo.00341.2018

67. Imbaby S, Matsuda N, Tomita K, Hattori K, Palikhe S, Yokoo H, et al. Beneficial effect of STAT3 decoy oligodeoxynucleotide transfection on organ injury and mortality in mice with cecal ligation and puncture-induced sepsis. *Sci Rep* (2020) 10:15316. doi: 10.1038/s41598-020-72136-x

68. Balic JJ, Albargy H, Luu K, Kirby FJ, Jayasekara WSN, Mansell F, et al. STAT3 serine phosphorylation is required for TLR4 metabolic reprogramming and IL-1β expression. *Nat Commun* (2020) 11:3816. doi: 10.1038/s41467-020-17669-5

69. Zhao J, Yu H, Liu Y, Gibson SA, Yan Z, Xu X, et al. Protective effect of suppressing STAT3 activity in LPS-induced acute lung injury. *Am J Physiol Lung Cell Mol Physiol* (2016) 311:L868–80. doi: 10.1152/ajplung.00281.2016

70. Carling D, Viollet B. Beyond energy homeostasis: the expanding role of AMP-activated protein kinase in regulating metabolism. *Cell Metab* (2015) 21(6):799–804. doi: 10.1016/j.cmet.2015.05.005

71. Kwon C, Sun JL, Jeong JH, Jung TW. Humanin attenuates palmitate-induced hepatic lipid accumulation and insulin resistance *via* AMPK-mediated suppression of the mTOR pathway. *Biochem Biophys Res Commun* (2020) 526:539–45. doi: 10.1016/j.bbrc.2020.03.128

72. Muzumdar RH, Huffman DM, Calvert JW, Jha S, Weinberg Y, Cui L, et al. Acute humanin therapy attenuates myocardial ischemia and reperfusion injury in mice. *Arterioscler Thromb Vasc Biol* (2010) 30:1940–8. doi: 10.1161/ATVBAHA.110.205997

73. Gong H, Tai H, Huang N, Xiao P, Mo C, Wang X, et al. Nrf2-SHP cascade-mediated STAT3 inactivation contributes to AMPK-driven protection against endotoxic inflammation. *Front Immunol* (2020) 11:414. doi: 10.3389/fimmu.2020.00414

74. Inata Y, Kikuchi S, Samraj RS, Hake PW, O'Connor M, Ledford JR, et al. Autophagy and mitochondrial biogenesis impairment contributes to age-dependent liver injury in experimental sepsis: dysregulation of AMP-activated protein kinase pathway. *FASEB J* (2018) 32:728–41. doi: 10.1096/fj.201700576R74

75. Inata Y, Piraino G, Hake PW, O'Connor M, Lahni P, Wolfe V, et al. Age-dependent cardiac function during experimental sepsis: effect of pharmacological activation of AMP-activated protein kinase by AICAR. *Am J Physiol Heart Circ Physiol* (2018) 315:H826–37. doi: 10.1152/ajpheart.00052.2018

76. Evangelou A, Zikos C, Benaki D, Pelecanou M, Bouziotis P, Papadopoulos M, et al. *In vitro* binding and *in vivo* biodistribution studies of the neuroprotective peptide humanin using [^{125}I]humanin derivatives. *Peptides* (2009) 30:2409–17. doi: 10.1016/j.peptides.2009.07.028

frontiers | Frontiers in Immunology

TYPE Original Research
PUBLISHED 02 September 2022
DOI 10.3389/fimmu.2022.992614

Check for updates

OPEN ACCESS

EDITED BY
Laura Dugo,
Campus Bio-Medico University, Italy

REVIEWED BY
Rosanna Di Paola,
University of Messina, Italy
Valerio Chiurchiù,
National Research Council, CNR, Italy

*CORRESPONDENCE
Massimo Collino
massimo.collino@unito.it

†These authors have contributed equally to this work

SPECIALTY SECTION
This article was submitted to Inflammation, a section of the journal Frontiers in Immunology

RECEIVED 12 July 2022
ACCEPTED 08 August 2022
PUBLISHED 02 September 2022

CITATION
Alves GF, Stoppa I, Aimaretti E, Monge C, Mastrocola R, Porchietto E, Einaudi G, Collotta D, Bertocchi I, Boggio E, Gigliotti CL, Clemente N, Aragno M, Fernandes D, Cifani C, Thiemermann C, Dianzani C, Dianzani U and Collino M (2022) ICOS-Fc as innovative immunomodulatory approach to counteract inflammation and organ injury in sepsis.
Front. Immunol. 13:992614.
doi: 10.3389/fimmu.2022.992614

COPYRIGHT
© 2022 Alves, Stoppa, Aimaretti, Monge, Mastrocola, Porchietto, Einaudi, Collotta, Bertocchi, Boggio, Gigliotti, Clemente, Aragno, Fernandes, Cifani, Thiemermann, Dianzani, Dianzani and Collino. This is an open-access article distributed under the terms of the Creative Commons Attribution License (CC BY). The use, distribution or reproduction in other forums is permitted, provided the original author(s) and the copyright owner(s) are credited and that the original publication in this journal is cited, in accordance with accepted academic practice. No use, distribution or reproduction is permitted which does not comply with these terms.

ICOS-Fc as innovative immunomodulatory approach to counteract inflammation and organ injury in sepsis

Gustavo Ferreira Alves[1], Ian Stoppa[2], Eleonora Aimaretti[3], Chiara Monge[4], Raffaella Mastrocola[3], Elisa Porchietto[5], Giacomo Einaudi[5], Debora Collotta[1], Ilaria Bertocchi[1], Elena Boggio[2], Casimiro Luca Gigliotti[2], Nausicaa Clemente[2], Manuela Aragno[3], Daniel Fernandes[6], Carlo Cifani[5], Christoph Thiemermann[7], Chiara Dianzani[4], Umberto Dianzani[2†] and Massimo Collino[1*†]

[1]Department of Neurosciences (Rita Levi Montalcini), University of Turin, Turin, Italy, [2]Department of Health Sciences, Università del Piemonte Orientale, Novara, Italy, [3]Department of Clinical and Biological Sciences, University of Turin, Turin, Italy, [4]Department of Drug Science and Technology, University of Turin, Turin, Italy, [5]Pharmacology Unit, School of Pharmacy, University of Camerino, Camerino, Italy, [6]Department of Pharmacology, Federal University of Santa Catarina, Florianópolis, Brazil, [7]William Harvey Research Institute, Bart's and The London School of Medicine and Dentistry, Queen Mary University of London, London, United Kingdom

Inducible T cell co-stimulator (ICOS), an immune checkpoint protein expressed on activated T cells and its unique ligand, ICOSL, which is expressed on antigen-presenting cells and non-hematopoietic cells, have been extensively investigated in the immune response. Recent findings showed that a soluble recombinant form of ICOS (ICOS-Fc) can act as an innovative immunomodulatory drug as both antagonist of ICOS and agonist of ICOSL, modulating cytokine release and cell migration to inflamed tissues. Although the ICOS-ICOSL pathway has been poorly investigated in the septic context, a few studies have reported that septic patients have reduced ICOS expression in whole blood and increased serum levels of osteopontin (OPN), that is another ligand of ICOSL. Thus, we investigated the pathological role of the ICOS-ICOSL axis in the context of sepsis and the potential protective effects of its immunomodulation by administering ICOS-Fc in a murine model of sepsis. Polymicrobial sepsis was induced by cecal ligation and puncture (CLP) in five-month-old male wild-type (WT) C57BL/6, $ICOS^{-/-}$, $ICOSL^{-/-}$ and $OPN^{-/-}$ mice. One hour after the surgical procedure, either CLP or Sham (control) mice were randomly assigned to receive once ICOS-Fc, ^{F119S}ICOS-Fc, a mutated form uncapable to bind ICOSL, or vehicle intravenously. Organs and plasma were collected 24 h after surgery for analyses. When compared to Sham mice, WT mice that underwent CLP developed within 24 h a higher clinical severity score, a reduced body temperature, an increase in plasma cytokines (TNF-α, IL-1β, IL-6, IFN-γ and IL-10), liver injury (AST and ALT) and kidney (creatinine and urea) dysfunction. Administration of ICOS-Fc to WT CLP mice reduced all of these abnormalities caused by sepsis. Similar beneficial effects were not seen in CLP-mice

treated with ^{F119S}ICOS-Fc. Treatment of CLP-mice with ICOS-Fc also attenuated the sepsis-induced local activation of FAK, P38 MAPK and NLRP3 inflammasome. ICOS-Fc seemed to act at both sides of the ICOS-ICOSL interaction, as the protective effect was lost in septic knockout mice for the ICOS or ICOSL genes, whereas it was maintained in OPN knockout mice. Collectively, our data show the beneficial effects of pharmacological modulation of the ICOS-ICOSL pathway in counteracting the sepsis-induced inflammation and organ dysfunction.

KEYWORDS

sepsis, inflammation, ICOS (inducible co-stimulatory molecule), cecal ligation and puncture, osteopontin (OPN)

Introduction

Sepsis is a life-threatening medical emergency characterized by a complex interplay of pro- and anti-inflammatory host responses, resulting in multiple organ dysfunction that can ultimately lead to death (1). Currently, deaths from sepsis correspond to nearly 20% of all deaths worldwide, and there is still no specific treatment available (2). The inducible T cell co-stimulator (ICOS, also known as CD278) belongs to the CD28 family of co-stimulatory immunoreceptors. It is a type I transmembrane glycoprotein whose expression is rapidly upregulated upon T cells activation (3). ICOS binds to its unique ligand (ICOSL, also known as CD275 or B7h), a member of the B7 family highly expressed on antigen-presenting cells (APCs) and non-hematopoietic cells under inflammatory stimuli (4–5). Thus far, the role of ICOS-ICOSL interaction has been poorly investigated in sepsis, although recent findings report that ICOS expression is reduced in whole blood of septic patients (6), and that reduced ICOS levels are strongly associated with organ dysfunction (7). To date, it is very well documented that the ICOS-ICOSL axis may display bidirectional effects. On the one hand, ICOS triggering modulates cytokine production in activated T cells and contributes to T regulatory (Treg) cells differentiation and survival (8–9). Given the fact that both animals and septic patients have an increased percentage of circulating Treg cells (10–12), it is suggestive that ICOS triggering may play a role in the septic immunosuppressive status. On the other hand, ICOSL triggering by ICOS may exert anti-inflammatory effects *via* responses, such as modulating the maturation and migration of macrophage and dendritic cells and the endothelial cell adhesiveness (13).

Recently, another ligand for ICOSL has been identified, osteopontin (OPN), an inflammatory mediator that binds to ICOSL in an alternative binding domain to that used by ICOS. Intriguingly, ICOS and OPN exert different and often opposite effects upon ICOSL triggering since OPN stimulates, whereas ICOS inhibits, migration of several cell types and tumor angiogenesis (14–16). Conventionally, a soluble recombinant form of ICOS (ICOS-Fc) has been designed by fusing a cloned extracellular portion of human or mouse ICOS with an Fc IgG1 portion and this molecule has been shown to trigger ICOSL thus promoting down-stream responses (17).

In vitro, ICOS-Fc inhibits adhesiveness of endothelial cells toward polymorphonuclear cells and tumor cells and migration of endothelial cells and tumor cells (15). These ICOS-Fc effects can also be recorded in dendritic cells (DC), along with modulated cytokine release and antigen cross-presentation in class I major histocompatibility complex molecules (13), while in osteoclasts, ICOS-Fc inhibits differentiation and function (18). *In vivo*, ICOS-Fc inhibits tumor growth and metastasis, development of osteoporosis, liver damage induced by acute inflammation following treatment with CCl4, and it favors skin wound healing (18–21). Nevertheless, little is known about the molecular mechanism(s) involved in ICOSL-mediated inflammatory response. The p38 MAPK, a well-known mediator that drives inflammation through upregulation of several pro-inflammatory cytokines such as TNF-α and IL-6 (22), and the NOD-like receptor protein 3 (NLRP3) inflammasome, able to induce the release of IL-1β and IL-18 and promote cell death by pyroptosis (23), are two of the most well characterized signaling pathways involved in the activation of the cytokine storm that contributes to organ dysfunction during sepsis. Furthermore, their pharmacological or genetic inhibition has been shown to reduce sepsis-related mortality (22–24). Finally, a non-receptor protein kinase namely Focal adhesion kinase (FAK) has been recently reported to signal inflammation downstream of the Toll-like receptor 4 upon lipopolysaccharide (LPS) challenge in macrophages and lung tissues (25). Therefore, here we investigated, for the first time, the pathological role of ICOS-ICOSL axis in the context of sepsis, its impact on selective inflammatory pathways and the potential protective effects of its

immunomodulation by administering ICOS-Fc in an experimental model of sepsis.

Material and methods

Animals and ethical statement

Inbred wild-type (WT, C57BL/6) mice, ICOSL knockout mice (ICOSL$^{-/-}$, B6.129P2-*Icosl*^{tm1Mak}/J), ICOS knockout mice (ICOS$^{-/-}$, B6.129P2-*Icos*^{tm1Mak}/J) and OPN knockout mice (OPN$^{-/-}$, B6.129S6(Cg)-*Spp1*^{tm1Blh}/J) were purchased from Envigo laboratories, (IT) and The Jackson Laboratory (Bar Harbor, ME, USA). Mice were housed under standard laboratory conditions, such as room temperature (25 ± 2°C) and light-controlled with free access to water and rodent chow for four weeks prior starting the experimental procedures. All animal protocols reported in this study followed the ARRIVE guidelines (26) and the recommendations for preclinical studies of sepsis provided by the MQTiPSS (27) The procedures were approved by the University's Institutional Ethics Committee as well as the National Authorities (Protocol number: 855/2021).

Cecal ligation and puncture (CLP)-induced sepsis model

Polymicrobial sepsis was carried out by CLP surgery in male, five-month-old mice. Mice were initially placed in an anesthetisia chamber (3% isoflurane -IsoFlo, Abbott Laboratories – delivered in oxygen 0.4 L/min), then kept under anaesthesia throughout surgery with 2% isoflurane delivered in oxygen 0.4 L/min *via* a nosecone. The body temperature was maintained at 37 °C through a homoeothermic blanket and constantly monitored by a rectal thermometer. Briefly, a mid-line laparotomy (~1.0 cm) was performed in the abdomen, exposing the cecum. The cecum was then totally ligated just below the ileocecal valve and a G-21 needle was used to puncture the ligated cecum in a single through-and-through manner. A small amount (droplet, ~3mm) of fecal content was released from the cecum which was carefully relocated into the peritoneum. Sham mice underwent the same surgical procedure, but without CLP. All animals received Carprofen (5 mg/kg, s.c.) as an analgesic agent and resuscitation fluid (0.9% NaCl, 50 mL/kg, s.c.) at 37°C. Mice were constantly monitored post-surgical and then placed back into fresh clean cages.

At 24 h, body temperature and a clinical score to assess symptoms consistent with murine sepsis were recorded blindly. The following 6 criteria were used for the clinical score: lethargy, piloerection, tremors, periorbital exudates, respiratory distress and diarrhea. An observed clinical score >3 was considered as severe sepsis, while a score between 3 and 1 was considered as moderate sepsis (28).

Study design

Seventy-two mice were randomized into eight groups (9 mice per group): Sham + Vehicle, CLP + Vehicle, CLP + ICOS-Fc, CLP + ^{F119S}ICOS-Fc, CLP ICOSL$^{-/-}$ + Vehicle, CLP ICOS$^{-/-}$ + Vehicle, CLP ICOS$^{-/-}$ + ICOS-Fc and OPN$^{-/-}$ + Vehicle. Treatment was given once one hour after surgery, where mice received either ICOS-Fc (100 µg each), ^{F119S}ICOS-Fc (100 µg each) or Vehicle (PBS, pH 7.4, 100 µl each) by intravenous injection (Figure 1).

Blood collection and organ harvesting

Twenty-four h after surgery all mice were anesthetized with isoflurane (3%) delivered in oxygen (0.4 L/min) and euthanized by cardiac exsanguination. Whole blood was withdrawn from each mouse in vials (EDTA 17.1 µM/mL) and plasma content was obtained after centrifugation (13,000 *g*, 10 min at R.T.). Organ samples (liver and kidney) were harvested and placed in cryotubes which were snap frozen in liquid nitrogen for storage at freezer -80°C. The samples were then analyzed in a blinded fashion (Figure 1).

Biomarkers of organ injury and systemic inflammation

Plasma samples were used to measure systemic levels of aspartate aminotransferase (AST) (#7036) and alanine aminotransferase (ALT) (#7018) (as markers of hepatocellular injury), creatinine (#7075) and urea (#7144) (as markers of renal dysfunction) using colorimetric clinical assay kits (FAR Diagnostics, Verona, Italy) according to the manufacturer's instructions. Systemic cytokine levels were determined in plasma using the Luminex suspension bead-based multiplexed Bio-Plex Pro™ Mouse Cytokine Th17 Panel A 6-Plex (#M6000007NY) assay (Bio-Rad, Kabelsketal, Germany). The cytokines (IL-1β, IL-6, TNF-α, IFN-γ, IL-17 and IL-10) were measured following the manufacturer's instructions.

Myeloperoxidase (MPO) activity analysis

MPO activity analysis was carried out in liver and kidney samples as previously described (29). Tissue samples (~100 mg) were homogenized (1:5 w-v) in 20 mM PBS (pH 7.4) and then centrifuged at 4°C (13,000 g, 10 min). Pellets were resuspended in

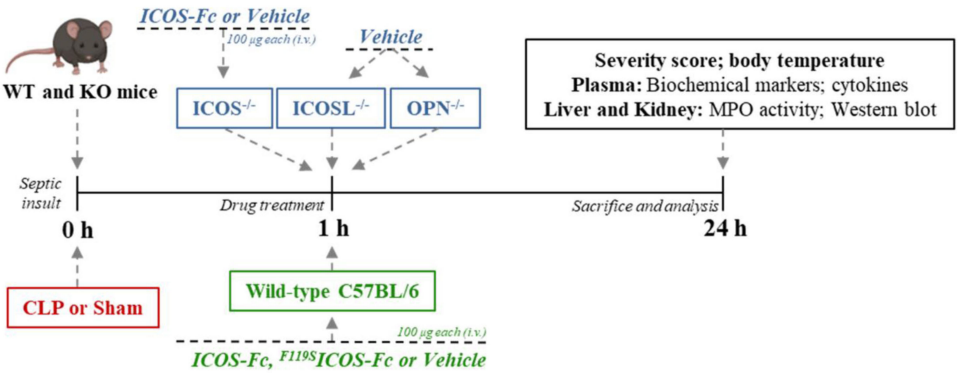

FIGURE 1
Timeline of the experimental design to investigate the role of ICOS-Fc in sepsis. Wild-type mice and/or ICOSL, ICOS and OPN knockout mice were randomly selected to undergo either Sham or CLP surgery. One hour later, mice received once either Vehicle (PBS, 100 µL), ICOS-Fc (100 µg) or ^{F119S}ICOS-Fc (100 µg) intravenously. At 24 h all parameters were analyzed.

500 µL of hexadecyltrimethylammonium bromide buffer (0.5% HTAB in 50 mM PBS, pH 6.0). A second centrifugation at 4°C (13,000 g, 10 min was performed and the supernatants (30 µL) were assessed for MPO activity by measuring spectrophotometrically (650 nm) the H_2O_2-dependent oxidation of 3,3′,5,5′-tetramethylbenzidine (TMB). Bicinchoninic acid (BCA) protein assay (Pierce Biotechnology Inc., Rockford, IL, USA) was used to quantify the protein content in the final supernatant. MPO activity was expressed as optical density (O.D.) at 650 nm per mg of protein.

Western blot analysis

Semi-quantitative immunoblot technique was carried out in hepatic and renal tissue samples as previously described (30). Total proteins were extracted from 50 mg of each tissue and the total content was quantified using BCA protein method following the manufacturer's instructions. Briefly, total proteins (50 µg/well) were separated by 8 and 10% sodium dodecyl sulphate-polyacrylamide gel electrophoresis (SDS-PAGE) and transferred to a polyvinylidene difluoride (PVDF) membrane, which was then blocked with 5% non-fat dry milk prepared in TBS-T buffer for 1 h at RT, followed by incubation with primary antibodies at the dilution 1:1000., rabbit anti-Thr^{180}/anti-Tyr^{182} p38 (Cell Signaling #9211); rabbit anti-total p38 (Cell Signaling #9212); mouse anti-NRLP3 (Adipogen- AG-20B-0014-C100); rabbit anti-Caspase-1 (Cell Signaling #24232); rabbit anti-Tyr^{397} FAK (Cell Signaling #3283); rabbit anti-total FAK (Cell Signaling #3285). The membranes were then incubated with a secondary antibody conjugated with horseradish peroxidase (HRP) at the dilution 1:10000 for 1 h at RT (anti-mouse or anti-rabbit, Cell Signaling #7076 and #7074, respectively). Afterwards, the membranes were stripped and incubated with rabbit anti-β-actin (Cell Signaling #4970). Immune complexes were visualized by chemiluminescence and the densitometric analysis was performed using Bio-Rad Image Lab Software 6.0.1. Results were normalized to sham bands.

Statistical analysis and data presentation

Sample size was determined on the basis of prior power calculations using G-Power 3.1^{TM} software (31). Data are expressed as dot plots (for each mouse) and as mean ± S.E.M of 9 mice per group. Shapiro-Wilk and Bartlett tests were used to verify data distribution and the homogeneity of variances, respectively. The statistical analysis was performed by one-way ANOVA, followed by Bonferroni's *post-hoc* test. Data not normally distributed, a non-parametric statistical analysis was applied through Kruskal-Wallis followed by Dunn's *post hoc*-test as indicated in the figure legends. Statistical significance was set at $P < 0.05$. Statistical analysis was performed using GraphPad Prism® software version 7.05 (San Diego, California, USA).

Materials

Unless otherwise stated, all reagents were purchased from the Sigma-Aldrich Company Ltd. (St. Louis, Missouri, USA).

Results

ICOS-Fc-mediated immunomodulation attenuates clinical status and organ injury/dysfunction triggered by sepsis

Sepsis was induced by CLP in WT mice treated with vehicle, ICOS-Fc or ^{F119S}ICOS-Fc (unable to bind ICOSL) and clinical scores and body temperature were recorded after 24 h. Moreover, sepsis was induced in mice deficient for ICOS, ICOSL, or OPN to assess the role the endogenous molecules of the ICOS/ICOSL/OPN system. Finally, a group of ICOS-deficient mice received ICOS-Fc treatment to evaluate the effect of the drug in the absence of the endogenous ICOS.

Results showed that, as expected, CLP-induced sepsis in WT mice led to a higher clinical severity score (Figure 2A) when compared to Sham WT mice, which was also associated with lower body temperature (Figure 2B). Intriguingly, treatment with ICOS-Fc improved both clinical score and hyphotermia in WT septic mice, whereas treatment with ^{F119S}ICOS-Fc had no effect (Figures 2A, B). Analysis of CLP knockout mice showed that ICOS$^{-/-}$ and ICOSL$^{-/-}$ mice showed similar clinical scores and decreased body temperatures as WT mice, whereas OPN$^{-/-}$ mice developed milder sepsis, with lower clinical scores and higher body temperature than WT mice. In ICOS$^{-/-}$ mice, treatment with ICOS-Fc induced similar positive effects as in WT mice (Figures 2A, B).

To investigate organ injury or dysfunction, plasma levels of ALT, AST, creatinine and urea were evaluated in these mice. Figure 3 shows that results mirrored those shown in Fig.2: CLP-induced sepsis caused striking increase of ALT, AST, creatinine and urea levels in WT type mice, and these levels were decreased by treatment with ICOS-Fc, but not ^{F119S}ICOS-Fc. Levels of these markers were increased also in CLP ICOS$^{-/-}$ and ICOSL$^{-/-}$ mice and urea levels were even higher in ICOS$^{-/-}$ than in WT mice. In CLP ICOS$^{-/-}$ mice, treatment with ICOS-Fc significantly decreased all these markers. In CLP OPN$^{-/-}$ mice, levels of these markers were significantly lower than in CLP WT mice.

ICOS-Fc administration modulates experimental sepsis-induced cytokine storm

The 6 cytokines were measured systemically in plasma samples by using a multiplex array. Figure 4 shows that, in WT mice, CLP-induced sepsis led to a cytokine storm with significant increase of levels of IL-1β, IL-6, IL-10, TNF-α, IFN-γ and a slight not significant increase of IL-17 compared to Sham mice. Administration of ICOS-Fc to WT CLP mice induced a significant decrease of IL-1β and TNF-α, whereas ^{F119S}ICOS-Fc had no effect. Levels of IL-1β, IL-6, IL-10, TNF-α, and IFN-γ were also increased in CLP ICOS$^{-/-}$ and ICOSL$^{-/-}$ mice at levels similar to those observed in CLP WT mice. Moreover, CLP ICOSL$^{-/-}$ mice showed higher levels of IL-17 than Sham mice, and CLP ICOS$^{-/-}$ mice displayed higher levels of TNF-α and, especially, IL-10 than CLP WT mice. The CLP ICOS$^{-/-}$ mice treated with ICOS-Fc significantly decreased levels of IL-1β, IL-6 and IL-10 compared to the untreated counterparts. In CLP OPN$^{-/-}$ mice, the increase of these cytokines was in general

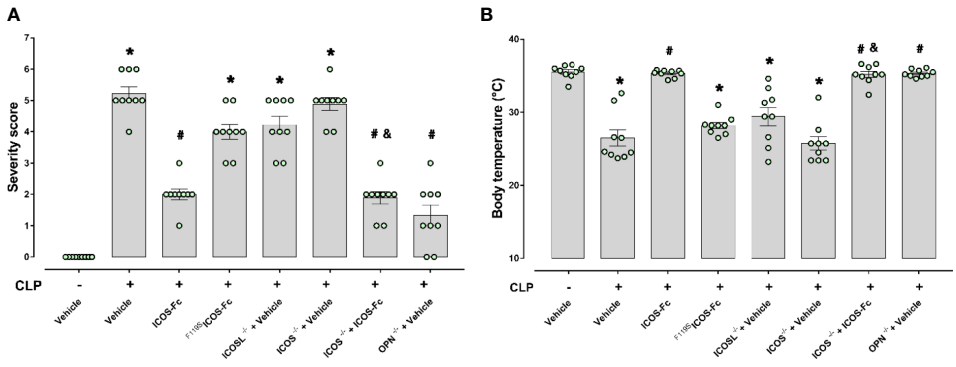

FIGURE 2
Role of the ICOS-ICOSL axis in the clinical status of experimental sepsis. Wild-type mice and/or ICOSL, ICOS and OPN knockout mice were randomly selected to undergo either Sham or CLP surgery. One hour later, mice received once either Vehicle (PBS, 100 µL), ICOS-Fc (100 µg) or ^{F119S}ICOS-Fc (100 µg) intravenously. At 24 h, severity score **(A)** and body temperature **(B)** were recorded. Data are expressed as dot plots (for each animal) and as mean ± S.E.M of 9 mice per group. Severity score was analyzed by a non-parametric test (Kruskal-Wallis) followed by Dunn's *post hoc*-test, whereas a parametric test (one-way ANOVA) followed by Bonferroni's *post hoc*-test was used for body temperature. *p<0.05 *vs* Sham + Vehicle; $^{\#}$p<0.05 *vs* CLP + Vehicle; $^{\&}$p<0.05 *vs* ICOS$^{-/-}$ + Vehicle.

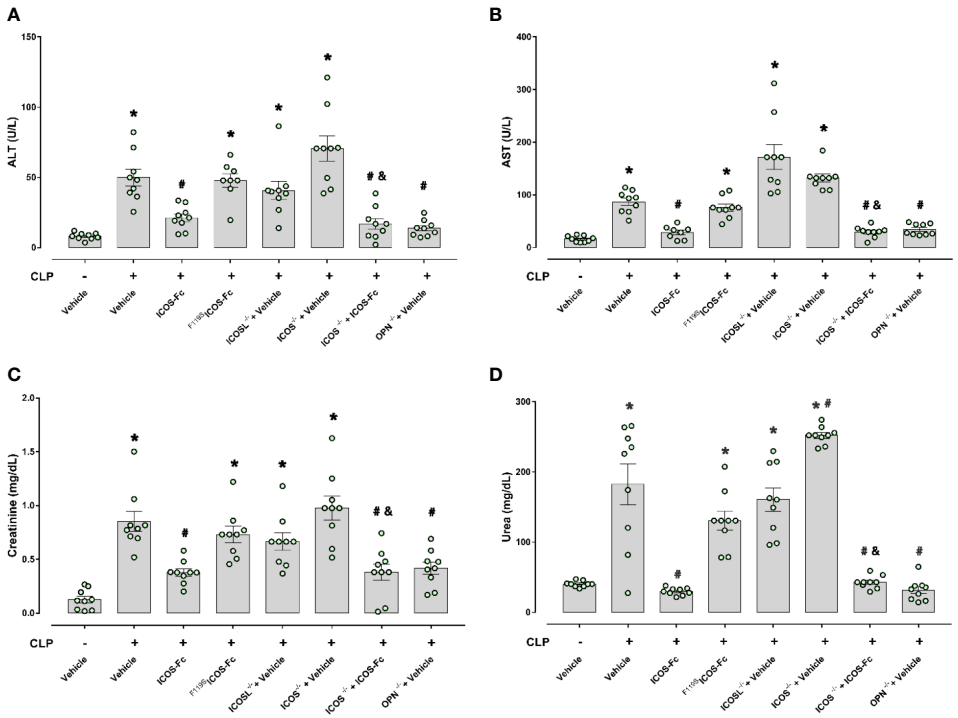

FIGURE 3
Effect of ICOS-ICOSL axis immunomodulation on sepsis-induced organ damage biomarkers. Wild-type mice and/or ICOSL, ICOS and OPN knockout mice were randomly selected to undergo either Sham or CLP surgery. One hour later, mice received once either Vehicle (PBS, 100 µL), ICOS-Fc (100 µg) or ^{F119S}ICOS-Fc (100 µg) intravenously. At 24 h, blood samples were withdrawn from each mouse and plasma levels of alanine transaminase (ALT) **(A)**, aspartate transaminase (AST) **(B)**, creatinine **(C)** and urea **(D)** were determined. Data are expressed as dot plots (for each animal) and as mean ± S.E.M of 9 mice per group. Statistical analysis was performed by one-way ANOVA followed by Bonferroni's *post hoc* test. *p<0.05 *vs* Sham + Vehicle; $^{\#}$p<0.05 *vs* CLP + Vehicle; $^{\&}$p<0.05 *vs* ICOS$^{-/-}$ + Vehicle.

moderate, with levels of IL-6, IL-10, TNF-α and IFN-γ higher than in Sham mice, and levels of IL-1β and IL-6 lower than in CLP WT mice.

ICOS-Fc treatment reduces sepsis-induced increase in MPO activity in the kidney

MPO activity was assessed in the liver and kidney, as an indirect biomarker of leukocyte tissue infiltration (Figure 5). When compared to Sham mice, CLP WT mice had increased MPO activity in both liver and kidney samples, and MPO activity was significanly decreased by ICOS-Fc (but not ^{F119S}ICOS-Fc treatment) in the kidney, but not in the liver. In the liver, MPO activity was similarly increased also in CLP ICOS$^{-/-}$, ICOSL$^{-/-}$, and OPN$^{-/-}$ mice, and it was not modified by ICOS-Fc treatment in CLP ICOS$^{-/-}$ mice. In the kidney, MPO activity was increased in CLP ICOS$^{-/-}$ and ICOSL$^{-/-}$ mice, and treatment with ICOS-Fc decreased MPO activity in CLP ICOS$^{-/-}$ mice. By contrast, CLP OPN$^{-/-}$ mice showed lower MPO levels in the kidney than CLP WT mice.

ICOS-Fc treatment reduces local FAK/p38 signalling and NLRP3 inflammasome activation in septic mice

In order to better elucidate the molecular mechanism underlying the beneficial effects evoked by ICOS-Fc administration, we focused on WT mice investigating the changes in some signaling cascades, previously documented to be affected by the ICOS-ICOSL axis and, at the same time, known to exert key role in sepsis pathogenesis. Western blot analysis showed that CLP mice showed significant increase of the phosphorylation of FAK at Tyr^{397} and p38 MAPK at Thr^{180}/Tyr^{182} in both hepatic (Figures 6A, C) and renal (Figures 6B, D) tissues, when compared to Sham mice. Interestingly, mice treatment with ICOS-Fc significantly attenuated the degree of phosphorylation of FAK/p38 axis in both tissues, thus suggesting reduced activation of these signaling pathways (Figures 6A–D).

We then assessed the activation of the inflammasome, by evaluating the expression of NLRP3 and cleaved caspase-1 in both liver and kidney samples (Figures 6E–H). Results showed that, in both tissues, CLP-induced sepsis significantly increased both

10.3389/fimmu.2022.992614

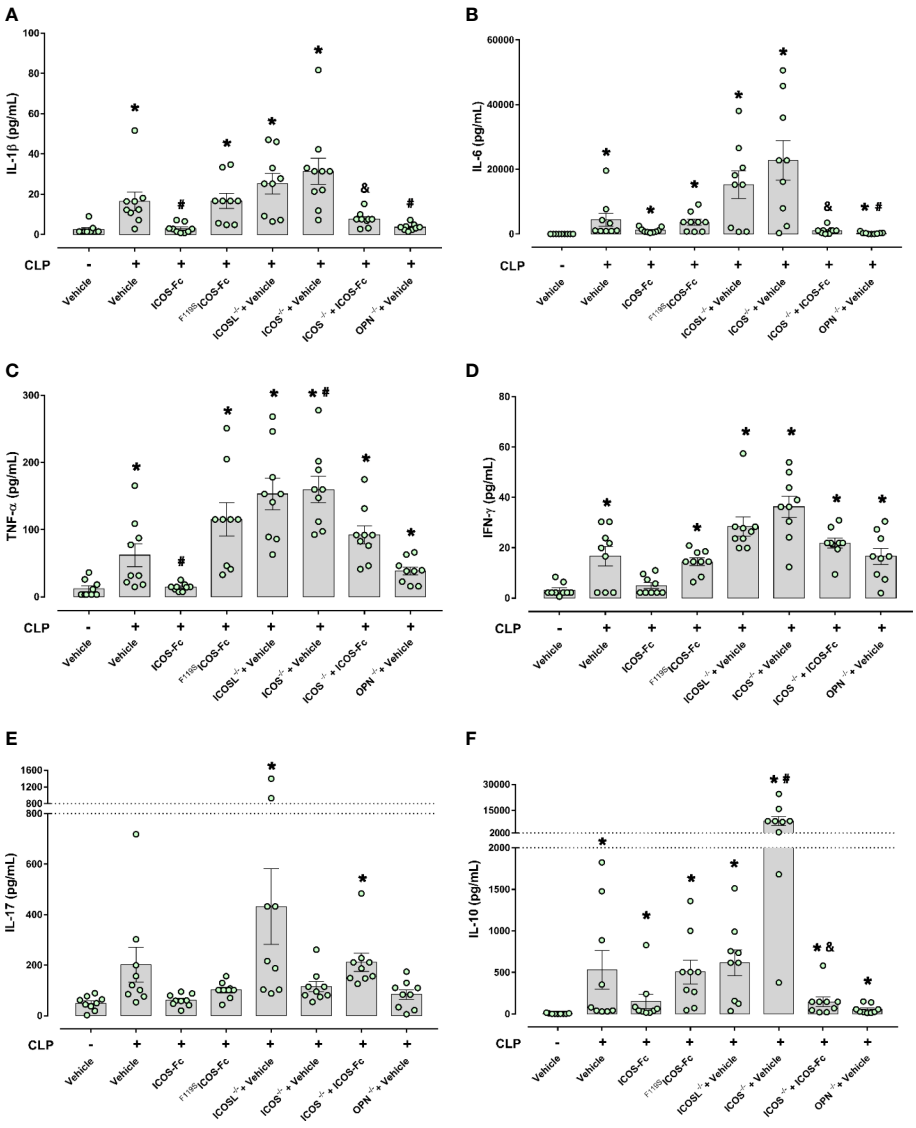

FIGURE 4
Effect of ICOS-ICOSL axis immunomodulation on systemic cytokines during experimental sepsis. Wild-type mice and/or ICOSL, ICOS and OPN knockout mice were randomly selected to undergo either Sham or CLP surgery. One hour later, mice received once either Vehicle (PBS, 100 µL), ICOS-Fc (100 µg) or ^{F119S}ICOS-Fc (100 µg) intravenously. At 24 h, blood samples were withdrawn from each mouse and plasma levels of IL-1β **(A)**, IL-6 **(B)**, TNF-α **(C)**, IFN-γ **(D)**, IL-17 **(E)** and IL-10 **(F)** were determined. Data are expressed as dot plots (for each animal) and as mean ± S.E.M of 9 mice per group. Statistical analysis was performed by one-way ANOVA followed by Bonferroni's *post hoc* test. *p<0.05 *vs* Sham + Vehicle; $^{\#}$p<0.05 *vs* CLP + Vehicle; $^{\&}$p<0.05 *vs* ICOS$^{-/-}$ + Vehicle.

molecules, and the increase was inhibited by mice treatment with ICOS-Fc (Figures 6E–H).

Discussion

Currently, most research on sepsis is focused on blocking the initial hyperinflammation, which in turn has resulted in promising outcomes. However, recent reports showed that both pro- and anti-inflammatory responses occur immediately and simultaneously after the onset of sepsis and most patients who survive this initial hyperinflammatory phase develop an immunosuppressive phase that can progress to late deaths (1, 32 and 33). Among the main causes of death in this immunosuppressive phase, the failure to control a primary infection and/or secondary hospital-acquired infections stands out (34). In the present study we report for the first time

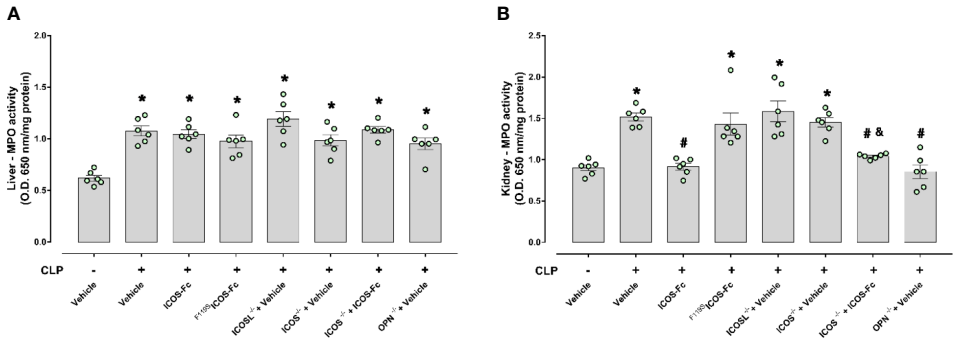

FIGURE 5
Effect of ICOS-ICOSL axis immunomodulation on sepsis-induced neutrophil (MPO activity) infiltration. Wild-type mice and/or ICOSL, ICOS and OPN knockout mice were randomly selected to undergo either Sham or CLP surgery. One hour later, mice received once either Vehicle (PBS, 100 µL), ICOS-Fc (100 µg) or ^{F119S}ICOS-Fc (100 µg) intravenously. At 24 h, liver and kidney samples were harvested. Through an *in vitro* assay, myeloperoxidase (MPO) activity was measured in liver **(A)** and kidney **(B)**. Data are expressed as dot plots (for each animal) and as mean ± S.E.M of 6 mice per group. Statistical analysis was performed by one-way ANOVA followed by Bonferroni's *post hoc* test. *p<0.05 *vs* Sham + Vehicle; $^{\#}$p<0.05 *vs* CLP + Vehicle; $^{\&}$p<0.05 *vs* ICOS$^{-/-}$ + Vehicle.

that ICOS-ICOSL axis may play a role in regulation of uncontrolled inflammation and organ injury induced by sepsis and that treatment of septic mice with ICOS-Fc may represent a novel immunomodulatory pharmacological approach that can simultaneously counteract both sepsis-induced hyperinflammation and immunosuppression.

These findings were obtained by evoking polymicrobial sepsis in either WT mice and knockout mice for ICOS, ICOSL and OPN genes. As expected, severe sepsis (score ≥3) was observed in vehicle-treated septic mice, suggesting potential late deaths, since the clinical scoring system is used as a surrogate marker of mortality. This detrimental effect was also associated with low body temperature (~27°C), as similarly, hypothermia is another surrogate marker of mortality, as a 5°C decrease over time or <30°C has also been shown to predict death in CLP-induced septic mice (35). Moreover, septic mice showed liver and kidney damage, displayed by increase of plasma AST/ALT and creatinine/urea levels, respectively, which is in line with the notion that sepsis can cause multiple organ failure including hepatocellular injury and renal dysfunction.

Intriguingly, treatment with ICOS-Fc substantially ameliorated the clinical picture by significantly decreasing all these parameters of sepsis. The effect was specific since no protection was detected following administration of ^{F119S}ICOS-Fc (a mutated form of ICOS-Fc carrying a phenylalanine-to-serine substitution at position 119).

Theoretically, the protective activity of ICOS-Fc might be ascribed to a twofold mechanism, i.e. on the one hand to the inhibition of the endogenous ICOS activity and, on the other hand, to triggering of the endogenous ICOSL. However, the effectiveness of ICOS-Fc not only in WT mice but also in ICOS$^{-/-}$ mice, lacking the endogenous ICOS, strongly suggest that the main protective effect on sepsis is due to triggering of ICOSL, which is in line with previous works showing that ICOSL triggering by ICOS-Fc elicits several anti-inflammatory activities both *in vitro* and *in vivo* (13, 15, 16, 19).

These results are in keeping also with recent findings showing that ICOS-Fc protects against liver damage through a shift of pro-inflammatory monocyte-derived macrophages to an anti-inflammatory phenotype (20). In parallel, the direct renoprotective effect triggered by ICOS-Fc treatment is supported by a recent study showing a key role of ICOSL in preventing early kidney disease, possibly through a selective binding to podocyte αvβ3 integrin, in which ICOSL serves as an αvβ3-selective antagonist that maintains adequate glomerular filtration (36).

The use of knockout mice highlighted that, in sepsis, a key role may be played by OPN as all the above septic parameters were significantly decreased in OPN$^{-/-}$ mice, so that OPN deficiency mirrored the effect of ICOS-Fc in WT mice. This finding is in line with data showing that, in humans, OPN levels are increased in sepsis (37) and OPN might be involved in the sepsis pathogenesis, possibly by supporting IL-6 secretion (38). Moreover, several reports showed that ICOS-Fc inhibits several proinflammatory activities of OPN *in vitro* and *in vivo* (16, 37, 39 and 40). Our findings are in keeping also with recent data showing that macrophage-derived OPN promotes glomerular injury in an experimental model of inflammatory and progressive kidney disease (41). OPN is an heavily phosphorylated extracellular protein, expressed and secreted by several cell types, including macrophages,

10.3389/fimmu.2022.992614

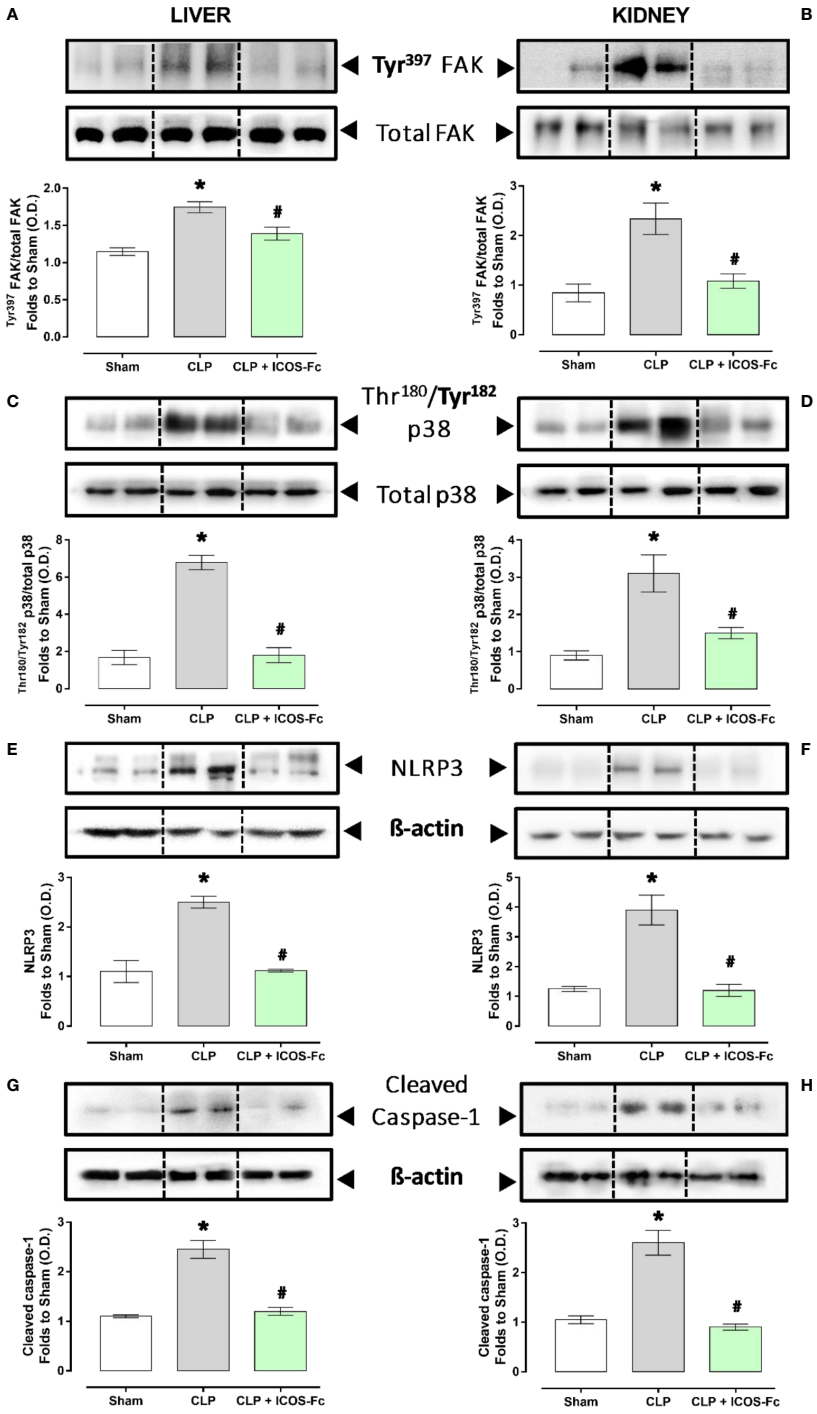

FIGURE 6
Effect of ICOS-ICOSL axis immunomodulation on tissue inflammatory pathways during experimental sepsis. Wild-type mice and/or ICOSL, ICOS and OPN knockout mice were randomly selected to undergo either Sham or CLP surgery. One hour later, mice received once either Vehicle (PBS, 100 µL), ICOS-Fc (100 µg) or ^{F119S}ICOS-Fc (100 µg) intravenously. At 24 h, liver and kidney samples were harvested, and total proteins were extracted from them. Western blotting analysis for phosphorylation of Tyr^{397} on FAK in the liver **(A)** and kidney **(B)** were normalized to total FAK; Phosphorylation of Thr^{180}/Tyr^{182} on p38 in the liver **(C)** and kidney **(D)** were normalized to total p38; NLRP3 expression in the liver **(E)** and kidney **(F)** were corrected against β-actin and normalized using the Sham related bands; Cleaved caspase-1 expression in the liver **(G)** and kidney **(H)** were corrected against β-actin and normalized using the Sham related bands. Densitometric analysis of the bands are expressed as relative optical density (O.D.). Data are expressed as dot plots (for each animal) and as mean ± S.E.M of 4-5 mice per group. Statistical analysis was performed by one-way ANOVA followed by Bonferroni's *post hoc* test. *p<0.05 *vs* Sham + Vehicle; $^{\#}$p<0.05 *vs* CLP + Vehicle.

endothelial cells, dendritic cells and T-cells. It can act as a cytokine mediating several biological functions, including cell migration, adhesion, activation of inflammatory cells, and modulation of T cell activation supporting differentiation of proinflammatory type 1 (Th1) and type 17 (Th17) Th cells (42).

Analysis of plasmatic cytokines showed that, in all mouse strains, sepsis was accompanied by increase of IL-1β, IL-6, IL-10, TNF-α and IFN-γ. Moreover, increase of TNF-α and, especially, IL-10 was particularly striking in $ICOS^{-/-}$ mice, which may point out that ICOS deficiency causes a dysregulation of activation of M1 and M2 macrophages. However, treatment with ICOS-Fc significantly decreased IL-1β and TNF-α in WT mice and IL-1β, IL-6 and IL-10 in $ICOS^{-/-}$ mice indicating that ICOS-Fc substantially downmodulates the cytokine storm in sepsis. In $OPN^{-/-}$ mice, increase of these cytokines was in general moderate, with a significant decrease of IL-1β and IL-6, in line with the mild sepsis developed by these mice.

Among the main inflammatory pathways activated during sepsis, we report a local (liver and kidney) overactivation of the FAK and p38 MAPK pathways in CLP mice. Previously, we have shown that the FAK pathway mediates inflammation through p38 MAPK and that this inflammatory axis plays a role in exacerbating inflammation (28). Activation of this axis promotes increased expression/secretion of pro-inflammatory cytokines such as TNF-α, IL-6, IL-1β and IL-17, which in turn contribute to the cytokine storm and multiple organ failure (MOF) associated with sepsis (43). Intriguingly, treatment of septic mice with ICOS-Fc significantly attenuated FAK and p38 MAPK phosphorylation, thus reducing their activation during septic insult, with a following impact on the development of the above-mentioned cytokine storm. These findings are in accordance with previous studies focused on tumor cell migration, whose treatment with ICOS-Fc reduces FAK and p38 MAPK activation both *in vitro* and *in vivo* (15, 19). As we and other have recently shown, FAK activation may also affect the overexpression and activation of another peculiar inflammatory pathway, NLRP3 inflammasome complex (28, 44). Thus, we wondered here whether ICOS-Fc could also infer with this cross-talk mechanism linking FAK to NLRP3 activation within the septic context. We report here that experimental sepsis led to an overactivation of the NLRP3 complex and consequent activation of its downstream mediator caspase-1, which were significantly reduced by treatment with ICOS-Fc, thus leading to reduced systemic release of IL-1β. In addition to the impact on the aforementioned inflammatory pathways, ICOS-Fc administration seems to directly affect leukocyte migration in CLP mice, as documented by the changes in MPO activity, a well-known biomarker of neutrophil infiltration, in both liver and kidney homogenates (45). Specifically, we documented that the sepsis-induced increase in MPO activity in renal tissues, was significantly counteracted by ICOS-Fc treatment. This effect, on the other hand, was absent when CLP mice were treated with ^{F119S}ICOS-Fc. Intriguingly, increased MPO activity was recorded in liver homogenates from septic mice, regardless of drug treatment or genetic intervention, when compared to Sham mice. Despite ICOS-Fc has been shown to reduce the migration of polymorphonuclear cells into inflamed tissues (15), these discrepant events observed in liver and kidney tissue may be the result of different levels of ICOSL expression. This finding corroborates a previous study reporting that hepatocytes did not express ICOSL, when compare to other organs, such as the kidney (46). Thus, suggesting that the hepatic protection induced by ICOS-Fc in septic mice is mainly due to a local and systemic resolution of inflammation rather than a reduction in leukocyte infiltration. A schematic representation summarizing the role of ICOS-ICOSL axis in the pathogenesis of sepsis and the protective effects of ICOS-Fc following sepsis-induced multiple organ failure is shown in Figure 7.

Despite the originality of our findings, we are aware of several limitations of our study, including the lack of extension of these findings to other important functional organs related to MOF during sepsis, such as the lungs and the cardiac tissue, along with the lack of analysis suggestive of the direct effect of ICOS-Fc treatment in preventing immunosuppression. Albeit the *in vivo* protocol described here is in accordance with the main recommendations provided by MQTiPSS consensus guidelines (27), we are not authorized to perform a survival study to assess the long-term effect of ICOS-Fc due to ethical reasons. Thus, further studies are needed to extend the clinical relevance of our findings as well as to gain a better insight into the safety profile of the proposed drug treatment.

Conclusions

In conclusion, we demonstrate here, for the first time, that the ICOS-ICOSL axis plays a crucial role in the development of systemic inflammation and organ damage induced by a clinically relevant sepsis model. These findings were confirmed by an exacerbation of septic injury in mice knockout for the ICOS and ICOSL genes. Interestingly, we also documented its draggability by showing protection when ICOS-Fc, a recombinant protein which act as an antagonist of ICOS and an agonist of ICOSL, was administered during sepsis. The beneficial effects of this innovative pharmacological approach are likely due to a potential cross-talk mechanisms involving the FAK-p38-NLRP3 inflammasome axis. A greater

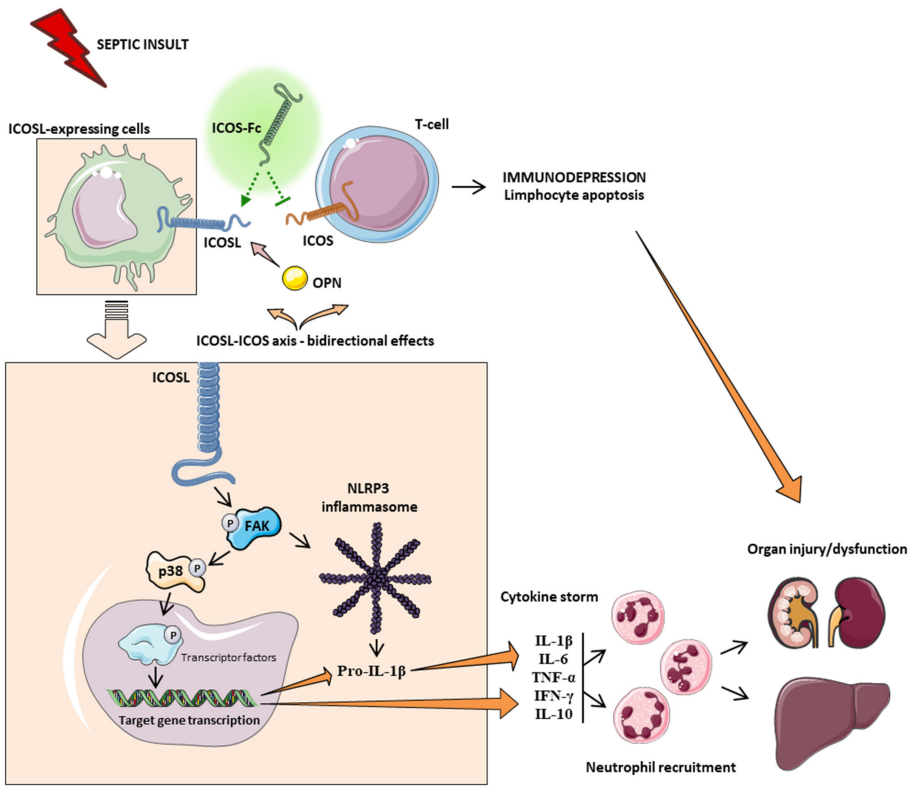

FIGURE 7
Schematic representation on the role of ICOS-ICOSL axis in the pathogenesis of sepsis. Septic insult results in an imbalance in the ICOS-ICOSL axis, leading to bidirectional harmful effects, where, on the one hand, the triggering of ICOS can induce immunosuppression, while, on the other hand, the signaling pathway downstream of the ICOSL protein leads to overactivation of FAK-p38-NLRP3 axis, promoting the transcription of pro-inflammatory genes, as well as the cleavage of pro IL-1β into IL-1β and subsequent production of pro-inflammatory cytokines. Leukocyte recruitment is also stimulated by the release of cytokines. Systemic hyperinflammation (cytokine storm), along with polymorphonuclear cell recruitment, contributes to the onset of multiple organ failure. Treatment with ICOS-Fc can attenuate sepsis-induced hyperinflammation and therefore MOF to improve clinical outcomes.

understanding of the molecular basis of ICOS-Fc-mediated effects is needed to harness its actions as a potentially powerful immunomodulatory tool for counteracting inflammation and organ injury in sepsis.

Data availability statement

The raw data supporting the conclusions of this article will be made available by the authors, without undue reservation.

Ethics statement

The animal study was reviewed and approved by Ethical committee OPBA University of Turin and Italian Ministry of Health, Italy.

Author contributions

GA, CD, UD, and MC conceived and designed the experiments. GA, IS, EA, CM, RM, EP, GE, DC, and NC performed the experiments. GA, EA, CM, RM, IB, EB, CG, NC, MA, DF, CT, CC, CD, UD, and MC analyzed the data. GA, CD, UD, CT, and MC, writing - review and editing. All authors have read and agreed to the published version of the manuscript.

Funding

The Università degli Studi di Torino has supported and funded this work (Ricerca Locale 2020 and 2021) and by the Associazione Italiana Ricerca sul Cancro (IG20714), Milan Italy.

Acknowledgments

Parts of the Figure 7 were drawn by using pictures from Servier Medical Art. Servier Medical Art by Servier is licensed

under a Creative Commons Attribution 3.0 Unported License (https://creativecommons.org/licenses/by/3.0/).

Conflict of interest

The authors declare that the research was conducted in the absence of any commercial or financial relationships that could be construed as a potential conflict of interest.

Publisher's note

All claims expressed in this article are solely those of the authors and do not necessarily represent those of their affiliated organizations, or those of the publisher, the editors and the reviewers. Any product that may be evaluated in this article, or claim that may be made by its manufacturer, is not guaranteed or endorsed by the publisher.

References

1. Hotchkiss RS, Monneret G, Payen D. Sepsis-induced immunosuppression: From cellular dysfunctions to immunotherapy. *Nat Rev Immunol* (2013) 13:862–74. doi: 10.1038/nri3552

2. Rudd KE, Johnson SC, Agesa KM, Shackelford KA, Tsoi D, Kievlan DR, et al. Global, regional, and national sepsis incidence and mortality, 1990 – 2017 : analysis for the global burden of disease study. *Lancet* (2020) 395:200–11. doi: 10.1016/S0140-6736(19)32989-7

3. Hutloff A, Dittrich AM, Beier KC, Eljaschewitsch B, Kraft R, Anagnostopoulos I, et al. ICOS is an inducible T-cell co-stimulator structurally and functionally related to CD28. *Nature* (1999) 100:263–6. doi: 10.1038/16717

4. Yoshinaga SK, Whoriskey JS, Khare SD, Sarmiento U, Guo J, Horan T, et al. T-Cell co-stimulation through B7RP-1 and ICOS. *Nature* (1999) 1:827–32. doi: 10.1038/45582

5. Swallow MM, Wallin JJ, Sha WC. B7h, a novel costimulatory homolog of B7.1 and B7.2, is induced by TNFa. *Immunity* (1999) 11:423–32. doi: 10.1016/s1074-7613(00)80117-x

6. Möhnle P, Hirschberger S, Hinske LC, Briegel J, Hübner M, Weis S, et al. MicroRNAs 143 and 150 in whole blood enable detection of T-cell immunoparalysis in sepsis. *Mol Med* (2018) 24:1–14. doi: 10.1186/s10020-018-0056-z

7. Menéndez R, Méndez R, Almansa R, Ortega A, Alonso R, Suescun M, et al. Simultaneous depression of immunological synapse and endothelial injury is associated with organ dysfunction in community-acquired pneumonia. *J Clin Med* (2019) 8:1–10. doi: 10.3390/jcm8091404

8. Burmeister Y, Lischke T, Dahler AC, Mages HW, Lam K-P, Coyle AJ , et al. ICOS controls the pool size of effector-memory and regulatory T cells. *J Immunol* (2008) 180:774–82. doi: 10.4049/jimmunol.180.2.774

9. Chen Q, Mo L, Cai X, Wei L, Xie Z, Li H, et al. ICOS signal facilitates Foxp3 transcription to favor suppressive function of regulatory T cells. *Int J Med Sci* (2018) 15:666–73. doi: 10.7150/ijms.23940

10. Luan Y, Yin C, Qin Q, Dong N, Zhu X, Sheng Z. Effect of regulatory T cells on promoting apoptosis of T lymphocyte and its regulatory mechanism in sepsis. *J Interf Cytokine Res* (2015) 35:969–80. doi: 10.1089/jir.2014.0235

11. Saito K, Wagatsuma T, Toyama H, Ejima Y, Hoshi K, Shibusawa M, et al. Sepsis is characterized by the increases in percentages of circulating CD4 + CD25 + regulatory T cells and plasma levels of soluble CD25. *J Exp Med* (2008) 216:61–8. doi: 10.1620/tjem.216.61

12. Leng F, Liu J, Liu Z, Yin J, Qu H-P. Increased proportion of CD4 d CD25 d Foxp3 d regulatory T cells during early-stage sepsis in ICU patients. *J Microbiol Immunol Infect* (2013) 46:338–44. doi: 10.1016/j.jmii.2012.06.012

13. Occhipinti S, Dianzani C, Chiocchetti A, Boggio E, Clemente N, Gigliotti CL, et al. Triggering of B7h by the ICOS modulates maturation and migration of monocyte-derived dendritic cells. *J Immunol* (2013) 190:1125–34. doi: 10.4049/jimmunol.1201816

14. Lund SA, Giachelli CM. The role of osteopontin in inflammatory processes. *J Cell Commun Signal* (2009) 3:311–22. doi: 10.1007/s12079-009-0068-0

15. Dianzani C, Minelli R, Mesturini R, Chiocchetti A, Barrera G, Boscolo S, et al. B7h triggering inhibits umbilical vascular endothelial cell adhesiveness to tumor cell lines and polymorphonuclear cells. *J Immunol* (2010) 185:3970–9. doi: 10.4049/jimmunol.0903269

16. Raineri D, Dianzani C, Cappellano G, Maione F, Baldanzi G, Iacobucc I, et al. Osteopontin binds ICOSL promoting tumor metastasis,". *Commun Biol* (2020) 3:1–15. doi: 10.1038/s42003-020-01333-1

17. Di Niro R, Ziller F, Florian F, Crovella S, Stebel M, Bestagno M, et al. Construction of miniantibodies for the *in vivo* study of human autoimmune diseases in animal models. *BMC Biotechnol* (2007) 7:1–10. doi: 10.1186/1472-6750-7-46

18. Gigliotti CL, Boggio E, Clemente N, Shivakumar Y, Toth E, Sblattero D, et al. ICOS-ligand triggering impairs osteoclast differentiation and function *In vitro* and *In vivo*. *J Immunol* (2016) 197:3905–16. doi: 10.4049/jimmunol.1600424

19. Dianzani C, Minelli R, Gigliotti CL, Occhipinti S, Giovarelli M, Conti LM, et al. B7h triggering inhibits the migration of tumor cell lines. *J Immunol* (2014) 192:4921–31. doi: 10.4049/jimmunol.1300587

20. Ramavath NN, Gadipudi LL, Provera A, Gigliotti LC, Boggio E, Bozzola C, et al. Inducible T-cell costimulator mediates Lymphocyte/Macrophage interactions during liver repair. *Front Immunol* (2021) 12:786680. doi: 10.3389/fimmu.2021.786680

21. Stoppa I, Gigliotti CL, Clemente N, Pantham D, Dianzani C, Monge C, et al. ICOSL stimulation by ICOS-fc accelerates cutaneous wound healing *In vivo*. *Int J Mol Sci* (2022) 23:1–12. doi: 10.3390/ijms23137363

22. O'Sullivan AW, Wang JH, Redmond HP. NF-κB and P38 MAPK inhibition improve survival in endotoxin shock and in a cecal ligation and puncture model of sepsis in combination with antibiotic therapy. *J Surg Res* (2009) 152:46–53. doi: 10.1016/j.jss.2008.04.030

23. Cornelius DC, Travis OK, TramelI RW, Borges-Rodriguez M, Baik CH, Greer M, et al, et al. NLRP3 inflammasome inhibition attenuates sepsis-induced platelet activation and prevents multi-organ injury in cecal-ligation puncture. *PLoS One* (2020) 15:1–15. doi: 10.1371/journal.pone.0234039

24. Lee S, Nakahira K, Dalli J, Siempos II, Norris PC, Colas RA, et al. NLRP3 inflammasome deficiency protects against microbial sepsis *via* increased lipoxin B4 synthesis. *Am J Respir Crit Care Med* (2017) 196:713–26. doi: 10.1164/rccm.201604-0892OC

25. Chen X, Zhao Y, Wang X, Lin Y, Zhao W, Wu D, et al. FAK mediates LPS-induced in fl ammatory lung injury through interacting TAK1 and activating TAK1-NF κ b pathway. *Cell Death Differ* (2022) 13:1–12. doi: 10.1038/s41419-022-05046-7

26. du Sert NP, Hurst V, Ahluwalia A, Alam S, Avey MT, Baker M, et al. The arrive guidelines 2.0: Updated guidelines for reporting animal research. *PloS Biol* (2020) 18:1–12. doi: 10.1371/journal.pbio.3000410

27. Osuchowski MF, Ayala A, Bahrami S, Bauer M, Boros M, Cavaillon J-M, et al. Minimum quality threshold in pre-clinical sepsis studies (mqtipss): An international expert consensus initiative for improvement of animal modeling in sepsis. *Shock* (2018) 50:377–80. doi: 10.1097/SHK.0000000000001212

28. Alves GF, Aimaretti E, Einaudi G, Mastrocola R, Oliveira JG, Collotta D, et al. Pharmacological inhibition of FAK-Pyk2 pathway protects against organ damage and prolongs the survival of septic mice. *Front Immunol* (2022) 13:837180. doi: 10.3389/fimmu.2022.837180

29. Kovalski V, Prestes AP, Oliveira JG, Alves GF, Colarites D, El Mattos J, et al. Protective role of cGMP in early sepsis. *Eur J Pharmacol* (2017) 807:174–81. doi: 10.1016/j.ejphar.2017.05.012

30. Nandra KK, Collino M, Rogazzo M, Fantozzi R, Patel NSA, Thiemermann C. "Pharmacological preconditioning with erythropoietin attenuates the organ injury and dysfunction induced in a rat model of hemorrhagic shock,". *DMM Dis Model Mech* (2013) 6:701–9. doi: 10.1242/dmm.011353

31. Faul F, Erdfelder E, Lang A-G, Buchner A. G*Power 3: A flexible statistical power analysis program for the social, behavioral, and biomedical sciences. *Behav Res Methods* (2007) 39:175–91. doi: 10.3758/bf03193146

32. Tsirigotis P, Chondropoulos S, Gkirkas K, Meletiadis J, Dimopoulou I. "Balanced control of both hyper and hypo-inflammatory phases as a new treatment paradigm in sepsis,". *J Thorac Dis* (2016) 8:E312–6. doi: 10.21037/jtd.2016.03.47

33. Boomer JS, To K, Chang KC, Takasu O, Osborne DF, Walton AH, et al. Immunosuppression in patients who die of sepsis and multiple organ failure. *J Am Med Assoc* (2011) 306:2594–605. doi: 10.1001/jama.2011.1829

34. Otto GP, Sossdorf M, Claus RA, Rödel J, Menge K, Reinhart K, et al. The late phase of sepsis is characterized by an increased microbiological burden and death rate. *Crit Care* (2011) 15:1–8. doi: 10.1186/cc10332

35. Mai SHC, Sharma N, Kwong AC, Dwivedi DJ, Khan M, Grin PM, et al. Body temperature and mouse scoring systems as surrogate markers of death in cecal ligation and puncture sepsis. *Intensive Care Med Exp* (2018) 6:1–14. doi: 10.1186/s40635-018-0184-3

36. Koh KH, Cao Y, Mangos S, Tardi NJ, Dande RR, Lee HW, et al. Nonimmune cell–derived ICOS ligand functions as a renoprotective αvβ3 integrin–selective antagonist. *J Clin Invest* (2019) 129:1713–26. doi: 10.1172/JCI123386

37. Castello LM, Baldrighi M, Molinari L, Salmi L, Cantaluppi V, Vaschetto R, et al. The role of osteopontin as a diagnostic and prognostic biomarker in sepsis and septic shock. *Cells* (2019) 8:1–12. doi: 10.3390/cells8020174

38. Uchibori T, Matsuda K, Shimodaira T, Sugano M, Uehara T, Honda T. IL-6 trans-signaling is another pathway to upregulate osteopontin. *Cytokine* (2017) 90:88–95. doi: 10.1016/j.cyto.2016.11.006

39. Hirano Y, Aziz M, Yang W-L, Wang Z, Zhou M, Ochani M, et al. Neutralization of osteopontin attenuates neutrophil migration in sepsis-induced acute lung injury. *Crit Care* (2015) 19:1–15. doi: 10.1186/s13054-015-0782-3

40. Fortis S, Khadaroo RG, Haitsma JJ, Zhang H. Osteopontin is associated with inflammation and mortality in a mouse model of polymicrobial sepsis. *Acta Anaesthesiol Scand* (2015) 59:170–5. doi: 10.1111/aas.12422

41. Trostel J, Truong LD, Roncal-Jimenez C, Miyazaki M, Miyazaki-Anzai S, Kuwabara M, et al. Disease different effects of global osteopontin and macrophage osteopontin in glomerular injury. *Am J Physiol - Ren Physiol* (2018) 315:F759–68. doi: 10.1152/ajprenal.00458.2017

42. Boggio E, Dianzani C, Gigliotti CL, Soluri MF, Clemente N, Cappellano G, et al. Thrombin cleavage of osteopontin modulates its activities in human cells *in vitro* and mouse experimental autoimmune encephalomyelitis *in vivo*. *J Immunol Res* (2016) 2016:1–13. doi: 10.1155/2016/9345495

43. Chaudhry H, Zhou J, Zhong Y, Ali MM, Mcguire F, Nagarkatti PS, et al. Role of cytokines as a double-edged sword in sepsis. *In Vivo (Brooklyn)* (2013) 27:669–84.

44. Chung IC, OuYang C-N, Yuan S-N, Li H-P, Chen J-T, Shieh H-R, et al. Pyk2 activates the NLRP3 inflammasome by directly phosphorylating ASC and contributes to inflammasome-dependent peritonitis. *Sci Rep* (2016) 6:1–13. doi: 10.1038/srep36214

45. Yu H, Liu Y, Wang M, Restrepo RJ, Wang D, Kalogeris TJ, et al. Myeloperoxidase instigates proinflammatory responses in a cecal ligation and puncture rat model of sepsis. *Am J Physiol - Hear Circ Physiol* (2020) 319:H705–21. doi: 10.1152/ajpheart.00440.2020

46. Wahl C, Bochtler P, Chen L, Schirmbeck R, Reimann J. B7-H1 on hepatocytes facilitates priming of specific cd8 t cells but limits the specific recall of primed responses. *Gastroenterology* (2008) 135:980–8. doi: 10.1053/j.gastro.2008.05.076

frontiers | Frontiers in Immunology

TYPE Original Research
PUBLISHED 23 September 2022
DOI 10.3389/fimmu.2022.1010882

Check for updates

OPEN ACCESS

EDITED BY
Manuela Mengozzi,
Brighton and Sussex Medical School, United Kingdom

REVIEWED BY
Adrien Joseph,
Assistance Publique Hopitaux De Paris, France
Massimo Collino,
University of Turin, Italy

*CORRESPONDENCE
Sina M. Coldewey
sina.coldewey@med.uni-jena.de

SPECIALTY SECTION
This article was submitted to Inflammation, a section of the journal Frontiers in Immunology

RECEIVED 03 August 2022
ACCEPTED 30 August 2022
PUBLISHED 23 September 2022

CITATION
Dennhardt S, Pirschel W, Wissuwa B, Imhof D, Daniel C, Kielstein JT, Hennig-Pauka I, Amann K, Gunzer F and Coldewey SM (2022) Targeting the innate repair receptor axis *via* erythropoietin or pyroglutamate helix B surface peptide attenuates hemolytic-uremic syndrome in mice. *Front. Immunol.* 13:1010882. doi: 10.3389/fimmu.2022.1010882

COPYRIGHT
© 2022 Dennhardt, Pirschel, Wissuwa, Imhof, Daniel, Kielstein, Hennig-Pauka, Amann, Gunzer and Coldewey. This is an open-access article distributed under the terms of the Creative Commons Attribution License (CC BY). The use, distribution or reproduction in other forums is permitted, provided the original author(s) and the copyright owner(s) are credited and that the original publication in this journal is cited, in accordance with accepted academic practice. No use, distribution or reproduction is permitted which does not comply with these terms.

Targeting the innate repair receptor axis *via* erythropoietin or pyroglutamate helix B surface peptide attenuates hemolytic-uremic syndrome in mice

Sophie Dennhardt[1,2,3], Wiebke Pirschel[1,2], Bianka Wissuwa[1,2], Diana Imhof[4], Christoph Daniel[5], Jan T. Kielstein[6], Isabel Hennig-Pauka[7], Kerstin Amann[5], Florian Gunzer[8] and Sina M. Coldewey[1,2,3]*

[1]Department of Anesthesiology and Intensive Care Medicine, Jena University Hospital, Jena, Germany, [2]Septomics Research Center, Jena University Hospital, Jena, Germany, [3]Center for Sepsis Control and Care, Jena University Hospital, Jena, Germany, [4]Pharmaceutical Biochemistry and Bioanalytics, Pharmaceutical Institute, University of Bonn, Bonn, Germany, [5]Department of Nephropathology, Friedrich-Alexander University (FAU) Erlangen-Nürnberg, Erlangen, Germany, [6]Medical Clinic V, Nephrology | Rheumatology | Blood Purification, Academic Teaching Hospital Braunschweig, Braunschweig, Germany, [7]Field Station for Epidemiology, University of Veterinary Medicine Hannover, Bakum, Germany, [8]Department of Hospital Infection Control, University Hospital Carl Gustav Carus, TU Dresden, Dresden, Germany

Hemolytic-uremic syndrome (HUS) can occur as a systemic complication of infections with Shiga toxin (Stx)-producing *Escherichia coli* and is characterized by microangiopathic hemolytic anemia and acute kidney injury. Hitherto, therapy has been limited to organ-supportive strategies. Erythropoietin (EPO) stimulates erythropoiesis and is approved for the treatment of certain forms of anemia, but not for HUS-associated hemolytic anemia. EPO and its non-hematopoietic analog pyroglutamate helix B surface peptide (pHBSP) have been shown to mediate tissue protection *via* an innate repair receptor (IRR) that is pharmacologically distinct from the erythropoiesis-mediating receptor (EPO-R). Here, we investigated the changes in endogenous EPO levels in patients with HUS and in piglets and mice subjected to preclinical HUS models. We found that endogenous EPO was elevated in plasma of humans, piglets, and mice with HUS, regardless of species and degree of anemia, suggesting that EPO signaling plays a role in HUS pathology. Therefore, we aimed to examine the therapeutic potential of EPO and pHBSP in mice with Stx-induced HUS. Administration of EPO or pHBSP improved 7-day survival and attenuated renal oxidative stress but did not significantly reduce renal dysfunction and injury in the employed model. pHBSP, but not EPO, attenuated renal nitrosative stress and reduced tubular dedifferentiation. In conclusion, targeting the EPO-R/IRR axis reduced mortality and renal oxidative stress in murine HUS without occurrence of thromboembolic complications or other adverse side effects. We therefore suggest that repurposing EPO for the

10.3389/fimmu.2022.1010882

treatment of patients with hemolytic anemia in HUS should be systematically investigated in future clinical trials.

KEYWORDS

erythropoietin, hemolytic-uremic syndrome, shiga toxin, mice, pyroglutamate helix B surface peptide, microangiopathic hemolytic anemia, thrombotic microangiopathy

Introduction

Hemolytic-uremic syndrome (HUS) belongs to the group of thrombotic microangiopathies and includes atypical and typical HUS. The latter accounts for approximately 90% of HUS cases and is a life-threatening systemic complication of infections with certain bacterial pathogens, most commonly Shiga toxin (Stx)-producing *Escherichia coli* (STEC) (1).

STEC-infections can cause diarrhea or hemorrhagic colitis with bloody diarrhea. STEC-HUS typically presents with microangiopathic hemolytic anemia, thrombocytopenia, acute kidney injury (AKI) and other organ dysfunctions (1). One-third of patients with STEC-HUS also develop long-term renal and up to 4%, long-term neurological sequelae (2). Renal oxidative stress was shown to be an important factor in HUS pathogenesis in pediatric HUS (3, 4). Its pathophysiological relevance was also demonstrated in a murine model of Stx2-induced HUS (5).

To date, organ supportive therapy in the intensive care unit (ICU), including hemodialysis, fluid resuscitation as well erythrocyte transfusion if indicated, has been the standard of care in patients with STEC-HUS (6). In the absence of targeted therapeutic options, there is a medical need to further investigate molecular therapeutic approaches for the treatment of this life-threatening systemic syndrome.

Due to the low incidence – of e. g. 0.07 per 100,000 persons/year for Germany (7) up to 0.67 per 100,000 persons/year for Argentina (8) – conducting prospective randomized clinical trials has proven difficult. To provide tools for preclinical studies, we have recently introduced and characterized several animal models for STEC-HUS, including an infection model employing the Northern German outbreak strain O104:H4 of 2011 and the well-characterized outbreak strain O157:H7 86-24 in gnotobiotic piglets (9), as well as a clinically relevant mouse model (10–12) reflecting most aspects of human pathology by repeatedly exposing animals to low doses of Stx isolated from an EHEC O157:H7 86-24. All previously described small animal models of STEC-HUS mimic well the critical illness, renal failure and microangiopathy seen in humans, while being limited in their modeling of hemolytic anemia, which is oftentimes masked by hemoconcentration secondary to fluid deficiency (10, 13, 14).

Erythropoietin (EPO), a pleiotropic hormone that has been shown to exert tissue-protective effects *via* the innate repair receptor (IRR) independent of its hematopoietic properties *via* the EPO receptor (EPO-R) homodimer (15, 16), appears to be a promising candidate to be further evaluated in HUS. Preclinical trials usually use one magnitude higher doses of EPO compared with clinical trials (1000-5000 IU/kg versus 300 IU/kg) (17). This could explain why preclinical tissue protection following EPO administration could often not be translated into the clinical setting. Furthermore, beside its potential beneficial effects, the thrombogenic effect of this erythropoiesis-stimulating hormone was critically discussed in the context of clinical studies (18, 19), as tissue-protective effects require high levels of EPO and administration of high EPO doses can increase the risk of thrombosis (16) and hypertension (17). For this reason, EPO-derived non-hematopoietic small peptide activators of the IRR, such as the pyroglutamate helix B surface peptide (pHBSP), have been developed (15). Preclinically, pHBSP has been shown to convey tissue protection in numerous disease models (20), such as nephroprotection in ischemia-reperfusion models of AKI (21, 22). Furthermore, pHBSP has been successfully employed in phase II studies in patients with diabetes or sarcoidosis and neuropathic pain (23, 24).

HUS can be considered as a specific phenotype of sepsis, as it represents a combination of infection and organ dysfunction. We previously reported that EPO attenuated AKI (25) and cardiac dysfunction (26) in mouse models of endotoxemia and cecal ligation and puncture-induced sepsis. There is no clinical evidence on the beneficial or harmful effects of EPO in patients with sepsis and there is only little evidence regarding the beneficial or harmful effects of EPO in ICU patients in general (27, 28). To our knowledge, the tissue-protective effects of EPO or pHBSP in HUS have not been investigated, yet. One trial that aimed to investigate the effects of EPO on the microcirculation of patients with severe sepsis was discontinued due to lack of recruitment (NCT01087450). We did not find the results of a study that examined the immunomodulatory effects of activated protein C and/or EPO in sepsis (NCT00229034). A third study

examining the effects of EPO on renal function in critically ill patients with and without multiorgan failure appears to be not completed (EudraCT number: 2008-003733-24). Altogether, there is no evidence from randomized controlled trials regarding the effects of EPO administration in sepsis and HUS. Despite this lack of evidence, it is however conceivable, that in the presence of severe hemolytic anemia in patients with HUS, the stimulation of hematopoiesis by EPO could be beneficial by reducing the need for allogenic erythrocyte transfusion, which carry non-negligible risks (29, 30).

Anemia is usually accompanied by a regulatory increase in endogenous EPO production due to hypoxia-mediated feedback mechanisms. In patients with iron deficiency or hemolytic anemia, serum EPO levels exceeding 2000 mU/ml (two orders of magnitude above normal range) have been reported (31). In contrast, renal anemia is often accompanied by insufficient EPO production due to direct damage to EPO-producing cells in the kidney (32) or inhibition of EPO production by various cytokines (33). Already in the early 1990's, it was hypothesized that anemias associated with low serum EPO levels might respond to treatment with recombinant EPO (34).

Currently, EPO can be considered in the treatment of anemia associated with chemotherapy (35) and chronic kidney disease (36). The current national guideline for the treatment of HUS in pediatric patients states that EPO can be considered in the treatment of HUS-associated hemolytic anemia as expert consensus without citing evidence (37). So far, no adverse effects have been observed in children receiving EPO for the treatment of hemolytic anemias (38–41). However, a reduction of red blood cell transfusion could not be shown in two small studies (38, 39). Hitherto, there are no sufficiently powered clinical studies in this context. Even a neutral effect of EPO in terms of nephroprotection in the absence of side effects might positively impact the therapy of HUS-associated hemolytic anemia and save the need for red blood cell transfusions.

In view of the above, we consider it necessary and promising to assess the role of EPO in this orphan disease which comprises a specific form of septic organ failure. The first objective of this study is to further elucidate the role of endogenous EPO and its potential clinical relevance in HUS by measuring endogenous EPO levels in different species: human patients (infection with EHEC O104:H4, 2011 German outbreak), gnotobiotic piglets (subjected to EHEC O104:H4 or EHEC O157:H7 86-24) and mice (subjected to Stx2 derived from EHEC O157:H7 86-24). The second objective of this study is to examine the effect of EPO and the non-hematopoietic peptide pHBSP in a murine model of HUS by measuring surrogate parameters of kidney injury and dysfunction, intrarenal barrier integrity, microangiopathy, oxidative and nitrosative stress and metabolome. Hereby, we aim to provide preclinical evidence to assess whether treatment of HUS with EPO or pHBSP should be considered and further investigated, particularly for HUS-associated hemolytic anemia.

Material and methods

Study design

Plasma samples of patients with STEC-HUS (n = 27, median age 47, 24 female) were provided by the German STEC-HUS Registry (42). These samples were taken within 10 d after admission to the hospital (HUS acute stage) and at the day of the last plasmapheresis (HUS pre-discharge). We analyzed the subcohort of 7 patients of which samples were available from day 1 to day 3 after hospital admission and within 3 d before hospital discharge. Age- and sex-matched samples of healthy controls (n = 21, median age 63.5, 15 female) were provided by Jena University Hospital [ICROS study (43)]. Ethic approval was obtained by the primary investigators from the Ethics Committee of Hannover Medical School (1123-2011) and of the Friedrich Schiller University Jena (5276-09/17). Participants provided written informed consent prior to inclusion in the respective studies.

Samples from gnotobiotic piglets (9) were collected 4 to 6 days after STEC-infection or mock infection (sham). Experimental procedures in gnotobiotic piglets were approved by the local permitting authorities in the Lower Saxony State Office for Consumer Protection and Food Safety and in accordance with the requirements of the national animal welfare law (Approval Number: 33.9-42502-04-13/1149) in accordance with the German legislation following the guidelines of FELASA and ARRIVE (9).

All procedures performed in mice were approved by the regional animal welfare committee and the Thuringian State Office for Consumer Protection (registration number 02-058/14) and performed in accordance with the German legislation. HUS-like disease in mice was induced by repetitive doses of Stx2 as described previously (10). Briefly, wild-type C57BL/6J mice aged 10-16 weeks weighing 20-30 g were randomly assigned to one of four groups (sham n = 16, Stx+vehicle n = 26, Stx+EPO n = 22, or Stx+pHBSP n = 21) and received 3x25 ng/kg body weight (BW) Stx or 0.9% NaCl i.v. on days 0, 3, and 6. EPO (1000 IU/kg BW) was applied s.c. 1 h after initial Stx injection. Due to its short plasma half-life, pHBSP (30 µg/kg BW) was applied s.c. every 24 h starting 1 h after initial Stx injection. Vehicle (Ringer's solution) was applied s.c. starting 1 h after initial Stx injection. Mice received 3x800 µl Ringer's solution each day for volume replacement. In compliance with ethical regulations, survival was monitored for 7 days using humane endpoints (mice were euthanized when reaching a high-grade disease state, Figure 3). Disease progression was monitored by weight loss and activity-based HUS score (ranging from 1-normally active, 2-active with slight restrictions, 3-active with clear intermissions, 4-slowed, 5-lethargic, 6-moribund, to 7-dead) as described previously (10). Animals were exsanguinated in deep ketamine/xylazine anesthesia (10). Renal tissue, blood and plasma samples were collected on day 7. An additional experiment with a

comparable survival rate including sham and Stx+vehicle mice was performed to compensate for the lower survival rate in the Stx+vehicle group and to increase the statistical power in the analysis of day-7-samples for plasma urea and creatinine and all histological [Schiff's periodic acid (PAS), acid fuchsin orange G (SFOG)] and immunohistochemistry (IHC) stainings (kidney-injury molecule 1 (KIM-1), cluster of differentiation 31 (CD31), E-cadherin, glycoprotein 1b (GP1b), nitrotyrosine and NADPH oxygenase 1 (NOX-1), Figures 4–7). Plasma EPO levels (Figure 2B) and plasma metabolome (Figure 8) were measured in an independent experimental setup with comparable survival rates since availability of plasma per animal was limited.

Compounds

Stx purification was performed as described previously (10). Human recombinant EPO (Epoeitin beta, Hoffmann-La Roche) was diluted to 1000 U/kg BW in Ringer's solution (vehicle). A standard N-(9-fluorenyl)methoxycarbonyl protocol for automated solid-phase peptide synthesis was implemented for pHBSP synthesis (Supplementary Methods). pHBSP was diluted to 30 µg/kg BW in Ringer's solution (vehicle).

Blood and plasma sample analysis

Human (42), piglet (9) and murine (10) blood samples were taken as described elsewhere. Hematology and analysis of laboratory chemistry parameters in murine samples were performed as recently described (10). Briefly, blood counts were analyzed using impedance technology implemented in the pocH100iv system (Sysmex, Kobe, Japan). Laboratory parameters were analyzed by an Architect™ c16200/ci8200 automated clinical chemistry system (Abbott Diagnostics, Abbott. Park, USA). This system uses the Jaffè method for plasma creatinine measurements and the urease/nicotinamide adenine dinucleotide hydrogen method for plasma urea measurements. The following parameters were measured using commercially available ELISA kits: serum or plasma EPO and murine plasma neutrophil-gelatinase-associated lipocalin (NGAL, Supplementary Table S1).

Tissue preparation, histopathology and IHC staining

Processing of kidney samples, histopathological analysis and IHC stainings were performed as described previously (10). SFOG and thrombocyte (GP1b) staining was performed as described recently (11). Until antigen demasking, sections for E-cadherin, NOX-1 and nitrotyrosine staining were treated similarly. The Vector M.O.M. Immunodetection kit (Vector Laboratories) was used for E-cadherin staining. Blocking of nitrotyrosine staining was performed in normal goat serum. IHC sections were washed with Tris(hydroxymethyl) aminomethan (TRIS) buffer during staining [50 mM TRIS, 300 mM NaCl, pH was adjusted to 7.6 with HCl (all Carl Roth); 0.04% Tween®20 (Sigma Aldrich)], incubated with primary antibodies overnight at 4°C in appropriate dilutions (Supplementary Table S2) and subsequently incubated for 30 min with secondary antibodies (Supplementary Table S3). NOX-1 sections were incubated in primary antibody directly after antigen retrieval. Nitrotyrosine sections were stained using the CSA kit and rabbit Link (Dako).

Histology and IHC quantification

Quantification and scoring of histopathological and IHC stainings were performed as described previously (10). For quantification of renal E-cadherin expression, all cut and completely positively stained tubules (with entirely visible lumen, excluding those with spotty staining) were counted in 12 adjacent cortical fields [one cortical field = region of interest (ROI)] per section in 400x magnification. Nitrotyrosine staining was quantified by superimposing a 10x10 grid (area of 0.0977 mm^2) over each field and counting positively stained fields in 20 adjacent cortical fields per section in 400x magnification (blinded). NOX-1 staining was analyzed using a scoring system (0 to 3; 0: < 25%, 1: 25-50%, 2: 50-75%, 3: > 75% positive staining per field, 12 fields/section, magnification 200x, blinded). Quantification of SFOG and thrombocyte staining was performed as described recently (11).

Targeted metabolomics and statistical analysis

Targeted metabolomics from heparinized plasma was performed at Biocrates Life Sciences by mass spectrometry using an MxP® Quant 500 kit. Data analysis was performed using R version 3.4.4 (R Core Team) as follows: Readings below detection level were set to half of detection level for each analyte separately. Metabolome data was then log 2 transformed without any further normalization. Z scores were calculated using mean and standard deviation of all samples. Trends along the four sample groups were tested using linear regression models where sample group assignment was used as the independent variable and each analyte as the dependent variable in a separate model. Prior to linear regression, the independent variable sample group assignment was transformed to a pseudo-continuous variable where all samples of group "sham" were set to 0, samples of group "Stx+pHBSP" were set to 1/3, samples of group "Stx+EPO" were set to 2/3 and samples of group "Stx+vehicle" were set to 1. Applying this transformation, the linear regression models test

whether there is an increasing or decreasing trend along the four groups in the assigned order. P-values for all models were Benjamini-Hochberg adjusted (44). Analytes with adjusted P-values below 0.05 and an absolute effect of one or bigger were considered significantly changing along the four sample groups.

Statistics

Data are depicted as mean ± SD for n observations. GraphPad Prism 7.05 (GraphPad Software) was used for data analysis applying Student's t-test and Wilcoxon signed rank test for comparisons between 2 groups. One-way ANOVA with Holm-Sidak *post hoc* test (parametric data) or Kruskal-Wallis test with Dunn's *post hoc* test (nonparametric data) were used for comparisons between more than 2 groups. Survival was depicted as Kaplan-Meier curve and analyzed by Mantel-Cox test. Association between EPO levels in patients with STEC-HUS and hematological and laboratory parameters and piglet samples was performed with GraphPad Prism 7.05 implementing non-parametric Spearman's rank correlation coefficients. A P-value < 0.05 was considered significant. Mean ± SD and P-values for all analyses are given in Supplementary Table S4.

Results

Elevated EPO levels in humans suffering from HUS

In patients with STEC-HUS, EPO serum levels were elevated in the acute stage of disease compared with healthy controls (Figure 1A, upper panel, Supplementary Tables S5, S6 for individual values). Pre-discharge, EPO levels decreased compared to the acute phase, yet continued to be higher than in healthy controls. In a subgroup, in which blood samples were consequently taken within 3 days after admission and 3 days before discharge from the hospital, a reduction of serum EPO levels was observed in 6 out of 7 HUS patients (Figure 1A, lower panel). Several hematological, laboratory and clinical parameters at hospital admission are listed in Table 1 and EPO values were correlated with these parameters. Anemia was present in 6 out of 7 patients (Figures 1B, C) and there was a trend towards a negative correlation between endogenous EPO levels and hemoglobin (Hb; r = -0.5357, P = 0.2357) or hematocrit (r = -0.6071, P = 0.1667) at hospital admission. No correlation was observed between endogenous EPO levels and lactate dehydrogenase (LDH) or creatinine at hospital admission (Figures 1D, E), although intriguingly, the lowest endogenous EPO levels were observed in patients with pronounced kidney dysfunction (Figure 1E).

While anemia appears to be a major driver of increased EPO secretion in patients with STEC-HUS, we wondered whether other mechanisms might also play a role. Considering that – at least in our limited subcohort-endogenous EPO was lowest in those patients with pronounced kidney dysfunction and injury, we hypothesize that these patients might profit from therapeutic EPO administration.

Elevated EPO levels in animal models of HUS

To further assess the role of EPO in HUS, we measured endogenous EPO levels in two well-characterized animal models of this condition. In gnotobiotic piglets with STEC-HUS, EPO levels were elevated in EHEC O104:H4- and EHEC O157:H7-infected piglets compared with sham piglets (Figure 2A). STEC-infected gnotobiotic piglets did not display clear signs of anemia or kidney injury compared with mock-infected sham animals (Table 2). No correlations were observed between EPO-levels and hematological parameters (Supplementary Table S7). In O157:H7-infected piglets, although LDH was comparably low, there was a trend towards negative correlation with EPO levels (Supplementary Table S7). In C57BL/6 mice subjected to Stx, slight hemoconcentration was observed (Supplementary Table 3, significant increase in Hb in Stx+vehicle compared with sham mice). Despite the absence of anemia in Stx+vehicle mice, EPO plasma levels were elevated compared with sham mice (Figure 2B). There was no correlation between plasma EPO levels and plasma NGAL as surrogate parameter for kidney damage in mice (Supplementary Figure S1).

As anemia appears not to be the sole driver of increased EPO levels during HUS and patients with pronounced kidney damage showed the lowest EPO levels, we next wanted to analyze the therapeutic potential of EPO and the non-hematopoietic EPO derivative pHBSP in a murine model of HUS.

Effect of EPO and pHBSP treatment on survival and clinical presentation of mice with HUS

7-day survival was significantly increased in Stx+EPO (68.2%) and Stx+pHBSP mice (76.2%) compared with Stx+vehicle mice (42.3%; Figure 3A). Consistently, disease progression was reduced on days 6 and 7 in these treatment groups (Figure 3B). All surviving Stx-challenged animals lost up to 20% weight until the end of the experiment. Statistical comparison of weight loss was performed until the first animals had to be euthanized at day 5 (Figure 3C). Weight loss in Stx+EPO mice was less pronounced compared with Stx+vehicle mice on days 4 and 5 (Figure 3C). While neurological involvement assessed by hind limb clasping reflex frequently occurred in Stx+vehicle mice (approx. 39%, P = 0.0067 vs. sham, Table 3), it was less common in Stx+EPO (approx. 27%; Table 3) and Stx+pHBSP mice (approx. 24%; Table 3). No differences were observed in plasma alanine aminotransferase (ALAT) and aspartate aminotransferase (ASAT), while Hb and/or hematocrit as

10.3389/fimmu.2022.1010882

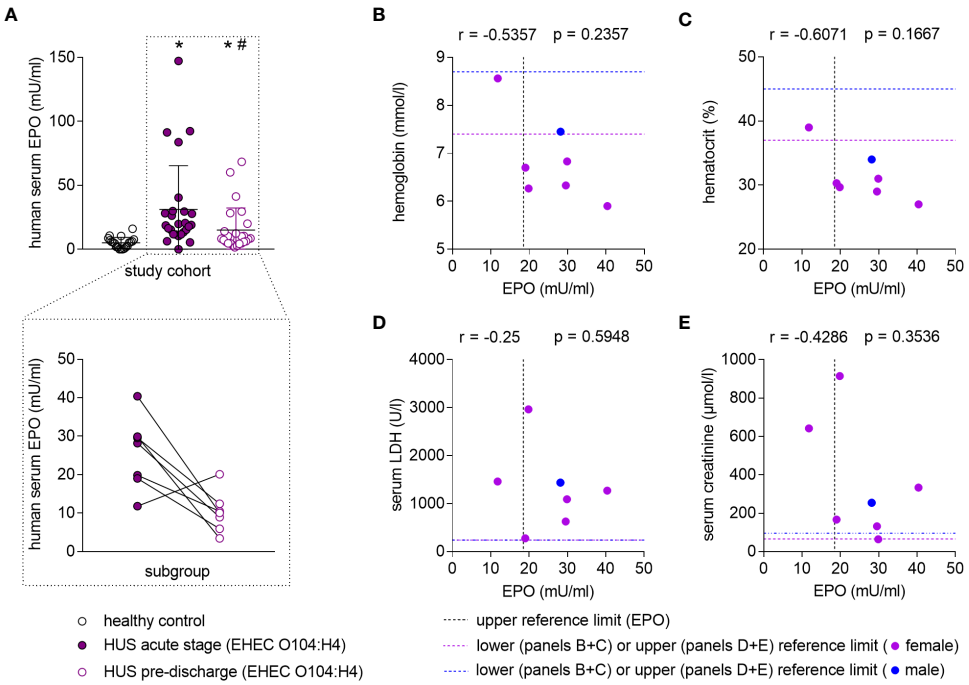

FIGURE 1
Endogenous EPO levels in patients with STEC-HUS and their correlation with anemia and kidney damage. **(A)** Upper panel: EPO serum levels in healthy controls (n = 20) and HUS patients (n = 26) within 10 d after admission to the hospital (HUS acute stage) and the last plasmapheresis (HUS pre-discharge) determined by ELISA. Data are expressed as scatter dot plot with mean ± SD. *P < 0.05 vs. healthy control (Mann-Whitney U-test), #P < 0.05 vs. HUS acute stage (Wilcoxon signed-rank test). Lower panel: Pairwise comparison of EPO serum levels of a subcohort of patients (n = 7) in which blood samples were available from day 1 to 3 after hospital admission and within 3 days before hospital discharge. Data are expressed as scatter dot plot with connecting line between respective measurements. **(B-E)** Correlation analysis implementing Spearman's correlation coefficient (r) for correlations of endogenous EPO levels with **(B)** hemoglobin (n = 7), **(C)** hematocrit (n = 7), **(D)** lactate dehydrogenase (LDH, n = 7) and **(E)** creatinine (n = 7) in the subcohort. The upper reference limit for EPO in health are indicated by dashed vertical lines. Gender-specific lower or upper reference limits for the respective parameters of anemia and kidney damage are indicated by dashed horizontal lines.

indicators of hemoconcentration were increased in all Stx-challenged mice (Table 3). Compared with sham mice, Hb was elevated in Stx+EPO mice, while it was not in Stx+pHBSP mice. However, there was no significant difference between Stx+EPO mice and Stx-vehicle mice. The effects of EPO-treatment on Hb might be masked by the slight hemoconcentration observed in all Stx-challenged groups.

Effect of EPO and pHBSP treatment on kidney injury and dysfunction in mice with HUS

After observing significantly increased survival rates in EPO- and pHBSP-treated animals, we analyzed the impact of both treatments on kidney injury and dysfunction. Stx+vehicle,

TABLE 1 Hematological, laboratory and renal function parameters in the subgroup of patients with STEC-HUS assessed at hospital admission.

Patient no.	Sex	Age	EPO (T1, mU/ml)	Hb (g/dl)	Hct (%)	LDH (U/l)	Crea (mg/dl)	Dialysis	Plasmapheresis (number)	RBC
5	m	26	28.194	12.0	34.0	1437	2.88	no	yes (6)	no
9	f	74	19.856	10.1	29.7	2966	10.35	yes	yes (4)	n/a
11	f	29	40.382	9.5	27.0	1273	3.78	yes	yes (6)	yes
12	f	39	29.546	10.2	29.0	627	1.49	no	no	no
13	f	44	19.034	10.8	30.3	279	1.89	no	yes (4)	yes
15	f	50	29.914	11.0	31.0	1091	0.73	yes	yes (7)	yes
25	f	73	11.820	13.8	39.0	1460	7.26	yes	yes (5)	yes

Hb, hemoglobin; Hct, hematocrit; LDH, lactate dehydrogenase; Crea, creatinine; RBC, red blood cell transfusion.

10.3389/fimmu.2022.1010882

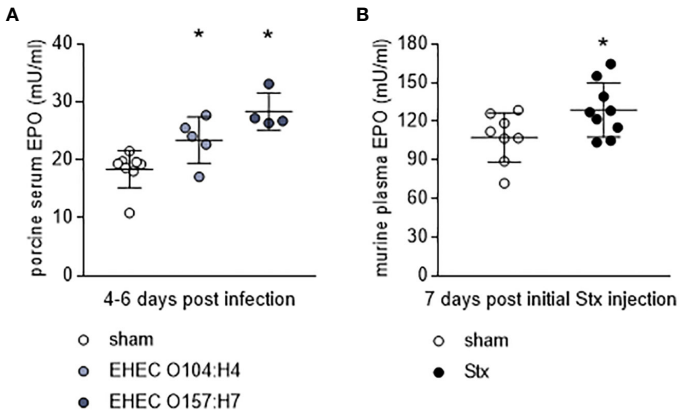

FIGURE 2
Endogenous EPO levels in animal models of HUS. **(A)** EPO serum levels in gnotobiotic piglets that were either mock-infected (sham) or infected with EHEC O157:H7 or EHEC O104:H4 determined by ELISA. Samples were taken 4-6 d after infection (sham n = 8, EHEC O104:H4 n = 5, EHEC O157:H7 n = 4). Data are expressed as scatter dot plot with mean ± SD. *P < 0.05 vs. sham (one-way ANOVA, Holm-Sidak's multiple comparison test). **(B)** EPO plasma levels in mice with HUS on day 7 of experiment (sham n = 8, Stx n = 10) determined by ELISA. Data are expressed as scatter dot plot with mean ± SD, *P < 0.05 vs. sham (unpaired t-test).

Stx+EPO and Stx+pHBSP mice presented with increased plasma urea, creatinine and NGAL compared with sham mice (Figures 4A–C). PAS staining revealed renal tissue damage in all Stx-challenged groups irrespective of treatment (Figure 4D). KIM-1 expression was elevated in Stx+vehicle, Stx+EPO and Stx+pHBSP mice compared with sham mice (Figure 4E). In Stx+pHBSP compared with Stx+vehicle mice, KIM-1 expression was reduced (Figure 4E).

Effects of EPO and pHBSP treatment on intrarenal barriers in mice with HUS

The integrity of endothelial and epithelial barriers in the kidney is crucial for its function. It was demonstrated before that Stx can damage both endothelial as well as epithelial cells in the kidney and thereby influence the integrity of these barriers (1). We stained kidney sections for endothelial and epithelial cell

TABLE 2 Hematological, laboratory and renal function parameters in STEC-infected piglets and mock-infected controls (sham) assessed 4-6 days after infection.

-	ID	EPO (U/l)	Hb (g/l)	Hct (L/l)	LDH (U/l)	Crea (µmol/l)
sham	16	17.983	94.9	0.25	702	59
	32	19.211	95.86	0.27	1105	63
	33	10.827	79.3	0.24	901	57
	44	19.726	124.02	0.19	1445	67
	46	19.331	60.35	0.19	884	74
	47	21.491	69.92	0.21	924	73
	48	18.587	54.46	0.17	1145	60
	49	19.578	60.72	0.18	808	70
O104:H4	18	17.048	69.6	0.21	909	54
	19	25.473	97.5	0.27	997	59
	36	27.684	78.2	0.22	1767	73
	42	24.029	116.66	0.24	977	53
	43	22.659	96.42	0.29	1761	63
O157:H7	20	33.098	78.8	0.23	538	61
	21	26.325	97.9	0.26	804	52
	34	26.667	65.14	0.33	740	65
	35	27.173	*n.d.*	*n.d.*	680	72

Hb and Hct could not be assessed in one piglet of the O157:H7 group (n.d.). Hb, hemoglobin; Hct, hematocrit; LDH, lactate dehydrogenase; Crea, creatinine.

10.3389/fimmu.2022.1010882

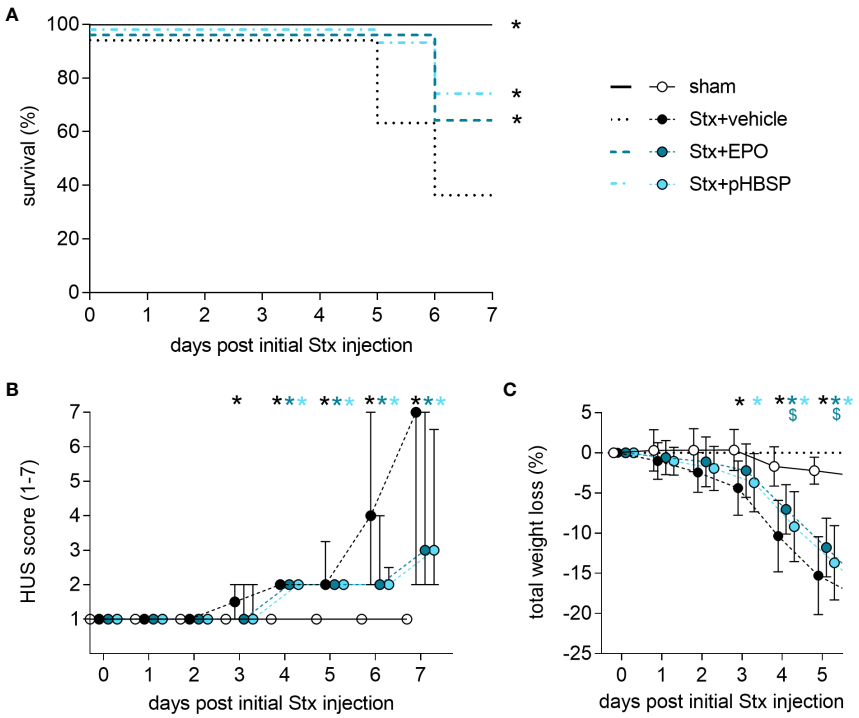

FIGURE 3
Effect of EPO and pHBSP treatment on survival and clinical presentation of mice with HUS. **(A-C)** Mice received either Stx or vehicle intravenously to induce experimental HUS. Mice with HUS were treated with vehicle (Ringer's solution 1 h post HUS induction s.c.), EPO (1 h post HUS induction s.c., 1000 IU/kg BW once) or pHBSP (1 h post HUS induction s.c., 30 µg/kg BW every 24 h; sham n = 15, Stx+vehicle n = 26, Stx+EPO n = 22, Stx+pHBSP n = 21). **(A)** Kaplan-Meier 7-day survival curves of sham mice, Stx-challenged mice treated with vehicle, Stx-challenged mice treated with EPO and Stx-challenged mice treated with pHBSP with humane endpoints. *P < 0.05 vs. Stx+vehicle (log-rank Mantel-Cox test). **(B)** Activity-based HUS score (ranging from 1-normally active, 2-active with slight restrictions, 3-active with clear intermissions, 4-slowed, 5-lethargic, 6-moribund, to 7-dead) was assessed three times daily and is depicted every 24 h until day 7 starting with first Stx injection. Data are expressed as median ± interquartile range. *P < 0.05 vs. sham (Kruskal-Wallis test, Dunn's multiple comparison test at every single time point). **(C)** Total weight loss referred to day 0 was assessed every 24 h and is depicted until day 5. Data are expressed as mean ± SD. *P < 0.05 sham vs. the respective color-coded group, $^{\$}$P < 0.05 vs. Stx+vehicle (two-way ANOVA, Holm-Sidak's multiple comparison test).

markers to assess the influence of EPO and pHBSP treatment on intrarenal barriers. Loss of renal CD31-positive endothelial cells (Figure 5A) and reduced E-cadherin expression was detected in kidneys of all Stx-challenged groups compared with sham mice (Figure 5B). However, E-cadherin expression was less decreased in Stx+pHBSP compared with Stx+vehicle and Stx+EPO mice (Figure 5B).

Effect of EPO and pHBSP treatment on microangiopathy in mice with HUS

GP1b was stained to highlight thrombocytes in the kidneys as indicators of microangiopathy (Figure 6A). An insignificant elevation of thrombocytes was observed in all Stx-challenged animals regardless of treatment, although it was weakest in the Stx+pHBSP group (Figure 6A). SFOG staining was performed to visualize fibrin deposits as indicators of microthrombi in renal sections (Figure 6B). Fibrin deposits were observed in all Stx-challenged groups compared with sham animals. There was an insignificant trend towards lower mean values of fibrin deposition in Stx+EPO and Stx+pHBSP mice compared with Stx+vehicle mice (Figure 6B).

Effects of EPO and pHBSP treatment on nitrosative and oxidative stress in mice with HUS

To further characterize the potential protective mechanism of EPO and pHBSP in HUS, surrogate parameters of nitrosative (nitrotyrosin formation) and oxidative (NOX-1 expression) stress were analyzed. Renal nitrotyrosine formation was elevated in all Stx-challenged groups compared with sham mice (Figure 7A). Compared with Stx+vehicle mice, formation of nitrotyrosine was decreased in the kidneys of Stx+EPO and Stx+pHBSP mice (Figure 7A). Compared with Stx+EPO mice, nitrotyrosine staining was even further decreased in Stx+pHBSP

10.3389/fimmu.2022.1010882

TABLE 3 Hematological and laboratory parameters of mice with HUS and effects of EPO and pHBSP treatment.

		sham	Stx+vehicle	Stx+EPO	Stx+pHBSP	P-values
clinical appearance	neurological symptoms	0/15 (0%)	10/26 (39%)	6/22 (27%)	5/21 (24%)	sham vs. Stx+vehicle: P = 0.0067
hematology	Hct (%)	34.8 ± 1.6	38.7 ± 2.5	39.1 ± 3.3	37.8 ± 2.3	sham vs. Stx+EPO: P = 0.005
	erythrocytes (cells/µl)	8162000 ± 337817	9196667 ± 477521	9200000 ± 811640	8926000 ± 546150	sham vs. Stx+vehicle: P = 0.0261
	Hb (g/dl)	11.3 ± 0.4	12.5 ± 0.6	12.6 ± 1	12.1 ± 0.8	sham vs. Stx+vehicle: P = 0.0374 sham vs. Stx+EPO: P = 0.0374
	thrombocytes (cells/µl)	890600 ± 71853	1078833 ± 123106	858167 ± 144950	1026400 ± 113372	Stx+vehicle vs. Stx+EPO: P = 0.0279
	leukocytes (cells/µl)	2500 ± 686	833.3 ± 151	1617 ± 799	1700 ± 957	sham vs. Stx+vehicle: P = 0.0059
	hemolysis score	0 ± 0	1.6 ± 1.4	1.3 ± 1.3	0.8 ± 1.1	sham vs. Stx+vehicle: P = 0.0023 sham vs. Stx+EPO: P = 0.013
laboratory markers	plasma ALAT (µmol/l*s)	0.6 ± 0.1	0.7 ± 0.2	0.6 ± 0.2	0.6 ± 0.2	ns
	plasma ASAT (µmol/l*s)	1.8 ± 1.1	2.6 ± 1.6	1.9 ± 1.1	1.3 ± 0.3	ns
	plasma LDH (µmol/l*s)	7.4 ± 2.9	16.4 ± 8.3	10.4 ± 4.6	8.1 ± 2.5	sham vs. Stx+vehicle: P = 0.0412
	plasma bilirubin (µmol/l)	2.0 ± 1.1	4.5 ± 1.5	5.0 ± 0.0	4.2 ± 1.1	sham vs. Stx+vehicle: P = 0.0153 sham vs. Stx+EPO: P = 0.0222
	plasma albumin (mg/dl)	13.5 ± 0.6	14.4 ± 1.0	15.0 ± 1.2	15.0 ± 0.7	sham vs. Stx+pHBSP: P = 0.0386

Hct, hematocrit; Hb, hemoglobin; ALAT, alanine aminotransferase; ASAT, aspartate aminotransferase; LDH, lactate dehydrogenase.

mice (Figure 7A). Of note, the predominantly glomerular staining of nitrotyrosine in Stx+vehicle mice was mitigated in Stx+EPO mice and attenuated in Stx+pHBSP mice (Figure 7A, arrowheads). NOX-1 expression was increased only in Stx+vehicle compared with sham mice, whereas Stx+pHBSP mice displayed lower NOX-1 expression compared with Stx +vehicle and Stx+EPO mice (Figure 7B).

Effect of EPO and pHBSP treatment on metabolome in mice with HUS

Oxidative stress and metabolism are closely interrelated and studies on the metabolome have not yet been reported in animal models of HUS. Therefore, we performed targeted metabolomics in the plasma of all four groups. Of the 630 metabolites analyzed in plasma, 426 were within the limit of detection. These 426 metabolites were analyzed using a linear regression model to test whether their abundance increases or decreases in the assigned order: sham–Stx+pHBSP–Stx+EPO–Stx+vehicle. 32 metabolites fitted this hypothesis, they are highlighted in heatmaps (Figures 8A, B) and assigned to the following substance classes: amino acids and derivatives (7/32), alkaloids (1/32), aminoxides (1/32, heatmap A) and lipids (23/32, triacylglycerides in heatmap B).

Discussion

To date, the role of EPO in HUS, a systemic orphan disease with occurrence of microangiopathic hemolytic anemia and AKI, has not been systematically investigated. We hypothesized that EPO treatment may be beneficial in patients with HUS-mediated hemolytic anemia and, targeting the IRR axis with EPO or non-hematopoietic EPO analogs, such as pHBSP, may convey nephroprotection in HUS.

The role of endogenous EPO levels in patients, piglets and mice with STEC-HUS

In response to cellular hypoxia (46), a regulatory increase in renal EPO secretion in patients with anemia would be expected. To our knowledge, there are no systematic studies on changes in endogenous EPO levels in adult patients with STEC-HUS and

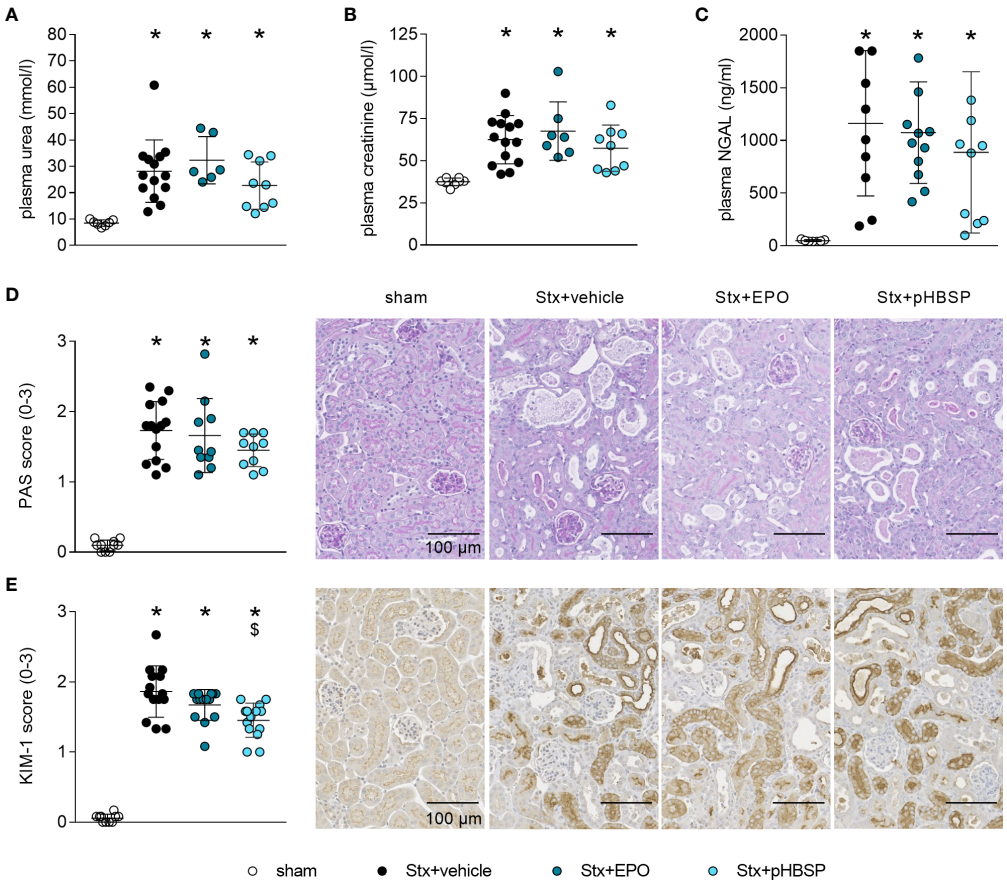

FIGURE 4
Effect of EPO and pHBSP treatment on kidney dysfunction and tubular injury in mice with HUS. Kidney injury and dysfunction was assessed on day 7 of HUS experiment. Plasma samples of mice with HUS and sham mice were analyzed for the kidney dysfunction parameters **(A)** urea and **(B)** creatinine (sham n = 7, Stx+vehicle n = 14, Stx+EPO n = 6, Stx+pHBSP n = 9) by an Architect^{TM} ci16200 System (Abbott), as well as the kidney injury marker **(C)** NGAL (sham n = 7, Stx+vehicle n = 10, Stx+EPO n = 12, Stx+pHBSP n = 10) by ELISA. **(A-C)** Data are expressed as scatter dot plot with mean ± SD. *P < 0.05 vs. sham (one-way ANOVA, Holm-Sidak's multiple comparison test). Quantification data as well as representative images (scale bar 100 µm) of **(D)** PAS staining (sham n = 10, Stx+vehicle n = 14, Stx+EPO n = 10, Stx+pHBSP n = 10, 10 fields per slide, score 0: no damage, 1: < 25% damaged, 2: 25–50% damaged, 3: > 50% damaged) and **(E)** immunohistochemical KIM-1 staining (score 0: < 25%, 1: 25–50%, 2: 50–75%, 3: > 75% strong positive staining per visual field, sham n = 10, Stx+vehicle n = 14, Stx+EPO n = 14, Stx+pHBSP n = 14, 12 fields per slide) in renal sections of sham and Stx-challenged mice. **(D, E)** Data are expressed as scatter dot plot with mean ± SD. *P < 0.05 vs. sham, $^{\$}$P < 0.05 vs. Stx+vehicle, (Kruskal-Wallis test, Dunn's multiple comparison test).

only one brief report in pediatric patients (32). We observed increased EPO serum levels in a small cohort of adult patients with STEC-HUS compared to healthy controls already at a reduced Hb level of about 11 g/dl. Our data showed no correlation between the degree of anemia and EPO levels. This observation is consistent with the above-mentioned report in children with STEC-HUS (32) and in critically ill patients with AKI of other origins (47–50). However, we cannot exclude a gender bias, as our patient cohort was mainly female as women were more frequently affected in the 2011 EHEC outbreak (51). Therefore, our observations should be validated in a larger, gender balanced cohort.

In the kidneys, EPO is produced by fibroblast-like type I interstitial cells located between peritubular capillaries and the proximal convoluted tubule (52). Thus, EPO expression is likely to be impaired when EPO-producing cells are damaged. Consistent with these considerations, patients with very high LDH or creatinine levels as surrogate parameters for tissue damage and renal dysfunction had the lowest EPO levels in our study. However, we found no correlation between LDH or creatinine levels and EPO levels in patients with HUS. We attribute this to the small number of patients studied. Nevertheless, clinical data suggests that EPO response appears to be impaired in STEC-HUS and EPO regulation may play an important role in the pathogenesis and disease resolution. Analyzing serum EPO levels in a larger cohort of patients with HUS and acute kidney injury of other origins may help to further elucidate whether the degree of renal dysfunction and/or injury

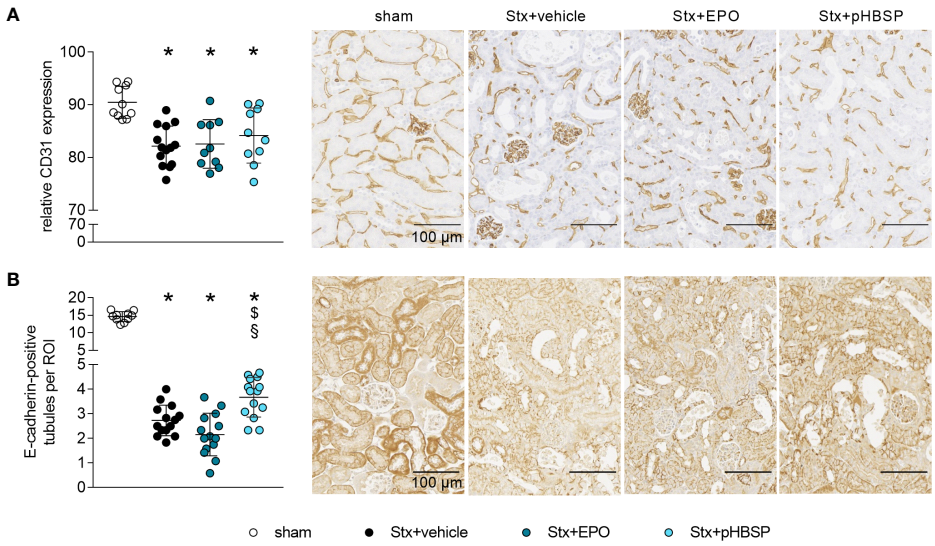

FIGURE 5
Effect of EPO and pHBSP treatment on intrarenal barriers in mice with HUS. Intrarenal barriers were assessed on day 7 of HUS experiment. Quantification data as well as representative images (scale bar 100 µm) of immunohistochemical **(A)** CD31 staining (sham n = 10, Stx+vehicle n = 14, Stx+EPO n = 10, Stx+pHBSP n = 10) and **(B)** E-cadherin (sham n = 10, Stx+vehicle n = 14, Stx+EPO n = 14, Stx+pHBSP n = 14), in renal sections of sham mice and mice subjected to Stx. **(A, B)** Data are expressed as scatter dot plot with mean ± SD. *P < 0.05 vs. sham, $P < 0.05 vs. Stx+vehicle, §P < 0.05 vs. Stx+EPO (one-way ANOVA, Holm-Sidak's multiple comparison test).

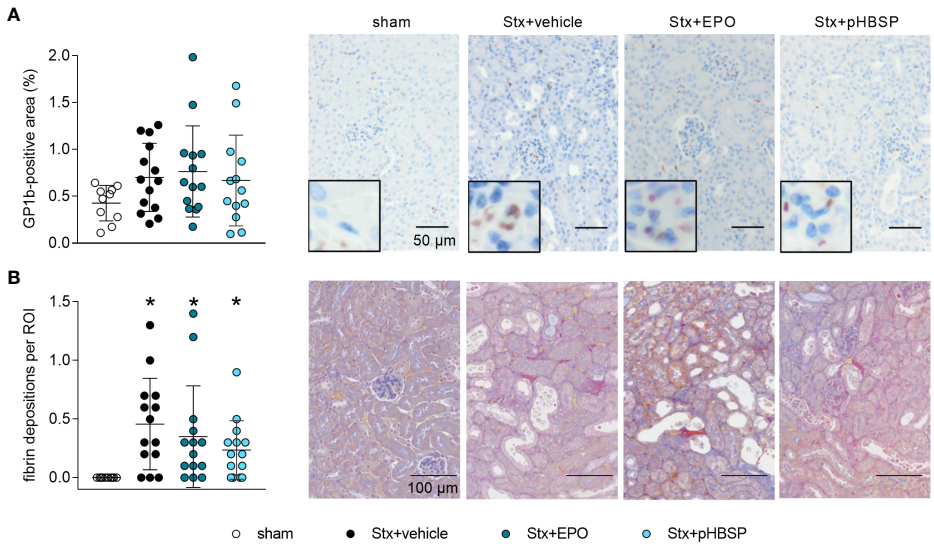

FIGURE 6
Effects of EPO and pHBSP treatment on microangiopathy in mice with HUS. Thrombocytes (indicated by glycoprotein 1b (GP1b) staining) and renal fibrin depositions (indicated by acid fuchsin orange G (SFOG) staining) were assessed on day 7 of HUS experiment. Quantification data and representative images of **(A)** immunohistochemical staining of thrombocytes (sham n = 10, Stx+vehicle n = 14, Stx+EPO n = 14, Stx+pHBSP n = 13) and **(B)** fibrin depositions (sham n = 10, Stx+vehicle n = 14, Stx+EPO n = 14, Stx+pHBSP n = 14) in kidney sections of sham mice and Stx-challenged mice. Quantitative data are expressed as scatter dot plot with mean ± SD. *P < 0.05 vs. sham (Kruskal-Wallis test, Dunn's multiple comparison test), scale bar 100 µm.

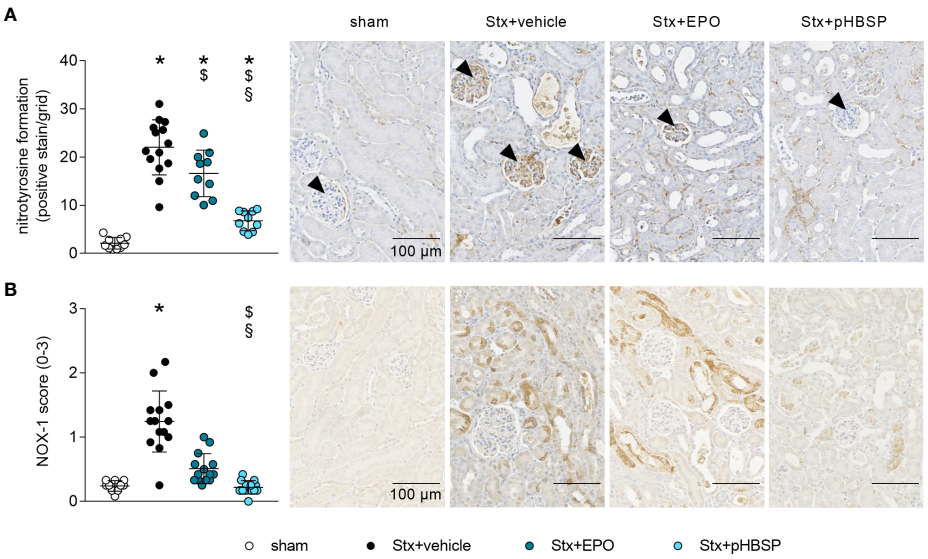

FIGURE 7
Effects of EPO and pHBSP treatment on nitrosative and oxidative stress in mice with HUS. Nitrosative and oxidative stress were assessed on day 7 of HUS experiment. Quantification data and representative images of immunohistochemical staining of **(A)** nitrotyrosine (sham n = 10, Stx+vehicle n = 14, Stx+EPO n = 10, Stx+pHBSP n = 10, arrowheads indicating glomeruli) and **(B)** NOX-1 (sham n = 10, Stx+vehicle n = 14, Stx+EPO n = 14, Stx+pHBSP n = 14) in kidney sections of sham mice and Stx-challenged mice. Quantitative data are expressed as scatter dot plot with mean ± SD. *P < 0.05 vs. sham, $P < 0.05 vs. Stx+vehicle, §P < 0.05 vs. Stx+EPO (A: one-way ANOVA, Holm-Sidak's multiple comparison test, B: Kruskal-Wallis test, Dunn's multiple comparison test), scale bar 100 µm.

correlates with the endogenous EPO production. Here, we pursued our line of thought by further conducting studies in animals with experimental HUS.

In gnotobiotic piglets with EHEC infection (9) and in mice after Stx challenge, we found an increase in EPO expression despite an absence of anemia in these animal models. We and others reported earlier that the extent of systemic hemolysis and subsequent anemia in experimental HUS is not as pronounced as in patients with HUS (9, 10, 14, 53, 54).

Based on pathophysiological considerations and evidence, these findings could imply that EPO expression in HUS does not increase proportionally to the extent of anemia but rather depends on the degree of renal hypoxia as first mechanistically described by Semenza et al. (55, 56). Microthrombotic occlusion in the kidneys can result in

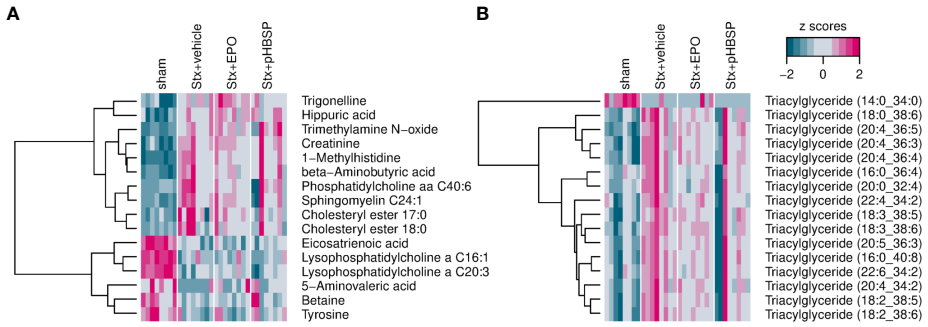

FIGURE 8
Effect of EPO and pHBSP treatment on plasma metabolome in mice with HUS. Metabolites in plasma of sham mice and Stx-challenged mice were assessed on day 7 of HUS experiment. Statistic modelling was performed to test the hypothesis that their abundance either increases or decreases in the following order: sham–Stx+pHBSP–Stx+EPO–Stx+vehicle **(A)** Small metabolites in murine plasma showing a significant trend for the four groups under investigation. **(B)** Triacylglyceroles in murine plasma showing a significant trend for the four groups under investigation. Data are shown as heatmaps depicting z-scores for all samples. The analytes were hierarchically clustered using Ward's minimum variance method (45) and an euclidian distance between z scores. Dendograms provide information about distances between clusters.

local hypoxia increasing the expression of the master regulator hypoxia-induced factor 1α (HIF-1α) and thereby EPO (57). However, direct damage to the EPO-expressing cells in the kidneys of HUS patients with hemolytic anemia may, especially in cases with severe renal injury, also result in insufficient EPO production to adequately stimulate hematopoiesis. Thus, patients with severe renal injury could benefit from treatment with exogenous EPO (58, 59).

EPO and pHBSP in the context of anemia correction and tissue protection

In our experimental setting, we observed a survival benefit in mice with HUS treated with either EPO or pHBSP. Tissue-protective effects of EPO and non-hematopoietic analogs have been the subject of discussion in the literature for nearly two decades (15, 16). Despite the observed beneficial effects of EPO in preclinical models of endotoxemia, sepsis, hemorrhagic shock and ischemia-reperfusion induced AKI (60–63), EPO failed to convey nephroprotection in several clinical trials that included patients following cardiac surgery (64, 65), cardiac arrest (66), kidney-transplantation (67) as well as ICU patients at risk for the development of AKI (EARLYARF trial) (68). However, in a small pilot trial with patients suffering from AKI after coronary artery bypass grafting surgery, treatment with EPO had a beneficial effect on all-cause mortality (69). Corwin et al. reported that administration of high-dose EPO (40,000 IU) to intensive care patients reduced the number of red blood cell transfusions without affecting mortality or clinical outcome (27). In a follow-up study of ICU patients, a subcohort of trauma patients treated with high-dose EPO showed no reduced need for red blood cell transfusions, however mortality was significantly reduced (18). Notably, an increase in thrombotic vascular events was noted in ICU patients who had not received thromboprophylaxis at baseline (18).

In the subset of mice surviving up to day 7 of the HUS experiments, we further investigated surrogate parameters for renal dysfunction and injury as well as barrier integrity, microangiopathy, oxidative and nitrosative stress and metabolome in plasma and/or renal tissue samples. As we have observed previously that AKI is accompanied by electrolyte imbalances, we propose that, in this model, mice die due to a severe AKI-induced hyperkalemia with subsequent cardiac arrhythmias and cardiac arrest (unpublished data). As fewer animals survived up to day 7 in the Stx+vehicle group (11/26, 42.3% survival) compared with the Stx+EPO (15/22, 68.2% survival) and Stx+pHBSP (16/21, 76.2% survival) group, the results need to be carefully interpreted in the light of a reverse survivorship bias, that might explain why we did not observe an effect of treatment with EPO or pHBSP on plasma creatinine, urea and NGAL, as surrogate parameters for AKI and renal dysfunction. However, we observed significant effects of EPO and/or pHBSP treatment on barrier integrity, oxidative and nitrosative stress and on selected metabolites in the samples studied.

Intact renal endothelial and epithelial barriers are important for the physiological function of the kidneys. We observed a pronounced Stx-induced damage of renal endothelial cells independent of treatment. Treatment with pHBSP, but not EPO led to a decrease in KIM-1 and an increase in E-cadherin expression in Stx-challenged mice in our setting. This could indicate less renal damage and enhanced epithelial barrier integrity, as tubular dedifferentiation – an important step in AKI progression – is characterised by a downregulation of E-cadherin (70). Although not resulting in amelioration of AKI in our model, this could have contributed to the increased survival observed after pHBSP treatment in Stx-challenged mice. In line with our results, the pharmaceutical upregulation of E-cadherin expression also proved nephroprotective in preclinical studies of cis-platin-induced AKI (71, 72).

In our recent study, we observed survival benefits in animals with reduced microangiopathy (11). Microangiopathy is a pathophysiological hallmark of HUS. As EPO can exert pro-thrombogenic effects, we consequently assessed the effects of EPO or pHBSP treatment on fibrin deposition and thrombocytes as surrogate parameters of microangiopathy to evaluate the potential of adverse treatment effects in HUS. Notably, we did not observe an aggravation of microthrombi formation or fibrin deposition in mice with HUS treated with either EPO or pHBSP.

Oxidative stress is involved in the pathogenesis of STEC-HUS (3–5). Nitrosative stress resembles a subtype of oxidative stress that has been shown to contribute to cell death (73). We observed an intense glomerular staining of nitrotyrosine in Stx+vehicle mice. Nitrotyrosine results from the reaction of the peroxynitrite radical – created when excess nitric oxide (NO) and superoxide radicals combine (74) – with accessible tyrosine residues (75). While basal NO plays a critical role in the regulation of the perfusion and vascular tone in glomeruli (74), it has been shown previously that inducible NO synthase (iNOS) induction and overproduction of NO had deleterious effects in ischemic AKI (76). In mice, iNOS is – among others – expressed in macrophages and glomerular mesangial cells and inducible by various pro-inflammatory stimuli (77). EPO and pHBSP have been demonstrated to reduce the expression of iNOS either on protein level in AKI of different etiologies (63, 78) or on mRNA level in lung and brain injury (79, 80). Thus, the reduction in renal nitrotyrosine staining in Stx+EPO and Stx+pHBSP mice could result from an inhibition of iNOS in the glomeruli of these mice.

Due to its critical role in the reabsorption of nutrients and maintenance of homeostasis, energy demand and metabolic activity are high in the kidneys (81). By analyzing the plasma metabolome, we observed an increase in triglycerides and cholesteryl esters in Stx-challenged mice that was consistently reported in HUS patients (82). Notably, we observed that alterations in some metabolites associated with kidney injury, e. g. trimethylamine N-oxide (83, 84) and trigonelline (85, 86) as well as lipid compounds were less distinct in mice with HUS after EPO or pHBSP treatment. In line with our results, a recent study demonstrated that EPO reduces lipidemia by stimulating lipid catabolism in peripheral adipose tissue (87). Further studies are required to examine the complex metabolic changes in animals and patients with HUS.

Taken together, we found that treatment with EPO or pHBSP positively affects several pathomechanisms of STEC-HUS which might explain the observed improvement in clinical outcome of mice with HUS. Further systematic studies in this context in animal models and even more importantly larger patient cohorts are needed to provide sufficient evidence to adjust clinical management.

Conclusion

We report here for the first time, that I) EPO levels in patients with STEC-HUS, STEC-infected piglets and Stx-challenged mice are elevated in a uniform manner, II) EPO or pHBSP treatment of mice with HUS improves survival and disease outcome, III) protective effects of pHBSP and EPO are associated with reduced renal oxidative stress, and IV) treatment with pHBSP in Stx-challenged mice is additionally associated with ameliorated nitrosative stress, less KIM-1 expression and tubular dedifferentiation. In the light of our results demonstrating favourable tissue-protective effects of EPO in a preclinical model, treatment of HUS-induced hemolytic anemia with EPO should be considered in patients. Further studies are needed to evaluate the effect of EPO and pHBSP treatment in clinical studies in patients with STEC-HUS.

Data availability statement

The metabolomics dataset presented in this study can be found in online repositories. The names of the repository/repositories and accession number(s) can be found below: https://www.ebi.ac.uk/biostudies/BioStudies accession number S-BSST657. Original data can be requested from sina.coldewey@med.uni-jena.de.

Ethics statement

The studies involving human participants were reviewed and approved by Ethics Committee of Hannover Medical School (1123-2011) and Ethics Committee of Friedrich Schiller University Jena (5276-09/17). The patients/participants provided their written informed consent to participate in this study. The animal studies were reviewed and approved by the Lower Saxony State Office for Consumer Protection and Food Safety (Approval Number: 33.9-42502-04-13/1149) and the regional animal welfare committee and the Thuringian State Office for Consumer Protection (registration number 02-058/14).

Author contributions

SC designed and planned the study; planned, performed and analyzed experiments and wrote the manuscript. SD planned, performed and analyzed experiments and wrote the manuscript. WP planned and performed histology and immunohistochemistry and analyzed data. BW planned and performed animal experiments. FG provided purified Stx and gnotobiotic piglet samples and contributed important intellectual content. DI synthesized and purified pHBSP and contributed important intellectual content. CD and KA performed histology and immunohistochemistry and contributed important intellectual content to histology and immunohistochemistry. JK provided HUS patient samples. IH-P provided gnotobiotic piglet samples. All authors provided important intellectual content and revised the manuscript prior to submission.

Funding

The research leading to these results has received funding from the German Research Foundation (DFG; Research Unit FOR1738, grant no. CO912/2-1 to SC and IM97/7-2 to DI) and the Federal Ministry of Education and Research (BMBF; ZIK Septomics Research Center, Translational Septomics, grant no. 03Z22JN12 to SC and Center for Sepsis Control and Care, project TaSep, grant no. 01EO1502 to SC).

Acknowledgments

We would like to thank J. Fischer (Septomics Research Center, Jena) and Dr. H. H. Brewitz (University of Bonn) for technical assistance, Prof. Dr. J. Menne (KRH Klinikum Siloah, Hannover) for provision of HUS patient samples and D. Driesch (BioControl) for support in metabolomics data analysis.

Conflict of interest

The authors declare that the research was conducted in the absence of any commercial or financial relationships that could be construed as a potential conflict of interest.

Publisher's note

All claims expressed in this article are solely those of the authors and do not necessarily represent those of their affiliated organizations, or those of the publisher, the editors and the reviewers. Any product that may be evaluated in this article, or claim that may be made by its manufacturer, is not guaranteed or endorsed by the publisher.

Supplementary material

The Supplementary Material for this article can be found online at: https://www.frontiersin.org/articles/10.3389/fimmu.2022.1010882/full#supplementary-material

References

1. Joseph A, Cointe A, Mariani Kurkdjian P, Rafat C, Hertig A. Shiga toxin-associated hemolytic uremic syndrome: A narrative review. *Toxins (Basel)* (2020) 12(2):32. doi: 10.3390/toxins12020067

2. Spinale JM, Ruebner RL, Copelovitch L, Kaplan BS. Long-term outcomes of shiga toxin hemolytic uremic syndrome. *Pediatr Nephrol* (2013) 28:2097–105. doi: 10.1007/s00467-012-2383-6

3. Ferraris V, Acquier A, Ferraris JR, Vallejo G, Paz C, Mendez CF. Oxidative stress status during the acute phase of haemolytic uraemic syndrome. *Nephrol Dial Transplant* (2011) 26:858–64. doi: 10.1093/ndt/gfq511

4. Kanzelmeyer NK, Pape L, Chobanyan-Jurgens K, Tsikas D, Hartmann H, Fuchs AJ, et al. L-arginine/NO pathway is altered in children with haemolytic-uraemic syndrome (HUS). *Oxid Med Cell Longev* (2014) 2014:203512. doi: 10.1155/2014/203512

5. Gomez SA, Abrey-Recalde MJ, Panek CA, Ferrarotti NF, Repetto MG, Mejias MP, et al. The oxidative stress induced *in vivo* by shiga toxin-2 contributes to the pathogenicity of haemolytic uraemic syndrome. *Clin Exp Immunol* (2013) 173:463–72. doi: 10.1111/cei.12124

6. Adamski J. Thrombotic microangiopathy and indications for therapeutic plasma exchange. *Hematol Am Soc Hematol Educ Program* (2014) 2014:444–9. doi: 10.1182/asheducation-2014.1.444

7. RKI. *Infektionsepidemiologisches jahrbuch meldepflichtiger krankheiten für 2020*. Robert Koch Institut (2020). Available at: https://www.rki.de/DE/Content/Infekt/Jahrbuch/Jahrbuch_2020.html.

8. Ministerio de Salud. *Boletín integrado de vigilancia N560 SE30 2021* (2021). Available at: https://bancos.salud.gob.ar/recurso/boletin-integrado-de-vigilancia-n560-se30-2021.

9. Wöchtl B, Gunzer F, Gerner W, Gasse H, Koch M, Bago Z, et al. Comparison of clinical and immunological findings in gnotobiotic piglets infected with escherichia coli O104:H4 outbreak strain and EHEC O157:H7. *Gut Pathog* (2017) 9:30. doi: 10.1186/s13099-017-0179-8

10. Dennhardt S, Pirschel W, Wissuwa B, Daniel C, Gunzer F, Lindig S, et al. Modeling hemolytic-uremic syndrome: In-depth characterization of distinct murine models reflecting different features of human disease. *Front Immunol* (2018) 9:1459. doi: 10.3389/fimmu.2018.01459

11. Pirschel W, Mestekemper AN, Wissuwa B, Krieg N, Kroller S, Daniel C, et al. Divergent roles of haptoglobin and hemopexin deficiency for disease progression of shiga-toxin-induced hemolytic-uremic syndrome in mice. *Kidney Int* (2022) 101(6):1171–85. doi: 10.1016/j.kint.2021.12.024

12. Sobbe IV, Krieg N, Dennhardt S, Coldewey SM. Involvement of NF-kappaB1 and the non-canonical NF-kappaB signaling pathway in the pathogenesis of acute kidney injury in shiga-toxin-2-induced hemolytic-uremic syndrome in mice. *Shock* (2021) 56:573–81. doi: 10.1097/SHK.0000000000001558

13. Keepers TR, Psotka MA, Gross LK, Obrig TG. A murine model of HUS: Shiga toxin with lipopolysaccharide mimics the renal damage and physiologic response of human disease. *J Am Soc Nephrol* (2006) 17:3404–14. doi: 10.1681/ASN.2006050419

14. Sauter KA, Melton-Celsa AR, Larkin K, Troxell ML, O'Brien AD, Magun BE. Mouse model of hemolytic-uremic syndrome caused by endotoxin-free shiga toxin 2 (Stx2) and protection from lethal outcome by anti-Stx2 antibody. *Infect Immun* (2008) 76:4469–78. doi: 10.1128/IAI.00592-08

15. Brines M, Patel NS, Villa P, Brines C, Mennini T, De Paola M, et al. Nonerythropoietic, tissue-protective peptides derived from the tertiary structure of erythropoietin. *Proc Natl Acad Sci United States America* (2008) 105:10925–30. doi: 10.1073/pnas.0805594105

16. Brines M, Grasso G, Fiordaliso F, Sfacteria A, Ghezzi P, Fratelli M, et al. Erythropoietin mediates tissue protection through an erythropoietin and common beta-subunit heteroreceptor. *Proc Natl Acad Sci United States America* (2004) 101:14907–12. doi: 10.1073/pnas.0406491101

17. Pearl RG. Erythropoietin and organ protection: lessons from negative clinical trials. *Crit Care* (2014) 18:526. doi: 10.1186/s13054-014-0526-9

18. Corwin HL, Gettinger A, Fabian TC, May A, Pearl RG, Heard S, et al. Efficacy and safety of epoetin alfa in critically ill patients. *N Engl J Med* (2007) 357:965–76. doi: 10.1056/NEJMoa071533

19. Ehrenreich H, Weissenborn K, Prange H, Schneider D, Weimar C, Wartenberg K, et al. Recombinant human erythropoietin in the treatment of acute ischemic stroke. *Stroke* (2009) 40:e647–56. doi: 10.1161/STROKEAHA.109.564872

20. Collino M, Thiemermann C, Cerami A, Brines M. Flipping the molecular switch for innate protection and repair of tissues: Long-lasting effects of a non-erythropoietic small peptide engineered from erythropoietin. *Pharmacol Ther* (2015) 151:32–40. doi: 10.1016/j.pharmthera.2015.02.005

21. Netrebenko AS, Gureev VV, Pokrovskii MV, Gureeva AV, Tsuverkalova YM, Rozhkov IS. Assessment of the nephroprotective properties of the erythropoietin mimetic peptide and infliximab in kidney ischemia-reperfusion injury in rats. *Arch Razi Inst* (2021) 76:995–1004. doi: 10.22092/ari.2021.355849.1728

22. Patel NS, Kerr-Peterson HL, Brines M, Collino M, Rogazzo M, Fantozzi R, et al. Delayed administration of pyroglutamate helix b surface peptide (pHBSP), a novel nonerythropoietic analog of erythropoietin, attenuates acute kidney injury. *Mol Med* (2012) 18:719–27. doi: 10.2119/molmed.2012.00093

23. Brines M, Dunne AN, van Velzen M, Proto PL, Ostenson CG, Kirk RI, et al. ARA 290, a nonerythropoietic peptide engineered from erythropoietin, improves metabolic control and neuropathic symptoms in patients with type 2 diabetes. *Mol Med* (2015) 20:658–66. doi: 10.2119/molmed.2014.00215

24. Dahan A, Dunne A, Swartjes M, Proto PL, Heij L, Vogels O, et al. ARA 290 improves symptoms in patients with sarcoidosis-associated small nerve fiber loss and increases corneal nerve fiber density. *Mol Med* (2013) 19:334–45. doi: 10.2119/molmed.2013.00122

25. Coldewey SM, Khan AI, Kapoor A, Collino M, Rogazzo M, Brines M, et al. Erythropoietin attenuates acute kidney dysfunction in murine experimental sepsis by activation of the beta-common receptor. *Kidney Int* (2013) 84:482–90. doi: 10.1038/ki.2013.118

26. Khan AI, Coldewey SM, Patel NS, Rogazzo M, Collino M, Yaqoob MM, et al. Erythropoietin attenuates cardiac dysfunction in experimental sepsis in mice *via* activation of the beta-common receptor. *Dis Model Mech* (2013) 6:1021–30. doi: 10.1242/dmm.011908

27. Corwin HL, Gettinger A, Pearl RG, Fink MP, Levy MM, Shapiro MJ, et al. Efficacy of recombinant human erythropoietin in critically ill patients: A randomized controlled trial. *JAMA* (2002) 288:2827–35. doi: 10.1001/jama.288.22.2827

28. MacLaren R, Gasper J, Jung R, Vandivier RW. Use of exogenous erythropoietin in critically ill patients. *J Clin Pharm Ther* (2004) 29:195–208. doi: 10.1111/j.1365-2710.2004.00552.x

29. Pasricha SR, Frazer DM, Bowden DK, Anderson GJ. Transfusion suppresses erythropoiesis and increases hepcidin in adult patients with beta-thalassemia major: A longitudinal study. *Blood* (2013) 122:124–33. doi: 10.1182/blood-2012-12-471441

30. Rasmussen SR, Kandler K, Nielsen RV, Jakobsen PC, Ranucci M, Ravn HB. Association between transfusion of blood products and acute kidney injury following cardiac surgery. *Acta Anaesthesiol Scand* (2020) 64:1397–404. doi: 10.1111/aas.13664

31. Schrezenmeier H, Noe G, Raghavachar A, Rich IN, Heimpel H, Kubanek B. Serum erythropoietin and serum transferrin receptor levels in aplastic anaemia. *Br J Haematol* (1994) 88:286–94. doi: 10.1111/j.1365-2141.1994.tb05020.x

32. Exeni R, Donato H, Rendo P, Antonuccio M, Rapetti MC, Grimoldi I, et al. Low levels of serum erythropoietin in children with endemic hemolytic uremic syndrome. *Pediatr Nephrol* (1998) 12:226–30. doi: 10.1007/s004670050443

33. Faquin WC, Schneider TJ, Goldberg MA. Effect of inflammatory cytokines on hypoxia-induced erythropoietin production. *Blood* (1992) 79:1987–94. doi: 10.1182/blood.V79.8.1987.1987

34. Erslev AJ. Erythropoietin. *N Engl J Med* (1991) 324:1339–44. doi: 10.1056/NEJM199105093241907

35. Deutsche Krebsgesellschaft, AWMF. *Supportive therapie bei onkologischen PatientInnen - langversion 1.0* (2016). Available at: http://leitlinienprogramm-onkologie.de/Supportive-Therapie.95.0.html.

36. K.D.I.O.K.A.W. Group. KDIGO clinical practice guideline for anemia in chronic kidney disease. *Kidney Inter Supplement* (2012) pp:279–335. doi: 10.1038/kisup.2012.35

37. Gesellschaft für Pädiatrische Nephrologie e.V. (GPN), AWMF. *Hämolytisch-urämisches syndrom im kindesalter* (2022). Available at: https://www.awmf.org/leitlinien/detail/ll/166-002.html.

38. Balestracci A, Capone MA, Meni Battaglia L, Toledo I, Martin SM, Beaudoin L, et al. Erythropoietin in children with hemolytic uremic syndrome: A pilot randomized controlled trial. *Pediatr Nephrol* (2022) 37(10):2383–92. doi: 10.1007/s00467-022-05474-9

39. Balestracci A, Martin SM, Toledo I, Alvarado C, Wainsztein RE. Early erythropoietin in post-diarrheal hemolytic uremic syndrome: A case-control study. *Pediatr Nephrol* (2015) 30:339–44. doi: 10.1007/s00467-014-2911-7

40. Pape L, Ahlenstiel T, Kreuzer M, Drube J, Froede K, Franke D, et al. Early erythropoietin reduced the need for red blood cell transfusion in childhood hemolytic uremic syndrome: a randomized prospective pilot trial. *Pediatr Nephrol* (2009) 24:1061–4. doi: 10.1007/s00467-008-1087-4

41. Woo da E, Lee JM, Kim YK, Park YH. Recombinant human erythropoietin therapy for a jehovah's witness child with severe anemia due to hemolytic-uremic syndrome. *Korean J Pediatr* (2016) 59:100–3. doi: 10.3345/kjp.2016.59.2.100

42. Kielstein JT, Beutel G, Fleig S, Steinhoff J, Meyer TN, Hafer C, et al. Best supportive care and therapeutic plasma exchange with or without eculizumab in shiga-toxin-producing e. coli O104:H4 induced haemolytic-uraemic syndrome: an analysis of the German STEC-HUS registry. *Nephrol Dial Transplant* (2012) 27:3807–15. doi: 10.1093/ndt/gfs394

43. Coldewey SM, Neu C, Baumbach P, Scherag A, Goebel B, Ludewig K, et al. Identification of cardiovascular and molecular prognostic factors for the medium-term and long-term outcomes of sepsis (ICROS): protocol for a prospective monocentric cohort study. *BMJ Open* (2020) 10:e036527. doi: 10.1136/bmjopen-2019-036527

44. Hochberg Y, Benjamini Y. More powerful procedures for multiple significance testing. *Stat Med* (1990) 9:811–8. doi: 10.1002/sim.4780090710

45. Murtagh F, Legendre P. Ward's hierarchical agglomerative clustering method: Which algorithms implement ward's criterion? *J Classif* (2014) 31:274–95. doi: 10.1007/s00357-014-9161-z

46. Lee P, Chandel NS, Simon MC. Cellular adaptation to hypoxia through hypoxia inducible factors and beyond. *Nat Rev Mol Cell Biol* (2020) 21:268–83. doi: 10.1038/s41580-020-0227-y

47. Matsuura R, Doi K, Komaru Y, Miyamoto Y, Yoshida T, Isegawa T, et al. Endogenous erythropoietin and hepatic dysfunction in acute kidney injury requiring renal replacement therapy. *Nephron* (2019) 142:10–6. doi: 10.1159/000496618

48. Morgera S, Heering P, Szentandrasi T, Niederau C, Grabensee B. Erythropoietin in patients with acute renal failure and continuous veno-venous haemofiltration. *Int Urol Nephrol* (1997) 29:245–50. doi: 10.1007/BF02551350

49. Tamion F, Le Cam-Duchez V, Menard JF, Girault C, Coquerel A, Bonmarchand G. Erythropoietin and renin as biological markers in critically ill patients. *Crit Care* (2004) 8:R328–35. doi: 10.1186/cc2902

50. Yamashita T, Noiri E, Hamasaki Y, Matsubara T, Ishii T, Yahagi N, et al. Erythropoietin concentration in acute kidney injury is associated with insulin-like growth factor-binding protein-1. *Nephrol (Carlton)* (2016) 21:693–9. doi: 10.1111/nep.12656

51. Frank C, Werber D, Cramer JP, Askar M, Faber M, an der Heiden M, et al. Epidemic profile of shiga-toxin-producing escherichia coli O104:H4 outbreak in Germany. *N Engl J Med* (2011) 365:1771–80. doi: 10.1056/NEJMoa1106483

52. Maxwell PH, Osmond MK, Pugh CW, Heryet A, Nicholls LG, Tan CC, et al. Identification of the renal erythropoietin-producing cells using transgenic mice. *Kidney Int* (1993) 44:1149–62. doi: 10.1038/ki.1993.362

53. Gunzer F, Hennig-Pauka I, Waldmann KH, Sandhoff R, Grone HJ, Kreipe HH, et al. Gnotobiotic piglets develop thrombotic microangiopathy after oral infection with enterohemorrhagic escherichia coli. *Am J Clin Pathol* (2002) 118:364–75. doi: 10.1309/UMW9-D06Q-M94Q-JGH2

54. Walsh PR, Johnson S. Treatment and management of children with haemolytic uraemic syndrome. *Arch Dis Child* (2018) 103:285–91. doi: 10.1136/archdischild-2016-311377

55. Semenza GL, Koury ST, Nejfelt MK, Gearhart JD, Antonarakis SE. Cell-type-specific and hypoxia-inducible expression of the human erythropoietin gene in transgenic mice. *Proc Natl Acad Sci United States America* (1991) 88:8725–9. doi: 10.1073/pnas.88.19.8725

56. Semenza GL, Nejfelt MK, Chi SM, Antonarakis SE. Hypoxia-inducible nuclear factors bind to an enhancer element located 3' to the human erythropoietin gene. *Proc Natl Acad Sci United States America* (1991) 88:5680–4. doi: 10.1073/pnas.88.13.5680

57. Corrado C, Fontana S. Hypoxia and HIF signaling: One axis with divergent effects. *Int J Mol Sci 21* (2020) 21(66):5611. doi: 10.3390/ijms21165611

58. Fishbane S, Coyne DW. How I treat renal anemia. *Blood* (2020) 136:783–9. doi: 10.1182/blood.2019004330

59. Mikhail A, Brown C, Williams JA, Mathrani V, Shrivastava R, Evans J, et al. Renal association clinical practice guideline on anaemia of chronic kidney disease. *BMC Nephrol* (2017) 18:345. doi: 10.1186/s12882-017-0688-1

60. Heitrich M, Garcia DM, Stoyanoff TR, Rodriguez JP, Todaro JS, Aguirre MV. Erythropoietin attenuates renal and pulmonary injury in polymicrobial induced-sepsis through EPO-r, VEGF and VEGF-R2 modulation. *BioMed Pharmacother* (2016) 82:606–13. doi: 10.1016/j.biopha.2016.05.045

61. Kwak J, Kim JH, Jang HN, Jung MH, Cho HS, Chang SH, et al. Erythropoietin ameliorates Ischemia/Reperfusion-induced acute kidney injury *via* inflammasome suppression in mice. *Int J Mol Sci 21* (2020) 21(10):3453. doi: 10.3390/ijms21103453

62. Ranjbaran M, Kadkhodaee M, Seifi B, Adelipour M, Azarian B. Erythropoietin attenuates experimental haemorrhagic shock-induced renal damage through an iNOS- dependent mechanism in male wistar rats. *Injury* (2017) 48:262–9. doi: 10.1016/j.injury.2017.01.010

63. Stoyanoff TR, Rodriguez JP, Todaro JS, Colavita JPM, Torres AM, Aguirre MV. Erythropoietin attenuates LPS-induced microvascular damage in a murine model of septic acute kidney injury. *BioMed Pharmacother* (2018) 107:1046–55. doi: 10.1016/j.biopha.2018.08.087

64. de Seigneux S, Ponte B, Weiss L, Pugin J, Romand JA, Martin PY, et al. Epoetin administrated after cardiac surgery: effects on renal function and inflammation in a randomized controlled study. *BMC Nephrol* (2012) 13:132. doi: 10.1186/1471-2369-13-132

65. Kim JH, Shim JK, Song JW, Song Y, Kim HB, Kwak YL. Effect of erythropoietin on the incidence of acute kidney injury following complex valvular heart surgery: a double blind, randomized clinical trial of efficacy and safety. *Crit Care* (2013) 17:R254. doi: 10.1186/cc13081

66. Guillemet L, Jamme M, Bougouin W, Geri G, Deye N, Vivien B, et al. Effects of early high-dose erythropoietin on acute kidney injury following cardiac arrest: exploratory *post hoc* analyses from an open-label randomized trial. *Clin Kidney J* (2020) 13:413–20. doi: 10.1093/ckj/sfz068

67. Sureshkumar KK, Hussain SM, Ko TY, Thai NL, Marcus RJ. Effect of high-dose erythropoietin on graft function after kidney transplantation: a randomized, double-blind clinical trial. *Clin J Am Soc Nephrol* (2012) 7:1498–506. doi: 10.2215/CJN.01360212

68. Endre ZH, Walker RJ, Pickering JW, Shaw GM, Frampton CM, Henderson SJ, et al. Early intervention with erythropoietin does not affect the outcome of acute kidney injury (the EARLYARF trial). *Kidney Int* (2010) 77:1020–30. doi: 10.1038/ki.2010.25

69. Oh SW, Chin HJ, Chae DW, Na KY. Erythropoietin improves long-term outcomes in patients with acute kidney injury after coronary artery bypass grafting. *J Korean Med Sci* (2012) 27:506–11. doi: 10.3346/jkms.2012.27.5.506

70. Zheng G, Lyons JG, Tan TK, Wang Y, Hsu TT, Min D, et al. Disruption of e-cadherin by matrix metalloproteinase directly mediates epithelial-mesenchymal transition downstream of transforming growth factor-beta1 in renal tubular epithelial cells. *Am J Pathol* (2009) 175:580–91. doi: 10.2353/ajpath.2009.080983

71. Gao L, Liu MM, Zang HM, Ma QY, Yang Q, Jiang L, et al. Restoration of e-cadherin by PPBICA protects against cisplatin-induced acute kidney injury by attenuating inflammation and programmed cell death. *Lab Invest* (2018) 98:911–23. doi: 10.1038/s41374-018-0052-5

72. Ni J, Hou X, Wang X, Shi Y, Xu L, Zheng X, et al. 3-deazaneplanocin a protects against cisplatin-induced renal tubular cell apoptosis and acute kidney injury by restoration of e-cadherin expression. *Cell Death Dis* (2019) 10:355. doi: 10.1038/s41419-019-1589-y

73. Wang F, Yuan Q, Chen F, Pang J, Pan C, Xu F, et al. Fundamental mechanisms of the cell death caused by nitrosative stress. *Front Cell Dev Biol* (2021) 9:742483. doi: 10.3389/fcell.2021.742483

74. Goligorsky MS, Brodsky SV, Noiri E. NO bioavailability, endothelial dysfunction, and acute renal failure: new insights into pathophysiology. *Semin Nephrol* (2004) 24:316–23. doi: 10.1016/j.semnephrol.2004.04.003

75. Korkmaz A, Kolankaya D. Inhibiting inducible nitric oxide synthase with rutin reduces renal ischemia/reperfusion injury. *Can J Surg* (2013) 56:6–14. doi: 10.1503/cjs.004811

76. Noiri E, Peresleni T, Miller F, Goligorsky MS. *In vivo* targeting of inducible NO synthase with oligodeoxynucleotides protects rat kidney against ischemia. *J Clin Invest* (1996) 97:2377–83. doi: 10.1172/JCI118681

77. Sharma K, Danoff TM, DePiero A, Ziyadeh FN. Enhanced expression of inducible nitric oxide synthase in murine macrophages and glomerular mesangial cells by elevated glucose levels: possible mediation *via* protein kinase c. *Biochem Biophys Res Commun* (1995) 207:80–8. doi: 10.1006/bbrc.1995.1156

78. Yang FL, Subeq YM, Chiu YH, Lee RP, Lee CJ, Hsu BG. Recombinant human erythropoietin reduces rhabdomyolysis-induced acute renal failure in rats. *Injury* (2012) 43:367–73. doi: 10.1016/j.injury.2011.11.013

79. Chen H, Luo B, Yang X, Xiong J, Liu Z, Jiang M, et al. Therapeutic effects of nonerythropoietic erythropoietin analog ARA290 in experimental autoimmune encephalomyelitis rat. *J Neuroimmunol* (2014) 268:64–70. doi: 10.1016/j.jneuroim.2014.01.006

80. Liu Y, Lu J, Wang X, Chen L, Liu S, Zhang Z, et al. Erythropoietin-derived peptide protects against acute lung injury after rat traumatic brain injury. *Cell Physiol Biochem* (2017) 41:2037–44. doi: 10.1159/000475434

81. Bhargava P, Schnellmann RG. Mitochondrial energetics in the kidney. *Nat Rev Nephrol* (2017) 13:629–46. doi: 10.1038/nrneph.2017.107

82. Kaplan BS, Gale D, Ipp T. Hyperlipidemia in the hemolytic-uremic syndrome. *Pediatrics* (1971) 47:776–9. doi: 10.1542/peds.47.4.776

83. Sun G, Yin Z, Liu N, Bian X, Yu R, Su X, et al. Gut microbial metabolite TMAO contributes to renal dysfunction in a mouse model of diet-induced obesity. *Biochem Biophys Res Commun* (2017) 493:964–70. doi: 10.1016/j.bbrc.2017.09.108

84. Tang WH, Wang Z, Kennedy DJ, Wu Y, Buffa JA, Agatisa-Boyle B, et al. Gut microbiota-dependent trimethylamine n-oxide (TMAO) pathway contributes to both development of renal insufficiency and mortality risk in chronic kidney disease. *Circ Res* (2015) 116:448–55. doi: 10.1161/CIRCRESAHA.116.305360

85. Chihanga T, Ma Q, Nicholson JD, Ruby HN, Edelmann RE, Devarajan P, et al. NMR spectroscopy and electron microscopy identification of metabolic and ultrastructural changes to the kidney following ischemia-reperfusion injury. *Am J Physiol Renal Physiol* (2018) 314(2)F154–66. doi: 10.1152/ajprenal.00363.2017

86. Won AJ, Kim S, Kim YG, Kim KB, Choi WS, Kacew S, et al. Discovery of urinary metabolomic biomarkers for early detection of acute kidney injury. *Mol Biosyst* (2016) 12:133–44. doi: 10.1039/C5MB00492F

87. Li J, Yang M, Yu Z, Tian J, Du S, Ding H. Kidney-secreted erythropoietin lowers lipidemia *via* activating JAK2-STAT5 signaling in adipose tissue. *EBioMedicine* (2019) 50:317–28. doi: 10.1016/j.ebiom.2019.11.007

frontiers | Frontiers in Immunology

TYPE Original Research
PUBLISHED 21 October 2022
DOI 10.3389/fimmu.2022.1034821

Check for updates

OPEN ACCESS

EDITED BY
Borna Relja,
Otto von Guericke University,
Germany

REVIEWED BY
Yukihiro Yamaguchi,
University of North Carolina at Chapel Hill, United States
Balachandar Selvakumar,
University of Sharjah, United Arab Emirates

*CORRESPONDENCE
Yufeng Liu
lyf6012@163.com
Tianyou Wang
Wangty999@sohu.com
Yong Zhong
1332388787@qq.com
Lian Ma
malian8965@sina.com

†These authors have contributed equally to this work and share first authorship

SPECIALTY SECTION
This article was submitted to Inflammation, a section of the journal Frontiers in Immunology

RECEIVED 02 September 2022
ACCEPTED 10 October 2022
PUBLISHED 21 October 2022

CITATION
Wang H, Luo J, Li A, Su X, Fang C, Xie L, Wu Y, Wen F, Liu Y, Wang T, Zhong Y and Ma L (2022) Proteomic and phosphorylated proteomic landscape of injured lung in juvenile septic rats with therapeutic application of umbilical cord mesenchymal stem cells. *Front. Immunol.* 13:1034821. doi: 10.3389/fimmu.2022.1034821

Proteomic and phosphorylated proteomic landscape of injured lung in juvenile septic rats with therapeutic application of umbilical cord mesenchymal stem cells

Hongwu Wang[1,2,3†], Junlin Luo[1†], Aijia Li[1], Xing Su[1], Chuiqin Fang[1], Lichun Xie[2,3,4], Yi Wu[1], Feiqiu Wen[2,3,5], Yufeng Liu[6*], Tianyou Wang[7*], Yong Zhong[8*] and Lian Ma[2,3,4,5*]

[1]Department of Pediatrics, The Second Affiliated Hospital of Shantou University Medical College, Shantou, China, [2]Department of Hematology and Oncology, Shenzhen Children's Hospital of China Medical University, Shenzhen, China, [3]Department of Hematology and Oncology, Shenzhen Children's Hospital, Shenzhen, China, [4]Department of Pediatrics, The Third Affiliated Hospital of Guangzhou Medical University (The Women and Children's Medical Hospital of Guangzhou Medical University), Guangzhou, China, [5]Department of Hematology and Oncology, Shenzhen Public Service Platform of Molecular Medicine in Pediatric Hematology and Oncology, Shenzhen, China, [6]Department of Pediatrics, The First Affiliated Hospital of Zhengzhou University, Zhengzhou, China, [7]Department of Hematology and Oncology, Beijing Children's Hospital, Capital Medical University, Beijing, China, [8]Department of Pediatrics, The Southeast General Hospital of Dongguan, Dongguan, China

Acute lung injury (ALI) is the most common complication of sepsis. Intravenous injection of HUMSCs can regulate the level of circulating endothelial cytokines and alleviate lung injury in juvenile septic rats. In this study, we performed proteomic and phosphorylated proteomic analysis of lung tissue of juvenile septic rats after Human Umbilical Cord Mesenchymal Stem Cells (HUMSCs) intervention for the first time, and screened the potential proteins and pathways of HUMSCs for therapeutic effect. The 4D proteome quantitative technique was used to quantitatively analyze the lung tissues of septic rats 24 hours (3 biological samples) and 24 hours after HUMSCs intervention (3 biological samples). A total of 213 proteins were identified as differentially expressed proteins, and 971 phosphorylation sites changed significantly. Based on the public database, we analyzed the functional enrichment of these proteins and phosphorylated proteins. In addition, Tenascin-C may be the key differential protein and ECM receptor interaction pathway may be the main signal pathway by using various algorithms to analyze the protein-protein interaction network. Phosphorylation analysis showed that tight junction pathway was closely related to immune inflammatory reaction, and EGFR interacted most, which may be the key differential phosphorylated protein. Finally, 123 conserved motifs of serine phosphorylation site (pS) and 17 conserved motifs of threonine (pT) phosphorylation sites were identified by motif analysis of phosphorylation sites. Results from proteomics and

phosphorylated proteomics, the potential new therapeutic targets of HUMSCs in alleviating lung injury in juvenile septic rats were revealed.

KEYWORDS

sepsis, pediatric, rat, cecal contents, umbilical cord mesenchymal stem cells, lung injury, proteomics, protein phosphorylation

Introduction

Lung is the main target organ of multiple organ dysfunction in sepsis (1). It has been reported in the literature that more than 50% of septic patients will have septic-induced acute lung injury (ALI) (2). At present, the main treatment for sepsis is still glucocorticoid, gamma globulin and symptomatic support treatment. There is no effective drug for septic lung injury except lung protective ventilation and fluid management strategy (3).

MSCs (Mesenchymal Stem Cells, MSCs) have immunomodulatory and paracrine functions (4, 5). In recent years, it has been reported that MSCs intervention can promote the repair of septic ALI and play a positive role (6–8). Studies have preliminarily confirmed that MSCs can effectively inhibit the secretion of cellular inflammatory factors and improve the prognosis of COVID-19 (9). The in-depth mechanism of MSCs-based therapy for septic lung injury is still not well defined. The therapeutic effect is affected by many factors, among which the interaction mechanism between MSCs and lung injury is an important factor (10).

Protein phosphorylation is the most common type of post-translational modification, and more than 30% of proteins in cells are phosphorylated, which is the most common and important mechanism to regulate protein function (11). Studies have found that MSCs can improve chronic inflammatory diseases such as chronic complications of diabetes, nerve cells and spinal cord injury by regulating key signaling pathways or protein phosphorylation (12–15).

Abbreviation: VEGFA, Vascular Endothelial Growth Factor A; ICAM1, Intercellular Adhesion Molecule 1; HUMSCs, Human Umbilical Cord Mesenchymal Stem Cells; DEPs, Differentially Expressed Proteins; DDPs, Differentially Phosphorylated Proteins; GO, Gene Ontology; KEGG, Kyoto Encyclopedia of Genes and Genomes; PPI, Protein Protein Interaction; PKs, Protein Kinase; ECM, Extracellular matrix; TNC, Tenascin-C; MIF, Macrophage migration Inhibitory Factor; PEG2, Prostaglandin E2; EGFR, Epidermal Growth Factor Receptor; mTOR, Rapamycin; pS, Phosphorylated Serine; pT, Phosphorylated Threonine; vWF, von Willebrand Factor; HMG-Box, High Mobility Group Box; CEs, Carboxylesterases; SEV, Small Extracellular Vesicles; MAPK, Mitogen Activated Protein Kinase; ALI, acute lung injury; UPLC, Ultra Performance Liquid Chromatography.

It has been reported that the phosphorylation level of nuclear factor (NF) -κB p65 in the lung tissue of septic mice decreased after the intervention of bone marrow stromal cell conditioned medium (MSC-CM), and the mechanism may be related to the inhibition of phosphorylation of NF-κB pathway by MSC-CM (16). The results showed that the intervention of HUMSCs reduced the expression of MyD88 mRNA and protein in the liver tissue of septic mice induced by cecal ligation and puncture (CLP), as well as the proportion of NFκB phosphorylation, which was closely related to the phosphorylation of MyD88-NFκB pathway (17). Pedrazza et al. found that MSCs can inhibit the activation of MAPK (mitogen-activated protein kinase, MAPK) pathway and regulate the inflammatory response in sepsis, and its mechanism may be directly related to the ability of BMMSCs to inhibit the phosphorylation of ERK, RSK and p38 in the MAPK family (18). Chen et al. showed that MSC SEV (Small Extracellular Vesicles, SEV) could improve the pulmonary microvascular permeability of ALI induced by sepsis, inhibit the pathological changes of lung tissue and the infiltration of neutrophils into lung tissue, and found that the protective effect of MSC SEV on lung may be related to its inhibition of phosphorylation of MAPK/NF-κB pathway and degradation of IκB (19).

Our study initially confirmed that HUMSCs can regulate the expression of endothelial cytokines through its immunomodulatory function, reduce inflammatory injury, and thus improve the symptoms and survival rate of juvenile septic rats. However, whether HUMSCs treatment can improve lung injury in juvenile septic rats, and which key proteins or protein phosphorylation modifications play a role still need further study.

Therefore, this study will use 4D proteome quantitative technology to quantitatively analyze the lung tissue proteome and protein phosphorylation modification group of 24 hours after sepsis (SIRs24) and 24 hours after HUMSCs intervention (MS24) in juvenile septic rats. Constructing a lung tissue-specific protein database, annotating common functions of the identified proteins, performing quantitative analysis of phosphorylation modification sites, performing difference screening according to the quantitative analysis result, performing motif analysis on the modification sites based on the difference analysis result, and

performing functional classification statistical analysis on the differentially modified proteins; Based on the statistical results of different classification methods, Fisher's exact test was used for enrichment analysis, and enrichment cluster analysis was used to compare the functional links of differentially modified proteins after HUMSCs intervention; Finally, protein interaction network (PPI) analysis was used to screen out the potential key regulatory modification proteins and reveal the potential molecular mechanism of HUMSCs to alleviate septic lung injury.

Materials and methods

Preparation of juvenile septic rats

Forty-one SPF grade 3-week-old SD rats were fed adaptively for one week, including 2 cecal contents donor rats, 6 normal rats (including 3 for sampling and 3 for mortality study), and 36 rats in the sepsis group of intraperitoneal injection of cecal contents solution (including 18 for sampling at different time points and 15 for mortality study). The pediatric sepsis rat model was induced by intraperitoneal injection of cecal content. When sepsis symptoms appeared after intraperitoneal injection of cecal contents (0 hour), the general condition of rats were evaluated at 3 hours, 9 hours, 24 hours, 48 hours and 72 hours after symptoms appeared. 3 rats were sacrificed at each observation time point to evaluate the sepsis model from the aspects of blood routine, biochemical indexes, immune cells, endothelial cytokines, nonspecific inflammatory factors, mortality, and pathological morphology of important organs such as lung and liver.The animal experiment was approved by the Ethics Committee of Shenzhen Topu Biological Laboratory Animal Center (Ethics Approval No.: TOP-IACUC-2021-0003).

Preparation of HUMSCs

Primary culture of HUMSCs: The acquisition and culture of fetal umbilical cord has been approved by the Ethics Committee of the Second Affiliated Hospital of Shantou University School of Medicine (Ethical Approval No.: 2021-89). After the birth of a healthy full-term newborn by cesarean section, the fetal umbilical cord was obtained under aseptic operation, placed in a 50ml centrifuge tube containing sterile PBS, and quickly transported to the laboratory in ice cubes. Clean and disinfect the ultra-clean table operated by a single person for at least 30 min, move the umbilical cord to another 50ml centrifuge tube filled with iodophor, and soak completely for 2-3min. Rinse the umbilical cord twice with 0.9% sterile saline, peel off the two umbilical arteries, umbilical vein and amniotic membrane, tear off Walton gum (umbilical cord matrix) with tweezers, cut it into 1-3mm3 tissue pieces, then lay the plates evenly, add DMEM/F12 medium containing 10% FBS, and culture it in a 5% CO_2 at 37 °C. After 7-14 days, cells can be observed under inverted phase contrast microscope, and cells can be changed or passaged according to the density of cell growth adherence.

Subculture of HUMSCs: When the primary cells of HUMSCs grow to 80-90% density in Petri dish under inverted phase contrast microscope, cell subculture can be carried out (taking 100 mm Petri dish as an example). Absorb and discard the old culture medium in a single-person ultra-clean table, gently wash it with sterile PBS preheated at 37 °C for 2 times, wash off dead cells, add 1 mL of EDTA trypsin containing 0.25%, shake well, put it at 37 °C, and incubate it in a 5% CO_2 for 1-2 min. Blow with a pipette gun until the adherent cells separate and fall off to form cell suspension. The 4 mL cell suspension was transferred into a 15 mL sterile centrifuge tube and whipped evenly. The 2 mL cell suspension was sucked out and placed in a new 100 mm cell culture dish at a ratio of 1: 2 or 1: 3. Each dish was supplemented to 8-10 mL, and then placed in a CO_2 culture dish to continue culture. When the cell density reached 90% again, cell passage could be carried out again. The third generation of HUMSCs (3×10^6/kg) was injected into juvenile septic rats *via* tail vein.

Experimental grouping

HUMSCs treatment group: The third generation HUMSCs (3×10^6/kg) were injected into juvenile septic rats through tail vein; Sepsis model group: The same amount of normal saline was injected into juvenile septic rats through tail vein. In this study, the lung tissue of septic rats 24 hours after sepsis (SIRs24) and 24 hours after HUMSCs intervention (MS24) were analyzed quantitatively in proteomic and phosphorylated groups.

Experimental materials and reagents

The materials and reagents required for sample preparation are shown in Supplementary Table 1.

Protein extraction

Take out the lung tissue sample to be tested from -80 °C, weigh a proper amount of lung tissue sample into a mortar precooled by liquid nitrogen, and add liquid nitrogen to fully grind it into powder. Samples in both groups were sonicated with four volumes of lysis buffer (8 M urea, 1% protease inhibitor, and 1% phosphatase inhibitor). Cell debris was removed by centrifugation at 12000 G for 10 min at 4 °C, and the supernatant was transferred to a new centrifuge tube for protein concentration determination by BCA kit.

Pancreatin enzymolysis

Take the same amount of protein from the lung tissue of the two groups for enzymolysis, and adjust to the same volume with the lysis solution. Slowly add TCA to a final concentration of 20%, vortex and mix, and precipitate at 4 °C for 2 hours. Then apply 4500 g, centrifuge for 5 min, discard the supernatant, and wash the precipitate 2-3 times with precooled acetone. After the precipitate was air-dried, TEAB with a final concentration of 200 mM was added, the precipitate was broken up by ultrasound, and trypsin was added at a ratio of 1:50 (protease: protein, m/m) for enzymolysis overnight. Dithiothreitol (DTT) was added to a final concentration of 5 mM and reduced at 56 °C for 30 min. Then iodoacetamide (IAA) was added to a final concentration of 11 mM and incubated at room temperature for 15 min in the dark.

Modification and enrichment

Dissolve the obtained peptide in the enrichment buffer solution (50% acetonitrile/6% trifluoroacetic acid), transfer the supernatant to the IMAC material washed in advance, and place it on a rotary shaker for incubation with mild shaking. After completion of the incubation, the resin was washed three times sequentially with the buffer solutions 50% acetonitrile/6% trifluoroacetic acid and 30% acetonitrile/0.1% trifluoroacetic acid. Finally, the modified peptide was eluted with 10% ammonia, and the eluate was collected and vacuum-frozen. Desalting was performed according to the instructions of C18 ZipTips after pumping, and the samples were subjected to liquid chromatography-mass spectrometry after vacuum freezing and pumping.

Liquid chromatography-mass spectrometry

Peptides were dissolved in the mobile phase A of liquid chromatography and separated by NanoElute UPLC (Ultra Performance Liquid Chromatography, UPLC) system. Mobile phase A was an aqueous solution containing 0.1% formic acid and 2% acetonitrile, and mobile phase B was a solution containing 0.1% formic acid and 100% acetonitrile. Liquid gradient setting: 0-78 min, 2% -22% B; 78-84 min, 22% -35% B; 84-87 min, 35% -90% B; 87-90 min, 90% B, flow rate maintained at 450 nL/min. Peptides were separated by UPLC and injected into Capillary ion source for ionization and then analyzed by timsTOF Pro mass spectrometry. The ion source voltage was set to 1.7 kV, and both the peptide parent ion and its secondary fragments were detected and analyzed using high-resolution TOFs. The scanning range of the secondary mass spectrum is set to be 100-1700. Data acquisition was performed using the Parallel Accumulation Serial Fragmentation (PASEF) mode. After a primary mass spectrum is collected, the secondary spectrum with the charge number of the parent ion in the range of 0-5 is collected in PASEF mode for 10 times, and the dynamic exclusion time of tandem mass spectrum scanning is set to 30 s to avoid repeated scanning of the parent ion.

Bioinformatics analysis methods

Annotation methods

GO annotation

The Gene Ontology, or GO, is a major bioinformatics initiative to unify the representation of gene and gene product attributes across all species. More specifically, the project aims to: 1. Maintain and develop its controlled vocabulary of gene and gene product attributes; 2. Annotate genes and gene products, and assimilate and disseminate annotation data; 3. Provide tools for easy access to all aspects of the data provided by the project. The ontology covers three domains: 1. Cellular component: A cellular component is just that, a component of a cell, but with the proviso that it is part of some larger object; this may be an anatomical structure (e.g. rough endoplasmic reticulum or nucleus) or a gene product group (e.g. ribosome, proteasome or a protein dimer). 2. Molecular function: Molecular function describes activities, such as catalytic or binding activities, that occur at the molecular level. GO molecular function terms represent activities rather than the entities (molecules or complexes) that perform the actions, and do not specify where or when, or in what context, the action takes place. 3. Biological process: A biological process is series of events accomplished by one or more ordered assemblies of molecular functions. It can be difficult to distinguish between a biological process and a molecular function, but the general rule is that a process must have more than one distinct steps. GO annotation proteome was derived from the UniProt-GOA database (http://www.ebi.ac.uk/GOA/). Firstly, Converting identified protein ID to UniProt ID and then mapping to GO IDs by protein ID. If some identified proteins were not annotated by UniProt-GOA database, the InterProScan soft would be used to annotated protein's GO functional based on protein sequence alignment method. Then proteins were classified by GO annotation based on three categories: biological process, cellular component and molecular function.

Domain annotation

A protein domain is a conserved part of a given protein sequence and structure that can evolve, function and exist independently of the rest of the protein chain. Each domain forms a compact three-dimensional structure and often can be

independently stable and folded. Many proteins consist of several structural domains. One domain may appear in a variety of differentially expressed proteins. Molecular evolution uses domains as building blocks and these may be recombined in different arrangements to create proteins with different functions. Domains vary in length from between about 25 amino acids up to 500 amino acids in length. The shortest domains such as zinc fingers are stabilized by metal ions or disulfide bridges. Domains often form functional units, such as the calcium-binding EF hand domain of calmodulin. Because they are independently stable, domains can be "swapped" by genetic engineering between one protein and another to make chimeric proteins.Identified proteins domain functional description were annotated by InterProScan (a sequence analysis application) based on protein sequence alignment method, and the InterPro domain database was used. InterPro (http://www.ebi.ac.uk/interpro/) is a database that integrates diverse information about protein families, domains and functional sites, and makes it freely available to the public *via* Web-based interfaces and services. Central to the database are diagnostic models, known as signatures, against which protein sequences can be searched to determine their potential function. InterPro has utility in the large-scale analysis of whole genomes and meta-genomes, as well as in characterizing individual protein sequences.

KEGG pathway annotation

KEGG connects known information on molecular interaction networks, such as pathways and complexes (the "Pathway" database), information about genes and proteins generated by genome projects (including the gene database) and information about biochemical compounds and reactions (including compound and reaction databases). These databases are different networks, known as the "protein network", and the "chemical universe" respectively. There are efforts in progress to add to the knowledge of KEGG, including information regarding ortholog clusters in the KEGG Orthology database. KEGG Pathways mainly including: Metabolism, Genetic Information Processing, Environmental Information Processing, Cellular Processes, Rat Diseases, Drug development. Kyoto Encyclopedia of Genes and Genomes (KEGG) database was used to annotate protein pathway. Firstly, using KEGG online service tools KAAS to annotated protein's KEGG database description. Then mapping the annotation result on the KEGG pathway database using KEGG online service tools KEGG mapper.

Subcellular localization

The cells of eukaryotic organisms are elaborately subdivided into functionally distinct membrane bound compartments. Some major constituents of eukaryotic cells are: extracellular space, cytoplasm, nucleus, mitochondria, Golgi apparatus, endoplasmic reticulum (ER), peroxisome, vacuoles, cytoskeleton, nucleoplasm, nucleolus, nuclear matrix and ribosomes. Bacteria also have subcellular localizations that can be separated when the cell is fractionated. The most common localizations referred to include the cytoplasm, the cytoplasmic membrane (also referred to as the inner membrane in Gram-negative bacteria), the cell wall (which is usually thicker in Gram-positive bacteria) and the extracellular environment. Most Gram-negative bacteria also contain an outer membrane and periplasmic space. Unlike eukaryotes, most bacteria contain no membrane-bound organelles, however there are some exceptions. There, we used wolfpsort a subcellular localization predication soft to predict subcellular localization. Wolfpsort is an updated version of PSORT/PSORT II for the prediction of eukaryotic sequences. Special for protokaryon species, Subcellular localization prediction soft CELLO was used.

Functional enrichment

Enrichment of gene ontology analysis

Proteins were classified by GO annotation into three categories: biological process, cellular compartment and molecular function. For each category, a two-tailed Fisher's exact test was employed to test the enrichment of the differentially expressed protein against all identified proteins. The GO with a corrected p-value < 0.05 is considered significant. Enrichment of pathway analysis: Encyclopedia of Genes and Genomes (KEGG) database was used to identify enriched pathways by a two-tailed Fisher's exact test to test the enrichment of the differentially expressed protein against all identified proteins. The pathway with a corrected p-value < 0.05 was considered significant. These pathways were classified into hierarchical categories according to the KEGG website. Enrichment of protein domain analysis: For each category proteins, InterPro (a resource that provides functional analysis of protein sequences by classifying them into families and predicting the presence of domains and important sites) database was researched and a two-tailed Fisher's exact test was employed to test the enrichment of the differentially expressed protein against all identified proteins. Protein domains with a corrected p-value < 0.05 were considered significant.

Enrichment-based clustering

For further hierarchical clustering based on differentially expressed protein functional classification (such as: GO, Domain, Pathway, Complex). We first collated all the categories obtained after enrichment along with their P values, and then filtered for those categories which were at least enriched in one of the clusters with P value <0.05. This filtered P value matrix was transformed by the function x = –log10 (P value). Finally these x values were z-transformed for each functional category. These z scores were then clustered by

one-way hierarchical clustering (Euclidean distance, average linkage clustering) in Genesis. Cluster membership were visualized by a heat map using the "heatmap.2" function from the "gplots" R-package.

Protein-protein interaction network

All differentially expressed protein database accession or sequence were searched against the STRING database version 11.0 for protein-protein interactions. Only interactions between the proteins belonging to the searched data set were selected, thereby excluding external candidates. STRING defines a metric called "confidence score" to define interaction confidence; we fetched all interactions that had a confidence score ≥ 0.7 (high confidence). Interaction network form STRING was visualized in R package "networkD3".

Results

Intraperitoneal injection of cecal contents to establish juvenile septic rat

About 4 hours after intraperitoneal injection of cecal content solution, 4-week-old SD rats have poor mental state, erect hair, accelerated breathing, curled up body, decreased vitality, reduced intake of water and slow response to stimulation, suggesting that pediatric rats have clinical manifestations of sepsis. Fifteen 4-week-old SD rats were intraperitoneally injected with cecal contents. 9 rats died within the observation time (72 hours), and the mortality was 60%. (Supplementary Figure 1A). Compared with the normal group, leukocytes, neutrophils and lymphocytes of rats with sepsis symptoms after intraperitoneal injection of cecal contents decreased significantly ($P < 0.05$), began to increase at 24 hours ($P < 0.05$), and monocytes decreased when pediatric rats had sepsis symptoms ($P < 0.05$), and began to rise at 9 hours. Platelets remained lower than normal level after the symptoms of sepsis in pediatric rats until the end of the observation period ($P < 0.05$) (Supplementary Figure 1B). Compared with the normal group, the expression of CRP, SAA, E-selectin, VEGFA, ICAM1 and NGAL at each time point after intraperitoneal injection of cecal content increased significantly ($P < 0.05$).and PGE2 decreased ($P < 0.05$) (Supplementary Figure 1C). After sepsis symptoms occurred in juvenile rats after intraperitoneal injection of cecal contents, HE staining of lung tissue showed thickening of alveolar wall, accompanied by granulocyte infiltration and falling cell fragments in local bronchus. 24 hours after the onset of sepsis symptoms occurred, HE staining of liver tissue showed that granular degeneration, loose cytoplasm and light staining of hepatocytes were widely seen around the central vein and portal area and in the liver parenchyma (Supplementary Figure 1D).

Culture, amplification and identification of HUMSCs

When human umbilical cord tissue mass was incubated in mesenchymal stem cell culture medium for 5-7 days, it can be seen that some tissue mass adhered to the wall and became round, and new cells crawled out around it, showing spindle shape and sparse distribution (Supplementary Figure 2A). After incubating for 7-10 days, the density of primary cells increased obviously, and tended to fuse. The cells were slender and enlarged in size, similar to fibroblasts. The growth rate of primary cells is slow, about 10-14 days, and the fusion degree of cells reaches 80%-90%, which can be passed. After passage, the cells grew rapidly, with 1: 3 passage. In this experiment, the third generation cells were used. At this stage, the cells were long spindle-shaped and had good growth vitality (Supplementary Figure 2B). Eight surface markers of MSCs were selected as the surface markers for detecting HUMSCs, which were CD 73, CD 90, CD 105, CD 11B, CD 34, CD 45 and HLA-DR. In this experiment, the surface markers of MSCs were selected from the third generation cells. The results showed that HUMACs stably expressed CD73 (99.01%), CD90 (95.6%) and CD105 (96.2%), and expressed CD11B (0.80%), CD19 (0.6%), CD34 (0.4%), CD45 (0.6%) and HLA-DR (0.6%) (Supplementary Figure 2C).

Proteomics dimension analysis of the mechanism of HUMSCs in the treatment of lung injury in juvenile septic rat

Difference of protein expression in lung tissue of juvenile septic rats treated with HUMSCs

In order to fully understand the mechanism of lung injury repair in juvenile septic rats after HUMSCs intervention, quantitative information was obtained by label-free quantitative proteomics. Based on the results of database search, the quality control analysis of peptides and modification sites was carried out on the lung tissues of juvenile septic rats 24 hours after HUMSCs intervention (MS24) and the lung tissues of juvenile septic rats without intervention (SIRs24). Most of the peptides were distributed in 7-20 amino acids, which was consistent with the general rules based on enzymatic digestion and mass spectrometry fragmentation. The distribution of peptide lengths identified by mass spectrometry met quality control requirements (Figure 1A); most proteins corresponded to more than two peptides. During quantification, one protein corresponding to multiple specific peptides (or corresponding to multiple spectra) is conducive to increasing the accuracy and credibility of the quantification results (Figure 1B); the coverage of most proteins is below 30% (Figure 1C); the molecular weight of the identified

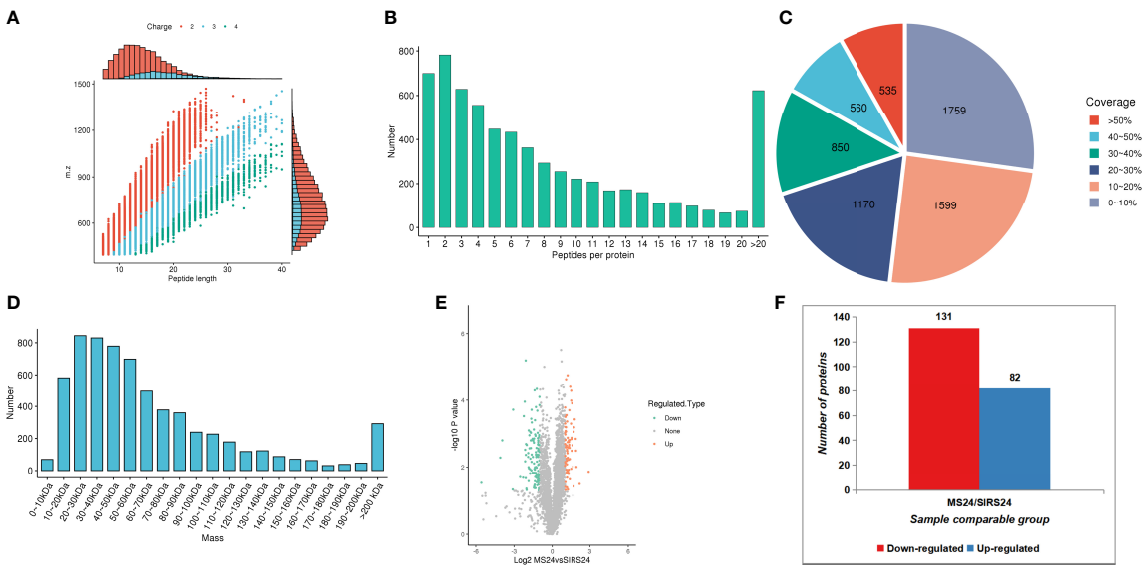

FIGURE 1
Proteomic quality control and DEPS identification after HUMSCs intervention. Peptide length distribution: most of the peptides were distributed in 7-20 amino acids **(A)**. Peptide number distribution: most proteins corresponded to more than two peptides **(B)**. Protein coverage distribution: the coverage of most proteins is below 30% **(C)**. Protein molecular weight distribution: the molecular weight of the identified protein is present at different stages and is evenly distributed **(D)**. Volcanogram showed the difference of protein expression between MS24 and SIRs24 group in lung tissue of juvenile septic rats **(E)**. The DEPS comparison between MS24 and SIRs24. 213 proteins were identified as DEPS (3.3% of 6438 proteins), of which 82 proteins were up-regulated and 131 proteins were down-regulated **(F)**.

protein is present at different stages and is evenly distributed (Figure 1D). The peptide length distribution, peptide number distribution, protein coverage distribution and protein molecular weight distribution all meet the quality control requirements. Volcanogram showed the difference of protein expression between MS24 and SIRs24 group in lung tissue of juvenile septic rats(Figure 1E). A total of 213 proteins (3.3% of 6438 proteins) were identified as difference of protein expression (DEPS) after HUMSCs intervention, of which 82 proteins were up-regulated and 131 proteins were down-regulated (Figure 1F), the top 20 proteins up-regulated and the top 20 proteins down-regulated (Supplementary Table 2).

Main functional protein mechanism of HUMSCs in treating lung injury in juvenile septic rats

GO annotation classification

The analysis according to GO classification (Figure 2A) shows that in the classification of biological processes, most proteins are involved in cellular processes and biological regulation; cellular components are dominated by intracellular fluid and protein-containing complexes; and molecular functions are classified in the categories of binding, catalytic activity, and molecular regulators. The immune system process categories contained 42 DEPSs, Mx1 (ratio 4.5, up-regulated), Rap2c (ratio 2.9481, up-regulated), TNC (ratio 2.8903, up-regulated), Arrdc1 (ratio 2.8117, up-regulated), AIF1 (ratio 0.4886, Down-regulation), MIF (ratio 0.4862, down-regulation) and UBXN1 (ratio 0.4776, down-regulation) were involved in the process of immune inflammation.

Subcellular structure annotation classification

In the subcellular structure annotation classification, the subcellular structure is dominated by cytoplasm (30.99%) and nucleus (29.11%) (Figure 2B).

COG functional classification

In the COG functional classification (Figure 2C), most of the proteins are in the signal transduction mechanism category (including 33 DEPS).

Main protein pathway mechanism and protein interaction network of HUMSCs in the treatment of lung injury in juvenile septic rats

Enrichment analysis of GO, KEGG pathways and protein domains of DEPs

GO classification, KEGG pathway and protein domain were used to analyze the differentially expressed proteins in the two groups.

The GO enrichment analysis showed (Figures 3A, B), based on the up-regulated protein enrichment in the biological process, the positive regulation of GTPase activity, pinocytosis,

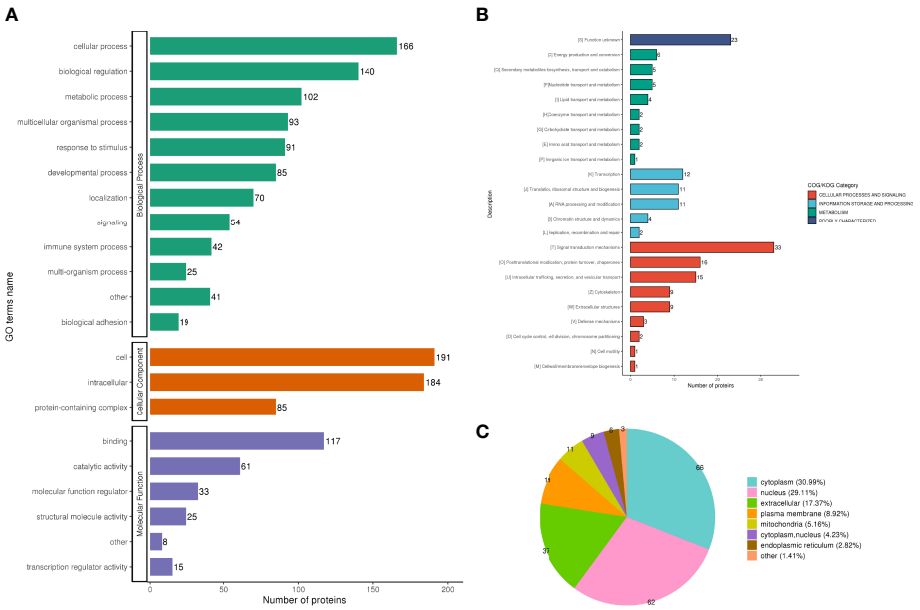

FIGURE 2
Functional classification of DEPS. GO classification, in the biological process classification, most proteins are involved in cellular processes and biological regulation; in the cellular component classification, most proteins are distributed in intracellular fluid and protein-containing complexes; in the molecular function classification, most of the proteins are in the categories of binding, catalytic activity and molecular regulators **(A)**. The subcellular structure was dominated by cytoplasm and nucleus **(B)**. COG functional classification showed that most of the proteins were in the signal transduction machinery category **(C)**.

antigen-stimulated inflammatory response, regulation of GTPase activity, regulation of mesenchymal stem cell proliferation, and regulation of B cell activation involved in immune response were enriched after the intervention of HUMSCs. The enrichment of down-regulated proteins in biological processes, including extracellular matrix organization, positive regulation of cell-matrix adhesion, positive regulation of cell-matrix adhesion, negative regulation of signal transduction, negative regulation of transferase activity, blood coagulation, fibrin clot formation, etc. Enrichment of up-regulated proteins based on molecular functions, such as class four-way junction DNA binding, DNA secondary structure binding, non-sequence-specific DNA binding, bending supercoiled DNA binding, GTPase activator activity, DNA binding and bending GTPase regulatory activity, molecular function regulators were enriched; Down-regulated proteins including structural molecule activity, 5.8 S rRNA binding, extracellular matrix structural components, ion channel inhibitor activity, channel inhibitor activity, structural components of ribosomes, and integrin binding were significantly present. In the classification of cell components, the up-regulated proteins were mainly enriched in the circulating endoplast membrane, and the down-regulated proteins were enriched in the extracellular matrix, extracellular zone, collagen-containing extracellular matrix, basement membrane, supramolecular polymers, supramolecular complexes, cytoplasmic ribosomes, extracellular space and other categories.

For KEGG enrichment of DEPS, we identified only 1 pathway from upregulated DEPS (Figure 3C) and 11 pathways from downregulated DEPs (Figure 3D). All of the significantly enriched pathways, ECM receptor interaction, PI3K-Akt signaling, and oxidative phosphorylation appear to be involved in the regulation of inflammatory responses.

Protein domain enrichment analysis, finding enrichment of important protein domains in upregulated DEPs, such as carboxylesterase family, HMG (High Mobility Group) box, trypsin, Dynamin family, homeobox domain (Figure 3E); The enrichment of important protein domains in down-regulated DEPs, It mainly includes von Willebrand factor type a domain, RNA recognition motif, C-terminal tandem repeat domain of type 4 procollagen, Lipocalin/cytoplasmic fatty acid-binding protein family, Cofilin/tropomyosin-type actin-binding protein, laminin-EGF-like domain (III and V), Laminin G domain (Figure 3F).

Cluster analysis of differentially expressed proteins

Go cluster analysis showed that DEPS was related to the positive regulation of cell-matrix adhesion, and the main cellular components were collagen-containing extracellular matrix, extracellular matrix and basement membrane. KEGG pathway

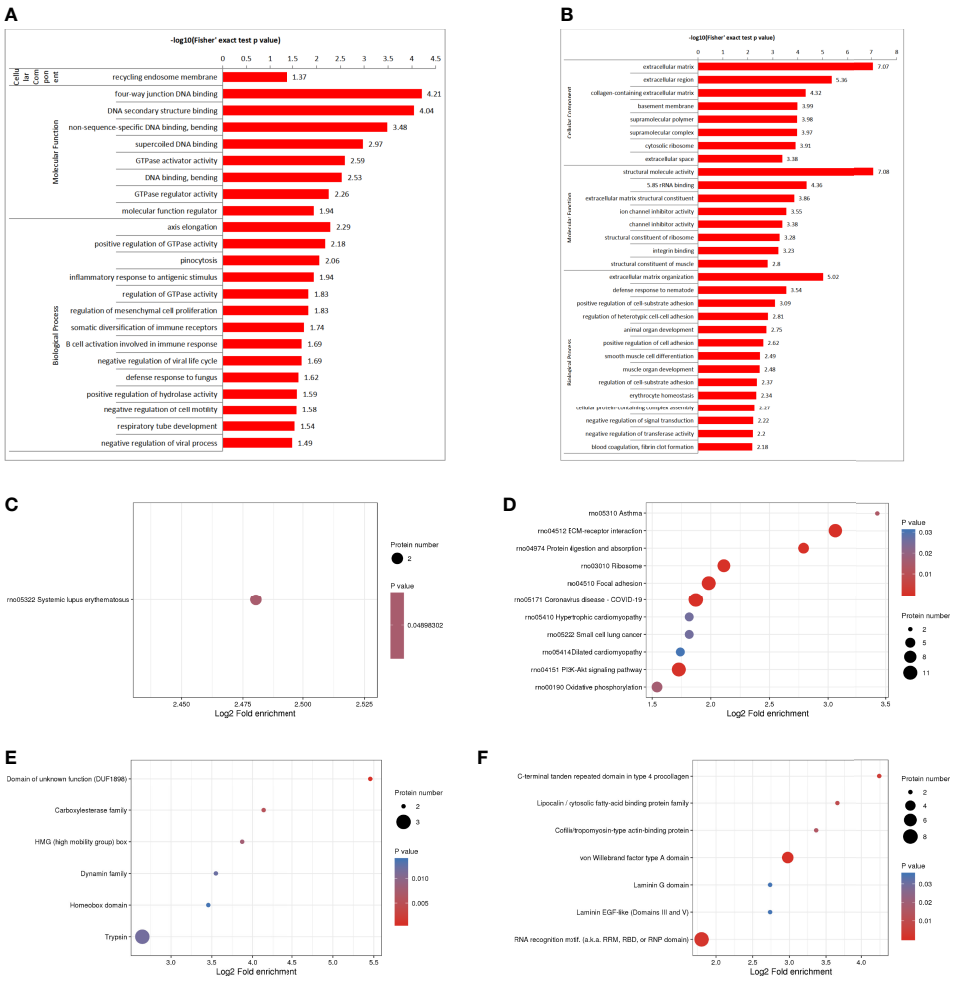

FIGURE 3
DEPS enrichment analysis. GO enrichment, up-regulated DEPS enrichmen **(A)**. GO enrichment, down-regulated protein enrichment **(B)**. KEGG enrichment of up-regulated DEPS **(C)**. KEGG enrichment of down-regulated DEPS **(D)**. Enrichment of important protein domains in upregulated DEPS **(E)**. Enrichment of important protein domains in downregulated DEPs **(F)**.

cluster analysis showed that most proteins were related to ECM receptor interaction and PI3K-Akt signaling pathway; Cluster analysis of protein domains revealed a predominance of EFG-like laminin (Figure 4).

PPI of differentially expressed proteins

PPI networks can identify and characterize relevant protein complexes, which is essential for understanding the molecular events involved. In order to clearly show the interaction between proteins, we selected the top 50 proteins with the closest interaction, and selected the top 15 proteins as hub proteins according to the degree (Supplementary Table 3). We found that some proteins were involved in the regulation of immune inflammatory response.

To perform PPI topology analysis, we combined known biomarker DEPs and applied them to plug-ins in the Molecular Complex Detection (MCODE) cellular landscape. Separation of dense regions and prediction of protein complexes by PPI subnetworks. MCODE got 36 modules and extracted 1 up-regulated DEP module (Figure 5A) and 3 most significant down-regulated DEP modules (Figures 5B–D).

Mechanism of HUMSCs in the treatment of lung injury in juvenile septic rats by phosphorylation modification omics dimension analysis

Difference of protein phosphorylation modification of HUMSCs in the treatment of lung injury in juvenile septic rats

Quality control evaluation is required for the data of mass spectrometry after the database search is completed. Most of the peptides are distributed in 7-20 amino acids, which is in line with

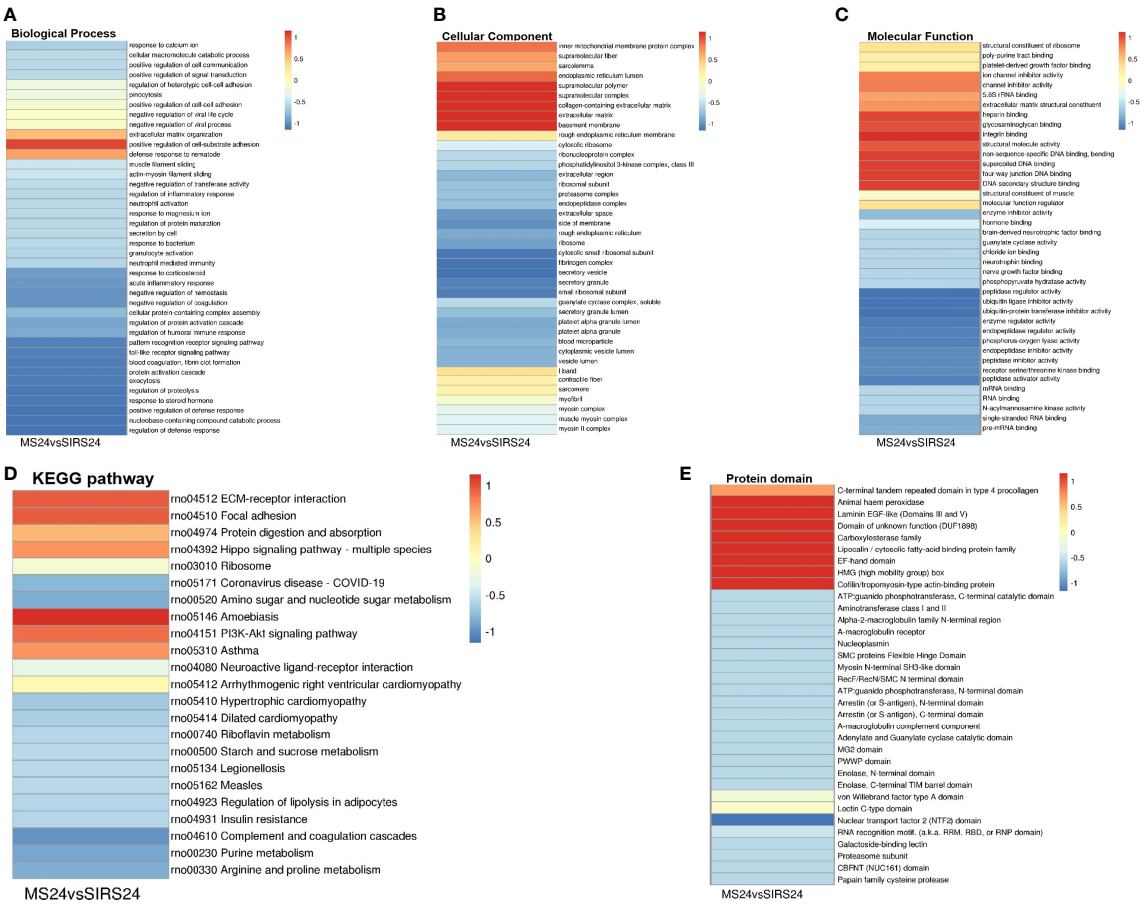

FIGURE 4
Cluster analysis of DEPS. The biological process cluster analysis of GO **(A)**. The cellular component analysis of GO **(B)**. The molecular function analysis **(C)**. The KEGG pathway cluster analysis **(D)**. Tthe protein domain cluster analysis **(E)**.

the general law based on enzymolysis and mass spectrometry fragmentation. The distribution of peptide lengths identified by mass spectrometry met the quality control requirements (Figure 6A). Phosphorylation changes in lung injury of juvenile septic rats after HUMSCs intervention were analyzed by protein phosphoromics, and 4840 phosphorylation sites were identified, of which 1725 sites were quantified (Figure 6B). Among all the quantified phosphorylation sites, 971 phosphorylation sites were significantly changed, of which 101 sites were up-regulated and 870 sites were down-regulated (Figure 6C).

Functional mechanism of DDPs in the treatment of lung injury in juvenile septic rats with HUMSCs

To investigate the protein phosphorylation modification group in the lung tissue of juvenile septic rats after HUMSCs intervention, we classified the phosphorylated proteins by GO, subcellular localization, and COG.

GO annotation classification

The two biological processes with the greatest changes in DPPs are cellular progression and biological regulation, the cellular components are mainly cells and intracellular fluids, and the molecular functions are mainly protein binding and catalytic activity (Figure 7A); The immune system process categories contained 95 DPPs, among which Rps17 (ratio 3.4465, up-regulated), ifitm3 (ratio 2.1523, up-regulated), Psme2 (ratio 2.2593, up-regulate), Snap29 (ratio 2.1905, up-regulate), Dync1i2 (ratio 0.2828, Down), Cd93 (ratio 0.2958, down), Cav1 (ratio 0.173, down), Pik3r4 (ratio 0.3905, down Down-regulation) and Lrrc8a (ratio 0.1174, down-regulation) were involved in the process of immune inflammation.

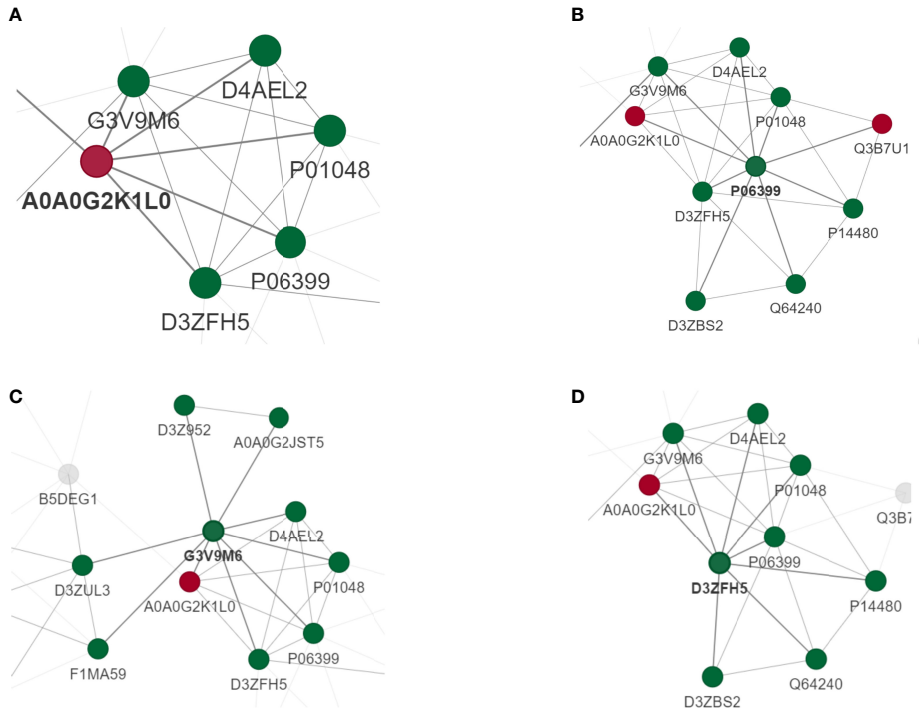

FIGURE 5
PPI analysis of DEPS. MCODE obtained 36 modules and extracted 1 up-regulated DEP module **(A)** and 3 most significant down-regulated DEP modules **(B–D)**.

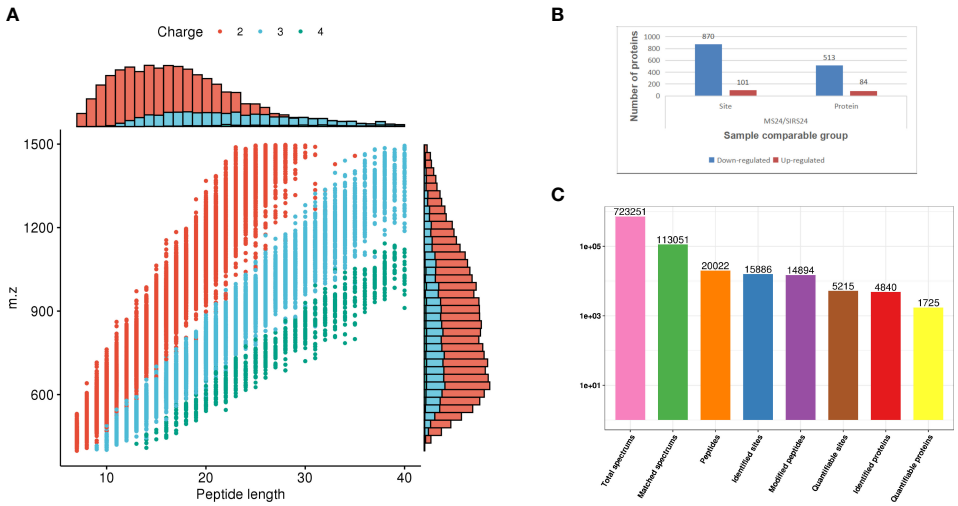

FIGURE 6
Data quality control and quantitative analysis of phosphorylation sites. The distribution of peptide length identified by mass spectrometry meets the quality control requirements **(A)**. 4840 phosphorylation sites were identified by protein phosphorylation analysis, of which 1725 were quantified **(B)**. 971 phosphorylation sites were significantly changed among all the quantified phosphorylation sites, of which 101 sites were up-regulated and 870 sites were down-regulated **(C)**.

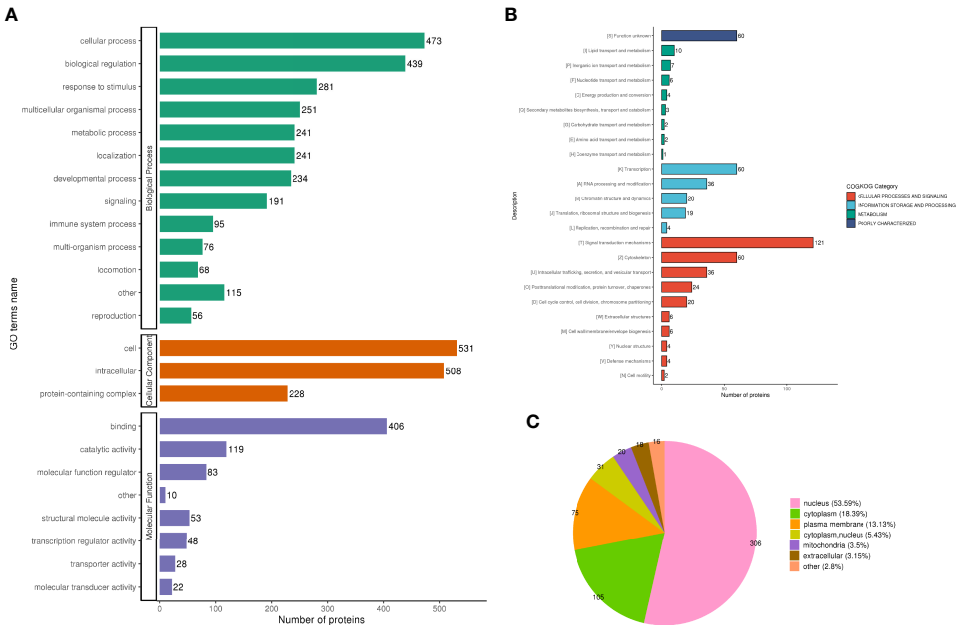

FIGURE 7
Functional classification of DPPs. GO classification analysis, the two biological processes with the greatest changes in DPPs are cellular progression and biological regulation, the cellular components are mainly cells and intracellular fluids, and the molecular functions are mainly protein binding and catalytic activity **(A)**. subcellular localization analysis, 571 phosphorylated proteins were quantitatively distributed in the nucleus (53.59%), cytoplasm (18.39%), and plasma membrane (13.13%) **(B)**. COG functional classification, most of the phosphorylated proteins that can be quantified are mainly in the categories of signal transduction mechanism (121 DPPs), transcription (60 DPPs), and cytoskeleton (60 Dpps) **(C)**.

Subcellular localization analysis

Five hundred and seventy-one phosphorylated proteins were quantitatively distributed in the nucleus (53.59%), cytoplasm (18.39%), and plasma membrane (13.13%) (Figure 7B).

Functional classification of COG

Most of the phosphorylated proteins that can be quantified are mainly in the categories of signal transduction mechanism (containing 121 DPPs), transcription (containing 60 DPPs), and cytoskeleton (containing 60 Dpps) (Figure 7C).

Key differential phosphorylated protein pathway mechanism and protein interaction network of HUMSCs in the treatment of lung injury in juvenile septic rats

GO and KEGG pathway enrichment analysis of DPPS

GO enrichment analysis of DPPs (Figures 8A, B)

In the HUMSCs intervention group, according to the classification of biological process enrichment, the response to rapamycin, plasma membrane repair, assembly of protein-containing complexes, oxidative phosphorylation, cortical cytoskeleton organization, RNA metabolic process, striated muscle contraction, and modification of synaptic structure were all enriched in the up-regulated phosphorylated proteins. In contrast, the regulation of cytoskeletal organization, organelle organization, supramolecular fiber organization, actin cytoskeletal organization, organelle organization and cell-substrate junction assembly is largely enriched in down-regulated phosphorylated proteins. Molecular function enrichment analysis showed that the binding categories were significantly enriched, such as RNA binding, complex-containing binding proteins, mRNA binding, actin filament binding, actin binding and structural molecular activity, which were enriched in up-regulated phosphorylated proteins. The down-regulated phosphorylated proteins mainly include structural components of the cytoskeleton, structural molecular activity, cytoskeletal protein binding, actin filament binding, and intercellular adhesion mediator activity. In cell component enrichment classification analysis, highly enriched categories included protein-containing complexes of upregulated phosphorylated proteins, ribonucleoprotein complexes, actin-based cell projection clusters, erect cilia, spliceosome complexes, erect cilia bundles, plasma membrane regions and cell division sites. For down-regulated

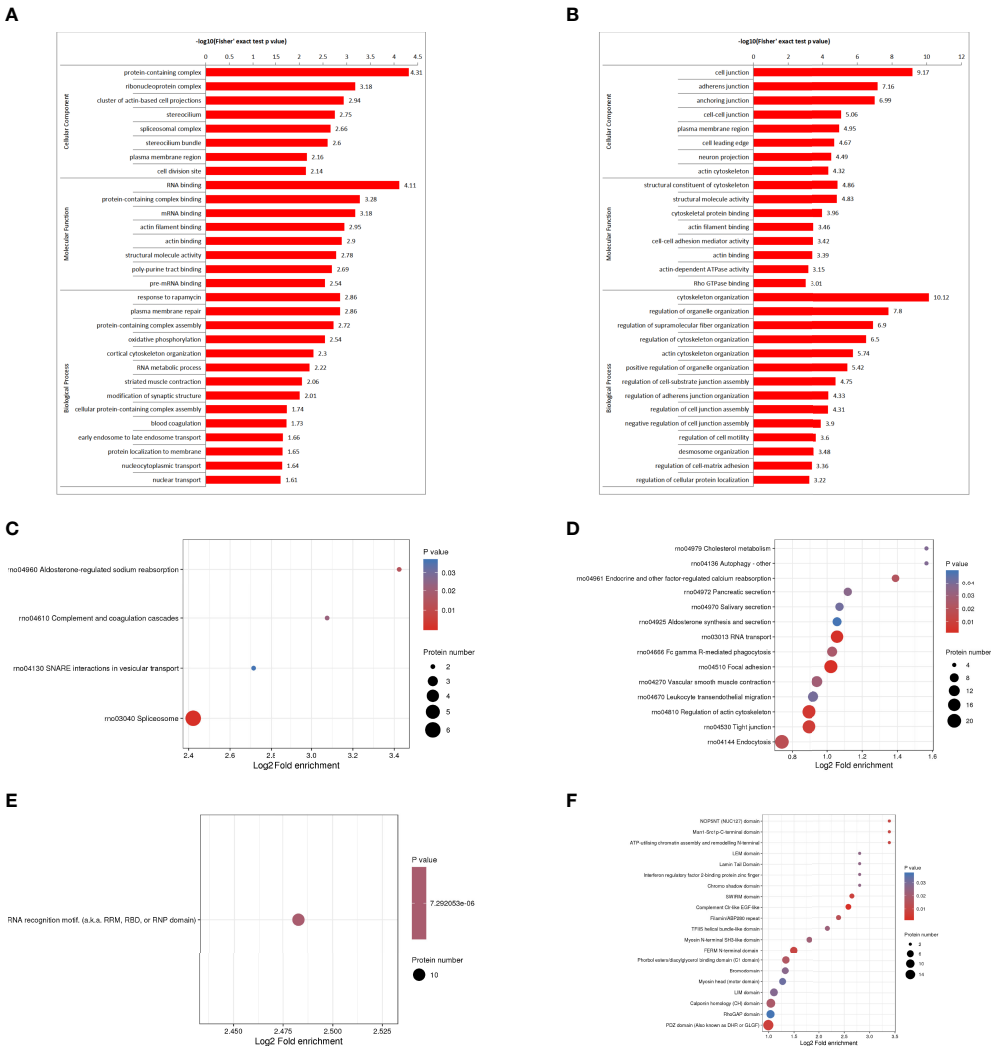

FIGURE 8
Functional enrichment analysis of DDPs. GO enrichment, up-regulated differentially phosphorylated protein enrichment **(A)**. GO enrichment, down-regulated differentially phosphorylated protein enrichment **(B)**. KEGG enrichment of up-regulated differently phosphorylated proteins **(C)**. KEGG enrichment of down-regulated differently phosphorylated proteins **(D)**. Enrichment of important protein domains in up-regulated differentially phospho-proteins **(E)**. Enrichment of important protein domains in down-regulated DDPs **(F)**.

phosphorylated proteins, cell junctions, adherens junctions, anchor junctions, intercellular junctions, and plasma membrane regions were largely enriched.

KEGG pathway enrichment analysis of DPPs (Figures 8C, D)

KEGG pathway analysis was performed on DPPs, and 4 pathways were identified from the upregulated DPPs, including spliceosome, aldosterone-regulated sodium reabsorption, complement and coagulation cascade, and trap interaction pathway in vesicular transport. Phosphoproteome data showed that phosphorylation levels were down-regulated in focal adhesion pathway, RNA transport pathway, actin cytoskeleton regulation pathway, tight junction pathway, endocytosis pathway, endocrine and other factors regulating calcium reabsorption pathway and FcγR-mediated phagocytosis pathway. Tight junctions encode genes for epithelial intercellular connexins, indicating that there is interference in the permeability between epithelial barriers, which may be closely related to the regulation of intercellular barriers in septic lung injury (Supplementary Figure 4).

Protein domain enrichment analysis of DPPs

We found that only RNA recognition motifs (RNP domains) were enriched in upregulated DPPs (Figure 8E). Enrichment of important protein domains in down-regulated DPPs, mainly including complement CLR-like EGF-like, PDZ domain,

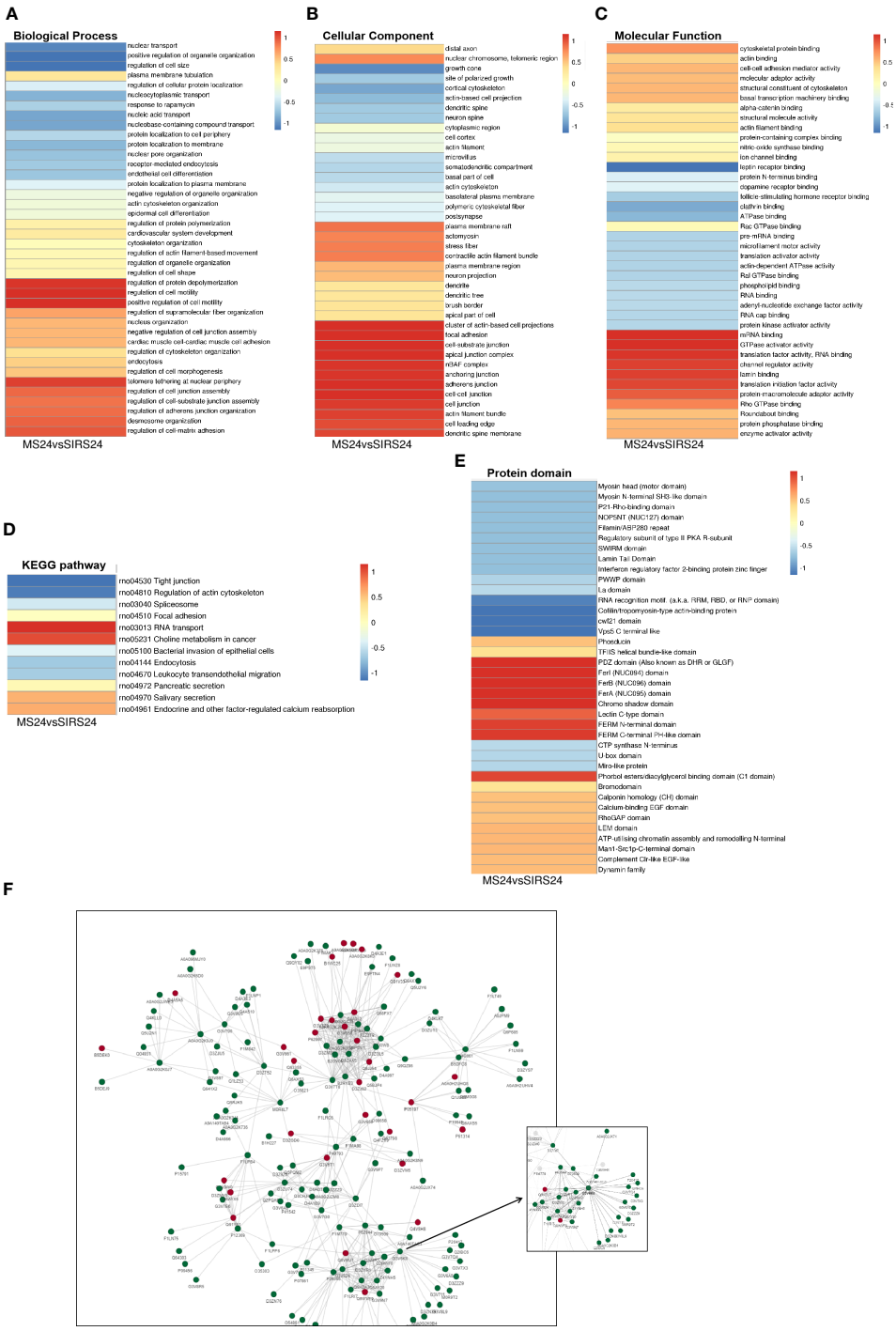

FIGURE 9
Cluster Analysis and Protein interaction network (PPI) of DDPs. Biological process cluster analysis of GO **(A)**. Cell component analysis of GO **(B)**. Molecular function analysis **(C)**. Cluster analysis of KEGG pathway **(D)**. Cluster analysis of protein domains **(E)**. The top 50 phosphorylated proteins with the closest interaction were selected, and a network containing a total of 173 related phosphorylated proteins was generated. G3V6K6 (EGFR) has 29 nodes **(F)**.

SWIRM domain, FERM N-terminal domain, NOP5NT (NUC127) domain, Man1-Src1p-C-terminal domain, ATP-utilizing chromatin assembly, and N-terminal remodeling (Figure 8F).

Cluster analysis and protein interaction network (PPI) of DDPs

Go cluster analysis showed that DPPs were associated with the regulation of protein unwinding and polymerization, the regulation of cell motility, and the positive regulation of cell motility (Figure 9A). Cellular components are dominated by actin-based cell projection clusters, focal adhesions, cell-base junctions, apical junction complexes, nBAF complexes, anchored junctions, adherens junctions, intercellular junctions, etc. (Figure 9B). Molecular function analysis showed that most of the phosphorylated proteins were associated with mRNA binding, GTPase activating factor activity, translation factor activity, RNA banding, channel regulator activity, etc. (Figure 9C). Cluster analysis of the KEGG pathway revealed that most of the phosphorylated proteins were involved in RNA transport (Figure 9D). Cluster analysis of the protein structural domains showed that they were closely related to the PDZ domain, FerI domain, FerB domain, FerA domain, chromosome shadow domain, etc. (Figure 9E).

We selected the top 50 phosphorylated proteins with the closest interaction and generated a network containing a total of 173 related phosphorylated proteins (Figure 9F). The Phosphorylated proteins with more interactions include Egfr, Sf3b1, U2af2, Srsf1, Srrm1, Arrb1, Hnrnpd, Igf2r, Srsf11 and Srrm2. Among them, G3V6K6 (EGFR) has 29 nodes, D4A9L2 (SRSF1) has 24 nodes, Q9JJ54 (Hnrnpd) has 21 nodes and G3V824 (Igf2r) has 21 nodes. It is also valuable for other analyses in this study. G3V6K6 (EGFR) interaction is the most (29 nodes), which may be involved in the repair process of septic lung injury.

Motif analysis of key phosphorylation sites of HUMSCs in the treatment of lung injury in juvenile septic rats

Protein phosphorylation is regulated by protein kinases (PKs), and different PKs prefer specific substrates with conserved motifs. We performed a bioinformatic analysis to identify novel phosphorylation motifs using a large number of phosphorylation sites found in this study. We performed intensive sequence analysis of hyperphosphorylated site motifs around the phosphate groups (10 amino acids upstream and 10 amino acids downstream of each phosphate group) of serine and threonine residues using the Motify-X program.

Among the 1316 phosphorylation sites, we identified 123 conserved motifs based on phosphorylated serine (pS) phosphorylation sites and 17 conserved motifs based on phosphorylated threonine (pT) phosphorylation sites.

We generated heat maps (Figure 10A) to show the enrichment or depletion of specific amino acids near the serine phosphorylation site. D, E, P, R and S have a tendency to move to the vicinity of serine phosphorylation sites. P, R, S are largely represented in the proximal region of the threonine phosphorylation site (Figure 10B). These amino acids close to the phosphorylation sites preferentially reflect the specific recognition of enzymes that catalyze phosphorylation in septic lung tissue after HUMSCs intervention. Further studies are

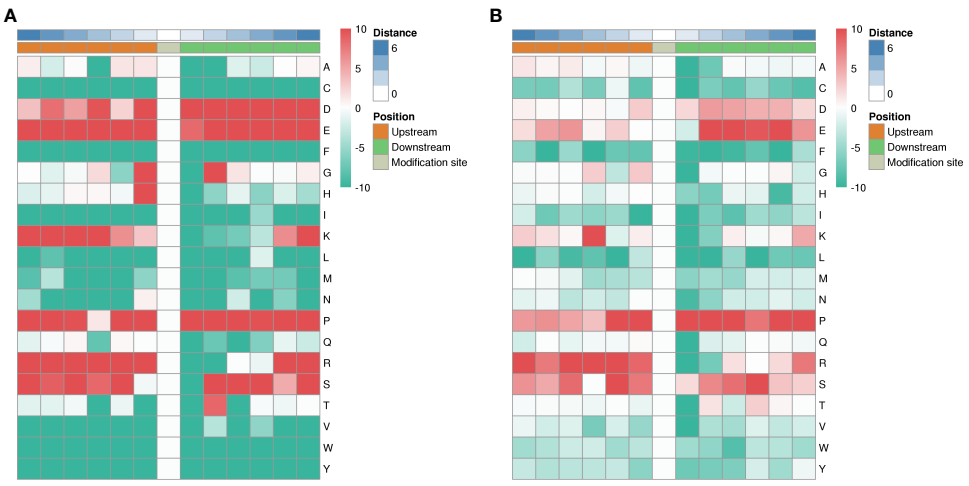

FIGURE 10
Motif analysis of phosphorylation sites. Heat map showing enrichment or depletion of specific amino acids near the serine phosphorylation site. D, E, P, R, and S tend to be near the serine phosphorylation site **(A)**. P, R, S are largely represented in the proximal region of the threonine phosphorylation site **(B)**.

needed to investigate whether different types of enzymes and kinases are active in regulating phosphorylation.

Discussion

Sepsis is a systemic inflammatory response syndrome caused by external pathogenic microorganism infection. The development of children's immune system is still imperfect, which can easily lead to multiple organ failure. The most common complications of ALI (20, 21), which can lead to bronchial epithelial cell injury, inflammatory cell infiltration in alveolar wall, and severe damage of lung blood barrier-capillary barrier. Cause respiratory failure (22). Studies have shown that MSC can alleviate ALI in sepsis through direct or paracrine effects (23, 24). In recent years, studies have confirmed that HUMSCs have immunomodulatory properties (4), and have made progress in the treatment of sepsis preclinical research (25).

The results of our study showed that the swelling of bronchial epithelial cells and the inflammatory cells on the alveolar wall were reduced by he staining after 24 hours of HUMSCs intervention (Supplementary Figure 1); the damage of lung blood and air barrier-capillary was reduced by transmission electron microscopy (Supplementary Figure 4). Endothelial cytokines E-selectin, VEGFA, ICAM1, and NGAL were significantly decreased, and PGE2 was elevated (Supplemental Figure 5). In conclusion, HUMSCs intervention can significantly reduce the inflammation of endothelial cells in blood circulation and lung tissue, improve the lung gas-blood barrier, and promote the repair of lung injury in juvenile septic rats. However, its molecular mechanism still needs to be further studied and clarified.

Phosphorylation modification is the most basic, common and important mechanism to regulate protein activity and function (11). Phosphorylation modification is the most basic, common and important mechanism to regulate protein activity and function (11). In order to comprehensively understand the mechanism of lung injury repair after HUMSCs intervention in juvenile septic rats, we performed proteomics and phosphoromics analysis of lung tissues of juvenile septic rats 24 hours after HUMSCs intervention (MS24) and those of unintervened septic juvenile rats (SIRs24) to further clarify its molecular mechanism.

First, we analyzed the mechanism of HUMSCs in the treatment of lung injury in juvenile septic rats from the perspective of proteomics. The results showed that 213 proteins were identified as differentially expressed proteins after HUMSCs intervention, of which 82 proteins were up-regulated and 131 proteins were down-regulated compared with the lung tissues of juvenile septic rats without intervention. It may be a potential key protein for the intervention of HUMSCs to alleviate septic lung injury.

According to GO classification analysis, in the classification of biological processes, most proteins are involved in cellular processes and biological regulation; they are mainly distributed in intracellular fluid and protein-containing complexes; their functions are mainly in the categories of binding and catalytic activity. It is worth noting that there are 42 DEPS in the immune system process category, among which the up-regulated differential proteins Mx1, Rap2c, TNC and Arrdc1 and the down-regulated differential proteins AIF1, MIF and UBXN1 are involved in the immune inflammatory response process. It has been reported that MX1 shows the key structural motif of GTPase family and is activated by rhabdovirus vaccination and bacterial RNA stimulation (26), and up-regulated with anti-inflammatory effect (27). Rap2c encodes a protein that is a member of the Ras-associated protein subfamily of the Ras-GTPase superfamily and acts as a molecular switch to regulate cell proliferation, differentiation, and apoptosis (28). TNC is an extracellular matrix (ECM) glycoprotein whose regulation is closely related to inflammation (29). Arrdc1 is involved in a variety of processes including cellular protein metabolism, extracellular vesicle biogenesis, and negative regulation of the Notch signaling pathway (30).The down-regulated differential protein AIF1 has been identified as an up-regulated protein of infection (31). The ubiquitin-regulated X (UbX) protein UbXN1, which contains a ubiquitin-associated domain, is a negative regulator of nuclear factor-κB (NF-κB) signaling (32, 33). It is suggested that the immune inflammatory response is important in the proteome of septic lung tissue. Our results showed that E-selectin, VEGFA, ICAM1 and NGAL were significantly decreased and PGE2 was increased after HUMSCs intervention (Supplementary Figure 5). It has been reported that TNC is an extracellular matrix (ECM) glycoprotein, and its upregulation can induce the expression of PGE2 (34), Macrophage migration inhibitory factor (MIF) is a multifunctional pro-inflammatory factor, and its overexpression can up-regulate the amount of ICAM-1, promote leukocyte adhesion to vascular endothelium, and mediate endothelial cell injury (35). After the intervention of HUMSCs, the content of ICAM-1 decreased and the content of PGE2 increased in juvenile septic rats, which participated in tissue repair, suggesting that HUMSCs may promote the repair of endothelial barrier injury in lung tissue by up-regulating the expression of TNC and PGE2, and (or) down-regulating the expression of MIF and ICAM-1. Studies have found that TNC is an ECM glycoprotein, and its regulation is closely related to inflammation. HUMSCs could significantly increase the level of PGE2 after intervention, while the up-regulation of TNC could induce the expression of PGE2. Therefore, we speculate that TNC may be the key protein for HUMSCs to promote the repair of lung injury in juvenile septic rats.

According to the results of go enrichment analysis, HUMSCs intervention participates in the regulation of antigen-stimulated inflammatory response and other biological processes, and is closely related to immune inflammatory response (36–38). For KEGG enrichment of differentially expressed proteins (DEPs), we identified only 1 pathway from upregulated DEPs and 11 pathways from downregulated DEPs. The main pathways related

to immune inflammatory response are ECM receptor interaction pathway, focal adhesion pathway and other signaling pathways (39–41).

Protein domain refers to a specific component that appears repeatedly in different protein molecules, with similar sequence, structure and function, and is a conserved unit in the process of protein evolution (42). We found an enrichment of important protein domains, such as carboxylesterase family, HMG (high mobility group) box, in upregulated DEPs and an enrichment of important protein domains, mainly including von Willebrand factor type A domain, in downregulated DEPs. Studies have reported that the expression and activity of carboxylesterases (CEs) are down-regulated under inflammatory conditions (43). The high mobility group (HMG-Box) protein family is a class of nuclear proteins that are secreted from the nucleus to the outside of the cell during systemic inflammatory response and mediate the inflammatory response as a proinflammatory cytokine (44). Von Willebrand factor (von Willebrand factor, vWF) is a multi-domain synthesized by vascular endothelial cells and bone marrow megakaryocytes, which can be used as an important indicator of endothelial cell activation and endothelial dysfunction, and participate in the process of body inflammation, tissue injury and repair, and immune regulation (45). The results showed that CEs and HMG-Box were up-regulated and vWF domain was down-regulated after HUMSCs intervention, suggesting that HUMSCs played a regulatory role.

Cluster analysis showed that the DEPs were related to the positive regulation of cell-matrix adhesion.The KEGG pathway cluster analysis showed that most of the proteins were related to the ECM receptor interaction pathway and focal adhesion signaling pathway. The protein domain cluster analysis showed that EFG-like laminin was the main protein.

GO enrichment analysis showed that HUMSCs intervened in regulating GTPase activity and antigen-stimulated inflammatory response, and B cell activation participated in immune response, extracellular matrix tissue, cell-matrix adhesion and other biological processes, which were closely related to immune inflammatory response. The results of DEPs enrichment and cluster analysis suggested that HUMSCs may regulate the expression of CEs, HMG-Box and von Willebrand factor type a domains through ECM receptor interaction pathway signaling pathway, and regulate the immune inflammatory response in the lung tissue of juvenile septic rats.

PPI networks can identify and characterize relevant protein complexes, which is crucial for understanding the molecular events involved (46). We use the string to determine the relation for PPI (47). In order to clearly show the interaction between proteins, we selected the top 50 proteins with the closest interaction, and we selected the top 15 proteins as hub proteins according to the degree. These proteins, due to their high degree of interaction, separate dense regions and predict protein complexes through the PPI subnetwork. MCODE obtained 36 modules and found that one up-regulated DEP module was TNC and the three most significant down-regulated DEP modules were (Fga, Fbn1, Itih2). Therefore, we speculate that HUMSCs may activate TNC-mediated PGE2 release through ECM-receptor interaction pathway.

In addition, our study also analyzed the mechanism of HUMSCs intervention in reducing lung injury in juvenile septic rats from the perspective of protein phosphorylation. Protein phosphorylation plays an important role in the process of cell signal transduction and is the most common and important mechanism to regulate protein function (11). To investigate the phosphoproteome of lung tissue in juvenile septic rats after HUMSCs intervention, we performed GO, subcellular localization, and COG classification of phosphoproteins. The two biological processes with the greatest changes in DPPs are cellular progression and biological regulation, which are mainly distributed in intracellular fluid, and their molecular functions are mainly protein binding and catalytic activity. The up-regulated phosphorylated proteins ifitm3 and Snap29 and the down-regulated proteins Cd93, Mx1, Cmklr1, Adam17 and Lrrc8a are involved in the immune inflammatory response. Studies have reported that IFITM3 is involved in cell adhesion, apoptosis, immunity, and antiviral activity. In addition, the IFITM3 gene is considered to be a preferred marker for inflammatory diseases (48). SARS-CoV-2 infection hinders autophagic flux by upregulating GSK3B in lung cell lines or downregulating autophagic genes, SNAP29, and lysosomal acidification genes in human samples, resulting in increased viral replication, suggesting that SNAP29 upregulation after HUMSCs intervention contributes to the repair of lung tissue cells (49). DPPs such as Cd93, Mx1, Cmklr1, Adam17 and Lrrc8a were significantly down-regulated after HUMSCs intervention, suggesting that the repair of septic lung injury is also closely related to the down-regulation of Cd93, Mx1, Cmklr1, Adam17 and Lrrc8a after HUMSCs intervention (50–54). In this study, the down-regulated phosphorylated proteins were more obvious than the up-regulated ones. In the phosphoproteomic analysis, the above proteins may be potential phosphorylated proteins for intervention of HUMSCs to alleviate septic lung injury.

In order to better understand the function of the identified phosphorylated proteins, we performed enrichment analysis of DPPs in the two groups at three levels of GO classification, KEGG pathway, and protein domain, respectively. In the HUMSCs intervention group, regarding the enrichment of phosphorylated proteins based on biological processes, response to rapamycin (mTOR) was significantly enriched for up-regulated proteins and cytoskeletal organization was significantly enriched for down-regulated proteins. For the HUMSCs intervention group, phosphorylated proteins were enriched based on molecular function upregulation, such as RNA binding, complex-containing binding proteins, mRNA binding, etc. In cell component enrichment classification analysis, the highly enriched categories included protein-

containing complexes of up-regulated phosphorylated proteins, ribonucleoprotein complexes, and for down-regulated phosphorylated proteins, cell junctions, adherens junctions, anchor knots, etc. Were significantly enriched.

Site occupancy of phosphorylation correlates with cell signaling status (55). KEGG pathway analysis was performed on DPPs to assess the pathways significantly represented in the intervention of HUMSCs in septic lung injury. We identified 4 pathways from upregulated DEPs and 14 pathways from downregulated DEPs. The down-regulated genes encoding epithelial intercellular connexin in the tight junction pathway and focal adhesion pathway indicate that there is interference in the permeability between epithelial barriers, which may be closely related to the regulation of intercellular barriers in septic lung injury (56–58).

Protein domain enrichment analysis found that only RNA recognition motif (RNP domain) was enriched in up-regulated DPPs, which was closely related to inflammatory regulation (59). As one of the important domains mediating the interaction between proteins, PDZ domain is enriched in down-regulated DPPs, participating in various biological processes such as intracellular transport, ion channels, and various signal transduction pathways, and its down-regulation can reduce the binding of inflammatory signals (60).

GO cluster analysis showed that DPPs were involved in the regulation of protein unfolding and polymerization. Cellular components are dominated by actin-based cell projection clusters, focal adhesions, cell-substrate junctions, etc. Analysis of molecular function revealed association with mRNA binding. Cluster analysis of KEGG pathway showed that most of the phosphorylated proteins were related to RNA transport, and the down-regulated proteins were related to the regulation of tight junction pathway and actin cytoskeleton. Our experimental results showed that E-selectin, VEGFA, ICAM1 and NGAL were significantly decreased after HUMSCs intervention (Supplementary Figure 5), and the expression of endothelial vascular growth factor VEGFA was closely related to tight junction pathway and focal adhesion pathway. VEGF is a key factor in the increased permeability of inflammation-related capillaries in patients with sepsis. VEGF can phosphorylate and dissociate intercellular connection-type molecules, such as vascular endothelial adhesion proteins, thereby promoting endothelial leakage. It is suggested that HUMSCs may regulate the phosphorylation of VEGFA through tight junction pathway or focal adhesion pathway, improve the permeability of endothelial barrier in lung tissue, and alleviate inflammatory injury.

We selected the top 50 phosphorylated proteins with the closest interaction and generated a network containing a total of 173 related phosphorylated proteins. There are many interactions between phosphorylated proteins, which can be considered as pivotal phosphorylated proteins according to the degree score. G3V6K6 (EGFR) found in this study has the most interactions (29 nodes), suggesting that it may be involved in the repair process of septic lung injury. EGFR is widely distributed on the cell surface, and this signaling pathway plays an important role in cell growth, proliferation, and differentiation (61). It has been reported that the inhibition of EGFR can improve the organ dysfunction induced by sepsis (62, 63). Therefore, it is suggested that G3V6K6 (EGFR) may be involved in the repair process of septic lung injury.

Protein phosphorylation is regulated by protein kinases (PKs), and different PKs prefer specific substrates with conserved motifs (64). We performed a bioinformatic analysis using the phosphorylation sites found in this study to identify novel phosphorylation motifs. We performed intensive sequence analysis of hyperphosphorylated site motifs around the phosphate groups of serine and threonine residues using the Motify-X program.

Among the 1316 phosphorylation sites, we identified 123 conserved motifs based on phosphorylated serine (pS) phosphorylation sites and 17 conserved motifs based on phosphorylated threonine (pT) phosphorylation sites. Heat maps were generated showing enrichment or depletion of specific amino acids near the serine phosphorylation site. D, E, P, R and S have a tendency to move to the vicinity of the serine phosphorylation site. P, R, S are largely represented in the proximal region of the threonine phosphorylation site. These amino acids near the phosphorylation sites preferentially reflect the specific recognition of the enzymes that catalyze phosphorylation in septic lung tissue after HUMSCs intervention. Further studies are needed to investigate whether different types of enzymes and kinases are active in regulating phosphorylation.In conclusion, from the perspective of protein phosphorylation modification, we speculate that HUMSCs may regulate the phosphorylation of VEGFA through EGFR-mediated tight junction pathway, improve the permeability of endothelial barrier in lung tissue and alleviate inflammatory injury.

Conclusion and prospect

Based on proteomics and phosphorylation modification analysis, it was confirmed that HUMSCs intervention could alleviate septic lung injury by regulating specific proteins or phosphorylation modification of proteins, and its basic molecular characteristics were described. Proteomic analysis revealed that TNC may be the key DEPs for HUMSCs to promote the repair of lung injury in juvenile septic rats. HUMSCs may activate TNC-mediated PGE2 release through ECM receptor interaction pathway, improve endothelial cell functional barrier, and promote the recovery of gas-blood barrier function in lung tissue. From the perspective of protein phosphorylation modification, it is suggested that HUMSCs may regulate the phosphorylation of VEGFA through EGFR tight junction pathway, improve the permeability of endothelial barrier in lung tissue, and alleviate inflammatory injury.

Results from proteomics and phosphorylated proteomics, the potential new therapeutic targets of HUMSCs in alleviating lung injury in juvenile septic rats were revealed.

However, there are also limitations. Our study is limited to bioinformatics analysis, and the key differential proteins, signaling pathways and phosphorylation sites have not been further verified. In the next step, proteins with significant differences in protein expression or modification levels will be selected for validation and research.

Data availability statement

The datasets presented in this study can be found in online repositories. The names of the repository/repositories and accession number(s) can be found in the article/Supplementary Material.

Ethics statement

The acquisition and culture of human umbilical cord tissue was approved by the Ethics Committee of the Second Affiliated Hospital of Medical College of Shantou University (Ethics Approval No.: 2021-89). The patients/participants provided their written informed consent to participate in this study. The animal experiment was approved by the Ethics Committee of Shenzhen Topu Biological Laboratory Animal Center (Ethics Approval No.: TOP-IACUC-2021-0003).

Author contributions

HW and JL: Writing- Original draft preparation, Visualization, Software. AL: experimental design. XS: Methodology. CF: Methodology, Visualization, Software. LX, YW and FW: Writing – review & editing. YL, TW, YZ and LM: Supervision. All authors contributed to the article and approved the submitted version.

Funding

This research was funded by grants from the National Natural Science Foundation of China (No. 81671525 and No. 8107047), Shenzhen Key Projects of Basic Research (No. JCYJ20200109150618539), Science and technology projects of Guangdong Province (No. 2020-53-112 and No. 2021-88-34), National Science and Technology Major Project (No. 2017ZX09304029004), and Promote special projects for emergency research for epidemic prevention and control technology of COVID-19 of science and technology bureau in Dongguan, China(No. 202071715032116).

Conflict of interest

The authors declare that the research was conducted in the absence of any commercial or financial relationships that could be construed as a potential conflict of interest.

Publisher's note

All claims expressed in this article are solely those of the authors and do not necessarily represent those of their affiliated organizations, or those of the publisher, the editors and the reviewers. Any product that may be evaluated in this article, or claim that may be made by its manufacturer, is not guaranteed or endorsed by the publisher.

Supplementary material

The Supplementary Material for this article can be found online at: https://www.frontiersin.org/articles/10.3389/fimmu.2022.1034821/full#supplementary-material

References

1. Kumar V. Pulmonary innate immune response determines the outcome of inflammation during pneumonia and sepsis-associated acute lung injury. *Front Immunol* (2020) 11:1722. doi: 10.3389/fimmu.2020.01722

2. Mikkelsen ME, Shah CV, Meyer NJ, Gaieski DF, Lyon S, Miltiades AN, et al. The epidemiology of acute respiratory distress syndrome in patients presenting to the emergency department with severe sepsis. *Shock* (2013) 40(5):375–81. doi: 10.1097/SHK.0b013e3182a64682

3. ARDS Definition Task Force, Ranieri VM, Rubenfeld GD, Thompson BT, Ferguson ND, Caldwell E, et al. Acute respiratory distress syndrome: the Berlin definition. *JAMA* (2012) 307(23):2526–33. doi: 10.1001/jama.2012.5669

4. Ding DC, Chang YH, Shyu WC, Lin SZ. Human umbilical cord mesenchymal stem cells: a new era for stem cell therapy. *Cell Transplant* (2015) 24(3):339–47. doi: 10.3727/096368915X686841

5. Li N, Hua J. Interactions between mesenchymal stem cells and the immune system. *Cell Mol Life Sci* (2017) 74(13):2345–60. doi: 10.1007/s00018-017-2473-5

6. Chan MC, Kuok DI, Leung CY, Hui KP, Valkenburg SA, Lau EH, et al. Human mesenchymal stromal cells reduce influenza a H5N1-associated acute lung injury *in vitro* and *in vivo*. *Proc Natl Acad Sci U.S.A.* (2016) 113(13):3621–6. doi: 10.1073/pnas.1601911113

7. Hoseinnia S, Ghane M, Norouzi J, Hosseini F. Mesenchymal stem cell and endothelial progenitor cells coinjection improves LPS-induced lung injury *via* Tie2 activation and downregulation of the TLR4/MyD88 pathway. *J Cell Biochem* (2021) 122(12):1791–804. doi: 10.1002/jcb.30133

8. Shi L, Wang L, Xu R, Zhang C, Xie Y, Liu K, et al. Mesenchymal stem cell therapy for severe COVID-19. *Signal Transduct Target Ther* (2021) 6(1):339. doi: 10.1038/s41392-021-00754-6

9. Leng Z, Zhu R, Hou W, Feng Y, Yang Y, Han Q, et al. Transplantation of ACE2(-) mesenchymal stem cells improves the outcome of patients with COVID-19 pneumonia. *Aging Dis* (2020) 11(2):216–28. doi: 10.14336/AD.2020.0228

10. Xiao K, Xie LX. Advances in mesenchymal stem cell-mediated tissue repair of lung injury. *Chronic Dis Transl Med* (2021) 7(2):75–8. doi: 10.1016/j.cdtm.2021.02.002

11. Tan CS. Sequence, structure, and network evolution of protein phosphorylation. *Sci Signal* (2011) 4(182):mr6. doi: 10.1126/scisignal.2002093

12. Liu W, Yu M, Xie D, Wang L, Ye C, Zhu Q, et al. Melatonin-stimulated MSC-derived exosomes improve diabetic wound healing through regulating macrophage M1 and M2 polarization by targeting the PTEN/AKT pathway. *Stem Cell Res Ther* (2020) 11(1):259. doi: 10.1186/s13287-020-01756-x

13. Chen J, Chen J, Cheng Y, Fu Y, Zhao H, Tang M, et al. Mesenchymal stem cell-derived exosomes protect beta cells against hypoxia-induced apoptosis *via* miR-21 by alleviating ER stress and inhibiting p38 MAPK phosphorylation. *Stem Cell Res Ther* (2020) 11(1):97. doi: 10.1186/s13287-020-01610-0

14. Na L, Wang S, Liu T, Zhang L. Ultrashort wave combined with human umbilical cord mesenchymal stem cell (HUC-MSC) transplantation inhibits NLRP3 inflammasome and improves spinal cord injury *via* MK2/TTP signalling pathway. *BioMed Res Int* (2020) 2020:3021750. doi: 10.1155/2020/3021750

15. Zhou W, Silva M, Feng C, Zhao S, Liu L, Li S, et al. Exosomes derived from human placental mesenchymal stem cells enhanced the recovery of spinal cord injury by activating endogenous neurogenesis. *Stem Cell Res Ther* (2021) 12(1):174. doi: 10.1186/s13287-021-02248-2

16. Su VY, Lin CS, Hung SC, Yang KY. Mesenchymal stem cell-conditioned medium induces neutrophil apoptosis associated with inhibition of the NF-kappaB pathway in endotoxin-induced acute lung injury. *Int J Mol Sci* (2019) 20(9):2208. doi: 10.3390/ijms20092208

17. Wu KH, Wu HP, Chao WR, Lo WY, Tseng PC, Lee CJ, et al. Time-series expression of toll-like receptor 4 signaling in septic mice treated with mesenchymal stem cells. *Shock* (2016) 45(6):634–40. doi: 10.1097/SHK.0000000000000546

18. Pedrazza L, Cubillos-Rojas M, de Mesquita FC, Luft C, Cunha AA, Rosa JL, et al. Mesenchymal stem cells decrease lung inflammation during sepsis, acting through inhibition of the MAPK pathway[J]. *Stem Cell Res Ther* (2017) 8(1):289. doi: 10.1186/s13287-017-0734-8

19. Chen J, Li C, Liang Z, Li C, Li Y, Zhao Z, et al. Human mesenchymal stromal cells small extracellular vesicles attenuate sepsis-induced acute lung injury in a mouse model: the role of oxidative stress and the mitogen-activated protein kinase/nuclear factor kappa b pathway. *Cytotherapy* (2021) 23(10):918–30. doi: 10.1016/j.jcyt.2021.05.009

20. Fleisher TA, Bleesing JJ. Immune function. *Pediatr Clin North Am* (2000) 47 (6):1197–209. doi: 10.1016/S0031-3955(05)70267-4

21. Qian M, Lou Y, Wang Y, Zhang M, Jiang Q, Mo Y, et al. PICK1 deficiency exacerbates sepsis-associated acute lung injury and impairs glutathione synthesis *via* reduction of xCT. *Free Radic Biol Med* (2018) 118:23–34. doi: 10.1016/j.freeradbiomed.2018.02.028

22. Matute-Bello G, Frevert CW, Martin TR. Animal models of acute lung injury. *Am J Physiol Lung Cell Mol Physiol* (2008) 295(3):L379–99. doi: 10.1152/ajplung.00010.2008

23. Lian J, Lin J, Zakaria N, Yahaya BH. Acute lung injury: Disease modelling and the therapeutic potential of stem cells. *Adv Exp Med Biol* (2020) 1298:149–66. doi: 10.1007/5584_2020_538

24. Feng B, Zhu J, Xu Y, Chen W, Sheng X, Feng X, et al. Immunosuppressive effects of mesenchymal stem cells on lung b cell gene expression in LPS-induced acute lung injury. *Stem Cell Res Ther* (2020) 11(1):418. doi: 10.1186/s13287-020-01934-x

25. Zhou Q, Xie M, Zhu J, Yi Q, Tan B, Li Y, et al. PINK1 contained in huMSC-derived exosomes prevents cardiomyocyte mitochondrial calcium overload in sepsis *via* recovery of mitochondrial Ca(2+) efflux. *Stem Cell Res Ther* (2021) 12 (1):269. doi: 10.1186/s13287-021-02325-6

26. Samanta M, Satapathy S, Paichha M, Choudhary P. Labeo rohita Mx1 exhibits the critical structural motifs of the family of large GTPases of mammals and is activated by rhabdovirus vaccination and bacterial RNA stimulations. *Anim Biotechnol* (2022) 33(1):22–42. doi: 10.1080/10495398.2020.1759612

27. Bizzotto J, Sanchis P, Abbate M, Lage-Vickers S, Lavignolle R, Toro A, et al. SARS-CoV-2 infection boosts MX1 antiviral effector in COVID-19 patients. *iScience* (2020) 23(10):101585. doi: 10.1016/j.isci.2020.101585

28. Zhou H, Chen D, Xie G, Li J, Tang J, Tang L, et al. LncRNA-mediated ceRNA network was identified as a crucial determinant of differential effects in periodontitis and periimplantitis by high-throughput sequencing. *Clin Implant Dent Relat Res* (2020) 22(3):424–50. doi: 10.1111/cid.12911

29. Meijer MT, de Vos AF, Scicluna BP, Roelofs JJ, Abou Fayçal C, Orend G, et al. Tenascin-c deficiency is associated with reduced bacterial outgrowth during klebsiella pneumoniae-evoked pneumosepsis in mice. *Front Immunol* (2021) 12:600979. doi: 10.3389/fimmu.2021.600979

30. Mackenzie K, Foot NJ, Anand S, Dalton HE, Chaudhary N, Collins BM, et al. Regulation of the divalent metal ion transporter *via* membrane budding. *Cell Discovery* (2016) 2:16011. doi: 10.1038/celldisc.2016.11

31. Gong X, Li X, You X, Hu A, Liu M, Yao H, et al. AIF1 was identified as an up-regulated gene contributing to CSFV shimen infection in porcine alveolar macrophage 3D4/21 cells. *PeerJ* (2020) 8:e8543. doi: 10.7717/peerj.8543

32. Wang YB, Tan B, Mu R, Chang Y, Wu M, Tu HQ, et al. Ubiquitin-associated domain-containing ubiquitin regulatory X (UBX) protein UBXN1 is a negative regulator of nuclear factor kappaB (NF-kappaB) signaling. *J Biol Chem* (2015) 290(16):10395–405. doi: 10.1074/jbc.M114.631689

33. Yuan P, Huang S, Yang Z, Xie L, Wang K, Yang Y, et al. UBXN1 interacts with the S1 protein of transmissible gastroenteritis coronavirus and plays a role in viral replication. *Vet Res* (2019) 50(1):28. doi: 10.1186/s13567-019-0648-9

34. Patel L, Sun W, Glasson SS, Morris EA, Flannery CR, Chockalingam PS, et al. Tenascin-c induces inflammatory mediators and matrix degradation in osteoarthritic cartilage. *BMC Musculoskelet Disord* (2011) 12:164. doi: 10.1186/1471-2474-12-164

35. Wu Y, Xu W, Hou J, Liu Y, Li R, Liu J, et al. Porphyromonas gingivalis-induced MIF regulates intercellular adhesion molecule-1 expression in EA.hy926 cells and monocyte-endothelial cell adhesion through the receptors CD74 and CXCR4. *Inflammation* (2019) 42(3):874–83. doi: 10.1007/s10753-018-0942-0

36. Buttenschon A, Liu Y, Edelstein-Keshet L. Cell size, mechanical tension, and GTPase signaling in the single cell. *Bull Math Biol* (2020) 82(2):28. doi: 10.1007/s11538-020-00702-5

37. Pilla-Moffett D, Barber MF, Taylor GA, Coers J. Interferon-inducible GTPases in host resistance, inflammation and disease. *J Mol Biol* (2016) 428 (17):3495–513. doi: 10.1016/j.jmb.2016.04.032

38. Zhang Y, He F, Chen Z, Su Q, Yan M, Zhang Q, et al. Melatonin modulates IL-1beta-induced extracellular matrix remodeling in human nucleus pulposus cells and attenuates rat intervertebral disc degeneration and inflammation. *Aging (Albany NY)* (2019) 11(22):10499–512. doi: 10.18632/aging.102472

39. Mardpour S, Hamidieh AA, Taleahmad S, Sharifzad F, Taghikhani A, Baharvand H, et al. Interaction between mesenchymal stromal cell-derived extracellular vesicles and immune cells by distinct protein content. *J Cell Physiol* (2019) 234(6):8249–58. doi: 10.1002/jcp.27669

40. Zhang L, Li Y, Dong YC, Guan CY, Tian S, Lv XD, et al. Transplantation of umbilical cord-derived mesenchymal stem cells promotes the recovery of thin endometrium in rats. *Sci Rep* (2022) 12(1):412. doi: 10.1038/s41598-021-04454-7

41. Nagai T, Ishida C, Nakamura T, Iwase A, Mori M, Murase T, et al. Focal adhesion kinase-mediated sequences, including cell adhesion, inflammatory response, and fibrosis, as a therapeutic target in endometriosis. *Reprod Sci* (2020) 27(7):1400–10. doi: 10.1007/s43032-019-00044-1

42. Aziz MF, Caetano-Anolles G. Evolution of networks of protein domain organization[J]. *Sci Rep* (2021) 11(1):12075. doi: 10.1038/s41598-021-90498-8

43. Szafran B, Borazjani A, Lee JH, Ross MK, Kaplan BL. Lipopolysaccharide suppresses carboxylesterase 2g activity and 2-arachidonoylglycerol hydrolysis: A possible mechanism to regulate inflammation. *Prostaglandins Other Lipid Mediat* (2015) 121(Pt B):199–206. doi: 10.1016/j.prostaglandins.2015.09.005

44. Wu X, Yang Z, Wang H, Zhao Y, Gao X, Zang B. High-mobility group box protein-1 induces acute pancreatitis through activation of neutrophil extracellular trap and subsequent production of IL-1beta. *Life Sci* (2021) 286:119231. doi: 10.1016/j.lfs.2021.119231

45. Choi SJ, Lillicrap D. A sticky proposition: The endothelial glycocalyx and von willebrand factor. *J Thromb Haemost* (2020) 18(4):781–5. doi: 10.1111/jth.14743

46. Zaki N, Berengueres J, Efimov D. Detection of protein complexes using a protein ranking algorithm. *Proteins* (2012) 80(10):2459–68. doi: 10.1002/prot.24130

47. Szklarczyk D, Franceschini A, Wyder S, Forslund K, Heller D, Huerta-Cepas J, et al. STRING v10: protein-protein interaction networks, integrated over the tree of life. *Nucleic Acids Res* (2015) 43(Database issue):D447–52. doi: 10.1093/nar/gku1003

48. Li HP, Chen PG, Liu FT, Zhu HS, Jiao XQ, Zhong K, et al. Characterization and anti-inflammation role of swine IFITM3 gene. *Oncotarget* (2017) 8(43):73579–89. doi: 10.18632/oncotarget.20568

49. Singh K, Chen YC, Hassanzadeh S, Han K, Judy JT, Seifuddin F, et al. Network analysis and transcriptome profiling identify autophagic and mitochondrial dysfunctions in SARS-CoV-2 infection. *Front Genet* (2021) 12:599261. doi: 10.3389/fgene.2021.599261

50. Fantone S, Tossetta G, Di Simone N, Tersigni C, Scambia G, Marcheggiani F, et al. CD93 a potential player in cytotrophoblast and endothelial cell migration. *Cell Tissue Res* (2022) 387(1):123–30. doi: 10.1007/s00441-021-03543-3

51. Andolfo I, Russo R, Lasorsa VA, Cantalupo S, Rosato BE, Bonfiglio F, et al. Common variants at 21q22.3 locus influence MX1 and TMPRSS2 gene expression

and susceptibility to severe COVID-19. *iScience* (2021) 24(4):102322. doi: 10.1016/j.isci.2021.102322

52. Xie Y, Huang Y, Ling X, Qin H, Wang M, Luo B. Chemerin/CMKLR1 axis promotes inflammation and pyroptosis by activating NLRP3 inflammasome in diabetic cardiomyopathy rat. *Front Physiol* (2020) 11:381. doi: 10.3389/fphys.2020.00381

53. Zipeto D, Palmeira J, Arganaraz GA, Argañaraz ER. ACE2/ADAM17/TMPRSS2 interplay may be the main risk factor for COVID-19. *Front Immunol* (2020) 11:576745. doi: 10.3389/fimmu.2020.576745

54. Choi H, Ettinger N, Rohrbough J, Dikalova A, Nguyen HN, Lamb FS. LRRC8A channels support TNFalpha-induced superoxide production by Nox1 which is required for receptor endocytosis. *Free Radic Biol Med* (2016) 101:413–23. doi: 10.1016/j.freeradbiomed.2016.11.003

55. Sharma K, D'Souza RC, Tyanova S, Schaab C, Wiśniewski JR, Cox J, et al. Ultradeep human phosphoproteome reveals a distinct regulatory nature of tyr and Ser/Thr-based signaling. *Cell Rep* (2014) 8(5):1583–94. doi: 10.1016/j.celrep.2014.07.036

56. Buckley A, Turner JR. Cell biology of tight junction barrier regulation and mucosal disease. *Cold Spring Harb Perspect Biol* (2018) 10(1):a029314. doi: 10.1101/cshperspect.a029314

57. Cong X, Kong W. Endothelial tight junctions and their regulatory signaling pathways in vascular homeostasis and disease. *Cell Signal* (2020) 66:109485. doi: 10.1016/j.cellsig.2019.109485

58. Bo H, He J, Wang X, Du R, Bei H, Chen J, et al. Danggui buxue tang promotes the adhesion and migration of bone marrow stromal cells *via* the focal adhesion pathway *in vitro*. *J Ethnopharmacol* (2019) 231:90–7. doi: 10.1016/j.jep.2018.11.018

59. Maris C, Dominguez C, Allain FH. The RNA recognition motif, a plastic RNA-binding platform to regulate post-transcriptional gene expression. *FEBS J* (2005) 272(9):2118–31. doi: 10.1111/j.1742-4658.2005.04653.x

60. Liu X, Fuentes EJ. Emerging themes in PDZ domain signaling: Structure, function, and inhibition. *Int Rev Cell Mol Biol* (2019) 343:129–218. doi: 10.1016/bs.ircmb.2018.05.013

61. Sabbah DA, Hajjo R, Sweidan K. Review on epidermal growth factor receptor (EGFR) structure, signaling pathways, interactions, and recent updates of EGFR inhibitors. *Curr Top Med Chem* (2020) 20(10):815–34. doi: 10.2174/1568026620666200303123102

62. Xu X, Wang J, Yang R, Dong Z, Zhang D. Genetic or pharmacologic inhibition of EGFR ameliorates sepsis-induced AKI. *Oncotarget* (2017) 8 (53):91577–92. doi: 10.18632/oncotarget.21244

63. Zheng WJ, Yan Q, Ni YS, Zhan SF, Yang LL, Zhuang HF, et al. Examining the effector mechanisms of xuebijing injection on COVID-19 based on network pharmacology. *BioData Min* (2020) 13:17. doi: 10.1186/s13040-020-00227-6

64. Goldsmith EJ, Cobb MH. Protein kinases. *Curr Opin Struct Biol* (1994) 4 (6):833–40. doi: 10.1016/0959-440X(94)90264-X

COPYRIGHT

© 2022 Wang, Luo, Li, Su, Fang, Xie, Wu, Wen, Liu, Wang, Zhong and Ma. This is an open-access article distributed under the terms of the Creative Commons Attribution License (CC BY). The use, distribution or reproduction in other forums is permitted, provided the original author(s) and the copyright owner(s) are credited and that the original publication in this journal is cited, in accordance with accepted academic practice. No use, distribution or reproduction is permitted which does not comply with these terms.

frontiers | Frontiers in Immunology

TYPE Original Research
PUBLISHED 02 November 2022
DOI 10.3389/fimmu.2022.1015577

Check for updates

OPEN ACCESS

EDITED BY
Christoph Thiemermann,
Queen Mary University of London,
United Kingdom

REVIEWED BY
Borna Relja,
Otto von Guericke University,
Germany
Basilia Zingarelli,
Cincinnati Children's Hospital Medical
Center, United States

*CORRESPONDENCE
Elisabetta Liverani
elisabetta.liverani@ndsu.edu

SPECIALTY SECTION
This article was submitted to
Inflammation,
a section of the journal
Frontiers in Immunology

RECEIVED 09 August 2022
ACCEPTED 10 October 2022
PUBLISHED 02 November 2022

CITATION
Amoafo EB, Entsie P, Albayati S,
Dorsam GP, Kunapuli SP, Kilpatrick LE
and Liverani E (2022) Sex-related
differences in the response of anti-
platelet drug therapies targeting
purinergic signaling pathways in sepsis.
Front. Immunol. 13:1015577.
doi: 10.3389/fimmu.2022.1015577

COPYRIGHT
© 2022 Amoafo, Entsie, Albayati,
Dorsam, Kunapuli, Kilpatrick and
Liverani. This is an open-access article
distributed under the terms of the
Creative Commons Attribution License
(CC BY). The use, distribution or
reproduction in other forums is
permitted, provided the original
author(s) and the copyright owner(s)
are credited and that the original
publication in this journal is cited, in
accordance with accepted academic
practice. No use, distribution or
reproduction is permitted which does
not comply with these terms.

Sex-related differences in the response of anti-platelet drug therapies targeting purinergic signaling pathways in sepsis

Emmanuel Boadi Amoafo[1], Philomena Entsie[1], Samara Albayati[2], Glenn P. Dorsam[3], Satya P. Kunapuli[2], Laurie E. Kilpatrick[4] and Elisabetta Liverani[1,2]*

[1]Department of Pharmaceutical Sciences, School of Pharmacy, College of Health Professions, North Dakota State University, Fargo, ND, United States, [2]Sol Sherry Thrombosis Research Center, Temple University School of Medicine, Temple University Hospital, Philadelphia, PA, United States, [3]Center for Inflammation and Lung Research, Department of Microbiology, Immunology and Inflammation, Lewis Katz School of Medicine, Temple University, Philadelphia, PA, United States, [4]Department of Microbiological Sciences, College of Agriculture, Food Systems and Natural Resources, North Dakota State University, Fargo, ND, United States

Sepsis, a complex clinical syndrome resulting from a serious infection, is a major healthcare problem associated with high mortality. Sex-related differences in the immune response to sepsis have been proposed but the mechanism is still unknown. Purinergic signaling is a sex-specific regulatory mechanism in immune cell physiology. Our studies have shown that blocking the ADP-receptor $P2Y_{12}$ but not $P2Y_1$ receptor was protective in male mice during sepsis, but not female. We now hypothesize that there are sex-related differences in modulating $P2Y_{12}$ or $P2Y_1$ signaling pathways during sepsis. Male and female wild-type (WT), $P2Y_{12}$ knock-out (KO), and $P2Y_1$ KO mice underwent sham surgery or cecal ligation and puncture (CLP) to induce sepsis. The $P2Y_{12}$ antagonist ticagrelor or the $P2Y_1$ antagonist MRS2279 were administered intra-peritoneally after surgery to septic male and female mice. Blood, lungs and kidneys were collected 24 hours post-surgery. Sepsis-induced changes in platelet activation, secretion and platelet interaction with immune cells were measured by flow cytometry. Neutrophil infiltration in the lung and kidney was determined by a myeloperoxidase (MPO) colorimetric assay kit. Sepsis-induced platelet activation, secretion and aggregate formation were reduced in male CLP $P2Y_{12}$ KO and in female CLP $P2Y_1$ KO mice compared with their CLP WT counterpart. Sepsis-induced MPO activity was reduced in male CLP $P2Y_{12}$ KO and CLP $P2Y_1$ KO female mice. CLP males treated with ticagrelor or MRS2279 showed a decrease in sepsis-induced MPO levels in lung and kidneys, aggregate formation, and platelet activation as compared to untreated male CLP mice. There were no differences in platelet activation, aggregate formation, and neutrophil infiltration in lung and kidney between female CLP mice and female CLP mice treated with ticagrelor or MRS2279. In human T lymphocytes, blocking $P2Y_1$ or $P2Y_{12}$ alters cell growth and secretion *in vitro* in a sex-dependent manner, supporting the data obtained in mice. In conclusion, targeting purinergic signaling represents a promising

10.3389/fimmu.2022.1015577

therapy for sepsis but drug targeting purinergic signaling is sex-specific and needs to be investigated to determine sex-related targeted therapies in sepsis.

KEYWORDS

platelets (PLT), purinergic signaling, sex-related differences, sepsis, platelet activation

Introduction

Sepsis, a complex clinical syndrome resulting from a serious infection, is a major healthcare problem associated with high morbidity and mortality (1). Current sepsis treatments are limited to supportive therapies (2), and specific pharmacologic treatments that could greatly improve patient outcomes have not yet been developed (2, 3). With hospital mortality rates of affected patients reportedly as high as 50%, there is a critical need for improved methods for treating sepsis (1).

Sex-related differences in the morbidity and mortality of sepsis have been observed in animal models and human diseases (4–8). To date, females has shown decreased mortality and organ failure in mice and humans compared to their male counterpart (4, 7). However, the lack of studies comparing both sexes limit our capacity to evaluate the extent of sex-related differences. Hence sex should be taken into account when identifying the optimal pharmacological intervention for sepsis. Sex-related differences have been observed in other diseases, such as cardiovascular diseases (4), Alzheimer's (9), cancer (10), and ulcerative colitis (11). In some cases, such as ulcerative colitis (11) and cardiovascular diseases (4) sex-specific treatment has been identified, improving the patient outcome. But there is a gap in knowledge for other diseases.

Purinergic signaling represents a novel regulatory mechanism in immune cell physiology (12). Cells respond to activation with the release of cellular ATP, which regulates cell functions (13). In sepsis, large amounts of ADP are released by tissue damage and immune cells. This leads to over-activation of purinergic signaling contributing to immune dysfunction (13). As a result, regulating purinergic signaling can reveal new avenues in the treatment of sepsis.

Changes in purinergic receptors has been investigated within sexes. For instance, changes in purinergic signaling response may be hormone-dependent (14–17) and they vary in the sex organs (18–20). Indeed, in a murine menopause model, ovarian protein levels of purinergic receptor P2X2 increased with ageing, suggesting that the P2X2 receptor is involved with menopause/ageing-related decline in ovarian function in females (21). Beaucage and coworkers revealed that the P2X7 receptor subtype might be involved in an age- and sex-dependent regulation of adipogenesis and lipid metabolism (14, 16).

Platelet ADP-induced activation is regulated by the $P2Y_{12}$ and $P2Y_1$ signaling pathways (22, 23). $P2Y_{12}$ is a G_i protein coupled receptor (24), while $P2Y_1$ is a G_q protein coupled receptor (23, 24). Activation of the $P2Y_{12}$ signaling pathway leads to platelet aggregation and potentiation of platelet secretion (25) while $P2Y_1$ activation leads to shape change and aggregation (23, 24). We have previously shown that blockade of the $P2Y_{12}$ signaling pathway in a murine model of sepsis results in improved outcomes in male mice (26), through decreased α-granule secretion of inflammatory mediators and reduced mobilization of P-selectin to the plasma membrane of platelets (26). We have shown that by blocking specific signaling pathways in platelets, we can regulate inflammation without compromising platelet functions. However, $P2Y_1$ deficiency did not alter inflammation levels or lung injury in a murine model of sepsis in male mice. However, there are sex-related differences in how platelet respond to activation. In fact, female platelets are more reactive to agonists, especially ADP than male (27, 28) suggesting sex-related differences in ADP- induced platelet activation. Sex-related differences in the expression of $P2Y_1$ or $P2Y_{12}$ have been shown to vary within sexes in the murine brain (29) but information about the expression of these receptors in other organs is limited.

In this study, we aim to investigate whether either deficiency or blocking the ADP-receptors $P2Y_1$ or $P2Y_{12}$ alters inflammation levels in sepsis in a sex-specific manner. To achieve this aim, we used a well-recognized murine model of sepsis (cecal ligation and double puncture) and compared male and female mice upon $P2Y_1$ or $P2Y_{12}$ deficiency or blockade. Our data show that $P2Y_{12}$ but not $P2Y_1$ deficiency, decreased the activity of MPO in lungs and kidneys, platelet-leukocyte interaction and platelet activation in male but not female mice. Either $P2Y_{12}$ or $P2Y_1$ blockade could decrease activity of MPO in lungs and kidneys and platelet-leukocyte interaction in male mice. On the other hand, $P2Y_1$ deficiency but not blockade decreased activity of MPO in lungs and platelet-leukocyte interaction in female mice. In human T lymphocytes, blocking $P2Y_1$ or $P2Y_{12}$ alters cell growth and secretion *in vitro* in a sex-dependent manner, supporting the data obtained in mice. Thus, drug targeting purinergic signaling

Abbreviations: CLP, cecal ligation and double puncture; IL-1β, interleukin-1 β; MPO, myeloperoxidase; PBMCs, peripheral blood mononuclear cells; PBS, phosphate-buffered saline; PF4, platelet factor 4.

appears to be sex-specific and needs to be investigated to determine sex-related targeted therapies in sepsis.

Materials and methods

Materials

All reagents were of analytical grade and were obtained from Thermo Fisher Scientific (Waltham, MA) unless stated otherwise. Ficoll-Paque was from GE Healthcare Bio-Sciences AB (Uppsala, SE). FITC-conjugated anti-mouse CD11b (clone M1/70) was obtained from Invitrogen (Waltham, MA). PE-conjugated anti-mouse CD4 (clone GK 1.5), FITC- conjugated anti-mouse CD41 (clone MWreg30) and FITC-conjugated mouse anti p-selectin (clone RB40.34) were obtained from BD Bioscience (San Jose, CA). FITC-conjugated anti-mouse CD14 (clone MEM-18) were obtained from Sigma-Aldrich (St. Louis, MO). PE-conjugated anti-human CD4 (clone OKT4) was purchased from BioLegend (San Diego, CA) and APC-conjugated anti-human CD8 (clone HIT8a) antibodies was obtained from eBioscience (San Diego, CA) Invitrogen (Waltham, MA). Rat IgG2a κ isotype control FITC [clone eBR2a), rat IgG2b K isotype control PE (clone eB149/10H5)] were purchased from eBioscience (San Diego, CA). Ticagrelor and MRS2279 was obtained from TOCRIS (Pittsburgh, PA).

Animals and treatments

Animal procedures and handling adhered to the National Institutes of Health standards and were approved by the Institutional Animal Care and Use Committee Protocol #A21040 at North Dakota State University (Fargo, ND, USA). Male and female wild-type and $P2Y_{12}$ deficient pathogen-free C57BL/6 mice (weight, 25-30 g; 8-10 weeks of age) were obtained from Schering-Plough Corporation (Kenilworth, NJ)1-4. P2Y1 deficient pathogen-free C57BL/6 male and female mice were generated by subcontract with Lexicon Genetics Inc. (Woodlands, TX) through knockout constructs as described previously (22, 25, 30). Only 8-10-week homozygote animals were included. Male and female mice were housed in a climate-controlled pathogen free environment and given free access to food and water.

The cecal ligation and double puncture (CLP) procedures were performed on under anesthesia with isoflurane (2 ± 4% induction in chamber and 1 ± 2% maintenance in mask) as described previously (26, 31–33). Following midline laparotomy, the cecum was identified, the mesentery trimmed, and the stalk joining the cecum to the large intestine ligated. Care was taken to assure the intestinal continuity was not interrupted. The cecum was punctured twice with a 24-gauge needle on the anti-mesenteric border, stool expressed, and the cecum returned to the abdomen. Sham control animals underwent a laparotomy without ligation or double puncture. Experiments were performed in $P2Y_{12}$, $P2Y_1$ KO, and wild-type (WT) male and female mice that were randomly assigned to one of four groups for wild-type or KO: wild-type and KO sham control group (6 animals per group); wild-type and KO undergoing CLP (CLP group, 6 animals per group).

Ticagrelor and MRS2279 were administrated intraperitoneally to WT male and female mice (6 animals per group) with a dose of 30 mg/kg (ticagrelor) (34–36) and 50mg/kg (MRS2279) (37, 38) at the time of surgery. Sham mice received the same doses of Ticagrelor and MRS2279. After the procedure but prior to emergence, sham and CLP mice were fluid-resuscitated (1 ml/mouse sterile saline, subcutaneously).

At 24 hours post-surgery, mice were anesthetized and blood samples were collected by cardiac puncture (10:1 in 3.8% sodium citrate) for hematology studies (Hemavet® Multispecies Hematology System, Drew Scientific, Inc. Oxford, CT). All mice were euthanized by cardiac puncture and exsanguination. Lungs and kidneys were collected and fixed or frozen immediately in liquid nitrogen.

Myeloperoxidase activity

Lungs and kidneys were homogenized and sonicated. After centrifugation (10,000 for 10 minutes at 4°C), myeloperoxidase (MPO) levels were detected using a MPO calorimetric assay kit (BioVision, USA). The assay was performed as described by the manufacturer. Briefly, perfused lung and kidney tissues were homogenized rapidly on ice upon addition of myeloperoxidase (MPO) Assay buffer and the supernatant collected after centrifugation (10,000 for 10 minutes at 4°C). Resorufin standard and MPO positive control were prepared. Standards, positive controls, and samples were transferred into different wells of the 96-well plate. Reaction mix prepared with MPO assay buffer, MPO peroxidation substrate, and hydrogen peroxidase (0.88M) was added to each well and thoroughly mixed after which fluorescence (Ex/Em=535/587 nm) was kinetically measured at 37°C for 10 minutes. A resorufin standard curve was plotted and the MPO activity of the test samples was calculated.

Blood urea nitrogen and creatinine measurement

Plasma aliquots from each animal were obtained by blood centrifugation (2,000 x g for 10 minutes) and immediately frozen. Blood urea nitrogen levels were measured using the urea nitrogen (BUN) colorimetric detection kit (ThermoFisher Scientific, USA). The assay was performed as described by the manufacturer. The plasma samples were diluted with deionized water (1:30) prior to use. The urea nitrogen standard (100 mg/dL urea nitrogen) was used. Samples and standards were added to a 96-well plate. Acidic solutions coded as color reagents A and B in

the kit were each added to all wells and incubated for 30 minutes, and the absorbance was immediately read at 450 nm using a microplate reader. Plasma creatinine was determined by an enzymatic assay kit (Mouse Creatinine Assay Kit no. 80350, Crystal Chem, Downers Grove, IL). The assay was performed as described by the manufacturer. Samples were added to a 96-well plate and incubated with the sarcosine oxidase solution provided. Following a 5-minute incubation at 37°C, a peroxidase solution was added to the samples and the plate was incubated for 5 minutes. The absorbance was immediately read at 550 nm using a microplate reader.

Platelet-leukocyte aggregate formation and P-selectin expression in whole blood

Murine blood samples were diluted 1:2 in PBS and incubated with either FITC-conjugated anti-mouse CD11b (dilution 1:100 in PBS) or CD4 (dilution 1:100 in PBS) or CD14 (dilution 1:100 in PBS) and PE-conjugated anti-mouse CD41 (dilution 1:100 in PBS) or with FITC-conjugated anti-mouse P-selectin (dilution 1:100 in PBS) for 20 minutes at 25°C. The reaction was stopped by adding BD FACSTM lysing solution (1:10 in PBS). Samples were kept in the dark and at 4°C prior to analysis. Flow cytometry was performed using Accuri-C6 System and data were analyzed with FlowJo software. Platelet ($CD41^+$) and leukocyte ($CD11b^+$) or T lymphocyte ($CD4^+$) or monocyte ($CD14^+$) aggregates were discriminated by forward and side light scatter and identified by their positive staining for PE-CD41 or FITC-CD11b, or FITC-CD4, or FITC-CD14 respectively. Events double positive for PE and FITC were identified aggregates and were recorded as a percentage of a total of 20,000 gated neutrophils or monocytes or T lymphocytes. Gating strategies are shown in Supplemental Figures 1A–C.

Platelet factor 4 and soluble P-selectin measurement

Plasma aliquots from each animal were obtained by centrifugation (2,000g for 10 minutes) of the blood samples and the plasma was immediately frozen. To detect PF4 and soluble p-selectin concentrations, corresponding ELISA kits (Sigma) were used. The assay was performed as described by the manufacturer. Briefly, Standard protein of mouse PF4 and P-selectin were reconstituted and diluted accordingly to provide a standard stock solution. Samples and standard were added to a 96-well plate coated with either anti-human PF4 or anti-P-selectin antibody, covered and incubated at room temperature for 2.5 hours and overnight at 4°C respectively with gentle shaking. The plates were washed and biotinylated mouse P-selectin or biotinylated anti-mouse PF-4 detection antibodies was added to each well and incubated at room temperature for an hour with gentle shaking. After washing, HRP conjugated streptavidin was added to each well and incubated for 45 minutes at room temperature. Then 3,3,5,5'-tetramethylbenzidine (TMB) in buffer solution was added to each well and incubated in the dark at room temperature for 30 minutes. The reaction was stopped by adding stop solution (0.2M sulfuric acid) to each well and the absorbance immediately read at 450nm using a micro-plate reader.

Thromboxane generation assay

Plasma aliquots from each animal were obtained by blood centrifugation (2,000g for 10 minutes). Samples were used to evaluate thromboxane generation using a TXB_2 EIA kit from Enzo Life Sciences (catalog no. ADI-901-002). The assay was performed as described by the manufacturer. Briefly, TXB_2 standard was prepared using Assay Buffer (tris buffered saline solution supplemented with proteins and sodium azide). Standards and unknown samples were pipetted into the appropriate wells. Blue conjugate (alkaline phosphatase-conjugated with TXB_2) and antibody solution (rabbit polyclonal antibody to TXB_2) was pipetted into each well. The plate was incubated at room temperature for 2 hours and washed using a wash solution (tris buffered saline containing detergents). pNpp substrate solution (p-nitrophenyl phosphate in buffer) was added to each well and incubated at room temperature for 45 minutes. The reaction was stopped using trisodium phosphate in water and the optical density read immediately at 405nm.

Cytokine measurements

Plasma aliquots from each animal were obtained by blood centrifugation (2,000g for 10 minutes). Levels of RANTES, Il-1β, IL-17, TNF-α, and IFN-γ were determined using the high sensitivity mouse cytokine discovery array 32-plex (Eve Technologies, Calgary, Canada).

Human peripheral blood mononuclear cell isolation

Human blood was obtained from healthy volunteers following informed consent. The Institutional Review Board of North Dakota State University approved the study (#3735). The age of the donors is 39.4 ± 3.0 for females and 38.5 ± 3.6 for males. Blood was collected in 3.2% sodium citrate vacutainers. Blood was diluted with RPMI1640, added to 10 ml of Ficoll-Paque, and centrifuged at 300 g for 30 minutes at RT. Peripheral blood mononuclear cells (PBMC) were collected from the interphase and washed twice in PBS. Viable cell numbers were

determined using Eve Automatic Cell counter (NanoEntek, Walthan, MA). Cells with viability higher than 85% were selected and viability was taken into account when the cell number was calculated. Cells ($0.5x10^6$ cells/mL) were then cultured at 37°C and 5% CO_2 in RPMI 1640 media, fully supplemented with penicillin-streptomycin (each at 0.8 mM) and L-glutamine (2 mM).

Peripheral blood mononuclear cell culture and treatments

PBMC were co-cultured for 3 days at 37°C in the presence or absence of LPS (1μM). To block the $P2Y_{12}$ signaling pathway *in vitro*, we used Ticagrelor (100μg/mL), a well-established selective $P2Y_{12}$ antagonist, which has been used in multiple *in vitro* studies (32, 33, 39, 40). To block the $P2Y_1$ signaling pathway *in vitro*, we used MRS2279 (MRS, 100μg/mL), a well-established selective $P2Y_1$ antagonist, which has been used in multiple *in vitro* studies (41–44). Negative control cells received an equivalent amount of vehicle (saline). Three-days after LPS exposure, cells were collected and analyzed using flow cytometry. The supernatant was collected and stored at -20°C prior to analysis.

$CD4^+$ and $CD8^+$ cell population

CD4 and CD8 phenotyping were measured *via* flow cytometry. Isolated PBMC (0.5×10^6 cells) were incubated with FITC-conjugated anti-human CD4 (1:100 dilution in saline) and PE-conjugated anti-human CD8 antibodies (1:100 dilution in saline) for 1 hour at room temperature. Cells were washed in PBS and kept in PBS at 4°C prior to analysis. Cells were then acquired using Accuri-C6 System and analyzed using the Flow Jo software. The total number of events acquired was 20,000 for each sample. Data are shown as a % of positive events as compared to the total number of events acquired (20,000) (Figure 1). Rat IgG2a κ isotype control FITC (clone eBR2a), rat IgG2b κ isotype control PE (clone eB149/10H5) were included as negative isotype controls. Gating strategies are shown now in Supplemental Figures 1D, E.

TNF-α measurement

Supernatant from human cell samples were collected by centrifugation (5,000g for 10 minutes) at day 3. TNF-α levels were determined by ELISA (Invitrogen - Waltham, MA). The assay was performed following manufacturer instructions. Briefly, samples and standards were incubated with Biotin-conjugate antibody (anti-human TNF-α polyclonal antibody) at room temperature for 2 hours and washed with assay buffer (PBS with 1% Tween 20, 10% BSA). Then samples were incubated with Streptavidin-HRP for 1 hour at room temperature. The wells were washed using the assay buffer and TMB substrate solution (tetramethyl-benzidine) was added to all wells and incubated at room temperature for 10 minutes. The reaction was stopped using Phosphoric acid (1M) and the absorbance was read immediately at 450 nm using a spectrophotometer.

IFN- γ measurement

Supernatant from human cell samples were collected by centrifugation (5,000g for 10 minutes) at day 3. IFN-γ concentrations were determined by ELISA (Invitrogen - Waltham, MA). The assay was performed following manufacturer instructions. Standards and samples were added to the wells, and incubated overnight at 4°C with gentle shaking. The wells were washed with the wash buffer provided and standards and samples were incubated with biotin conjugate for 1 hour at room temperature. After washing the plate, standards and samples were incubated with streptavidin-HRP for 45 minutes at room temperature. After washing the plate, standards and samples were incubated with TMB substrate solution (tetramethyl-benzidine) in the dark at room temperature for about 30 minutes. The stop solution was added, and the absorbance read immediately at 450 nm.

Statistical analysis

Differences among groups were statistically analyzed using one-way ANOVA; Bonferroni's Multiple Comparison Test was used as a *post-hoc* analysis. Each treatment group included four or more experiments ($n \geq 4$), based on power calculations and work performed previously (45–47). For human cell experiments: each independent experiment was performed using platelets and PBMCs isolated from one donor. PBMCs and platelets from 4 donors were isolated, co-cultured, stimulated and analyzed. Differences among groups were analyzed using a one-way ANOVA test. The analysis was performed in an unpaired fashion. $P < 0.05$ was considered to be significant. Data are reported as mean ± standard error of the mean (S.E.M.) for each group.

Results

Inflammation-induced elevation in circulating white blood cells counts is decreased in male $P2Y_{12}$ and female $P2Y_1$ null mice

First, we analyzed the number of circulating white blood cells (WBC), lymphocytes (LY) and neutrophils (PMN) in blood

10.3389/fimmu.2022.1015577

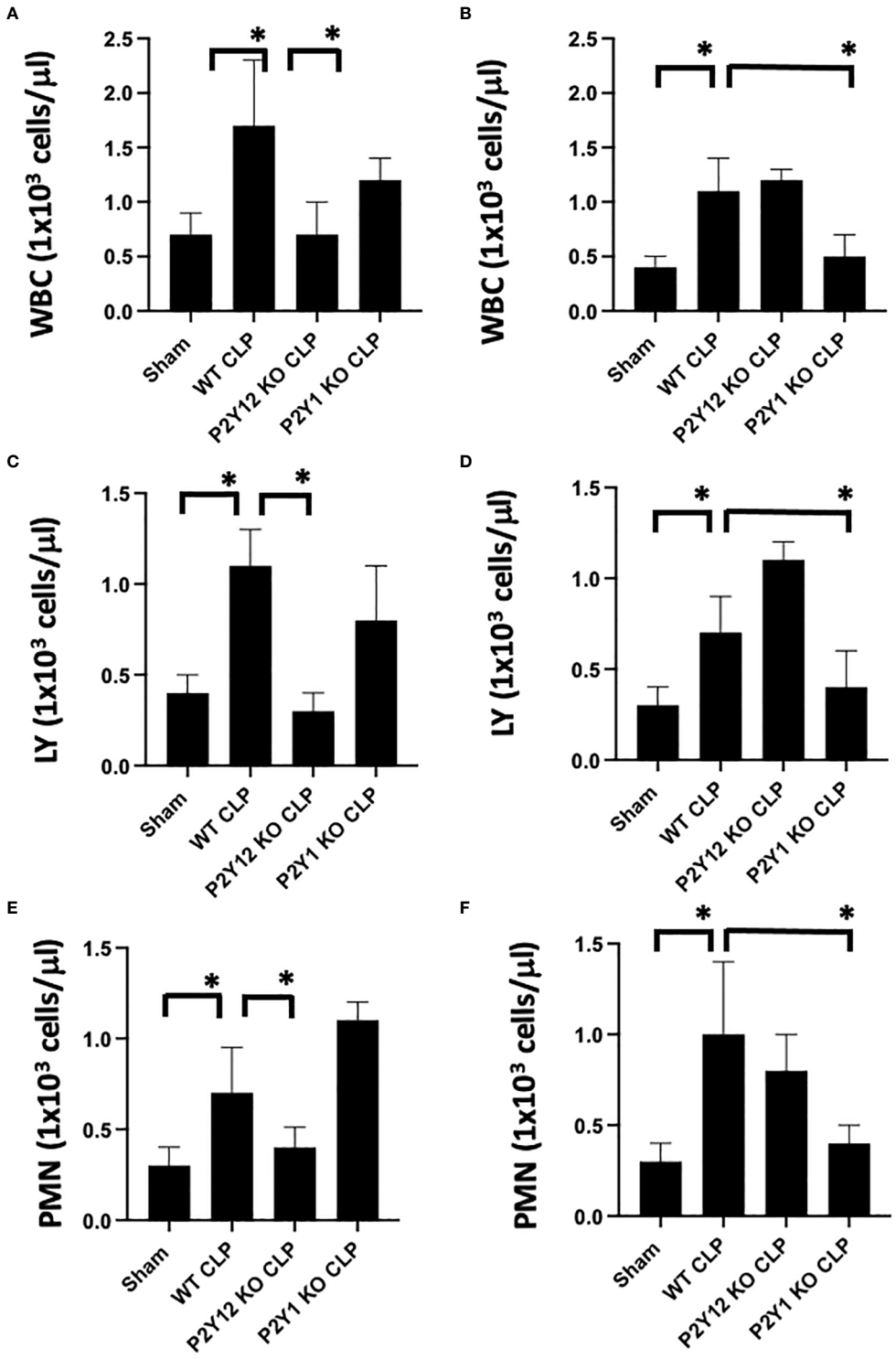

FIGURE 1
Inflammation-induced elevation in circulating white blood cell counts is decreased in male $P2Y_{12}$ and female $P2Y_1$ KO mice. Blood samples were collected by cardiac puncture in 3.8% sodium citrate (10:1), and hematology studies were performed. Graphs show counts of White blood cells (WBC, **A, B**) lymphocytes (LY; **C, D**), and neutrophils (PMN; **E, F**). Sham and CLP in wild-type (WT) and $P2Y_{12}$ KO and $P2Y_1$ mice of male **(A, C E)** and female **(B, D, F)** mice. Values are expressed as $1x10^3$cells/µL, mean ± S.E.M. n = 5). (*P < 0.05). No differences between WT, $P2Y_{12}$ KO, and $P2Y_1$ KO sham were noted in both male and female mice (data not shown).

samples (Figure 1) from WT, $P2Y_1$ KO and $P2Y_{12}$ KO male and female mice. Upon CLP surgery, we observed a significant increase in leukocyte count (white blood cells (A-B), lymphocytes (C-D) and neutrophils (E-F) in septic mice as compared with the Sham group in both male (A-C-E) and female (B-D-F) mice (Figure 1, $P<0.05$; male CLP vs male sham or CLP vs female CLP vs female sham). Interestingly, the increase was more pronounced in male septic mice as compared with the female counterpart (Figure 1, $P<0.05$; male CLP vs female CLP) for white blood cells, lymphocytes, and neutrophils. However, the sepsis-induced leukocyte count (white blood cells, lymphocytes, and neutrophils) was not increased in the CLP $P2Y_{12}$ KO male mice compared to WT CLP male mice (Figures 1A, C, E $P<0.05$; male CLP vs male $P2Y_{12}$ KO CLP) but no change in CLP $P2Y_1$ KO male mice was noted (Figures 1A, C, E). In female mice, no difference was noted between CLP $P2Y_{12}$ KO mice and WT CLP mice, while leukocyte count (lymphocytes and neutrophils) was not increased in the CLP $P2Y_1$ KO female mice compared to WT CLP female (Figures 1B, D, F) $P<0.05$; female CLP vs female $P2Y_1$ KO CLP. Platelet count did not change in all the groups analyzed (data not shown).

Sepsis-induced increase of MPO activity in the lungs is reduced in male septic $P2Y_{12}$ and female septic $P2Y_1$ KO mice

As the lung is one of the most affected organs during sepsis (48–50), we investigated MPO activity in lung tissue as an indication of neutrophil infiltration in the tissue (Figure 2). Lung samples from Sham and CLP mice were analyzed for male and female mice in WT, $P2Y_1$, and $P2Y_{12}$ KO. Although MPO activity was significantly increased in both male (Figure 2A) and female (Figure 2B) WT mice following CLP as compared with the Sham counterpart (Figure 2, $P<0.05$; male CLP vs male sham and female CLP vs female sham), a higher increase in MPO activity was noted in male WT CLP mice as compared with female WT CLP mice (Figure 2, $P<0.05$; male CLP vs female CLP). MPO activity was not elevated in the lungs of KO $P2Y_{12}$ CLP mice as compared to the activity in CLP WT mice in males (Figure 2. A $P<0.05$; male CLP vs male $P2Y_{12}$ KO CLP), while no difference between WT and $P2Y_{12}$ KO was seen in female mice (Figure 2B). These data suggest that $P2Y_{12}$ deficiency alter pulmonary inflammation and inflammatory cell recruitment in male but not in female mice during sepsis. In $P2Y_1$ mice, we did not see any difference in MPO activity in male $P2Y_1$ KO CLP mice as compared with male WT CLP mice (Figure 2A). However, in female mice, MPO activity is significantly reduced in female $P2Y_1$ KO CLP compared with WT CLP mice (Figure 2B, $P<0.05$; female CLP vs female $P2Y_1$ KO CLP). These data suggest that $P2Y_1$ deficiency alter sepsis-induced pulmonary inflammation and inflammatory cell recruitment in female mice but not male mice.

Sepsis induced- platelet activation was decreased in male septic $P2Y_{12}$ and female septic $P2Y_1$ KO mice

To determine whether sepsis-induced platelet activation was sex-dependent or required $P2Y_{12}$ or $P2Y_1$ signaling, we

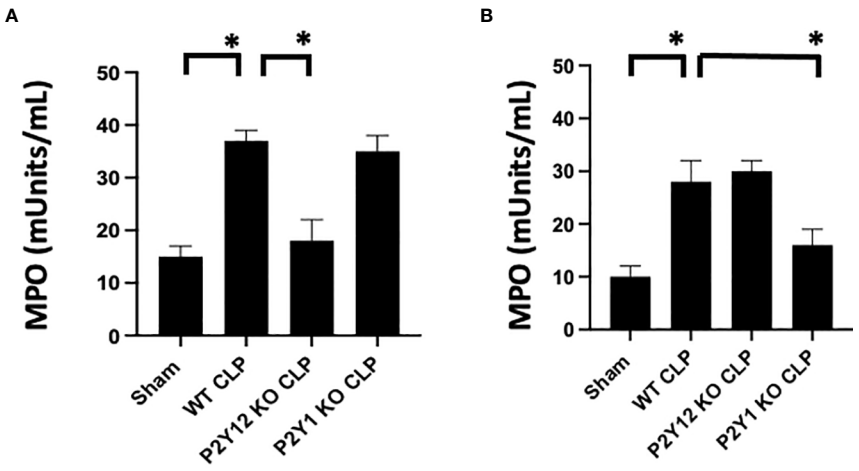

FIGURE 2
Sepsis-induced increase of activity of MPO in the lungs is reduced in male septic $P2Y_{12}$ and female septic $P2Y_1$ KO mice. MPO analysis was performed in lung samples of Sham and CLP in wild-type (WT) and $P2Y_{12}$ KO and $P2Y_1$ mice of male **(A)** and female **(B)** mice. Values are expressed as mUnits/mL, mean ± SEM. (*P < 0.05) (n = 5). No differences between WT, $P2Y_{12}$ KO, and $P2Y_1$ KO sham were noted in both male and female mice (data not shown).

measured p-selectin platelet surface expression in septic mice (WT, $P2Y_{12}$ KO CLP and $P2Y_1$ KO CLP) for both male (Figure 3A) and female (Figure 3B). P-selectin was increased in both WT CLP male and female mice as compared with Sham counterparts (Figure 3, $P<0.05$; male CLP vs male sham and female CLP vs female sham, $P<0.05$; male CLP vs female CLP). In $P2Y_{12}$ KO CLP mice, sepsis-induced p-selectin values were lower than the WT CLP (Figure 3A $P<0.05$, male CLP vs male $P2Y_{12}$ KO CLP) while no difference between WT CLP and $P2Y_{12}$ KO CLP was noted in female mice. Similarly, to what was noted in Figures 1 and 2, no difference in p-selectin values was reported between WT CLP and $P2Y_1$ KO CLP in male mice, but p-selectin was significantly reduced in $P2Y_1$ KO CLP in female mice (Figure 3B, $P<0.05$, female CLP vs female $P2Y_1$ KO CLP).

Sepsis induced- platelet-leukocyte aggregate formation in whole blood was reduced in male septic $P2Y_{12}$ and female septic $P2Y_1$ KO mice

As platelet-leukocyte interaction is a key step in sepsis, we analyzed platelet-leukocyte aggregate formation in the whole blood and we investigated whether targeting the receptor $P2Y_{12}$ or $P2Y_1$ can modulate platelet-leukocyte interaction differently in male and female mice (Figures 3C, D). First, we measured interaction between platelets (CD41) and leukocyte (CD11b). The percentage of $CD41^+/CD11b^+$ aggregate was increased in male CLP and female CLP as compared with their Sham counterpart (Figures 3C, D, $P<0.05$, male CLP vs male Sham and female CLP vs female sham). Female CLP-induced platelet-leukocyte aggregates was lower than CLP males (Figures 3C, D, $P<0.05$, male CLP vs female CLP). In $P2Y_{12}$ KO CLP mice, sepsis-induced platelet-leukocyte aggregates values were lower than the WT CLP (Figure 3C; $P<0.05$, male CLP vs male $P2Y_{12}$ KO CLP) while no difference between WT CLP and $P2Y_{12}$ KO CLP was noted in female mice (Figure 3D). However, no difference in platelet-leukocyte aggregates was reported between WT CLP and $P2Y_1$ KO CLP in male mice (Figure 3C), but $CD41^+/CD11b^+$ aggregates were significantly reduced in $P2Y_1$ KO CLP in female mice (Figure 3D, $P<0.05$, female CLP vs female $P2Y_1$ KO CLP).

Second, we analyzed the aggregate formation of circulating platelets ($CD41^+$) and T helper ($CD4^+$) cells. The percent of platelet-CD4 lymphocytes aggregate was increased during sepsis as compared with the sham control group in male and female mice (Figure 3C $P<0.05$, male CLP vs male Sham and female CLP vs female sham), but in $P2Y_{12}$ KO male mice platelets-$CD4^+$ T cells aggregates were diminished, suggesting decreased platelets and $CD4^+$ T cells interactions (Figure 3C $P<0.05$, male CLP vs male $P2Y_{12}$ KO CLP). In female mice, no change was noted in platelets and $CD4^+$ T cells interaction upon $P2Y_{12}$ deficiency. No change in platelets-$CD4^+$ T cells aggregate was noted in male CLP $P2Y_1$ KO mice as compared with male CLP WT mice. But in female mice, platelets and CD4+ T cells aggregate is reduced in female CLP $P2Y_1$ KO mice as compared with female CLP WT mice (Figure 3C $P<0.05$, female CLP vs female $P2Y_1$ KO CLP). These data suggest that $P2Y_{12}$ and $P2Y_1$ deficiency reduce platelet-leukocyte and T cell-platelet interactions in a sex-dependent manner.

$P2Y_{12}$ or $P2Y_1$ antagonism attenuates lung and renal MPO activity in sepsis in a sex-related manner

Next, we investigated whether $P2Y_{12}$ or $P2Y_1$ antagonism alters sepsis-induced MPO activity similarly to receptor deficiency. Leukocyte trafficking to the lungs and kidneys are among the most affected organs during sepsis (51, 52). At 24 hours post-CLP, there is evidence of both lung and kidney damage associated with increased leukocyte influx (MPO activity) (31, 53, 54). Next, we determined whether blocking the $P2Y_{12}$ or $P2Y_1$ receptors alters MPO activity in the lung (Figures 4A, B) and kidney (Figures 4C, D) of septic male (4A and C) or female (4B and D) mice. Figure 4A shows that MPO activity was increased during sepsis in the lung (Figure 4A) in male mice as compared with the Sham group ($P<0.05$; male CLP vs male sham). However, when male mice were treated with either MRS2279 or ticagrelor, a significant reduction in MPO was noted in septic male mice as compared with untreated CLP mice ($P<0.05$; CLP vs CLP + MRS2279 or CLP vs CLP + ticagrelor). MPO activity was also increased during sepsis in the lung (Figure 4B) in female mice as compared with the Sham group ($P<0.05$; female CLP vs female sham). However, when female mice were treated with either MRS2279 or ticagrelor, no change was noted in MPO levels in the lung in septic female as compared with untreated female CLP (Figure 4B). Similarly in kidney samples (Figure 4C), when male mice were treated with either MRS2279 or ticagrelor, a significant reduction in MPO was noted in septic mice as compared with untreated mice ($P<0.05$; CLP vs CLP + MRS2279 or CLP vs CLP + ticagrelor). When female mice were treated with either MRS2279 or ticagrelor, no change was noted in MPO levels in the kidney in septic females as compared with untreated female CLP (Figure 4D). These data suggest that blocking either $P2Y_1$ or $P2Y_{12}$ receptors decreased activity of MPO in the lungs and kidneys of male, but not female mice.

We also investigate a plasma indicator of kidney injury such as blood urea nitrogen (BUN)/creatinine ratios. The ratio was elevated in the CLP group in both males (Figure 4E) and females (Figure 4F) as compared to their sham control, demonstrating increased levels of blood urea nitrogen BUN/creatinine ratios upon sepsis. Importantly, in male mice (Figure 4E), exposure to ticagrelor and MRS2279 resulted in a significant decrease in BUN/creatinine ratios ($P<0.05$; CLP vs CLP + MRS2279 or CLP

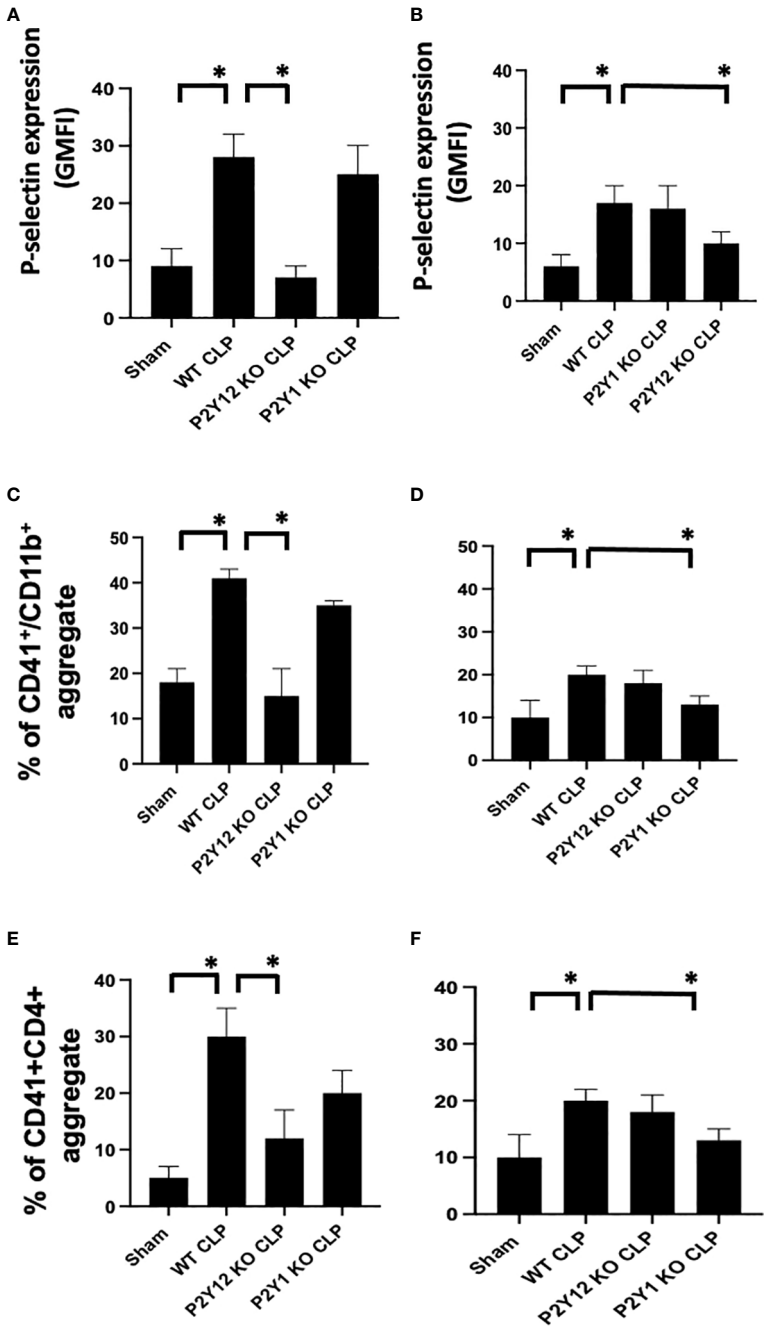

FIGURE 3
Sepsis-induced platelet activation and CD41+/CD11b or CD41+/CD4+ aggregates were decreased in male septic $P2Y_{12}$ and female septic $P2Y_1$ KO mice. Blood samples were collected by cardiac puncture in 3.8% sodium citrate (10:1) **(A, B)** P-selectin expression on the platelet surface was evaluated using flow cytometry in whole blood. Data were collected from WT, $P2Y_{12}$ KO, and $P2Y_1$ mice of male **(A)** and female **(B)** mice. Both Sham and CLP were analyzed. (n=6) (*P<0.05) Values are expressed as Geometric Mean of fluorescence intensity (GMFI), mean ± S.E.M No differences between WT, $P2Y_{12}$ KO, and $P2Y_1$ KO sham were noted in both male and female mice. **(C, D)** Peripheral blood collected from WT, $P2Y_{12}$ KO, and $P2Y_1$ mice of male **(C)** and female **(D)** mice were incubated with antibodies against CD41 (platelet marker) and CD11B (leukocyte marker). Activated leukocytes were gated based on CD11b expression, and cell shape and data were analyzed as a percentage of aggregates expressing both CD41 and CD11b. Values are expressed as the percentage of CD41+/CD11b+ cells, mean ± SEM, n=5). No differences between WT, $P2Y_{12}$ KO, and $P2Y_1$ KO sham were noted in both male and female mice. (*P<0.05). **(E, F)** Peripheral blood collected from WT, $P2Y_{12}$ KO, and $P2Y_1$ mice of male **(E)** and female **(F)** mice was incubated with antibodies against CD41 (platelet marker) and CD4 (T cell marker). T cells were gated based on CD4 expression and cell shape, and data were analyzed based on the percentage of aggregates that express both CD41 and CD4 (n = 6). No differences between WT, $P2Y_{12}$ KO, and $P2Y_1$ KO sham were noted in both male and female mice (data not shown). (*P < 0.05).

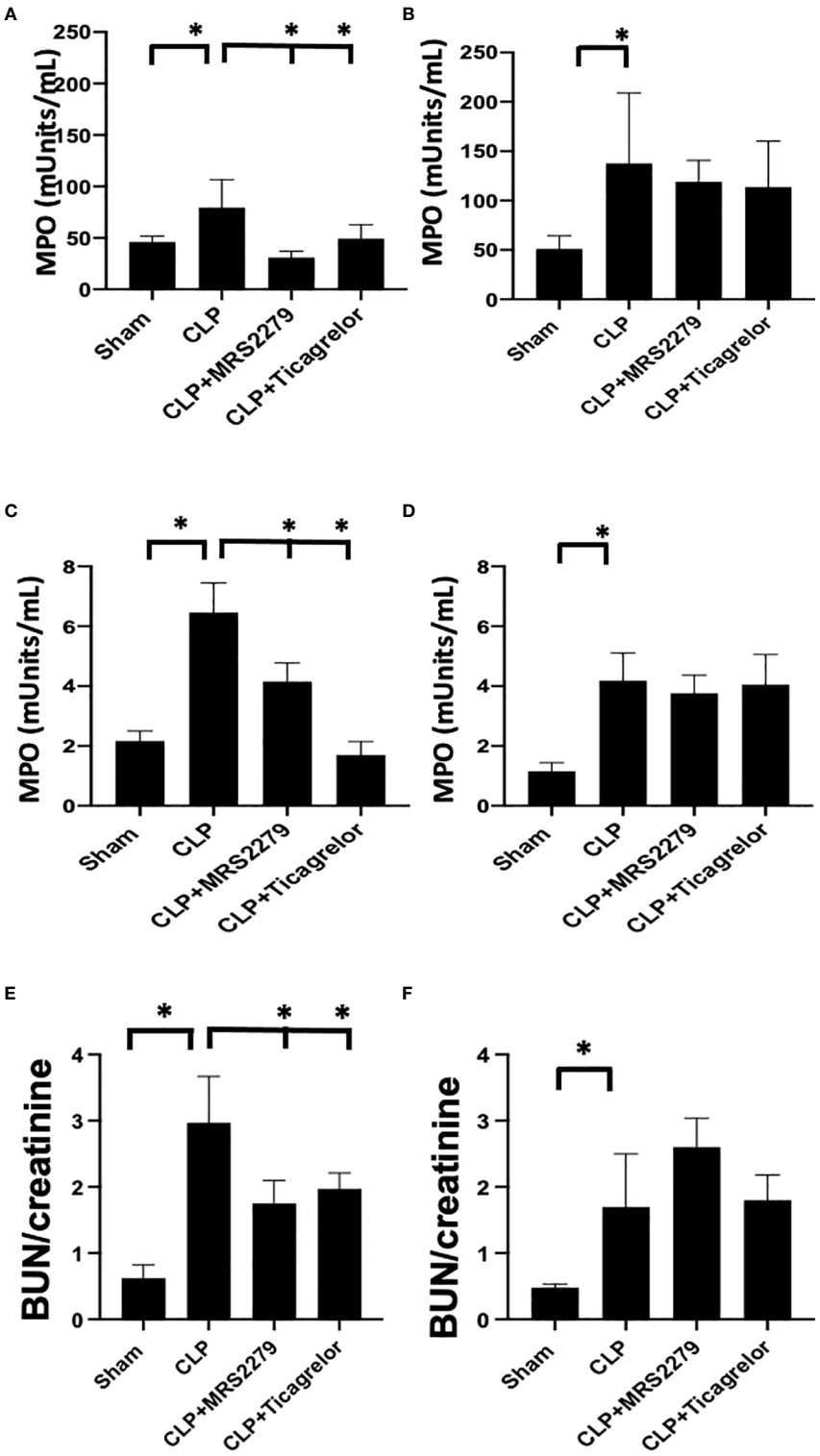

FIGURE 4
$P2Y_{12}$ or $P2Y_1$ antagonism attenuates lung and renal MPO activity in sepsis in a sex-related manner. **(A–D)** MPO analysis was performed in the lung **(A, B)** and kidney **(C, D)** samples of Sham, CLP, MRS2279-treated CLP, and ticagrelor-treated CLP in male **(A, C)** and female mice **(B, D)**. Values are expressed as mUnits/mL, mean ± SEM. (n = 5). (*P < 0.05). **(E, F)** Blood urea nitrogen (BUN)/Creatinine ratios were determined 24 hours post-surgery in plasma samples of Sham, CLP + CLP, MRS2279-treated CLP, and ticagrelor-treated CLP in male **(E)** and female mice **(F)**.

vs CLP + ticagrelor). No changes were noted in female mice upon treatments (Figure 4F).

$P2Y_{12}$ or $P2Y_1$ antagonism alters sepsis-induced platelet activation, and platelet–leukocyte aggregate formation in a sex-specific manner

We investigated whether $P2Y_{12}$ or $P2Y_1$ antagonism can influence platelet activation in male and female mice during sepsis. We analyzed P-selectin expression on the surface of circulating platelets (Figures 5A, B) and the levels of soluble p-selectin in the plasma (Figures 5C, D). In both male (Figure 5A) and female (Figure 5B) mice, sepsis augmented p-selectin expression on platelet surface as compared with their Sham control ($P<0.05$; male Sham vs male CLP or female Sham vs female CLP). P-selectin expression was higher in septic males as compared with septic female mice ($P<0.05$; male CLP vs female CLP). In male mice, treatment with MRS2279 p-selectin surface expression was not changed in response to CLP, while ticagrelor treatment significantly prevented the sepsis induced elevation of p-selectin surface expression as compared with untreated CLP ($P<0.05$; CLP vs CLP + ticagrelor). In female mice, no change was noted in p-selectin expression upon treatment with either MRS2279 or ticagrelor as compared with untreated CLP (Figure 5B). Similar results were noted for soluble p-selectin in the plasma of septic mice. (Figures 5C, D). Again, soluble p-selectin was higher in untreated septic male mice as compared with septic female mice ($P<0.05$; male CLP vs female CLP). In male mice, treatment with MRS2279 or ticagrelor lowered sepsis-elevated soluble p-selectin as compared with untreated CLP (Figure 5C; $P<0.05$; CLP vs CLP + MRS2279; CLP vs CLP + ticagrelor). In female mice, no change was noted in p-selectin expression upon treatment with either MRS2279 or ticagrelor as compared with untreated CLP (Figure 5D).

Aggregates of platelets and other immune cells have been observed in peripheral whole blood during other diseases [22, 23], including sepsis (26, 31). Hence, we investigated the aggregates of platelets and CD4+ T cells (Figures 5E, F) or CD14+ cells (Figures 5G, H) circulating in the whole blood of sham control, CLP mice, and CLP mice treated with MRS2179 or ticagrelor in both male and female (Figure 5). Aggregates were analyzed using flow cytometry. CD4+ or CD14+ cells were gated, and the percent of aggregates as events positive for both CD41 and CD4 Figures 5E, F) or CD41 and CD14 (Figures 5G, H) respectively was determined. Platelet-CD4+ T cell aggregate formation was increased during sepsis as compared with the sham control group in both male and female mice (Figures 5E, F, $P<0.05$; male Sham vs male CLP, female Sham vs female CLP). The % of platelet-CD4+ T cell aggregate was significantly higher in male CLP mice as compared with CLP female mice ($P<0.05$; male CLP vs female CLP). Treatment with either MRS2279 or ticagrelor dramatically diminished aggregate formation in male mice (Figure 5E; $P<0.05$; CLP vs CLP + MRS2279; CLP vs CLP + ticagrelor), suggesting that blockade of either $P2Y_{12}$ or $P2Y_1$ signaling pathway contribute to decrease platelets and CD4+ T cells interactions in male mice. No change was noted in female mice when either $P2Y_{12}$ or $P2Y_1$ were blocked (Figure 5H).

$P2Y_{12}$ or $P2Y_1$ antagonism decreased sepsis-induced platelet secretion in both male and female mice

We and other groups have previously observed an increase in platelet secretion during sepsis in animal models and patient samples (26, 31, 55, 56). Hence, we determined platelet secretion in septic male and female mice with and without blockade of either $P2Y_{12}$ or $P2Y_1$ signaling pathway (Figure 6). We measured plasma levels of platelet-factor 4 (PF-4) and Thromboxane (TBX-B2). As previously observed, both PF-4 and Thromboxane were elevated in male or female septic mice as compared with Sham control (Figure 6) $P<0.05$; Sham vs CLP in male and female). Interestingly, in contrast with the data obtained in KO mice (Figure 4), levels of both PF-4 and Thromboxane upon sepsis were comparable between male and female mice. Septic-induced Thromboxane increase was not noted in CLP male mice when mice were treated with either MRS2279 or ticagrelor as compared with untreated male CLP mice (Figure 6A, $P<0.05$; CLP vs CLP + MRS2279; CLP vs CLP + ticagrelor). Similar data were noted in female mice (Figure 6B), where either MRS2279 or ticagrelor treatment prevented the sepsis- elevated level of Thromboxane ($P<0.05$; CLP vs CLP + MRS2279; CLP vs CLP + ticagrelor). Similarly, PF-4 levels were not elevated in CLP male mice when mice were treated with either MRS2279 or ticagrelor as compared with untreated male CLP mice (Figure 6C; $P<0.05$; CLP vs CLP + MRS2279; CLP vs CLP + ticagrelor). Similar data were noted in female mice, where either MRS2279 or ticagrelor treatment prevented the elevated level of PF-4 (Figure 6D; $P<0.05$; CLP vs CLP + MRS2279; CLP vs CLP + ticagrelor). These data suggest that blocking either $P2Y_{12}$ or $P2Y_1$ signaling pathway prevents sepsis-elevated platelet secretion in a sex-independent manner.

$P2Y_{12}$ or $P2Y_1$ antagonism selectively alter cytokine levels in the plasma in a sex-specific manner

As an increase in circulating cytokines has been observed in patient samples (49, 57) and it has been related to the severity of the disease (58, 59), we investigated levels of RANTES, IL-10, IL-1β, IL-17, TNF-α and IFN-γ in plasma samples (Figure 7). As expected, all

10.3389/fimmu.2022.1015577

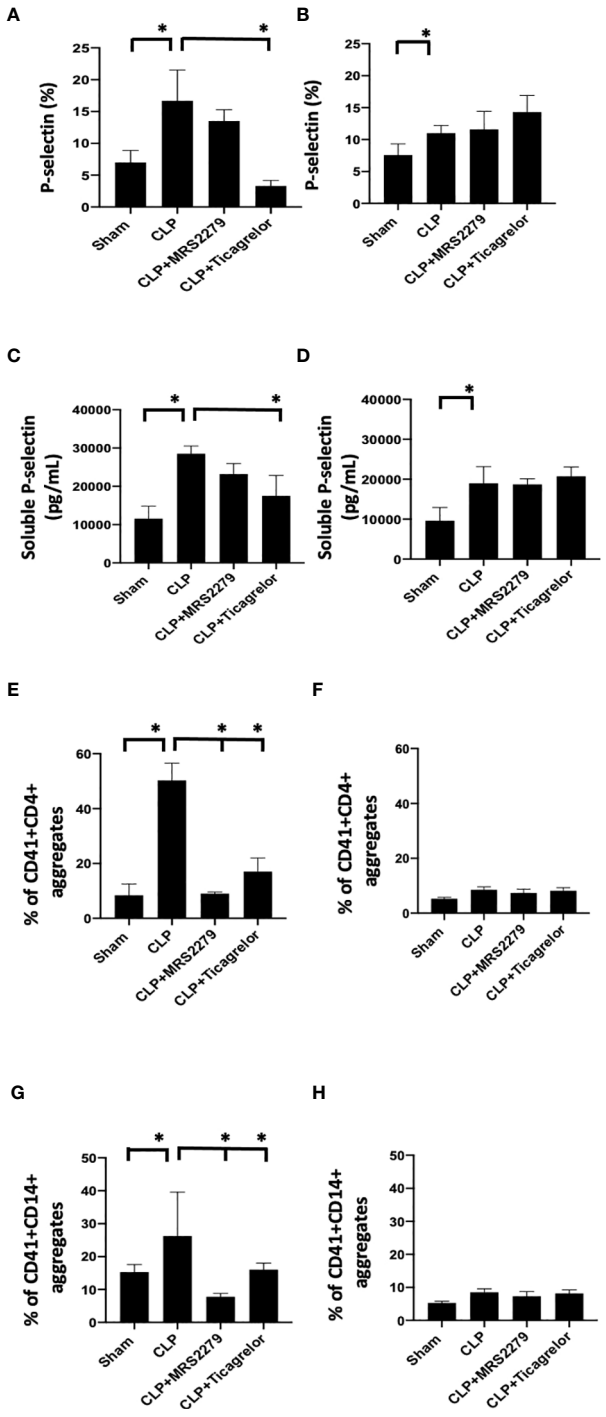

FIGURE 5
$P2Y_{12}$ or $P2Y_1$ antagonism alters sepsis-induced platelet activation, and platelet–leukocyte aggregate formation in a sex-specific manner. **(A, B)**_Blood samples were collected by cardiac puncture in 3.8% sodium citrate (10:1) P-selectin expression on platelet surface was evaluated using flow cytometry in whole blood. Data were collected from Sham and CLP in male **(A)** and female mice **(B)**. Mice were untreated or treated with MRS (50mg/kg) or ticagrelor (30 mg/kg). Values are expressed as % of platelets positive to p-selectin, mean ± S.E.M. (*P < 0.05). **(C, D)** Soluble p-selectin was analyzed in the plasma collected from Sham and CLP male **(C)** and female **(D)** mice using an ELISA kit. Mice were untreated or treated with MRS (10mg/kg) or ticagrelor (10mg/kg). Values are expressed as pg/mL, mean ± S.E.M. (*P < 0.05). **(E-H)** Samples were collected from Sham and CLP male **(E–G)** and female **(F–H)** mice. Samples were incubated with antibodies against CD41 (platelet marker) and CD4 (T cell marker, **E, F**) or CD14 (monocyte marker, **G, H**). T cells or monocytes were gated based on CD4 or CD14 expression respectively and cell shape. Data were analyzed based on the percentage of aggregates that express both CD41 and CD4 **(E, F)** or CD14 **(G, H)**. Values are expressed as the percentage of CD41+/CD11b+ cells, mean ± SEM n = 7).

10.3389/fimmu.2022.1015577

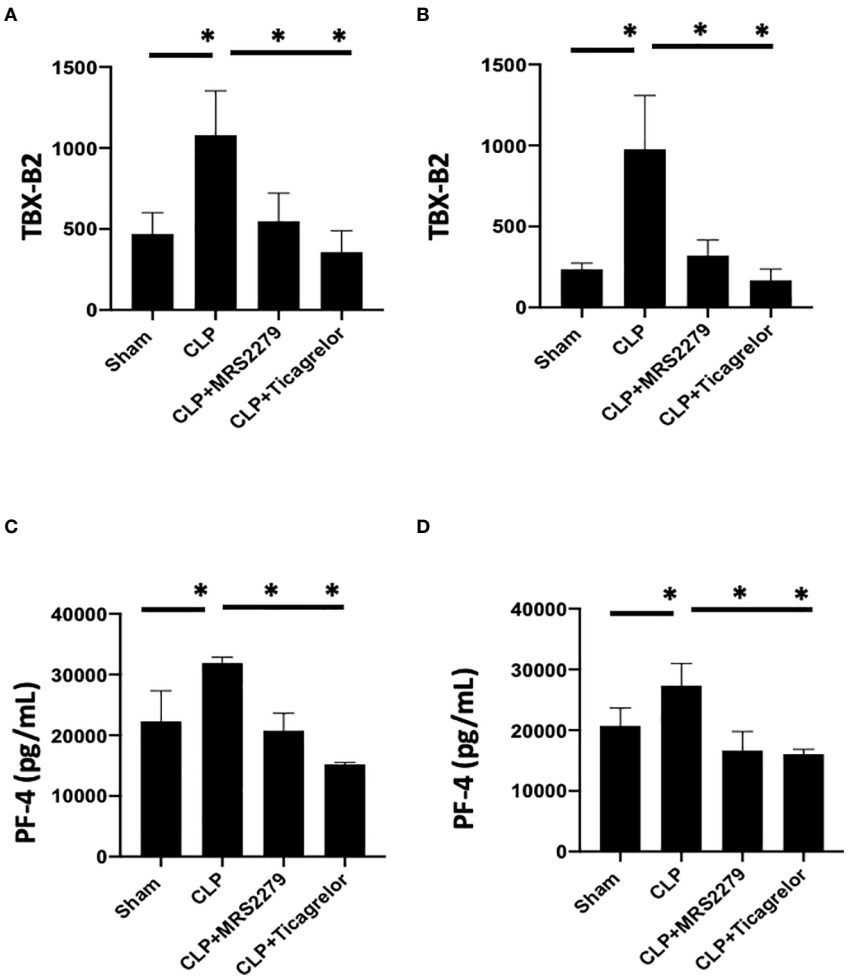

FIGURE 6
$P2Y_{12}$ or $P2Y_1$ antagonism decreased sepsis-induced platelet secretion in both male and female mice. Plasma levels of Thromboxane (TBX-B2) **(A, B)** or PF4 **(C, D)** were evaluated in female (left) and male (right) mice that underwent Sham or CLP surgery. Mice were treated with MRS2279 (MRS) or ticagrelor. Values are expressed as pmol/mL (*p < 0.05, n = 6).

cytokines' levels were significantly higher in septic mice as compared with their Sham counterpart for males (Figures 7A, C, E, G, I, K) and female (Figures 7B, D, F, H, J, L) mice.

For male mice, the sepsis-induced increase in RANTES plasma levels was decreased in mice treated with ticagrelor (Figure7A, $P<0.05$; CLP vs CLP + ticagrelor), while no change was noted when septic male mice were exposed to MRS2279. On the other hand, in female mice, the sepsis-induced increase in RANTES plasma levels was decreased when mice were exposed to MRS2279 (Figure 7B, $P<0.05$; CLP vs CLP MRS2279), while no change between septic mice was noted when mice were exposed to ticagrelor. Similar data were observed for IL-10 (Figures 7C, D) and IL-1β (E-F).

On the contrary, IL-17 levels were non increased in septic male mice treated with either ticagrelor or MRS2279 (Figure 7G, $P<0.05$; CLP vs CLP MRS2279 and CLP vs CLP + ticagrelor). On the other hand, in female mice, the sepsis-induced increase in IL-1β plasma levels was noted while mice were exposed to MRS2279 (Figure 7F, $P<0.05$; CLP vs CLP MRS2279), while an increase in IL-17 was noted in septic female mice exposed to ticagrelor as compared with septic untreated female mice (Figure 7H, $P<0.05$; CLP vs CLP MRS2279 and CLP vs CLP + ticagrelor).

No change was noted in both male and female mice in TNF-α levels in any of the treated groups as compared with septic males and females (Figures 7I, J).

Similarly, for male mice, the sepsis-induced increase in IFN-γ plasma levels were noted while mice were exposed to ticagrelor (Figure 7K, $P<0.05$; CLP vs CLP + ticagrelor), while no change between septic mice was noted when mice were exposed to MRS2279. On the other hand, in female mice, no change

10.3389/fimmu.2022.1015577

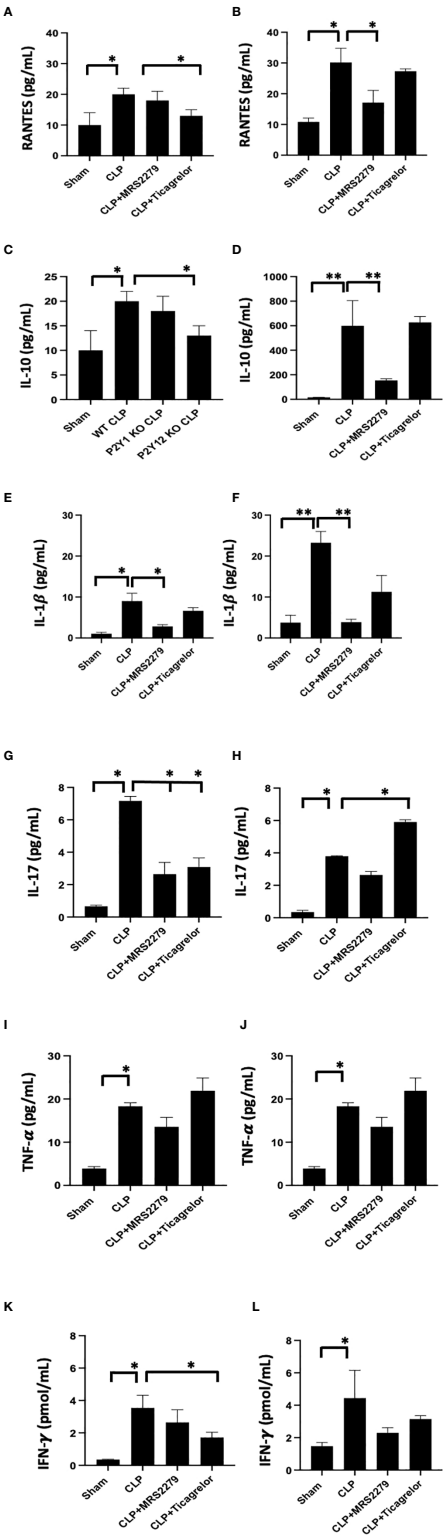

FIGURE 7
P2Y12 or P2Y1 antagonism selectively alters cytokine plasma levels in a sex-specific manner. Plasma samples obtained from each animal were used for detection levels of RANTES **(A, B)**, IL-10 **(C, D)**, IL-1β **(E, F)**, IL-17 **(G, H)**, TNF-α **(I,J)**, and IFN-γ **(K, L)**. Both Sham and CLP samples were analyzed for male and female mice. Mice were treated with MRS2279 (MRS) or ticagrelor. Values are expressed as pg/mL (*P < 0.05; **P < 0.01; n = 5).

between treated septic mice and their treated counterpart was noted (Figure 7L).

$P2Y_1$ antagonism selectively alters CD4 and CD8 cell populations in female but not male human PBMCs

To determine whether the sex-specific effects of purinergic signaling blockage that we noted in mice during sepsis is also observed in human cells, we investigated whether blocking $P2Y_1$ or $P2Y_{12}$ signaling pathways influence CD4 and CD8 differentiation when PBMCs cells are stimulated with LPS (Figure 8). PBMCs were isolated from male and female donors and $P2Y_1$ or $P2Y_{12}$ signaling pathways were blocked using MRS2179 and ticagrelor respectively (Figure 8, 100μg/mL). PBMCs were incubated with LPS (1μM) for 72 hours. Percentage of CD4 and CD8 cells (Figures 8A, B) was determined using flow cytometry and cytokine secretion was determined by ELISA (Figures 8C, D).

In PBMCs isolated from male donors, in unstimulated PBMCs the % of CD8+ cells increased in unstimulated cells when treated with either MRS2179 or ticagrelor as compared with untreated unstimulated cells (Figure 8A, $P<0.05$; Unstim vs Unstim + MRS2279; Unstim vs Unstim + ticagrelor). No changes were noted in LPS-stimulated PBMCs isolated from male donors. Interestingly in unstimulated PBMC from female subjects, exposure to MRS2279 increased the % of CD8+ cells as compared with untreated cells (Figure 8B, $P<0.05$; Unstim vs Unstim + MRS2279; LPS vs LPS + MRS2279). No change was noted when unstimulated cells from female donors were incubated with ticagrelor (Figure 8B). Similar results were noted in LPS-stimulated PBMC from female donors (Figure 8B). Indeed, exposure to MRS2279 increased the % of CD8+ cells as compared with untreated cells (Figure 8B, $P<0.05$; LPS vs LPS + MRS2279). No change was noted when LPS-stimulated cells from female donors were incubated with ticagrelor (Figure 8B).

In PBMC isolated from male donors, no change was noted in the CD4+ population in unstimulated PBMCs cells when the cells were incubated with MRS2279 or ticagrelor (Figure 8C). However, in LPS-stimulated male PBMCs, the % of CD4+ cells decreased in LPS-stimulated cells when treated with MRS2179 but not ticagrelor compared with untreated LPS-stimulated cells (Figure 8C, $P<0.05$; LPS vs LPS + MRS2279). When female PBMCs were incubated with MRS2279, the % of CD4+ cells increased in unstimulated cells as compared with untreated cells (Figure 8D, $P<0.05$; Unstim vs Unstim + MRS2279). In contrast, in LPS-stimulated PBMCs the % of CD4+ cells decreased in LPS-stimulated cells when treated with either MRS2179 or ticagrelor as compared with untreated LPS-stimulated cells (Figure 8D, $P<0.05$; LPS vs LPS + MRS2279; LPS vs LPS + ticagrelor). These data indicate that blocking purinergic signaling alters the % of the CD8 and CD4 population depending on LPS stimulation in a sex-specific manner.

$P2Y_1$ antagonism selectively alters IFN-γ and TNF-α levels in female but not male PBMCs

Next, we measured the concentration of TNF-α (Figure 8C) and IFN-γ (Figure 8D) in the supernatant of PBMCs cultured in the presence and absence of LPS (1μM - 72 hours) (Figures 8E–H). In male unstimulated cells, TNF-α content was significantly increased when PBMCs were exposed to either MRS or ticagrelor (Figure 8E). In female unstimulated cells, we noted a significant increase TNF-α when cells were treated with MRS, but not ticagrelor (Figure 8E, $P<0.05$; Unstim vs Unstim + MRS; Unstim vs Unstim + ticagrelor). In male LPS-stimulated cells, a significant decrease was noted when cells were incubated with either MRS or ticagrelor (Figure 8E, $P<0.05$; LPS vs LPS + MRS; LPS vs LPS + ticagrelor). In female LPS-stimulated cells, no change was noted in TNF-α in the supernatant when cells were treated with MRS, but a significant decrease was noted when cells were incubated with ticagrelor (Figure 8F, $P<0.05$; LPS vs LPS + ticagrelor). In unstimulated cells from male donors, INF-γ content was significantly increased when PBMCs were exposed to either MRS or ticagrelor (Figure 8G, $P<0.05$; Unstim vs Unstim + MRS, Unstim vs Unstim + ticagrelor). In unstimulated cells from female donors, no change was noted in INF-γ content between the supernatant collected from unstimulated cells as compared with unstimulated cells treated with either MRS or ticagrelor (Figure 8H). In LPS-stimulated cells from male donors, a significant increase was noted when cells were incubated with MRS but not ticagrelor as compared with the LPS-treated control (Figure 8G, $P<0.05$; LPS vs LPS + MRS). In LPS-stimulated cells from female donors, INF-γ was significantly decreased in cells treated with either MRS or ticagrelor as compared with untreated LPS control (Figure 7H, $P<0.05$; LPS vs LPS + MRS; LPS vs LPS + ticagrelor).

Discussion

Sex differences in the morbidity and mortality of sepsis have been observed in animal models and human diseases (4–8). To date, females have shown decreased mortality and organ failure in mice and humans compared to their male counterparts (4, 7). However, the lack of studies comparing both sexes limits our capacity to evaluate the extent of sex-related differences and to determine a sex-specific treatment as a result. Our previous studies revealed that platelets are important in sepsis and blocking purinergic signaling in platelets alters the outcome of sepsis in male mice (23, 26, 31). However, we are aware of sex-related differences in purinergic signaling responses (41, 60–63) and in platelet activation (20). Hence, it is essential to investigate how female mice respond to sepsis and whether blocking purinergic signaling alters platelets' response in a sex-dependent manner. Our data suggest for the first time that the purinergic receptor $P2Y_{12}$ and $P2Y_1$ influence sepsis-

10.3389/fimmu.2022.1015577

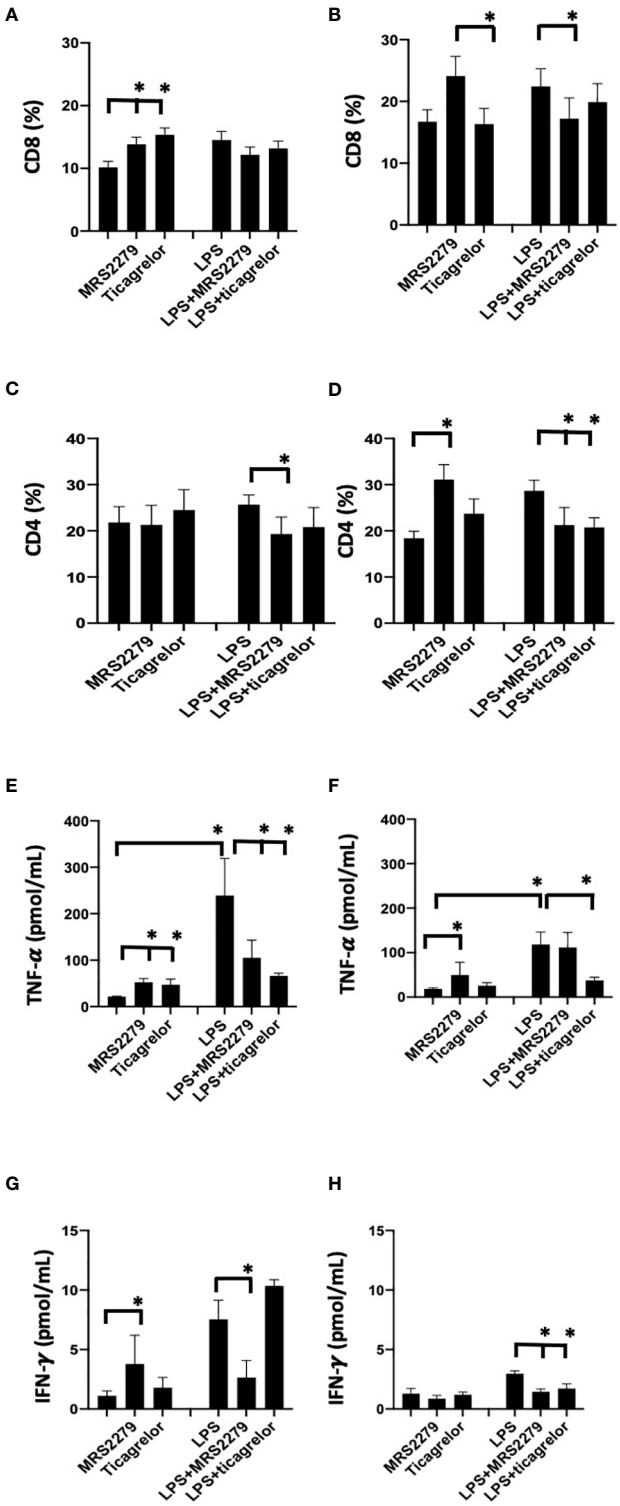

FIGURE 8
P2Y12 or P2Y1 antagonism selectively alter CD4 and CD8 cell populations and cytokine secretion in human PBMCs. Cells isolated from female (black) and male (white) donors were stimulated with LPS (right panel) or left unstimulated (left panel) for 72 h. Cells isolated from male **(A-C-E-G)** and female **(B-D-F-H)** donors were stimulated with LPS (right panel) or left unstimulated (left panel) for 72 hours. Unstimulated cells were cultured without stimuli. Cells were exposed MRS2279 (100μg/mL) or ticagrelor (100μg/mL). Negative control did not receive any treatment. Cell populations positive to CD8 **(A-B)** or CD4 **(C-D)** were determined using flow cytometry. Data are expressed as % of expression ± S.E.M. (*$p < 0.05$, n=6). Cytokine levels in the culture supernatants were determined for TNF-alpha **(E-F)** and IFN-γ **(G-H)**. The groups analyzed were: negative control, MR2279-treated, and ticagrelor-treated cells. Cells were stimulated with LPS (right panel) or left unstimulated (left panel) for 72 h. Values are expressed in pg/ml; means ± S.E.M. are plotted (*$p < 0.05$, n = 6).

induced activity of MPO in lungs and kidneys, circulating cytokines, platelet activation and platelet-leukocyte interaction differently in male and female mice. Hence targeting platelets and the purinergic receptor $P2Y_{12}$ and $P2Y_1$ may be an appropriate therapeutic strategy that is sex dependent.

In our previous studies in male mice using a CLP model of sepsis (19, 21), $P2Y_{12}$ but not $P2Y_1$ deficiency diminished platelet activation and ameliorated the outcome of sepsis (26). When we compared these data with data obtained from female mice, we noted that $P2Y_1$ but not $P2Y_{12}$ deficiency could improve the outcome of sepsis, in terms of neutrophil infiltration in the lungs and kidney, platelet activation, and platelet interaction with other immune cells. Previous data have also shown that purinergic signaling is activated differently in male and female mice (27, 28), and the expression of $P2Y_1$ and $P2Y_{12}$ receptor varies between sexes (29). Ticagrelor is currently used as anti-platelet therapy (64–66) and clinical studies have confirmed that the effects of ticagrelor in preventing cardio-vascular diseases in patients were comparable between men and women (67–69), hence a sex-related therapy may not be required for cardiovascular disease treatment. However, other studies identified significant changes between male and female patients suggesting a discrepancy in the literature that needs to be clarified (70, 71). The effects of ticagrelor on inflammatory conditions have been studied in a variety of animal models (35, 72–75), although most of the studies were performed exclusively on male mice (36, 73–75). Moreover, clinical trials investigating the effects of ticagrelor in patients during inflammatory conditions, such as inflammatory factors during myocardial infarction (76) or pneumonia (75) has started but they have not provided definitive answers. So far, our data suggest that targeting $P2Y_{12}$ may not be the most appropriate approach to treating females in sepsis, and more data are required to determine whether there is any sex-specificity.

Interestingly, in male mice, blocking $P2Y_1$ shows a decrease in activity of MPO in lungs and kidney and platelet-leukocyte interaction, similarly, to blocking $P2Y_{12}$. This was observed in animal models of other diseases, such as colitis (38), Alzheimer (42) and multiple sclerosis (44) when blocking $P2Y_1$ improved the outcome of the disease. However, the data are different from what we observed upon $P2Y_1$ deficiency. In previous studies, $P2Y_1$ blockade and $P2Y_1$ deficiency did show comparable results (38, 77, 78), suggesting that the discrepancy we have observed now could be due to sepsis in general or the CLP model. As previous studies investigating either $P2Y_1$ deficiency or antagonism were performed almost exclusively in male mice (37, 38, 44, 77), our experiments were the first to investigate changes in inflammation levels in sepsis in female mice upon $P2Y_1$ blockade and compare them with the male counterpart. In this model of sepsis, $P2Y_1$ blockade did not improve activity of MPO in lungs and kidneys nor altered platelet interaction with other cells. Surprisingly, this is different from what we observed upon $P2Y_1$ deficiency. This discrepancy could be due to the dose of MRS2279 used or the off-target effects of MRS2279. We have previously noted $P2Y_{12}$-independent effects upon $P2Y_{12}$ antagonism *in vivo* (26) and *in vitro* (79, 80) but so far, no studies have reported similar results when targeting $P2Y_1$. Moreover, the discrepancy could be due to the fact that the $P2Y_1$ antagonist is administered at surgery, while $P2Y_1$ deficiency may alter organ and/or tissue during development. However, it is interesting to notice that the data appear to be sex-specific as we noted the opposite in male mice. Sex-related differences in the immune response have been reported, indicating that some sex-related differences may be germline encoded. Sex-related differences in purinergic signaling expression and responses in female mice as compared with male mice have been reported (41, 60–63). Cytokine secretion upon inflammation has shown to vary between sexes (81). Indeed, we have observed that cytokine levels such as RANTES, IL-1β, IL-10, and IL-17 are altered by blocking $P2Y_1$ or $P2Y_{12}$ differently in septic male and female mice. Hence, purinergic signaling may regulate cytokine secretion in sepsis in a sex-related manner. Blocking $P2Y_{12}$ or $P2Y_1$ has shown to change cytokine secretion in several previous studies (26, 31, 74, 82, 83) but changes between male and female mice have not been measured. It would be interesting to investigate thoroughly whether $P2Y_1$ and $P2Y_{12}$ are expressed differently in the immune system of males and females. One study investigated LPS-induced lung injury in female mice that revealed platelet activation and neutrophil infiltration is dependent on $P2Y_1$ (41). This is a different sepsis model than the one used in this study, but it may suggest that modulating the $P2Y_1$ receptor alters platelet response during LPS-induced inflammation. Furthermore, changes in purinergic signaling may be hormonal-dependent. Indeed, other purinergic receptors such as a P2X7 appeared to be hormonal-dependent (14, 16), hence it would be interesting to determine whether the expression of $P2Y_1$ or $P2Y_{12}$ is related to hormone secretion.

To determine whether this sex-specificity of $P2Y_1$ and $P2Y_{12}$ activation was observed in human cells, we investigated whether PBMCs respond to purinergic signaling blockade *in vitro* when stimulated to LPS. We have previously investigated $P2Y_{12}$ signaling pathways in human T cells and reported that human T cells express $P2Y_{12}$ and $P2Y_{12}$ receptors and blockade altered T cell proliferation and activation in a stimuli-dependent manner (80). However, no experiments have compared $P2Y_1$ or $P2Y_{12}$ blockade in LPS-activated PBMCs obtained from male and female donors. Our data exhibited that PBMCs obtained from male donors blocked by either $P2Y_1$ or $P2Y_{12}$ inhibitors similarly altered $CD4^+$ and $CD8^+$ populations, and these changes depended on whether the cells had been activated with LPS. These observations are supportive of our *in vivo* data, where blocking either $P2Y_1$ or $P2Y_{12}$ improved the outcome of sepsis similarly. However, in PBMCs obtained from female donors, the CD8+ population growth was altered only when $P2Y_1$ was blocked. This is in line with the data we obtained in septic female $P2Y_1$ deficient mice. Data on female mice have shown that $P2Y_1$ blockade but not $P2Y_{12}$ could decrease leukocyte chemotaxis and platelet-leukocyte interaction (41). Taken together the data support that blocking $P2Y_1$ could be a more effective strategy to

modulate the immune response in female mice. In future studies, it will be important to evaluate whether these changes are due to sex-related differences in $P2Y_1$ and $P2Y_{12}$ receptor expression. There are studies investigating how $P2Y_1$ can regulate CD4+ differentiation *in vivo* and *in vitro*. $P2Y_1$ deficiency decreased CD4+ population growth and in particular Th17 differentiation during colonic inflammation (77). *In vitro* experiments in human PBMCs have shown that blocking $P2Y_1$ could modulate CD4+ cell activation (84). Indeed, mRNA levels of $P2Y_1$ are higher than $P2Y_{12}$ (84). In all the studies, no differentiation between male and female cells was analyzed so more data are required before we can identify the most appropriate therapeutic strategy for treating sepsis in both sexes.

The current study has several limitations. First, we have selected the time point of 24 hours post-CLP. It has been shown that at 24 hours organ injury (such as lungs, kidneys, and heart) (48, 50, 85–87), and cytokine levels increase in blood samples of CLP mice (48, 85) are comparable to that noted in septic patients (49, 57). However, to deepen our understanding of sex-related differences in sepsis, exploring a variety of time points is essential. Second, it is true that sepsis can occur at any age, but infants, people with chronic conditions, people with weakened immune systems, and older adults are at high risk (as stated by the Center for Disease Control and Prevention). Indeed, the incidence of sepsis increases with age and is associated with extremely high mortality rates (88, 89). Here, we have selected 8-10-week-old mice, which is comparable to a fertile adult in humans, however, it would be interesting to investigate older or younger male and female mice. These experiments could also investigate whether hormonal changes could be related to $P2Y_1$ and $P2Y_{12}$ expression. Finally, exploring a range of doses for both antagonists will also be an essential future study to determine whether the sex-related effects are dose-dependent.

In conclusion, modulating $P2Y_{12}$ or $P2Y_1$ receptors can be effective in improving sepsis outcomes, depending on the sex. Targeting purinergic signaling represents a promising therapy for sepsis and identifying sex-specific purinergic signaling may lead to more sex-related targeted therapies in sepsis.

Data availability statement

The raw data supporting the conclusions of this article will be made available by the authors, without undue reservation.

Ethics statement

The Institutional Review Board of North Dakota State University approved the study (#3735). The patients/participants provided their written informed consent to participate in this study. The animal study was reviewed and approved by Institutional Animal Care and Use Committee Protocol #A21040 at North Dakota State University (Fargo, ND, USA).

Author contributions

EA collected materials, performed experiments, and analyzed data. PE collected materials performed experiments and analyzed data. SA analyzed data and wrote the manuscript. GPD analyzed data and wrote the manuscript. SPK analyzed data and wrote the manuscript. LEK analyzed data and wrote the manuscript. EL designed the research study, analyzed data, and wrote the manuscript. All authors contributed to the article and approved the submitted version.

Funding

This work was supported by the National Institute of Health, grant AI156627-01 to EL, grant HL155694 to SPK, and by the Defense Threat Reduction Agency (Grant #HDTRA11910012) to LEK.

Acknowledgments

We would like to thank Jamie Brown and Kimberly Peterson from Lillestol Research LLC (Fargo, ND) for collaborating with us in obtaining the human blood samples.

Conflict of interest

The authors declare that the research was conducted in the absence of any commercial or financial relationships that could be construed as a potential conflict of interest.

Publisher's note

All claims expressed in this article are solely those of the authors and do not necessarily represent those of their affiliated organizations, or those of the publisher, the editors and the reviewers. Any product that may be evaluated in this article, or claim that may be made by its manufacturer, is not guaranteed or endorsed by the publisher.

Supplementary material

The Supplementary Material for this article can be found online at: https://www.frontiersin.org/articles/10.3389/fimmu.2022.1015577/full#supplementary-material

SUPPLEMENTARY FIGURE 1
Flow cytometric gating strategy. Gating strategies are shown to define **(A)** platelet-CD4+ T cell aggregates, **(B)** platelet-CD41+ cell aggregates **(C)** p-selectin surface expression, and **(D, E)** T cell populations.

References

1. Singer M, Deutschman CS, Seymour CW, Shankar-Hari M, Annane D, Bauer M, et al. The third international consensus definitions for sepsis and septic shock (Sepsis-3). *JAMA* (2016) 315(8):801–10. doi: 10.1001/jama.2016.0287

2. Martin-Loeches I, Levy MM, Artigas A. Management of severe sepsis: advances, challenges, and current status. *Drug Des Devel Ther* (2015) 9:2079–88. doi: 10.2147/DDDT.S78757

3. Dejager L, Pinheiro I, Dejonckheere E, Libert C. Cecal ligation and puncture: the gold standard model for polymicrobial sepsis? *Trends Microbiol* (2011) 19 (4):198–208. doi: 10.1016/j.tim.2011.01.001

4. Angele MK, Pratschke S, Hubbard WJ, Chaudry IH. Gender differences in sepsis: cardiovascular and immunological aspects. *Virulence* (2014) 5(1):12–9. doi: 10.4161/viru.26982

5. Diodato MD, Knoferl MW, Schwacha MG, Bland KI, Chaudry IH. Gender differences in the inflammatory response and survival following haemorrhage and subsequent sepsis. *Cytokine* (2001) 14(3):162–9. doi: 10.1006/cyto.2001.0861

6. Eachempati SR, Hydo L, Barie PS. Gender-based differences in outcome in patients with sepsis. *Arch Surg* (1999) 134(12):1342–7. doi: 10.1001/archsurg.134.12.1342

7. Failla KR, Connelly CD. Systematic review of gender differences in sepsis management and outcomes. *J Nurs Scholarsh.* (2017) 49(3):312–24. doi: 10.1111/jnu.12295

8. Schroder J, Kahlke V, Book M, Stuber F. Gender differences in sepsis: genetically determined? *Shock* (2000) 14(3):307–10. doi: 10.1097/00024382-200014030-00011

9. Ferretti MT, Iulita MF, Cavedo E, Chiesa PA, Schumacher Dimech A, Santuccione Chadha A, et al. Sex differences in Alzheimer disease - the gateway to precision medicine. *Nat Rev Neurol* (2018) 14(8):457–69. doi: 10.1038/s41582-018-0032-9

10. Dorak MT, Karpuzoglu E. Gender differences in cancer susceptibility: an inadequately addressed issue. *Front Genet* (2012) 3:268. doi: 10.3389/fgene.2012.00268

11. Sceats LA, Morris AM, Bundorf MK, Park KT, Kin C. Sex differences in treatment strategies among patients with ulcerative colitis: A retrospective cohort analysis of privately insured patients. *Dis Colon Rectum.* (2019) 62(5):586–94. doi: 10.1097/DCR.0000000000001342

12. Cekic C, Linden J. Purinergic regulation of the immune system. *Nat Rev Immunol* (2016) 16(3):177–92. doi: 10.1038/nri.2016.4

13. Ledderose C, Bao Y, Kondo Y, Fakhari M, Slubowski C, Zhang J, et al. Purinergic signaling and the immune response in sepsis: A review. *Clin Ther* (2016) 38(5):1054–65. doi: 10.1016/j.clinthera.2016.04.002

14. Beaucage KL, Xiao A, Pollmann SI, Grol MW, Beach RJ, Holdsworth DW, et al. Loss of P2X7 nucleotide receptor function leads to abnormal fat distribution in mice. *Purinergic Signal* (2014) 10(2):291–304. doi: 10.1007/s11302-013-9388-x

15. Lu Y, Jiang Q, Yu L, Lu ZY, Meng SP, Su D, et al. 17beta-estradiol rapidly attenuates P2X3 receptor-mediated peripheral pain signal transduction *via* ERalpha and GPR30. *Endocrinol* (2013) 154(7):2421–33. doi: 10.1210/en.2012-2119

16. Madec S, Rossi C, Chiarugi M, Santini E, Salvati A, Ferrannini E, et al. Adipocyte P2X7 receptors expression: a role in modulating inflammatory response in subjects with metabolic syndrome? *Atherosclerosis* (2011) 219(2):552–8. doi: 10.1016/j.atherosclerosis.2011.09.012

17. Sivcev S, Slavikova B, Rupert M, Ivetic M, Nekardova M, Kudova E, et al. Synthetic testosterone derivatives modulate rat P2X2 and P2X4 receptor channel gating. *J Neurochem* (2019) 150(1):28–43. doi: 10.1111/jnc.14718

18. Bjorkgren I, Lishko PV. Purinergic signaling in testes revealed. *J Gen Physiol* (2016) 148(3):207–11. doi: 10.1085/jgp.201611676

19. Burnstock G. Purinergic signalling in endocrine organs. *Purinergic Signal* (2014) 10(1):189–231. doi: 10.1007/s11302-013-9396-x

20. Martinez-Ramirez AS, Vazquez-Cuevas FG. Purinergic signaling in the ovary. *Mol Reprod Dev* (2015) 82(11):839–48. doi: 10.1002/mrd.22537

21. Zimon A, Erat A, Von Wald T, Bissell B, Koulova A, Choi CH, et al. Genes invoked in the ovarian transition to menopause. *Nucleic Acids Res* (2006) 34 (11):3279–87. doi: 10.1093/nar/gkl387

22. Kim S, Kunapuli SP. P2Y12 receptor in platelet activation. *Platelets* (2011) 22(1):56–60. doi: 10.3109/09537104.2010.497231

23. Liverani E, Kilpatrick LE, Tsygankov AY, Kunapuli SP. The role of P2Y(1) (2) receptor and activated platelets during inflammation. *Curr Drug Targets.* (2014) 15(7):720–8. doi: 10.2174/1389450115666140519162133

24. Murugappa S, Kunapuli SP. The role of ADP receptors in platelet function. *Front Biosci* (2006) 11:1977–86. doi: 10.2741/1939

25. Kahner BN, Shankar H, Murugappan S, Prasad GL, Kunapuli SP. Nucleotide receptor signaling in platelets. *J Thromb Haemost* (2006) 4(11):2317–26. doi: 10.1111/j.1538-7836.2006.02192.x

26. Liverani E, Rico MC, Tsygankov AY, Kilpatrick LE, Kunapuli SP. P2Y12 receptor modulates sepsis-induced inflammation. *Arterioscler Thromb Vasc Biol* (2016) 36(5):961–71. doi: 10.1161/ATVBAHA.116.307401

27. Coleman JR, Moore EE, Kelher MR, Samuels JM, Cohen MJ, Sauaia A, et al. Female platelets have distinct functional activity compared with male platelets: Implications in transfusion practice and treatment of trauma-induced coagulopathy. *J Trauma Acute Care Surg* (2019) 87(5):1052–60. doi: 10.1097/TA.0000000000002398

28. Leng XH, Hong SY, Larrucea S, Zhang W, Li TT, Lopez JA, et al. Platelets of female mice are intrinsically more sensitive to agonists than are platelets of males. *Arterioscler Thromb Vasc Biol* (2004) 24(2):376–81. doi: 10.1161/01.ATV.0000110445.95304.91

29. Crain JM, Nikodemova M, Watters JJ. Expression of P2 nucleotide receptors varies with age and sex in murine brain microglia. *J Neuroinflammation.* (2009) 6:24. doi: 10.1186/1742-2094-6-24

30. Quinton TM, Murugappan S, Kim S, Jin J, Kunapuli SP. Different G protein-coupled signaling pathways are involved in alpha granule release from human platelets. *J Thromb Haemost.* (2004) 2(6):978–84. doi: 10.1111/j.1538-7836.2004.00741.x

31. Albayati S, Vemulapalli H, Tsygankov AY, Liverani E. P2Y12 antagonism results in altered interactions between platelets and regulatory T cells during sepsis. *J Leukoc Biol* (2021) 110(1):141–53. doi: 10.1002/JLB.3A0220-097R

32. Bentur OS, Li J, Jiang CS, Martin LH, Kereiakes DJ, Coller BS. Application of auxiliary VerifyNow point-of-Care assays to assess the pharmacodynamics of RUC-4, a novel alphaIIbbeta3 receptor antagonist. *TH Open* (2021) 5(3):e449–e60. doi: 10.1055/s-0041-1732343

33. Pavlovic N, Kopsida M, Gerwins P, Heindryckx F. Inhibiting P2Y12 in macrophages induces endoplasmic reticulum stress and promotes an anti-tumoral phenotype. *Int J Mol Sci* (2020) 21(21):8177. doi: 10.3390/ijms21218177

34. Huang B, Qian Y, Xie S, Ye X, Chen H, Chen Z, et al. Ticagrelor inhibits the NLRP3 inflammasome to protect against inflammatory disease independent of the P2Y12 signaling pathway. *Cell Mol Immunol* (2021) 18(5):1278–89. doi: 10.1038/s41423-020-0444-5

35. Ye Y, Birnbaum GD, Perez-Polo JR, Nanhwan MK, Nylander S, Birnbaum Y. Ticagrelor protects the heart against reperfusion injury and improves remodeling after myocardial infarction. *Arterioscler Thromb Vasc Biol* (2015) 35 (8):1805–14. doi: 10.1161/ATVBAHA.115.305655

36. Yu C, Gao CM, Xie N, Wang XQ, Ma YQ. Effect of ticagrelor on acute kidney injury in septic rats and its underlying mechanism. *Exp Ther Med* (2021) 21 (5):475. doi: 10.3892/etm.2021.9906

37. Tian G, Zhou J, Quan Y, Kong Q, Wu W, Liu X. P2Y1 receptor agonist attenuates cardiac fibroblasts activation triggered by TGF-beta1. *Front Pharmacol* (2021) 12:627773. doi: 10.3389/fphar.2021.627773

38. Zhang C, Qin J, Zhang S, Zhang N, Tan B, Siwko S, et al. ADP/P2Y1 aggravates inflammatory bowel disease through ERK5-mediated NLRP3 inflammasome activation. *Mucosal Immunol* (2020) 13(6):931–45. doi: 10.1038/s41385-020-0307-5

39. Banka AL, Eniola-Adefeso O. Method article: an *in vitro* blood flow model to advance the study of platelet adhesion utilizing a damaged endothelium. *Platelets* (2022) 33(5):692–9. doi: 10.1080/09537104.2021.1988550

40. Wang P, Hu XX, Li YH, Gao NY, Chen GQ, Chen JL. Inhibitory effect of resveratrol on the pharmacokinetics of ticagrelor *in vivo* and *in vitro*. *Can J Physiol Pharmacol* (2021) 99(8):821–6. doi: 10.1139/cjpp-2020-0512

41. Amison RT, Arnold S, O'Shaughnessy BG, Cleary SJ, Ofoedu J, Idzko M, et al. Lipopolysaccharide (LPS) induced pulmonary neutrophil recruitment and platelet activation is mediated *via* the P2Y1 and P2Y14 receptors in mice. *Pulm Pharmacol Ther* (2017) 45:62–8. doi: 10.1016/j.pupt.2017.05.005

42. Delekate A, Fuchtemeier M, Schumacher T, Ulbrich C, Foddis M, Petzold GC. Metabotropic P2Y1 receptor signalling mediates astrocytic hyperactivity *in vivo* in an alzheimer's disease mouse model. *Nat Commun* (2014) 5:5422. doi: 10.1038/ncomms6422

43. Martorell A, Wellmann M, Guiffa F, Fuenzalida M, Bonansco C. P2Y1 receptor inhibition rescues impaired synaptic plasticity and astroglial Ca(2+)-dependent activity in the epileptic hippocampus. *Neurobiol Dis* (2020) 146:105132. doi: 10.1016/j.nbd.2020.105132

44. Nobili P, Shen W, Milicevic K, Bogdanovic Pristov J, Audinat E, Nikolic L. Therapeutic potential of astrocyte purinergic signalling in epilepsy and multiple sclerosis. *Front Pharmacol* (2022) 13:900337. doi: 10.3389/fphar.2022.900337

45. Gerdes N, Zhu L, Ersoy M, Hermansson A, Hjemdahl P, Hu H, et al. Platelets regulate CD4(+) T-cell differentiation *via* multiple chemokines in humans. *Thromb Haemost* (2011) 106(2):353–62. doi: 10.1160/TH11-01-0020

46. Hamzeh-Cognasse H, Cognasse F, Palle S, Chavarin P, Olivier T, Delezay O, et al. Direct contact of platelets and their released products exert different effects on human dendritic cell maturation. *BMC Immunol* (2008) 9:54. doi: 10.1186/1471-2172-9-54

47. Tan S, Li S, Min Y, Gistera A, Moruzzi N, Zhang J, et al. Platelet factor 4 enhances CD4(+) T effector memory cell responses *via* akt-PGC1alpha-TFAM signaling-mediated mitochondrial biogenesis. *J Thromb Haemost* (2020) 18 (10):2685–700. doi: 10.1111/jth.15005

48. Fang Z, Zhang X, Huang Y, Zhou H, Lu Y, Sun Y, et al. Piperlongumin improves survival in the mouse model of sepsis: Effect on coagulation factors and lung inflammation. *Inflammation* (2022). doi: 10.1007/s10753-022-01709-x

49. Gong W, Wen H. Sepsis induced by cecal ligation and puncture. *Methods Mol Biol* (2019) 1960:249–55. doi: 10.1007/978-1-4939-9167-9_22

50. Qiu W, An S, Wang T, Li J, Yu B, Zeng Z, et al. Melatonin suppresses ferroptosis *via* activation of the Nrf2/HO-1 signaling pathway in the mouse model of sepsis-induced acute kidney injury. *Int Immunopharmacol* (2022) 112:109162. doi: 10.1016/j.intimp.2022.109162

51. Kim WY, Hong SB. Sepsis and acute respiratory distress syndrome: Recent update. *Tuberc Respir Dis (Seoul).* (2016) 79(2):53–7. doi: 10.4046/trd.2016.79.2.53

52. Peerapornratana S, Manrique-Caballero CL, Gomez H, Kellum JA. Acute kidney injury from sepsis: current concepts, epidemiology, pathophysiology, prevention and treatment. *Kidney Int* (2019) 96(5):1083–99. doi: 10.1016/j.kint.2019.05.026

53. Khan AA, Alsahli MA, Rahmani AH. Myeloperoxidase as an active disease biomarker: Recent biochemical and pathological perspectives. *Med Sci (Basel).* (2018) 6(2):33. doi: 10.3390/medsci6020033

54. Liverani E, Mondrinos MJ, Sun S, Kunapuli SP, Kilpatrick LE. Role of protein kinase c-delta in regulating platelet activation and platelet-leukocyte interaction during sepsis. *PloS One* (2018) 13(4):e0195379. doi: 10.1371/journal.pone.0195379

55. Russwurm S, Vickers J, Meier-Hellmann A, Spangenberg P, Bredle D, Reinhart K, et al. Platelet and leukocyte activation correlate with the severity of septic organ dysfunction. *Shock* (2002) 17(4):263–8. doi: 10.1097/00024382-200204000-00004

56. Shimoyama Y, Umegaki O, Kadono N, Minami T. Presepsin and platelet to lymphocyte ratio predict the progression of septic subclinical acute kidney injury to septic acute kidney injury: a pilot study. *BMC Res Notes.* (2022) 15(1):212. doi: 10.1186/s13104-022-06103-2

57. Wen H. Sepsis induced by cecal ligation and puncture. *Methods Mol Biol* (2013) 1031:117–24. doi: 10.1007/978-1-62703-481-4_15

58. Fajgenbaum DC, June CH. Cytokine storm. *N Engl J Med* (2020) 383 (23):2255–73. doi: 10.1056/NEJMra2026131

59. Moriyama K, Nishida O. Targeting cytokines, pathogen-associated molecular patterns, and damage-associated molecular patterns in sepsis *via* blood purification. *Int J Mol Sci* (2021) 22(16):8882. doi: 10.3390/ijms22168882

60. Amison RT, Jamshidi S, Rahman KM, Page CP, Pitchford SC. Diverse signalling of the platelet P2Y1 receptor leads to a dichotomy in platelet function. *Eur J Pharmacol* (2018) 827:58–70. doi: 10.1016/j.ejphar.2018.03.014

61. Burnstock G. Pathophysiology and therapeutic potential of purinergic signaling. *Pharmacol Rev* (2006) 58(1):58–86. doi: 10.1124/pr.58.1.5

62. Burnstock G. Purinergic signalling in the reproductive system in health and disease. *Purinergic Signal* (2014) 10(1):157–87. doi: 10.1007/s11302-013-9399-7

63. Crain JM, Watters JJ. Estrogen and P2 purinergic receptor systems in microglia: Therapeutic targets for neuroprotection. *Open Drug Discovery J* (2010) 2:148–67. doi: 10.2174/1877381801002010148

64. Ozaki AF, Jackevicius CA, Chong A, Sud M, Fang J, Austin PC, et al. Hospital-level variation in ticagrelor use in patients with acute coronary syndrome. *J Am Heart Assoc* (2022) 11(13):e024835. doi: 10.1161/JAHA.121.024835

65. Lee YJ, Suh Y, Kim JS, Cho YH, Yun KH, Kim YH, et al. Ticagrelor monotherapy after 3-month dual antiplatelet therapy in acute coronary syndrome by high bleeding risk: The subanalysis from the TICO trial. *Korean Circ J* (2022) 52 (4):324–37. doi: 10.4070/kcj.2021.0321

66. Gargiulo G, Serino F, Esposito G. Cardiovascular mortality in patients with acute and chronic coronary syndrome: insights from the clinical evidence on ticagrelor. *Eur Rev Med Pharmacol Sci* (2022) 26(7):2524–42. doi: 10.26355/eurrev_202204_28490

67. Vogel B, Baber U, Cohen DJ, Sartori S, Sharma SK, Angiolillo DJ, et al. Sex differences among patients with high risk receiving ticagrelor with or without aspirin after percutaneous coronary intervention: A subgroup analysis of the TWILIGHT randomized clinical trial. *JAMA Cardiol* (2021) 6(9):1032–41. doi: 10.1001/jamacardio.2021.1720

68. Schreuder MM, Badal R, Boersma E, Kavousi M, Roos-Hesselink J, Versmissen J, et al. Efficacy and safety of high potent P2Y12 inhibitors prasugrel and ticagrelor in patients with coronary heart disease treated with dual antiplatelet therapy: A sex-specific systematic review and meta-analysis. *J Am Heart Assoc* (2020) 9(4):e014457. doi: 10.1161/JAHA.119.014457

69. Husted S, James SK, Bach RG, Becker RC, Budaj A, Heras M, et al. The efficacy of ticagrelor is maintained in women with acute coronary syndromes participating in the prospective, randomized, PLATelet inhibition and patient outcomes (PLATO) trial. *Eur Heart J* (2014) 35(23):1541–50. doi: 10.1093/eurheartj/ehu075

70. Ranucci M, Aloisio T, Di Dedda U, Menicanti L, de Vincentiis C, Baryshnikova E, et al. Gender-based differences in platelet function and platelet reactivity to P2Y12 inhibitors. *PloS One* (2019) 14(11):e0225771. doi: 10.1371/journal.pone.0225771

71. Waissi F, Dekker M, Bank IEM, Korporaal SJA, Urbanus RT, de Borst GJ, et al. Sex differences in flow cytometry-based platelet reactivity in stable outpatients suspected of myocardial ischemia. *Res Pract Thromb Haemost.* (2020) 4(5):879–85. doi: 10.1002/rth2.12344

72. Mansour A, Bachelot-Loza C, Nesseler N, Gaussem P, Gouin-Thibault I. P2Y12 inhibition beyond thrombosis: Effects on inflammation. *Int J Mol Sci* (2020) 21(4):174793. doi: 10.3390/ijms21041391

73. Mansour SM, Abd El-Aal SA, El-Abhar HS, Ahmed KA, Awny MM. Repositioning of ticagrelor: Renoprotection mediated by modulating renin-angiotensin system, inflammation, autophagy and galectin-3. *Eur J Pharmacol* (2022) 918:174793. doi: 10.1016/j.ejphar.2022.174793

74. Rahman M, Gustafsson D, Wang Y, Thorlacius H, Braun OO. Ticagrelor reduces neutrophil recruitment and lung damage in abdominal sepsis. *Platelets* (2014) 25(4):257–63. doi: 10.3109/09537104.2013.809520

75. Sexton TR, Zhang G, Macaulay TE, Callahan LA, Charnigo R, Vsevolozhskaya OA, et al. Ticagrelor reduces thromboinflammatory markers in patients with pneumonia. *JACC Basic Transl Sci* (2018) 3(4):435–49. doi: 10.1016/j.jacbts.2018.05.005

76. Gao CZ, Ma QQ, Wu J, Liu R, Wang F, Bai J, et al. Comparison of the effects of ticagrelor and clopidogrel on inflammatory factors, vascular endothelium functions and short-term prognosis in patients with acute ST-segment elevation myocardial infarction undergoing emergency percutaneous coronary intervention: a pilot study. *Cell Physiol Biochem* (2018) 48(1):385–96. doi: 10.1159/000491768

77. Chang YY, Huan QC, Peng J, Bi WC, Zhai LX, Chen Y, et al. P2Y1R ligation suppresses Th17 cell differentiation and alleviates colonic inflammation in an AMPK-dependent manner. *Front Immunol* (2022) 13:820524. doi: 10.3389/fimmu.2022.820524

78. Gao YY, Gao ZY. Extracellular adenosine diphosphate stimulates CXCL10-mediated mast cell infiltration through P2Y1 receptor to aggravate airway inflammation in asthmatic mice. *Front Mol Biosci* (2021) 8:621963. doi: 10.3389/fmolb.2021.621963

79. Liverani E, Rico MC, Garcia AE, Kilpatrick LE, Kunapuli SP. Prasugrel metabolites inhibit neutrophil functions. *J Pharmacol Exp Ther* (2013) 344(1):231–43. doi: 10.1124/jpet.112.195883

80. Vemulapalli H, Albayati S, Patwa VC, Tilley DG, Tsygankov AY, Liverani E. ADP exerts P2Y12 -dependent and P2Y12 -independent effects on primary human T cell responses to stimulation. *J Cell Commun Signal* (2020) 14(1):111–26. doi: 10.1007/s12079-019-00540-8

81. Takahashi T, Iwasaki A. Sex differences in immune responses. *Science* (2021) 371(6527):347–8. doi: 10.1126/science.abe7199

82. Kuboyama K, Harada H, Tozaki-Saitoh H, Tsuda M, Ushijima K, Inoue K. Astrocytic P2Y(1) receptor is involved in the regulation of cytokine/chemokine transcription and cerebral damage in a rat model of cerebral ischemia. *J Cereb Blood Flow Metab* (2011) 31(9):1930–41. doi: 10.1038/jcbfm.2011.49

83. Noguchi Y, Shinozaki Y, Fujishita K, Shibata K, Imura Y, Morizawa Y, et al. Astrocytes protect neurons against methylmercury *via* ATP/P2Y(1) receptor-mediated pathways in astrocytes. *PloS One* (2013) 8(2):e57898. doi: 10.1371/journal.pone.0057898

84. Woehrle T, Ledderose C, Rink J, Slubowski C, Junger WG. Autocrine stimulation of P2Y1 receptors is part of the purinergic signaling mechanism that regulates T cell activation. *Purinergic Signal* (2019) 15(2):127–37. doi: 10.1007/s11302-019-09653-6

85. Anter A, Ahmed AF, Hammad ASA, Almalki WH, Abdel Hafez SMN, Kasem AW, et al. The severity of acute kidney and lung injuries induced by cecal ligation and puncture is attenuated by menthol: Role of proliferating cell nuclear antigen and apoptotic markers. *Front Med (Lausanne)* (2022) 9:904286. doi: 10.3389/fmed.2022.904286

86. Mao S, Lv J, Chen M, Guo N, Fang Y, Tong J, et al. Serinc2 deficiency causes susceptibility to sepsis-associated acute lung injury. *J Inflamm (Lond)* (2022) 19 (1):9. doi: 10.1186/s12950-022-00306-x

87. Mohammad S, O'Riordan CE, Verra C, Aimaretti E, Alves GF, Dreisch K, et al. RG100204, a novel aquaporin-9 inhibitor, reduces septic cardiomyopathy and multiple organ failure in murine sepsis. *Front Immunol* (2022) 13:900906. doi: 10.3389/fimmu.2022.900906

88. Bicen C, Akdemir M, Turken MA, Cekok K, Ekin A, Turan AC. Analysis of risk factors affecting mortality in elderly patients operated on for hip fractures: A retrospective comparative study. *Acta Orthop Traumatol Turc* (2021) 55(6):493–9. doi: 10.5152/j.aott.2021.21004

89. Lu P, Xie T, Dai G, Li Y, Zou J, Chen H, et al. [Risk factors analysis for postoperative mortality of elderly patients with femoral neck fracture undergoing hemiarthroplasty]. *Zhongguo Xiu Fu Chong Jian Wai Ke Za Zhi* (2021) 35(2):217–20. doi: 10.7507/1002-1892.202009122

frontiers | Frontiers in Immunology

TYPE Original Research
PUBLISHED 10 November 2022
DOI 10.3389/fimmu.2022.1010263

Check for updates

OPEN ACCESS

EDITED BY
Pietro Ghezzi,
University of Urbino Carlo Bo, Italy

REVIEWED BY
Kazue Takahashi,
Harvard Medical School, United States
Kentaro Hatano,
University of Tsukuba, Japan
Serenella Anzilotti,
University of Sannio, Italy

*CORRESPONDENCE
Dima A. Hammoud
hammoudd@cc.nih.gov

SPECIALTY SECTION
This article was submitted to Inflammation, a section of the journal Frontiers in Immunology

RECEIVED 02 August 2022
ACCEPTED 17 October 2022
PUBLISHED 10 November 2022

CITATION
Martinez-Orengo N, Tahmazian S, Lai J, Wang Z, Sinharay S, Schreiber-Stainthorp W, Basuli F, Maric D, Reid W, Shah S and Hammoud DA (2022) Assessing organ-level immunoreactivity in a rat model of sepsis using TSPO PET imaging. *Front. Immunol.* 13:1010263. doi: 10.3389/fimmu.2022.1010263

COPYRIGHT
© 2022 Martinez-Orengo, Tahmazian, Lai, Wang, Sinharay, Schreiber-Stainthorp, Basuli, Maric, Reid, Shah and Hammoud. This is an open-access article distributed under the terms of the Creative Commons Attribution License (CC BY). The use, distribution or reproduction in other forums is permitted, provided the original author(s) and the copyright owner(s) are credited and that the original publication in this journal is cited, in accordance with accepted academic practice. No use, distribution or reproduction is permitted which does not comply with these terms.

Assessing organ-level immunoreactivity in a rat model of sepsis using TSPO PET imaging

Neysha Martinez-Orengo[1], Sarine Tahmazian[1], Jianhao Lai[1], Zeping Wang[1], Sanhita Sinharay[1], William Schreiber-Stainthorp[1], Falguni Basuli[2], Dragan Maric[3], William Reid[1], Swati Shah[1] and Dima A. Hammoud[1]*

[1]Center for Infectious Disease Imaging, Radiology and Imaging Sciences, Clinical Center, National Institutes of Health, Bethesda, MD, United States, [2]Chemistry and Synthesis Center, National Heart, Lung, and Blood Institute, National Institutes of Health, Rockville, MD, United States, [3]Flow and Imaging Cytometry Core Facility, National Institute of Neurological Disorders and Stroke, National Institutes of Health, Bethesda, MD, United States

There is current need for new approaches to assess/measure organ-level immunoreactivity and ensuing dysfunction in systemic inflammatory response syndrome (SIRS) and sepsis, in order to protect or recover organ function. Using a rat model of systemic sterile inflammatory shock (intravenous LPS administration), we performed PET imaging with a translocator protein (TSPO) tracer, [^{18}F]DPA-714, as a biomarker for reactive immunoreactive changes in the brain and peripheral organs. *In vivo* dynamic PET/CT scans showed increased [^{18}F]DPA-714 binding in the brain, lungs, liver and bone marrow, 4 hours after LPS injection. Post-LPS mean standard uptake values (SUV_{mean}) at equilibrium were significantly higher in those organs compared to baseline. Changes in spleen [^{18}F]DPA-714 binding were variable but generally decreased after LPS. SUV_{mean} values in all organs, except the spleen, positively correlated with several serum cytokines/chemokines. *In vitro* measures of TSPO expression and immunofluorescent staining validated the imaging results. Noninvasive molecular imaging with [^{18}F]DPA-714 PET in a rat model of systemic sterile inflammatory shock, along with *in vitro* measures of TSPO expression, showed brain, liver and lung inflammation, spleen monocytic efflux/lymphocytic activation and suggested increased bone marrow hematopoiesis. TSPO PET imaging can potentially be used to quantify SIRS and sepsis-associated organ-level immunoreactivity and assess the effectiveness of therapeutic and preventative approaches for associated organ failures, *in vivo*.

KEYWORDS

sepsis, TSPO (18 kda translocator protein), 18F-DPA-714, whole body PET/CT, organ-level immunoreactivity

Introduction

Sepsis is an abnormal response by the host immune system to microbial infections which frequently results in multi-organ dysfunction and death. As reported by the CDC, 1.7 million adults develop sepsis and more than 200,000 die in the USA every year in addition to millions of adults and children around the world (1, 2). Globally, sepsis is responsible for 20% of all-cause deaths and since 2017 it has been recognized by the World Health Organization as a global health concern (3, 4). Despite the vast improvement in septic patient outcomes over the last few decades, physical and psychological post-sepsis symptoms persist and remain a major problem affecting the quality of life of recovered patients (5, 6). The exact etiologies underlying neurocognitive and other systems' dysfunctions in this patient population, including more recently, the survivors of moderate to severe COVID-19 infection, have been difficult to pinpoint (7).

Although an inflammatory circulatory process is an established manifestation of systemic inflammatory response syndrome (SIRS) and sepsis, the degree of direct organ-level inflammation is not easily inferred until late in the disease process when irreversible organ failure is impending (8). In 2016, the society of Critical Care Medicine and the European Society of Intensive Care Medicine prioritized organ dysfunction in their new definition of sepsis (Sepsis-3) which uses a sequential organ failure assessment (SOFA) score as an index (9). This led to calls for a new direction of research where assessing organ level inflammation and ensuing dysfunction becomes a priority along with attempts to protect or recover organ function (10). In this context, imaging studies using pre-clinical models of sepsis and biomarkers of peripheral immunoreactivity can be used to detect and gauge organ-level inflammation and consequently the effectiveness of various therapeutic and preventative approaches for SIRS/sepsis *in vivo*.

The 18kDa translocator protein (TSPO), formerly known as peripheral benzodiazepine receptor (PBR), is an outer mitochondrial membrane receptor expressed in many cell types, but especially known to be expressed in brain microglia (11, 12). Due to increased expression in activated microglia, TSPO is widely used as a PET imaging target in the detection and *in vivo* quantification of neuroinflammation in a variety of neuropathologies, and as therapeutics (13–20). However, as we have recently shown, TSPO is expressed not just in microglia, monocytes, and macrophages but also in dendritic cells, neutrophils, B- and T-cells, both in humans and macaques (21, 22). Extracranially, TSPO is also expressed in various cell types in the bone marrow (23) and other peripheral tissues (24) including heart (25), colon (26), liver (27), and lungs (28). Nevertheless, TSPO targeting in PET has been sparsely used to evaluate peripheral inflammation in preclinical and clinical models, with only a handful of published studies (26, 28–32), none of which focus on sepsis-induced inflammation in peripheral organs, beyond the lungs.

In this study, we evaluated the well-known TSPO PET ligand [^{18}F]DPA-714 to quantify organ level immunoreactivity *in vivo*, after intravenous LPS injection. We corroborated our imaging findings with *ex-vivo* assessment of TSPO gene expression and correlated binding with various biomarkers of disease and inflammatory changes. Tissue sections of the brain, lung, and spleen were also assessed by immunofluorescence staining to explain our *in vivo* findings. Only one time point after LPS injection was used since our study is meant as a proof of concept.

Methods

Animals

Male Fisher rats were purchased from Charles River Laboratory (Wilmington, MA) and were housed in a temperature-controlled environment with free access to food and water with a 12-hour dark/light cycle. A total of 13 animals (Age range: 3.7-4.2 months, mean age: 3.96 ± 0.17 months; Weight range: 0.29-0.36 kg, mean weight 0.32 ± 0.01 kg) were used for all PET imaging experiments. An additional set of 15 animals (5 controls and 10 LPS-treated) were used to increase sample size for molecular experiments including cytokines/chemokines panels, qPCR, and immunohistochemistry (IHC).

LPS administration

The LPS was extracted from E. coli serotype O111:B4 and purified by gel filtration (Sigma Aldrich #L3012). This serotype can stimulate B-cells and other cells of the immune system mainly *via* activation of Toll-like receptor 4 (TLR4), a receptor that recognizes Pathogen-associated molecular patterns (PAMPs).

The administration of either intraperitoneal (IP) or intravenous (IV) injection of LPS in rodents is commonly used to induce a systemic sterile inflammatory shock and organ failure that simulates sepsis. Although IP injections are easier and more convenient, IV injections allow for more consistent levels of LPS in the blood as well as faster induction of an immune response and neuroinflammation (33). Acute LPS injections in rats have shown to induce significant systemic and central inflammation, including different regions of the brain, as early as 2 hours after inoculation (34, 35). In human studies, the typical route of LPS injection is IV as well. In our study, we used the IV injection method in rats as described by others (36, 37), using 5mg/kg LPS dose. Since the main focus of our study was to evaluate organ level inflammation, LPS injection of rats *via* the IV route was deemed a suitable model to induce an immune response with increased cytokine levels in serum and tissues. In our hands, this resulted in all animals developing a measurable systemic and organ-level inflammatory syndrome within 4 hours.

[^{18}F]DPA-714 radioligand synthesis

[^{18}F]DPA-714 was synthesized as previously reported (38). In a typical reaction, starting with 9600 MBq of fluorine-18, we obtained 3100 MBq of the product with a radiochemical purity > 99%. The molar activity was 125000 MBq/μmol.

[^{18}F]DPA-714 PET imaging

Prior to each scan, the animal was anesthetized (3-4% isoflurane) and the lateral tail vein was cannulated with a butterfly catheter connected to a heparin lock. Once the animal was properly positioned, [^{18}F]DPA-714 was injected slowly through the tail vein catheter (mean dose 1.13 ± 0.1 mCi) over a period of 30 seconds as a bolus followed by a quick saline flush (300 μL). PET imaging using Inveon PET/CT scanner (Siemens Medical Solutions, USA) with a transaxial and axial field of view (FOV) of 10 and 12.7 cm, full width at half maximum spatial resolution at 1.4 mm center FOV, was initiated immediately after the injection. Dynamic PET scans were performed for 60 minutes.

Baseline [^{18}F]DPA-714 scans were obtained for each animal. Two days following the baseline scan, animals received a prophylactic subcutaneous injection of buprenorphine (0.1 mg/kg) one hour before LPS was administered *via* intravenous tail vein (5mg/kg). After a 4-hour waiting period, [18F]DPA-714 PET/CT imaging was performed. Whole blood was also collected before and 4 hours after LPS injections. After completion of the baseline PET imaging session, the animals were allowed to recover whereas following the post-LPS scans, the animals were immediately euthanized and perfused with saline for whole blood and organ collection. Following this, various organs were collected and immediately snap frozen in liquid nitrogen. The tissues were stored at -80°C until further use for downstream procedures such as RNA extraction and lysate preparation. A separate group of animals (control n=4; LPS n=4) were used for immunohistochemistry. The detailed procedures for organ collection and tissue treatments prior to staining are mentioned below under "multiplex fluorescence immunohistochemistry".

[^{18}F]DPA-714 PET image analysis

The images were reconstructed using OSEM-3D and were analyzed using PMOD 3.8 (PMOD Technologies, Ltd., Zurich, Switzerland). The PET images were co-registered to the CT image, and volumes of interest (VOIs) were drawn for the whole brain, liver, lungs, spleen, and bone marrow. Time activity curves (TACs) were derived from the dynamic images for each VOI. The mean standardized uptake at equilibrium was averaged from 26-40 min and reported as the SUV_{mean}.

It is known that TSPO is expressed in the kidneys and can be upregulated in inflammatory conditions. These changes can usually be quantified by PET when kidney function is otherwise intact. In our study, however, we did not assess kidney binding, mainly because many of our animals showed decreased kidney function after LPS administration, a commonly seen phenomenon in SIRS and sepsis patients (sepsis-induced acute kidney injury (AKI)) (39). As a result of the secondary reduced glomerular filtration rate and tubular dysfunction in the kidneys, the effective excretion of our ligand and its metabolites was delayed, resulting in ligand retention in the parenchyma of the kidneys, as has been described with 99mTc-Mag3 scans (40). We thus assumed that the increased radioactivity in the kidneys four hours post-LPS likely reflects a combination of upregulated TSPO expression (due to inflammatory changes) and ligand retention within the renal parenchyma, and as such is unreliable as a measure of immune activation after LPS administration.

Serum and lysate preparation

Serum from whole blood, as well as liver, brain, spleen, and lung lysates were collected from 13 LPS injected rats and 5 control rats. Pre- and post-LPS inoculation serum was collected for 8 animals and only post-LPS serum was collected for 10 animals. Sectional tissues with a total weight of 50 mg were obtained from each organ (lung, liver, spleen, and basal ganglia of the brain) and homogenized to perform RNA and protein extraction. Total cellular RNA from LPS treated rats and controls were isolated using the Zymo ZR-Duet DNA/RNA MiniPrep Plus Kit (Catalog No. D7003) according to the manufacturer's instructions. The RNase-Free DNase Set (Qiagen No.79254) was used to remove genomic DNA from the RNA samples. The protein lysates were obtained by homogenizing the tissues in a protein extraction buffer and then collecting the supernatants after centrifugation. Total protein concentrations of the lysates were measured using the BCA assay (Pierce cat#23225) prior to performing enzyme-linked immunoassay (ELISA).

Enzyme-linked immunoassay

Cytokine/chemokine levels were measured in the brain, liver, spleen, lung lysates, and in the serum of LPS treated and control rats. A multiplex ELISA kit (Millipore Sigma #RECYMAG65K27PMX) for 27 analytes was used following the manufacturer's instructions. The panel included G-CSF, Eotaxin, GM-CSF, IL-1α, Leptin, MIP-1α, IL-4, IL-1B, IL-2, IL-6, EGF, IL-13, IL-10, IL-12p70, IFNγ, IL-5, IL-17, IL-18, MCP-1, IP-10, GRO/KC, VEGF, Fractalkine, LIX, MIP-2,

TNFα, and RANTES analytes. The protein concentrations for the organ lysates were adjusted to 2mg/ml before analysis by ELISA. The serum samples were not diluted before the run. The plates were read on Bioplex 200™ (Bio-Rad) and the analyte concentrations were determined for all the organs and serum.

Quantitative polymerase chain reaction of organ tissues

Synthesis of first-strand cDNA from total RNA was performed using RT² First Strand Kit and the cDNA was amplified with RT² SYBR®Green qPCR Mastermix (Qiagen, Hilden, Germany). The housekeeping gene for the ribosomal protein lateral stalk subunit P1, *Rplp1* (Qiagen #PPR42363C-200) was used as an internal control. Samples for the gene of interest, *Tspo* (Qiagen #PPR06787A-200), were run in triplicates. Using CFX96 Real-time qPCR System (Bio-Rad, Hercules, CA), relative changes in mRNA expression levels were quantified. The Ct values were normalized to the housekeeping gene.

Multiplex fluorescence immunohistochemistry

Animals were perfused with saline followed by 4% PFA. Tissues were cryoprotected using 10-30% sucrose gradient before being embedded in optimal cutting temperature compound (OCT), frozen, and cut in 10 µm-thick sections. Tissue slices from the brain, spleen, and lungs of a group of LPS injected animals (n=4) and control animals (n=3) were stained using different combinations of up to 5 primary antibodies to detect specific immunoinflammatory cell types using MF-IHC. These antibodies respectively included CD3 for T-cells (Thermo Fisher Scientific # MA1-7630), B220 for B-cells (Thermo Fisher Scientific # 14-0460-82), granulocyte marker for neutrophils (Thermo Fisher Scientific # 14-0570-82), CD68 for monocytes/macrophages (Abcam # ab125212), MHCII for dendritic cells (Thermo Fisher Scientific # 14-0920-82), and Iba1 for microglia (Cedarlane Labs # 234006(SY)). TSPO antibody (Abcam #ab109497) was used to stain for the protein. Each of the above primary immunoreactions was visualized using appropriate fluorophore-conjugated secondary antibodies obtained either from Jackson ImmunoResearch (DyLight 405 # 115-475-075) or Thermo Fisher Scientific/Invitrogen (Alexa Fluor 546 # A21123, Alexa Fluor 594 # A21145, Alexa Fluor 488 # A21151, Alexa Fluor 430 # A11064, Alexa Fluor 555 # A21435, Pacific Orange # P31584) and all antibodies were diluted based on the manufacturer's recommendation. The cell nuclei were counterstained using 1 µg/ml DAPI to facilitate cell counting. All fluorescence signals were imaged using an Axio Imager.Z2 upright scanning wide field fluorescence microscope (Zeiss) equipped with Orca Flash 4.0 high resolution sCMOS camera (Hamamatsu), 200W X-cite 200DC broadband light source (Lumen Dynamics) and standard DAPI, and various Alexa Fluor filter sets (Semrock). After imaging, the multichannel image datasets were processed for image stitching, illumination correction, and the images were imported into Adobe Photoshop CS6 to produce pseudo-colored multi-channel composites.

Staining quantification

Quantification of percent fluorescence intensities was performed using NIH ImageJ 1.53a software. For the lungs, a single ROI encompassing the whole tissue region was drawn. For the spleen, the white pulp and red pulp were analyzed with four ROIs drawn on each region and then combined. In the brain, ROIs were also drawn by region, including either the striatum, cortex, or corpus callosum; with multiple small ROIs drawn in each region. Liver IHC could not be performed due to high levels of autofluorescence prohibiting meaningful staining of different cell markers.

ImageJ was also used to quantify microglial length using the free hand lines tool to measure 80 ramifications per animal and the free hand selections tool to delineate 20 somas per animal from different ROIs of brain tissues.

Statistics

Paired t-test was used to evaluate the differences in average [^{18}F]DPA-714 binding (SUV_{mean}) at baseline and post LPS administration for each organ. Unpaired t-test was used to compare TSPO mRNA expression between controls and LPS groups and to analyze the differences in TSPO and various cell marker stains by IHC. For those tests, p-values <0.05 were considered statistically significant. Even though we found colocalization of TSPO with different cell markers, we felt that our histopathology sample size was too small (controls n=3, LPS n=4) for an accurate and reliable Pearson analysis of TSPO binding.

Non-parametric Mann Whitney test was used to compare cytokine expression in serum and organ lysates between controls and LPS groups since many datasets were not normally distributed. p-values <0.01 were considered statistically significant.

Repeated measures correlations between SUV values and serum cytokine levels were performed using the *rmcorr* program in R (version 3.5.1). In order to account for multiple comparisons in this analysis, correlations with p-values < 0.01 were considered to reflect positive or negative associations.

Study approval

All procedures were approved by the Animal Care and Use Committee (ACUC) of the Clinical Center (CC) at the National

Institutes of Health (NIH) and were performed in an AAALAC International accredited facility in accordance with relevant NIH policies and the Animal Welfare Act and Regulations.

Results

Assessment of whole body TSPO distribution by [^{18}F]DPA-714 PET imaging

The animals underwent PET/CT scans at baseline and 4 hours post-LPS injection. Post-LPS inoculation, the rats displayed reduced physical activity and slower respiratory rate (avg 30-35 breaths per minute) during the scan compared to baseline scans (breath rate 40-50 breaths per minute) under similar levels of anesthesia (1.5- 2% isoflurane-O_2 mixture). Some of the animals also had diarrhea after LPS treatment.

The post-LPS scans showed increased [^{18}F]DPA-714 binding in the brain, lungs, liver, and bone marrow as demonstrated in the time activity curves (TACs) (Figure 1). In the spleen, most animals (10 out of 13) showed decreased binding rather than increased binding. On average, binding was decreased compared to baseline on the mean TAC. Mean TACs for whole brain, liver, lungs, and bone marrow showed higher [^{18}F]DPA-714 binding in the post-LPS rats when compared to baseline. Post-LPS SUV_{mean} were significantly higher for brain ($p = 0.007$), lungs ($p = 0.023$), liver ($p < 0.0001$), and bone marrow ($p = 0.002$) with an average of 2-3-fold increase. There were no significant differences in spleen SUV_{mean} values with most animals instead showing decreased SUV_{mean} compared to baseline (Figures 1A-C).

Changes in blood cell counts and cytokine levels reflect systemic inflammation

In our animals, there were significant decreases in platelets, white blood cells counts as well as monocytes, eosinophils and lymphocyte counts (Supplementary Figure 1).

It has been demonstrated that both pro- and anti-inflammatory cytokines play an important role during sepsis and that serum levels increase in patients with sepsis. In our model, serum cytokine levels increased in the LPS group when compared to controls (Figure 2). The following list of serum cytokines showed significantly increased expression after LPS exposure: IL-1β, IL-4, IL-6, MIP-1α, MIP-2, IL-10, IL-17A, IL-18, GRO/KC, IFNγ, Fractalkine, VEGF, TNFα, MCP-1, RANTES, and IP-10 (all $p < 0.0001$). Rats that did not have baseline measures also showed increased cytokine levels when compared to controls. At the organ level, increased expression of various cytokines in organ lysates from brain, lungs, liver, and spleen was also observed in the LPS group when compared to controls (Figure 3).

Multiple serum cytokine levels positively correlated with SUV_{mean} of the brain, lungs, liver, and bone marrow (Figure 4). Some of the most relevant and frequently expressed cytokines that showed significant associations include IL-2, IL-17A, TNFα, IL-6, IL-1β, MCP-1, and IL-4. These cytokines have been associated with severity of sepsis, organ dysfunction, and mortality in septic shock patients (41). Additional serum cytokines that correlated with SUVs in specific organs included EGF (brain); GM-CSF, IL-10, IL-18, VEGF (lungs); IL-1α, Leptin, MIP-1α, IL-12p70, IFNγ, IP-10, GRO/KC, Fractalkine, LIX, MIP-2, and RANTES (liver); and MIP-1α, MIP-2, IL-5, IL-10, IFNγ, IP-10, GRO/KC, VEGF, and Fractalkine (bone marrow). No correlations were observed between cytokine levels in serum and spleen SUV_{mean} values.

Ex-vivo assessment of organ level changes in TSPO expression

Real time PCR performed to assess the changes in TSPO expression at the transcriptional level showed one to two-fold upregulation of TSPO mRNA expression in the lung ($p = 0.0497$), liver ($p = 0.0121$), and brain ($p = 0.0462$) when compared to controls, but not in the spleen ($p = 0.5529$), which is consistent with the PET imaging results (Figure 5).

Based on immunohistochemistry, there was significantly increased expression of TSPO ($p = 0.0361$), CD68 (macrophage marker) ($p = 0.001$) and CD3 (T cell marker) ($p = 0.0305$) in the lungs of LPS treated animals when compared to controls (Figure 6). Additionally, the expression of B cells -B220 ($p = 0.1510$), neutrophils -granulocytes ($p = 0.0626$), and dendritic cells -MHCII ($p = 0.1018$) was also higher compared to controls, although the differences did not reach statistical significance (Figure 6). While co-localization of TSPO staining with macrophages was the most noticeable, we also found co-localization of TSPO staining with dendritic cells, neutrophils (Supplementary Figure 2) and lymphocytes (Supplementary Figure 3).

We also analyzed the spleen by IHC using combined ROIs equally distributed between the red pulp and white pulp. There was decreased expression of monocytes/macrophages -CD68 ($p = 0.0121$) and increased expression of B cells -B220 ($p = 0.0256$) (Figure 7). Due to mixed response patterns, there were no statistically significant differences in the expression of TSPO, neutrophils -granulocytes, or T cells -CD3 in the spleen of LPS rats when compared to controls (Figure 7). Increased proliferating B cells in the lymphoid white pulp most likely represents the initiation of immune responses. This increase could have offset the loss of monocytes, resulting in no appreciable change in total TSPO expression in two out of four animals. The other two animals showed increased TSPO staining despite decreased CD68 staining. At the same time, they showed increased granulocyte and lymphocyte staining, possibly offsetting the decreased monocyte staining (Figure 7).

10.3389/fimmu.2022.1010263

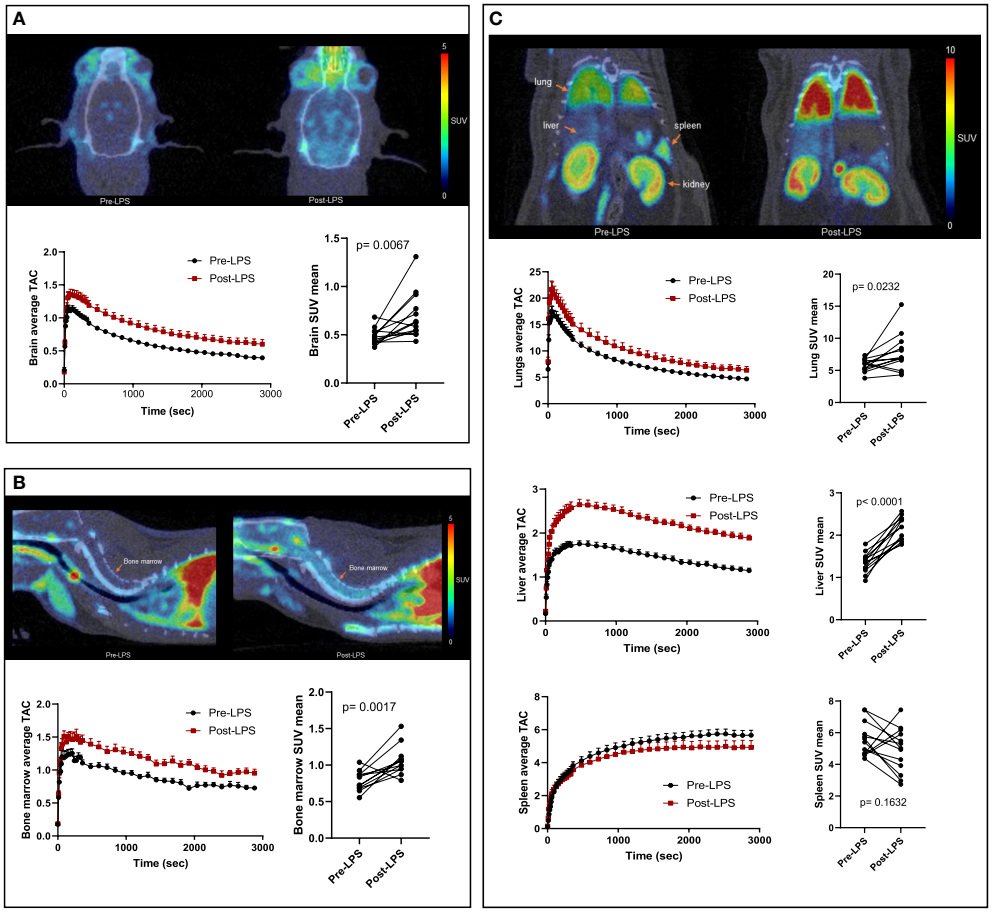

FIGURE 1
[^{18}F]DPA-714 binding in the brain and peripheral organs of LPS-treated rats. Representative PET/CT scans (top), average time activity curves (TACs) (bottom left) and mean standardized uptake values (SUVs) of [^{18}F]DPA-714 averaged from 26-40 minutes (bottom right) are shown in the brain **(A)**, bone marrow **(B)**, and peripheral organs- lungs, liver and spleen **(C)**. Representative PET images and mean TACs show increased binding in brain, lungs, liver, and bone marrow, but not in spleen, compared to baseline (n=13). Statistical analysis was performed using paired t-test to evaluate the differences in average [^{18}F]DPA-714 binding by PET at baseline and post-LPS for each organ. p-values <0.05 are considered statistically significant. *p<0.05, **p<0.01, ****p<0.0001.

In the brain, while there was generally higher expression of TSPO protein in the LPS treated animals when compared to controls in the striatum (mean 2.334 vs 0.6130) and corpus callosum (mean 1.783 vs 0.54) regions, it did not achieve statistical significance possibly due to the limited sample size. However, we observed distinct changes in the morphological characteristics of the microglia such as the length of the glial processes and the size of the soma (Figure 8). The microglial processes were shorter and the cell bodies were larger in LPS treated rats (p<0.0001) indicating there was early microglial activation in these animals.

Discussion

The sequential organ failure assessment (SOFA) or the shorter bedside clinical tool quickSOFA, have been implemented to evaluate groups of patients with SIRS/sepsis and better predict the severity of resulting organ dysfunction, morbidity, and mortality (42, 43). However, these tools are still limited in sensitivity and performance (44, 45), creating the need for more accurate measures of organ-level inflammation in septic patients. The effectiveness of [^{18}F]DPA-714 as a biomarker of peripheral inflammation has previously been validated in different diseases (46–49). In this study, we used [^{18}F]DPA-714 in a rat model of LPS-induced systemic inflammation, showing that *in vivo* whole-body PET imaging with the TSPO biomarker [^{18}F]DPA-714 can be used to quantify organ-level immunoreactivity. As expected, [^{18}F]DPA-714 PET imaging indicated increased expression of TSPO in the brain, lungs, bone marrow, and liver, and a variable change in TSPO expression in the spleen when compared to baseline (prior to LPS treatment) (Figure 1).

10.3389/fimmu.2022.1010263

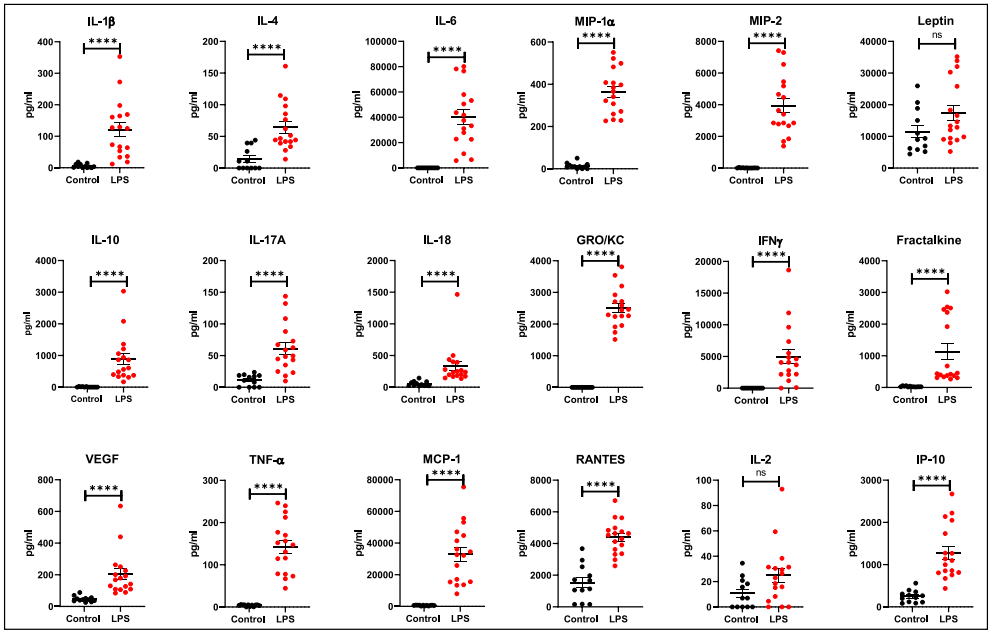

FIGURE 2
Expression of serum cytokines and chemokines. Increased expression (pg/mL) of various cytokines and chemokines is seen after LPS treatment (Control n=12, LPS n=17). Statistical analysis was performed using unpaired Mann Whitney test to evaluate changes in serum cytokines and chemokines between controls and LPS groups. Mean with SEM are shown. p-values <0.01 are considered statistically significant. ****p<0.0001, not significant (ns).

Sepsis is initially associated with an overwhelming release of cytokines and later on a phase of immune suppression with substantial immune cell depletion as a result of constant exposure to pro- and anti-inflammatory cytokines (50, 51). The production of IL-6, TNFα, IL-18, and IL-1 pro-inflammatory cytokines along with IL-10 (anti-inflammatory cytokine) is a hallmark response to sepsis. Our model of systemic sterile inflammatory shock follows this characteristic cytokine profile of sepsis showing increased expression of cytokines in the serum (Figure 2) and organ lysates (Figure 3). More importantly, we found a significant positive correlation between TSPO SUV_{mean} values in brain, lungs, bone marrow, and liver with the expression of these inflammatory cytokines in serum (Figure 4).

Our findings in the lungs are consistent with the current understanding of acute respiratory distress syndrome (ARDS) in severe SIRS and sepsis. In these patients, higher plasma levels of anti-inflammatory IL-10 during early course of disease correlate with severity of illness regardless of the use of oxygen support (52, 53) while higher expression of pro-inflammatory cytokines IL-1 and IL-6 at the onset of ARDS predicts unfavorable outcomes (54). After initial recovery from sepsis, continuous deployment of functionally impaired macrophages from lymphoid reservoirs to the lungs can further prevent lung recovery and increase negative outcomes during secondary infections (55, 56). In a previous study, [^{18}F]FDG PET lung uptake was found to precede increased CT attenuation (lung edema) in a model of sepsis and ARDS, which was accompanied by neutrophil influx reflected by increased myeloperoxidase activity (57). In our model, we showed increased [^{18}F]DPA-714 binding in the lungs of the LPS rats when compared to controls (Figure 1C) which correlated with systemic cytokines and was accompanied by increased staining for immune cell markers, namely macrophages, neutrophils, dendritic cells and lymphocytes (Figure 6), even though some of the differences in staining did not reach statistical significance. The latter however could be attributed to the small sample number used for IHC staining. As expected, TSPO staining colocalized mainly with macrophages (CD68), and to a lesser extent with other activated myeloid and lymphoid immune cells (Supplementary Figures 2, 3). Our imaging findings thus support an inflammatory reaction induced in the lungs through the systemic administration of LPS, similar to what occurs in sepsis, that is measurable using [^{18}F] DPA-714.

SIRS and sepsis can also affect the cell components of the bone marrow in the early stages, making it susceptible to inflammation, and showing increased proliferating cells in response to peripheral immune cell depletion (58). Using a repeated measures correlation to analyze bone marrow SUV_{mean} with serum cytokines, we showed a positive correlation with IL-6, IL-10, IL-1β, and VEGF, among others (Figure 4). The correlation between SUV and VEGF is most

10.3389/fimmu.2022.1010263

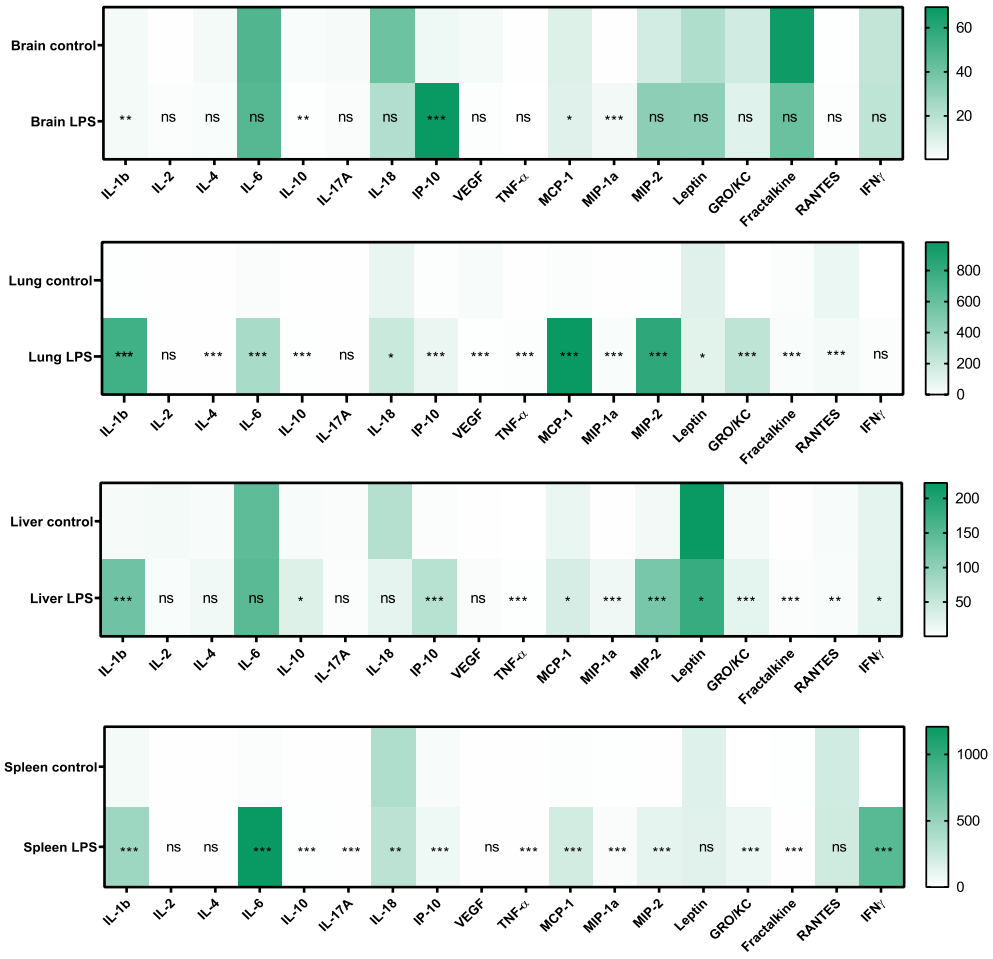

FIGURE 3
Expression of cytokines and chemokines in organ lysates. Changes in the expression (pg/mL) of various cytokines and chemokines in brain, lung, liver, and spleen lysates due to LPS treatment is shown (Control n=4, LPS n=14). Statistical analysis was performed using Mann-Whitney test to evaluate changes in tissue cytokines and chemokines between controls and LPS groups. p-values <0.01 are considered statistically significant. *p<0.05, **p<0.01, ***p<0.001, not significant (ns).

relevant as increased expression of this cytokine mediates morbidity and mortality in patients with severe sepsis. IL-18 shares similar characteristics with IL-1β and is increased in septic patients, particularly in those with thrombocytopenia (59, 60). In addition, we found negative correlations between bone marrow SUV_{mean} values and white blood counts (WBC (K/uL r= -0.86, p= 0.003), platelets (K/uL; r= -0.97, p= 0.00001) and lymphocytes (K/uL; r= -0.87, p= 0.002). Increased TSPO expression in the bone marrow is thus likely to reflect a combination of inflammation and increased hematopoiesis in response to peripheral leukopenia and thrombocytopenia, which were seen in our animal model and are commonly encountered in septic patients (Supplementary Figure 1).

Another peripheral organ evaluated in this study was the liver where we found an agreement between the PET imaging results and TSPO gene expression changes (Figures 1, 5). Similarly, the imaging data correlated with increased Leptin and MIP-2 in serum which is an important finding since increased levels of Leptin and MIP-2 in septic patients also correlate with disease severity (61, 62). We did not assess liver enzyme levels in our study due to logistical limitations, however liver dysfunction is a well-known complication of sepsis. The association between the degree of liver inflammation and acute/chronic dysfunction is thus an important potential use for our quantitative noninvasive *in vivo* imaging approach.

When assessing the spleen, our PET data showed generally mixed change in binding of [^{18}F]DPA-714 in the LPS group, with most animals showing decreased binding and some animals showing increased binding (Figure 1). No significant difference in TSPO gene expression (Figure 5C) were observed in the spleens of the LPS injected rats when compared to controls. Similar to PET imaging, IHC showed a mixed picture where two

10.3389/fimmu.2022.1010263

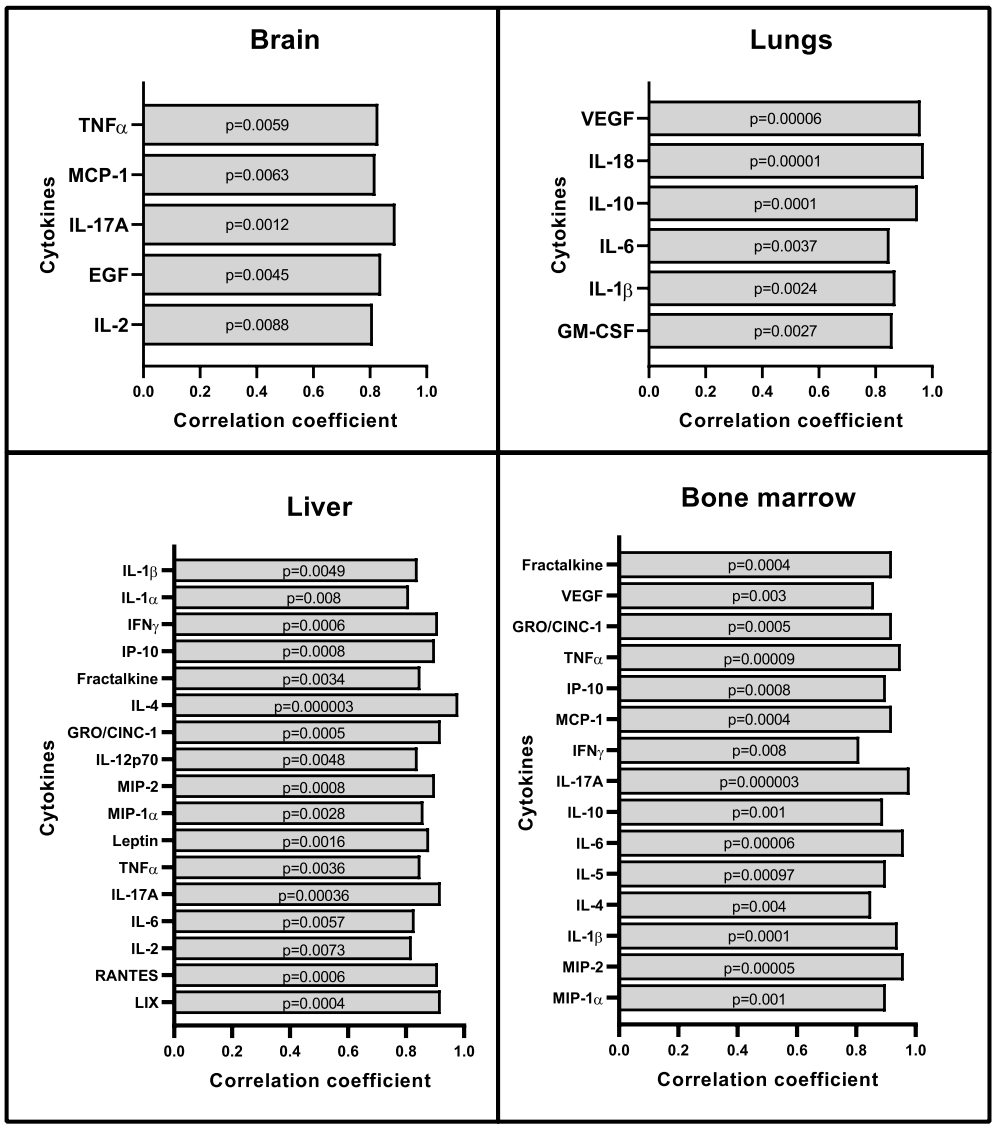

FIGURE 4
Correlation between organ SUV_{mean} with serum cytokines and chemokines. Repeated measures correlations analysis shows positive correlations between cytokines in serum and SUV_{mean} values from brain, lungs, liver, and bone marrow (n=8). No correlations were seen with the spleen. Statistical analysis was performed using the rmcorr package in R. In order to account for multiple comparisons in this analysis, correlations with p-values < 0.01 were considered to reflect positive or negative association.

out of four animals showed increased TSPO staining. In one animal with increased TSPO staining despite decreased CD68 staining (Figure 7) we found increased $B220^+$ cells and mixed changes of granulocytes and $CD3^+$ cells. Increased TSPO staining in this case could be explained by lymphocytic proliferation despite migration of monocytes to other organs such as the lungs.

[^{18}F]DPA-714 PET imaging of TSPO in the brain has been very well characterized in different models of neuroinflammation (17, 63–72). Our study shows a significant positive correlation between [^{18}F]DPA-714 brain binding and levels of MCP-1, IL-2, EGF, IL-17A, and TNFα in serum. These cytokines are neuroregulatory molecules that penetrate the blood brain barrier and regulate interactions between peripheral tissues and the CNS (73, 74). They promote neutrophil mobilization to sites of inflammation and are increased in septic encephalopathy (75–77). Furthermore, IL-17A has been described as a main player in the immunological dysfunction during sepsis, with increased levels in serum of pediatric and adult patients during early stage of sepsis, making it an attractive biomarker and therapeutic target (78). When staining microglia with Iba1, we did not find differences in staining intensity between controls and LPS animals. We are aware that, despite being

10.3389/fimmu.2022.1010263

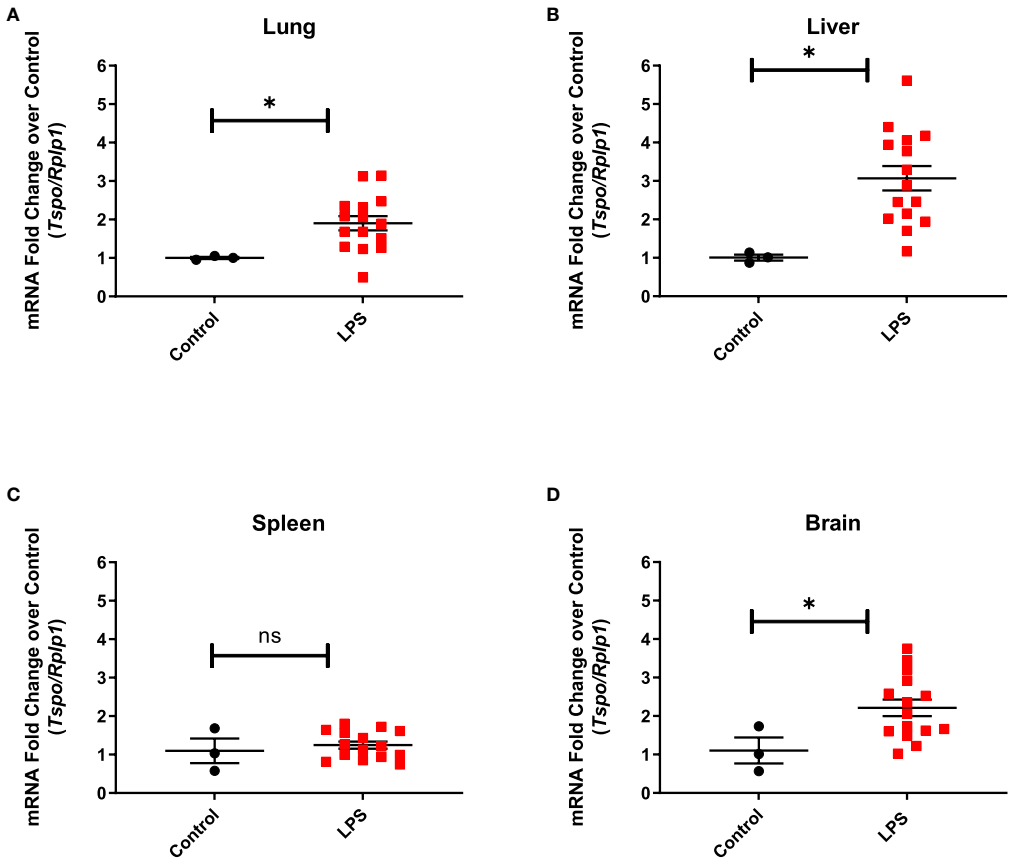

FIGURE 5
TSPO gene expression in organ lysates. Increased TSPO mRNA levels in the lung. **(A)** (p=0.0497), liver **(B)** (p=0.0121), and brain **(D)** (0.0462) from LPS treated rats (n=15), but not in the spleen **(C)** (p=0.5529), when compared to controls (n=3). Statistical analysis was performed using unpaired t-test. Mean with SEM are shown. p-values <0.05 are considered statistically significant. Tspo is target gene and ribosomal protein lateral stalk subunit P1 (Rplp1) is the housekeeping gene used for normalization. *p<0.05; not significant (ns).

commonly used as a marker of microglial activation, Iba1 protein is not always specific enough to discriminate between activated and non-activated microglia, or to distinguish microglia from macrophages. Instead, we relied on the detection of subtle morphological changes in Iba1 stained microglia which are generally believed to specifically reflect stages of microglial activation. Our LPS animal model shows the morphological transformation of resting microglia into cells with less complex ramifications, thickening of the cell body, and presentation of an amoebic phenotype which are characteristic of microglial activation and phagocytic stage (Figure 8). This is similar to findings of microglial activation in the white matter of patients with systemic sepsis (enlarged and amoebic microglial phenotypes) when compared to non-septic controls (79). Sepsis survivors also can show clinical manifestations of delirium or long-term cognitive decline (5, 80), and other studies correlate these manifestations with white matter disruption (81). Neuroinflammatory changes in association with LPS administration and increased cytokine levels in the serum in our model could thus simulate brain-specific inflammatory changes in the setting of SIRS and sepsis. Whether those changes are associated with permanent damage, however, remains unclear and requires further evaluation.

In three animals who were imaged with [^{18}F] DPA-714, we noted that responses were different from the rest of the cohort: one animal showed decreased TSPO binding both in the brain and lungs after LPS administration compared to baseline, and manifested only mild immune activation based on serum cytokines, one animal had mildly decreased binding in the brain and one animal showed lower binding in the lungs. The immune response of those last two animals, however, were within the range or on the higher end of cytokine expression levels. We thus believe these findings are due to natural variability in the immune response to LPS as well as variability in organ response to inflammatory signals, a phenomenon that has been previously described (82–84). By using a relatively larger sample number, we have confidence we have encompassed the whole spectrum of immune activation.

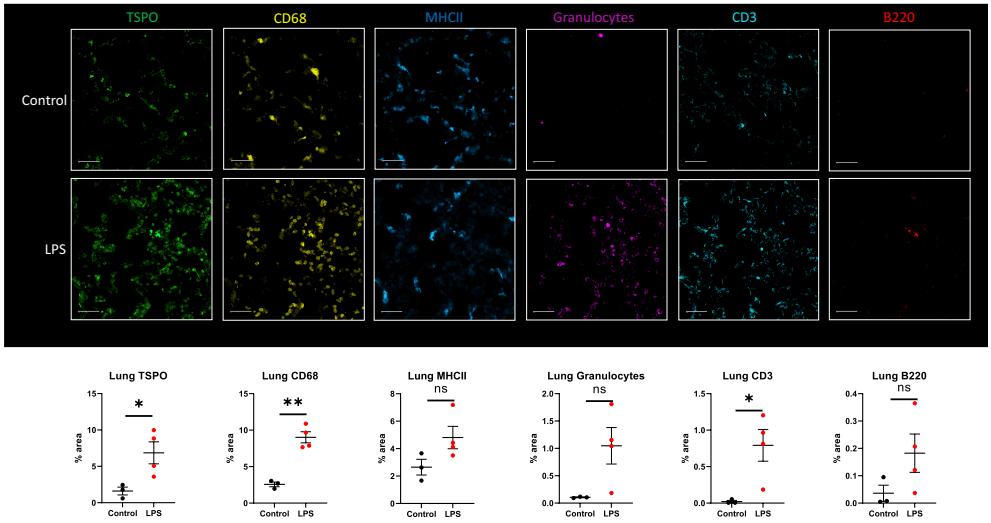

FIGURE 6
Immunohistochemistry in lung tissue sections. Representative MF-IHC images of a single lung section from control (top panels) and LPS treated rat (bottom panels). Quantification of the various stains was obtained by measuring whole lung section using Image J. Percentage area values are shown under each panel for TSPO, CD68 (macrophages), MHCII (dendritic cells), Granulocytes (neutrophils), CD3 (T cells), and B220 (B cells). There is increased TSPO (p=0.0361), CD68-monocytes/macrophages (p=0.001), and CD3-T cells (p=0.0305) staining in the lungs of LPS-treated rats (n=4) compared to controls (n=3). In this specific animal, staining for TSPO, macrophages, MHCII, granulocytes and lymphocytes was increased. Statistical analysis was performed using unpaired t-test. Mean with SEM are shown. p-values <0.05 are considered statistically significant. *p<0.05, **p<0.01, not significant (ns.)

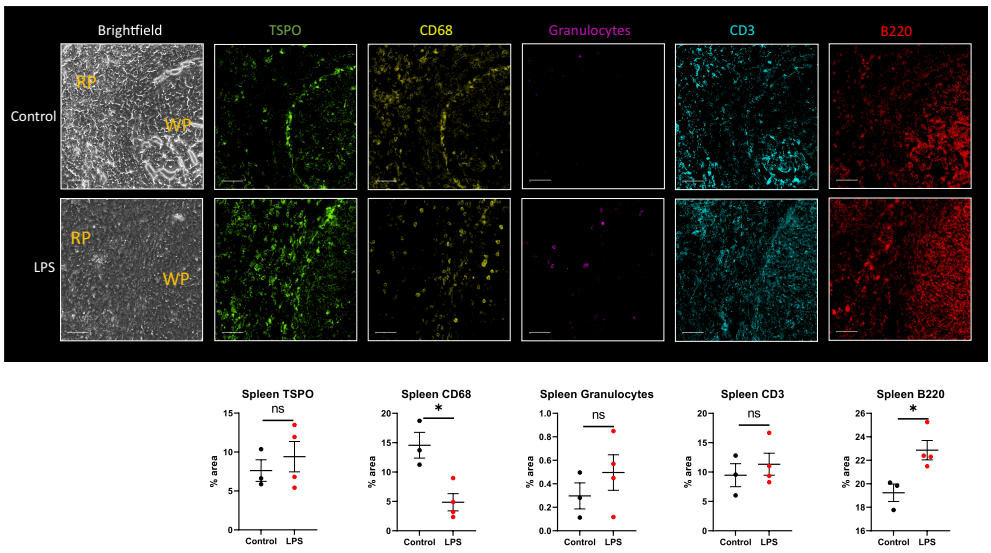

FIGURE 7
Immunohistochemistry in spleen tissue sections. Representative MF-IHC images of a single spleen section from control (top panels) and LPS-treated rat (bottom panels). The regions shown here include both the red pulp (RP) and white pulp (WP) areas as indicated in the brightfield images. Quantification of the various stains was obtained by measuring multiple ROIs in the red and white pulp spleen section using Image J. Percentage area values are shown under each panel for TSPO, CD68 (macrophages), MHCII (dendritic cells), Granulocytes (neutrophils), CD3 (T cells), and B220 (B-cells). No significant statistical difference in TSPO expression between groups is seen with two out of four animals showing increased staining, as shown. This is seen despite significant decreased immunoreactivity for CD68-monocytes/macrophages (p=0.0003), likely due to increased lymphocytic expression in the LPS group (n=4) compared to controls (n=3). Statistical analysis was performed using unpaired t-test. Mean with SEM are shown. p-values <0.05 are considered statistically significant. *p<0.05, not significant (ns).

10.3389/fimmu.2022.1010263

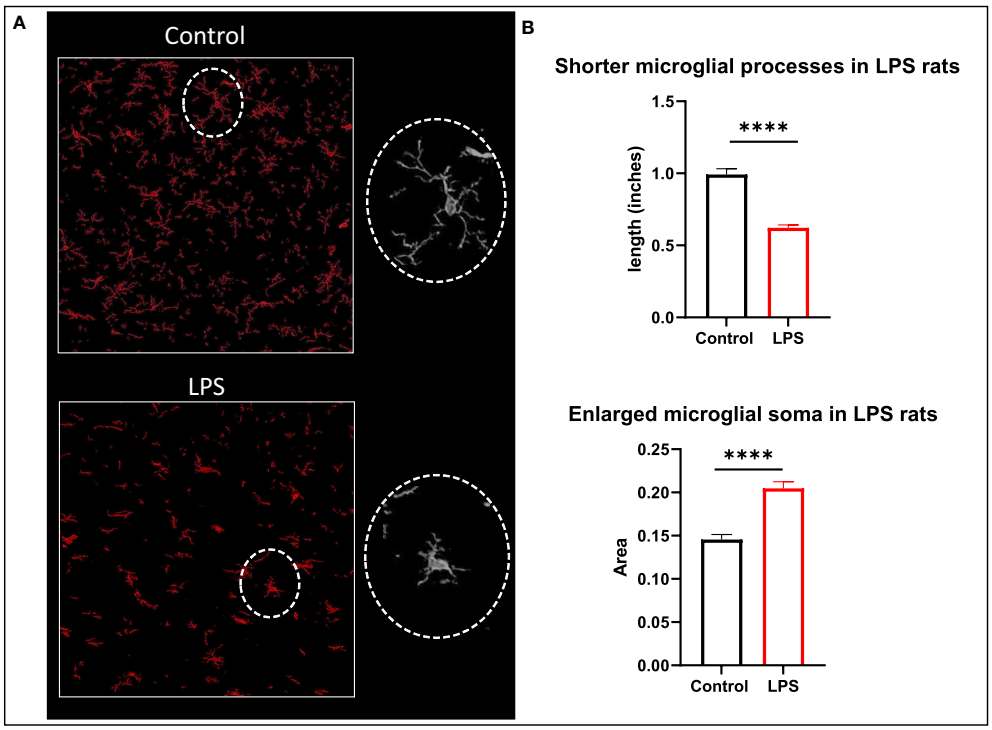

FIGURE 8
Morphological changes in microglia. **(A)** Representative images of microglia (Iba1 in red) in the corpus callosum of control and LPS treated rats. **(B)** Animals with systemic inflammation (LPS) show shorter microglial processes and thicker cell body compared to controls. Quantification was performed using the free hand selection tool from Image J to measure the length of 80 microglial processes and to delineate 20 somas from several ROIs in brain sections for each animal (control n=3; LPS-treated n=4). Statistical analysis was performed using unpaired t-test. Mean with SEM are shown. ****p <0.0001.

It is important to clarify here that although LPS can induce a systemic sterile inflammatory shock that can be similar in some aspects to what happens in SIRS and sepsis, direct translation of rodent findings into human findings in the setting of bacterial sepsis is not straightforward. LPS is an endotoxin present in the outer membrane of Gram-negative bacteria and extracted LPS has been broadly used in animal models and human studies to mimic the systemic inflammation caused by bacterial infections. There are however still differences in innate and adaptive responses between LPS and bacterial induced shock, including variability in serum cytokines and primary type of circulating leukocytes (85). To this end, however, our study is meant as a proof of concept that TSPO imaging can be useful in assessing organ-level inflammation, irrespective of the type of systemic inflammation.

One limitation of this study is that collection of tissues at baseline and after LPS administration for further biological analyses from the same animal is not possible. This forced us to use another set of animals for additional biological studies to support the PET data. Also, the small sample size (controls=3, LPS=4) used for immunohistochemistry could have limited the statistical analysis. However, with the promising results presented herein, additional studies with a larger sample size are warranted. Although [^{18}F]DPA-714 has shown better affinity and specificity to TSPO than previous ligands, assessment of TSPO gene polymorphisms and binding status (86) should be performed in human studies for accurate quantitative analysis. This will allow further evaluation of correlations between [^{18}F] DPA-714 uptake (or other TSPO ligands) and other molecular and clinical scores.

In conclusion, while the use of blood biomarkers and scoring systems can help predict organ dysfunction and mortality in patients with sepsis (87, 88), our study demonstrated that immunoreactivity in different organs (lung, liver, bone marrow, brain, and spleen) can be measured *in vivo* using the PET radiotracer [^{18}F]DPA-714. Inflammatory changes in the lungs, liver, brain, and bone marrow correlated with peripheral inflammation (increased pro- and anti-inflammatory cytokines in serum such as TNFα, IL-1, IL-6, IL-17A, IL-18, and IL-10). Our study is a proof of concept of the feasibility of using PET to assess organ level immunoreactivity in systemic sterile inflammatory response and the same approach could potentially be used in sepsis to evaluate the effectiveness of

preventative and therapeutic approaches in decreasing/controlling organ-level inflammation.

Data availability statement

The original contributions presented in the study are included in the article/Supplementary Material. Further inquiries can be directed to the corresponding author.

Ethics statement

The animal study was reviewed and approved by the Animal Care and Use Committee (ACUC) of the Clinical Center (CC) at the (NIH) and were performed in an AAALAC International accredited facility in accordance with relevant NIH policies and the Animal Welfare Act and Regulations.

Author contributions

There are eleven co-authors who have contributed significantly to this paper: DH, SwS, WR and SaS conceived of and designed the study. WR, SwS, SaS, WS-S, NM-O, JL and ZW evaluated the animals, performed the scans, and collected/or analyzed the data. NM-O, ST and SwS performed *in vitro* experiments and analysis. FB synthesized and validated the radioactive compounds. DM performed IHC experiments and associated data preparation. ST, NM-O, SwS and DH wrote the first draft of the paper. All authors participated in drafting the article and/or revising it critically for intellectual content. All authors contributed to the article and approved the submitted version.

Funding

Funding for this study was provided by the Intramural Research Program of the Clinical Center, NIH (Center for Infectious Disease Imaging (CIDI), Radiology and Imaging Sciences).

Conflict of interest

The authors declare that the research was conducted in the absence of any commercial or financial relationships that could be construed as a potential conflict of interest.

Publisher's note

All claims expressed in this article are solely those of the authors and do not necessarily represent those of their affiliated organizations, or those of the publisher, the editors and the reviewers. Any product that may be evaluated in this article, or claim that may be made by its manufacturer, is not guaranteed or endorsed by the publisher.

Supplementary material

The Supplementary Material for this article can be found online at: https://www.frontiersin.org/articles/10.3389/fimmu.2022.1010263/full#supplementary-material

SUPPLEMENTARY DATA SHEET 2
Graphical abstract.

References

1. Kramarow EA. Sepsis-related mortality among adults aged 65 and over: United states, 2019. *NCHS Data Brief* (2021) 422):1–8. doi: 10.15620/cdc:110542

2. Mayr FB, Yende S, Angus DC. Epidemiology of severe sepsis. *Virulence* (2014) 5(1):4–11. doi: 10.4161/viru.27372

3. Kilpatrick C, Saito H, Allegranzi B, Pittet D. Preventing sepsis in health care - it's in your hands: A world health organization call to action. *J Infect Prev* (2018) 19 (3):104–6. doi: 10.1177/1757177418769146

4. Rudd KE, Johnson SC, Agesa KM, Shackelford KA, Tsoi D, Kievlan DR, et al. Global, regional, and national sepsis incidence and mortality, 1990-2017: Analysis for the global burden of disease study. *Lancet* (2020) 395(10219):200–11. doi: 10.1016/S0140-6736(19)32989-7

5. Iwashyna TJ, Ely EW, Smith DM, Langa KM. Long-term cognitive impairment and functional disability among survivors of severe sepsis. *JAMA* (2010) 304(16):1787–94. doi: 10.1001/jama.2010.1553

6. van der Slikke EC, An AY, Hancock REW, Bouma HR. Exploring the pathophysiology of post-sepsis syndrome to identify therapeutic opportunities. *EBioMedicine* (2020) 61:103044. doi: 10.1016/j.ebiom.2020.103044

7. Gritte RB, Souza-Siqueira T, Curi R, Machado MCC, Soriano FG. Why septic patients remain sick after hospital discharge? *Front Immunol* (2020) 11:605666. doi: 10.3389/fimmu.2020.605666

8. Chakraborty RK, Burns B. Systemic inflammatory response syndrome. In: *StatPearls*. Treasure Island FL: StatPearls (2022).

9. Singer M, Deutschman CS, Seymour CW, Shankar-Hari M, Annane D, Bauer M, et al. The third international consensus definitions for sepsis and septic shock (Sepsis-3). *JAMA* (2016) 315(8):801–10. doi: 10.1001/jama.2016.0287

10. Fujishima S. Organ dysfunction as a new standard for defining sepsis. *Inflammation Regener* (2016) 36:24. doi: 10.1186/s41232-016-0029-y

11. Yao R, Pan R, Shang C, Li X, Cheng J, Xu J, et al. Translocator protein 18 kDa (TSPO) deficiency inhibits microglial activation and impairs mitochondrial function. *Front Pharmacol* (2020) 11:986. doi: 10.3389/fphar.2020.00986

12. Bonsack F, Sukumari-Ramesh S. TSPO: An evolutionarily conserved protein with elusive functions. *Int J Mol Sci* (2018) 19(6), 1694. doi: 10.3390/ijms19061694

13. Xu J, Sun J, Perrin RJ, Mach RH, Bales KR, Morris JC, et al. Translocator protein in late stage alzheimer's disease and dementia with lewy bodies brains. *Ann Clin Transl Neurol* (2019) 6(8):1423–34. doi: 10.1002/acn3.50837

14. Rupprecht R, Papadopoulos V, Rammes G, Baghai TC, Fan J, Akula N, et al. Translocator protein (18 kDa) (TSPO) as a therapeutic target for neurological and psychiatric disorders. *Nat Rev Drug Discov* (2010) 9(12):971–88. doi: 10.1038/nrd3295

15. Hammoud DA, Endres CJ, Chander AR, Guilarte TR, Wong DF, Sacktor NC, et al. Imaging glial cell activation with [11C]-R-PK11195 in patients with AIDS. *J Neurovirol* (2005) 11(4):346–55. doi: 10.1080/13550280500187351

16. Sinharay S, Tu TW, Kovacs ZI, Schreiber-Stainthorp W, Sundby M, Zhang X, et al. In vivo imaging of sterile microglial activation in rat brain after disrupting the blood-brain barrier with pulsed focused ultrasound: [18F]DPA-714 PET study. *J Neuroinflamm* (2019) 16(1):155. doi: 10.1186/s12974-019-1543-z

17. Lee DE, Yue X, Ibrahim WG, Lentz MR, Peterson KL, Jagoda EM, et al. Lack of neuroinflammation in the HIV-1 transgenic rat: an [(18)F]-DPA714 PET imaging study. *J Neuroinflamm* (2015) 12(1):171. doi: 10.1186/s12974-015-0390-9

18. Alam MM, Lee J, Lee SY. Recent progress in the development of TSPO PET ligands for neuroinflammation imaging in neurological diseases. *Nucl Med Mol Imaging* (2017) 51(4):283–96. doi: 10.1007/s13139-017-0475-8

19. Cumming P, Burgher B, Patkar O, Breakspear M, Vasdev N, Thomas P, et al. Sifting through the surfeit of neuroinflammation tracers. *J Cereb Blood Flow Metab* (2018) 38(2):204–24. doi: 10.1177/0271678X17748786

20. Werry EL, Bright FM, Piguet O, Ittner LM, Halliday GM, Hodges JR, et al. Recent developments in TSPO PET imaging as a biomarker of neuroinflammation in neurodegenerative disorders. *Int J Mol Sci* (2019) 20(13), 3161. doi: 10.3390/ijms20133161

21. Blevins LK, Crawford RB, Azzam DJ, Guilarte TR, Kaminski NE. Surface translocator protein 18 kDa (TSPO) localization on immune cells upon stimulation with LPS and in ART-treated HIV(+) subjects. *J Leukoc Biol* (2021) 110(1):123–40. doi: 10.1002/JLB.3A1219-729RR

22. Shah S, Sinharay S, Patel R, Solomon J, Lee JH, Schreiber-Stainthorp W, et al. PET imaging of TSPO expression in immune cells can assess organ-level pathophysiology in high-consequence viral infections. *Proc Natl Acad Sci USA* (2022) 119(15):e2110846119. doi: 10.1073/pnas.2110846119

23. Verweij SL, Stiekema LCA, Delewi R, Zheng KH, Bernelot Moens SJ, Kroon J, et al. Prolonged hematopoietic and myeloid cellular response in patients after an acute coronary syndrome measured with (18)F-DPA-714 PET/CT. *Eur J Nucl Med Mol Imaging* (2018) 45(11):1956–63. doi: 10.1007/s00259-018-4038-8

24. Largeau B, Dupont AC, Guilloteau D, Santiago-Ribeiro MJ, Arlicot N. TSPO PET imaging: From microglial activation to peripheral sterile inflammatory diseases? *Contrast Media Mol Imaging* (2017) 2017:6592139. doi: 10.1155/2017/6592139

25. Borchert T, Hess A, Lukacevic M, Ross TL, Bengel FM, Thackeray JT. Angiotensin-converting enzyme inhibitor treatment early after myocardial infarction attenuates acute cardiac and neuroinflammation without effect on chronic neuroinflammation. *Eur J Nucl Med Mol Imaging* (2020) 47(7):1757–68. doi: 10.1007/s00259-020-04736-8

26. Bernards N, Pottier G, Theze B, Dolle F, Boisgard R. In vivo evaluation of inflammatory bowel disease with the aid of muPET and the translocator protein 18 kDa radioligand [18F]DPA-714. *Mol Imaging Biol* (2015) 17(1):67–75. doi: 10.1007/s11307-014-0765-9

27. Hatori A, Yui J, Xie L, Kumata K, Yamasaki T, Fujinaga M, et al. Utility of translocator protein (18 kDa) as a molecular imaging biomarker to monitor the progression of liver fibrosis. *Sci Rep* (2015) 5:17327. doi: 10.1038/srep17327

28. Hatori A, Yui J, Yamasaki T, Xie L, Kumata K, Fujinaga M, et al. PET imaging of lung inflammation with [18F]FEDAC, a radioligand for translocator protein (18 kDa). *PloS One* (2012) 7(9):e45065. doi: 10.1371/journal.pone.0045065

29. Jones HA, Marino PS, Shakur BH, Morrell NW. In vivo assessment of lung inflammatory cell activity in patients with COPD and asthma. *Eur Respir J* (2003) 21(4):567–73. doi: 10.1183/09031936.03.00048502

30. Xie L, Yui J, Hatori A, Yamasaki T, Kumata K, Wakizaka H, et al. Translocator protein (18 kDa), a potential molecular imaging biomarker for non-invasively distinguishing non-alcoholic fatty liver disease. *J Hepatol* (2012) 57(5):1076–82. doi: 10.1016/j.jhep.2012.07.002

31. Pugliese F, Gaemperli O, Kinderlerer AR, Lamare F, Shalhoub J, Davies AH, et al. Imaging of vascular inflammation with [11C]-PK11195 and positron emission tomography/computed tomography angiography. *J Am Coll Cardiol* (2010) 56(8):653–61. doi: 10.1016/j.jacc.2010.02.063

32. van der Laken CJ, Elzinga EH, Kropholler MA, Molthoff CF, van der Heijden JW, Maruyama K, et al. Noninvasive imaging of macrophages in rheumatoid synovitis using 11C-(R)-PK11195 and positron emission tomography. *Arthritis Rheum* (2008) 58(11):3350–5. doi: 10.1002/art.23955

33. Sly LM, Krzesicki RF, Brashler JR, Buhl AE, McKinley DD, Carter DB, et al. Endogenous brain cytokine mRNA and inflammatory responses to lipopolysaccharide are elevated in the Tg2576 transgenic mouse model of alzheimer's disease. *Brain Res Bull* (2001) 56(6):581–8. doi: 10.1016/S0361-9230(01)00730-4

34. Doursout MF, Schurdell MS, Young LM, Osuagwu U, Hook DM, Poindexter BJ, et al. Inflammatory cells and cytokines in the olfactory bulb of a rat model of neuroinflammation; insights into neurodegeneration? *J Interferon Cytokine Res* (2013) 33(7):376–83. doi: 10.1089/jir.2012.0088

35. Friedrich T, Schalla MA, Goebel-Stengel M, Kobelt P, Rose M, Stengel A. Inflammatory stress induced by intraperitoneal injection of LPS increases phoenixin expression and activity in distinct rat brain nuclei. *Brain Sci* (2022) 12(2), 135. doi: 10.3390/brainsci12020135

36. Wolff S, Klatt S, Wolff JC, Wilhelm J, Fink L, Kaps M, et al. Endotoxin-induced gene expression differences in the brain and effects of iNOS inhibition and norepinephrine. *Intensive Care Med* (2009) 35(4):730–9. doi: 10.1007/s00134-009-1394-7

37. Huang ZS, Xie DQ, Xu LJ, Huang CS, Zheng M, Chen YJ, et al. Tetramethylpyrazine ameliorates lipopolysaccharide-induced sepsis in rats via protecting blood-brain barrier, impairing inflammation and nitrous oxide systems. *Front Pharmacol* (2020) 11:562084. doi: 10.3389/fphar.2020.562084

38. Kuhnast B, Damont A, Hinnen F, Catarina T, Demphel S, Le Helleix S, et al. [18F]DPA-714, [18F]PBR111 and [18F]FEDAA1106-selective radioligands for imaging TSPO 18 kDa with PET: Automated radiosynthesis on a TRACERLAb FX-FN synthesizer and quality controls. *Appl Radiat Isot* (2012) 70(3):489–97. doi: 10.1016/j.apradiso.2011.10.015

39. Zarbock A, Gomez H, Kellum JA. Sepsis-induced acute kidney injury revisited: pathophysiology, prevention and future therapies. *Curr Opin Crit Care* (2014) 20(6):588–95. doi: 10.1097/MCC.0000000000000153

40. Kanazawa H, Kotoda A, Akimoto T, Shinozaki T, Inoue M, Sugimoto H, et al. Serial Tc-99m MAG3 renography evaluating the recovery of acute kidney injury associated with minimal change nephrotic syndrome. *Intern Med* (2013) 52(9):987–91. doi: 10.2169/internalmedicine.52.9204

41. Bozza FA, Salluh JI, Japiassu AM, Soares M, Assis EF, Gomes RN, et al. Cytokine profiles as markers of disease severity in sepsis: a multiplex analysis. *Crit Care* (2007) 11(2):R49. doi: 10.1186/cc5783

42. Raith EP, Udy AA, Bailey M, McGloughlin S, MacIsaac C, Bellomo R, et al. Prognostic accuracy of the SOFA score, SIRS criteria, and qSOFA score for in-hospital mortality among adults with suspected infection admitted to the intensive care unit. *JAMA* (2017) 317(3):290–300. doi: 10.1001/jama.2016.20328

43. Delano MJ, Ward PA. The immune system's role in sepsis progression, resolution, and long-term outcome. *Immunol Rev* (2016) 274(1):330–53. doi: 10.1111/imr.12499

44. Kaneko N, Kuo HH, Boucau J, Farmer JR, Allard-Chamard H, Mahajan VS, et al. Loss of bcl-6-Expressing T follicular helper cells and germinal centers in COVID-19. *Cell* (2020) 183(1):143–157 e13. doi: 10.1016/j.cell.2020.08.025

45. Askim A, Moser F, Gustad LT, Stene H, Gundersen M, Asvold BO, et al. Poor performance of quick-SOFA (qSOFA) score in predicting severe sepsis and mortality - a prospective study of patients admitted with infection to the emergency department. *Scand J Trauma Resusc Emerg Med* (2017) 25(1):56. doi: 10.1186/s13049-017-0399-4

46. Zheng J, Winkeler A, Peyronneau MA, Dolle F, Boisgard R. Evaluation of PET imaging performance of the TSPO radioligand [18F]DPA-714 in mouse and rat models of cancer and inflammation. *Mol Imaging Biol* (2016) 18(1):127–34. doi: 10.1007/s11307-015-0877-x

47. Gent YY, Weijers K, Molthoff CF, Windhorst AD, Huisman MC, Kassiou M, et al. Promising potential of new generation translocator protein tracers providing enhanced contrast of arthritis imaging by positron emission tomography in a rat model of arthritis. *Arthritis Res Ther* (2014) 16(2):R70. doi: 10.1186/ar4509

48. Pottier G, Bernards N, Dolle F, Boisgard R. [(1)(8)F]DPA-714 as a biomarker for positron emission tomography imaging of rheumatoid arthritis in an animal model. *Arthritis Res Ther* (2014) 16(2):R69. doi: 10.1186/ar4508

49. Bruijnen STG, Verweij NJF, Gent YYJ, Huisman MC, Windhorst AD, Kassiou M, et al. Imaging disease activity of rheumatoid arthritis by macrophage targeting using second generation translocator protein positron emission tomography tracers. *PloS One* (2019) 14(9):e0222844. doi: 10.1371/journal.pone.0222844

50. Nedeva C, Menassa J, Puthalakath H. Sepsis: Inflammation is a necessary evil. *Front Cell Dev Biol* (2019) 7:108. doi: 10.3389/fcell.2019.00108

51. Cao C, Yu M, Chai Y. Pathological alteration and therapeutic implications of sepsis-induced immune cell apoptosis. *Cell Death Dis* (2019) 10(10):782. doi: 10.1038/s41419-019-2015-1

52. Liu CH, Kuo SW, Ko WJ, Tsai PR, Wu SW, Lai CH, et al. Early measurement of IL-10 predicts the outcomes of patients with acute respiratory distress syndrome receiving extracorporeal membrane oxygenation. *Sci Rep* (2017) 7(1):1021. doi: 10.1038/s41598-017-01225-1

53. Kim WY, Hong SB. Sepsis and acute respiratory distress syndrome: Recent update. *Tuberc Respir Dis (Seoul)* (2016) 79(2):53–7. doi: 10.4046/trd.2016.79.2.53

54. Meduri GU, Headley S, Kohler G, Stentz F, Tolley E, Umberger R, et al. Persistent elevation of inflammatory cytokines predicts a poor outcome in ARDS. plasma IL-1 beta and IL-6 levels are consistent and efficient predictors of outcome over time. *Chest* (1995) 107(4):1062–73. doi: 10.1378/chest.107.4.1062

55. Baudesson de Chanville C, Chousterman BG, Hamon P, Laviron M, Guillou N, Loyher PL, et al. Sepsis triggers a late expansion of functionally impaired tissue-

vascular inflammatory monocytes during clinical recovery. *Front Immunol* (2020) 11:675. doi: 10.3389/fimmu.2020.00675

56. Davis FM, Schaller MA, Dendekker A, Joshi AD, Kimball AS, Evanoff H, et al. Sepsis induces prolonged epigenetic modifications in bone marrow and peripheral macrophages impairing inflammation and wound healing. *Arterioscler Thromb Vasc Biol* (2019) 39(11):2353–66. doi: 10.1161/ATVBAHA.119.312754

57. Rodrigues RS, Bozza FA, Hanrahan CJ, Wang LM, Wu Q, Hoffman JM, et al. (18)F-fluoro-2-deoxyglucose PET informs neutrophil accumulation and activation in lipopolysaccharide-induced acute lung injury. *Nucl Med Biol* (2017) 48:52–62. doi: 10.1016/j.nucmedbio.2017.01.005

58. Yin F, Qian H, Duan C, Ning B. The bone marrow niche components are adversely affected in sepsis. *Mol BioMed* (2020) 1(1):10. doi: 10.1186/s43556-020-00010-3

59. Grobmyer SR, Lin E, Lowry SF, Rivadeneira DE, Potter S, Barie PS, et al. Elevation of IL-18 in human sepsis. *J Clin Immunol* (2000) 20(3):212–5. doi: 10.1023/A:1006641630904

60. Cui YL, Wang B, Gao HM, Xing YH, Li J, Li HJ, et al. Interleukin-18 and miR-130a in severe sepsis patients with thrombocytopenia. *Patient Prefer Adherence* (2016) 10:313–9. doi: 10.2147/PPA.S95588

61. Shapiro NI, Khankin EV, Van Meurs M, Shih SC, Lu S, Yano M, et al. Leptin exacerbates sepsis-mediated morbidity and mortality. *J Immunol* (2010) 185 (1):517–24. doi: 10.4049/jimmunol.0903975

62. Walley KR, Lukacs NW, Standiford TJ, Strieter RM, Kunkel SL. Elevated levels of macrophage inflammatory protein 2 in severe murine peritonitis increase neutrophil recruitment and mortality. *Infect Immun* (1997) 65(9):3847–51. doi: 10.1128/iai.65.9.3847-3851.1997

63. Wang Y, Yue X, Kiesewetter DO, Niu G, Teng G, Chen X. PET imaging of neuroinflammation in a rat traumatic brain injury model with radiolabeled TSPO ligand DPA-714. *Eur J Nucl Med Mol Imaging* (2014) 41(7):1440–9. doi: 10.1007/s00259-014-2727-5

64. Hagens MHJ, Golla SV, Wijburg MT, Yaqub M, Heijtel D, Steenwijk MD, et al. In vivo assessment of neuroinflammation in progressive multiple sclerosis: a proof of concept study with [(18)F]DPA714 PET. *J Neuroinflamm* (2018) 15 (1):314. doi: 10.1186/s12974-018-1352-9

65. Kuszpit K, Hollidge BS, Zeng X, Stafford RG, Daye S, Zhang X, et al. [(18)F] DPA-714 PET imaging reveals global neuroinflammation in zika virus-infected mice. *Mol Imaging Biol* (2018) 20(2):275–83. doi: 10.1007/s11307-017-1118-2

66. Vieira IF, Ory D, Casteels C, Lima FRA, Van Laere K, Bormans G, et al. Volume-of-interest-based supervised cluster analysis for pseudo-reference region selection in [(18)F]DPA-714 PET imaging of the rat brain. *EJNMMI Res* (2018) 8 (1):112. doi: 10.1186/s13550-018-0467-4

67. Sridharan S, Lepelletier FX, Trigg W, Banister S, Reekie T, Kassiou M, et al. Comparative evaluation of three TSPO PET radiotracers in a LPS-induced model of mild neuroinflammation in rats. *Mol Imaging Biol* (2017) 19(1):77–89. doi: 10.1007/s11307-016-0984-3

68. Chauveau F, Van Camp N, Dolle F, Kuhnast B, Hinnen F, Damont A, et al. Comparative evaluation of the translocator protein radioligands 11C-DPA-713, 18F-DPA-714, and 11C-PK11195 in a rat model of acute neuroinflammation. *J Nucl Med* (2009) 50(3):468–76. doi: 10.2967/jnumed.108.058669

69. Boutin H, Prenant C, Maroy R, Galea J, Greenhalgh AD, Smigova A, et al. [18F]DPA-714: Direct comparison with [11C]PK11195 in a model of cerebral ischemia in rats. *PloS One* (2013) 8(2):e56441. doi: 10.1371/journal.pone.0056441

70. Arlicot N, Vercouillie J, Ribeiro MJ, Tauber C, Venel Y, Baulieu JL, et al. Initial evaluation in healthy humans of [18F]DPA-714, a potential PET biomarker for neuroinflammation. *Nucl Med Biol* (2012) 39(4):570–8. doi: 10.1016/j.nucmedbio.2011.10.012

71. Peyronneau MA, Saba W, Goutal S, Damont A, Dolle F, Kassiou M, et al. Metabolism and quantification of [(18)F]DPA-714, a new TSPO positron emission tomography radioligand. *Drug Metab Dispos* (2013) 41(1):122–31. doi: 10.1124/dmd.112.046342

72. Vicidomini C, Panico M, Greco A, Gargiulo S, Coda AR, Zannetti A, et al. In vivo imaging and characterization of [(18)F]DPA-714, a potential new TSPO ligand, in mouse brain and peripheral tissues using small-animal PET. *Nucl Med Biol* (2015) 42(3):309–16. doi: 10.1016/j.nucmedbio.2014.11.009

73. Jiang CL, Lu CL. Interleukin-2 and its effects in the central nervous system. *Biol Signals Recept* (1998) 7(3):148–56. doi: 10.1159/000014541

74. Petitto JM, Meola D, Huang Z. Interleukin-2 and the brain: Dissecting central versus peripheral contributions using unique mouse models. *Methods Mol Biol* (2012) 934:301–11. doi: 10.1007/978-1-62703-071-7_15

75. Alexander JJ, Jacob A, Cunningham P, Hensley L, Quigg RJ. TNF is a key mediator of septic encephalopathy acting through its receptor, TNF receptor-1. *Neurochem Int* (2008) 52(3):447–56. doi: 10.1016/j.neuint.2007.08.006

76. Ye B, Tao T, Zhao A, Wen L, He X, Liu Y, et al. Blockade of IL-17A/IL-17R pathway protected mice from sepsis-associated encephalopathy by inhibition of microglia activation. *Mediators Inflammation* (2019) 2019:8461725. doi: 10.1155/2019/8461725

77. Siddiqui S, Fang M, Ni B, Lu D, Martin B, Maudsley S. Central role of the EGF receptor in neurometabolic aging. *Int J Endocrinol* (2012) 2012:739428. doi: 10.1155/2012/739428

78. Morrow KN, Coopersmith CM, Ford ML. IL-17, IL-27, and IL-33: A novel axis linked to immunological dysfunction during sepsis. *Front Immunol* (2019) 10:1982. doi: 10.3389/fimmu.2019.01982

79. Zrzavy T, Hoftberger R, Berger T, Rauschka H, Butovsky O, Weiner H, et al. Pro-inflammatory activation of microglia in the brain of patients with sepsis. *Neuropathol Appl Neurobiol* (2019) 45(3):278–90. doi: 10.1111/nan.12502

80. Bruck E, Schandl A, Bottai M, Sackey P. The impact of sepsis, delirium, and psychological distress on self-rated cognitive function in ICU survivors-a prospective cohort study. *J Intensive Care* (2018) 6:2. doi: 10.1186/s40560-017-0272-6

81. Morandi A, Rogers BP, Gunther ML, Merkle K, Pandharipande P, Girard TD, et al. The relationship between delirium duration, white matter integrity, and cognitive impairment in intensive care unit survivors as determined by diffusion tensor imaging: the VISIONS prospective cohort magnetic resonance imaging study*. *Crit Care Med* (2012) 40(7):2182–9. doi: 10.1097/CCM.0b013e318250acdc

82. Jacobsen S, Andersen PH, Toelboell T, Heegaard PM. Dose dependency and individual variability of the lipopolysaccharide-induced bovine acute phase protein response. *J Dairy Sci* (2004) 87(10):3330–9. doi: 10.3168/jds.S0022-0302(04)73469-4

83. Fang H, Jin H, Hua C, Liu A, Song Z, Chen X, et al. The LPS responsiveness in BN and LEW rats and its severity are modulated by the liver. *J Immunol Res* (2018) 2018:6328713. doi: 10.1155/2018/6328713

84. Somann JP, Wasilczuk KM, Neihouser KV, Sturgis J, Albors GO, Robinson JP, et al. Characterization of plasma cytokine response to intraperitoneally administered LPS & subdiaphragmatic branch vagus nerve stimulation in rat model. *PloS One* (2019) 14(3):e0214317. doi: 10.1371/journal.pone.0214317

85. Stortz JA, Raymond SL, Mira JC, Moldawer LL, Mohr AM, Efron PA. Murine models of sepsis and trauma: Can we bridge the gap? *ILAR J* (2017) 58 (1):90–105. doi: 10.1093/ilar/ilx007

86. Owen DR, Yeo AJ, Gunn RN, Song K, Wadsworth G, Lewis A, et al. An 18-kDa translocator protein (TSPO) polymorphism explains differences in binding affinity of the PET radioligand PBR28. *J Cereb Blood Flow Metab* (2012) 32(1):1–5.

87. Liu J, Bai C, Li B, Shan A, Shi F, Yao C, et al. Mortality prediction using a novel combination of biomarkers in the first day of sepsis in intensive care units. *Sci Rep* (2021) 11(1):1275. doi: 10.1038/s41598-020-79843-5

88. Hebert PC, Drummond AJ, Singer J, Bernard GR, Russell JA. A simple multiple system organ failure scoring system predicts mortality of patients who have sepsis syndrome. *Chest* (1993) 104(1):230–5. doi: 10.1378/chest.104.1.230

frontiers | Frontiers in Immunology

TYPE Original Research
PUBLISHED 02 December 2022
DOI 10.3389/fimmu.2022.994295

Check for updates

OPEN ACCESS

EDITED BY
Borna Relja,
Otto von Guericke University,
Germany

REVIEWED BY
Na Cui,
Peking Union Medical College Hospital (CAMS), China
Yi Yang,
Southeast University, China

*CORRESPONDENCE
Yimin Li
dryiminli@vip.163.com

†These authors have contributed equally to this work

SPECIALTY SECTION
This article was submitted to Inflammation, a section of the journal Frontiers in Immunology

RECEIVED 14 July 2022
ACCEPTED 11 November 2022
PUBLISHED 02 December 2022

CITATION
Zheng Y, Liu B, Deng X, Chen Y, Huang Y, Zhang Y, Xu Y, Sang L, Liu X and Li Y (2022) Construction and validation of a robust prognostic model based on immune features in sepsis. *Front. Immunol.* 13:994295. doi: 10.3389/fimmu.2022.994295

COPYRIGHT
© 2022 Zheng, Liu, Deng, Chen, Huang, Zhang, Xu, Sang, Liu and Li. This is an open-access article distributed under the terms of the Creative Commons Attribution License (CC BY). The use, distribution or reproduction in other forums is permitted, provided the original author(s) and the copyright owner(s) are credited and that the original publication in this journal is cited, in accordance with accepted academic practice. No use, distribution or reproduction is permitted which does not comply with these terms.

Construction and validation of a robust prognostic model based on immune features in sepsis

Yongxin Zheng[1,2†], Baiyun Liu[1,2†], Xiumei Deng[1,2†], Yubiao Chen[1,2†], Yongbo Huang[1,2], Yu Zhang[1,2], Yonghao Xu[1,2], Ling Sang[1,2], Xiaoqing Liu[1,2] and Yimin Li[1,2*]

[1]State Key Laboratory of Respiratory Diseases, National Clinical Research Center for Respiratory Disease, Guangzhou Institute of Respiratory Health, Department of Critical Care Medicine, The First Affiliated Hospital of Guangzhou Medical University, Guangzhou, China, [2]The First Affiliated Hospital, Guangzhou Medical University, Guangzhou, China

Purpose: Sepsis, with life-threatening organ failure, is caused by the uncontrolled host response to infection. Immune response plays an important role in the pathophysiology of sepsis. Immune-related genes (IRGs) are promising novel biomarkers that have been used to construct the diagnostic and prognostic model. However, an IRG prognostic model used to predict the 28-day mortality in sepsis was still limited. Therefore, the study aimed to develop a prognostic model based on IRGs to identify patients with high risk and predict the 28-day mortality in sepsis. Then, we further explore the circulating immune cell and immunosuppression state in sepsis.

Materials and methods: The differentially expressed genes (DEGs), differentially expressed immune-related genes (DEIRGs), and differentially expressed transcription factors (DETFs) were obtained from the GEO, ImmPort, and Cistrome databases. Then, the TFs-DEIRGs regulatory network and prognostic prediction model were constructed by Cox regression analysis and Pearson correlation analysis. The external datasets also validated the reliability of the prognostic model. Based on the prognostic DEIRGs, we developed a nomogram and conducted an independent prognosis analysis to explore the relationship between DEIRGs in the prognostic model and clinical features in sepsis. Besides, we further evaluate the circulating immune cells state in sepsis.

Results: A total of seven datasets were included in our study. Among them, GSE65682 was identified as a discovery cohort. The results of GSEA showed that there is a significant correlation between sepsis and immune response. Then, based on a P value <0.01, 69 prognostic DEIRGs were obtained and the potential molecular mechanisms of DEIRGs were also clarified. According to multivariate Cox regression analysis, 22 DEIRGs were further identified to construct the prognostic model and identify patients with high risk. The Kaplan–Meier survival analysis showed that high-risk groups have higher 28-day mortality than low-risk groups (P=1.105e-13). The AUC value was 0.879 which symbolized that the prognostic model had a better accuracy to predict

the 28-day mortality. The external datasets also prove that the prognostic model had an excellent prediction value. Furthermore, the results of correlation analysis showed that patients with Mars1 might have higher risk scores than Mars2-4 (P=0.002). According to the previous study, Mars1 endotype was characterized by immunoparalysis. Thus, the sepsis patients in high-risk groups might exist the immunosuppression. Between the high-risk and low-risk groups, circulating immune cells types were significantly different, and risk score was significantly negatively correlated with naive CD4+ T cells (P=0.019), activated NK cells (P=0.0045), monocytes (P=0.0134), and M1 macrophages (P=0.0002).

Conclusions: Our study provides a robust prognostic model based on 22 DEIRGs which can predict 28-day mortality and immunosuppression status in sepsis. The higher risk score was positively associated with 28-day mortality and the development of immunosuppression. IRGs are a promising biomarker that might facilitate personalized treatments for sepsis.

KEYWORDS

sepsis, immune, prognostic model, 28-day mortality, immunosuppression

Introduction

Sepsis is a complex disorder that develops as a severe systemic inflammatory response to infection, and is associated with high mortality (1). According to the US report, there were 48.9 (38.9-62.9) million incident cases of sepsis in the world annually and 11.0 (10·1-12·0) million patients died with sepsis (2). Sepsis was recognized as the most expensive burden and threat to human health. Increased mortality was associated with delay in initiating early treatments. The previous study estimated that the survival rate decreases by roughly 10% every hour that appropriate antimicrobial medication is delayed, emphasizing the urgent need for early identification and precise treatments to improve clinical outcomes (1, 3, 4). In 2017, World Health Organization (WHO) also declared that the improvement of sepsis early prevention, early recognition, and treatment is a global health priority (5). Therefore, the identification of septic patients at high risk may help clinicians to screen and identify individuals who are most likely to have poor prognosis, or to detect immunosuppressed states which could benefit from targeted immunostimulating therapies, and eventually improve patients' prognosis.

Sepsis is an uncontrolled inflammatory response to invasive infection which can disturb homeostasis. After infection, the immune response can eliminate the pathogens but sometimes the host will release damage-associated molecular patterns (DAMPs) to damage organs. However, in late sepsis, sepsis patients have immune suppression which is characterized the lymphocyte exhaustion and the reprogramming of antigen–presenting cells (6, 7). In face of the complex pathophysiology of sepsis and its often challenging clinical evaluation, promising diagnostic biomarkers in sepsis are emerging with the application of blood genomics. Scicluna et al. (8) established endotypes for patients with sepsis through genome-wide blood gene expression profiles. The study provided a method to classify sepsis patients into four different endotypes and the detection of sepsis endotypes may assist in the precise treatments. Besides, increasing studies have identified novel immune biomarkers for early diagnosis and guide immunotherapies in oncology research. The immune related-genes (IRGs) model had been successfully applied in oncology to identify patients at high risk and estimate overall survival (9, 10). However, a robust IRGs model to identify high-risk patients and predict prognosis for adult patients with all-cause sepsis is still lacking.

The primary objective of this study was to construct an IRGs model to predict the prognosis of adult patients with all-cause sepsis. To achieve this aim, we obtain the differentially expressed IRGs (DEIRGs) that we can establish the Cox prediction model based on DEIRGs to predict the patients at high risk and the prognosis for patients with sepsis. Then, we construct a regulatory network between differentially expressed transcription factors (DETFs) and DEIRGs to explore the underlying molecular mechanisms. Besides, we further analyze the immune microenvironment in sepsis patients. Finally, we tested the robustness of the predictive model across the other datasets, and we provided a quantitative tool for predicting the individual probability of death.

10.3389/fimmu.2022.994295

Materials and methods

Datasets selection, data acquisition, and processing

A workflow is shown in Figure 1. The Gene Expression Omnibus (GEO) (https://www.ncbi.nlm.nih.gov/geo/) and ArrayExpress (https://www.ebi.ac.uk/arrayexpress/) databases were comprehensively searched from inception to April 2022 to obtain the relevant datasets. The inclusion criteria of datasets were: (1) diagnosis of patients with sepsis; (2) sample size more than 50; (3) age ≥18 years; (4) the endpoints included 28-day mortality; (5) the patient's specimens were collected before 24h on ICU admission and anti-inflammation treatments. Therefore, the 7 datasets were included in the study. Among them, GSE65682 was recognized as a training set because it was a large cohort study, and the other datasets were retained for model validation. The details of these datasets are shown in Table 1. To identify IRGs, we downloaded 2,483 IRGs from the Immunology Database and Analysis Portal (ImmPort) (http://www.immport.org/). Moreover, to construct the regulatory network, we obtained the transcription factors (TFs) from Cistrome Project (http://www.cistrome.org/).

Differential expression analysis in sepsis

All the genes in GSE65682 were differentially analyzed by using limma R packages (http://www.bioconductor.org/packages/release/bioc/html/limma.html) (11). The parameter for DEGs screened was $|\text{Log2Foldchange}| \geq 0.5$ and P-value < 0.05. The Volcano plots were drawn by 'ggplot2' R package. Then, the IRGs that were overlapping with DEGs were identified as DEIRGs. Similarly, DETFs were obtained by matching TFs with DEGs.

DEGs and gene set enrichment analysis

GSEA was used to assess related pathways and molecular mechanisms in sepsis. We performed the GSEA by the R package 'clusterProfiler'. Normalized enrichment score (NES) and false discovery rate (FDR) were used to quantify enrichment magnitude and statistical significance, respectively (12, 13).

Identification of prognostic DEIRGs and construction of the regulatory network

To identify the prognostic DEIRGs (P <0.01), R package 'survival R' was used to perform univariate Cox regression analysis. Then, it is important to further explore the mechanisms of TFs to regulate the prognostic DEIRGs. Thus, we further analyzed the coexpression relationship between TFs and prognostic DEIRGs by calculating Pearson's correlation coefficient. A regulatory network was constructed based on the filter thresholds (P value <0.001 and |cor| > 0.5). The network was visualized by using Cytoscape software.

Construction of the prognostic prediction model in sepsis and development of nomogram

Based on the univariate Cox regression analysis, prognostic DEIRGs were recognized as the biomarkers for multivariate Cox regression analysis. According to the median risk score value, conducted between low-risk and high-risk groups by using 'survival' R package. To evaluate the sensitivity and specificity of the prediction model, the receiver operating characteristics (ROC) curve was calculated using the 'survivalROC' package. The area under the ROC curve (AUC) was used to evaluate the prognostic model: 0.5-0.7 (moderate), 0.7-0.8 (better), and >0.9 (excellent).

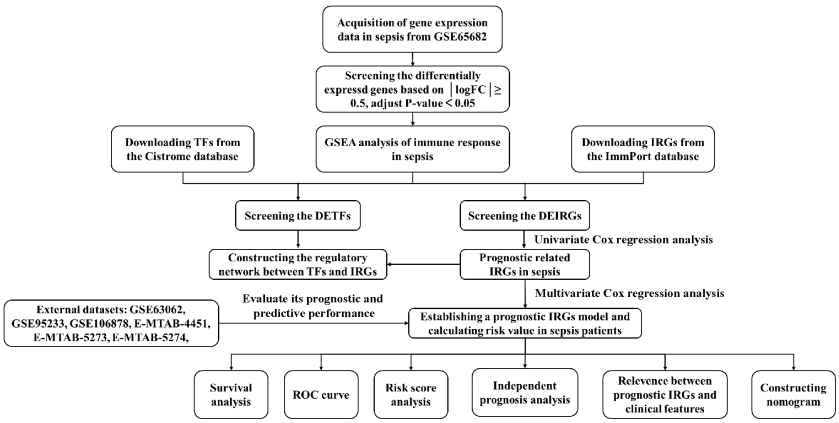

FIGURE 1
Flowchart of data analysis and validation.

TABLE 1 Basic information of the datasets included in this study.

Accession	Study population	Sample type	Country	Timing of gene expression profiling	Mortality / Total patients
GSE65682	Patient diagnoses sepsis due to cap, hap and non-infectious control.	Blood	Netherlands and England	On ICU admission	114 / 802
GSE63042	Patients with SIRS or sepsis	Blood	America	The day of enrollment upon presentation to the ED.	28 / 129
GSE95233	Patients with septic shock and healthy volunteers	Blood	France	Day 1 of ICU admission	34 / 124
GSE106878	septic shock patients from the CORTICUS-trial	Circulating leukocytes	International	Before hydrocortisone application	26 / 94
E-MTAB-4451	Patients with severe sepsis due to CAP	Circulating leukocytes	England	On ICU admission	52 / 106
E-MTAB-5273	Patients with sepsis due to CAP or faecal peritonitis.	Circulating leukocytes	England	First day of ICU stay	43 / 221
E-MTAB-5274	Patients with sepsis due to CAP or faecal peritonitis.	Circulating leukocytes	England	First day of ICU stay	14 / 106

To provide a quantitative tool for predicting probability of 28-day mortality in septic patients, we construct a nomogram according to the DEIRGs in the prognostic model and clinic features. The patients' clinic features are shown in Supplementary Table 1.

Validation in multiple external datasets

To evaluate the predictive performance of the prognostic model, 6 datasets (GSE63062, GSE95233, GSE106878, E-MTAB-4451, E-MTAB-5273, and E-MTAB-5274) were included according to the inclusion criteria. The prognostic model was used to predict the 28-day mortality of external datasets. Furthermore, the ROC curve was generated to determine sensitivity and specificity in the prognostic model.

Gene ontology and pathway enrichment analysis for DEIRGs in the prognostic model

To explore the mechanisms and functions of DEIRGs in the prognostic model, we performed Gene Ontology (GO) and Pathway Enrichment Analysis (KEGG) through the DAVID database (https://david.ncifcrf.gov/). Upon GO analysis and KEGG analysis, a P value <0.05 was recognized as statistical significance. The results of GO analysis were classified into three functional groups: biological process (BP), molecular function (MF), and cellular component (CC).

Correlation analysis between clinical features and DEIRGs in prognostic model

The correlation between risk score, gene expression value, and clinical features (age, gender, diabetes, ICU acquired infection (ICUA), and endotype class) were analyzed by using the 'beeswarm' R package. A P value <0.05 indicated statistical significance.

Exploration of circulating immune cells between low-risk and high-risk groups

CIBERSORTx (https://cibersort.stanford.edu/), an online analytical tool based on a kind of deconvolution algorithm iterated 1000 times, was available to provide an estimation of the abundances of member cell types in a mixed cell population by using gene expression data (14). Then, the content of 22 types of circulating immune cells in each sample was visualized by a vertical stack bar. Furthermore, the difference analysis of immune cells between low-risk and high-risk groups was shown by drawing barplot diagrams. Additionally, we explored the correlation between immune cells and risk score by Spearman correlation analyses. A P value <0.05 was considered statistical significance.

Statistical analysis

All statistical analyses were performed using R software and Grapad prism 9.0. The 'limma R' package was used to conduct differential expression analysis. The R package 'clusterProfiler' was adopted for assessing related pathways and molecular mechanisms in sepsis. The prognostic prediction model was constructed by univariate and multivariate Cox regression analysis. Besides, the 'survival', 'survival ROC', and 'risk Plot' R packages were applied to evaluate the survival difference between the high-risk and low-risk groups and assess the sensitivity and specificity in the prognostic model. Then, the 'beeswarm' R package was used to explore the correlation

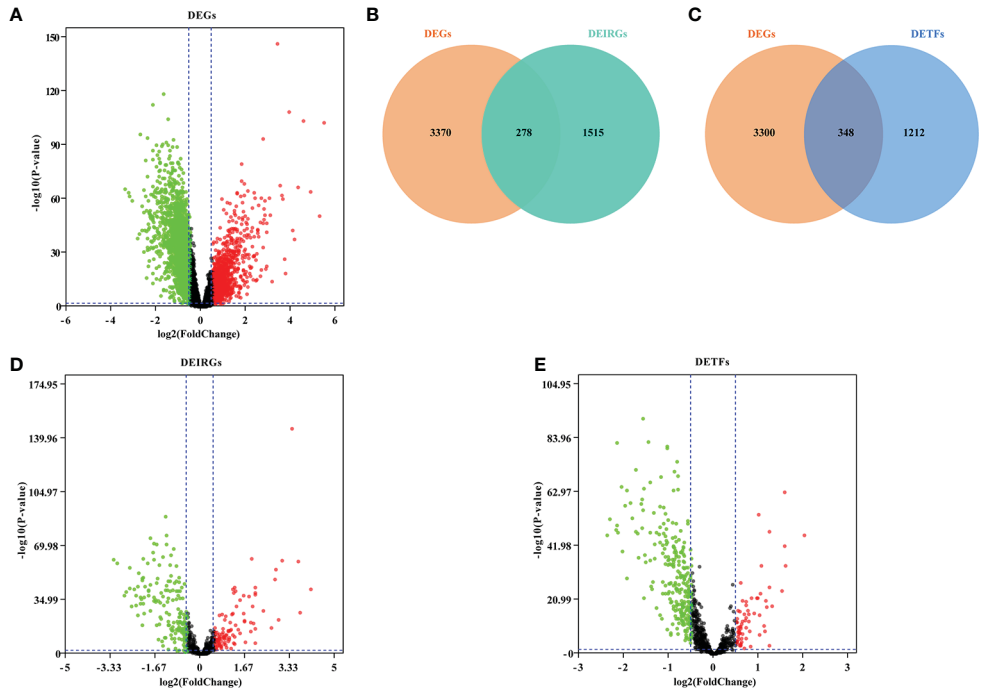

FIGURE 2
Screening DEGs, DEIRGs and DETFs. **(A)** Volcano plot showing DEGs in GSE66890; **(B)** Venn diagram showed DEIRGs; **(C)** Venn diagram showed DETFs; **(D)** Volcano plot showing DEIRGs; **(E)** Volcano plot showing DETFs. Based on the |fold change|>0.5 and FDR<0.05, the red points represent upregulated genes and the green points represent downregulated genes. No significant differences are showed in black.

between clinical features and DEIRGs in the prognostic model. P value < 0.05 was considered statistically significant.

Results

DEGs, DEIRGs, DETFs and GSEA analysis

After the differential expression analysis of GSE65682, we obtained 3,648 DEGs (FDR <0.05, $|\text{Log2FC}| \geq 0.5$) (Figure 2A; Supplementary Table 2). To identify the DEIRGs, we downloaded all 2,483 immune genes from the ImmPORT database. Then, we matched IRGs with DEGs and obtained 278 DEIRGs (Figures 2B, D; Supplementary Table 3). Similarly, we searched and downloaded all 1,560 TFs from the Cistrome database. We matched TFs with DEGs and obtained 348 DETFs (Figures 2C, E; Supplementary Table 4).

In order to explore the immune response in sepsis, we downloaded the KEGG gene sets and all GO gene sets from MsigDB. Then, the changes of these pathways and functions in gene sets were analyzed, namely Healthy vs Sepsis. According to our analysis, we found that immune response played an important role in the development of sepsis. In GO gene sets, we found that adaptive immune response was significantly upregulated in sepsis. However, cell activation involved in immune response, immune effector process, and myeloid leukocyte activation were upregulated in healthy and sepsis (Figures 3A, B). In KEGG gene sets, antigen processing and presentation, natural killer cell-mediated cytotoxicity, and primary immunodeficiency were most significantly increased (Figures 3C, D). Our results showed that there is a significant correlation between sepsis and immune response, and provide a theoretical basis for the construction of immune genes model to predict the prognosis of sepsis patients.

Identification of prognostic DEIRGs and construction of regulatory network

Univariate Cox regression analysis was applied to screen and identify the prognostic genes in sepsis. According to P value <0.01, 69 prognostic DEIRGs were obtained (Figure 4A; Supplementary Table 5). Among them, 11 prognostic DEIRGs were high-risk and the others were low-risk. Then, to explore the molecular mechanisms between DETFs and prognostic DEIRGs, a regulatory network between DETFs and prognostic DEIRGs was constructed (Figure 4B; Supplementary Table 6). A total of 69 prognostic DEIRGs and 10 TFs were shown in the regulatory network (Figure 4B). As shown in the regulatory network, almost all expression level of high-risk DEIRGs (MPO, PTX3, DEFA4, CTSG, AZU1, ELANE, and RNASE3) were upregulated

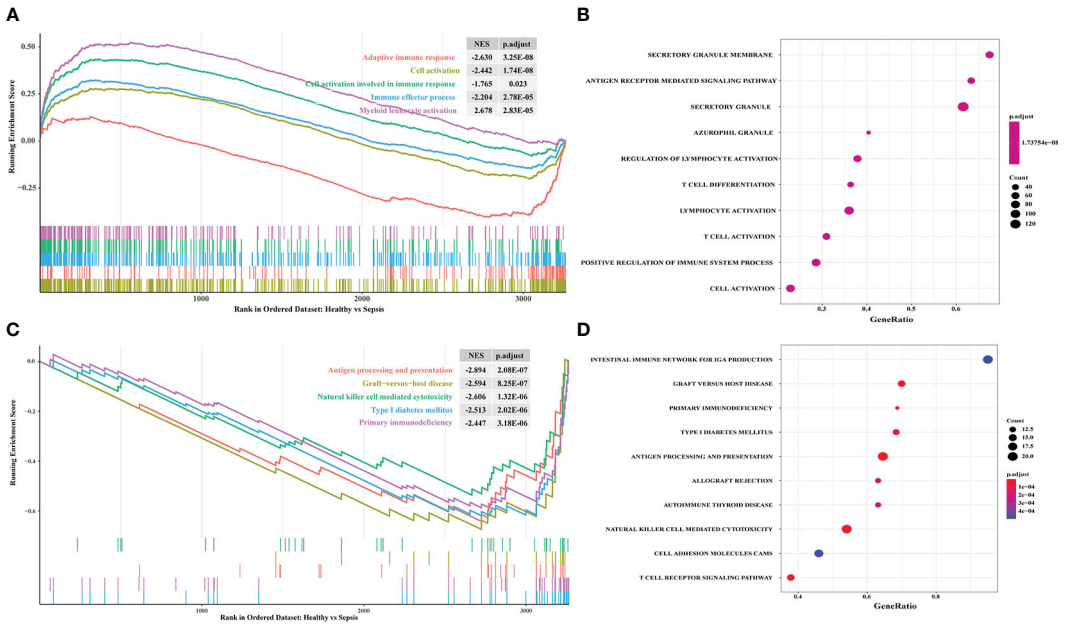

FIGURE 3
Exploring the difference of immune response between sepsis and healthy by using GSEA. **(A)** The enriched gene sets in GO collection; **(B)** The results of GO analysis from GSEA; **(C)** The enriched gene sets in KEGG collection; **(D)** The results of KEGG analysis from GSEA. The enrichment score of curve above 0 points indicates that the gene sets were activated in healthy. The curve below 0 points indicates that the gene sets were activated in sepsis. p.adjust, adjusted p-value; NES, normalized enrichment score.

by CEBPE. Additionally, IL1R2 was upregulated by BCL11B, and FURIN was regulated by KLF1, TFDP1, and MX11. Besides, most low-risk DEIRGs had a positive relationship with BCL11B, MYC, POLB, STAT1, RUNX2, and KLF10. The other low-risk DEIRGs (HCK, IL17RA, ISG20L2, and ITGAL) were negatively regulated by KLF1, TFDP1, and MX11. The coefficient filter >0.5 and the P value <0.001 were set as the threshold to indicate statistical significance.

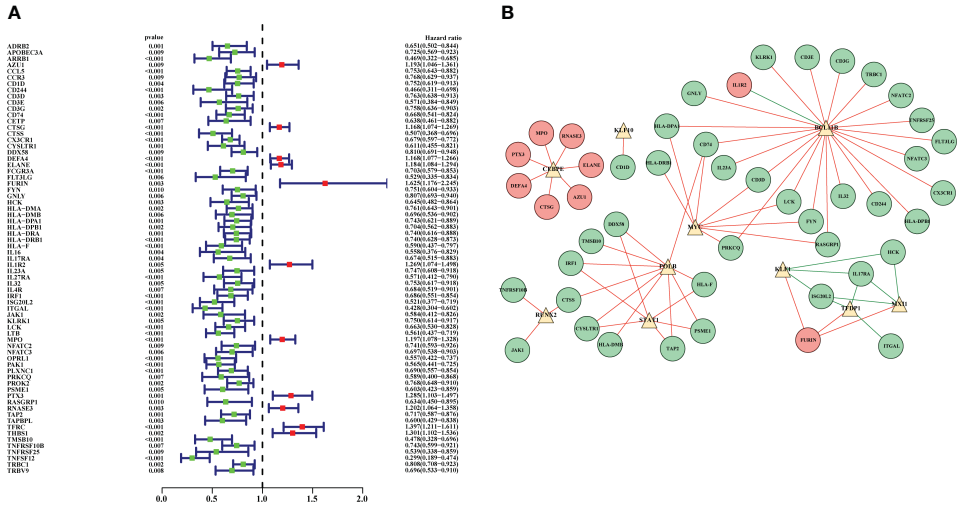

FIGURE 4
Prognostic DEIRGs and regulatory network between DETFs and prognostic DEIRGs. **(A)** Forest plot for prognostic DEIRGs in sepsis. Red and green dots were recognized as high-risk and low-risk, respectively; **(B)** Regulatory network between prognostic DEIRGs and DETFs. The red and green circles indicate high-risk DEIRGs and low-risk DEIRGs, respectively. The yellow triangles were applied to symbolize the DETFs. Moreover, the red and green lines were used to indicate a positive and negative correlation between prognostic DEIRGs and DETFs.

Construction of prognostic prediction model in sepsis

The 69 prognostic DEIRGs were obtained by univariate Cox regression analysis. Then, these prognostic DEIRGs were further incorporated into multivariate Cox regression analysis. Finally, 22 DEIRGs might serve to be the prognostic factors to independently predict the prognosis of sepsis patients (Table 2). Thus, the expression profiles of 22 DEIRGs were applied to construct the prognostic model to predict the 28-day mortality in sepsis patients. To obtain the survival risk score, the expression value and relative coefficients of 22 DEIRGs were used to calculate. The formulas was shown in Supplementary Table 7. Based on the median risk score value, 479 septic patients were classified into a high-risk group (n= 239) and a low-risk group (n=240) (Supplementary Table 7).

Then, Kaplan–Meier survival analysis was performed to analyze the 28-day mortality of high-risk groups (n= 239) and low-risk groups (n=240). As expected, the 28-day mortality of high-risk groups was significantly higher than low-risk group (Figure 5A; Supplementary Table 8). Furthermore, we drew an ROC curve to evaluate the sensitivity and specificity of the prognostic model. The results showed that the AUC value was 0.879 which symbolized that the prognostic model had a better accuracy to predict the 28-day mortality of high-risk and low-risk groups (Figure 5B). Additionally, the riskscope curve was constructed (Figure 5C) and the survival status of the two groups is shown in Figure 5D. The differential expression analysis of 22 DEIRGs are shown in Figure 5E.

Validation of prognostic model by external datasets

To further evaluate the accuracy and reliability of the prognostic model, six datasets in line with the inclusion criteria were chosen to perform external validation. ROC analysis was performed to investigate the prognostic value of the prediction model. The AUC was 0.805 in E-MTAB-4451 (Figure 6A), AUC was 0.783 in E-MTAB-5273 (Figure 6B), AUC was 0.913 in E-MTAB-5274 (Figure 6C), AUC was 0.917 in GSE95233 (Figure 6D), AUC was 0.796 in GSE106878 (Figure 6E) and AUC was 0.915 in GSE63042 (Figure 6F), respectively. Therefore, the IRGs prognostic model had an excellent prediction value.

TABLE 2 Multivariate Cox regression analyses of 22 IRGs of risk model in sepsis.

DEIRGs	coef	HR	HR.95L	HR.95H	pvalue
ADRB2	-0.693479	0.499834	0.3647514	0.6849434	1.60E-05
CD1D	-0.394755	0.6738449	0.4833991	0.9393211	0.0198413
CD74	0.7029737	2.0197499	1.102899	3.6987881	0.0227718
CETP	-1.176492	0.3083585	0.2045131	0.4649334	1.96E-08
ELANE	0.3804079	1.4628811	0.9891965	2.1633934	0.0567083
FYN	0.4151731	1.5146329	0.9758725	2.3508326	0.0641593
GNLY	-0.244232	0.7833063	0.6309512	0.9724504	0.0268901
HLA-DRA	-0.761003	0.4671977	0.2847489	0.7665478	0.0025925
IL16	1.0580916	2.8808678	1.2936444	6.4155183	0.0095908
IL17RA	-0.54816	0.5780126	0.3256761	1.0258613	0.0611051
IL1R2	0.2860863	1.3312073	1.0111484	1.7525746	0.0414519
LTB	-0.651796	0.5211092	0.3413782	0.7954661	0.0025252
MPO	-0.615383	0.540434	0.3689694	0.7915804	0.0015765
PLXNC1	-0.488971	0.613257	0.3999037	0.9404368	0.0249953
PSME1	0.7359292	2.0874208	0.9682696	4.500116	0.0604232
TAP2	-0.386602	0.6793615	0.453822	1.0169892	0.0603643
TFRC	0.1729455	1.1888014	0.9450299	1.4954539	0.1396536
THBS1	0.3465734	1.4142134	1.1220993	1.782373	0.0033265
TNFRSF10B	0.7411038	2.0982502	1.4481151	3.0402651	8.97E-05
TNFSF12	-0.898271	0.4072731	0.230409	0.7198997	0.0019965
TRBV9	-0.336649	0.7141593	0.4942263	1.0319634	0.0730621
DEFA4	0.1906303	1.210012	0.9676379	1.513096	0.0946212

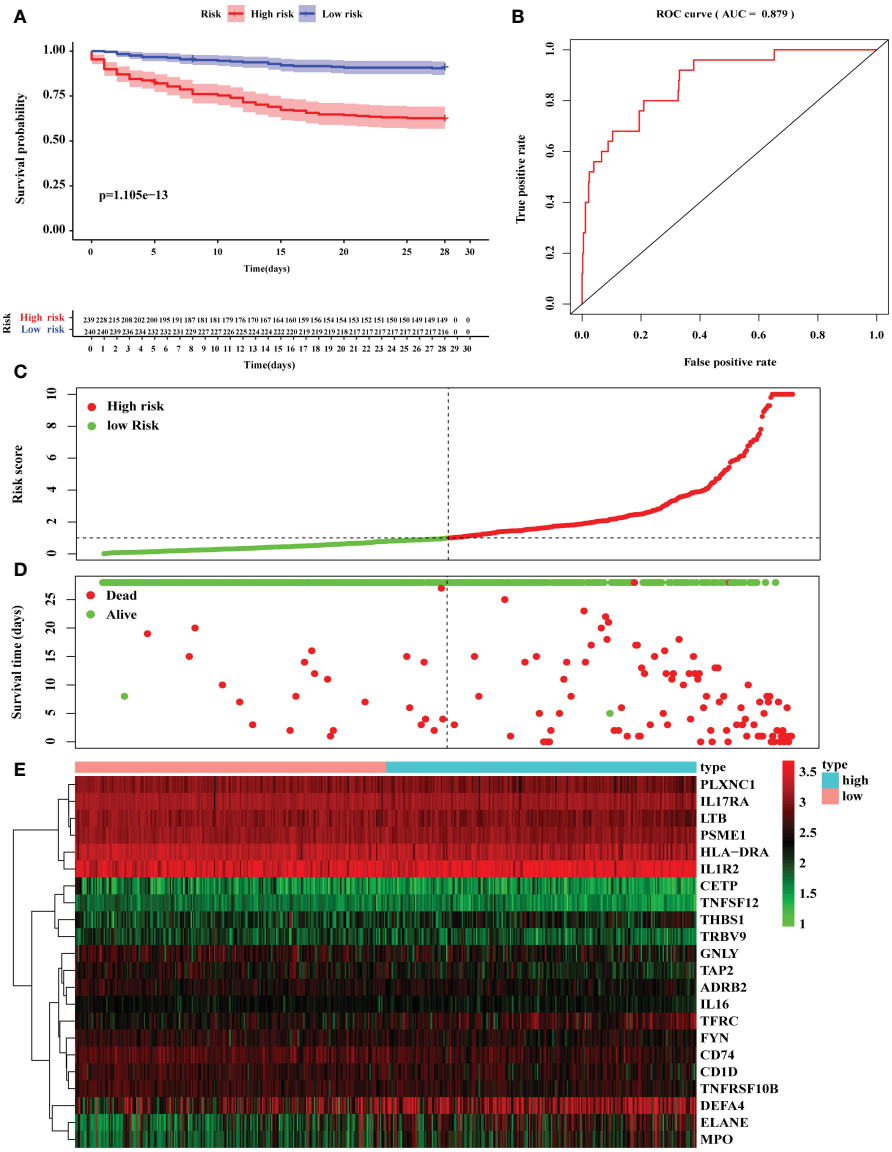

FIGURE 5
Construction of prognostic model based on 22 DEGs. **(A)** Kaplan–Meier survival analysis of 28-day mortality between high-risk groups (red) and low-risk groups (blue). The color of each survival line indicated the 95% CI of probability of survival at each time point. **(B)** The ROC curve showed the AUC value of prognostic model. **(C)** The risk score analysis between high-risk and low-risk groups. **(D)** The survival status analysis between high-risk and low-risk groups. **(E)** The differentially expression analysis of 22 DEIRGs in prognostic model from 479 sepsis patients.

Independent prognosis analysis and exploring the relationships between DEIRGs in prognostic model and clinical features in sepsis

The 22 DEIRGs in the prognostic model had a better predictive ability to investigate the 28-day mortality in sepsis. Then, we further conducted the univariate independent prognostic analysis and multivariate independent prognostic analysis to explore the correlation between clinical features and 28-day mortality in sepsis. The results of the univariate independent prognostic analysis showed that age (P = 0.019) and risk score (P <0.001) were related to the 28-day mortality, respectively (Supplementary Table 9; Figure 7A). The results of the multivariate independent prognostic analysis also showed that age (P = 0.005) and risk score (P <0.001) were the independent prognostic factors to predict the 28-day mortality in sepsis (Supplementary Table 10; Figure 7B).

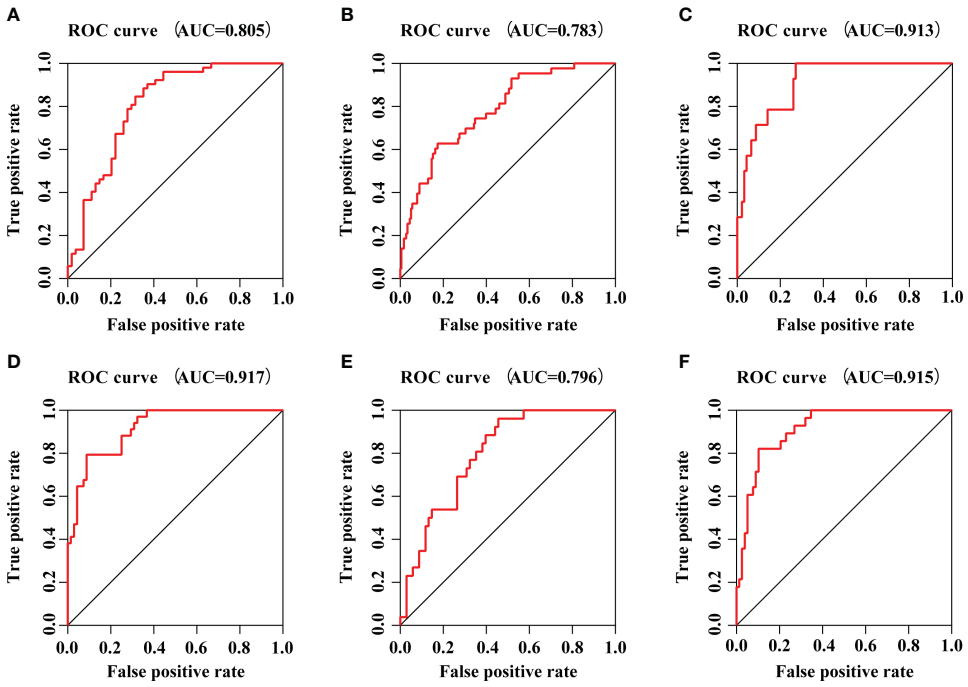

FIGURE 6
The prognostic efficacy of IRGs prognostic model. **(A)** The ROC curve of E-MTAB-4451 dataset. **(B)** The ROC curve of E-MTAB-5273 dataset. **(C)** The ROC curve of E-MTAB-5274 dataset. **(D)** The ROC curve of GSE95233 dataset. **(E)** The ROC curve of GSE106878 dataset. **(F)** The ROC curve of GSE63042 dataset.

Then, the correlation between clinical features and DEIRGs in the prognostic model was further explored (Supplementary Material 11). Among the clinical features, the endotype class was classified into four classes, including Mars1, Mars2, Mars3, and Mars4 (8). According to the research, the Mars1 endotype was characterized by a pronounced decrease in the expression of genes corresponding to key innate and adaptive immune cell functions such as Toll-like receptor, nuclear factor κB (NFκB1) signaling, antigen presentation, and T-cell receptor signaling, which might be characterized by immune paralysis. The other endotypes (Mars2-4) were characterized by high expression of genes involved in pro-inflammatory (eg, NF-κB signaling) and innate (eg, interferon signaling) immune reactions, which are characterized as pro-inflammatory and innate immune response. As shown in Figure 8, the expression level of CD1D was higher in ICU-acquired infection (ICUA). Besides, the expression levels of ADRB2, CD1D, CD74, FYN, GNLY, IL16, IL17RA, PLXNC1, PSME1, TAP2, TNFRSF10B

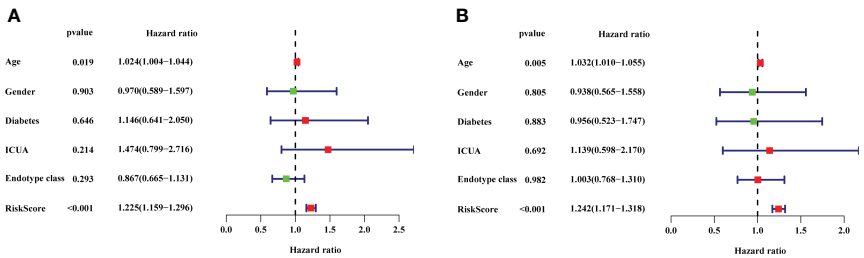

FIGURE 7
The results of univariate independent prognostic analysis and multivariate independent prognostic analysis. **(A)** Univariate independent prognostic analysis. **(B)** Multivariate independent prognostic analysis. The red dots and green dots in the forest map indicated that the clinical feature was a high-risk factor and low-risk factor, respectively. ICUA, ICU acquired infection.

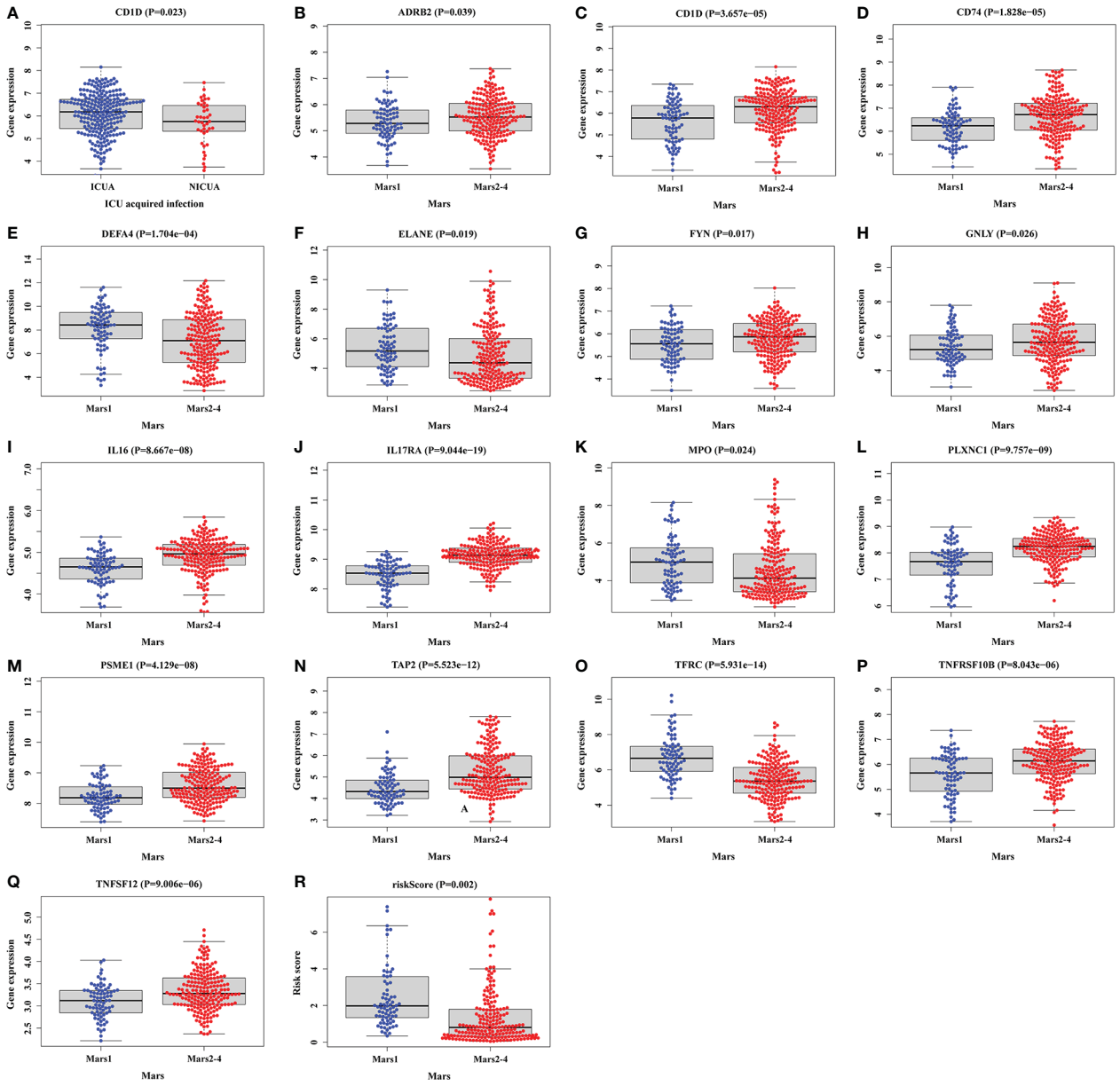

FIGURE 8
Relationships between clinical features and DEIRGs in prognostic model. **(A)** Different expression of CD1D between the ICUA/NICUA in sepsis. **(B–R)** Different expression of DEIRGs in prognostic model between Mars1 and Mars2-4 in sepsis. ICUA, ICU acquired infection; NICUA, No ICU acquired infection; Mars, molecular diagnosis and risk stratification of sepsis.

and TNFSF12 in Mars2-4 were significantly higher than Mars1. The expression levels of DEFA4, ELANE, MPO, and TFRC were significantly lower in Mars1 compared to those in Mars2-4. Therefore, DEFA4, ELANE, MPO, and TFRC might be related to immune paralysis in sepsis. Additionally, patients with Mars1 might have higher risk scores than Mars2-4 (Figure 8R) which was consistent with the results of Scicluna et al. (8).

Development of nomogram to predict the 28-day mortality in sepsis

We constructed a nomogram to predict the 28-day mortality in sepsis according to clinical features and DEIRGs in the prognostic model (Figure 9). The value of each of the variables was given a score based on the points scale axis. The total score was calculated by adding each single score. Then, the total points

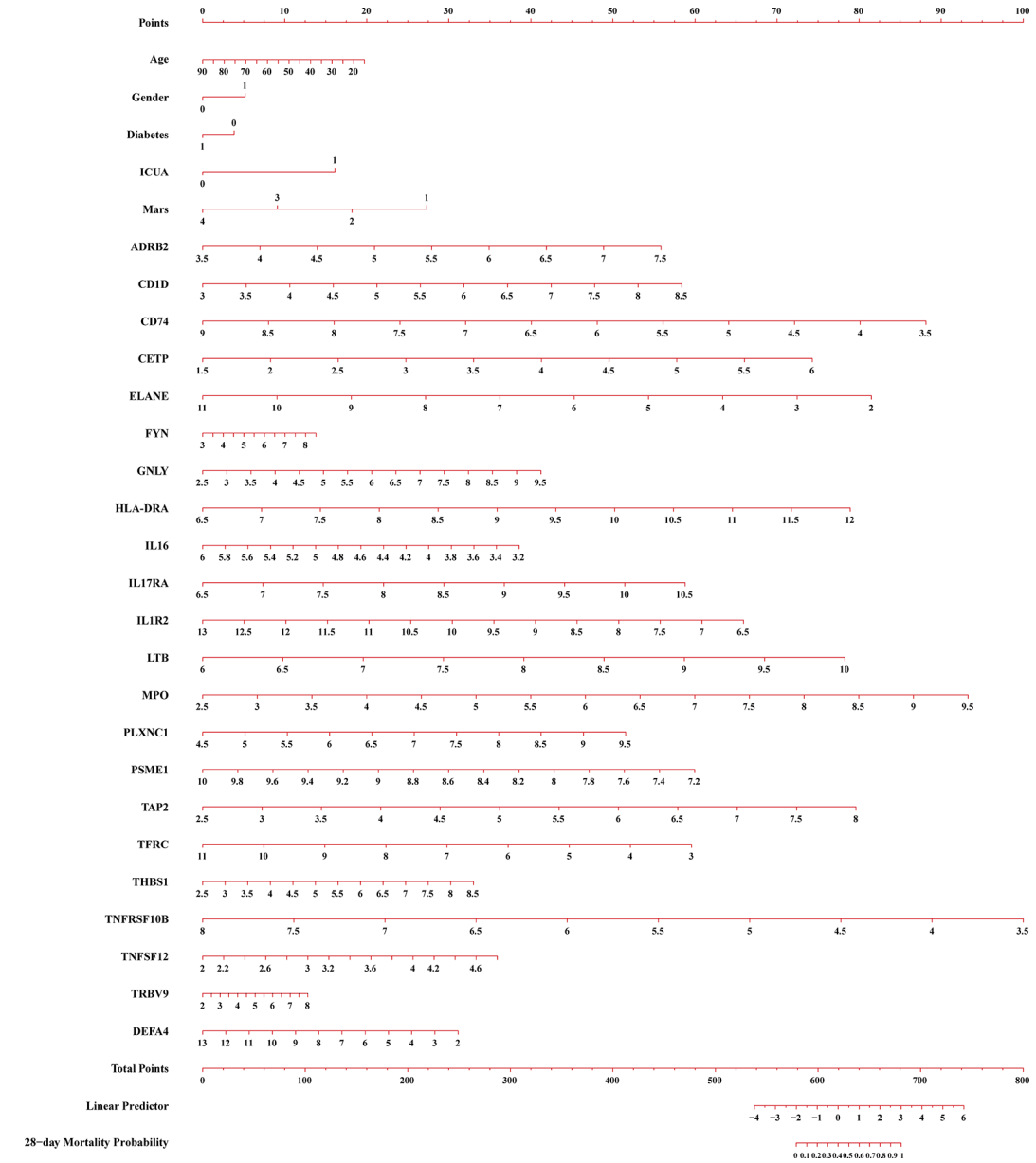

FIGURE 9
A constructed nomogram for 28-day mortality prediction of a patients with sepsis. ICUA, ICU acquired infection; Mars, molecular diagnosis and risk stratification of sepsis.

were projected to the 28-day mortality probability scale axis to estimate the probability of death in sepsis.

Functional analysis for DEIRGs in prognostic model

To explore the functional changes for DEIRGs in the prognostic model, we performed the functional enrichment analysis. The GO terms were divided into three functional groups, including biological process (BP), cell component (CC), and molecular function (MF). The top 10 significant enrichment results are shown in Figure 10. In BP groups, DEIRGs were mainly enriched in antigen processing and presentation, positive regulation of cytokine production and positive regulation of leukocyte cell–cell adhesion (Figure 10A). In CC groups, DEIRGs were mainly involved in MHC class II protein complex, MHC protein complex and

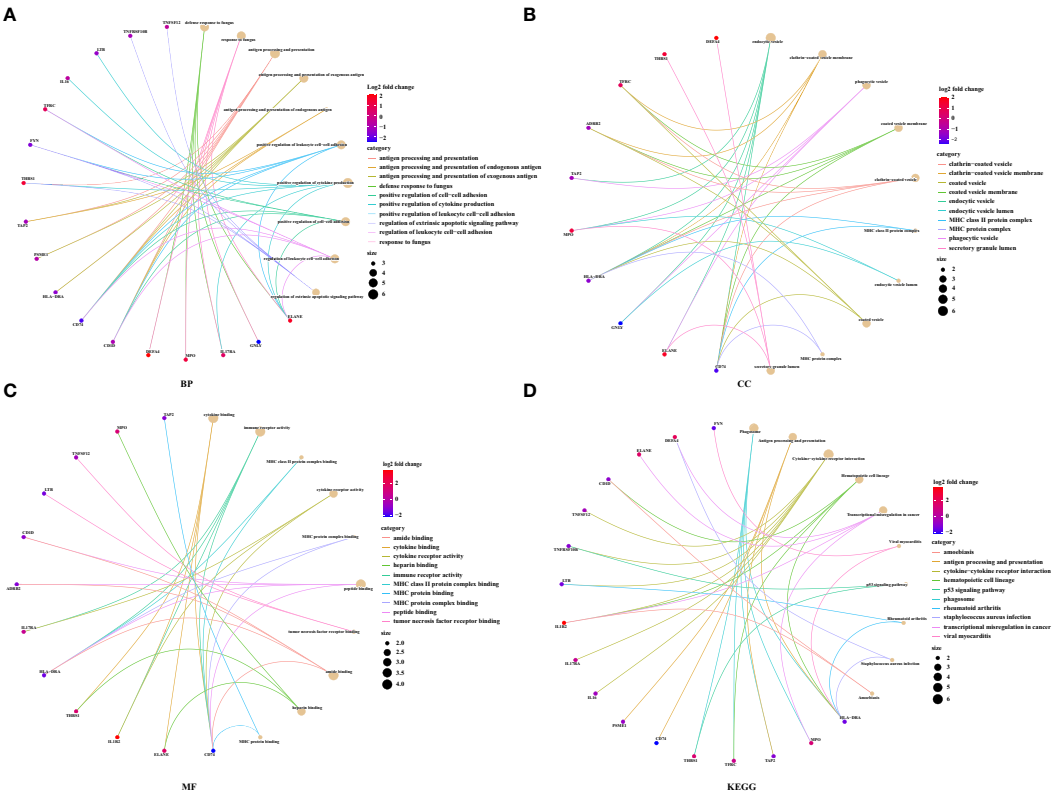

FIGURE 10
The functional enrichment analysis for DEIRGs in prognostic model. **(A)** Biological process. **(B)** Cell component. **(C)** Molecular function. **(D)** KEGG pathway enrichment analysis.

phagocytic vesicle (Figure 10B). In MF groups, DEIRGs mainly enriched in cytokine binding, cytokine receptor activity and immune receptor activity (Figure 10C). As for the KEGG analysis, DEIRGs were mainly involved in antigen processing and presentation, cytokine–cytokine receptor interaction and hematopoietic cell lineage (Figure 10D).

Correlation analysis between DEIRGs and circulating immune cells

Numerous studies had demonstrated that circulating immune cells levels were associated with the prognosis of patients (15, 16). Therefore, we wanted to explore the different status of circulating immune cells between low-risk and high-risk groups. As shown in Supplementary Figure 1, the status of immune cells was significantly different in low-risk groups compared to the high-risk groups. Then, we further analyzed the composition of immune cells between low-risk and high-risk groups. The results of CIBERSORTx demonstrated that compared to the high-risk groups, CD8+ T cells (P=0.0135), resting (P=0.0005), and activated NK cells (P<0.0001), monocytes (P<0.0001), and M1 macrophages (P<0.0001) were more abundant in low-risk groups, while naive CD4+ T cells (P=0.0257), follicular helper T cells (P=0.0489) and activated dendritic cells (P<0.0001) were significantly enriched in high-risk groups (Figure 11A). Besides, we also analyzed the correlation of risk score and 22 immune cell types *via* Spearman correlation analyses. The results showed that risk scores were significantly positively correlated with follicular helper T cells (P=0.0437), gamma delta T cells (P=0.0004), resting NK cells (P=0.0259), activated dendritic cells (P<0.0001), and activated mast cells (P<0.0001), whereas were significantly negatively correlated with naive CD4+ T cells (P=0.019), activated NK cells (P=0.0045), monocytes (P=0.0134) and M1 macrophages (P=0.0002).

Discussion

Sepsis, with high heterogeneity, is characterized by aberrant immune responses, including hyperinflammation and immune suppression (17). Increasingly, studies have pointed out that

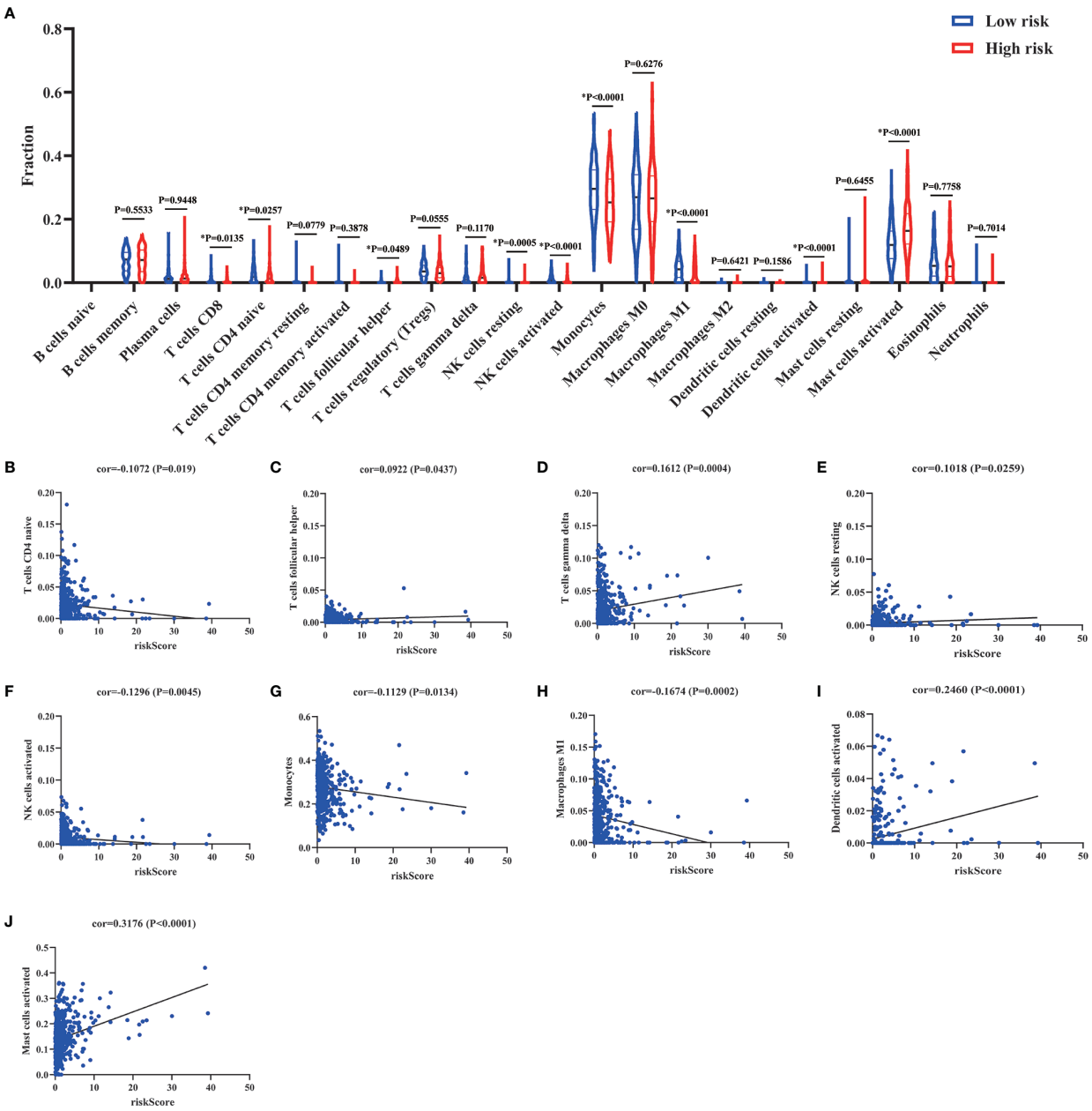

FIGURE 11
Comparison and correlation of circulating immune cells between low-risk and high-risk groups. **(A)** Comparison of circulating immune cells between low-risk and high-risk groups *via* CIBERSORTx. **(B–J)** Correlation between risk scores and circulating immune cells *via* Spearman correlation analysis. *p < 0.05.

IRGs are promising novel biomarkers that may have important predictive and prognostic value (8, 18, 19). Thus, our research demonstrates that immune response played an important role in the development of sepsis. Then, the Cox prediction model obtained the 22 DEIRGs to classify the patients into low-risk and high-risk groups and construct the prognostic model. The regulatory network between TFs and prognostic DEIRGs was constructed to reveal the potential novel molecular mechanisms in sepsis. In this study, the prognostic model had a better accuracy to predict the 28-day mortality in sepsis. The external datasets also validated that the prognostic model had an excellent prediction value. Besides, we further developed a nomogram to provide a tool for predicting the probability of 28-day mortality in sepsis. We further explore the functional changes *via* functional enrichment analysis. Finally, the circulating immune cells were evaluated by CIBERSORTx.

As we know, the biomarkers to diagnose and predict the prognosis of sepsis were lacking due to the complex pathogenesis and high heterogeneity in sepsis. The unbalanced immune response of sepsis was initially activated to release tremendous damage-associated molecular patterns (DAMPs) such as cytokines. The cytokine storm will further lead to organ damage and even death (20). However, longitudinal analyses of immune response showed that patients developed persistent inflammation and immunosuppression in the late stage of sepsis (21). Therefore, the aberrant immune responses during sepsis might reflect the disease progression. The results of GSEA in this study also showed that immune responses were significantly related to the development of sepsis (Figure 3).

IRGs, promising novel biomarkers, had been used to predict the prognosis in many diseases (22). Even in sepsis, Lu et al. demonstrated the immune genes exhibited superior diagnostic and predictive efficacy in mortality than clinical characteristics (18). However, the molecular mechanisms of prognostic DEIRGs in sepsis were still unclear. In our study, we have identified 11 prognostic DEIRGs with high risk and 58 prognostic DEIRGs with low risk *via* univariate Cox regression analysis (Figure 4A). TFs, as an enhancer or promoter, could regulate the genes' expression by binding to a particular DNA region. The regulatory network was constructed between TFs and prognostic DEIRGs (Figure 4B). We found key TFs (CEBPE, BCL11B, MYC, POLB, and STAT1) which had the most downstream DEIRGs and relatively high correlation coefficients. CEBPE has been demonstrated to be involved in the generation and proliferation of neutrophils (23). Besides, CEBPE was an important target to promote the innate immune system (e.g. neutrophil) to kill the bacteria (24). In this study, almost high-risk DEIRGs (MPO, PTX3, DEFA4, CTSG, AZU1, ELANE, and RNASE3) were upregulated by CEBPE which indicated that these high-risk DEIRGs might promote the inflammation and innate immune responses. Additionally, the BCL11B gene was essential for T cell and NK cell development and function (25). MYC, POLB, and STAT1 have also been described as having a strong relationship to the functions of the immune system and the clearance of pathogens (26–28). Therefore, most low-risk DEIRGs had a positive relationship with BCL11B, MYC, POLB and STAT1 might have an important role in regulating immune responses and defending against pathogens.

To construct the prognostic model, we further conducted the multivariate Cox regression analysis to identify the prognostic DEIRGs (Table 2). Then, the prognostic model could predict the 28-day mortality in sepsis with better accuracy (Figures 5B, 6). Among them, we obtained 4 high-risk genes (ELANE, IL1R2, MPO, and DEFA4) and 18 low-risk genes. ELANE and MPO had been demonstrated to involve in neutrophil protease activity. The expression levels of ELANE and MPO were correlated directly with organ failure and mortality which was in line with our results (29, 30). Besides, IL1R2, a decoy receptor for IL-1, has been implicated in sepsis (31). Previous studies have proven that IL1R2 was a biomarker to distinguish septic shock from non-septic shock postsurgical patients. The high expression of IL1R2 was significantly correlated to death in patients with postsurgical shock (32, 33). Interestingly, Liang et al. (34) pointed out that IL1R2 could distinguish gram-negative/gram-positive bacterial infection. The elevation of serum IL1R2 could be a biomarker to diagnose septic patients infected by gram-negative bacteria.

As we know, numerous studies have provided prognostic models/biomarkers for predicting overall survival in sepsis. However, these predictive factors were not applied to all sepsis patients due to the high heterogeneity. Thus, it is critical to stratify patients to guide treatments. A VANISH randomized trial categorized patients into SRS (sepsis response signatures) 1 and SRS2 according to transcriptomic profile. Patients with the immunocompetent SRS2 endotype might have significantly higher mortality when treated with corticosteroids than with placebo (35). Additionally, Scicluna et al. (8) classified patients with sepsis into four different endotypes (Mars1, Mars2, Mars3 and Mars4) upon ICU admission. According to the research, Mars1, with TAP2 transcripts denoting, was characterized by immune paralysis and poor prognosis, whereas Mars2-4 were characterized by high expression of pro-inflammatory genes. Our research also demonstrated that TAP2 was significantly downregulated in Mars1 compared to Mars2-4 (Figure 8N). TAP2 was a subunit of major histocompatibility complex class I (MHC-I) molecules involved in antigen processing (36). TAP2 has the potential to inhibit lipopolysaccharide-induced proinflammation by negative regulation of toll-like receptor-4 (TLR4) (37). Besides, our research also showed that most sepsis patients with high risk might have the Mars1 endotype which indicated the poor prognosis of patients with the Mars1 endotype (Figure 8R). This result was also in line with the previous study. Therefore, patients with sepsis in immunosuppression might be associated with an increased risk of mortality.

As we know, patients who survive early sepsis often develop a hypoinflammatory state and nosocomial infections which lead to high mortality (7, 17). Immune suppression in patients with sepsis is characterized by enhanced apoptosis of immune cells, T cell exhaustion, and reduced expression of activating cell surface molecules. Previous studies have proven that T cell exhaustion in immunosuppression was related to poor outcomes (38). The apoptosis of T cells (CD4+, CD8+, and Th17) will result in immunosuppression and is associated with higher mortality (39). Besides, nature killer (NK) cells could clear the pathogens and promote inflammation through the production of IFN-γ. However, NK cells will become tolerant and cytokine production

of IFN-γ and TNF-α will be impaired in the late stage of sepsis. The proportion of NK cells in lymphocytes was negatively associated with 28-day mortality in septic patients (40, 41). Monocytes and macrophages are important components of the immune system that can remove pathogens and contribute to the immune response by antigen presentation. The M1 macrophages were characterized by the production of proinflammatory cytokines and antimicrobial activity. However, the polarization of M1 macrophages will be inhibited in immunosuppression. The M1 macrophage reprogramming will develop a pathological anti-inflammatory response to sepsis and increase the risk of immunosuppression (42, 43). In our research, CD8+ T cells (P=0.0135), resting (P=0.0005) and activated NK cells (P<0.0001), monocytes (P<0.0001), and M1 macrophages (P<0.0001) were more abundant in low-risk groups which indicated a hyperinflammatory state in low-risk groups (Figure 11A). Besides, the results of correlation analyses also showed that risk scores were significantly negatively correlated with naive CD4+ T cells (P=0.019), activated NK cells (P=0.0045), monocytes (P=0.0134), and M1 macrophages (P=0.0002) (Figure 11). In toto, the patients with high risk scores might be associated with immunosuppression. The risk score was positively associated with the development of immunosuppression in sepsis. The risk score might provide assistance for distinguishing sepsis patients with immunosuppression.

However, in spite of the remarkable results, there are several limitations that we could not ignore. First, a lot of publicly available sepsis datasets were excluded for lacking the mortality outcome. These datasets might concentrate on the differential diagnosis or other poor outcomes. The exclusion of these datasets might cause potential selection bias. Second, our prognostic model had a better performance in distinguishing patients with high risk, evaluating 28-day mortality in sepsis, and identifying sepsis patients with immunosuppression. However, it still needs large prospective cohorts to validate the performance before the prognostic model was applied to general use. Third, the datasets we included did not provide the details of comorbidities or other diseases. Therefore, we can't exclude the impact of these factors on the prognostic model. Fourth, it may not accurately identify the immune cell types in sepsis according to bulk RNA-Seq data and the CIBERSORTx deconvolution algorithm. It still required further experiments (e.g. Flow Cytometry) to validate the results. Finally, the *vivo* and *vitro* experiments may help us identify the hub genes to predict the prognosis of sepsis and identify the patients with immunosuppression.

Conclusion

Our study demonstrated that immune response played an important role in the development of sepsis. IRGs, as promising novel biomarkers, were used to construct the TFs-DEIRGs regulatory network and prognostic prediction model, respectively. The TF-DEIRGs regulatory network has revealed the potential molecular mechanisms for DEIRGs in sepsis. The prognostic model, with great performance, could identify the patients with high risk and predict the 28-day mortality in patients with sepsis. Besides, the prognostic DEIRGs were also related to the immune cell circulating and immunosuppression state, which might promote individualized therapy for sepsis patients.

Data availability statement

The datasets presented in this study can be found in online repositories. The names of the repository/repositories and accession number(s) can be found in the article/Supplementary Material.

Author contributions

YoZ and YH analysed and interpreted the data. YoZ, YuZ, YC and BL performed the bioinformatics analyses. XD, YX and LS performed data acquisition and figure preparations. YoZ and YH wrote the manuscript. XL and YL revised and edited this paper. All authors contributed to the article and approved the submitted version.

Funding

This work was supported by the National Natural Science Foundation of China (81870069, 81970071, 82070084, 82270085), the Natural Science Foundation of Guangdong Province (2020A1515011459, 2021A1515012565), the Science and Technology Program of Guangzhou (202102010366, 202201020444), the State Key Laboratory of Respiratory Disease Independent Program (SKLRD-Z-202108), Guangdong Marine Economy Development Special Project (GDNRC[2022]35).

Conflict of interest

The authors declare that the research was conducted in the absence of any commercial or financial relationships that could be construed as a potential conflict of interest.

Publisher's note

All claims expressed in this article are solely those of the authors and do not necessarily represent those of their affiliated

organizations, or those of the publisher, the editors and the reviewers. Any product that may be evaluated in this article, or claim that may be made by its manufacturer, is not guaranteed or endorsed by the publisher.

Supplementary material

The Supplementary Material for this article can be found online at: https://www.frontiersin.org/articles/10.3389/fimmu.2022.994295/full#supplementary-material

SUPPLEMENTARY TABLE 1
The clinic features of GSE65682.

SUPPLEMENTARY TABLE 2
The differential expression analysis of GSE65682.

SUPPLEMENTARY TABLE 3
The differential expression analysis of IRGs.

SUPPLEMENTARY TABLE 4
The differential expression analysis of TFs.

SUPPLEMENTARY FIGURE 1
The status of circulating immune cells between low-risk and high-risk groups.

References

1. Singer M, Deutschman CS, Seymour CW, Shankar-Hari M, Annane D, Bauer M, et al. The third international consensus definitions for sepsis and septic shock (Sepsis-3). *JAMA* (2016) 315(8):801–10. doi: 10.1001/jama.2016.0287

2. Rudd KE, Johnson SC, Agesa KM, Shackelford KA, Tsoi D, Kievlan DR, et al. Global, regional, and national sepsis incidence and mortality, 1990-2017: analysis for the global burden of disease study. *Lancet* (2020) 395(10219):200–11. doi: 10.1016/S0140-6736(19)32989-7

3. Kumar A, Roberts D, Wood KE, Light B, Parrillo JE, Sharma S, et al. Duration of hypotension before initiation of effective antimicrobial therapy is the critical determinant of survival in human septic shock. *Crit Care Med* (2006) 34(6):1589–96. doi: 10.1097/01.CCM.0000217961.75225.E9

4. Ferrer R, Martin-Loeches I, Phillips G, Osborn TM, Townsend S, Dellinger RP, et al. Empiric antibiotic treatment reduces mortality in severe sepsis and septic shock from the first hour: results from a guideline-based performance improvement program. *Crit Care Med* (2014) 42(8):1749–55. doi: 10.1097/CCM.0000000000000330

5. World Health Organization. *World health assembly 70, resolution 70.7: improving the prevention, diagnosis and clinical management of sepsis* (2017). Available at: http://apps.who.int/gb/ebwha/pdf_files/WHA70/A70_R7-en.pdf.

6. van der Poll T, van de Veerdonk FL, Scicluna BP, Netea MG. The immunopathology of sepsis and potential therapeutic targets. *Nat Rev Immunol* (2017) 17(7):407–20. doi: 10.1038/nri.2017.36

7. Cecconi M, Evans L, Levy M, Rhodes A. Sepsis and septic shock. *Lancet* (2018) 392(10141):75–87. doi: 10.1016/S0140-6736(18)30696-2

8. Scicluna BP, van Vught LA, Zwinderman AH, Wiewel MA, Davenport EE, Burnham KL, et al. Classification of patients with sepsis according to blood genomic endotype: a prospective cohort study. *Lancet Respir Med* (2017) 5 (10):816–26. doi: 10.1016/S2213-2600(17)30294-1

9. Li B, Cui Y, Diehn M, Li R. Development and validation of an individualized immune prognostic signature in early-stage nonsquamous non-small cell lung cancer. *JAMA Oncol* (2017) 3(11):1529–37. doi: 10.1001/jamaoncol.2017.1609

10. Pages F, Mlecnik B, Marliot F, Bindea G, Ou FS, Bifulco C, et al. International validation of the consensus immunoscore for the classification of colon cancer: a prognostic and accuracy study. *Lancet* (2018) 391(10135):2128–39. doi: 10.1016/S0140-6736(18)30789-X

11. Ritchie ME, Phipson B, Wu D, Hu Y, Law CW, Shi W, et al. Limma powers differential expression analyses for RNA-sequencing and microarray studies. *Nucleic Acids Res* (2015) 43(7):e47. doi: 10.1093/nar/gkv007

12. Eraso-Pichot A, Braso-Vives M, Golbano A, Menacho C, Claro E, Galea E, et al. GSEA of mouse and human mitochondriomes reveals fatty acid oxidation in astrocytes. *Glia* (2018) 66(8):1724–35. doi: 10.1002/glia.23330

13. Subramanian A, Tamayo P, Mootha VK, Mukherjee S, Ebert BL, Gillette MA, et al. Gene set enrichment analysis: A knowledge-based approach for interpreting genome-wide expression profiles. *Proc Natl Acad Sci U.S.A.* (2005) 102(43):15545–50. doi: 10.1073/pnas.0506580102

14. Newman AM, Liu CL, Green MR, Gentles AJ, Feng W, Xu Y, et al. Robust enumeration of cell subsets from tissue expression profiles. *Nat Methods* (2015) 12 (5):453–7. doi: 10.1038/nmeth.3337

15. Yang S, Liu T, Nan H, Wang Y, Chen H, Zhang X, et al. Comprehensive analysis of prognostic immune-related genes in the tumor microenvironment of cutaneous melanoma. *J Cell Physiol* (2020) 235(2):1025–35. doi: 10.1002/jcp.29018

16. Song Q, Shang J, Yang Z, Zhang L, Zhang C, Chen J, et al. Identification of an immune signature predicting prognosis risk of patients in lung adenocarcinoma. *J Transl Med* (2019) 17(1):70. doi: 10.1186/s12967-019-1824-4

17. van der Poll T, Shankar-Hari M, Wiersinga WJ. The immunology of sepsis. *Immunity* (2021) 54(11):2450–64. doi: 10.1016/j.immuni.2021.10.012

18. Lu J, Chen R, Ou Y, Jiang Q, Wang L, Liu G, et al. Characterization of immune-related genes andimmune infiltration features for early diagnosis, prognosis and recognition of immunosuppression in sepsis. *Int Immunopharmacol* (2022) 107:108650. doi: 10.1016/j.intimp.2022.108650

19. Liu S, Li Y, She F, Zhao X, Yao Y. Predictive value of immune cell counts and neutrophil-to-lymphocyte ratio for 28-day mortality in patients with sepsis caused by intra-abdominal infection. *Burns Trauma* (2021) 9:tkaa040. doi: 10.1093/burnst/tkaa040

20. Wiersinga WJ, Leopold SJ, Cranendonk DR, van der Poll T. Host innate immune responses to sepsis. *Virulence* (2014) 5(1):36–44. doi: 10.4161/viru.25436

21. Darden DB, Kelly LS, Fenner BP, Moldawer LL, Mohr AM, Efron PA. Dysregulated immunity and immunotherapy after sepsis. *J Clin Med* (2021) 10 (8):1742. doi: 10.3390/jcm10081742

22. Li J, Liu C, Chen Y, Gao C, Wang M, Ma X, et al. Tumor characterization in breast cancer identifies immune-relevant gene signatures associated with prognosis. *Front Genet* (2019) 10:1119. doi: 10.3389/fgene.2019.01119

23. Evrard M, Kwok IWH, Chong SZ, Teng KWW, Becht E, Chen J, et al. Developmental analysis of bone marrow neutrophils reveals populations specialized in expansion, trafficking, and effector functions. *Immunity* (2018) 48 (2):364–379 e368. doi: 10.1016/j.immuni.2018.02.002

24. Kyme P, Thoennissen NH, Tseng CW, Thoennissen GB, Wolf AJ, Shimada K, et al. C/EBPepsilon mediates nicotinamide-enhanced clearance of staphylococcus aureus in mice. *J Clin Invest* (2012) 122(9):3316–29. doi: 10.1172/JCI62070

25. Holmes TD, Pandey RV, Helm EY, Schlums H, Han H, Campbell TM, et al. The transcription factor Bcl11b promotes both canonical and adaptive NK cell differentiation. *Sci Immunol* (2021) 6(57):eabc9801. doi: 10.1126/sciimmunol.abc9801

26. Xu H, Jiang Y, Xu X, Su X, Liu Y, Ma Y, et al. Inducible degradation of lncRNA Sros1 promotes IFN-gamma-mediated activation of innate immune responses by stabilizing Stat1 mRNA. *Nat Immunol* (2019) 20(12):1621–30. doi: 10.1038/s41590-019-0542-7

27. Wang S, Liu R, Yu Q, Dong L, Bi Y, Liu G. Metabolic reprogramming of macrophages during infections and cancer. *Cancer Lett* (2019) 452:14–22. doi: 10.1016/j.canlet.2019.03.015

28. Alshalchi SA, Anderson GG. Involvement of stress-related genes polB and PA14_46880 in biofilm formation of pseudomonas aeruginosa. *Infect Immun* (2014) 82(11):4746–57. doi: 10.1128/IAI.01915-14

29. Guirgis FW, Leeuwenburgh C, Moldawer L, Ghita G, Black LP, Henson M, et al. Lipid and lipoprotein predictors of functional outcomes and long-term mortality after surgical sepsis. *Ann Intensive Care* (2021) 11(1):82. doi: 10.1186/s13613-021-00865-x

30. Almansa R, Heredia-Rodriguez M, Gomez-Sanchez E, Andaluz-Ojeda D, Iglesias V, Rico L, et al. Transcriptomic correlates of organ failure extent in sepsis. *J infection* (2015) 70(5):445–56. doi: 10.1016/j.jinf.2014.12.010

31. Peters VA, Joesting JJ, Freund GG. IL-1 receptor 2 (IL-1R2) and its role in immune regulation. *Brain Behav Immun* (2013) 32:1–8. doi: 10.1016/j.bbi.2012.11.006

32. Martinez-Paz P, Aragon-Camino M, Gomez-Sanchez E, Lorenzo-Lopez M, Gomez-Pesquera E, Fadrique-Fuentes A, et al. Distinguishing septic shock from non-septic shock in postsurgical patients using gene expression. *J infection* (2021) 83(2):147–55. doi: 10.1016/j.jinf.2021.05.039

33. Martinez-Paz P, Aragon-Camino M, Gomez-Sanchez E, Lorenzo-Lopez M, Gomez-Pesquera E, Lopez-Herrero R, et al. Gene expression patterns distinguish mortality risk in patients with postsurgical shock. *J Clin Med* (2020) 9(5):1276. doi: 10.3390/jcm9051276

34. Lang Y, Jiang Y, Gao M, Wang W, Wang N, Wang K, et al. Interleukin-1 receptor 2: A new biomarker for sepsis diagnosis and gram-Negative/Gram-Positive bacterial differentiation. *Shock* (2017) 47(1):119–24. doi: 10.1097/SHK.0000000000000714

35. Antcliffe DB, Burnham KL, Al-Beidh F, Santhakumaran S, Brett SJ, Hinds CJ, et al. Transcriptomic signatures in sepsis and a differential response to steroids. from the VANISH randomized trial. *Am J Respir Crit Care Med* (2019) 199(8):980–6. doi: 10.1164/rccm.201807-1419OC

36. Blees A, Januliene D, Hofmann T, Koller N, Schmidt C, Trowitzsch S, et al. Structure of the human MHC-I peptide-loading complex. *Nature* (2017) 551 (7681):525–8. doi: 10.1038/nature24627

37. Park S, Shin HJ, Shah M, Cho HY, Anwar MA, Achek A, et al. TLR4/MD2 specific peptides stalled *in vivo* LPS-induced immune exacerbation. *Biomaterials* (2017) 126:49–60. doi: 10.1016/j.biomaterials.2017.02.023

38. Le Tulzo Y, Pangault C, Gacouin A, Guilloux V, Tribut O, Amiot L, et al. Early circulating lymphocyte apoptosis in human septic shock is associated with poor outcome. *Shock* (2002) 18(6):487–94. doi: 10.1097/00024382-200212000-00001

39. Wu HP, Chung K, Lin CY, Jiang BY, Chuang DY, Liu YC. Associations of T helper 1, 2, 17 and regulatory T lymphocytes with mortality in severe sepsis. *Inflammation Res* (2013) 62(8):751–63. doi: 10.1007/s00011-013-0630-3

40. Feng T, Liao X, Yang X, Yang C, Lin F, Guo Y, et al. A shift toward inhibitory receptors and impaired effector functions on NK cells contribute to immunosuppression during sepsis. *J Leukoc Biol* (2020) 107(1):57–67. doi: 10.1002/JLB.4A0818-313RR

41. Souza-Fonseca-Guimaraes F, Parlato M, Fitting C, Cavaillon JM, Adib-Conquy M. NK cell tolerance to TLR agonists mediated by regulatory T cells after polymicrobial sepsis. *J Immunol* (2012) 188(12):5850–8. doi: 10.4049/jimmunol.1103616

42. Essandoh K, Li Y, Huo J, Fan GC. MiRNA-mediated macrophage polarization and its potential role in the regulation of inflammatory response. *Shock* (2016) 46(2):122–31. doi: 10.1097/SHK.0000000000000604

43. Rackov G, Hernandez-Jimenez E, Shokri R, Carmona-Rodriguez L, Manes S, Alvarez-Mon M, et al. p21 mediates macrophage reprogramming through regulation of p50-p50 NF-kappaB and IFN-beta. *J Clin Invest* (2016) 126 (8):3089–103. doi: 10.1172/JCI83404

frontiers | Frontiers in Immunology

TYPE Correction
PUBLISHED 06 March 2023
DOI 10.3389/fimmu.2023.1146121

Check for updates

OPEN ACCESS

EDITED AND REVIEWED BY
Pietro Ghezzi,
University of Urbino Carlo Bo, Italy

*CORRESPONDENCE
Yimin Li
dryiminli@vip.163.com

†These authors have contributed equally to this work

SPECIALTY SECTION
This article was submitted to Inflammation, a section of the journal Frontiers in Immunology

RECEIVED 17 January 2023
ACCEPTED 13 February 2023
PUBLISHED 06 March 2023

CITATION
Zheng Y, Liu B, Deng X, Chen Y, Huang Y, Zhang Y, Xu Y, Sang L, Liu X and Li Y (2023) Corrigendum: Construction and validation of a robust prognostic model based on immune features in sepsis. *Front. Immunol.* 14:1146121. doi: 10.3389/fimmu.2023.1146121

COPYRIGHT
© 2023 Zheng, Liu, Deng, Chen, Huang, Zhang, Xu, Sang, Liu and Li. This is an open-access article distributed under the terms of the Creative Commons Attribution License (CC BY). The use, distribution or reproduction in other forums is permitted, provided the original author(s) and the copyright owner(s) are credited and that the original publication in this journal is cited, in accordance with accepted academic practice. No use, distribution or reproduction is permitted which does not comply with these terms.

Corrigendum: Construction and validation of a robust prognostic model based on immune features in sepsis

Yongxin Zheng[1,2†], Baiyun Liu[1,2†], Xiumei Deng[1,2†], Yubiao Chen[1,2†], Yongbo Huang[1,2], Yu Zhang[1,2], Yonghao Xu[1,2], Ling Sang[1,2], Xiaoqing Liu[1,2] and Yimin Li[1,2*]

[1]State Key Laboratory of Respiratory Diseases, National Clinical Research Center for Respiratory Disease, Guangzhou Institute of Respiratory Health, Department of Critical Care Medicine, The First Affiliated Hospital of Guangzhou Medical University, Guangzhou, China, [2]The First Affiliated Hospital, Guangzhou Medical University, Guangzhou, China

KEYWORDS

sepsis, immune, prognostic model, 28-day mortality, immunosuppression

A Corrigendum on:

Construction and validation of a robust prognostic model based on immune features in sepsis.

By Zheng Y, Liu B, Deng X, Chen Y, Huang Y, Zhang Y, Xu Y, Sang L, Liu X and Li Y (2022) *Front. Immunol.* 13:994295. doi: 10.3389/fimmu.2022.994295

In the published article, there was an error. The 'pheatmap' R package should be corrected to 'ggplot2' R package; false discovery rate (FDR) should be corrected to P-value.

A correction has been made to **Materials and Methods, Differential expression analysis in sepsis.** This sentence previously stated:

"All the genes in GSE65682 were differentially analyzed by using limma R packages (http://www.bioconductor.org/packages/release/bioc/html/limma.html) (11). The parameter for DEGs screened was |Log2Foldchange| ≥0.5 and false discovery rate (FDR) < 0.05. The Volcano plots were drawn by 'pheatmap' R package. Then, the IRGs that were overlapping with DEGs were identified as DEIRGs. Similarly, DETFs were obtained by matching TFs with DEGs."

The corrected sentence appears below:

"All the genes in GSE65682 were differentially analyzed by using limma R packages (http://www.bioconductor.org/packages/release/bioc/html/limma.html) (11). The parameter for DEGs screened was |Log2Foldchange| ≥0.5 and P-value <0.05. The Volcano plots were drawn by 'ggplot2' R package. Then, the IRGs that were overlapping with DEGs were identified as DEIRGs. Similarly, DETFs were obtained by matching TFs with DEGs."

In the published article, there was an error. The 'survival R' package should be corrected to 'survival' R package.

A further correction has been made to **Materials and Methods, Construction of the prognostic prediction model in sepsis and development of nomogram**, paragraph 1. This section previously stated:

TABLE 1 Basic information of the datasets included in this study.

Accession	Study population	Sample type	Country	Timing of gene expression profiling	Mortality/Total patients
GSE65682	Patient diagnoses sepsis due to cap, hap and non-infectious control.	Blood	Netherlands and England	On ICU admission	114/802
GSE63042	Patients with SIRS or sepsis	Blood	America	The day of enrollment upon presentation to the ED.	28/129
GSE95233	Patients with septic shock and healthy volunteers	Blood	France	Day 1 of ICU admission	34/124
GSE106878	septic shock patients from the CORTICUS-trial	Circulating leukocytes	International	Before hydrocortisone application	26/94
E-MTAB-4451	Patients with severe sepsis due to CAP	Circulating leukocytes	England	On ICU admission	52/106
E-MTAB-5273	Patients with sepsis due to CAP or faecal peritonitis.	Circulating leukocytes	England	First day of ICU stay	43/221
E-MTAB-5274	Patients with sepsis due to CAP or faecal peritonitis.	Circulating leukocytes	England	First day of ICU stay	14/106

"Based on the univariate Cox regression analysis, prognostic DEIRGs were recognized as the biomarkers for multivariate Cox regression analysis. According to the median risk score value, conducted between low-risk and high-risk groups by using 'survival R' package. To evaluate the sensitivity and specificity of the prediction model, the receiver operating characteristics (ROC) curve was calculated using the 'survivalROC' package. The area under the ROC curve (AUC) was used to evaluate the prognostic model: 0.5-0.7 (moderate), 0.7-0.8 (better), and >0.9 (excellent)."

The corrected sentence appears below:

"Based on the univariate Cox regression analysis, prognostic DEIRGs were recognized as the biomarkers for multivariate Cox regression analysis. According to the median risk score value, conducted between low-risk and high-risk groups by using 'survival' R package. To evaluate the sensitivity and specificity of the prediction model, the receiver operating characteristics (ROC) curve was calculated using the 'survivalROC' package. The area under the ROC curve (AUC) was used to evaluate the prognostic model: 0.5-0.7 (moderate), 0.7-0.8 (better), and >0.9 (excellent)."

In the published article, there was an error in Table 1 as published. The name of dataset "GSE63062" was wrong, and it should be changed to "GSE63042". The corrected Table 1 and its caption "Basic information of the datasets included in this study." appear below.

The authors apologize for these errors and state that they do not change the scientific conclusions of the article in any way. The original article has been updated.

Publisher's note

All claims expressed in this article are solely those of the authors and do not necessarily represent those of their affiliated organizations, or those of the publisher, the editors and the reviewers. Any product that may be evaluated in this article, or claim that may be made by its manufacturer, is not guaranteed or endorsed by the publisher.

frontiers | Frontiers in Immunology

TYPE Original Research
PUBLISHED 23 February 2023
DOI 10.3389/fimmu.2023.1105181

Check for updates

OPEN ACCESS

EDITED BY
Marijn M. Speeckaert,
Ghent University Hospital, Belgium

REVIEWED BY
Stephan Immenschuh,
Hannover Medical School, Germany
Massimo Collino,
University of Turin, Italy

*CORRESPONDENCE
Sina M. Coldewey
sina.coldewey@med.uni-jena.de

SPECIALTY SECTION
This article was submitted to Inflammation, a section of the journal Frontiers in Immunology

RECEIVED 22 November 2022
ACCEPTED 08 February 2023
PUBLISHED 23 February 2023

CITATION
Kröller S, Wissuwa B, Dennhardt S, Krieg N, Thiemermann C, Daniel C, Amann K, Gunzer F and Coldewey SM (2023) Bruton's tyrosine kinase inhibition attenuates disease progression by reducing renal immune cell invasion in mice with hemolytic-uremic syndrome. *Front. Immunol.* 14:1105181. doi: 10.3389/fimmu.2023.1105181

COPYRIGHT
© 2023 Kröller, Wissuwa, Dennhardt, Krieg, Thiemermann, Daniel, Amann, Gunzer and Coldewey. This is an open-access article distributed under the terms of the Creative Commons Attribution License (CC BY). The use, distribution or reproduction in other forums is permitted, provided the original author(s) and the copyright owner(s) are credited and that the original publication in this journal is cited, in accordance with accepted academic practice. No use, distribution or reproduction is permitted which does not comply with these terms.

Bruton's tyrosine kinase inhibition attenuates disease progression by reducing renal immune cell invasion in mice with hemolytic-uremic syndrome

Sarah Kröller[1,2], Bianka Wissuwa[1,2], Sophie Dennhardt[1,2], Nadine Krieg[1,2], Christoph Thiemermann[3], Christoph Daniel[4], Kerstin Amann[4], Florian Gunzer[5] and Sina M. Coldewey[1,2,6*]

[1]Department of Anesthesiology and Intensive Care Medicine, Jena University Hospital, Jena, Germany, [2]Septomics Research Center, Jena University Hospital, Jena, Germany, [3]William Harvey Research Institute, Barts and The London School of Medicine and Dentistry, Queen Mary University of London, London, United Kingdom, [4]Department of Nephropathology, Friedrich-Alexander University (FAU) Erlangen-Nürnberg, Erlangen, Germany, [5]Department of Hospital Infection Control, University Hospital Carl Gustav Carus, TU Dresden, Dresden, Germany, [6]Center for Sepsis Control and Care (CSCC), Jena University Hospital, Jena, Germany

Hemolytic-uremic syndrome (HUS) can occur as a complication of an infection with Shiga-toxin (Stx)-producing *Escherichia coli*. Patients typically present with acute kidney injury, microangiopathic hemolytic anemia and thrombocytopenia. There is evidence that Stx-induced renal damage propagates a pro-inflammatory response. To date, therapy is limited to organ-supportive strategies. Bruton's tyrosine kinase (BTK) plays a pivotal role in recruitment and function of immune cells and its inhibition was recently shown to improve renal function in experimental sepsis and lupus nephritis. We hypothesized that attenuating the evoked immune response by BTK-inhibitors (BTKi) ameliorates outcome in HUS. We investigated the effect of daily oral administration of the BTKi ibrutinib (30 mg/kg) and acalabrutinib (3 mg/kg) in mice with Stx-induced HUS at day 7. After BTKi administration, we observed attenuated disease progression in mice with HUS. These findings were associated with less BTK and downstream phospholipase-C-gamma-2 activation in the spleen and, subsequently, a reduced renal invasion of BTK-positive cells including neutrophils. Only ibrutinib treatment diminished renal invasion of macrophages, improved acute kidney injury and dysfunction (plasma levels of NGAL and urea) and reduced hemolysis (plasma levels of bilirubin and LDH activity). In conclusion, we report here for the first time that BTK inhibition attenuates the course of disease in murine HUS. We suggest that the observed reduction of renal immune cell invasion contributes – at least in part – to this effect. Further translational studies are needed to evaluate BTK as a potential target for HUS therapy to overcome currently limited treatment options.

KEYWORDS

hemolytic-uremic syndrome, acute kidney injury, inflammation, animal model, Bruton's tyrosine kinase, ibrutinib, acalabrutinib

1 Introduction

Food-borne infections with Shiga-toxin (Stx)-producing *Escherichia coli* (STEC) are the major cause of hemolytic-uremic syndrome (HUS). In 2020, 4446 cases of STEC infections were registered in 36 European countries of which 320 patients suffered from HUS (1). Thereby, HUS is a rare, but acute, renal disorder and clinically presents with a triad of acute kidney injury (AKI), microangiopathic hemolytic anemia and thrombocytopenia. With a mortality rate of 3% in young children, HUS survivors can suffer from persisting end-stage renal disease (ESRD) as well as frequently occurring long-term neurological sequelae (2, 3). After translocation of Stx across the human intestinal epithelium, Stx is transferred mainly by immune cells *via* extracellular vesicles to renal endothelial cells, which express the Stx receptor globotriasylceramide (Gb3) (4, 5). Following internalization, Stx exerts ribotoxic effects resulting in an apoptotic and proinflammatory environment. The profound renal injury and tissue destruction caused by Stx results in immune cell migration to kidney, originating from natural reservoirs such as spleen, leading to an amplification of the local and systemic inflammation (5). A specific disease-modifying therapy for HUS is not available and, hence, therapy is currently limited to supportive options including fluid resuscitation and renal replacement therapy (6). Moreover, prospective randomized clinical trials are not feasible due to generally low incidences and unpredictable epidemic HUS outbreaks.

Bruton's tyrosine kinase (BTK) is a cytoplasmic and non-receptor binding protein tyrosine kinase belonging to the TEC family of kinases. Although the function of the BTK was first described in B-cell development, all cells of hematopoietic origin, excluding T-cells, express BTK indicating its important role in innate and adaptive immunity (7–9). The pivotal role of BTK in the development, recruitment and function of innate immune cells is further highlighted by the fact that BTK-deficient mice or mice treated with BTK inhibitors (BTKi) present with a reduced number of macrophages and migration of immature neutrophil granulocytes to inflamed tissue (10–12).

As BTK takes an intermediary role in diverse signaling pathways *via* downstream targets such as phospholipase-C-gamma-2 (PLCγ2), that influences cell survival, proliferation, differentiation and activation, excessive activation of BTK has been linked to pathophysiological processes in many B-cell-mediated cancers (13). Therefore, intense efforts have been made to design reversible and irreversible BTKi of which the CYS-481-binding inhibitors ibrutinib and second-generation acalabrutinib have been approved by the FDA (14). Interestingly, BTKi also reduce the local and/or systemic inflammation, the associated renal injury and dysfunction in animal models of sepsis, metabolic inflammation and lupus nephritis as well as in patients with COVID-19 (12, 15–17).

The role of BTK in the pathophysiology of STEC-HUS remains unknown. However, the promising results in preclinical studies of inflammatory diseases as well as the findings of the gene expression analysis performed in our well-characterized model of murine HUS (Gene Expression Online - GSE99229) (18) led us to the hypothesis that BTK plays a pivotal role in the inflammatory response and the resulting disease progression in STEC-HUS. Therefore, we investigated the effect of the two FDA-approved, irreversible BTKi ibrutinib and acalabrutinib in a murine model of HUS.

2 Material and methods

2.1 Animal experiments and study design

The induction of murine HUS by repetitive doses of Stx purified from an O157:H7 EHEC strain 86-24 patient isolate was performed as described previously (18). Male C57BL/6J wild-type mice aged 10-14 weeks were randomly assigned to one of six groups (sham + vehicle; HUS + vehicle; sham + ibrutinib; HUS + ibrutinib; sham + acalabrutinib; HUS + acalabrutinib) (n = 16 per group). Briefly, mice received low doses of Stx (25 ng/kg BW in 0.9% NaCl; HUS groups) or 0.9% NaCl (sham groups) i.v. on day 0, 3 and 6 and BTKi treatment (ibrutinib, acalabrutinib or vehicle) every 24 h p.o. starting immediately after initial Stx injection. For fluid resuscitation, mice received 800 µl Ringer's Lactate solution subcutaneously three times daily. Body weight was monitored daily and disease progression was evaluated three times daily using an established HUS score (Supplementary Table S1), in which the disease severity was categorized from 1 = no signs of illness to 5 = dead. Survival was monitored up to day 7 using humane endpoints (18, 19). Animals were exsanguinated in deep anesthesia (100 mg/kg ketamine; 10 mg/kg xylazine) and perfused with 0.9% NaCl. All *in vivo* experiments were approved by the regional animal welfare committee and the Thuringian State Office for Consumer Protection (registration number UKJ-20-018) and were performed in accordance with German legislation and the approved guidelines.

2.2 BTK inhibitors

Ibrutinib and acalabrutinib (MedChemExpress) were diluted to 30 mg/kg BW or 3 mg/kg BW in vehicle, respectively. The vehicle was composed of 5% mannitol (Carl Roth), 0.5% gelantine (Sigma Aldrich) and 2.5% dimethyl sulfoxide (DMSO; Carl Roth) dissolved in injection-grade water (Fresenius Kabi).

2.3 Blood and plasma sample analysis

Blood withdrawal and plasma preparation (at 4°C) were performed as described previously (18). Plasma neutrophil gelatinase associated lipocalin (NGAL), urea, bilirubin and plasma activity of lactate dehydrogenase (LDH) were analyzed with commercial kits according to manufacturer's instructions

(Supplementary Table S2). Hemograms were determined using scil Vet abc Plus+ (scil animal care company GmbH).

2.4 Tissue preparation, histopathology, and immunohistochemical staining

Renal tissue was fixed for at least 72 h in 5% buffered formaldehyde solution (Fischar), before dehydration in descending alcohol solution and embedding in paraffin (Thermo Fisher Scientific) were performed as described previously (18). For all histological staining procedures, 2 µm renal sections were prepared. Histopathological evaluation of renal and splenic tissue using periodic acid Schiff (PAS) staining were performed as described previously (18). Staining for kidney injury molecule-1 (KIM-1), BTK, lymphocyte antigen 6 complex (Ly6g), F4-80, CD3, Ki67 and cleaved caspase-3 (CC-3) were used to evaluate renal sections immunohistochemically. Generally, sections were deparaffinized and hydrated as described previously (18). Blocking of endogenous peroxidase was performed using 3% H_2O_2 (Carl Roth) and target retrieval solution (pH 6; Dako) was utilized for antigen retrieval in a pressure cooker. Bovine serum albumin (BSA; Sigma Aldrich) or 20% serum (PAA Laboratories) as well as avidin and biotin solution (15 min each; Vector Laboratories) were used each to block unspecific binding sites (Supplementary Table S3). Renal sections were incubated with primary antibody (Supplementary Table S4) overnight at 4°C. Sections were further incubated with secondary antibody (Supplementary Table S5) and with VectaStain ABC kit (Vector Laboratories) for 30 min each (Supplementary Table S3 for detailed information). As substrate, 3,3-diaminobenzidine (DAB; Vector Laboratories) was used and sections were counterstained with hemalaun (Carl Roth). Finally, renal sections were dehydrated and mounted for observation. Tris(hydroxymethyl)aminomethan (TRIS) buffer (pH 7.6) containing 50 mM TRIS (Carl Roth), 300 mM sodium chloride (Carl Roth), 0.04% Tween® 20 (Sigma Aldrich) was used to wash renal sections between the staining processes. Staining of thrombocytes (glycoprotein-1b (GP1b)) and fibrin deposition (acid fuchsin–Orange G stain (SFOG)) was performed as described previously (18, 19).

2.5 Quantification of histopathology and immunohistochemical staining

PAS staining was used for evaluation of vacuolization of splenic cells. Splenic vacuolization was quantified by counting the number of vacuoles in a grid area (10 x 10 caskets; grid area: 0.0156 mm^2) for 20 adjacent areas (magnification 1000x). Quantification and evaluation for staining of KIM-1, F4-80, CD3, Ki67 and CC-3 with a grid area of 0.0977 mm^2 and 400x magnification was performed as described previously (18). Staining of BTK positive cells was quantified by counting the number of intersections overlapping the positive brown staining in a grid area (10 x 10 caskets; grid area: 0.0977 mm^2) for 20 adjacent cortical areas (magnification 400x). Staining of Ly6g was quantified by counting the number of caskets with positive brown staining in a grid area (10 x 10 caskets; grid area: 0.0977 mm^2) for 20 adjacent cortical areas (magnification 400x). Images were taken using KEYENCE BZ-X800 microscope and BZ-X800 viewer after performing white balance and auto exposure at magnification of 400x (1000x for spleen). Quantification of thrombocytes and fibrin deposition was performed as described previously (18, 19).

2.6 Immunoblot analysis

15 mg of frozen spleen were homogenized in 10 µl/mg lysis buffer as described previously (20). Concentration of proteins was assessed as described previously (20). 15 µg (for pBTK/BTK, NLRP3, pro-IL-1β) and 60 µg (for pPLCγ2/PLCγ2) of protein were reduced in Laemmli buffer at 95°C for 5 min and 300 rpm shaking, loaded onto 10% TGX Stain-Free FastCast gels (Bio-Rad Laboratories) and transferred as described previously (20). Membranes were blocked using 5% BSA in TRIS buffered saline with Tween-20 (TBS-T) at room temperature for 1 h. Membranes were incubated in primary antibody diluted in 5% BSA in TBS-T overnight at 4°C (Supplementary Table S6). Membranes were washed 5 times for 5 min each in TBS-T followed by the incubation in HRP-coupled secondary antibodies, diluted in 5% BSA in TBS-T, at room temperature for 1 h (Supplementary Table S6). Again, membranes were washed 5 times for 5 min each in TBS-T. Clarity Western ECL substrate (Bio-Rad Laboratories) and the ChemiDoc MP Imaging System (Bio-Rad Laboratories) were used for signal detection. Image Lab software (Bio-Rad Laboratories) was used for analysis of relative protein expression as described previously (20). Bands with normalization factors between 0.7 and 1.3 were considered for evaluation (21). Phosphorylation levels were determined by the division of relative phosphorylated protein by relative pan protein and subsequent normalization to vehicle-treated HUS group.

2.7 Statistics

Data were analyzed using GraphPad Prism 7.05 (GraphPad Software) and are depicted as mean + SD for n observations, where n represents the number of animals studied. Survival was analyzed generating Kaplan-Meier curves. Kruskal-Wallis test (non-parametric test) or ordinary one-way ANOVA (parametric test) was used to compare sham groups to their corresponding HUS groups, as well as HUS + vehicle compared with HUS + BTKi. Gaussian distribution was verified using Shapiro-Wilk normality test at 0.05 significance level. If necessary, values were converted to logarithmic values to achieve normality. For immunoblotting, Mann-Whitney-U test was used for comparison between two groups. A P-value < 0.05 was considered significant.

10.3389/fimmu.2023.1105181

3 Results

3.1 Disease severity is improved in BTKi-treated mice with HUS

Seven-day survival of vehicle-treated mice with HUS (81.25%) was decreased compared with vehicle-treated sham mice (100%) (Figure 1A). Mice with HUS treated with ibrutinib (87.5%) or acalabrutinib (93.75%) showed an increased, but not significantly altered, survival rate compared with vehicle-treated mice with HUS. During the experiment, all mice with HUS showed increasing disease progression (i.e. increase in morbidity), indicated by the clinical HUS score (Figure 1B). However, the HUS score on day 7 was only significantly increased in vehicle-treated mice with HUS compared with their corresponding sham group (Figure 1C). Mice with HUS of all groups lost a significant amount of weight during the 7-day experimental period (Figure 1D) compared with their corresponding sham group. Weight loss was highest in vehicle-treated mice with HUS (20.6%), followed by mice with HUS treated with acalabrutinib (17.2%) (Figure 1E). Comparison of the HUS groups revealed that mice with HUS treated with acalabrutinib lost significantly less weight compared with the vehicle-treated mice with HUS, while weight loss of ibrutinib-treated mice with HUS was reduced (P = 0.05), but not significantly altered, compared with the vehicle-treated HUS group.

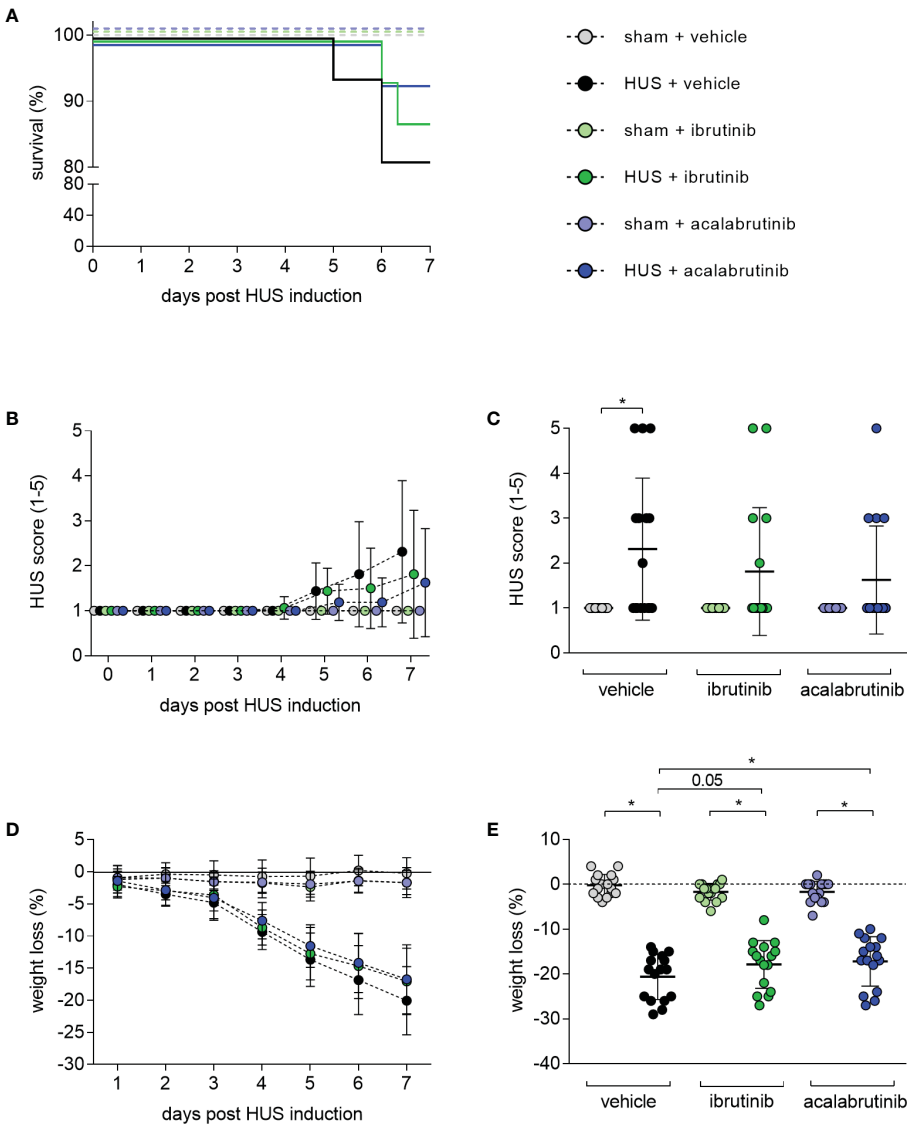

FIGURE 1
Clinical presentation of mice with HUS treated with ibrutinib or acalabrutinib. HUS followed up for 7 days in sham mice and mice subjected to HUS with daily oral application of vehicle, ibrutinib or acalabrutinib. **(A)** Survival by Kaplan-Meier survival analysis + *post hoc* test, analysis of **(B)** progression of HUS score in the course of the experiment (ranging from 1 = no signs of illness to 5 = dead), **(C)** HUS score on day 7, **(D)** progression of weight loss in the course of the experiment, **(E)** weight loss on humane endpoints or day 7 (n = 16 per group). Data are expressed as **(B, D)** dot blot and **(C, E)** scatter dot blot with mean + SD. **(C)** Kruskal-Wallis test + Dunn's multiple comparison test, **(E)** ordinary one-way ANOVA + Holm-Sidak's multiple comparison test. *P < 0.05. HUS, hemolytic uremic syndrome.

10.3389/fimmu.2023.1105181

3.2 Kidney injury, proliferation and apoptosis are partly ameliorated by BTKi treatment in mice with HUS

Mice with HUS treated with vehicle or acalabrutinib showed severe renal injury, indicated by significantly increased plasma NGAL compared with their corresponding sham group (Figure 2A). In contrast, ibrutinib-treated mice with HUS showed elevated, but not significantly altered, plasma NGAL compared with their corresponding sham group as well as significantly less plasma NGAL compared with vehicle-treated mice with HUS. Mice with HUS of all groups showed significantly increased plasma urea compared with their corresponding sham group (Figure 2B). However, ibrutinib-treated mice with HUS showed significantly less plasma urea when compared with mice with

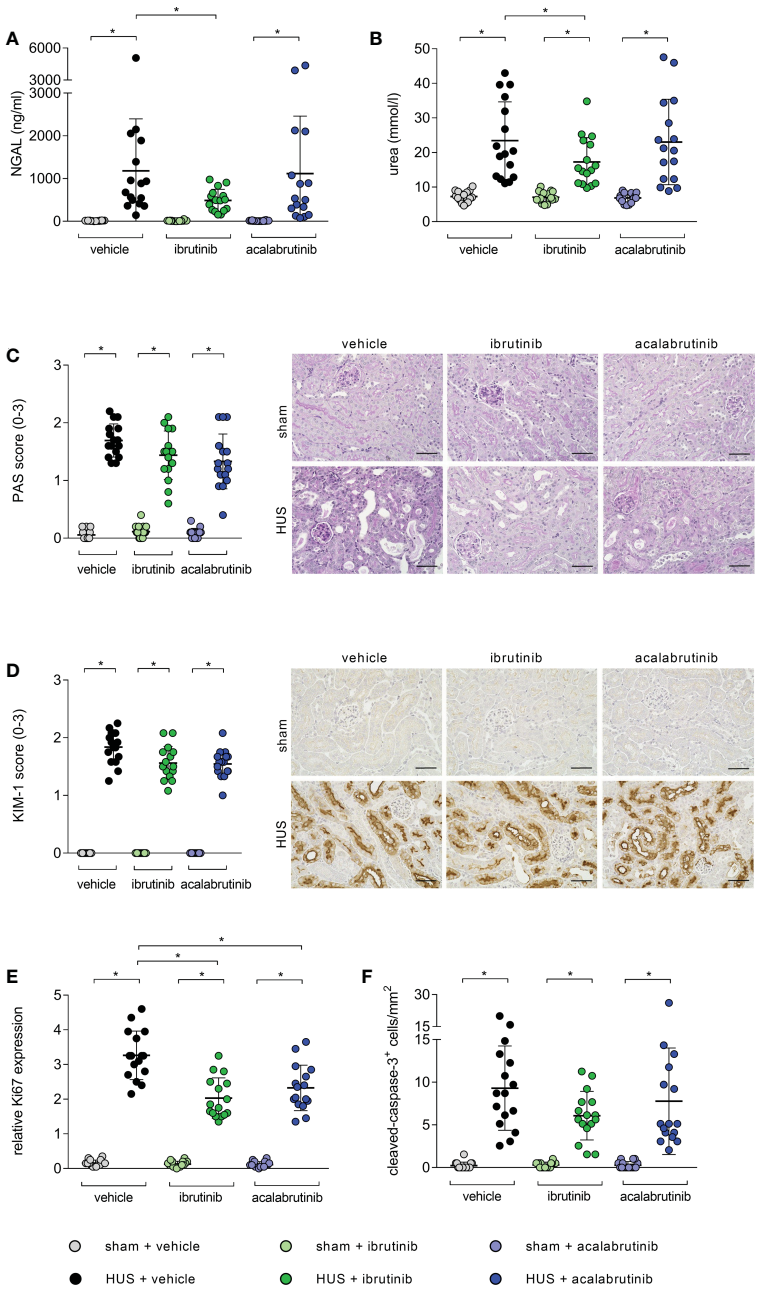

FIGURE 2
Parameters of kidney injury, proliferation and apoptosis of mice with HUS treated with ibrutinib or acalabrutinib. Determination of plasma **(A)** NGAL and **(B)** urea (n = 16 per group) on humane endpoint or day 7. Quantification and representative images of **(C)** PAS reaction and **(D)** relative KIM-1 expression in renal sections (n = 16 per group) on humane endpoint or day 7. Bars = 50 µm (400x magnification). Quantification of renal **(E)** Ki67 and **(F)** CC-3 expression (n = 16 per group) on humane endpoint or day 7. Data are expressed as scatter dot plot with mean + SD. **(A, B, E)** ordinary one-way ANOVA + Holm-Sidak's multiple comparison test, **(C, D, F)** Kruskal-Wallis test + Dunn's multiple comparison test. *P < 0.05. NGAL, neutrophil gelatinase-associated lipocalin; PAS, periodic acid Schiff; KIM-1, kidney injury molecule-1; HUS, hemolytic-uremic syndrome.

10.3389/fimmu.2023.1105181

HUS of the vehicle group. For further evaluation of tissue damage, PAS staining and analysis of KIM-1 expression was performed. Mice with HUS of all groups showed a significantly higher PAS score (Figure 2C) and KIM-1 (Figure 2D) score compared with their corresponding sham group. However, the highest PAS and KIM-1 scores were measured in vehicle-treated mice with HUS, while ibrutinib- and acalabrutinib-treated mice with HUS tended to have lower PAS and KIM-1 scores. Proliferation and apoptosis in renal tissue was evaluated using Ki67 and CC-3 staining, respectively. Mice with HUS of all groups showed significantly increased cell proliferation compared with their corresponding sham group (Figure 2E; Supplementary Figure 1A). Notably, treatment with ibrutinib or acalabrutinib significantly reduced the amount of proliferated cells in renal tissue compared with vehicle-treated mice with HUS. Similarly, mice with HUS of all groups showed significantly increased number of apoptotic cells compared with their corresponding sham group irrespective of their treatment (Figure 2F; Supplementary Figure 1B).

3.3 Surrogate parameters of hemolysis and fibrin deposition are reduced in ibrutinib-treated mice with HUS

As indirect hemolysis markers, plasma bilirubin and plasma LDH activity were measured. Mice with HUS of all groups showed significantly higher bilirubin levels compared with their corresponding sham group (Figure 3A). However, ibrutinib-treated mice with HUS showed significantly reduced plasma bilirubin when compared with the mice with HUS of the vehicle group. Similar results were seen for measurement of LDH activity in

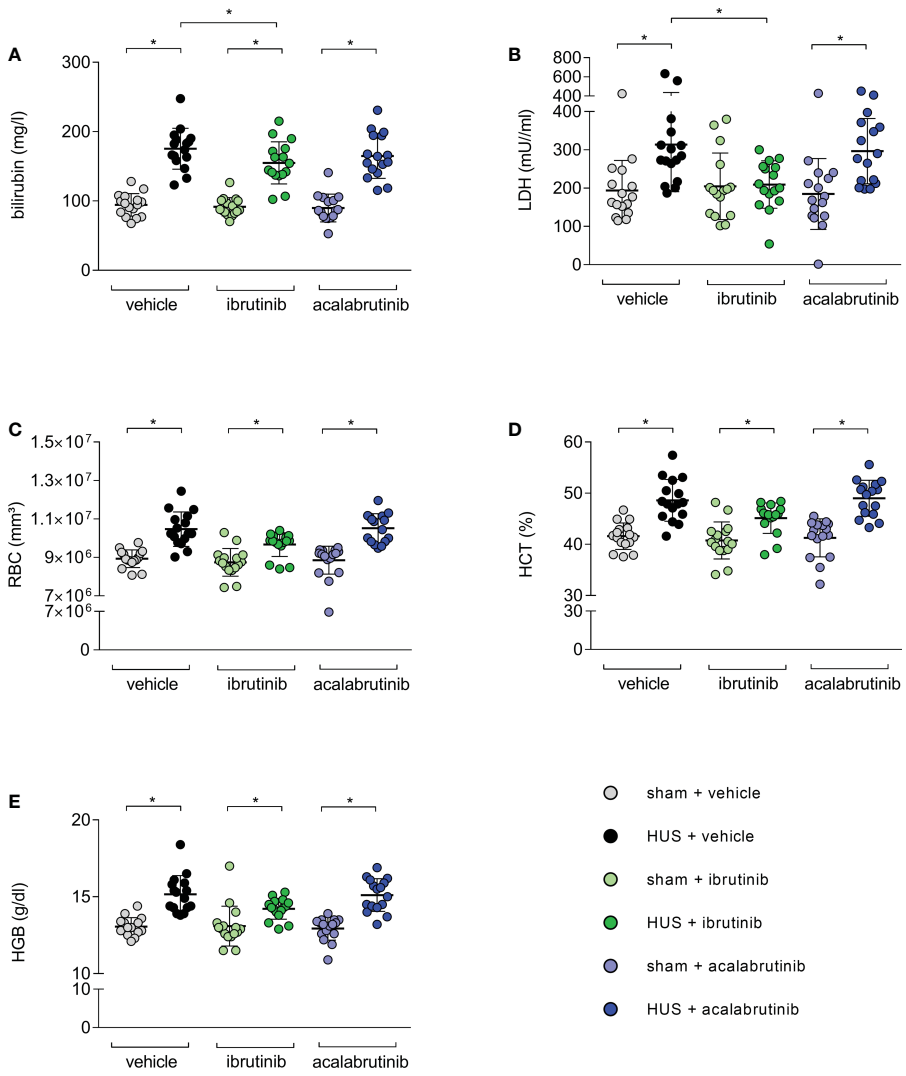

FIGURE 3
Surrogate parameters of hemolysis of mice with HUS treated with ibrutinib or acalabrutinib. Determination of plasma **(A)** bilirubin; **(B)** LDH activity and whole blood **(C)** erythrocytes, **(D)** hematocrit and **(E)** hemoglobin (n = 16 per group) on humane endpoint or day 7. Data are expressed as scatter dot plot with mean + SD. **(A)** ordinary one-way ANOVA + Holm-Sidak's multiple comparison test, **(B–E)** Kruskal-Wallis test + Dunn's multiple comparison test. *P < 0.05. RBC, erythrocytes; HCT, hematocrit; HGB, hemoglobin; LDH, lactate dehydrogenase; HUS, hemolytic-uremic syndrome.

plasma. Mice with HUS treated with vehicle or acalabrutinib showed increased plasma LDH activity compared with their corresponding sham group (Figure 3B), while ibrutinib-treated mice with HUS showed LDH activity equal to those seen in the corresponding sham animals. All mice with HUS showed significantly increased erythrocyte count (Figure 3C), hematocrit (Figure 3D) and hemoglobin (Figure 3E) in whole blood compared with their corresponding sham group, indicating the development of hemoconcentration as described previously (18). An insignificant trend towards lower mean values of hemoconcentration indicators was observed in ibrutinib-treated mice with HUS compared with vehicle-treated mice with HUS. Significant thrombocytopenia was not observed in mice with experimental HUS regardless of treatment (Supplementary Figure S2A). Surrogate parameters of red blood indices (mean corpuscular volume, mean corpuscular hemoglobin, mean corpuscular hemoglobin concentration) did not show any differences between vehicle-treated groups and BTKi-treated groups, indicating that treatment with BTKi in mice did not influence characteristics of erythrocytes in mice (Supplementary Figures S2B–D). To analyze thrombotic microangiopathy in the kidneys, thrombocytes counts in renal sections of all groups were assessed by GP1b staining, and fibrin deposition was assessed by SFOG staining. Renal thrombocyte counts were significantly increased in the kidney sections of all mice with HUS compared with the corresponding sham mice, regardless of treatment (Supplementary Figure S3A). Fibrin deposits were significantly increased in the kidney sections of vehicle- or acalabrutinib-treated mice with HUS compared with the corresponding sham mice, however not in ibrutinib-treated mice (Supplementary Figure S3B).

3.4 Dampened renal immune cell invasion by treatment with BTKi in mice with HUS

BTK is mainly expressed in infiltrating immune cells. Therefore, histological analysis for renal immune cell invasion was performed. In all stainings, mice with HUS of all groups showed significant increase of the evaluated immune cells compared with their corresponding sham group. However, histological staining for BTK revealed a significant reduction of BTK-positive cells in ibrutinib- and acalabrutinib-treated mice with HUS compared with mice with HUS of the vehicle group (Figure 4A). Moreover, the same effect was detected for the invasion of neutrophil granulocytes, indicated by Ly6g staining (Figure 4B). Quantification of F4-80 (surface marker for macrophages) revealed significantly reduced accumulation of macrophages only in ibrutinib-treated mice with HUS compared with vehicle-treated mice with HUS, while this effect was not seen for acalabrutinib treatment (Figure 4C). By contrast, the invasion of CD3-positive cells (surface marker for T-lymphocytes) remained unaffectedly high in mice with HUS of all groups irrespective of their treatment (Figure 4D).

3.5 Alternated BTK-downstream signaling and grade of vacuolization by BTKi treatment in mice with HUS

As the spleen is described as a natural reservoir of immune cells and BTK is known to have a major impact in the activation of immune cells (9, 22–24), the phosphorylation level of BTK was analyzed in whole-cell protein lysates. BTK phosphorylation was significantly reduced in mice with HUS treated with ibrutinib or acalabrutinib compared with vehicle-treated mice with HUS (Figure 5A). As a direct downstream target of BTK, phosphorylation level of PLCγ2 was analyzed in spleen. Ibrutinib-treated mice with HUS showed reduced, but not significantly altered, PLCγ2 phosphorylation compared with vehicle-treated mice with HUS (Figure 5B). In contrast, only acalabrutinib treatment in mice with HUS led to significantly reduced phosphorylation of PLCγ2 compared with the vehicle-treated mice with HUS. Since BTK has been described as an activator of the NLRP3 inflammasome, the relative protein expression of NLRP3 and pro-IL-1β in spleen tissue was analyzed. In the spleen, ibrutinib-treated mice with HUS showed a trend towards decreased NLRP3 (Figure 5C) and pro-IL-1β (Figure 5D) expression, while acalabrutinib-treated mice with HUS showed a significantly decreased protein expression of NLRP3 (Figure 5C) and pro-IL-1β (Figure 5D) compared with vehicle-treated mice with HUS. For analysis of spleen morphology, PAS staining was performed and vacuolization of cells was counted. Vehicle- and acalabrutinib-treated mice with HUS showed significantly increased vacuolization of cells compared with their corresponding sham group (Figure 5E). Moreover, treatment with ibrutinib and acalabrutinib lead to significantly reduced vacuolization of cells in mice with HUS compared with vehicle-treated mice with HUS.

4 Discussion

STEC-HUS is a rare, but life-threatening, disease causing acute kidney injury often followed by long-term sequelae. Hitherto, supportive therapy during acute phase of this disease is the mainstay and targeted therapy is still missing. In the present study, we report for the first time that the two FDA-approved BTKi ibrutinib and acalabrutinib attenuate disease progression seen by a reduction of renal immune cell infiltration in a murine model of HUS.

Critical steps in HUS pathophysiology, caused by Stx, are acute kidney injury, microangiopathic hemolytic anemia and thrombocytopenia as well as the evoked immune response. As the kidneys are the main target of Stx in HUS, we investigated the impact of the BTKi ibrutinib and acalabrutinib on renal pathology in our murine HUS model. Ibrutinib-treatment in mice with HUS slightly alleviated renal injury by reducing plasma NGAL and urea as well as proliferation of cells in renal tissue. Nevertheless, a profound improvement in renal tissue damage and dysfunction has not been observed for both inhibitors in the present study.

10.3389/fimmu.2023.1105181

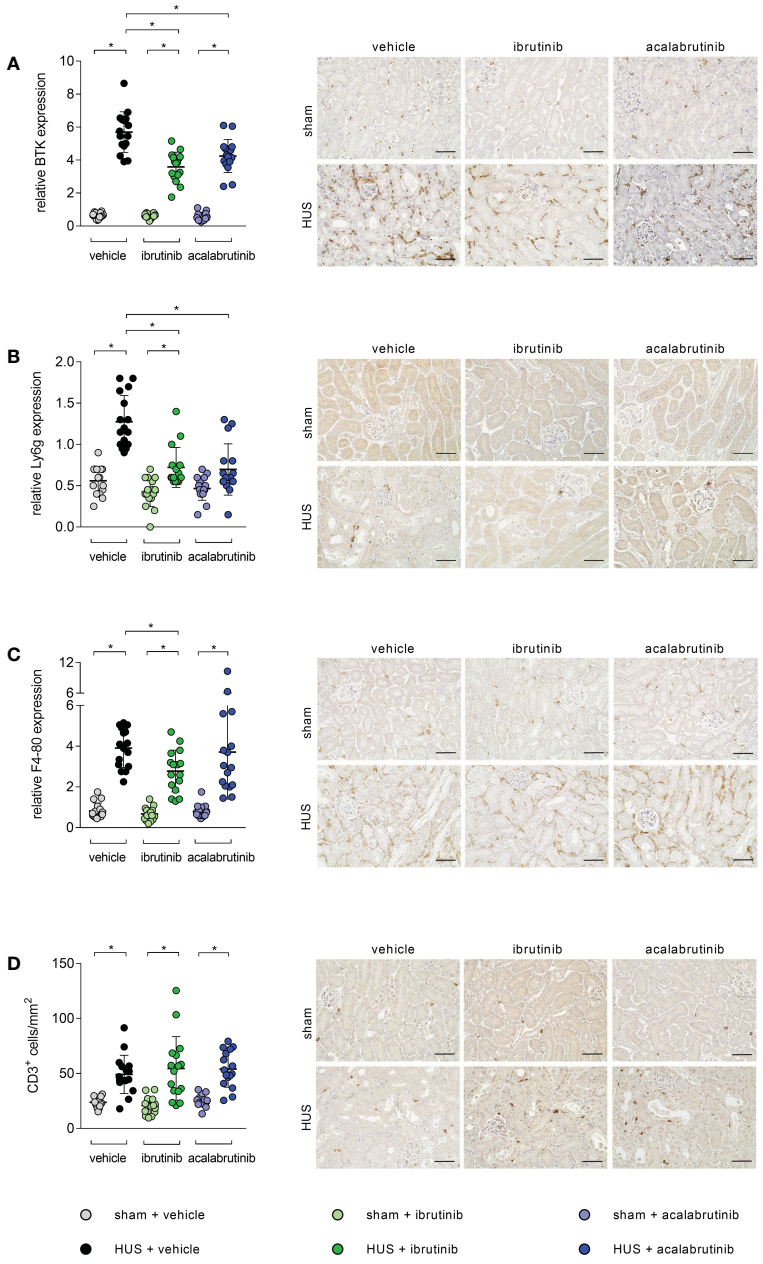

FIGURE 4
Renal immune response of mice with HUS treated with ibrutinib or acalabrutinib. Quantification and representative images of **(A)** BTK, **(B)** Ly6g, **(C)** F4-80 and **(D)** CD3 expression in renal sections (n = 16 per group) on humane endpoint or day 7. Bars = 50 µm (400x magnification). Data are expressed as scatter dot plot with mean + SD. **(A, C, D)** ordinary one-way ANOVA + Holm-Sidak's multiple comparison test. **(B)** Kruskal-Wallis test + Dunn's multiple comparison test. *P < 0.05. BTK, Bruton's tyrosine kinase; Ly6g, lymphocyte antigen 6 complex, locus G; HUS, hemolytic-uremic syndrome.

Conversely, ibrutinib and acalabrutinib have already been proven to ameliorate renal dysfunction in murine models of cecal ligation and puncture (CLP)-induced sepsis, sepsis-induced acute kidney injury as well as lupus nephritis (15, 16, 25). In the light of these studies, we hypothesize that inhibition of BTK in the pathophysiology of HUS does not primarily affect the ribotoxic function and subsequent destruction of renal tissue by Stx. Therefore, we analyzed the influence of BTKi on the aspect of hemolysis in the pathophysiology of HUS. In our HUS model, mice suffer from profound dehydration, indicated by increased hemoglobin and hematocrit, and show elevated hemolysis markers, which have been described before (18). In the present study, ibrutinib-treated mice with HUS showed positive impact on hemolysis while intervention with acalabrutinib did not. Interestingly, both inhibitors have already been described as therapeutic option for autoimmune hemolytic anemia and are currently tested in clinical stage 2 trials (ibrutinib: NCT03827603, NCT04398459; acalabrutinib: NCT-04657094) (26, 27). These contradicting results might be explained by different application regimes of ibrutinib (30 mg/kg BW) and acalabrutinib (3 mg/kg BW) in our

10.3389/fimmu.2023.1105181

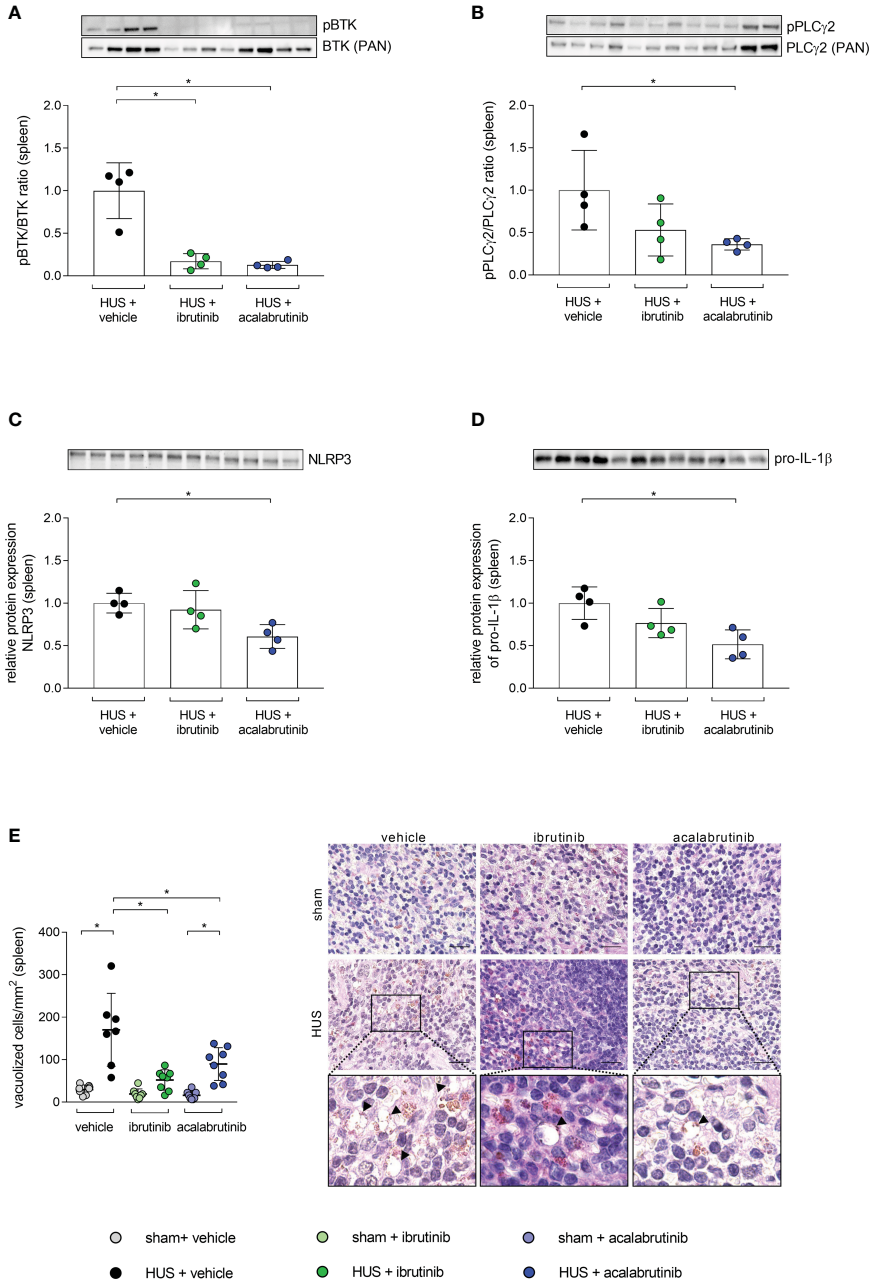

FIGURE 5
BTK-downstream signaling as well as vacuolization of cells in spleen of mice with HUS treated with ibrutinib or acalabrutinib. Ratio of relative phosphorylated protein expression to relative pan protein expression of **(A)** BTK and **(B)** PLCγ2 as well as relative protein expression of **(C)** NLRP3 and **(D)** pro-IL-1β in spleen (n = 4 per HUS group) in whole splenic protein lysates on humane endpoint or day 7. Quantification and representative images of **(E)** vacuolization of cells in splenic sections (n = 7 - 8 per group) on humane endpoint or day 7. Bars = 20 µm (1000x magnification). Arrows indicate sites of vacuolization. Data are expressed as scatter dot plot with mean + SD. **(A–D)** Mann-Whitney-U test. **(E)** ordinary one-way ANOVA + Holm-Sidak's multiple comparison test. *P < 0.05. BTK, Bruton's tyrosine kinase; PLCγ2, phospholipase-C-gamma2; HUS, hemolytic-uremic syndrome; NLRP3, NLR family pyrin domain containing 3; IL-1β, Interleukin-1beta.

study. Moreover, potential off-target activity of ibrutinib cannot be excluded. Ibrutinib has been shown to block other TEC family kinases such as epidermal growth factor receptor (EGFR), targeting interleukin-2 inducible T-cell kinase (ITK) and TEC. In contrast, acalabrutinib possesses a much higher selectivity, but reduced potency, for BTK compared with ibrutinib (27–29). Thrombocytopenia is another hallmark of HUS and we already previously described that mice with HUS did not develop a pronounced thrombocytopenia in the employed model. We hypothesized earlier that thrombocytopenia might be masked by hypovolemia and consecutive hemoconcentration (18). Recently published studies have reported antithrombotic properties of low doses of BTKi in mouse models and human volunteers (30–32). Therefore, we investigated the effects of BTKi on thrombotic microangiopathy in HUS by staining platelets and fibrin deposition. In our model acalabrutinib had no effect on surrogate

parameters of thrombotic events. However, in ibrutinib-treated mice with HUS, we observed a trend towards less fibrin deposition. Taken together, we observed an advantage for ibrutinib over acalabrutinib in the analysis of renal injury, hemolysis and fibrin deposition in our murine HUS model. However, the improvement of disease progression of HUS by BTKi, seen by decreased morbidity and lowered mortality, was observed for both inhibitors. As BTK is mainly expressed in cells of hematopoietic origin, we assume that treatment with ibrutinib and acalabrutinib mostly affects the evoked immune response after initial renal injury.

In the last decade, intense research has been performed to demonstrate that inflammation is a central part in the pathophysiology of HUS and not just an epiphenomenon (33). Renal destruction, induced by Stx, not only causes vascular damage but also the induction of cytokine and chemokine expression. Thereby, the secretion of interleukin-8 or monocyte chemotactic protein 1 of the Stx-affected cells generates an inflammatory environment, while simultaneously enhancing immune cell adhesion and their migration into renal tissue (33–35). Therefore, it is not surprising that recruitment of macrophages, neutrophils and other immune cells is well documented in murine kidneys of our HUS model as well as in HUS patients (18, 19, 36). Interestingly, binding of Stx to neutrophils prolongs their lifespan, increases reactive oxygen species production and neutrophil extracellular trap formation and thereby intensifying the inflammatory process, indicating neutrophils are an important player in HUS pathophysiology (37). In the present study, we observed that treatment with the BTKi ibrutinib and acalabrutinib significantly reduced the general amount of BTK-positive cells in renal tissue. Further analysis showed that especially neutrophils and macrophages (ibrutinib only) were affected by BTKi treatment in HUS, matching the fact that expression of BTK in both cell types was proven to play an important part in their maturation and function. Matching this, BTK deficiency has been associated with reduced number of monocytes, macrophages as well as granulocytes arresting in a pre-mature stage causing neutropenia in different studies (9, 11, 38, 39). We hypothesize that especially the reduced amount of neutrophils migrating into renal tissue through BTKi is the reason for the improved morbidity and mortality observed in the present study. Underlining this, Lill et al. recently observed that in mice with HUS, tissue-resident renal macrophages produce TNF-α, which is a crucial chemotactic molecule for recruitment of neutrophils (40). TNF-α depletion of these macrophages significantly reduced neutrophil migration into the kidney and significantly improved disease outcome (40). In addition, the functional state of neutrophils has been correlated with renal dysfunction and disease outcome in children with HUS, emphasizing a crucial role of neutrophils in the progression of this disease (36). Besides the role of BTK in the physiological function of immune cells, BTK has also a profound impact on the recruitment process of neutrophils and macrophages from the bloodstream or natural reservoirs into injured tissue, as BTK has been found to play a key role in E-selectin-mediated slow rolling and transmigration of neutrophils into tissue (41, 42). The concept of the spleen as a natural reservoir of immune cells is well established. Neutrophils can contribute to the marginating pool of granulocytes through localization in the spleen in absence of infection or injury (23). Especially the mobilization of splenic monocytes to injured tissue after coronary ligation highlights the ability of the spleen to make immune cells available after tissue destruction (24). To examine, whether inhibition of BTK affects other organs involved in the triggered immune cell activation and recruitment, we analyzed the activation status of splenic BTK and its direct downstream target PLCγ2 (43, 44) and observed a reduced activation of both proteins in splenic tissue by BTKi in mice with HUS. Furthermore, BTK has previously been described as a positive and direct regulator of the NLRP3 inflammasome and the production of pro-inflammatory IL-1β (45–48). We analyzed the protein expression of NLRP3 and pro-IL-1β and observed reduced expression of these proteins in spleen tissue of BTKi-treated mice with HUS. Therefore, we hypothesize that the BTK-downstream signaling, which leads to activation and recruitment of immune cells to the kidney and generation of pro-inflammatory stimuli, is blocked by the employed BTKi, particularly in the spleen of mice with HUS. Moreover, we observed vacuolization of cells in the red pulp of the spleen after HUS induction, which is significantly reduced by BTKi. To our knowledge, this phenomenon has not been described before in the pathophysiology of HUS. Extensive vacuolization in the red pulp has already been negatively associated with the outcome in studies analyzing murine infections with *Plasmodium berghei* or toxicity testing of elmiron (49, 50). Concluding this, we hypothesize that an improved outcome of HUS progression through BTKi could be achieved by a reduced immune cell recruitment from spleen to kidney and a reduced alternation of splenic tissue.

Hitherto, HUS therapy is limited to organ-supportive strategies. We report here for the first time that the commercially available BTKi ibrutinib and acalabrutinib alleviate disease progression in murine HUS by reducing renal immune cell invasion. Moreover, our results indicate less BTK-induced immune cell activation in spleen as potential explanation. The promising results of BTK as a new target in HUS therapy in our study are worth to be further validated.

Data availability statement

The original contributions presented in the study are included in the article/Supplementary Material. Further inquiries can be directed to the corresponding author.

Ethics statement

The animal study was reviewed and approved by the regional animal welfare committee and the Thuringian State Office for Consumer Protection (registration number UKJ-20-018).

Author contributions

SMC designed, planned, and supervised the study. SK and SMC wrote the manuscript. SK, BW, SD, and NK performed animal experiments. SK performed data analysis of animal experiments. SK performed and analyzed ELISA, histology, immunohistochemistry, and Western blots. CD performed staining of SFOG, staining and analysis of GP1b. FG provided Shiga toxin. SMC, SK, BW, SD, NK, CT, CD, KA, and FG provided important intellectual content and revised the manuscript. All authors contributed to the article and approved the submitted version.

Funding

The research work was funded by the Federal Ministry of Education and Research (BMBF, ZIK Septomics Research Center, Translational Septomics, award no. 03Z22JN12 to SMC).

Acknowledgments

We thank Jacqueline Fischer (Translational Septomics, Jena University Hospital, Jena, Germany) for technical assistance.

Conflict of interest

The authors declare that the research was conducted in the absence of any commercial or financial relationships that could be construed as a potential conflict of interest.

Publisher's note

All claims expressed in this article are solely those of the authors and do not necessarily represent those of their affiliated organizations, or those of the publisher, the editors and the reviewers. Any product that may be evaluated in this article, or claim that may be made by its manufacturer, is not guaranteed or endorsed by the publisher.

Supplementary material

The Supplementary Material for this article can be found online at: https://www.frontiersin.org/articles/10.3389/fimmu.2023.1105181/full#supplementary-material

References

1. European Food Safety AEuropean Centre for Disease P, Control. The European union one health 2020 zoonoses report. *EFSA J* (2021) 19(12):e06971. doi: 10.2903/j.efsa.2021.6971

2. Harkins VJ, McAllister DA, Reynolds BC, Shiga-Toxin E. Coli hemolytic uremic syndrome: Review of management and long-term outcome. *Curr Pediatr Rep* (2020) 8 (1):16–25. doi: 10.1007/s40124-020-00208-7

3. Spinale JM, Ruebner RL, Copelovitch L, Kaplan BS. Long-term outcomes of shiga toxin hemolytic uremic syndrome. *Pediatr Nephrol* (2013) 28(11):2097–105. doi: 10.1007/s00467-012-2383-6

4. Schuller S. Shiga toxin interaction with human intestinal epithelium. *Toxins (Basel)* (2011) 3(6):626–39. doi: 10.3390/toxins3060626

5. Bowen EE, Coward RJ. Advances in our understanding of the pathogenesis of hemolytic uremic syndromes. *Am J Physiol Renal Physiol* (2018) 314(3):F454–61. doi: 10.1152/ajprenal.00376.2017

6. Kavanagh D, Raman S, Sheerin NS. Management of hemolytic uremic syndrome. *F1000Prime Rep* (2014) 6:119. doi: 10.12703/P6-119

7. Bruton OC. Agammaglobulinemia. *Pediatrics* (1952) 9(6):722–8. doi: 10.1542/peds.9.6.722

8. Vetrie D, Vorechovsky I, Sideras P, Holland J, Davies A, Flinter F, et al. The gene involved in X-linked agammaglobulinaemia is a member of the src family of protein-tyrosine kinases. *Nature* (1993) 361(6409):226–33. doi: 10.1038/361226a0

9. Weber ANR, Bittner Z, Liu X, Dang TM, Radsak MP, Brunner C. Bruton's tyrosine kinase: An emerging key player in innate immunity. *Front Immunol* (2017) 8:1454. doi: 10.3389/fimmu.2017.01454

10. Marron TU, Rohr K, Martinez-Gallo M, Yu J, Cunningham-Rundles C. TLR signaling and effector functions are intact in XLA neutrophils. *Clin Immunol* (2010) 137(1):74–80. doi: 10.1016/j.clim.2010.06.011

11. Melcher M, Unger B, Schmidt U, Rajantie IA, Alitalo K, Ellmeier W. Essential roles for the tec family kinases tec and btk in m-CSF receptor signaling pathways that regulate macrophage survival. *J Immunol* (2008) 180(12):8048–56. doi: 10.4049/jimmunol.180.12.8048

12. Purvis GSD, Collino M, Aranda-Tavio H, Chiazza F, O'Riordan CE, Zeboudj L, et al. Inhibition of bruton's TK regulates macrophage NF-kappaB and NLRP3 inflammasome activation in metabolic inflammation. *Br J Pharmacol* (2020) 177 (19):4416–32. doi: 10.1111/bph.15182

13. Wang X, Kokabee L, Kokabee M, Conklin DS. Bruton's tyrosine kinase and its isoforms in cancer. *Front Cell Dev Biol* (2021) 9:668996. doi: 10.3389/fcell.2021.668996

14. Liang C, Tian D, Ren X, Ding S, Jia M, Xin M, et al. The development of bruton's tyrosine kinase (BTK) inhibitors from 2012 to 2017: A mini-review. *Eur J Med Chem* (2018) 151:315–26. doi: 10.1016/j.ejmech.2018.03.062

15. O'Riordan CE, Purvis GSD, Collotta D, Chiazza F, Wissuwa B, Al Zoubi S, et al. Bruton's tyrosine kinase inhibition attenuates the cardiac dysfunction caused by cecal ligation and puncture in mice. *Front Immunol* (2019) 10:2129. doi: 10.3389/fimmu.2019.02129

16. Chalmers SA, Glynn E, Garcia SJ, Panzenbeck M, Pelletier J, Dimock J, et al. BTK inhibition ameliorates kidney disease in spontaneous lupus nephritis. *Clin Immunol* (2018) 197:205–18. doi: 10.1016/j.clim.2018.10.008

17. Treon SP, Castillo JJ, Skarbnik AP, Soumerai JD, Ghobrial IM, Guerrera ML, et al. The BTK inhibitor ibrutinib may protect against pulmonary injury in COVID-19-infected patients. *Blood* (2020) 135(21):1912–5. doi: 10.1182/blood.2020006288

18. Dennhardt S, Pirschel W, Wissuwa B, Daniel C, Gunzer F, Lindig S, et al. Modeling hemolytic-uremic syndrome: In-depth characterization of distinct murine models reflecting different features of human disease. *Front Immunol* (2018) 9:1459. doi: 10.3389/fimmu.2018.01459

19. Pirschel W, Mestekemper AN, Wissuwa B, Krieg N, Kroller S, Daniel C, et al. Divergent roles of haptoglobin and hemopexin deficiency for disease progression of shiga-toxin-induced hemolytic-uremic syndrome in mice. *Kidney Int* (2022) 101 (6):1171–85. doi: 10.1016/j.kint.2021.12.024

20. Sobbe IV, Krieg N, Dennhardt S, Coldewey SM. Involvement of NF-kappaB1 and the non-canonical NF-kappaB signaling pathway in the pathogenesis of acute kidney injury in shiga-toxin-2-induced hemolytic-uremic syndrome in mice. *Shock* (2021) 56(4):573–81. doi: 10.1097/SHK.0000000000001558

21. Rivero-Gutierrez B, Anzola A, Martinez-Augustin O, de Medina FS. Stain-free detection as loading control alternative to ponceau and housekeeping protein immunodetection in Western blotting. *Anal Biochem* (2014) 467:1–3. doi: 10.1016/j.ab.2014.08.027

22. Bronte V, Pittet MJ. The spleen in local and systemic regulation of immunity. *Immunity* (2013) 39(5):806–18. doi: 10.1016/j.immuni.2013.10.010

23. Summers C, Rankin SM, Condliffe AM, Singh N, Peters AM, Chilvers ER. Neutrophil kinetics in health and disease. *Trends Immunol* (2010) 31(8):318–24. doi: 10.1016/j.it.2010.05.006

24. Swirski FK, Nahrendorf M, Etzrodt M, Wildgruber M, Cortez-Retamozo V, Panizzi P, et al. Identification of splenic reservoir monocytes and their deployment to inflammatory sites. *Science* (2009) 325(5940):612–6. doi: 10.1126/science.1175202

25. Nadeem A, Ahmad SF, Al-Harbi NO, Ibrahim KE, Alqahtani F, Alanazi WA, et al. Bruton's tyrosine kinase inhibition attenuates oxidative stress in systemic immune cells and renal compartment during sepsis-induced acute kidney injury in mice. *Int Immunopharmacol* (2021) 90:107123. doi: 10.1016/j.intimp.2020.107123

26. Jalink M, Berentsen S, Castillo JJ, Treon SP, Cruijsen M, Fattizzo B, et al. Effect of ibrutinib treatment on hemolytic anemia and acrocyanosis in cold agglutinin disease/cold agglutinin syndrome. *Blood* (2021) 138(20):2002–5. doi: 10.1182/blood.2021012039

27. Robak T, Witkowska M, Smolewski P. The role of bruton's kinase inhibitors in chronic lymphocytic leukemia: Current status and future directions. *Cancers (Basel)* (2022) 14(3). doi: 10.3390/cancers14030771

28. Honigberg LA, Smith AM, Sirisawad M, Verner E, Loury D, Chang B, et al. The bruton tyrosine kinase inhibitor PCI-32765 blocks b-cell activation and is efficacious in models of autoimmune disease and b-cell malignancy. *Proc Natl Acad Sci U S A.* (2010) 107(29):13075–80. doi: 10.1073/pnas.1004594107

29. von Hundelshausen P, Siess W. Bleeding by bruton tyrosine kinase-inhibitors: Dependency on drug type and disease. *Cancers (Basel)* (2021) 13(5). doi: 10.3390/cancers13051103

30. Nicolson PLR, Nock SH, Hinds J, Garcia-Quintanilla L, Smith CW, Campos J, et al. Low-dose btk inhibitors selectively block platelet activation by CLEC-2. *Haematologica* (2021) 106(1):208–19. doi: 10.3324/haematol.2019.218545

31. Busygina K, Jamasbi J, Seiler T, Deckmyn H, Weber C, Brandl R, et al. Oral bruton tyrosine kinase inhibitors selectively block atherosclerotic plaque-triggered thrombus formation in humans. *Blood* (2018) 131(24):2605–16. doi: 10.1182/blood-2017-09-808808

32. Busygina K, Denzinger V, Bernlochner I, Weber C, Lorenz R, Siess W. Btk inhibitors as first oral atherothrombosis-selective antiplatelet drugs? *Thromb Haemost* (2019) 119(8):1212–21. doi: 10.1055/s-0039-1687877

33. Exeni RA, Fernandez-Brando RJ, Santiago AP, Fiorentino GA, Exeni AM, Ramos MV, et al. Pathogenic role of inflammatory response during shiga toxin-associated hemolytic uremic syndrome (HUS). *Pediatr Nephrol* (2018) 33(11):2057–71. doi: 10.1007/s00467-017-3876-0

34. Morigi M, Zoja C, Figliuzzi M, Foppolo M, Micheletti G, Bontempelli M, et al. Fluid shear stress modulates surface expression of adhesion molecules by endothelial cells. *Blood* (1995) 85(7):1696–703. doi: 10.1182/blood.V85.7.1696.bloodjournal8571696

35. Morigi M, Galbusera M, Binda E, Imberti B, Gastoldi S, Remuzzi A, et al. Verotoxin-1-induced up-regulation of adhesive molecules renders microvascular endothelial cells thrombogenic at high shear stress. *Blood* (2001) 98(6):1828–35. doi: 10.1182/blood.V98.6.1828

36. Fernandez GC, Gomez SA, Ramos MV, Bentancor LV, Fernandez-Brando RJ, Landoni VI, et al. The functional state of neutrophils correlates with the severity of renal dysfunction in children with hemolytic uremic syndrome. *Pediatr Res* (2007) 61 (1):123–8. doi: 10.1203/01.pdr.0000250037.47169.55

37. Fernandez GC, Lopez MF, Gomez SA, Ramos MV, Bentancor LV, Fernandez-Brando RJ, et al. Relevance of neutrophils in the murine model of haemolytic uraemic syndrome: mechanisms involved in shiga toxin type 2-induced neutrophilia. *Clin Exp Immunol* (2006) 146(1):76–84. doi: 10.1111/j.1365-2249.2006.03155.x

38. Farrar JE, Rohrer J, Conley ME. Neutropenia in X-linked agammaglobulinemia. *Clin Immunol Immunopathol* (1996) 81(3):271–6. doi: 10.1006/clin.1996.0188

39. Kozlowski C, Evans DI. Neutropenia associated with X-linked agammaglobulinaemia. *J Clin Pathol* (1991) 44(5):388–90. doi: 10.1136/jcp.44.5.388

40. Lill JK, Thiebes S, Pohl JM, Bottek J, Subramaniam N, Christ R, et al. Tissue-resident macrophages mediate neutrophil recruitment and kidney injury in shiga toxin-induced hemolytic uremic syndrome. *Kidney Int* (2021) 100(2):349–63. doi: 10.1016/j.kint.2021.03.039

41. Volmering S, Block H, Boras M, Lowell CA, Zarbock A. The neutrophil btk signalosome regulates integrin activation during sterile inflammation. *Immunity* (2016) 44(1):73–87. doi: 10.1016/j.immuni.2015.11.011

42. Mueller H, Stadtmann A, Van Aken H, Hirsch E, Wang D, Ley K, et al. Tyrosine kinase btk regulates e-selectin-mediated integrin activation and neutrophil recruitment by controlling phospholipase c (PLC) gamma2 and PI3Kgamma pathways. *Blood* (2010) 115(15):3118–27. doi: 10.1182/blood-2009-11-254185

43. Tomlinson MG, Woods DB, McMahon M, Wahl MI, Witte ON, Kurosaki T, et al. A conditional form of bruton's tyrosine kinase is sufficient to activate multiple downstream signaling pathways *via* PLC gamma 2 in b cells. *BMC Immunol* (2001) 2:4. doi: 10.1186/1471-2172-2-4

44. Rodriguez R, Matsuda M, Perisic O, Bravo J, Paul A, Jones NP, et al. Tyrosine residues in phospholipase cgamma 2 essential for the enzyme function in b-cell signaling. *J Biol Chem* (2001) 276(51):47982–92. doi: 10.1074/jbc.M107577200

45. Ito M, Shichita T, Okada M, Komine R, Noguchi Y, Yoshimura A, et al. Bruton's tyrosine kinase is essential for NLRP3 inflammasome activation and contributes to ischaemic brain injury. *Nat Commun* (2015) 6:7360. doi: 10.1038/ncomms8360

46. Liu X, Pichulik T, Wolz OO, Dang TM, Stutz A, Dillen C, et al. LRR, and PYD domain-containing protein 3 (NLRP3) inflammasome activity is regulated by and potentially targetable through bruton tyrosine kinase. *J Allergy Clin Immunol* (2017) 140(4):1054–67 e10. doi: 10.1016/j.jaci.2017.01.017

47. Bittner ZA, Liu X, Mateo Tortola M, Tapia-Abellan A, Shankar S, Andreeva L, et al. BTK operates a phospho-tyrosine switch to regulate NLRP3 inflammasome activity. *J Exp Med* (2021) 218(11). doi: 10.1084/jem.20201656

48. Weber ANR. Targeting the NLRP3 inflammasome *via* BTK. *Front Cell Dev Biol* (2021) 9:630479. doi: 10.3389/fcell.2021.630479

49. Wang H, Li S, Cui Z, Qin T, Shi H, Ma J, et al. Analysis of spleen histopathology, splenocyte composition and haematological parameters in four strains of mice infected with plasmodium berghei K173. *Malar J* (2021) 20(1):249. doi: 10.1186/s12936-021-03786-z

50. Suttie AW. Histopathology of the spleen. *Toxicol Pathol* (2006) 34(5):466–503. doi: 10.1080/01926230600867750

Frontiers in Immunology

Explores novel approaches and diagnoses to treat immune disorders.

The official journal of the International Union of Immunological Societies (IUIS) and the most cited in its field, leading the way for research across basic, translational and clinical immunology.

Discover the latest Research Topics

See more →

Frontiers

Avenue du Tribunal-Fédéral 34
1005 Lausanne, Switzerland
frontiersin.org

Contact us

+41 (0)21 510 17 00
frontiersin.org/about/contact